THERMOCONSOLIDATION AND THERMAL DISPERSION IN DEFORMABLE POROUS MEDIA

by

CHEO K. LEE

B.S. in Engineering, Seoul National University, Seoul, Korea 1979
M.S. in Engineering, Seoul National University, Seoul, Korea 1981

SUBMITTED TO THE DEPARTMENT OF CIVIL AND ENVIRONMENTAL ENGINEERING
IN PARTIAL FULFILLMENT OF THE REQUIREMENTS
FOR THE DEGREE OF

DOCTOR OF PHILOSOPHY

at the

MASSACHUSETTS INSTITUTE OF TECHNOLOGY

May, 1994

Signature of the Author _____

Department of Civil and Environmental Engineering

Certified by _____ 5/10/94

Chiang C. Mei
Professor of Civil and Environmental Engineering
Thesis Supervisor

Accepted by _____

Joseph M. Sussman
Chairman, Departmental
Committee on Graduate Studies

THERMOCONSOLIDATION AND THERMAL DISPERION IN DEFORMABLE POROUS MEDIA

by

CHEO K. LEE

submitted to the Department of Civil and Environmental Engineering
on May 11th, 1994 in partial fulfillment of the requirements
for the degree of Doctor of Philosophy
at the Massachusetts Institute of Technology

ABSTRACT

Part A
Thermoconsolidation in Poroelastic Media

The theory of homogenization, which is a rigorous method of averaging with multiple-scale perturbation expansions, is applied to thermoconsolidation in porous media. The assumptions are the existence of disparate length scales and the periodicity of medium structure and material properties on the lower scales.

In Chapter I, we consider two-scale periodic porous media. The governing equations and constitutive coefficients on the macroscale are deduced without any empirical or closure assumptions starting from the basic conservation laws on the microscale. When the medium deformation is comparable to typical grain size, the governing equations are in general nonlinearly coupled due to nonlinear boundary conditions on the fluid-solid interfaces. Therefore the phenomenologically based Biot's linear theory of consolidation must be limited to the cases with solid displacement much smaller than the grain size. However, those nonlinear terms originating from the nonlinear interface boundary conditions vanish for special class of microcell geometries with three orthogonal planes of symmetry and Biot's theory is still valid. By extending Auriault and Sanchez-Palencia (1977), certain properties and constraints on the macroscale coefficients are established. For a cubic array of Wigner-Seitz grains the microcell boundary value problems are solved numerically to calculate the macroscale coefficients. The elastic coefficient tensor possesses cubic symmetry and other coefficients are isotropic. The macroscale equations are applied to the pumping of hot fluid from geothermal reservoirs. In the case of two-dimensional pumping through a small sink at the bottom, when the Rayleigh number is sufficiently large, the seepage flow develops cellular convective motion and the upper surface deforms in wavy pattern.

In Chapter II, the two-scale analysis is extended to three-scale media to deduce the macroscale governing equations and constitutive coefficients starting from the mesoscale equations. The theory is applied to layered medium on the mesoscale and the effects of the contrast of the mesoscale coefficients on the anisotropy of the macroscale coefficients are examined.

Part B
Thermal Dispersion in Poroelastic Media

The theory of homogenization is applied to thermal dispersion in relatively highly permeable and hard poroelastic media.

In Chapter I, thermal dispersion in two-scale media is investigated assuming that the microscale Peclét number and the Rayleigh number are finite. The microcell boundary value problem which is a convection-diffusion equation is defined and is identical to that for rigid media by Mei(1991). The dispersion tensor is in general non-symmetric. For a cubic array of Wiger-Seitz grains, by solving the microcell boundary value problem numerically for a mean flow direction along the symmetry axis the dispersion tensor is calculated. For such case there are two non-vanishing coefficients, the longtudinal D_L and the transvers D_T. For large Peclét number, both grow as the square of Peclét number. This is in contrast with the numerous experiments with natural granular media which shows as the first power of Peclét number.

In Chapter II, thermal dispersion in three-scale media is analyzed. It is assumed that the mesoscale Peclét number is finite but the Rayleigh number is large. Due to buoyancy the flow and heat transport on the macroscale are nonlinearly coupled. Also the mesoscale cell boundary value problem is nonlinearly coupled to the governing equations for flow and heat transport on the macroscale. For layered medium, the symmetric and anti-symmetric dispersion tensors are derived analytically. The longitudinal dispersion coefficient along the horizontal direction grows as the square of mesoscale Peclét number when the mean flow is parallel to the layers but reaches finite limit value when the mean flow is not parallel to the layers. The transverse dispersion coefficient in the vertical direction always reaches finite limit as the Peclét number increases. The off-diagonal and anti-symmetric dispersion coefficients are in general nonzero. The macroscale equations are applied to the dispersion of a thermal cloud released in a uniform seepage flow through a layered medium. For sufficiently large Rayleigh number the cloud rises across the depth due to strong buoyancy while it is being convected by the uniform flow. The variation of the longitudinal dispersion coefficient can be large. The Peclét number tends to decrease the effects of Rayleigh number.

Thesis supervisor : Chiang C. Mei

Title : Professor of Civil and Environmental Engineering

To my wife Kyung-Ok

and

children Sang-Hyub and Sang-Jee

ACKNOWLEDGEMENT

I am very much indebted to my advisor Professor Chiang C. Mei for his unfailing support, guidance and enthusiasm. Much of the work here would have not been possible without his keen insight and guidance. I owe much of myself present day to him. His scholarship and pursuit of thoroughness are the kind of standards I will always put forth in the future.

I am thankful to my committee members, Professors Lynn Gelhar, Borivoje Mikic, Howard Brenner, Rohan Abeyaratne and Daniel Rothman for their interests and encouragement.

The present research has been supported by the National Science Foundation, Geomechanics/ Geotechnical/ Geoenvironmental Program (Grant MSS-9019976, 'Modeling Porous and Deformable Media') and Fluid Mechanics/ Hydraulics/ Particles Program (Grant CTS-9115689, 'Water Wave Dynamics and Dispersion'). The support is greatly acknowledged.

I thank Pat Dixon who has been of great help in many ways. My thanks also go to Elaine, Karen, Carol and Dolores. Special thanks go to Mrs. Carol Mei for so many invitations to dinner and most of all the warmth and kindness she showed will always be with me and my family. Many of the Parsons Lab friends deserve my sincere appreciation for making this lab a memorable place. I especially thank friends in our group, former and present, for being there and sharing a diversity of different views and much more. I also thank Chin-Cheng Sun for kindly letting me use the data he gathered from literature. His extensive collection of experimental data on dispersion has provided me with very useful information and has been used in Chapter I, Part B in the thesis.

My family has been an invaluable source of encouragement and support. Hardly I can find words for my wife Kyung who has endured the long journey maintaining our home the most precious place. My children have been of great pleasure to me. Often they awakened me up to recognize some important aspects of life that I have been ignorant. Finally I thank my parents for their encouragement and support from remote home. Their life-long moral encouragement to pursue lofty ideal will always be incarved in me.

TABLE OF CONTENTS

PART B. THERMAL DISPERSION IN POROELASTIC MEDIA

PART A. THERMOCONSOLIDATION IN POROELASTIC MEDIA

NOTATIONS

a	elastic coefficient tensor of rank four $a_{ijk\ell}$ in solid
a_I	elastic coefficient a'_{zzzz} in a medium with cubic symmetry
a_{II}	elastic coefficient a'_{zzyy} in a medium with cubic symmetry
a_{III}	elastic coefficient a'_{zyzy} in a medium with cubic symmetry
a'	elastic coefficient tensor of rank four $a'_{ijk\ell}$ of porous medium on the ℓ' scale
a''	elastic coefficient tensor of rank four $a''_{ijk\ell}$ of porous medium on the ℓ'' scale
$\bar{a}$	average heat capacity of porous medium on the ℓ' scale
$A^{f,s}$	vector function for $\theta^{(1)}_{f,s}$
A'	vector function for $\theta^{(1)}$ (cf. (3.3.2) in Chapter II)
A_{ij}	coordinate transformation matrix (cf. (C.5) in Appendix C)
$\mathbf{A}_f, \mathbf{A}_s$	coefficient matrices in finite element equation for heat diffusion
b	ratio of thermal stress to pore pressure
$b_{\alpha\beta rr}$	compliance tensor of rank four
B	scale of thermal modulus
B_{ij}	coordinate transformation matrix (cf. (C.22) in Appendix C)
C'_j	vector coefficient (cf. (3.3.26) in Chapter I)
C_p	specific heat
$\mathbf{D}$	stiffness matrix for solid in finite element equation
e	extrapolation error in numerical results
$\mathbf{e}_i$	unit vector in i-th direction
E	Young's modulus
E'_j	vector coefficient (cf. (3.3.26) in Chapter I)
$\mathbf{E}$	elastic coefficient matrix in finite element equation
$\mathbf{f}_f, \mathbf{f}_s$	forcing vector terms in finite element equation for heat diffusion
F'_{jmngh}	fifth order tensor coefficient (cf. (3.3.13) in Chapter I)
$\mathbf{F}$	forcing vector in finite element equation for Stokes problem
g	gravitational acceleration
G'_{jmn}	third order tensor coefficient (cf. (3.3.13) in Chapter I)
H'_{jmn}	third order tensor coefficient (cf. (3.3.13) in Chapter I)
I	identity tensor
I'_j	vector coefficient (cf. (3.3.13) in Chapter I)
J_h	functional for heat diffusion problem in microcell
J_f	functional for Stokes problem in microcell

J_ϵ	functional for elastostatic problem in microcell
J'_{jmn}	third order tensor coefficient (cf. (3.3.26) in Chapter I)
$[J]$	Jacobian matrix in finite element equation
k	second order tensor k_{ij} (cf. (3.3.19) in Chapter I)
k'	permeability tensor k'_{ij} on the ℓ' scale
k''	permeability tensor k''_{ij} on the ℓ'' scale
K	hydraulic conductivity of porous medium or bulk modulus of solid
K'_j	vector coefficient (cf. (3.3.13) in Chapter I)
$\mathbf{K}_k, \mathbf{K}_S$	coefficient matrices in finite element equation for Stokes problem
$\mathbf{K}_\phi$	coefficient matrix in finite element equation for elasticity in microcell
ℓ	microscale length
ℓ'	macroscale length in two-scale medium or mesoscale length in three-scale medium
ℓ''	macroscale length in three-scale medium
L'_j	vector coefficient (cf. (3.3.26) in Chapter I)
$m_{f,s}$	thermal conductivity of fluid(f) or soild(s)
m'	thermal conductivity of porous medium on the ℓ' scale
m''	thermal conductivity of porous medium on the ℓ'' scale
$M_{f,s}$	scale of thermal conductivity of fluid(f) or soild(s)
M_r	M_s/M_f
M'_{jmn}	third order tensor (cf. (3.3.26) in Chapter I)
n'	porosity on the mesoscale ℓ'
n''	porosity on the macroscale ℓ''
N	unit normal vector
$N^{f,s}$	outward unit normal vector from fluid(f) or soild(s)
N_o	unit normal vector on the initial fluid-solid interface
N_ξ	unit normal vector on the fluid-solid interface in the moving frame
N'_j	vector coefficient (cf. (3.3.26) in Chapter I)
$\mathbf{N}$	shape function matrix in finite elements
O	order symbol
p	dynamic pressure variation
p_s	initial static pressure
P	total pressure ($= p_s + p$)
P'	scale of pressure drop over the length ℓ'
P''	scale of pressure drop over the length ℓ''
Pe	microscale Peclét number

$\hat{Pe}$	Pe/ϵ
Pe^*	Peclét number for porous medium layer (cf. (7.2.5) in Chapter I)
Pe'	mesoscale Peclét number
$\hat{Pe'}$	Pe'/ϵ
Pr	Prandtl number
$\mathbf{q}(k)$	nodal unknown vector fro k in finite element equation for Stokes problem
$\mathbf{q}(S)$	nodal unknown vector for S in finite element equation for Stokes problem
$\mathbf{q}(\phi)$	nodal unknown vector in finite element equation for elasticity in microcell
$\mathbf{Q}_\phi$	force vector in finite element equation for elasticity in microcell
R_c	critical Rayleigh number for a porous medium layer
R'_j	vector coefficient (cf. (3.3.13) in Chapter I)
Ra	mesoscale Rayleigh number
Ra'	macroscale Rayleigh number
Re	Reynolds number ($=U\ell/\nu$)
$\hat{Re}$	Re/ϵ
$s, (1-s)$	thickness of layers
S	vector coefficient (cf. (3.3.19) in Chapter I)
S'	vector coefficient (cf. (3.2.10) in Chapter II)
S'_{mnk}	third order tensor coefficient (cf. (3.4.13) in Chapter I)
$S_i^{\pm}$	symmetry plane in a microcell at $x_i = 0(-)$ or $x_i = \ell/2(+)$
t	time
T_c	consoildation time scale over ℓ' scale
T'_c	consoildation time scale over ℓ'' scale
T_d	heat diffusion time scale over ℓ' scale
T'_d	heat diffusion time scale over ℓ'' scale
T_v	heat convection time scale over ℓ' scale
T'_v	heat convection time scale over ℓ'' scale
$T_{f,s}$	total temperature for fluid fluid(f) or soild(s) ($= \overline{T}_{f,s} + \theta_{f,s}$)
$\overline{T}_{f,s}$	initial temperature for fluid fluid(f) or soild(s)
$\overline{T}_j$	traction force in j-th direction on the fluid-solid interface
T'_k	vector coefficient (cf. (3.4.13) in Chapter I)
u	fluid velocity vector
u_d	fluid velocity vector relative to the solid velocity
U	scale of fluid velocity on the microscale ℓ
U'	scale of seepage velocity on the ℓ' scale
U_x, U_z	heat convection velocity in a porous layer

U_k' vector coefficient (cf. (3.4.13) in Chapter I)

$\overline{U}$ heat convection velocity on the ℓ' scale

v solid displacement

V' scale of solid displacement over ℓ' scale

V'' scale of solid displacement over ℓ'' scale

W' vector coefficient (cf. (3.2.10) in Chapter II)

x microscale vector coordinates

X microscale vector coordinates ($=x-\ell/2$)

x' mesoscale vector coordinates

x'' macroscale vector coordinates

x_N horizontal extent of computational domain in x

x' mesoscale vector coordinates

x'' macroscale vector coordinates

x, y, z Cartesian coordinates

α linear expansion coefficient of solid

α' pressure coefficient tensor of porous medium in Hookes's law (cf. (3.3.15) in Chapter I)

α'' pressure coefficient tensor of porous medium in Hookes's law (cf. (3.2.8) in Chapter II)

$\alpha_{f,s}$ thermal diffusivity of fluid(f) or soild(s)

β thermal modulus of solid

β_p compressibility of fluid

β_T thermal expansion coefficient of fluid

β_c' scalar coefficient (cf.(3.3.28) in Chapter I)

β_t' thermal modulus tensor of porous medium in Hookes's law (cf. (3.3.15) in Chapter I)

β_c'' scalar coefficient (cf.(3.2.14) in Chapter II)

β_t'' thermal modulus tensor of porous medium in Hookes's law (cf. (3.2.8) in Chapter II)

γ' second order tensor coefficient (cf.(3.3.28) in Chapter I)

γ'' second order tensor coefficient (cf.(3.2.14) in Chapter II)

Γ fluid-solid interface

$\Gamma_{f,s}$ fluid(f) or soild(s) part on the periodic boundary

Γ_ξ fluid-solid interface in the moving frame

δ scale of solid strain over ℓ' scale

δ'	scale of solid strain over ℓ'' scale
δ''_c	second order tensor coefficient (cf.(3.2.14) in Chapter II)
δ_{ij}	Kronecker delta
Δ_x	dilation of porous medium matrix$(=\nabla' \cdot v^{(0)})$
ϵ	scale ratio $(\ell/\ell'$ or $\ell'/\ell'')$
ζ	vector coefficient (cf.(3.3.3) in Chapter I)
ζ'	vector coefficient (cf.(3.2.3) in Chapter II)
ζ'_c	scalar coefficient (cf.(3.3.28) in Chapter I)
ζ''_c	scalar coefficient (cf.(3.2.14) in Chapter II)
η	vector coefficient (cf.(3.3.3) in Chapter I)
η'	vector coefficient (cf.(3.2.3) in Chapter II)
θ	medium temperature
θ'	$(=\theta'/Ra)$
$\theta_{f,s}$	temperature variation in the fluid(f) or soild(s)
Θ'	scale of temperature variation over ℓ'
Θ''	scale of temperature variation over ℓ''
λ	Lamé constant
μ	Lamé constant for solid or absolute viscosity of fluid
μ_o, μ_1	shear moduli of porous medium with cubic symmetry
ν	kinematic viscosity of fluid or Poisson's ratio for solid
ξ	microscale vector coordinates in the moving frame$(=x - v^{(0)})$ or logarithmic horizontal coordinate (cf.(7.3.1) in Chapter I)
ξ_N	horizontal extent of computational domain in ξ
ξ'	mesoscale vector coordinates in the moving frame$(=x' - v^{(0)})$
$\rho_{f,s}$	density of fluid(f) or soild(s)
ρ_o	reference density of fluid at the initial state
$(\rho C_p)_r$	$(\rho C_p)_s/\rho C_p)_f$
$\sigma_{f,s}$	stress in fluid(f) or soild(s)
σ_T	total stress$(=\sigma_f$ in $\Omega_f)$ or $(=\sigma_s$ in $\Omega_s)$
τ	time in the moving frame$(=t)$
ϕ	third order tensor (cf.(3.3.3) in Chapter I)
ϕ'	third order tensor (cf.(3.2.3) in Chapter II)
Φ	viscous dissipation in fluid
ψ	ϕ in a rotated frame (cf. (C.6) in Appendix C)
ω	rotation tensor ω_{ij} in solid
Ω	periodic cell on the microscale

Ω'	periodic cell on the mesoscale
$\Omega_{f,s}$	fluid(f) or soild(s) region in a microcell
$\mathcal{D}$	scale of the elastic modulus of solid
Cof	cofactor of a matrix
det	determinant of a matrix
$e(\cdot)$	microscale strain operator
$e_\xi(\cdot)$	microscale strain operator in the moving frame
$e'(\cdot)$	macroscale strain operator(2-scale) or mesoscale strain operator(3-scale)
$e'_\xi(\cdot)$	macroscale strain operator(2-scale) or mesoscale gradient operator(3-scale)
$e''(\cdot)$	macroscale strain operator(3-scale)
$e''_\xi(\cdot)$	macroscale strain operator(3-scale) in the moving frame
$(\cdot)^{(n)}$	n-th order term in perturbation series
$(\cdot)^T$	transpose
:	second order contraction
$(\cdot)^*$	normalized quantity
$(\cdot)^\pm$	variables in the upper(+) or lower(-) layer
$\bar{(\cdot)}$	coefficients in physical units
$\langle\cdot\rangle$	unit cell volume average
$[\![\cdot]\!]$	difference of between layers $(=(\cdot)^+ - (\cdot)^-)$
∇	microscale gradient operator
∇_ξ	microscale gradient operator in the moving frame
∇'	macroscale gradient operator(2-scale) or mesoscale gradient operator(3-scale)
∇'_ξ	macroscale gradient operator(2-scale) or mesoscale gradient operator(3-scale) in the moving frame
∇''	macroscale gradient operator(3-scale)

GENERAL INTRODUCTION

Land subsidence as a consequence of water, gas and oil withdrawal from underground is a widespread phenomenon in the areas of heavy urban growth and industrialization. Many of the world's major cities have suffered subsidence and there are extensive reviews of case histories (Poland and Davis, 1969; Poland, 1984; Waltham, 1989). The damages caused by subsidence are sometimes so serious that the estimated remedial cost for protection can be tremendous (Waltham, 1989). Some well known cases are the San Joaquin Valley and the Wilmington oil field in California, the Ekofisk oil field in the North Sea, and the Mexico City.

On the other hand, the geothermal energy is being actively exploited for power generation and other industrial purposes in many parts of the world (Lunis and Lienan, 1988; Keller, 1984). One of the major concerns is the soil subsidence caused by the extraction of hot fluid. Of particular interest is the Wairakei geothermal field in New Zealand (Stilwell, 1975; Bixley, 1984) where the extraction of the hot geothermal fluid has resulted in subsidence of $4.5m$. Narasimhan and Goyal (1984) list some case histories related to geothermal systems from around the world.

Geothermal reservoirs are usually categorized as either liquid-dominated or vapor-dominated but in practice most reservoirs are liquid-dominated (Donaldson and Grant, 1981). In addition to the Wairakei field, the liquid-dominated system at Cerro Prieto geothermal field in Mexico where electric power generation began in 1973 showed negligibly small subsidence until 1978. But after the earthquake of June 8, 1980, approximately 45 cm of vertical subsidence was recorded (Zelwer and Grannel, 1982). A typical example of vapor-dominated reservoir is the Geysers field, California, where the maximum subsidence of only 14 cm as of 1977 after four years of heavy production was measured (Lofgren, 1978). The above contrast shows that it is crucial to use appropriate data locally available in the prediction of subsidence (Narasimhan and Goyal, 1984).

In the present study, we shall particularly be interested in the thermoconsolidation of porous media. In fact, the isothermal consolidation is a subset of thermoconsolidation when the effects due to thermal changes are ignored.

LITERATURE REVIEW

Isothermal Consolidation

Starting from the linear theory of consolidation by Biot(1941) who deduced the three-dimensional theory of small strain deformation in porous media, there have been many works to model the ground subsidence. Extensive reviews can be found in Fallou et al(1992) and Lee et al(1992). We give only a brief review.

The most common approach is to model the soil body as multilayer system composed of highly permeable aquifers and less permeable aquitards. In some models (Verruijt, 1969; Corapcioglu and Brutsaert, 1977; Bear and Corapcioglu, 1981a,b; Corapcioglu and Bear, 1983), aquifers are assumed to be primarily responsible for the soil deformation so that aquitards are treated only as thin film across which pressure drop occurs. However, the deformation in aquitards is also known to cause subsidence because of the relatively large compressibility (Poland and Davis, 1969) and have been included in later models (Gambolati and Freeze, 1973; Gambolati et al, 1974; Helm, 1975, 1976). On the other hand, by invoking the quasi-three dimensional approximation introduced by Hantush(1960) and Hantush and Jacob(1955a,b) i.e. the flow is mainly horizontal and vertical respectively in aquifers and aquitards, other models have been developed (Herrera and Figueroa, 1969; Frind, 1983; Gambolati et al, 1986; Neumann and Witherspoon, 1969; Neumann et al, 1982).

When the aquitards are sufficiently soft and thick, the self-weight effect of the soil is also important (Gibson et al, 1967, 1981; and Mei, 1985). For pumping from a layered soil, Fallou et al(1992) have examined the self-weight effects on the decline of pore pressure and the subsidence. It has been extended by Lee et al(1992) to the case of finite strain including soil hysteresis by employing the Lagrangian approach

introduced by Cooper(1966) and used by Gambolati(1973a,b), Gibson et al(1967, 1981).

Thermoconsolidation

By allowing thermal effects in both fluid and solid, Schiffman(1971) first formulated the linearized thermoelastic theory of consolidation for porous medium in which the classical laws of Hooke, Fourier and Darcy were incorporated, but the convective heat transport due to fluid motion was not included. Later Derski and Kowalski(1979) derived the governing equations for thermoconsolidation which include the heat convection. They assumed that the medium is identically homogeneous and isotropic.

Brownell et al(1977) also obtained the thermoelastic governing equations which take into account the coupling between fluid and solid matrix. By using some typical data from geothermal reservoirs they examined the inertia terms in the momentum equations, the pressure work and the viscous dissipation in the energy equation and showed that they are negligibly small. However, the heat convection due to solid movement, which is important when the consolidation and heat diffusion time scales are comparable, was not included. Later their equations were used to simulate the radial flow due to line source which penetrates across the depth of a confined hot water geothermal reservoir and two-phase flow in geothermal wells by Garg and Pritchett(1984a,b). Since the attention was focused on rocks with small compressibility, the subsidence has been discarded.

Bear and Corapcioglu(1981c) also proposed a model for thermoconsolidation in an aquifer by taking the coupling of poroelastic medium and fluid into account but their discussion was mainly on the variation of depth-averaged quantities in the horizontal direction. Many ad hoc assumptions are introduced which are hard to assess. Kurashige(1989) considered the linear thermoelastic behavior around a spherical cavity which is subject to hot (or cold) water injection. His results show that either the convective or the conductive transport of heat and pore pressure could be dominant depending on the permeability of the medium.

Consolidation due to Local Heat Source

Radioactive resources have long been used to generate nuclear power in many countries. The problem of how to treat the nuclear wastes became important and therefore many possible disposal concepts were considered (Frosch, 1977). One porposal is to store the nuclear wastes in canisters which are shot down deep into a mud sea bottom. The anticipated problems are thermostress around the canister which may fail and toxic material transport caused by fracture due to released heat (Hollister, 1977; Silva, 1977).

The thermoconsolidation around a point source in an infinite medium was studied by Booker and Savvidou(1985) with material properties homogeneous and isotropic both thermomechanically and hydraulically. Only conduction was allowed. After obtaining the fundamental solution due to point source, they simulated a cylindrical source such as heat generating canister and found that only a small fraction of the pore pressure which would be achieved in impermeable medium is reached. The same kind of approach was applied to layered medium of semi-infinite extent with a decaying heat source buried at finite depth from the top surface where traction forces and temperature variations are zero (Small and Booker, 1986). Again no flow was taken into account and only conduction was allowed. A homogeneous medium which is elastically isotropic but hydraulically anisotropic (greater permeability in horizontal direction than in vertical dirction) was analyzed similarly (Savvidou and Booker, 1989) and the results show that the increase in both pore pressure and compressional stress is significantly smaller than the case for isotropic soil with equal vertical permeability.

For one-dimensional thermoelastic responses in a porous half space, McTigue (1986) has examined the pressure and temperature distributions due to several conditions on the top surface such as drainage and impermeable and also constant temperature and heat flux. It is shown that, in all cases, both the pressure and temperature develop to higher level as the ratio of permeability to thermal diffusivity

decreases. On the other hand, a thick and soft soil layer was studied thermoelastically for temperature changes on the surface by taking the self-weight effects into account in one-dimensional problem by Mei and Tyvand(1988). It was shown that depending on a parameter which characterizes the relative importance of the gravity effect to the diffusional term in the solid momentum equation, the gound surface may swell up or settle down.

Convective Heat Transfer in Porous Media

On the basic side, there has been a vast literature on the natural convection in porous media starting from Lapwood(1948). Mainly the flow instability is considered in a porous layer heated from below, horizontal or inclined. Extensive reviews can be found in Cheng(1978), Combarnous and Bories(1975) and Nield and Bejan(1992).

Aquifers have also been recognized as a mean for storing thermal energy. The associated problems such as gorund water flow and heat transport were surveyed by Mercer et al(1982). Mercer et al (1975) used the finite element method for depth-averaged governing equations to simulate the areal distribution of heat and temperature at the Wairakei geothermal field within a numerical domain large enough to cover the actual field. The steady distributions of hydraulic head and temperature prior to exploitation were used as initial conditions for the transient problem after 1955. The calculated head distributions were not in good agreement with measured data.

The natural convection about a vertical impermeable wall or cylinder has been studied to model hot dikes, formed by magma intrusion into shallow depths of earth's crust, which can serve as energy source. Cheng and Minkowycz(1977) applied the boundary layer approximations for flow in porous media invoked by Wooding(1963) and McNabb(1965) to the vertical buoyant flow at a heated vertical wall. Minkowycz and Cheng(1976) used same approach for a cylindrical intrusion. Wooding (1963) idealized the Wairakei field as a geothermal plume with implicit assumption that the Prandtl number is finite i.e. restricting the region of thermal diffusion

to that of mixing between fluids at different temperatures. Yih(1965) considered the same problem in an infinite region and pointed out that Wooding's solutions are valid for all Prandtl numbers. On the other hand, Cheng(1978) demonstrates that the plume problem is a special case of free convection around a vertical wall if the wall temperature has special vertical distribution given by $T_w = T_\infty + Ax^{-1/3}$ where T_∞ is the uniform medium temperature in the outer field, A is a constant and x is the vertical coordinate positive upwards.

Rana et al(1979) computed the flow pattern and isotherms in a three-layer medium with one layer of low permeability sandwiched between two others in order to simulate the rock formations in Hawaii. The results show that a multi-cellular convection pattern may occur due to the presence of the lower permeability layer.

Theory of Homogenization for the Mechanics of Porous Media

The amount of work required to analyze problems such as flow through porous media or gorund subsidence either analytical or numerical becomes extremely large when the number of inclusions such as lenses,beds or in highly idealized terms thin layers increases. While these remain practically impossible tasks, the theory of homogenization introduced by Sanchez-Palencia (1974) and summarized in the books by Bensoussan et al (1978), Sanchez-Palencia (1980), Bakhvalov and Panasenko(1989) and Ene and Polisevski(1987), has been successful in providing a general scheme for deducing both macroscale governing equations and the effective constitutive coefficients for the mechanics and dynamics of rigid and deformable porous media from microscopic mechanics. The strength of this theory is that within the assumed framework even Darcy's law is computable and no empirical assumptions are made. The limitations are associated with the assumptions as discussed below.

In the original theory of homogenization, two key assumptions are made. One is the existence of two well separated spatial scales, namely the microscale ℓ and the macroscale ℓ' where $\ell/\ell' = \epsilon \ll 1$ and ϵ serves as ordering parameter which is used in the subsequent asymptotic expansions of physical variables. Secondly,

all unknowns and material properties are assumed to be periodic on the microscale so that averages over the microscale cell are well defined. In order to obtain the governing equations and constitutive coefficients at the macroscale, the standard multiple scale perturbation is then used.

For the fluid flow through rigid porous medium with two spatial scales, the phenomenological and empirically established Darcy's law can be rigorously derived from the microscale problems in terms of structural characterics at the microscale (Ene and Sanchez-Palencia, 1973, 1975). This has been extended to include the deformation of poroelastic medium for two scale by Auriault and Sanchez-Palencia (1977) and the dynamics of porous media by Levy(1979), Burridge and Keller(1981) and Auriault et al(1985).

The theory has also been applied to thermal flows in saturated rigid porous medium. Steady heat conduction was considered starting from the heat equations for both solid and fluid phases at the microscale and the macroscale conduction equation and thermal conductivity were obtained (Ene and Sanchez-Palencia, 1981). They also studied the steady convective heat transfer in a rigid porous medium (Ene and Sanchez-Palencia, 1982). It is noted that the pressure and temperature distributions at leading order depend macroscale coordinates only and correspond to the externally imposed pressure gradient and temperature difference. Interesting examples of application to geothermal engineering can be found in Ene and Polisevski(1987).

While these were all concerned with two spatial scales, the situations encountered in fields exhibit features of more than two spatial scales by the presence of lenses and layers. The extension of the theory to three or more scales for the mechanics of porous media was carried out recently by Mei and Auriault(1989) with the addition of intermediate mesoscale. The scale relations are such that $\ell/\ell' = \ell'/\ell'' = \epsilon \ll 1$, where ℓ, ℓ' and ℓ'' are the microscale, mesoscale and macroscale respectively. By solving some canonical boundary value problems defined on the lower scales, one gets the constitutive coefficients of the next larger

scale. Finally, after solving the macroscale problem, the solution can be used backwards to calculate the solutions on the finer scales. For an example, they specialized the three-scale theory of consolidation to a transversely isotropic medium on the mesoscale to find the macroscale coefficients.

SCOPE OF THE PRESENT WORK

We are concerned with thermoconsolidation in porous media. First, in Chapter I, the two scale medium is considered. While the micro length scale is comparable to typical pore or grain size, our interests in the physical processes in porous media are over much larger macroscale. However, the description on the macroscale should take account of the effects of microscale variations on the macroscale behavior. This is achieved for spatially periodic medium without making any empirical or closure assumptions by using the homogenization theory starting from the basic conservation laws on the microscale. Specifically on the macroscale, the equations of quasi-static equilibrium, Darcy's law, consolidation and heat transport are derived. Several canonical microcell boundary value problems are defined. For the elastic property, a set of elastostatic problems with prescribed traction forces on the fluid-solid interface in a given cell geomtry is defined. For the seepage flow, the Stokes problem is defined in the fluid phase. Similarly for heat transport, a coupled heat diffusion problem for both fluid and solid phases is obtained. By solving them numerically for a chosen microcell geometry, the macroscale coefficients are calculated.

In Chapter II, a porous medium with three disparate length scales is considered. Starting from the governing equations on the mesoscale derived in Chapter I, the homogenization procedure is applied to deduce the macroscale governing equations. They are in the same form as those on the mesoscale. However the effects of inhomogeneities in terms of the medium properties on the mesoscale are incorporated and can be determined by solving some canonical boundary value problems defined on the mesoscale. The elasticity, flow and heat diffuion problems are defined whose solutions are nontrivial only when the medium properties on the mesoscale

are nonuniform. Therefore in a medium uniform on the mesoscale the whole problem reduces to the two scale one identically. For periodically layered medium in alternating fashion on the mesoscale, the macroscale coefficients are examined in terms of the contrast in the mesoscale coefficients.

Chapter I. THERMOCONSOLIDATION IN TWO-SCALE POROUS MEDIA

1. Introduction

A two scale porous medium is characterized by the existence of two disparate length scales, the microscale ℓ and the macroscale ℓ'. The scale ratio $\epsilon = \ell/\ell'$ is assumed to be very small. The structure of the porous medium is assumed to be periodic on the microscale with periodic length ℓ. It is also assumed that the variables and material propertiers are periodic over the microscale.

It is shown that, in general, the macroscale equations which govern the deformation, flow and heat transport are nonlinearly coupled when the solid displacement is allowed to be comparable to a typical grain size. However, those nonlinear terms vanish for special class of cell geometry on the microscale with three orthogonal planes of symmetry. Even for such case, the governing equations are nonlinearly coupled via heat convection.

The general theory is applied to one-and two-dimensional thermoconsolidation in a porous layer due to pumping of pore fluid. The effects of buoyancy and nonlinear coupling in the heat convection are examined.

2. The Governing Equations and Boundary Conditions

The fluid is assumed to be slightly compressible with finite thermal expansion coefficient but with negligible compressibility under isothermal pressure. Viscous dissipation and compressional work will also be neglected from the outset. Errors due to omission will be examined a posteriori after deducing the macroscale governing equations in §3.

2.1 The Governing Equations, Boundary Conditions and Order Estimates

On the microscale the interstitial fluid is governed by the conservation laws of mass

$$\nabla \cdot u = 0 \quad \text{in} \quad \Omega_f \tag{2.1.1}$$

momentum

$$\rho_f \left(\frac{\partial u}{\partial t} + u \cdot \nabla u \right) = -\nabla P + \mu \nabla^2 u - \rho_f g \mathbf{e}_z \quad \text{in} \quad \Omega_f \tag{2.1.2}$$

and energy

$$(\rho C_p)_f \left(\frac{\partial T_f}{\partial t} + u \cdot \nabla T_f \right) = \nabla \cdot (m_f \cdot \nabla T_f) \quad \text{in} \quad \Omega_f \tag{2.1.3}$$

where u, p and T are the velocity, total pressure and total temperature and the subscript f denotes the fluid phase. Also, ρ, C_p and m denote the density, specific heat and thermal conductivity, respectively. Note that the total pressure P is the sum of initial static pressure p_s and the dynamic pressure p. Also T_f is the sum of the initial temperature $\overline{T}_f$ and the temperature variation θ_f from the initial state i.e.

$$T_f = \overline{T}_f + \theta_f \tag{2.1.4}$$

We adopt the following equation of state for the pore fluid

$$\rho_f = \rho_o (1 - \beta_T \theta_f) \tag{2.1.5}$$

where ρ_o is the reference density at $\theta_f = 0$ and β_T is the thermal expansion coefficient of fluid. Accordingly

$$\nabla p_s = -\rho_o(z)g \tag{2.1.6}$$

Substituting (2.1.5) and (2.1.6) into (2.1.2) and making use of Boussinesq approximation we obtain

$$\rho_o\left(\frac{\partial u}{\partial t} + u \cdot \nabla u\right) = -\nabla p + \mu\nabla^2 u + \rho_o g\beta_T\theta_f \mathbf{e}_z \quad \text{in} \quad \Omega_f \tag{2.1.7}$$

The last term represents the bouyant force due to gravity.

The momentum balance in the solid phase, for sufficiently slow motion, is governed by the equation of *quasi*-static equilibrium

$$\nabla \cdot \sigma_s = 0 \quad \text{in} \quad \Omega_s \tag{2.1.8}$$

The energy balance is governed by

$$(\rho C_p)_s\left(\frac{\partial T_s}{\partial t} + \frac{dv}{dt} \cdot \nabla T_s\right) = \nabla \cdot (m_s \cdot \nabla T_s) \quad \text{in} \quad \Omega_s \tag{2.1.9}$$

where σ_s is the solid stress, dv/dt is the velocity of solid phase and $T_s = \overline{T}_s + \theta_s$ is the total temperature of solid with θ_s being the variation from the initial state. As will be shown later, the convective transfer due to solid movement is needed in (2.1.9) in a consolidationg medium. Assuming linear elastic deformation, the solid stress σ_s is related to v via Hooke's law

$$\sigma_s = a : e(v) - \beta\theta_s \cdot I \tag{2.1.10}$$

where a is the elastic coefficient tensor of rank four and β is the thermal modulus tensor of rank two. The symbol I denotes the identity tensor.

Let $\Gamma(t)$ be the wetted surface of a grain. The kinematic boundary condition demands that the velocity vector be continuous across $\Gamma(t)$.

$$u = \frac{dv}{dt} \qquad \text{on} \quad \Gamma(t) \tag{2.1.11}$$

The dynamical condition requires that the normal stress be also continuous across $\Gamma(t)$, *i.e.*,

$$\sigma_s \cdot N = \sigma_f \cdot N \qquad \text{on} \quad \Gamma(t) \tag{2.1.12}$$

where N is the unit normal vector on Γ pointing from the fluid into the solid. The fluid stress σ_f is defined as

$$\sigma_f = -pI + 2\mu e(u) \tag{2.1.13}$$

where $e(\ )$ is the linear strain operator

$$e(u) = \frac{1}{2}\left[\nabla u + (\nabla u)^T\right] \tag{2.1.14}$$

In addition, the temperature and the normal heat flux must be continuous across Γ:

$$T_f = T_s \qquad \text{on} \quad \Gamma(t) \tag{2.1.15}$$

$$(m_f \cdot \nabla T_f) \cdot N = (m_s \cdot \nabla T_s) \cdot N \qquad \text{on} \quad \Gamma(t) \tag{2.1.16}$$

Consider the flow through pores of micro-length scale ℓ driven by a pressure drop P' over the macroscale ℓ'. We impose the basic assumptions that the length ratio $\epsilon = \ell/\ell' \ll 1$ is very small and that the fluid velocity is very low so that momentum balance is dominated by the driving pressure gradient of $O(P'/\ell')$ and the viscous stress of $O(\mu U/\ell^2)$ in (2.1.2) *i.e.*,

$$U = \frac{P'\ell^2}{\mu\ell'} \tag{2.1.17}$$

Correspondingly, Reynolds number $Re = U\ell/\nu$ is very small.

$$Re \leq O(\epsilon) \tag{2.1.18}$$

There are, in principle, three times scales inherent in the present problem. One is the consolidation time T_c given by

$$T_c = \frac{\rho_f g \ell'^2}{\mathcal{D}K} \tag{2.1.19}$$

where $\mathcal{D}$ and $K = O\left(g\ell^2/\nu\right)$ are the elastic modulus and the hydraulic conductivity of the medium respectively. The other two are the convection and diffusion (conduction) time scales of heat transfer

$$T_v = \frac{\ell'}{U} \qquad \text{and} \qquad T_d = \frac{\ell'^2}{\alpha_f} \tag{2.1.20}$$

where $\alpha_f = m_f/(\rho C_p)_f$ is the thermal diffusivity of the fluid. Combining (2.1.19) and (2.1.20) we have

$$\frac{T_c}{T_d} = \frac{\rho_f g \alpha_f}{\mathcal{D}K} \quad \text{and} \quad \frac{T_v}{T_d} = \frac{\ell}{\ell'}\frac{\alpha_f}{U\ell} = \frac{\epsilon}{Pe} \tag{2.1.21}$$

where $Pe = U\ell/\alpha_f$ is the Pelét number. By definition $Pe = Re \cdot Pr$ where $Pr = \nu/\alpha_f$ is the Prandtl number.

Reported values of $\mathcal{D}$ and K vary over a wide range depending on the medium, as shown in Table 2.1(Domenico and Schwartz,1990). Accordingly the estimated ratio of the consolidation time to the heat diffusion time T_c/T_d ranges from very small values for rock to finite values for clay. Typical values of $\rho_f = O(10^3 kg/m^3)$ and $\alpha_f = O(10^{-7}m^2/s)$ were taken in Table 2.1.

	$\mathcal{D}(N/m^2)$	$K(m/s)$	T_c/T_d
clay	$10^6 - 10^8$	$10^{-11} - 10^{-9}$	$10^{-2} - 10^2$
sand	$10^7 - 10^8$	$10^{-7} - 10^{-4}$	$10^{-7} - 10^{-3}$
rock	10^{10}	$10^{-9} - 10^{-4}$	$10^{-9} - 10^{-4}$

Table 2.1. Typical values of $\mathcal{D}$ and K for some common soils and the ratio T_c/T_d

While the ratio T_c/T_d is strongly affected by the material properties, T_v/T_d depends only on the Peclét number which is a measure of the relative importance of heat convection to diffusion.

Turning to the stress continuity condition (2.1.12), we see after using (2.1.10) and (2.1.13) in (2.1.12) that

$$\frac{\sigma_f}{\sigma_s} \sim \frac{P'}{a : e(v)} \sim \frac{P'}{\mathcal{D}\delta} = O(1) \tag{2.1.22}$$

where $\mathcal{D}$ and δ are the scales of the elastic modulus a and the solid strain $e(v)$. Since Hooke's law (2.1.10) is legitimate only for infinitesimal strain, we assume

$$\delta \sim \frac{P'}{\mathcal{D}} \ll 1 \tag{2.1.23}$$

In this part, we shall consider only weak convection and specifically assume that the Peclét number is very small:

$$Pr = O(1); \quad Pe = O(\epsilon); \quad T_v/T_d = O(1) \tag{2.1.24}$$

The interesting case of $Pe = O(1)$ in which the dispersion on the macroscale is important will be the topic of Part B. In the present case, the deformation of the medium due to changes in pressure and temperature is of great concern while heat is transported by convection and diffusion. We shall assume that $\delta = O(\epsilon)$ in (2.1.22) so that

$$\delta \sim \frac{P'}{\mathcal{D}} = O(\epsilon) \tag{2.1.25}$$

This allows the deformation to be comparable to the microscale length ℓ. Since the total global solid strain is $\delta = \Delta V'/\ell'$ to the leading order, the total solid displacement of any grain can be as large as ℓ. Also, in view of the wide variation of the ratio T_c/T_d from medium to medium, the macroscale governing equations are deduced by allowing $T_c/T_d = O(1)$. It will be shown later that the governing equations for porous media such as sand or rock with $T_c/T_d \leq O(\epsilon^2)$ are given as a special case of $T_c/T_d = O(1)$.

2.2 Normalized Governing Equations and Boundary Conditions

Based on the scale estimates in the previous section, the governing equations and boundary conditions are normalized as follows:

$$
\begin{aligned}
&x = \ell x^*, \quad t = Tt^* \\
&u = Uu^* = \frac{P'\ell^2}{\mu\ell'}u^*, \quad p = P'p^*, \quad T_{f,s} = \Theta' T^*_{f,s} \\
&\sigma_s = \mathcal{D}\sigma^*_s, \quad \sigma_f = P'\sigma^*_f \quad v = \ell v^* \\
&a = \mathcal{D}a^*, \quad \beta = B\beta^*, \quad m_f = M_f m^*_f, \quad m_s = M_s m^*_s
\end{aligned}
\tag{2.2.1}
$$

in which variables with the superscript * are dimensionless. The time scale T is such that

$$
T = T_v \sim T_d \sim T_c \tag{2.2.2}
$$

The symbol Θ' is for the characteristic temperature variation over the macroscale ℓ'. Also, B and M_f and M_s are the orders of magnitude for the thermal modulus β and the thermal conductivities of fluid and solid. From linear thermoelasticity for isotropic material (Sokolnikoff 1956, p. 359) we have

$$
\sigma_{ij} = 2\mu e_{ij}(v) + \lambda e_{kk}(v)\delta_{ij} - \alpha(3\lambda + 2\mu)\theta_s\delta_{ij} \tag{2.2.3}
$$

where λ and μ are the Lamé constants and α is the coefficient of linear thermal expansion. It follows then

$$
B \sim \alpha\mathcal{D} \tag{2.2.4}
$$

Substituting (2.2.2) into (2.1.1), (2.1.7) and (2.1.3) we obtain, in the fluid phase

$$
\nabla^* \cdot u^* = 0 \qquad \text{in} \quad \Omega_f \tag{2.2.5}
$$

$$
\left[\frac{\rho_f \ell^2}{\mu T}\epsilon\right]\frac{\partial u^*}{\partial t^*} + \epsilon Re u^* \cdot \nabla^* u^* = -\nabla^* p^* + \epsilon\nabla^{*2}u^* + \left[\frac{\epsilon^2}{Pe}Ra\right]\theta^*_f \mathbf{e}_z \qquad \text{in} \quad \Omega_f \tag{2.2.6}
$$

$$
\left[\frac{\ell^2}{\alpha_f T}\right]\frac{\partial T^*_f}{\partial t^*} + Pe u^* \cdot \nabla^* T^*_f = \nabla^* \cdot (m^*_f \cdot \nabla^* T^*_f) \qquad \text{in} \quad \Omega_f \tag{2.2.7}
$$

where

$$
Ra = \frac{g\beta_T \ell^2 \ell' \Theta}{\nu\alpha_f} \tag{2.2.8}
$$

is the Rayleigh number. The dynamic temperature variation θ' may at most be comparable to the temperature difference over the macroscale ℓ' at the initial state.

It is also assumed that there is no natural convection at the initial state which means that the initial temperature $\overline{T}_f$ is governed by the pure diffusion equation

$$0 = \nabla^* \cdot (m_f^* \cdot \nabla^* \overline{T}_f^*) \qquad \text{in} \quad \Omega_f \tag{2.2.9}$$

Since the critical Rayleigh number for the onset of natural convection in a porous layer is $4\pi^2 \sim 40$ (Lapwood, 1948), we take

$$Ra \leq O(1) \tag{2.2.10}$$

From (2.2.2) and (2.2.6), the fluid stress σ_f in (2.1.13) is scaled as

$$\sigma_f^* = -p^* I + \epsilon e^*(u^*) \tag{2.2.11}$$

Similarly, in the solid phase, equations (2.1.10), (2.1.8) and (2.1.9) are normalized to give

$$\sigma_s^* = a^* : e^*(v^*) - [\alpha\Theta]\beta^*\theta_s^* \qquad \text{in} \quad \Omega_s \tag{2.2.12}$$

$$\nabla^* \cdot \sigma_s^* = 0 \qquad \text{in} \quad \Omega_s \tag{2.2.13}$$

$$\frac{(\rho C_p)_s}{(\rho C_p)_f}\left(\left[\frac{\ell^2}{\alpha_f T}\right]\frac{\partial T_s^*}{\partial t^*} + \left[\frac{V'\ell}{\alpha_f T}\right]\frac{dv^*}{dt^*}\cdot\nabla^* T_s^*\right) = \left[\frac{M_s}{M_f}\right]\nabla^*\cdot(m_s^*\cdot\nabla^* T_s^*) \quad \text{in} \quad \Omega_s \tag{2.2.14}$$

For common rocks and quartz which constitute the solid phase, typical values of the linear expansion coefficient α are $O(10^{-6} - 10^{-5\circ}C^{-1})$ (Jumikis(1983); Franklin and Dusseault(1989)). Allowing $\Theta' < O(10^{2\circ})$ we get $\alpha\Theta' < 10^{-3}$. Since the thermal stress must be balanced by the medium strain via Hooke's law(e.g. $\delta \sim \alpha\Theta'$), we shall specifically assume that

$$\alpha\Theta' \sim \delta = O(\epsilon) \tag{2.2.15}$$

in view of (2.1.25). The solid stress σ_s is then scaled by

$$\sigma_s^* = a^* : e^*(v^*) - \epsilon\beta^*\theta_s^* \tag{2.2.16}$$

The initial temperature of solid phase $\overline{T}_s$ is also governed by pure diffudion equation like (2.2.9).

The interface boundary conditions (2.1.11), (2.1.12), (2.1.15) and (2.1.16) are also normalized to

$$u^* = \left[\frac{V'}{UT}\right]\frac{dv^*}{dt^*} \qquad \text{on} \quad \Gamma(t) \tag{2.2.17}$$

$$\sigma_s^* \cdot N = \left[\frac{P}{\mathcal{D}}\right]\sigma_f^* \cdot N \qquad \text{on} \quad \Gamma(t) \tag{2.2.18}$$

$$T_f^* = T_s^* \qquad \text{on} \quad \Gamma(t) \tag{2.2.19}$$

$$(m_f^* \cdot \nabla^* T_f^*) \cdot N = \left[\frac{M_s}{M_f}\right](m_s^* \cdot \nabla^* T_s^*) \cdot N \qquad \text{on} \quad \Gamma(t) \tag{2.2.20}$$

In the above normalized equations, the factors which include the time scale T should be further estimated as follows.

We first estimate V'/UT which is the order of magnitude of the convection velocity in Ω_s relative to the fluid velocity. Recall that the ratio T_c/T_d varies over the range of $O(\epsilon^{-2})$ to $O(1)$ due to wide variation of T_c from soil to soil(see Table 2.1). Therefore, in order to assure the condition of infinitesimal strain (2.1.25) and to allow wide enough range of T_c/T_d in later applications, we write

$$\frac{V'}{UT} = O\left(\frac{V'}{UT_c}\frac{T_c}{T_d}\right) = O\left(\frac{\mathcal{D}}{P'}\frac{\nu K}{\ell\ell' g}\frac{T_c}{T_d}\right) = O\left(\epsilon\frac{\mathcal{D}}{P'}\frac{T_c}{T_d}\right) = O(1) \tag{2.2.21}$$

where $v = O(\ell)$, which was expected in the sentence after (2.1.25), and $K = O(g\ell^2/\nu)$ have been used. The ratio T_c/T_d has been taken to be of $O(1)$ in (2.2.21) as assumed earlier.

The multiplying factor in the heat equation (2.2.14) then becomes, after using (2.2.21),

$$\frac{V'\ell}{\alpha_f T} = O\left(\frac{U\ell}{\alpha_f}\frac{V'}{UT}\right) = O(Pe) = O(\epsilon) \tag{2.2.22}$$

By using $T = T_d$, other factors in the local derivatives become

$$\frac{\rho_f \ell^2}{\mu T}\epsilon = O\left(\frac{\rho_f \ell^2 \alpha_f}{\mu \ell'^2}\epsilon\right) = O\left(\frac{\alpha_f}{\nu}\epsilon^3\right) = O\left(\frac{\epsilon^3}{Pr}\right) = O(\epsilon^3) \tag{2.2.23}$$

$$\frac{\ell^2}{\alpha_f T} = O\left(\frac{\ell^2}{\ell'^2}\right) = O(\epsilon^2) \tag{2.2.24}$$

Under the assumption of $T_c/T_d = O(1)$, $T_c \sim T_v \sim T_d$ (cf(2.1.24)) and there is only one time scale. A special case of $T_c/T_d = O(\epsilon^2)$ will be considered later in §3.

3. The Macroscale Governing Equations

A Galilean transformation is introduced in §3.1 so that in the moving frame the medium deformation becomes much smaller than the microcell size and the interface boundary conditions can be expanded about the initial position. By using the transformation the governing equations and boundary conditions are written in the moving frame in §3.2 and the multiple scale perturbation is introduced to obtain the approximate equations at various orders of ϵ. In §3.3 and §3.4, the macroscale governing equations are derived for the deformation, flow and heat transport. They are in general nonlinearly coupled because of the nonlinear boundary conditions on the fluid-solid interface. Several canonical microcell boundary value problems are defined whose solutions are needed to determine the macroscale coefficients. The macroscale governing equations in the Eulerian frame and in the physical variables are then discussed.

3.1 Galilean Transformation.

In view of (2.2.10), (2.2.22), (2.2.23) and (2.2.24), equations (2.2.5)-(2.2.7), (2.2.13) and (2.2.14) become

$$\nabla^* \cdot u^* = 0 \qquad \text{in} \quad \Omega_f \tag{3.1.1}$$

$$\Big[\frac{1}{Pr}\Big]\epsilon^3 \frac{\partial u^*}{\partial t^*} + \Big[\frac{Re}{\epsilon}\Big]\epsilon^2 u^* \cdot \nabla^* u^* = -\nabla^* p^* + \epsilon \nabla^{*2} u^* + \epsilon\Big[\frac{\epsilon}{Pe} Ra\Big]\theta_f^* \mathbf{e}_z \qquad \text{in} \quad \Omega_f \tag{3.1.2}$$

$$\epsilon^2 \frac{\partial T_f^*}{\partial t^*} + \Big[\frac{Pe}{\epsilon}\Big]\epsilon u^* \cdot \nabla^* T_f^* = \nabla^* \cdot (m_f^* \cdot \nabla^* T_f^*) \qquad \text{in} \quad \Omega_f \tag{3.1.3}$$

$$\nabla^* \cdot \sigma_s^* = 0 \qquad \text{in} \quad \Omega_s \tag{3.1.4}$$

$$\frac{(\rho C_p)_s}{(\rho C_p)_f}\left(\epsilon^2 \frac{\partial T_s^*}{\partial t^*} + \Big[\frac{Pe}{\epsilon}\Big]\epsilon \frac{dv^*}{dt^*} \cdot \nabla^* T_s^*\right) = \frac{M_s}{M_f}\nabla^* \cdot (m_s^* \cdot \nabla^* T_s^*) \quad \text{in} \quad \Omega_s \tag{3.1.5}$$

where the expressions in the brackets are of $O(1)$ and have been used to account the order of magnitude relation $Re = Pe = O(\epsilon)$ and $Pr = O(1)$. The following simpler notation will be used for the ratios:

$$\hat{Re} = \frac{Re}{\epsilon} = O(1), \quad \hat{Pe} = \frac{Pe}{\epsilon} = O(1), \quad (\rho C_p)_r = \frac{(\rho C_p)_s}{(\rho C_p)_f}, \quad M_r = \frac{M_s}{M_f} \tag{3.1.6}$$

The interface boundary conditions (2.2.17) to (2.2.20) become, after using (2.1.25) and (2.2.22),

$$u^* = \frac{dv^*}{dt^*} \qquad \text{on} \quad \Gamma(t) \tag{3.1.7}$$

$$\sigma_s^* \cdot N = \epsilon \sigma_f^* \cdot N \qquad \text{on} \quad \Gamma(t) \tag{3.1.8}$$

$$T_f^* = T_s^* \qquad \text{on} \quad \Gamma(t) \tag{3.1.9}$$

$$(m_f^* \cdot \nabla^* T_f^*) \cdot N = M_r (m_s^* \cdot \nabla^* T_s^*) \cdot N \qquad \text{on} \quad \Gamma(t) \tag{3.1.10}$$

We now assume a periodic structure on the microscale and divide the medium into periodic micro-cells (Ω-cell). All the variables are assumed to be Ω-periodic.

Introduce the multiple-scale vectors

$$x, \qquad x' = \epsilon x \tag{3.1.11}$$

in space. Since $T_c \sim T_v \sim T_d$ in this case, only one time scale is used. Accordingly the differential operators are expanded as

$$\begin{aligned} \nabla^* &= \nabla + \epsilon \nabla' \\ e^*(\cdot) &= e(\cdot) + \epsilon e'(\cdot) \end{aligned} \tag{3.1.12a,b}$$

We now introduce the perturbation expansions

$$\begin{aligned} v^* &= v^{(0)} + \epsilon v^{(1)} + \epsilon^2 v^{(2)} + \dots \\ \sigma_s^* &= \sigma_s^{(-1)} + \epsilon \sigma_s^{(0)} + \epsilon^2 \sigma_s^{(1)} \end{aligned} \tag{3.1.13a,b}$$

Hooke's law (2.2.16) is then expanded as

$$\sigma_s^* = a^* : e(v^{(0)}) + \epsilon \left\{ a^* : [e'(v^{(0)}) + e(v^{(1)})] - \beta^* \theta_s^{(0)} \right\} + \dots$$

so that

$$\begin{aligned} \sigma_s^{(-1)} &= a^* : e(v^{(0)}) \\ \sigma_s^{(0)} &= a^* : [e'(v^{(0)}) + e(v^{(1)})] - \beta^* \theta_s^{(0)} \end{aligned} \tag{3.1.14}$$

If we substitute (3.1.13) and (3.1.14) into (3.1.4) it follows that

$$\begin{aligned} \nabla \cdot \sigma_s^{(-1)} &= 0 \\ \sigma_s^{(-1)} \cdot N &= 0 \quad \text{on} \quad \Gamma(t) \end{aligned} \tag{3.15a,b}$$

Recall that the leading solid displacement $v^{(0)}$ is of $O(\ell)$ as estimated in §2. In view of (3.1.14) equations (3.1.15a and b) suggest that $v^{(0)}$ is independent of the microscale coordinates

$$v^{(0)} = v^{(0)}(x', t^*) \tag{3.1.16}$$

i.e., to leading order all grains move as a whloe. This will be confirmed later.

Since the solid displacement is comparable to a typical microcell size, the boundary conditions (3.1.7) to (3.1.10) can not be expanded about $\Gamma(t = 0)$. If observations are made in a frame from which the microscale independent mode $v^{(0)}$ is absent, the deviation $\Gamma(t)$-$\Gamma(t = 0)$ will be of $O(\epsilon\ell)$ and Taylor expansion of the interface boundary conditions is permitted. This suggests a Galilean transform which is introduced below.

As a consequence of the bodily translation of Ω-cell the instantaneous fluid-solid interface $\Gamma(t)$ is carried from $\Gamma(t = 0)$ by rectilinear motion $dv^{(0)}/dt$. In order to apply the boundary conditions (3.1.7) to (3.1.10) at the instantaneous interface $\Gamma(t)$, we introduce a new coordinate

$$\xi_i^*(x_i^*, t^*) = x_i^* - v_i^{(0)}(x_i^*, t^*) \tag{3.1.17}$$

In this new frame, $\Gamma(t)$ deviates from its initial location by a small amount $O(\epsilon)$ because of elastic deformation which depends on the microscale coordinates, and the boundary conditions can be expanded about the new initial position.

The time associated with ξ^* will be denoted by τ^* to be distinguished from t^*. We shall refer to (x^*, t^*) and (ξ^*, τ^*) as the Eulerian and the moving coordinate systems respectively.

In the moving frame, we introduce the multiple-scale vectors

$$\xi, \qquad \xi' = \epsilon\xi \tag{3.1.18}$$

and the spatial derivative is expanded accordingly as

$$\nabla_\xi^* = \nabla_\xi + \epsilon\nabla'_\xi \tag{3.1.19}$$

We now determine the transform relations between two frames. After using (3.1.17) the time derivative in the Eulerian frame is transformed to

$$\begin{aligned}\frac{\partial}{\partial t^*} &= \frac{\partial}{\partial \tau^*} + \frac{\partial \xi^*}{\partial t^*} \cdot \nabla_\xi^* = \frac{\partial}{\partial \tau^*} - \frac{\partial v^{(0)}}{\partial t^*} \cdot \nabla_\xi^* \\ &= \frac{\partial}{\partial \tau^*} - \left(\frac{\partial v^{(0)}}{\partial t^*} \cdot \nabla_\xi + \epsilon \frac{\partial v^{(0)}}{\partial t^*} \cdot \nabla'_\xi \right)\end{aligned} \tag{3.1.20}$$

The transform relation for spatial derivatives may be found as follows. We first note from (3.1.17)

$$\nabla_x^* = \left(I - \nabla_x^* v^{(0)} \right) \cdot \nabla_\xi^*$$

or

$$\begin{aligned}\nabla_\xi^* &= \left(I - \nabla_x^* v^{(0)} \right)^{-1} \cdot \nabla_x^* \\ &= \frac{\mathrm{Cof} \left(I - \nabla_x^* v^{(0)} \right)^T}{\det |I - \nabla_x^* v^{(0)}|} \cdot \nabla_x^*\end{aligned} \tag{3.1.21}$$

where Cof denotes the cofactor.

The determinant in (3.1.21) is

$$\det |I - \nabla_x^* v^{(0)}| = \begin{vmatrix} 1 - \frac{\partial v_1^{(0)}}{\partial x_1^*} & -\frac{\partial v_2^{(0)}}{\partial x_1^*} & -\frac{\partial v_3^{(0)}}{\partial x_1^*} \\ -\frac{\partial v_1^{(0)}}{\partial x_2^*} & 1 - -\frac{\partial v_2^{(0)}}{\partial x_2^*} & -\frac{\partial v_3^{(0)}}{\partial x_2^*} \\ -\frac{\partial v_1^{(0)}}{\partial x_3^*} & -\frac{\partial v_2^{(0)}}{\partial x_3^*} & 1 - \frac{\partial v_3^{(0)}}{\partial x_3^*} \end{vmatrix} \tag{3.1.22}$$

A typical element in (3.1.22) can be expanded according to (3.1.19) as

$$\frac{\partial v_j^{(0)}}{\partial x_i^*} = \frac{\partial v_j^{(0)}}{\partial x_i} + \epsilon \frac{\partial v_j^{(0)}}{\partial x_i'} = \epsilon \frac{\partial v_j^{(0)}}{\partial x_i'} \tag{3.1.23}$$

where (3.1.16) has been used. After the expansion, (3.1.22) then becomes

$$\det |I - \nabla_x^* v^{(0)}| = 1 - \epsilon \Delta_x + \epsilon^2 (\alpha_x - \beta_x) + O(\epsilon^3) \tag{3.1.24}$$

where

$$\begin{aligned}\Delta_x &= \nabla'_x \cdot v^{(0)} \\ \alpha_x &= \frac{\partial v_1^{(0)}}{\partial x_1'} \frac{\partial v_2^{(0)}}{\partial x_2'} + \frac{\partial v_2^{(0)}}{\partial x_2'} \frac{\partial v_3^{(0)}}{\partial x_3'} + \frac{\partial v_3^{(0)}}{\partial x_3'} \frac{\partial v_1^{(0)}}{\partial x_1'} \\ \beta_x &= \frac{\partial v_2^{(0)}}{\partial x_3'} \frac{\partial v_3^{(0)}}{\partial x_2'} + \frac{\partial v_3^{(0)}}{\partial x_1'} \frac{\partial v_1^{(0)}}{\partial x_3'} + \frac{\partial v_1^{(0)}}{\partial x_2'} \frac{\partial v_2^{(0)}}{\partial x_1'}\end{aligned} \tag{3.1.25a-c}$$

The cofactor matrix is similarly expanded with the result

$$\text{Cof}\left(I - \nabla_x^* v^{(0)}\right)^T = I - \epsilon\Delta_x I + \epsilon^2\left(\alpha_x I + S_x\right) + O(\epsilon^3) \tag{3.1.26a}$$

where S_x is the following matrix

$$S_x = \begin{bmatrix} -\frac{\partial v_2^{(0)}}{\partial x_2'}\frac{\partial v_2^{(0)}}{\partial x_2'} & -\frac{\partial v_1^{(0)}}{\partial x_2'}\frac{\partial v_2^{(0)}}{\partial x_1'} & -\frac{\partial v_1^{(0)}}{\partial x_2'}\frac{\partial v_2^{(0)}}{\partial x_1'} \\ & -\frac{\partial v_1^{(0)}}{\partial x_2'}\frac{\partial v_2^{(0)}}{\partial x_1'} & -\frac{\partial v_2^{(0)}}{\partial x_2'}\frac{\partial v_2^{(0)}}{\partial x_2'} \\ \text{sym.} & & -\frac{\partial v_1^{(0)}}{\partial x_2'}\frac{\partial v_2^{(0)}}{\partial x_1'} \end{bmatrix} \tag{3.1.26b}$$

Combining (3.1.24) and (3.1.26) we obtain

$$\begin{aligned} &\left(I - \nabla_x^* v^{(0)}\right)^{-1} \\ &= \left\{1 + [\epsilon\Delta_x - \epsilon^2(\alpha_x - \beta_x) + O(\epsilon^3)] + [\epsilon\Delta_x - \epsilon^2(\alpha_x - \beta_x) + O(\epsilon^3)]^2 + \ldots\right\} \\ &\times [I - \epsilon\Delta_x I + \epsilon^2(\alpha_x I + S_x) + O(\epsilon^3)] \\ &= I + \epsilon^2(S_x + \beta_x I) + O(\epsilon^3) \end{aligned} \tag{3.1.27}$$

and therefore (3.1.21) becomes

$$\nabla_\xi^* = \nabla_x^* + \epsilon^2(S_x + \beta_x I)\cdot\nabla_x^* + O(\epsilon^3) \tag{3.1.28a}$$

which is further written

$$\nabla_\xi + \epsilon\nabla_\xi' = \nabla_x + \epsilon\nabla_x' + \epsilon^2(S_x + \beta_x I)\cdot\nabla_x + O(\epsilon^3) \tag{3.1.28b}$$

after employing the multiple scale expansions. The transform relations (3.1.20) and (3.1.28) will be repeatedly used in the next subsection to transform the governing equations and boundary conditions to the moving frame (ξ^*, τ^*).

3.2 The Governing Equations and Boundary Conditions in the Moving Frame.

The normalized equations (3.1.1) to (3.1.5) in the Eulerian frame are now transformed according to (3.1.20) and (3.1.28b). The multiple-scale expansion (3.1.19) is then employed to obtain the approximate equations at successive orders of ϵ. On the other hand, the boundary conditions are first expanded in Taylor series about the moving interface and then expanded according to the multiple scale relations (3.1.18).

We further introduce the perturbation expansions

$$f^* = f^{(0)} + \epsilon f^{(1)} + \epsilon^2 f^{(2)} + ... \qquad (3.2.1a)$$

for

$$u^*, p^*, \sigma_f^*, \theta_f^* \quad \text{and} \quad \theta_s^* \qquad (3.2.1b)$$

3.2.1 Mass and Momentum Conservations.

The expansion of the governing equations (3.1.1), (3.1.2) and (3.1.4) is straightforward and the results are listed here.

The continuity equation (3.1.1) becomes

$$\begin{aligned} O(1) \qquad & \nabla_\xi \cdot u^{(0)} = 0 \\ O(\epsilon) \qquad & \nabla'_\xi \cdot u^{(0)} + \nabla_\xi \cdot u^{(1)} = 0 \end{aligned} \tag{3.2.1a,b}$$

The fluid momentum equation (3.1.2) similarly becomes

$$\begin{aligned} O(1) \qquad & 0 = -\nabla_\xi p^{(0)} =^{\text{def}} \nabla_\xi \cdot \sigma_f^{(0)} \\ O(\epsilon) \qquad & 0 = -(\nabla'_\xi p^{(0)} + \nabla_\xi p^{(1)}) + \nabla_\xi^2 u^{(0)} + \frac{Ra}{\hat{P}e}\theta_f^{(0)}\mathbf{e}_z \\ & = \nabla'_\xi \cdot \sigma_f^{(0)} + \nabla_\xi \cdot \sigma_f^{(1)} + \frac{Ra}{\hat{P}e}\theta_f^{(0)}\mathbf{e}_z \end{aligned} \tag{3.2.2a,b}$$

in which the fluid stress is given by

$$\begin{aligned} \sigma_f^{(0)} &= -\, p^{(0)} I \\ \sigma_f^{(1)} &= -\, p^{(1)} I + e_\xi(u^{(0)}) \end{aligned} \tag{3.2.3a,b}$$

after expanding (2.2.11) accordidng to (3.1.28) and (3.2.1).

The solid equilibrium equation (3.1.4) becomes

$$\begin{aligned} O(1) \qquad & \nabla_\xi \cdot \sigma_s^{(-1)} = 0 \\ O(\epsilon) \qquad & \nabla'_\xi \cdot \sigma_s^{(-1)} + \nabla_\xi \cdot \sigma_s^{(0)} = 0 \\ O(\epsilon^2) \qquad & \nabla'_\xi \cdot \sigma_s^{(0)} + \nabla_\xi \cdot \sigma_s^{(1)} = 0 \end{aligned} \tag{3.2.4a-c}$$

They are identical in form to those in the Eulerian frame except for the change from x to ξ.

Hooke's law (3.1.14) in the moving frame is written similarly as

$$\begin{aligned} \sigma_s^{(-1)} &= a^* : e_\xi(v^{(0)}) \\ \sigma_s^{(0)} &= a^* : [e'_\xi(v^{(0)}) + e_\xi(v^{(1)})] - \beta^* \theta_s^{(0)} \\ \sigma_s^{(1)} &= a^* : [e'_\xi(v^{(1)} + e_\xi(v^{(2)})] - \beta^* \theta_s^{(1)} \end{aligned} \tag{3.2.5a-c}$$

Note that at the leading order the stress continuity condition (3.1.15b) is imposed at the initial position of the interface in the moving frame. It then follows immediately from (3.2.3a) and (3.1.15b) that

$$\sigma_s^{(-1)} = 0; \quad e_\xi(v^{(0)}) = 0; \quad v^{(0)} = v^{(0)}(\xi', \tau^*) \tag{3.2.6}$$

In the fluid phase, we also have from (3.2.2a) that

$$p^{(0)} = p^{(0)}(\xi', \tau^*) \tag{3.2.7}$$

Therefore, the solid displacement $v^{(0)}$ and the pore pressure $p^{(0)}$ at leading order are independent of the microscale coordinate ξ. The same is true in the Eulerian frame since the translation is by an amount independent of the microscale. This confirms (3.1.16). In view of (3.2.6), the fluid momentum equation (3.2.2) and the equilibrium equation (3.2.3) may be combined to give

$$\begin{aligned} \nabla_\xi \cdot \sigma_T^{(0)} &= 0 \\ \nabla'_\xi \cdot \sigma_T^{(0)} + \nabla_\xi \cdot \sigma_T^{(1)} &= -\frac{Ra}{\hat{P}e}\theta_f^{(0)}\mathbf{e}_z \end{aligned} \tag{3.2.8a,b}$$

where $\sigma_T^{(n)}$ is the total stress and is defined by

$$\sigma_T^{(n)} = \left\{ \begin{array}{ll} \sigma_f^{(n)} & \text{in } \Omega_f \\ \sigma_s^{(n)} & \text{in } \Omega_s \end{array} \right\} \tag{3.2.9}$$

Note that the right-hand side of (3.2.8b) is due to the buoyancy in the fluid phase and serves as body force.

3.2.2 Energy Equations.

The energy equations (3.1.3) and (3.1.5) are similarly transformed to the moving coordinates by using (3.1.20) and (3.1.28b) and then expanded according to the multiple-scale relations (3.1.19).

In the fluid phase, equation (3.1.3) becomes

$$\epsilon^2\left(\frac{\partial T_f^*}{\partial \tau^*}-\frac{\partial v^{(0)}}{\partial t^*}\cdot\nabla_\xi^* T_f^*\right)+\epsilon\hat{P}eu^*\cdot\nabla_\xi^* T_f^*=\nabla_\xi^*\cdot[m_f^*\cdot(\nabla_\xi^* T_f^*)]+0(\epsilon^2) \qquad (3.2.10)$$

where the error terms of $O(\epsilon^2)$ is from those of the same order in (3.1.28b) and will be shown to be actually of $O(\epsilon^3)$ later. Expanding (3.37), we obtain

$$\begin{aligned}
O(1)\qquad & 0=\nabla_\xi\cdot(m_f^*\cdot\nabla_\xi T_f^{(0)})\\
O(\epsilon)\qquad & \hat{P}eu^{(0)}\cdot\nabla_\xi T_f^{(0)}=\nabla'_\xi\cdot(m_f^*\cdot\nabla_\xi T_f^{(0)})+\nabla_\xi\cdot[M_f^*\cdot(\nabla'_\xi T_f^{(0)}+\nabla_\xi T_f^{(1)})]\\
O(\epsilon^2)\qquad & \frac{\partial T_f^{(0)}}{\partial\tau^*}-\frac{\partial v^{(0)}}{\partial t^*}\cdot\nabla_\xi T_f^{(0)}+\hat{P}eu^{(0)}\cdot(\nabla'_\xi T_f^{(0)}+\nabla_\xi T_f^{(1)})+\hat{P}eu^{(1)}\cdot\nabla_\xi T_f^{(0)}\\
& \qquad=\nabla'_\xi\cdot[m_f^*\cdot(\nabla'_\xi T_f^{(0)}+\nabla_\xi T_f^{(1)})]+\nabla_\xi\cdot[m_f^*\cdot(\nabla'_\xi T_f^{(1)}+\nabla_\xi T_f^{(2)})]
\end{aligned} \qquad (3.2.11a-c)$$

In the same manner, the heat equation for the solid phase becomes

$$\begin{aligned}
(\rho C_p)_r[\epsilon^2\left(\frac{\partial T_s^*}{\partial\tau^*}-\frac{\partial v^{(0)}}{\partial t^*}\cdot\nabla_\xi^* T_s^*\right)+\hat{P}e\epsilon\left(\frac{\partial v^*}{\partial\tau^*}-\dot{v}^{(0)}\cdot\nabla_\xi^* v^*\right)\cdot\nabla_\xi^* T_s^* \\
=M_r\nabla_\xi^*\cdot(m_s^*\cdot\nabla_\xi^* T_s^*)+O(\epsilon^2)
\end{aligned} \qquad (3.2.12)$$

which yields

$$\begin{aligned}
O(1)\qquad & 0=M_r\nabla_\xi\cdot(m_s^*\cdot\nabla_\xi T_s^{(0)})\\
O(\epsilon)\qquad & (\rho Cp)_r\hat{P}e\left(\frac{\partial v^{(0)}}{\partial\tau^*}-\frac{\partial v^{(0)}}{\partial t^*}\cdot\nabla_\xi v^{(0)}\right)\cdot\nabla_\xi T_s^{(0)}\\
& \qquad=M_r\nabla'_\xi\cdot(m_s^*\cdot\nabla_\xi T_s^{(0)})+M_r\nabla_\xi\cdot[m_s^*\cdot(\nabla'_\xi T_s^{(0)}+\nabla_\xi T_s^{(1)})]\\
O(\epsilon^2)\qquad & (\rho Cp)_r\frac{\partial T_s^{(0)}}{\partial\tau^*}-\frac{\partial v^{(0)}}{\partial t^*}\cdot\nabla_\xi T_s^{(0)}+\hat{P}e\frac{\partial v^{(0)}}{\partial\tau^*}\cdot(\nabla'_\xi T_s^{(0)}+\nabla_\xi T_s^{(1)})\\
& \qquad+\hat{P}e\left(\frac{\partial v^{(1)}}{\partial\tau^*}-\frac{\partial v^{(0)}}{\partial t^*}\cdot(\nabla'_\xi v^{(0)}+\nabla_\xi v^{(1)})\right)\cdot\nabla_\xi Ts^{(0)}\\
& =M_r\nabla'_\xi\cdot[m_s^*\cdot(\nabla'_\xi Ts^{(0)}+\nabla_\xi T_s^{(1)})]+M_r\nabla_\xi\cdot[m_s^*\cdot(\nabla'_\xi T_s^{(1)}+\nabla_\xi T_s^{(2)})]
\end{aligned} \qquad (3.2.13a-c)$$

The total derivative dv^*/dt^* of the solid displacement in (3.1.5) has been replaced by $\partial v^*/\partial t^*$. This will be explained in the discussion of the interface boundary conditions below (cf. (3.2.4)).

3.2.3 Boundary Conditions on the Interface.

The boundary conditions (3.1.7) to (3.1.10) are now expanded about the initial position of the interface in the moving frame. This new interface will be denoted by $\Gamma_\xi^{(0)}$.

Kinematic Boundary Condition (3.1.7) :

The total derivative in the kinematic boundary condition (3.1.7) is the sum of local and convective terms

$$\frac{dv^*}{dt^*} = \frac{\partial v^*}{\partial t^*} + \frac{dv^*}{dt^*} \cdot \nabla^* v^*$$

which may be written after inversion

$$\frac{dv^*}{dt^*} = (I - \nabla^* v^*)^{-1} \frac{\partial v^*}{\partial t^*} = \frac{Cof(I - \nabla^* v^*)^T}{det|I - \nabla^* v^*|} \frac{\partial v^*}{\partial t^*} + = \frac{\partial v^*}{\partial t^*} + O(\epsilon^3) \qquad (3.2.14)$$

The last equality follows from (3.1.27) and the fact that the leading term $v^{(0)}$ of v^* is independent of the microscale (cf.(3.2.6)).

Let us transform the kinematic boundary condition (3.1.7) to the moving frame by using (3.1.20).

$$\begin{aligned} u^* &= \frac{\partial v^*}{\partial \tau^*} - \frac{\partial v^{(0)}}{\partial t^*} \cdot \nabla_\xi^* v^* + 0(\epsilon^3) \\ &= \frac{\partial v^*}{\partial \tau^*} - \left[\frac{\partial v^{(0)}}{\partial \tau^*} - \left(\frac{\partial v^{(0)}}{\partial t^*} \cdot \nabla_\xi^* v^{(0)} \right) \right] \cdot \nabla_\xi^* v^* + O(\epsilon^3) \qquad (3.2.15) \\ &= \frac{\partial v^*}{\partial \tau^*} - \frac{\partial v^{(0)}}{\partial \tau^*} \cdot \nabla_\xi^* v^* + O(\epsilon^2) \end{aligned}$$

where another use of (3.1.20) has been made for $\partial v^{(0)}/\partial t^*$ and (3.2.6) was used. We now Taylor expand (3.2.15) about the new initial interface $\Gamma_\xi(0)$.

$$\begin{aligned} &u^* + (v^* - v^{(0)}) \cdot \nabla_\xi^* u^{(0)} + ... \\ &\quad = \frac{\partial v^*}{\partial \tau^*} - \frac{\partial v^{(0)}}{\partial \tau^*} \cdot \nabla_\xi^* v^* + (v^* - v^{(0)}) \cdot \nabla_\xi \left(\frac{\partial v^*}{\partial \tau^*} - \frac{\partial v^{(0)}}{\partial \tau^*} \cdot \nabla_\xi^* v^* \right) + ... \end{aligned}$$

This result may be expanded by using (3.1.13a), (3.1.19) and (3.2.1) as

$$(u^{(0)} + \epsilon u^{(1)} + ...) + (\epsilon v^{(1)} + ...) \cdot (\nabla_\xi + \epsilon \nabla'_\xi)(u^{(0)} + \epsilon u^{(1)} + ...)$$

$$= \frac{\partial}{\partial \tau^*}(v^{(0)} + \epsilon v^{(1)} ...) - \frac{\partial v^{(0)}}{\partial \tau^*} \cdot (\nabla_\xi + \epsilon \nabla'_\xi)(v^{(0)} + \epsilon v^{(1)} + ...) + (\epsilon v^{(1)} + ...) \cdot$$

$$(\nabla_\xi + \epsilon \nabla'_\xi) \left[\frac{\partial}{\partial \tau^*}(v^{(0)} + \epsilon v^{(1)} + ...) - \frac{\partial v^{(0)}}{\partial \tau^*} \cdot (\nabla_\xi + \epsilon \nabla'_\xi)(v^{(0)} + \epsilon v^{(1)} + ...) \right] + ...$$

Collecting terms of like order and invoking (3.2.6), we obtain

$$\begin{aligned} O(1) \qquad & u^{(0)} = \frac{\partial v^{(0)}}{\partial \tau^*} \\ O(\epsilon) \qquad & u^{(1)} + v^{(1)} \cdot \nabla_\xi u^{(0)} = \frac{\partial v^{(1)}}{\partial \tau^*} - \frac{\partial v^{(0)}}{\partial \tau^*} \cdot (\nabla'_\xi v^{(0)} + \nabla_\xi v^{(1)}) \end{aligned} \qquad (3.2.16a, b)$$

Dynamic Boundary Condition :

The stress continuity (3.1.8) can be similarly expanded. We shall first show that the normal vector N on the instantaneous fluid-solid interface is altered from the initial normal vector N_o by a negligibly small amount.

Let $N_\xi(0)$ be the normal vector on the new initial interface. Obviously, $N_\xi(0) = N_o$ since the leading order translation $v^{(0)}$ is independent of the microscale coordinate ξ. Let the interface be described by $F(\xi^*, \tau^*) = 0$ in which $\xi^* = \xi_o^* + \epsilon v^{(1)} + O(\epsilon^2)$ with ξ_o^* being the initial position of the interface. Thus

$$F(\xi^*, \tau^*) = F(\xi_o^* + \epsilon v^{(1)} + O(\epsilon^2), \tau^*)$$

Taking the gradient, we get

$$\nabla_\xi^* F = \nabla_{\xi_o}^* F + \epsilon \nabla_\xi^* v^{(1)} \cdot \left[\nabla_\xi^* F \right]_{\xi = \xi_o} + O(\epsilon^2)$$

where $\nabla_{\xi_o}^* F$ is the gradient of F at the initial position in the moving frame. It follows then

$$\nabla_{\xi_o}^* F = (I + \epsilon \nabla_\xi^* v^{(1)})^{-1} \cdot \nabla_\xi^* F + O(\epsilon^2) = \nabla_\xi^* F + O(\epsilon^2) \qquad (3.2.17)$$

where (3.1.27) has been used. Therefore,

$$N_\xi(\tau) = N_\xi(0) + O(\epsilon^2) = N_o + O(\epsilon^2) \tag{3.2.18}$$

The stress continuity (3.1.8) is now expanded about $\Gamma_\xi(0)$ as

$$[\sigma_s^* + (v^* - v^{(0)}) \cdot \nabla_\xi^* \sigma_s^* + ...] \cdot N_\xi(0) = \epsilon[\sigma_f^* + (v^* - v^{(0)}) \cdot \nabla_\xi^* \sigma_f^*] \cdot N_\xi(0) + O(\epsilon^2) \tag{3.2.19}$$

By using the perturbation expansions (3.1.13a) and (3.2.1) and recalling (3.2.6) and (3.2.7), we obtain at various orders of ϵ

$$\begin{aligned} O(1) \qquad & \sigma_s^{(-1)} \cdot N_\xi = 0 \\ O(\epsilon) \qquad & \sigma_s^{(0)} \cdot N_\xi = \sigma_f^{(0)} \cdot N_\xi \\ O(\epsilon^2) \qquad & (\sigma_s^{(1)} + v^{(1)} \cdot \nabla_\xi \sigma_s^{(0)}) \cdot N_\xi = \sigma_f^{(1)} \cdot N_\xi \end{aligned} \tag{3.2.20a-c}$$

The thermal boundary conditions (3.1.9) and (3.1.10) are similarly expanded. We only give the results here.

Thermal Boundary Conditions :

The temperature continuity (3.1.9) becomes

$$\begin{aligned} O(1) \qquad & T_f^{(0)} = T_s^{(0)} \\ O(\epsilon) \qquad & T_f^{(1)} = T_s(1) \\ O(\epsilon^2) \quad & T_f^{(2)} + v^{(1)} \cdot (\nabla'_\xi T_f^{(0)} + \nabla_\xi T_f^{(1)}) = T_s^{(2)} + v^{(1)} \cdot (\nabla'_\xi T_s^{(0)} + \nabla_\xi T_s^{(1)}) \end{aligned} \tag{3.2.21a-c}$$

Note that the $O(1)$ equations (3.2.11a), (3.2.12a) and (3.2.21a) implies immediately that $\theta_f^{(0)}$ and $\theta_s^{(0)}$ are independent of ξ and are equal. This fact has been used in writting down ((3.2.21b and c). Also the heat flux continuity (3.1.10) gives

$$\begin{aligned} O(1) \qquad & m_f^* \cdot \nabla_\xi T_f^{(0)} \cdot N = M_r m_s^* \cdot \nabla_\xi T_s^{(0)} \cdot N_\xi \\ O(\epsilon) \qquad & m_f^* \cdot (\nabla'_\xi T_f^{(0)} + \nabla_\xi T_f^{(1)}) \cdot N = M_r m_s^* \cdot (\nabla'_\xi T_s^{(0)} + \nabla_\xi T_s^{(1)}) \cdot N_\xi \\ O(\epsilon^2) & m_f^* \cdot [\nabla'_\xi T_f^{(1)} + \nabla_\xi T_f^{(2)} + v^{(1)} \cdot \nabla_\xi (\nabla'_\xi T_f^{(0)} + \nabla_\xi T_f^{(1)})] \cdot N_\xi \\ & = M_r m_s^* \cdot [\nabla'_\xi T_s^{(1)} + \nabla_\xi T_s^{(2)} + v^{(1)} \cdot \nabla_\xi (\nabla'_\xi T_s^{(0)} + \nabla_\xi T_s^{(1)})] \cdot N_\xi \end{aligned} \tag{3.2.22a-c}$$

In the next subsection, we shall use the perturbation equations and boundary conditions governing microscale to deduce the effective macroscale constitutive equations in the moving frame.

3.3 Macrosale Equations for Solid and Fluid Motions.

The Solid Phase

In the solid phase, we have from (3.2.4b) and (3.2.5b)

$$\nabla_\xi \cdot \left\{ a^* : \left[e'_\xi(v^{(0)}) + e_\xi(v^{(1)}) \right] \right\} - \nabla_\xi \cdot (\beta^* \theta_s^{(0)} \cdot I) = 0 \quad \text{in} \quad \Omega_s \tag{3.3.1}$$

and from (3.32b), (3.31a) and (3.47b)

$$\left\{ a^* : \left[e'_\xi(v^{(0)}) + e(v^{(1)}) \right] - \beta^* \theta_s^{(0)} I \right\} \cdot N = -(p^{(0)} \cdot I) \cdot N \quad \text{on} \quad \Gamma \tag{3.3.2}$$

In addition, $v^{(1)}$ is Ω-periodic. The conditions define a boundary value problem for $v^{(1)}$.

Note that $\theta_s^{(0)}$ does not depend on x. Because of linearity, the solution for $v^{(1)}$ can be assumed to be of the form

$$v^{(1)} = \phi : e'_\xi(v^{(0)}) - \eta p^{(0)} - \zeta \theta_s^{(0)} \tag{3.3.3}$$

where $\phi(\xi, \xi', \tau)$ is a third order tensor and $\eta(\xi, \xi', \tau)$ and $\zeta(\xi, \xi', \tau)$ are vectors all of which yet to be determined. Substituting (3.3.3) into (3.3.1) and (3.3.2) we obtain a set of canonical cell problems for ϕ, η, and ζ

$$\begin{aligned} \nabla_\xi \cdot [a^* : e_\xi(\phi)] + (\nabla_\xi \cdot a^*) : II &= 0 \\ \nabla_\xi \cdot [a^* : e_\xi(\eta)] &= 0 \qquad \text{in} \quad \Omega_s \\ \nabla_\xi \cdot [a^* : e_\xi(\zeta)] + \nabla_\xi \cdot \beta^* &= 0 \end{aligned} \tag{3.3.4a-c}$$

with the boundary conditons

$$\begin{aligned} [a^* : e_\xi(\phi)] \cdot N + (a^* : II) \cdot N &= 0 \\ [a^* : e_\xi(\eta)] \cdot N &= I \cdot N \qquad \text{on} \quad \Gamma \\ [a^* : e_\xi(\zeta)] \cdot N + \beta^* \cdot N &= 0 \end{aligned} \tag{3.3.5a-c}$$

and that

$$\phi, \eta, \zeta \quad \text{are} \quad \Omega\text{-periodic.} \tag{3.3.6a}$$

For uniqueness we require that

$$\langle \phi \rangle = \langle \eta \rangle = \langle \zeta \rangle = 0 \tag{3.3.6b}$$

where the brackets denote the Ω-average of a quantity

$$\langle f \rangle = \frac{1}{\Omega} \int_{\Omega_i} f d\Omega \qquad (i = f \quad \text{or} \quad s) \tag{3.3.7}$$

Equations (3.3.4) to (3.3.7) can be solved numerically for any prescribed geometry in Ω-cell.

At the next order $O(\epsilon^2)$, we have from (3.2.8b) and (3.2.20c)

$$\begin{aligned} \nabla'_\xi \cdot \sigma_T^{(0)} + \nabla_\xi \cdot \sigma_T^{(1)} &= -\frac{Ra}{\hat{P}e} \theta_f^{(0)} \mathbf{e}_z \\ \left(\sigma_s^{(1)} + v^{(1)} \cdot \nabla_\xi \sigma_s^{(0)} \right) \cdot N_\xi &= \sigma_f^{(1)} \cdot N_\xi \end{aligned} \tag{3.3.8a,b}$$

Integrate (3.3.8a) over Ω-cell and use Ω-periodicity to obtain

$$\nabla'_\xi \cdot \langle \sigma_f^{(0)} \rangle + \nabla'_\xi \cdot \langle \sigma_s^{(0)} \rangle + \frac{1}{\Omega} \left(\int_\Gamma \sigma_f^{(1)} \cdot N^f dS + \int_\Gamma \sigma_s^{(1)} \cdot (-N^f) dS \right) = -\frac{Ra}{\hat{P}e} n' \theta_f^{(0)} \mathbf{e}_z \tag{3.3.9}$$

where n' is the porosity and N^f is the outward unit normal vector from the fluid phase. By using (3.3.8b) the integrals in (3.3.9) further become

$$\begin{aligned} &\frac{1}{\Omega} \left(\int_\Gamma \sigma_f^{(1)} \cdot N^f dS + \int_\Gamma \sigma_s^{(1)} \cdot (-N^f) dS \right) = -\frac{1}{\Omega} \int_\Gamma v^{(1)} \cdot \nabla_\xi \sigma_s^{(0)} \cdot (-N^f) dS \\ &= -\frac{1}{\Omega} \int_{\Omega_s} \nabla_\xi \cdot \left(v^{(1)} \cdot \nabla_\xi \sigma_s^{(0)} \right) d\Omega = -\frac{1}{\Omega} \int_{\Omega_s} \frac{\partial v_k^{(1)}}{\partial \xi_i} \frac{\partial \sigma_s^{(0)}{}_{ij}}{\partial \xi_k} d\Omega \end{aligned} \tag{3.3.10}$$

where (3.2.4b) has been used in the last step. Equation (3.3.10) is further manipulated by using Gauss theorem and Ω-periodicity to give

$$\begin{aligned} (3.3.10) &= -\frac{1}{\Omega} \int_{\Omega_s} \left[\frac{\partial}{\partial \xi_k} \left(\sigma_s^{(0)}{}_{ij} \frac{\partial v_k^{(1)}}{\partial \xi_i} \right) - \sigma_s^{(0)}{}_{ij} \frac{\partial}{\partial \xi_i} \left(\frac{\partial v_k^{(1)}}{\partial \xi_k} \right) \right] d\Omega \\ &= -\frac{1}{\Omega} \int_\Gamma \sigma_s^{(0)}{}_{ij} \frac{\partial v_k^{(1)}}{\partial \xi_i} N_k^s dS + \frac{1}{\Omega} \int_{\Omega_s} \frac{\partial}{\partial \xi_i} \left(\sigma_s^{(0)}{}_{ij} \frac{\partial v_k^{(1)}}{\partial \xi_k} \right) d\Omega \\ &= -\frac{1}{\Omega} \int_\Gamma \sigma_s^{(0)}{}_{ij} \left(\frac{\partial v_k^{(1)}}{\partial \xi_i} N_k^s - \frac{\partial v_k^{(1)}}{\partial \xi_k} N_i^s \right) dS \end{aligned} \tag{3.3.11}$$

Substituting (3.3.3) into (3.3.11), we have

(3.3.10)

$$
\begin{aligned}
&= -\frac{1}{\Omega}\int_\Gamma dS a^*_{ijpq}\left[\left(\delta_{pm}\delta_{qn}+e_{pq}(\phi^{mn})\right)e'_{mn}(v^{(0)})-e_{pq}(\eta)p^{(0)}-e_{pq}(\zeta)\theta^{(0)}\right]\\
&\quad\times\left[\frac{\partial\phi^{gh}_k}{\partial\xi_i}e'_{gh}(v^{(0)})-\frac{\partial\eta_k}{\partial\xi_i}p^{(0)}-\frac{\partial\zeta_k}{\partial\xi_i}\theta^{(0)}\right]N^s_k\\
&\quad+\frac{1}{\Omega}\int_\Gamma dS a^*_{ijpq}\left[\left(\delta_{pm}\delta_{qn}+e_{pq}(\phi^{mn})\right)e'_{mn}(v^{(0)})-e_{pq}(\eta)p^{(0)}-e_{pq}(\zeta)\theta^{(0)}\right]\\
&\quad\times\left[\frac{\partial\phi^{gh}_k}{\partial\xi_k}e'_{gh}(v^{(0)})-\frac{\partial\eta_k}{\partial\xi_k}p^{(0)}-\frac{\partial\zeta_k}{\partial\xi_k}\theta^{(0)}\right]N^s_i\\
&= -\left(F'_{jmngh}e'_{gh}(v^{(0)})+G'_{jmn}p^{(0)}+H'_{jmn}\theta^{(0)}\right)e'_{mn}(v^{(0)})\\
&\quad-I'_j p^{(0)^2}-R'_j p^{(0)}\theta^{(0)}-K'_j\theta^{(0)^2}
\end{aligned}
\tag{3.3.12}
$$

where

$$
\begin{aligned}
F'_{jmngh} &= \frac{1}{\Omega}\int_\Gamma a^*_{ijpq}\left(\delta_{pm}\delta_{qn}+e_{pq}(\phi^{mn})\right)\left(\frac{\partial\phi^{gh}_k}{\partial\xi_i}N^s_k-\frac{\partial\phi^{gh}_k}{\partial\xi_k}N^s_i\right)dS\\
G'_{jmn} &= -\frac{1}{\Omega}\int_\Gamma a^*_{ijpq}\left(\delta_{pm}\delta_{qn}+e_{pq}(\phi^{mn})\right)\left(\frac{\partial\eta_k}{\partial\xi_i}N^s_k-\frac{\partial\eta_k}{\partial\xi_k}N^s_i\right)dS\\
&\quad-\frac{1}{\Omega}\int_\Gamma\left(a^*_{ijpq}e_{pq}(\eta)\frac{\partial\phi^{mn}_k}{\partial\xi_i}N^s_k-\frac{\partial\phi^{mn}_k}{\partial\xi_k}N^s_i\right)dS\\
H'_{jmn} &= -\frac{1}{\Omega}\int_\Gamma a^*_{ijpq}\left(\delta_{pm}\delta_{qn}+e_{pq}(\phi^{mn})\right)\left(\frac{\partial\zeta_k}{\partial\xi_i}N^s_k-\frac{\partial\zeta_k}{\partial\xi_k}N^s_i\right)dS\\
&\quad-\frac{1}{\Omega}\int_\Gamma a^*_{ijpq}e_{pq}(\zeta)\left(\frac{\partial\phi^{mn}_k}{\partial\xi_i}N^s_k-\frac{\partial\phi^{mn}_k}{\partial\xi_k}N^s_i\right)dS\\
I'_j &= \frac{1}{\Omega}\int_\Gamma a^*_{ijpq}e_{pq}(\eta)\left(\frac{\partial\eta_k}{\partial\xi_i}N^s_k-\frac{\partial\eta_k}{\partial\xi_k}N^s_i\right)dS\\
R'_j &= \frac{1}{\Omega}\int_\Gamma a^*_{ijpq}e_{pq}(\eta)\left(\frac{\partial\zeta_k}{\partial\xi_i}N^s_k-\frac{\partial\zeta_k}{\partial\xi_k}N^s_i\right)dS\\
K'_j &= \frac{1}{\Omega}\int_\Gamma a^*_{ijpq}e_{pq}(\zeta)\left(\frac{\partial\zeta_k}{\partial\xi_i}N^s_k-\frac{\partial\zeta_k}{\partial\xi_k}N^s_i\right)dS
\end{aligned}
\tag{3.3.13a-f}
$$

Finally, upon substituting (3.3.12) and (3.3.13) into (3.3.9), and using (3.2.5b) for $\sigma^{(0)}_s$ with $v^{(1)}$ given by (3.3.3) and $\sigma^{(0)}_f = -p^{(0)}I$, the macroscale equilibrium

equation becomes

$$\nabla'_\xi \cdot \left[a' : e'_\xi(v^{(0)}) - \alpha' p^{(0)} - \beta'_t \theta^{(0)}\right] - \left(F' : e'_\xi(v^{(0)}) + G' p^{(0)} + H' \theta^{(0)}\right) : e'_\xi(v^{(0)}) - I' p^{(0)^2} - R' p^{(0)} \theta^{(0)} - K' \theta^{(0)^2} = -\frac{Ra}{\hat{P}e} n' \theta_f^{(0)} \mathbf{e}_z \tag{3.3.14}$$

where

$$a' = \langle a^* : [II + e_\xi(\phi)] \rangle$$

$$\alpha' = n' I + \langle a^* : e_\xi(\eta) \rangle \tag{3.3.15a-c}$$

$$\beta'_t = \langle \beta^* \rangle + \langle a^* : e_\xi(\zeta) \rangle$$

The symbol n' denotes the porosity. The expression in the brackets of (3.63) which is $\langle \sigma_T^{(0)} \rangle$ gives the macroscale Hooke's law

$$\langle \sigma_T^{(0)} \rangle = a' : e'_\xi(v^{(0)}) - \alpha' p^{(0)} - \beta'_t \theta^{(0)} \tag{3.3.16}$$

The right-hand side of (3.3.14) is from the buoyancy in the fluid, othe nonlinear terms originate from the nonlinear boundary condition on stress (3.3.8b) which is nonlinear because of the $O(\ell)$ movement of the interface. All of these coefficients can be determined in terms of the solutions to the canonical boundary value problems defined in (3.3.4) to (3.3.7).

The Fluid Phase

The fluid phase can be treated similarly. In the fluid phase, we first recall that $v^{(0)}$ is independent of ξ. If we replace $u^{(0)}$ in (3.2.2a) and (3.2.3b) by

$$u_d^{(0)} = u^{(0)} - \frac{\partial v^{(0)}}{\partial \tau^*} \tag{3.3.17}$$

it is seen that the equations remain valid. Thus

$$\nabla_\xi \cdot u_d^{(0)} = 0 \tag{3.3.18a}$$

$$0 = -(\nabla'_\xi p^{(0)} + \nabla_\xi p^{(1)}) + \nabla_\xi^2 u_d^{(0)} + \frac{Ra}{\hat{P}e} \theta_f^{(0)} \mathbf{e}_z \tag{3.3.18b}$$

In view of (3.2.7) and $\theta_f^{(0)} = \theta^{(0)}(\xi', \tau^*)$ (which will be shown shortly) and the linearity of (3.3.18), we assume in the fluid phase

$$u_d^{(0)} = u^{(0)} - \frac{\partial v^{(0)}}{\partial \tau^*} = -k \cdot \left(\nabla'_\xi p^{(0)} - \frac{Ra}{\hat{P}e} \theta^{(0)} \mathbf{e}_z \right)$$
$$p^{(1)} = S \cdot \left(\nabla'_\xi p^{(0)} - \frac{Ra}{\hat{P}e} \theta^{(0)} \mathbf{e}_z \right) \qquad (3.3.19a, b)$$

where $k(\xi, \xi')$ and $S(\xi, \xi')$ are a second-order tensor and a vector to be determined. Substituting (3.3.19a,b) into (3.3.17), (3.3.18) and (3.2.16a), we obtain the canonical cell boundary value problem which k and S must satisfy.

$$\begin{aligned} \nabla_\xi \cdot k &= 0 && \text{in} \quad \Omega_f \\ \nabla_\xi^2 \cdot k &= -\nabla_\xi S - I && \text{in} \quad \Omega_f \\ k &= 0 && \text{on} \quad \Gamma_\xi(0) \end{aligned} \qquad (3.3.20a - d)$$

k and S are Ω – periodic

(Ene and Sanchez-Palencia, 1974). This can also be solved numerically. Afterwards, the Ω-average of (3.3.19a) gives Darcy's law

$$\langle u_d^{(0)} \rangle = \langle u^{(0)} \rangle - n' \frac{\partial v^{(0)}}{\partial \tau^*} = -k' \cdot \left(\nabla'_\xi p^{(0)} - \frac{Ra}{\hat{P}e} \theta^{(0)} \mathbf{e}_z \right) \qquad (3.3.21)$$

where k' is the Ω-cell average of k, *e.g.*

$$k' = \langle k \rangle \qquad (3.3.22)$$

It is stressed that the flow is driven not only by pressure gradient, but also by bouyancy (see (3.3.18b)).

We now consider the continuity equation at $O(\epsilon)$ to derive the consolidation equation. From (3.2.2b) and (3.2.16b)

$$\nabla'_\xi \cdot u^{(0)} + \nabla_\xi \cdot u^{(1)} = 0$$
$$u^{(1)} + v^{(1)} \cdot \nabla_\xi u^{(0)} = \frac{\partial v^{(1)}}{\partial \tau^*} - \frac{\partial v^{(0)}}{\partial \tau^*} \cdot \left(\nabla'_\xi v^{(0)} + \nabla_\xi v^{(1)} \right) \qquad (3.3.23a, b)$$

Let us take the Ω-average of (3.72a) and use Gauss's theorem and Ω-periodicity to obtain

$$\nabla'_\xi \cdot \langle u^{(0)} \rangle + \frac{1}{\Omega} \int_\Gamma u^{(1)} \cdot N^f dS = 0 \tag{3.3.24}$$

After using (3.3.23b) the integral in (3.3.24) may be written as

$$\begin{aligned}
\frac{1}{\Omega} \int_\Gamma u^{(1)} \cdot N^f dS &= -\frac{1}{\Omega} \int_\Gamma \frac{\partial v^{(1)}}{\partial \tau^*} \cdot (-N^f) dS - \frac{1}{\Omega} \int_\Gamma v_j^{(1)} \frac{\partial u_i^{(0)}}{\partial \xi_j} N_i^f dS \\
&\quad + \frac{1}{\Omega} \int_\Gamma \frac{\partial v_j^{(0)}}{\partial \tau^*} \left(\frac{\partial v_i^{(0)}}{\partial \xi'_j} + \frac{\partial v_i^{(1)}}{\partial \xi_j} \right) (-N_i^f) dS \\
&= -\langle \nabla_\xi \cdot \frac{\partial v^{(1)}}{\partial \tau^*} \rangle - \frac{1}{\Omega} \int_\Gamma v_j^{(1)} \frac{\partial u_i^{(0)}}{\partial \xi_j} N_i^f dS + \frac{1}{\Omega} \int_{\Omega_s} \frac{\partial}{\partial \xi_i} \left(\frac{\partial v_j^{(0)}}{\partial \tau^*} \frac{\partial v_i^{(1)}}{\partial \xi_j} \right) d\Omega
\end{aligned}$$

where (3.2.6) has been used in the last step. If we use (3.3.13) for $v^{(1)}$ and (3.3.19) for $u^{(0)}$, the same integral further becomes after some manipulation

$$\begin{aligned}
&- \langle e_\xi(\phi) : I \rangle : e'_\xi \left(\frac{\partial v^{(0)}}{\partial \tau^*} \right) + \langle e_\xi(\eta) : I \rangle \frac{\partial p^{(0)}}{\partial \tau^*} + \langle e_\xi(\zeta) : I \rangle \frac{\partial \theta^{(0)}}{\partial \tau^*} \\
&+ \left(J'_{jmn} e'_{mn}(v^{(0)}) + L'_j p^{(0)} + C'_j \theta^{(0)} \right) \left(\frac{\partial p^{(0)}}{\partial \xi'_j} - \frac{Ra}{\hat{P}e} \delta_{jz} \theta^{(0)} \right) \\
&+ \left(M'_{jmn} e'_{mn}(v^{(0)}) + N'_j p^{(0)} + E'_j \theta^{(0)} \right) \frac{\partial v_j^{(0)}}{\partial \tau^*}
\end{aligned} \tag{3.3.25}$$

where

$$\begin{Bmatrix} J'_{jmn} \\ L'_j \\ C'_j \end{Bmatrix} = \frac{1}{\Omega} \int_\Gamma \frac{\partial k_{ij}}{\partial \xi_\ell} \begin{Bmatrix} \phi_\ell^{mn} \\ -\eta_\ell \\ -\zeta_\ell \end{Bmatrix} N_i^f dS \tag{3.3.26a}$$

$$\begin{Bmatrix} M'_{jmn} \\ N'_j \\ E'_j \end{Bmatrix} = \frac{1}{\Omega} \int_\Gamma \begin{Bmatrix} -\frac{\partial \phi_i^{mn}}{\partial \xi_i} \\ \frac{\partial \eta_i}{\partial \xi_i} \\ \frac{\partial \zeta_i}{\partial \xi_i} \end{Bmatrix} N_j^f dS \tag{3.3.26b}$$

Substituting (3.3.25) for the integral and (3.3.19) for $u^{(0)}$ in (3.3.24) we finally obtain

$$\begin{aligned}
\nabla'_\xi \cdot \left[k' \cdot \left(\nabla'_\xi p^{(0)} - \frac{Ra}{\hat{P}e} \delta_{jz} \theta^{(0)} \right) \right] &= (\nabla'_\xi n') \cdot \frac{\partial v^{(0)}}{\partial \tau^*} + \gamma' : e'_\xi \left(\frac{\partial v^{(0)}}{\partial \tau^*} \right) + \beta'_c \frac{\partial p^{(0)}}{\partial \tau^*} \\
&+ \zeta'_c \frac{\partial \theta^{(0)}}{\partial \tau^*} + \left(J' : e'_\xi \left(v^{(0)} \right) + L' p^{(0)} + C' \theta^{(0)} \right) \cdot \left(\nabla'_\xi p^{(0)} - \frac{Ra}{\hat{P}e} \delta_{jz} \theta^{(0)} \right) \\
&+ \left(M' : e'_\xi \left(v^{(0)} \right) + N' p^{(0)} + E' \theta^{(0)} \right) \cdot \frac{\partial v^{(0)}}{\partial \tau^*}
\end{aligned} \tag{3.3.27}$$

where

$$\gamma' = n'I - \langle e_\xi(\phi) : I \rangle$$

$$\beta'_c = \langle e_\xi(\eta) : I \rangle \qquad (3.3.28a - c)$$

$$\zeta'_c = \langle e_\xi(\zeta) : I \rangle$$

Equation (3.76) is the thermoconsolidation equation. It has nonlinear coupling terms which stem from the nonlinear boundary condition (3.3.23b).

We emphasize that, by allowing the solid displacement to be as large as the pore size or granular size, the effective macroscale equations coupling the solid and fluid are nonlinear in general. This means that Biot's linear theory must be limited to cases where the solid displacement is much smaller than the granular size. We shall however show in Appendix D that for a microcell with three planes of symmetry the nonlinear coefficients vanish. Therefore Biot's equations are valid for porous media isotropic on the microscale.

3.4 Macroscale Heat Transport

At $O(\epsilon)$, another set of micro-cell boundary value problems are defined for temperature fluctuations at the microscale level which are proportional to the macroscale thermal gradient. The heat transport equation will be found at $O(\epsilon^2)$.

The total temperature $T_{f,s}$ will be decomposed by the initial temperatures $\overline{T}_{f,s}$ and the dynamic variations $\theta_{f,s}$. The initial temperature is governed by the pure steady diffusion problem. The governing equations are simply (3.38) and (3.40) without the local and convective terms. Application of the homogenization theory to such elliptic problems has been treated elsewhere (Bensoussan et al (1978), Sanchez-Palencia (1980)) and will not be repeated here.

Let the temperature $T^{(n)}_{f,s}$ be

$$T^{(n)}_{f,s} = \overline{T}^{(n)}_{f,s} + \theta^{(n)}_{f,s} \quad (n = 0, 1, 2, ...)$$

3.4.1 The Canonical Cell Problems for Heat Transfer

At $O(1)$, we have from (3.2.11a), (3.2.13a), (3.2.21a) and (3.2.22a)

$$\begin{aligned} 0 &= \nabla_\xi \cdot (m_f^* \cdot \nabla_\xi \theta_f^{(0)}) \quad \text{in} \quad \Omega_f \\ 0 &= M_r \nabla_\xi \cdot (m_s^* \cdot \nabla_\xi \theta_s^{(0)}) \text{in} \quad \Omega_s \\ \theta_f^{(0)} &= \theta_s^{(0)} \qquad\qquad \text{on} \quad \Gamma(0) \\ (m_f^* \cdot \nabla_\xi \theta_f^{(0)}) \cdot N &= M_r (m_s^* \cdot \nabla_\xi \theta_s^{(0)}) \cdot N \qquad \text{on} \quad \Gamma(0) \end{aligned} \tag{3.4.1a-d}$$

which is a pure conduction problem. The initial temperatures $\overline{T}_f^{(0)}$ and $\overline{T}_s^{(0)}$ are governed by the same equations.

Multiply (3.4.1a) and (3.4.1b) by $\theta_f^{(0)}$ and $\theta_s^{(0)}$, integrate over Ω_f and Ω_s, and use Gauss's theorem and Ω−periodicity to get:

$$\begin{aligned} 0 = &\int_\Gamma \{m_f^* \cdot \theta_f^{(0)} \nabla_\xi \theta_f^{(0)} \cdot N^f + M_r m_s^* \cdot \theta_s^{(0)} \nabla_\xi \theta_s^{(0)} \cdot N^s\} dS \\ &- \int_{\Omega_f} m_f^* \cdot \nabla_\xi \theta_f^{(0)} \nabla_\xi \theta_f^{(0)} d\Omega - M_r \int_{\Omega_s} m_s^* \cdot \nabla_\xi \theta_s^{(0)} \nabla_\xi \theta_s^{(0)} d\Omega \end{aligned} \tag{3.4.2}$$

where N^f and N^s are the unit normal vectors on $\Gamma(0)$ pointing outwards from Ω_f and Ω_s, respectively. The surface integrals cancel out because of (3.4.1c) and (3.4.1d). Since the volume integrals are positive-definite, (3.4.2) gives

$$\nabla_\xi \theta_f^{(0)} = \nabla_\xi \theta_s^{(0)} = 0 \quad ; \quad \theta_f^{(0)} = \theta_s^{(0)} = \theta^{(0)}(\xi', \tau^*) \tag{3.4.3}$$

The same holds for the initial temperature, e.g.

$$\overline{T}_f^{(0)} = \overline{T}_s^{(0)} = \overline{T}^{(0)}(\xi', \tau^*) \tag{3.4.3}$$

So that the leading order temperature does not depend on the microscale. The subscripts f and s for leading component temperature can be omitted from here on.

At $O(\epsilon)$ we take (3.4.3) and (3.4.4) into account and rewrite (3.2.11b), (3.2.13b), (3.2.21b) and (3.2.22b) after subtracting the initial temperature as

$$
\begin{aligned}
0 &= \nabla_\xi \cdot \left[m_f^* \cdot (\nabla'_\xi \theta^{(0)} + \nabla_\xi \theta_f^{(1)} \right] \quad \text{in} \quad \Omega_f \\
0 &= M_r \nabla_\xi \cdot \left[m_s^* \cdot (\nabla'_\xi \theta^{(0)} + \nabla_\xi \theta_s^{(1)}) \right] \quad \text{in} \quad \Omega_s \\
\theta_f^{(1)} &= \theta_s^{(1)} \qquad \text{on} \qquad \Gamma(0) \\
m_f^* \cdot (\nabla'_\xi \theta^{(0)} + \nabla_\xi \theta_f^{(1)}) \cdot N &= M_r m_s^* \cdot (\nabla'_\xi \theta^{(0)} + \nabla_\xi \theta_s^{(1)}) \cdot N \quad \text{on} \quad \Gamma(0)
\end{aligned}
\tag{3.4.5a-d}
$$

This set of equations define a boundary value problem for $\theta_f^{(1)}$ and $\theta_s^{(1)}$ and again describes a pure conduction problem. Equations (3.4.5a) and (3.4.5b) immediately suggest

$$
\begin{aligned}
\theta_f^{(1)} &= A^f \cdot \nabla'_\xi \theta^{(0)} \qquad \text{in} \qquad \Omega_f \\
\theta_s^{(1)} &= A^s \cdot \nabla'_\xi \theta^{(0)} \quad \text{in} \quad \Omega_s
\end{aligned}
\tag{3.4.6a,b}
$$

The unknown vector functions $A^f(\xi, \xi')$ and $A^s(\xi, \xi')$ must satisfy the following inhomogeneous canonical boundary value problem

$$
\begin{aligned}
0 &= \nabla_\xi \cdot [m_f^* \cdot (I + \nabla_\xi A^f)] \quad \text{in} \quad \Omega_f \\
&= M_r \nabla_\xi \cdot [m_s^* \cdot (I + \nabla_\xi A^s)] \quad \text{in} \quad \Omega_s \\
A^f &= A^s \qquad \text{on} \quad \Gamma(0) \\
m_f^* \cdot (I + \nabla_\xi A^f) \cdot N &= M_r m_s^* \cdot (I + \nabla_\xi A^s) \cdot N \quad \text{on} \quad \Gamma(0) \\
A^f \quad &\text{and} \quad A^s \quad \text{are} \quad \Omega\text{-periodic}
\end{aligned}
\tag{3.4.7a-e}
$$

For uniqueness we require

$$
\langle A^f \rangle = \langle A^s \rangle = 0 \tag{3.4.7f}
$$

The coupling between A^f and A^s comes in the boundary condition (3.4.7c and d).

By the same reasoning, the initial temperature at $O(\epsilon)$ becomes

$$
\overline{T}_f^{(1)} = A^f \cdot \nabla'_\xi \overline{T}^{(0)}, \quad \overline{T}_s^{(1)} = A^s \cdot \nabla'_\xi \overline{T}^{(0)} \tag{3.4.8}
$$

We now move to $O(\epsilon^2)$ to obtain the macroscale heat transport.

3.4.2 The Heat Transport Equation

At the next order $O(\epsilon^2)$, we subtract the initial temperature for the conduction part from (3.2.11c) and (3.2.13c) and invoke (3.4.3) and (3.4.4), to get

$$\begin{aligned}
&\frac{\partial\theta^{(0)}}{\partial\tau^*} + \hat{P}e\,u^{(0)}\cdot(\nabla'_\xi\theta^{(0)} + \nabla'_\xi\overline{T}^{(0)}) + \hat{P}e\nabla_\xi\cdot\left[u^{(0)}(\theta_f^{(1)} + \overline{T}_f^{(1)})\right] \\
&\quad = \nabla'_\xi\cdot\left[m_f^*\cdot(\nabla'_\xi\theta^{(0)} + \nabla\theta_f^{(1)})\right] + \nabla_\xi\cdot\left[m_f^*\cdot(\nabla'_\xi\theta_f^{(1)} + \nabla_\xi\theta_f^{(2)})\right] \quad \text{in} \quad \Omega_f \\
&(\rho C_p)_r\left\{\frac{\partial\theta^{(0)}}{\partial\tau^*} + \hat{P}e\frac{\partial v^{(0)}}{\partial\tau^*}\cdot\left[(\nabla'_\xi\theta^{(0)} + \nabla'_\xi\overline{T}^{(0)}) + (\nabla_\xi\theta_s^{(1)} + \nabla_\xi\overline{T}_s^{(1)})\right]\right\} \\
&\quad = M_r\nabla'_\xi\cdot\left[m_s^*\cdot(\nabla'_\xi\theta^{(0)} + \nabla_\xi\theta_s^{(1)})\right] \\
&\qquad + M_r\nabla_\xi\cdot\left[m_s^*\cdot(\nabla'_\xi\theta_s^{(1)} + \nabla_\xi\theta_s^{(2)})\right] \quad \text{in} \quad \Omega_s
\end{aligned} \tag{3.4.9a,b}$$

where the mass conservation (3.2.1b) has been used in (3.4.9a). Similarly the boundary conditions (3.2.21c) and (3.2.22c) become

$$\begin{aligned}
&\theta_f^{(2)} + v^{(1)}\cdot\left[\nabla'_\xi(\theta^{(0)} + \overline{T}^{(0)}) + \nabla_\xi(\theta_f^{(1)} + \overline{T}_f^{(1)})\right] \\
&= \theta_s^{(2)} + v^{(1)}\cdot\left[\nabla'_\xi(\theta^{(0)} + \overline{T}^{(0)}) + \nabla_\xi(\theta_s^{(1)} + \overline{T}_s^{(1)})\right] \quad \text{on} \quad \Gamma_\xi(0) \\
&m_f^*\cdot\left[\nabla'_\xi\theta_f^{(1)} + \nabla_\xi\theta_f^{(2)} + v^{(1)}\cdot\nabla_\xi(\nabla_\xi\theta_f^{(1)} + \nabla_\xi\overline{T}_f^{(1)})\right]\cdot N \\
&= M_r m_s^*\cdot\left[\nabla'_\xi\theta_s^{(1)} + \nabla_\xi\theta_s^{(2)} + v^{(1)}\cdot\nabla_\xi(\nabla_\xi\theta_s^{(1)} + \nabla_\xi\overline{T}_s^{(1)})\right]\cdot N \quad \text{on} \quad \Gamma_\xi(0)
\end{aligned} \tag{3.4.9c,d}$$

Integrating (3.4.9a) and (3.4.9b) over Ω_f and Ω_s and using Gauss's theorem, Ω-periodicty and (3.4.9d), we obtain

$$\begin{aligned}
&\overline{a}\frac{\partial\theta^{(0)}}{\partial\tau^*} + \hat{P}e\langle u^{(0)}\rangle\cdot(\nabla'_\xi\theta^{(0)} + \nabla'_\xi\overline{T}^{(0)}) + \hat{P}e\langle\nabla_\xi\cdot[u^{(0)}(\theta_f^{(1)} + \overline{T}_f^{(1)})]\rangle \\
&\qquad + (\rho C_p)_r\hat{P}e\frac{\partial v^{(0)}}{\partial\tau^*}\cdot\langle I + \nabla_\xi A^s\rangle\cdot(\nabla'_\xi\theta^{(0)} + \nabla'_\xi\overline{T}^{(0)}) \\
&\qquad = \nabla'_\xi\cdot\left\{\left[\langle m_f^*\cdot(I + \nabla_\xi A^f)\rangle + M_r\langle m_s^*\cdot(I + \nabla_\xi A^s)\rangle\right]\cdot\nabla'_\xi\theta^{(0)}\right\} \\
&\qquad - \frac{1}{\Omega}m_f^*\cdot\int_\Gamma v^{(1)}\cdot\nabla_\xi(\nabla_\xi\theta_f^{(1)} + \nabla_\xi\overline{T}_f^{(1)})\cdot N^f dS \\
&\qquad - \frac{1}{\Omega}M_r m_s^*\cdot\int_\Gamma v^{(1)}\cdot\nabla_\xi(\nabla_\xi\theta_s^{(1)} + \nabla_\xi\overline{T}_s^{(1)})\cdot(-N^f)dS
\end{aligned} \tag{3.4.10}$$

in which (3.4.6) and (3.4.8) have been used and $\overline{a}$ is the average heat capacity of the medium given by

$$\overline{a} = n' + (1 - n')(\rho C_p)_r \tag{3.4.10a}$$

After using Gauss's theorem, (3.2.16a), (3.4.5c), (3.4.6) and (3.4.8), the third term on the left-hand side of (3.4.10) further becomes

$$\hat{P}e\langle \nabla_\xi \cdot [u^{(0)}(\theta_f^{(1)} + \overline{T}_f^{(1)})]\rangle = -\hat{P}e \frac{\partial v^{(0)}}{\partial \tau^*} \cdot \langle \nabla_\xi A^s \rangle \cdot \nabla'_\xi (\theta^{(0)} + \overline{T}^{(0)}) \tag{3.4.11}$$

After using (3.3.3), (3.4.6) and (3.4.8), the integrals on the right-hand side of (3.4.10) become

$$-\left(S'_{mnk} e'_{mn}(v^{(0)}) + T'_k p^{(0)} + U'_k \theta^{(0)}\right)\left(\frac{\partial \theta^{(0)}}{\partial \xi'_k} + \frac{\partial \overline{T}^{(0)}}{\partial \xi'_k}\right) \tag{3.4.12}$$

where

$$\begin{aligned}\begin{Bmatrix} S'_{mnk} \\ T'_k \\ U'_k \end{Bmatrix} =& \frac{1}{\Omega} m^*_{f\,i\ell} \int_\Gamma \begin{Bmatrix} \phi_{jmn} \\ -\eta_j \\ -\zeta_j \end{Bmatrix} \frac{\partial}{\partial \xi_j}\left(\frac{\partial A^f_k}{\partial \xi_\ell}\right) N^f_i \, dS \\ &- \frac{M_r}{\Omega} m^*_{s\,i\ell} \int_\Gamma \begin{Bmatrix} \phi_{jmn} \\ -\eta_j \\ -\zeta_j \end{Bmatrix} \frac{\partial}{\partial \xi_j}\left(\frac{\partial A^s_k}{\partial \xi_\ell}\right) N^f_i \, dS\end{aligned} \tag{3.4.13}$$

Substituting (3.4.11) to (3.4.13) into (3.4.10) the macroscale heat transport becomes

$$\begin{aligned}&\overline{a}\frac{\partial \theta^{(0)}}{\partial \tau^*} + \hat{P}e\overline{U} \cdot \nabla'_\xi (\theta^{(0)} + \overline{T}^{(0)}) \\ &\quad + [S' : e'(v^{(0)}) + T' p^{(0)} + U' \theta^{(0)}] \cdot (\nabla'_\xi \theta^{(0)} + \nabla'_\xi \overline{T}^{(0)}) \\ &\quad = \nabla'_\xi \cdot (m' \cdot \nabla'_\xi \theta^{(0)})\end{aligned} \tag{3.4.14}$$

where

$$\begin{aligned}\overline{U} &= \langle u^{(0)} \rangle + \frac{\partial v^{(0)}}{\partial \tau^*} \cdot [(\rho C_p)_r (1 - n') I - (1 - (\rho C_p)_r) \langle \nabla_\xi A^s \rangle] \\ m' &= \langle m^*_f \cdot (I + \nabla_\xi A^f) \rangle + M_r \langle m^*_s \cdot (I + \nabla_\xi A^s) \rangle\end{aligned} \tag{3.4.15a,b}$$

are the effective velocity of heat convection and the thermal conductivity of the medium. There are also nonlinear coupling terms which result from the finite displacement of the fluid solid interface. Note that convection velocity depends also on A^s which is the solution to the cell problem defined by (3.4.7). A^s depends only on the geometry and material properties in the microscale and can be computed a priori.

3.5 Macroscale Equations in Eulerian Coordinates

The macroscale governing equations (3.3.14), (3.3.21), (3.3.27) and (3.4.14) are now transformed back to the Eulerian frame by using (3.1.20) and (3.1.28). Note that the time derivative is applied, in (3.3.27) and (3.4.14), only on the microscale-independent variables $v^{(0)}$, $p^{(0)}$ and $\theta^{(0)}$. Therefore, $\partial/\partial\tau^*$, ∇_ξ and ∇'_ξ can be replaced by $\partial/\partial t^*$, ∇ and ∇' with an error of $O(\epsilon)$. In summary, we have

$$\nabla' \cdot [a' : e'(v^{(0)}) - \alpha' p^{(0)} - \beta'_t \theta^{(0)}] - (F' : e'(v^{(0)}) + G' p^{(0)} + H' \theta^{(0)}) : e'(v^{(0)}) - I' {p^{(0)}}^2 - R' p^{(0)} \theta^{(0)} - K' {\theta^{(0)}}^2 = -\frac{Ra}{\hat{P}e} n' \theta^{(0)} \mathbf{e}_z \tag{3.5.1}$$

$$\langle u^{(0)} \rangle - n' \frac{\partial v^{(0)}}{\partial t^*} = -k' \cdot \left(\nabla' p^{(0)} - \frac{Ra}{\hat{P}e} \theta^{(0)} \mathbf{e}_z \right) \tag{3.5.2}$$

$$\begin{aligned} \nabla' \cdot \left[k' \cdot \left(\nabla' p^{(0)} - \frac{Ra}{\hat{P}e} \theta^{(0)} \mathbf{e}_z \right) \right] &= (\nabla' n') \cdot \frac{\partial v^{(0)}}{\partial t^*} + \gamma' : e' \left(\frac{\partial v^{(0)}}{\partial t^*} \right) + \beta'_c \frac{\partial p^{(0)}}{\partial t^*} \\ &+ \zeta'_c \frac{\partial \theta^{(0)}}{\partial t^*} + (J' : e'(v^{(0)}) + L' p^{(0)} + C' \theta^{(0)}) \cdot \left(\nabla' p^{(0)} - \frac{Ra}{\hat{P}e} \theta^{(0)} \mathbf{e}_z \right) \\ &+ (M' : e'(v^{(0)}) + N' p^{(0)} + E' \theta^{(0)}) \cdot \frac{\partial v^{(0)}}{\partial t^*} \end{aligned} \tag{3.5.3}$$

$$\begin{aligned} &\overline{a} \frac{\partial \theta^{(0)}}{\partial t^*} + \hat{P}e \overline{U} \cdot \nabla' (\theta^{(0)} + \overline{T}^{(0)}) \\ &+ [S' : e'(v^{(0)}) + T' p^{(0)} + U' \theta^{(0)}] \cdot (\nabla' \theta^{(0)} + \nabla' \overline{T}^{(0)}) = \nabla' \cdot (m' \cdot \nabla' \theta^{(0)}) \end{aligned} \tag{3.5.4}$$

The macroscale coefficients are determined after solving the canonical boundary value problems summarized earlier for a given microcell geometry. However, as will

be shown later in §5, the tensor coefficients F', G', H', I', R', K', J', L', C', M', N', E', S', T' and U' of the nonlinearly coupled terms vanish for cell geometries which have three mutually orthogonal planes of symmetry.

3.6 A Special Case of Small T_c ; $T_c/T_d = O(\epsilon^2)$.

In practice, the transport of solute or heat is of greater concern in sand or rock. In such porous media, the ratio of the consolidation time to the heat diffusion time T_c/T_d is, as shown in Table 2.1, generally very small and the governing equations can be obtained as a special case of $T_c/T_d = O(1)$ treated in the previous subsections. Also, the elastic modulus $\mathcal{D}$ of such medium is relatively large so that $P'/\mathcal{D}$ is relatively small.

In order to be consistent with the scale estimates of Table 2.1 for sand or rock, we shall assume

$$T_c/T_d = O(\epsilon^2), \qquad P'/\mathcal{D} = O(\epsilon^2) \tag{3.6.1}$$

All other dimensionless parameters remain the same as before,e.g.

$$Pr = O(1), \quad Re = O(\epsilon), \quad Pe = O(\epsilon) \tag{3.6.2}$$

Accordingly the scale ratios in (2.2.21) and (2.2.22) become

$$\frac{V}{UT} = O(\epsilon^2) \quad ; \quad \frac{V\ell}{\alpha_f T} = O(\epsilon^3) \tag{3.6.3}$$

The energy equation in the solid phase (2.2.14), the kinematic boundary condition (2.2.17) and the stress continuity equation (2.2.18) now become respectively,

$$(\rho C_p)_r \left(\epsilon^2 \frac{\partial \theta_s^*}{\partial t^*} + \epsilon^3 \frac{dv^*}{dt^*} \cdot \nabla^* \theta_s^* \right) = M_r \nabla^* \cdot (m_s^* \cdot \nabla^* \theta_s^*) \quad \text{in} \quad \Omega_s \tag{3.6.4}$$

$$u^* = \epsilon^2 \frac{dv^*}{dt^*} \qquad \text{on} \quad \Gamma(0) \tag{3.6.5}$$

$$\sigma_s^* \cdot N = \epsilon^2 \sigma_f^* \cdot N \tag{3.6.6}$$

Therefore, the relative importance of solid velocity in the deformation of and the convection of heat in the medium is reduced by a factor of $O(\epsilon^2)$. This does not

imply that there is no consolidation as will be shown later. The scale relation for the stress continuity (3.6.6) at the fluid-solid interface implies that the solid displacement is independent of the microscale coordinates at not only the leading order $v^{(0)}$ but also the first order $v^{(1)}$. For (3.6.1) to be consistent with the relation (2.1.24),e.g. $\delta \sim P'/\mathcal{D}$, we set $v^{(0)} = 0$. Consequently the deviation of $\Gamma(t)$ from $\Gamma(0)$ is $O(\epsilon\ell)$ and the Galilean transformation is not necessary. Moreover, the reduced scale of solid displacement immediately shows that the boundary conditions on the interface are linear and all nonlinear coupling terms in the macroscale governing equations disappear.

As remarked earlier in §2, the scale relation (3.6.1) implies that T_c is not only the consolidation time scale but also the time scale for temperature changes over the macroscale. Since this shortest time scale is not relevant to the thermal changes over the macroscale, it is ignored and there remains one time scale $T_v = T_d$(cf.(2.2.2)).

According to (3.6.4) to (3.6.6) the convection terms on the left-hand side of (3.2.11a-c) and the solid velocity on the left-hand side of (3.2.13a-c) are moved to the equations at the orders of ϵ higher by two. The resulting governing equations at the macroscale become as follows.

$$\nabla' \cdot \left[a' : \epsilon'(v^{(1)}) - \alpha' p^{(0)} - \beta_t' \theta^{(0)} \right] = -\frac{Ra}{\hat{P}e} n' \theta^{(0)} \mathbf{e}_z \tag{3.6.7}$$

$$\langle u^{(0)} \rangle = -k' \cdot \left(\nabla' p^{(0)} - \frac{Ra}{\hat{P}e} \theta^{(0)} \mathbf{e}_z \right) \tag{3.6.8}$$

$$\nabla' \cdot [k' \cdot (\nabla' p^{(0)} - \frac{Ra}{\hat{P}e} \theta^{(0)} \mathbf{e}_z)] = 0 \tag{3.6.9}$$

$$\bar{a} \frac{\theta^{(0)}}{\partial t^*} + \hat{P}e \langle u^{(0)} \rangle \cdot \nabla' (\theta^{(0)} + \overline{T}^{(0)}) = \nabla' \cdot (m' \cdot \nabla' \theta^{(0)}) \tag{3.6.10}$$

in which the elastic coefficcients a', α' and β_t' were given in (3.3.15a-c) and the permeability k' and the thermal condictivity m' were given in (3.3.22) and (3.4.15b).

In contrast with (3.3.27) and (3.4.14), (3.6.9) and (3.6.10) no longer contain the nonlinear coupling terms and the terms involving the solid velocity $\partial v^{(1)}/\partial t^*$ also disappear. Note that the linear terms on the right-hand side of (3.5.3) originate

from $\partial v^{(2)}/\partial t^*$(cf.(3.3.24)) and $v^{(2)}$ is given by (3.3.3). This implies that, although $v^{(1)}$, $p^{(0)}$ and $\theta^{(0)}$ are coupled, the elastic response of the medium to pressure and thermal changes is instantaneous while the medium temperature varies in a transient manner as in (3.6.10). Thus the fluid flow and temperature variations can be solved first as if the solid were rigid. Afterwards the solid stress is found by accounting for the pre-existing fluid pressure and temperature distributions.

3.7 The Macroscale Governing Equations in Physical Variables.

It will be shown that the coefficients F', G', H', I', R', K', J', L', C', M', N', E', S', T' and U' of the nonlinearly coupled terms vanish for microcell geometry with three planes of symmetry which will be used for real computation of macroscale coefficients. Excluding those terms, we write the macroscale governing equations in physical variables.

With the normalization scalea of (2.2.1) the macroscale governing equations in physical variables are readily obtained. An overhead symbol ($\tilde{}$) is used to denote physical constitutive coefficients. Again the nonlinear coupling terms are not retained.

If we recall the definitions for Ra and $\hat{P}e$ from (2.2.8) and (3.1.6), the equilibrium equation (3.5.1) becomes

$$\nabla \cdot [\tilde{a} : e(v) - \tilde{\alpha} p - \tilde{\beta}_t \theta] = -\rho_f g \beta_T n' \theta \mathbf{e}_z \tag{3.7.1}$$

where the primes are now dropped and

$$\begin{aligned} \tilde{a} &= \langle a : [II + e(\tilde{\phi})] \rangle \\ \tilde{\alpha} &= n' I + \langle a : e(\tilde{\eta}) \rangle \\ \tilde{\beta}_t &= \langle \beta \rangle + \langle a : e(\tilde{\zeta}) \rangle \end{aligned} \tag{3.7.2a-c}$$

Darcy's law may be written from (3.5.2) as

$$\langle u_d \rangle = \langle u \rangle - n' \frac{\partial v}{\partial t} = -\tilde{k} \cdot (\nabla p - \rho_f g \beta_T \theta \mathbf{e}_z) \tag{3.7.3}$$

The thermoconsolidation equation (3.5.3) is similarly written as

$$\nabla \cdot [\tilde{k} \cdot (\nabla p - \rho_f g \beta_T \theta \mathbf{e}_z)] = (\nabla n') \cdot \frac{\partial v}{\partial t} + \tilde{\gamma} : e\left(\frac{\partial v}{\partial t}\right) + \tilde{\beta}_c \frac{\partial p}{\partial t} + \tilde{\zeta}_c \frac{\partial \theta}{\partial t} \qquad (3.7.4)$$

where

$$\begin{aligned} \tilde{\gamma} &= n' I - \langle e(\tilde{\phi}) \rangle : I \\ \tilde{\beta}_c &= \langle e(\tilde{\eta}) \rangle : I \\ \tilde{\zeta}_c &= \langle e(\tilde{\zeta}) \rangle : I \end{aligned} \qquad (3.7.5a-c)$$

After using (3.4.15a and b), the heat transport equation (3.5.4) is written

$$\overline{\rho C_p} \frac{\partial \theta}{\partial t} + \left\{ (\rho C_p)_f \left[\langle u \rangle - \frac{\partial v}{\partial t} \cdot \langle \nabla \tilde{A}^s \rangle \right] + (\rho C_p)_s \frac{\partial v}{\partial t} \cdot ((1 - n')I + \langle \nabla \tilde{A}^s \rangle) \right\} \cdot \left(\nabla \theta + \nabla \overline{T}\right) = \nabla \cdot (\widetilde{m}' \cdot \nabla \theta') \qquad (3.7.6)$$

where

$$\overline{\rho C_p} = n'(\rho C_p)_f + (1 - n')(\rho C_p)_s \qquad (3.7.7)$$

$$\widetilde{m}' = \langle m_f \cdot (I + \nabla \tilde{A}^f) \rangle + \langle m_s \cdot (I + \nabla \tilde{A}^s) \rangle \qquad (3.7.8)$$

are the macroscale heat capacity and thermal conductivity of the composite medium respectively.

Note that the heat transport equation is still nonlinear due to the finite displacement of the solid matrix compared to the pore size. The constitutive coefficients to be computed from the cell boundary value problems are $\tilde{a}$, $\tilde{\alpha}$, $\tilde{\beta}_t$ in Hooke's law, $\tilde{\gamma}$, $\tilde{\beta}_c$, $\tilde{\zeta}_c$ in the consolidation equation and $\widetilde{m}'$ in the heat transport equation. All the coefficients are associated with the linear terms.

4. Properties of Macroscale Coefficients.

By making use of the microcell boundary value problems defined previously, certain properties of the macroscale coefficients can be deduced.

For the isothermal case these properties have been thoroughly studied by Auriault and Sanchez-Palencia(1977). Their work is extended here to show that, the inter-relationship among ϕ, η and ζ implies certain constraints among the elastic coefficients a', α' and β_t' of (3.3.15). Also the coefficients γ', β_c' and ζ_c' of the consolidation equation (3.3.28) are shown to have certain properties and be related to a'. For the coefficients associated with flow and heat transport, symmetry and positive definite properties will be shown.

The coefficients F', G', H', I', R', K', J', L', C', M', N', E', S', T' and U' for the nonlinear terms are shown to vanish for a microcell geometry with three planes of symmetry in Appendix D. The discussions in this section are restricted to the coefficients of linear terms in the macroscale governing equations. The actual computations of the macroscale coefficients will be carried out in §5 for a special microcell geometry with three planes of symmetry for which only the constitutive coefficients associated with the linear terms need to be computed.

4.1 Elastic Coefficients.

With the normalization of (2.2.1), the dimensionless macroscale equilibrium equation is (cf. (3.7.1))

$$\nabla' \cdot \langle \sigma_T^{(0)} \rangle = -\frac{Ra}{\hat{P}e} n' \theta^{(0)} \mathbf{e}_z \tag{4.1.1}$$

where

$$\langle \sigma_T^{(0)} \rangle = a' : e'(v^{(0)}) - \alpha' p^{(0)} - \beta_t' \theta^{(0)} \tag{4.1.2}$$

is the total stress and the coefficients are given by(cf.(3.7.2(a-c))

$$\begin{aligned} a' &= a'_{ijk\ell} = \langle a^*_{ijpq}(\delta_{pk}\delta_{q\ell} + e_{pq}(\phi^{k\ell})) \rangle \\ \alpha' &= \alpha'_{ij} = n'\delta_{ij} + \langle a^*_{ijpq} e_{pq}(\eta) \rangle \\ \beta_t' &= (\beta_t')_{ij} = \langle \beta^*_{ij} \rangle + \langle a^*_{ijpq} e_{pq}(\zeta) \rangle \end{aligned} \tag{4.1.3a-c}$$

For convenience the second and third indices of ϕ_{ikl}, which are identical to those of the macroscale strain $e'(v^{(0)})$, are placed in the upper right corner as superscripts in (4.1.3a).

We shall first show that the elastic coefficient tensor of rank four a' possesses the symmetry properties of the elastic coefficients a^* (cf.(2.2.12)) known in linear elasticity. Relationships among a', α' and β'_i are then derived from the boundary value problems (3.3.4) to (3.3.6) after assuming isotropic material for the solid phase.

Suppose that the porous medium contains no pore fluid and is in isothermal condition. Equations (4.1.1) and (4.1.2) then reduce to

$$\nabla' \cdot \langle \sigma_T^{(0)} \rangle = \nabla' \cdot [a' : e'(v^{(0)})] = 0 \tag{4.1.4}$$

It is obvious, from the symmetry properties $\langle \sigma_T^{(0)} \rangle_{ij} = \langle \sigma_T^{(0)} \rangle_{ji}$ and $e'_{ij}(v^{(0)}) = e'_{ji}(v^{(0)})$, that

$$a'_{ijk\ell} = a'_{jik\ell} = a'_{ij\ell k} \tag{4.1.5a}$$

It is also known that(Fung, 1965)

$$a'_{ijk\ell} = a'_{k\ell ij} \tag{4.1.5b}$$

from the stress-strain relation derived from the strain energy density. Similarly it follows from (4.1.2) that

$$\alpha'_{ij} = \alpha'_{ji} \quad ; \quad (\beta'_i)_{ij} = (\beta'_i)_{ji} \tag{4.1.6}$$

In indicial form, the boundary value problems for ϕ, η and ζ are defined by (3.3.4) to (3.3.6)

$$\begin{aligned} \frac{\partial}{\partial x_i}[a^*_{ijpq}(\delta_{pm}\delta_{qn} + e_{pq}(\phi^{mn}))] &= 0 \quad \text{in} \quad \Omega_s \\ \frac{\partial}{\partial x_i}[a^*_{ijpq} e_{pq}(\eta)] &= 0 \quad \text{in} \quad \Omega_s \\ \frac{\partial}{\partial x_i}[a^*_{ijpq} e_{pq}(\zeta) + \beta^*_{ij}] &= 0 \quad \text{in} \quad \Omega_s \end{aligned} \tag{4.1.7a-c}$$

$$a^*_{ijpq}(\delta_{pm}\delta_{qn} + e_{pq}(\phi^{mn}))N^\varepsilon_i = 0 \qquad \text{on} \quad \Gamma(0)$$

$$a^*_{ijpq}e_{pq}(\eta)N^\varepsilon_i = \delta_{ij}N^\varepsilon_i \qquad \text{on} \quad \Gamma(0) \qquad (4.1.8a-c)$$

$$(a^*_{ijpq}e_{pq}(\zeta) + \beta^*_{ij})N^\varepsilon_i = 0 \qquad \text{on} \quad \Gamma(0)$$

and

$$\phi, \quad \eta \quad \text{and} \quad \zeta \quad \text{are} \quad \Omega - \text{periodic} \qquad (4.1.9a)$$

$$\langle\phi\rangle = \langle\eta\rangle = \langle\zeta\rangle = 0 \qquad (4.1.9b)$$

It has been shown in Auriault and Sanchez-Palencia(1977). that

$$\langle a^* : e(\eta)\rangle = -\langle e(\phi)\rangle : I \qquad (4.1.10)$$

Similar relationship is now extended to between ϕ and ζ and η and ζ here.

Multiply (4.1.7a) by ζ_j, integrate over Ω_ε and use Gauss theorem and Ω-periodicity to get

$$\int_\Gamma [a^*_{ijpq}(\delta_{pm}\delta_{qn} + e_{pq}(\phi^{mn}))]\zeta_j N^\varepsilon_i dS$$

$$- \int_{\Omega_\varepsilon} a^*_{ijpq}e_{pq}(\phi^{mn})e_{ij}(\zeta)d\Omega - \int_{\Omega_\varepsilon} a^*_{ijpq}e_{pq}(\phi^{mn})\delta_{pm}\delta_{qn}e_{ij}(\zeta)d\Omega = 0 \qquad (4.1.11)$$

The surface integral on Γ vanishes beacuse of (4.1.8a). Likewise, upon multiplying (4.1.7c) by ϕ^{mn}_j and integrating over Ω_ε we obtain

$$\int_{\Omega_\varepsilon} a^*_{ijpq}e_{pq}(\zeta)e_{ij}(\phi^{mn})d\Omega + \int_{\Omega_\varepsilon} \beta^*_{ij}e_{ij}(\phi^{mn})d\Omega = 0 \qquad (4.1.12)$$

Combining (4.1.11) and (4.1.12)

$$\langle a^* : e(\zeta)\rangle = \langle \beta^* : e(\phi)\rangle \qquad (4.1.13)$$

The same procedure applied to (4.7b and c) for η and ζ yields

$$\langle \beta^* : e(\eta)\rangle = -\langle e(\zeta)\rangle : I \qquad (4.1.14)$$

On the other hand, if we multiply (4.1.7b) by η_j and integrate over Ω_ε, it follows that

$$\langle \nabla \cdot \eta\rangle = \langle e(\eta)\rangle : I > 0 \qquad (4.1.15)$$

as shown by Auriault and Sanchez-Palencia(1977). After multiplying (4.1.7c) by ζ_j and integrating over Ω_s, similar relation can be found for ζ.

$$\int_\Gamma [a^*_{ijpq} e_{pq}(\zeta) + \beta^*_{ij}]\zeta_j N_i^s - \int_{\Omega_s} [a^*_{ijpq} e_{pq}(\zeta) + \beta^*_{ij}] e_{ij}(\zeta) d\Omega = 0$$

which gives

$$\int_{\Omega_s} \beta^*_{ij} e_{ij}(\zeta) d\Omega = -\int_{\Omega_s} a^*_{ijpq} e_{pq}(\zeta) e_{ij}(\zeta) d\Omega < 0$$

after using (4.1.8c) or

$$\langle \beta^* : e(\zeta) \rangle < 0 \tag{4.1.16}$$

Let us assume that the solid grains are isotropic so that there are two independent constants λ and μ or equivalently Young's modulus E and Poisson's ratio ν which are related by

$$\lambda^* = \frac{\lambda}{E} = \frac{\nu}{(1+\nu)(1-2\nu)}, \quad \mu^* = \frac{\mu}{E} = \frac{1}{2(1+\nu)} \tag{4.1.17}$$

Specifically

$$\begin{aligned} a^*_{xxxx} &= a^*_{yyyy} = a^*_{zzzz} = \lambda^* + 2\mu^* \\ a^*_{xxyy} &= a^*_{yyzz} = a^*_{zzxx} = \lambda^* \\ a^*_{xyxy} &= a^*_{yzyz} = a^*_{zxzx} = \mu^* \end{aligned} \tag{4.1.18}$$

If we recall (2.2.4), the dimensionless thermal modulus β^*_{ij} for isotropic solid is then

$$\beta^*_{ij} = \beta^* \delta_{ij} = \frac{\beta}{\alpha E} \delta_{ij} = (3\lambda^* + 2\mu^*)\delta_{ij} \quad ; \quad \beta^* = (3\lambda^* + 2\mu^*) \tag{4.1.19a,b}$$

Also the bulk modulus is given by

$$K^* = \frac{K}{E} = \frac{1}{3}(3\lambda^* + 2\mu^*) \tag{4.1.19c}$$

It is convenient to introduce the dimensionless compliance tensor of rank four $b_{\alpha\beta kh}$ (Auriault and Sanchez-Palencia, 1977) which is related to the elastic coefficients a^* by

$$a^*_{ijkh} b_{\alpha\beta kh} = \frac{1}{2}(\delta_{\alpha i}\delta_{\beta j} + \delta_{\alpha j}\delta_{\beta i}) \tag{4.1.20}$$

(see Appendix B). If the solid is isotropic, it can be shown that the tensor $b_{\alpha\beta kh}$ has the following property (cf.(B.11))

$$b_{\alpha\beta rr} = \frac{\delta_{\alpha\beta}}{3\lambda^* + 2\mu^*} = \frac{\delta_{\alpha\beta}}{3K^*} \tag{4.1.21}$$

We now express the coefficients α'_{ij} and $(\beta'_t)_{ij}$ in terms of $a'_{ijk\ell}$ for isotropic grains. In view of (4.1.20), equation (4.1.3a) may be written as

$$\langle e_{pq}(\phi^{k\ell})\rangle = [a'_{ijkl} - (1-n')a^*_{ijk\ell}]b_{ijpq} \tag{4.1.22}$$

after scalar multiplication by b_{ijpq}. Contracting by $p = q$ in (4.1.22), it becomes

$$\langle \phi^{k\ell}_{i,i}\rangle = a'_{ijk\ell}b_{ijrr} - (1-n')\delta_{k\ell} \tag{4.1.23}$$

Combining (4.1.3b), (4.1.10) and (4.1.23), we have

$$\alpha'_{ij} = n'\delta_{ij} - \langle \phi^{ij}_{\ell,\ell}\rangle = \delta_{ij} - a'_{pqij}b_{pqrr} = \delta_{ij} - \frac{a'_{pqij}\delta_{pq}}{3\lambda^* + 2\mu^*} = \delta_{ij} - \frac{a'_{pqij}\delta_{pq}}{3K^*} \tag{4.1.24}$$

where the last equality follows after using (4.1.21). Equation (4.1.24) has been obtained by Auriault and Sanchez-Palencia(1977) who further specialized it to an isotropic medium at the macroscale level to obtain

$$\alpha'_{ij} = \Big(1 - \frac{3\lambda' + 2\mu'}{3\lambda^* + 2\mu^*}\Big)\delta_{ij} = \alpha\delta_{ij}$$

where λ' and μ' are the Lame's constants of the medium and must be determined by solving the canonical cell problems (4.1.7) to (4.1.9).

In a later section, we shall choose a special micro-structure which has three orthogonal planes of symmetry so that it satisfies the requirements for cubic symmetry in crystalline structure. It will be shown that $a'_{ijk\ell}$ reduces to three distinct constants by using the symmetry of the solution ϕ.

After using (4.1.13), (4.1.19a,b) and (4.1.23), the effective macroscale thermal modulus β'_t of (4.1.3c) becomes

$$(\beta'_t)_{ij} = \beta^*\delta_{ij}(1-n') + \beta^*\langle e_{\ell\ell}(\phi^{ij})\rangle = \beta^* a'_{pqij}b_{pqrr} = \beta^*\frac{a'_{pqij}\delta_{pq}}{3\lambda^* + 2\mu^*} = a'_{pqij}\delta_{pq} \tag{4.1.25}$$

Alternatively, (4.1.14) and (4.1.24) can be used to obtain (4.1.25).

The significances of (4.1.24) and (4.1.25) are as follows. If the elastic coefficients a'_{ijpq} are determined for a given cell geometry, the coefficients α'_{ij} and $(\beta'_t)_{ij}$ are readily calculated by (4.1.24) and (4.1.25); the cell boundary value problems for η and ζ need not to be solved unless microscale variation of the stresses inside a micro-cell is required.

The relations (4.1.10) to (4.1.16) can also be used to establish the properties of the coefficients γ', β'_c and ζ'_c in (3.3.28). Auriault and Sanchez-Palencia(1977) have shown, after using (4.1.10),(4.1.20) and (4.1.21), that

$$\gamma' = n'I - \langle e(\phi)\rangle : I = n'I + \langle a^* : e(\eta)\rangle = \alpha' \tag{4.1.26}$$

$$\begin{aligned}\beta'_c &= \langle e_{\ell\ell}(\eta)\rangle = b_{\ell\ell ij}[(1-n')\delta_{ij} - a'_{pqij}b_{pqrr}] \\ &= \frac{1}{3\lambda^* + 2\mu^*}\Big[3(1-n') - a'_{ppjj}\frac{1}{3\lambda^* + 2\mu^*}\Big] \\ &= \frac{1}{3K^*}\Big[3(1-n') - a'_{ppjj}\frac{1}{3K^*}\Big]\end{aligned} \tag{4.1.27}$$

and also by using (4.1.15) that

$$\beta'_c > 0 \tag{4.1.28}$$

We extend it to express ζ'_c in terms of $a'_{ijk\ell}$. From (3.3.28c)

$$\zeta'_c = \langle e(\zeta)\rangle : I = \langle e_{\ell\ell}(\zeta)\rangle \tag{4.1.29}$$

Also from (4.1.3c) we have by using the compliance tensor and (4.1.25)

$$\langle e_{\ell m}(\zeta)\rangle = -b_{\ell mij}[\beta^*(1-n')\delta_{ij} - (\beta'_t)_{ij}] = -b_{\ell mij}[\beta^*(1-n')\delta_{ij} - \beta^* a'_{pqij}b_{pqrr}]$$

Contraction by setting $\ell = m$ and use of (4.1.21) give

$$\begin{aligned}\langle e_{\ell\ell}(\zeta)\rangle &= -b_{\ell\ell ij}\beta^*[(1-n')\delta_{ij} - a'_{pqij}b_{pqrr}] \\ &= -\frac{\delta_{ij}}{3\lambda^* + 2\mu^*}\beta^*\Big[(1-n')\delta_{ij} - a'_{pqij}\frac{\delta_{pq}}{3\lambda^* + 2\mu^*}\Big]\end{aligned} \tag{4.1.30}$$

Substituting (4.1.30) into (4.1.29) we have

$$\zeta_c' = -\frac{\beta^*}{3\lambda^* + 2\mu^*}\Big[3(1-n') - a'_{ppjj}\frac{1}{3\lambda^* + 2\mu^*}\Big] = -\beta^*\beta_c' \tag{4.1.31}$$

Since equation (4.1.16) implies for isotropic grains that

$$\langle \beta^* : e(\zeta)\rangle = \beta^*\langle e(\zeta)\rangle : I = \beta^*\zeta_c' < 0$$

it follows that

$$\zeta_c' < 0 \tag{4.1.32}$$

It is noted again that the coefficients γ', β_c' and ζ_c' are automatically determined, if a'_{pqij} are once given after solving ϕ problem, by (4.1.26),(4.1.27) and (4.1.31).

4.2 Permeability.

The symmetry and positive definiteness of the permability k' of (3.3.12) has been shown in Ene and Sanchez-Palencia(1975). For small Peclet number(§3), buoyancy also induces flow(cf.(3.3.21)) and we shall prove that the permability k' of (3.3.21) is still positive definite. The proof of symmetry is the same as for Darcy's law without buoyancy.

The fluid momentum equation (3.31b) is written in indicial form

$$0 = -\Big(\frac{\partial p^{(0)}}{\partial x_i'} + \frac{\partial p^{(1)}}{\partial x_i}\Big) + 2\frac{\partial}{\partial x_k}e_{ik}(u_d^{(0)}) + Ra\theta^{(0)}\delta_{iz} \tag{4.2.1}$$

where

$$e_{ik}(u_d^{(0)}) = \frac{1}{2}\Big(\frac{\partial (u_d^{(0)})_k}{\partial x_i} + \frac{\partial (u_d^{(0)})_i}{\partial x_k}\Big) \tag{4.2.2}$$

is the symmetric strain tensor for fluid velocity. Multiply (4.2.1) by $u_d^{(0)}$ and integrate over Ω_f:

$$\begin{aligned} &-\frac{2}{\Omega}\int_{\Omega_f} u_d^{(0)}\frac{\partial}{\partial x_k}e_{ik}(u_d^{(0)})d\Omega \\ &\quad = -\frac{1}{\Omega}\int_{\Omega_f} u_d^{(0)}\Big(\frac{\partial p^{(0)}}{\partial x_i'} + \frac{\partial p^{(1)}}{\partial x_i}\Big)d\Omega + \frac{Ra}{\Omega}\int_{\Omega_f} u_d^{(0)}\theta^{(0)}\delta_{iz}d\Omega \end{aligned} \tag{4.2.3}$$

The left-hand side becomes, after using Gauss theorem, the no-slip condition $u_d^{(0)} = 0$ on $\Gamma(0)$(cf.(3.2.16a)) and symmetry of (4.2.2),

$$
\begin{aligned}
&-\frac{2}{\Omega}\int_{\Omega_f}(u_d^{(0)})_i\frac{\partial}{\partial x_k}e_{ik}(u_d^{(0)})d\Omega \\
&=-\frac{2}{\Omega}\int_{\Omega_f}\Big(\frac{\partial}{\partial x_k}[(u_d^{(0)})_i e_{ik}(u_d^{(0)})]-e_{ik}(u_d^{(0)})\frac{\partial (u_d^{(0)})_i}{\partial x_k}\Big)d\Omega \\
&=\frac{1}{\Omega}\int_{\Omega_f}e_{ik}(u_d^{(0)})e_{ik}(u_d^{(0)})d\Omega
\end{aligned}
\tag{4.2.4}
$$

The right-hand side of (4.2.3) becomes, using (3.3.19a),

$$
\begin{aligned}
&-\frac{1}{\Omega}\int_{\Omega_f}\Big[(u_d^{(0)})_i\frac{\partial p^{(0)}}{\partial x_i'}+\frac{\partial}{\partial x_i}((u_d^{(0)})_i p^{(1)})\Big]d\Omega+\frac{Ra}{\Omega}\int_{\Omega_f}(u_d^{(0)})_i\theta^{(0)}\delta_{iz}d\Omega \\
&=\frac{1}{\Omega}\int_{\Omega_f}k_{ij}\Big(\frac{\partial p^{(0)}}{\partial x_j'}-Ra\theta^{(0)}\delta_{jz}\Big)\frac{\partial p^{(0)}}{\partial x_i'}d\Omega \\
&\qquad-\frac{Ra}{\Omega}\int_{\Omega_f}k_{ij}\Big(\frac{\partial p^{(0)}}{\partial x_j'}-Ra\theta^{(0)}\delta_{jz}\Big)\theta^{(0)}\delta_{iz}d\Omega \\
&=k_{ij}'\frac{\partial p^{(0)}}{\partial x_i'}\frac{\partial p^{(0)}}{\partial x_j'}-\Big[k_{ij}'\delta_{jz}\frac{\partial p^{(0)}}{\partial x_i'}+k_{ij}'\delta_{iz}\frac{\partial p^{(0)}}{\partial x_j'}\Big]Ra\theta^{(0)}+k_{ij}'\delta_{iz}\delta_{jz}Ra^2\theta^{(0)^2} \\
&=k_{ij}'\Big(\frac{\partial p^{(0)}}{\partial x_j'}-Ra\theta^{(0)}\delta_{jz}\Big)\Big(\frac{\partial p^{(0)}}{\partial x_i'}-Ra\theta^{(0)}\delta_{iz}\Big)
\end{aligned}
\tag{4.2.5}
$$

in which the symmetry $k_{ij}' = k_{ji}'$ has been used. Substituting (4.2.4) and (4.2.5) into (4.2.3) and invoking $e_{ik}(u_d^{(0)}) = e_{ik}(u_d^{(0)})$, we get

$$
\frac{1}{\Omega}\int_{\Omega_f}e_{ik}(u_d^{(0)})e_{ik}(u_d^{(0)})d\Omega=-k_{ij}\Big(\frac{\partial p^{(0)}}{\partial x_j'}-Ra\theta^{(0)}\delta_{jz}\Big)\Big[-\Big(\frac{\partial p^{(0)}}{\partial x_i'}-Ra\theta^{(0)}\delta_{iz}\Big)\Big]
\tag{4.2.6}
$$

The left-hand side is the viscous dissipation which is positive. The right-hand side is the product of the force due to both pressure gradient and buoyancy and the induced velocity . Therefore k_{ij}' is positive definite.

4.3 Thermal Conductivity.

In the case of weak convection $Pe = O(\epsilon)$(§3), the effective diffusion coefficient m_{ij}' of (3.4.15b) is the consequence of pure diffusion at both macro- and microscale and is symmetric and positive definite.

Rewriting (3.4.7) in indicial form, we have

$$0 = \frac{\partial}{\partial x_k}\Big[m^f_{k\ell}\Big(\delta_{\ell i} + \frac{\partial A^f_i}{\partial x_\ell}\Big)\Big] \qquad \text{in} \quad \Omega_f$$

$$0 = M_r \frac{\partial}{\partial x_k}\Big[m^s_{k\ell}\Big(\delta_{\ell i} + \frac{\partial A^s_i}{\partial x_\ell}\Big)\Big] \qquad \text{in} \quad \Omega_s \qquad (4.3.1a-d)$$

$$A^f_i = A^s_i \qquad \text{on} \quad \Gamma(0)$$

$$m^f_{k\ell}\Big(\delta_{\ell i} + \frac{\partial A^f_i}{\partial x_\ell}\Big)N_k = M_r m^s_{k\ell}\Big(\delta_{\ell i} + \frac{\partial A^s_i}{\partial x_\ell}\Big)N_k \qquad \text{on} \quad \Gamma(0)$$

Multiply (4.3.1a) and (4.3.1b) by A^f_j and A^s_j and integrate over Ω_f and Ω_s respectively. It then follows

$$0 = \frac{1}{\Omega}\int_\Gamma \Big[m^f_{k\ell}\Big(\delta_{\ell i} + \frac{\partial A^f_i}{\partial x_\ell}\Big)A^f_j N^f_k + M_r m^s_{k\ell}\Big(\delta_{\ell i} + \frac{\partial A^s_i}{\partial x_\ell}\Big)A^s_j N^s_k\Big]dS$$

$$-\frac{1}{\Omega}\int_{\Omega_f} m^f_{k\ell}\frac{\partial A^f_j}{\partial x_k}\Big(\delta_{\ell i} + \frac{\partial A^f_i}{\partial x_\ell}\Big)d\Omega - -\frac{1}{\Omega}M_r\int_{\Omega_s} m^s_{k\ell}\frac{\partial A^s_j}{\partial x_k}\Big(\delta_{\ell i} + \frac{\partial A^s_i}{\partial x_\ell}\Big)d\Omega$$

The integrals on Γ vanish because of (4.3.1c and d) and after using the symmetry $m^f_{k\ell} = m^f_{\ell k}$ and $m^s_{k\ell} = m^s_{\ell k}$, we get

$$\Big\langle m^f_{ik}\frac{\partial A^f_j}{\partial x_k}\Big\rangle + M_r\Big\langle m^s_{ik}\frac{\partial A^s_j}{\partial x_k}\Big\rangle = -\Big\langle m^f_{\ell k}\frac{\partial A^f_i}{\partial x_\ell}\frac{\partial A^f_j}{\partial x_k}\Big\rangle - M_r\Big\langle m^s_{\ell k}\frac{\partial A^s_i}{\partial x_\ell}\frac{\partial A^s_j}{\partial x_k}\Big\rangle \qquad (4.3.2)$$

The thermal conductivity tensor in (3.4.15b) then becomes

$$m'_{ij} = \Big\langle m^f_{\ell k}\Big(\delta_{\ell i}\delta_{kj} - \frac{\partial A^f_i}{\partial x_\ell}\frac{\partial A^f_j}{\partial x_k}\Big)\Big\rangle + M_r\Big\langle m^s_{\ell k}\Big(\delta_{\ell i}\delta_{kj} - \frac{\partial A^s_i}{\partial x_\ell}\frac{\partial A^s_j}{\partial x_k}\Big)\Big\rangle \qquad (4.3.3)$$

which shows the symmetry $m'_{ij} = m'_{ji}$. The positive definiteness is proven in Bensoussan et al(1978) in terms of ellipticity condition of the coefficient m'_{ij},e.g. $m'_{ij}\xi_i\xi_j \geq \gamma\xi_i\xi_i$ for any $\xi \in \mathbf{R}^3$ with $\gamma > 0$.

5. A Cubic Array of Wigner-Seitz Grains.

In this section, a simple microcell with three planes of symmetry is chosen for subsequent evelopment of our theory. As a specific model of microcell, we consider the Wigner-Seitz cell depicted in Fig 5.1. It is shown in Appendix C that, for such cell geometry with three planes of symmetry, the elastic coefficients $a^l_{ijk\ell}$ of (4.1.3a) exhibit cubic symmetry so that there are three distinct constants whereas α^l_{ij} and $(\beta^l_t)_{ij}$ of (4.1.3b and c) are isotropic. Similarly the permeability k^l_{ij} of (3.3.22) and the thermal conductivity m^l_{ij} of (3.4.16b) are isotropic. Only the final results are summarized in this section. Also, as mentioned before, the coefficients F', G', H', I', R', K', J', L', C', M', N', E', S', T' and U' for the nonlinear terms in the macroscale governing equations (3.5.1) to (3.5.4) vanish for a microcell geometry with three planes of symmetry. This is shown in Appendix D by making use of the symmetry properties of the solutions from Appendix C.

5.1 Symmetry of Elastic Coefficients

The elastic coefficient tensor of rank four a^l of (4.1.3a), which has 21 coefficients in the most general case, reduces to the following three distinct coefficients :

$$\begin{aligned} a_I &= a^l_{xxxx} = a^l_{yyyy} = a^l_{zzzz} \\ a_{II} &= a^l_{xxyy} = a^l_{yyzz} = a^l_{zzxx} \\ a_{III} &= a^l_{xyxy} = a^l_{yzyz} = a^l_{zxzx} \end{aligned} \tag{5.1.1}$$

All other coefficients vanish due to symmetry of the cell geometry. Material which has the elastic coefficients as (5.1.1) with three distinct constants is said to possess cubic symmetry property(Love(1944), Lekhnitskii(1963)). If further the relation $(a_I - a_{II}) = 2a_{III}$ holds, the material is called isotropic and there are only two independent coefficients.

The pressure coefficient α^l_{ij} and thermal moduli $(\beta^l_t)_{ij}$ in Hooke's law (4.1.2) reduce to isotropic tensors so that

$$\alpha^l_{ij} = \alpha' \begin{bmatrix} 1 & 0 & 0 \\ 0 & 1 & 0 \\ 0 & 0 & 1 \end{bmatrix} \qquad \text{and} \qquad (\beta^l_t)_{ij} = \beta^l_t \begin{bmatrix} 1 & 0 & 0 \\ 0 & 1 & 0 \\ 0 & 0 & 1 \end{bmatrix} \tag{5.1.2}$$

where

$$\alpha' = 1 - (a_I + 2a_{II})/(3\lambda^* + 2\mu^*)$$
$$\beta'_t = \beta^*(a_I + 2a_{II})/(3\lambda^* + 2\mu^*) \tag{5.1.3}$$

in which λ^* and μ^* are the normalized Lamé constants and have been given in (4.1.18).

The coefficients γ'_{ij}, β'_c and ζ' in (4.1.26), (4.1.27) and (4.1.31) of the linear terms in the consolidation equation (3.5.3) similarly become

$$\gamma'_{ij} = \alpha'\delta_{ij} = \alpha' \begin{bmatrix} 1 & 0 & 0 \\ 0 & 1 & 0 \\ 0 & 0 & 1 \end{bmatrix} \tag{5.1.4}$$

$$\beta'_c = \frac{3}{3\lambda^* + 2\mu^*}\left[1 - n' - \frac{a_I + 2a_{II}}{3\lambda^* + 2\mu^*}\right] > 0 \tag{5.1.5}$$

$$\zeta'_c = -\beta^*\beta'_c = -\frac{3\beta^*}{3\lambda^* + 2\mu^*}\left[1 - n' - \frac{a_I + 2a_{II}}{3\lambda^* + 2\mu^*}\right] < 0 \tag{5.1.6}$$

The coefficients γ'_{ij}, β'_c and ζ'_c also have been expressed in terms of only a_I and a_{II}.

5.2 Permeability k'_{ij} and Thermal Conductivity m'_{ij}

The permeability and thermal conductivity similarly reduce to isotropic tensors.

$$k'_{ij} = k' \begin{bmatrix} 1 & 0 & 0 \\ 0 & 1 & 0 \\ 0 & 0 & 1 \end{bmatrix} \quad \text{and} \quad m'_{ij} = m' \begin{bmatrix} 1 & 0 & 0 \\ 0 & 1 & 0 \\ 0 & 0 & 1 \end{bmatrix} \tag{5.2.1}$$

where

$$k' = \langle k_{xx} \rangle = \langle k_{yy} \rangle = \langle k_{zz} \rangle = \frac{1}{\Omega}\int_\Omega k_{xx} d\Omega$$
$$m' = m'_{xx} = m'_{yy} = m'_{zz} = \overline{m} + \frac{1}{\Omega}\left(m^*_f \int_{\Gamma(0)} A^f_x N^f_x dS + M_r m^*_s \int_{\Gamma(0)} A^s_x N^s_x dS\right) \tag{5.2.2}$$

For details of the reduction see Appendix C.

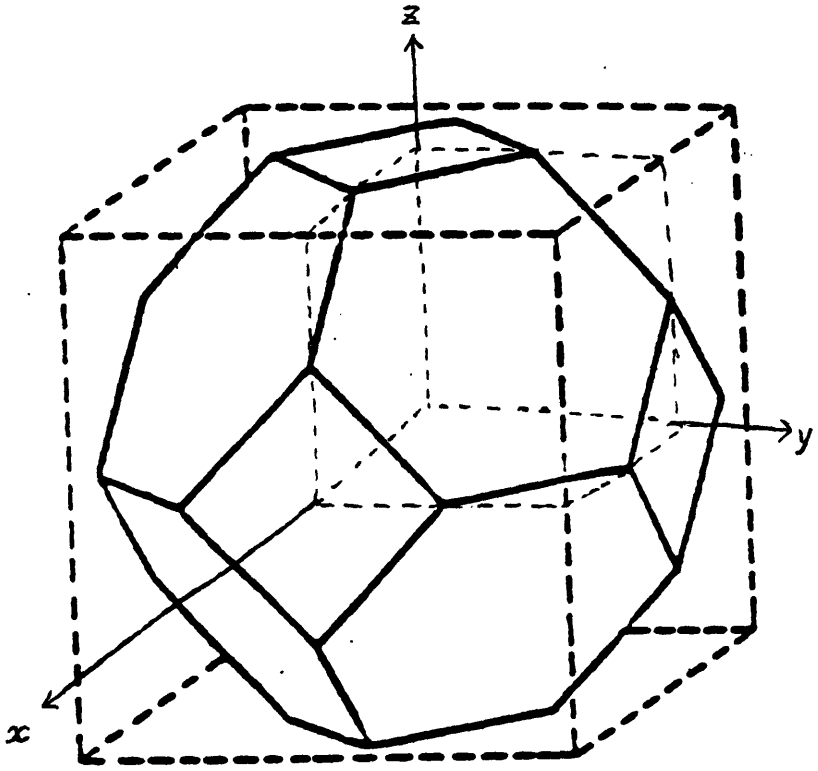

Fig. 5.1 A Wigner-Seitz microcell. The interior of the soccer ball shape is solid.

6. Numerical Computation of the Coefficients.

The microsale boundary value problems for the elastic deformation in the solid phase, the flow through pores and the heat diffusion through fluid and solid are now solved numerically for the periodic array of the Wigner-Seitz grains. We first derive the variational principles for these problems which are valid for arbitrary periodic cell geometry. It will be shown for Wigner-Seitz grains by using symmetry arguments that the computational domain is reduced to only 1/8-th of the microcell. Finite elements are then used to represent the functionals in terms of the nodal unknowns.

6.1 The Variational Principles.

In the elasticity part, as has been shown in §4.1, the elastostatic problems for ϕ_i^{mn} only need to be solved.

If we multiply (4.1.7a) by $\delta\phi_j^{mn}$ and integrate over the solid phase, it follows that

$$\int_{\Omega_s} \frac{\partial}{\partial x_i}\left[a^*_{ijpq}e_{pq}(\phi^{mn})\delta\phi_j^{mn}\right]d\Omega - \int_{\Omega_s} a^*_{ijpq}e_{pq}(\phi^{mn})\frac{\partial(\delta\phi_j^{mn})}{\partial x_i}d\Omega = 0 \qquad (6.1.1)$$

where no summation over the indices mn is assumed. The first integral becomes after using Gauss theorem and (4.1.8a)

$$\begin{aligned}\int_{\Omega_s} \frac{\partial}{\partial x_i}\left[a^*_{ijpq}e_{pq}(\phi^{mn})\delta\phi_j^{mn}\right]d\Omega &= \int_{\Gamma+\Gamma_s} a^*_{ijpq}e_{pq}(\phi^{mn})\delta\phi_j^{mn}N_i^s dS \\ = -\int_{\Gamma} a^*_{ijmn}\delta\phi_j^{mn}N_i^s dS &= -\delta\left(\int_{\Gamma} a^*_{ijmn}\phi_j^{mn}N_i^s dS\right)\end{aligned} \qquad (6.1.2)$$

where Γ_s is the solid part on the periodic boundaries (see Fig. 5.1). The integral on Γ_s has vanished since, if ϕ_j^{mn} is periodic on Γ_s, so are $\delta\phi_j^{mn}$ and $e_{pq}(\phi^{mn})$. The second integral in (6.1.1) can be written, inview of the symmetry relation

$$a^*_{ijpq} = a^*_{jipq} = a^*_{ijqp} = a^*_{pqij} \qquad (6.1.3)$$

as

$$\begin{aligned}
&\int_{\Omega_\epsilon} a^*_{ijpq} \frac{\partial(\delta\phi^{mn}_j)}{\partial x_i} e_{pq}(\phi^{mn}) d\Omega \\
&\quad = \int_{\Omega_\epsilon} a^*_{ijpq} \left[e_{ij}(\delta\phi^{mn}) + \omega_{ij}(\delta\phi^{mn}) \right] e_{pq}(\phi^{mn}) d\Omega \\
&\quad = \frac{1}{2} \int_{\Omega_\epsilon} \left(a^*_{ijpq} + a^*_{pqij} \right) e_{pq}(\delta\phi^{mn}) e_{pq}(\phi^{mn}) d\Omega \\
&\quad = \delta \left\{ \int_{\Omega_\epsilon} \frac{1}{2} a^*_{ijpq} e_{pq}(\phi^{mn}) e_{pq}(\phi^{mn}) \right\} d\Omega
\end{aligned} \tag{6.1.4}$$

where the fact that the product of a^*_{ijpq} (symmetric in i and j) and the anti-symmetric rotation tensor $\omega_{ij}(\delta\phi^{mn})$ yields zero and (6.1.3) have been used.

Substituting (6.1.2) and (6.1.4) into (6.1.1), we obtain

$$\delta J_\epsilon = 0 \tag{6.1.5}$$

where the functional J_ϵ is given by(no summation over mn)

$$J_\epsilon = \int_{\Omega_\epsilon} \frac{1}{2} a^*_{ijpq} e_{pq}(\phi^{mn}) e_{pq}(\phi^{mn}) d\Omega - \int_\Gamma a^*_{ijmn} \phi^{mn}_j N^\epsilon_i dS \tag{6.1.6}$$

Thus the solution of the boundary value problem (4.1.7a), (4.1.8a) and (4.1.9) is obtained by minimizing J_ϵ. Equations (6.1.5) and (6.1.6) appear to be the same as the principle of minimum potential energy in linear elasticity(Sokolnikoff, 1956) with zero body force and prescribed traction on Γ. It is noteworthy that the elastostatic problem (4.1.7a) with the Ω-periodicity condition, which is not essential boundary condition, leads to the same principle.

In the fluid phase, we first write the Stokes problem (3.3.20) in indicial form as

$$\begin{aligned}
\frac{\partial k_{ij}}{\partial x_i} &= 0 && \text{in} \quad \Omega_f \\
\frac{\partial^2 k_{ij}}{\partial x_n \partial x_n} &= -\frac{\partial S_j}{\partial x_i} - \delta_{ij} && \text{in} \quad \Omega_f \\
k_{ij} &= 0 && \text{on} \quad \Gamma(0) \\
k_{ij} \quad &\text{and} \quad S_j \quad \text{are} \quad \Omega - \text{periodic}
\end{aligned} \tag{6.1.7a-d}$$

Multiplying (6.1.7b) by δk_{ij} and then integrating over Ω_f and using comma to denote partial differentiation, we get after use of Gauss theorem and (6.1.7a)

$$\begin{aligned}
&\int_{\Omega_f} \left\{ [(\delta k_{ij}) k_{ij,n}]_{,n} - (\delta k_{ij})_{,n} k_{ij,n} + \delta(k_{ij} S_{j,i}) - k_{ij}\delta(S_{j,i}) + (\delta k_{ij})\delta_{ij} \right\} d\Omega \\
&= \int_{\Gamma+\Gamma_f} (\delta k_{ij}) k_{ij,n} N_n^f dS \\
&\quad + \int_{\Omega_f} \left[\delta\left(-\frac{1}{2} k_{ij,n} k_{ij,n} + k_{ij} S_{j,i} + k_{ij}\delta_{ij} \right) - (k_{ij}\delta S_j)_{,i} + k_{ij,i}\delta S_j \right] d\Omega \\
&= \int_{\Gamma+\Gamma_f} \left[(\delta k_{ij}) k_{ij,n} N_n^f - k_{ij}(\delta S_j) N_i^f \right] dS \\
&\quad + \delta \int_{\Omega_f} \left(-\frac{1}{2} k_{ij,n} k_{ij,n} + k_{ij} S_{j,i} + k_{ij}\delta_{ij} \right) d\Omega
\end{aligned} \tag{6.1.8}$$

Because of the Ω-periodicity condition (6.1.7d), quantities δk_{ij}, $k_{ij,n}$ and δS_j are also Ω-periodic. Thus the surface integral on Γ_f vanishes. Also, due to the no slip condition (6.1.7c), k_{ij} and δk_{ij} are zero on the interface. Accordingly the surface integral on Γ vanishes and (6.1.8) yields

$$\delta J_f = 0 \tag{6.1.9}$$

where

$$J_f = \int_{\Omega_f} \left(-\frac{1}{2} \frac{\partial k_{ij}}{\partial x_n} \frac{\partial k_{ij}}{\partial x_n} + k_{ij} \frac{\partial S_j}{\partial x_i} + k_{ij}\delta_{ij} \right) d\Omega \tag{6.1.10}$$

Minimization of J_f is equivalent to solving the Stokes problem (6.1.7).

The variational principle for heat diffusion in both fluid and solid phases is a special case of the convection diffusion problem to be treated in Part B when the Peclet number goes to zero. We only give the result here.

$$\delta J_h = 0 \tag{6.1.11}$$

where

$$J_h = \int_{\Omega_f} \left(m_f^* \frac{\partial A_\ell^f}{\partial x_k} \frac{\partial A_\ell^f}{\partial x_k} + m_f^* \frac{\partial A_\ell^f}{\partial x_\ell} \right) d\Omega + M_r \int_{\Omega_s} \left(m_s^* \frac{\partial A_\ell^s}{\partial x_k} \frac{\partial A_\ell^s}{\partial x_k} + m_s^* \frac{\partial A_\ell^s}{\partial x_\ell} \right) d\Omega \tag{6.1.12}$$

is the functional corresponding to the heat diffusion in two phases of (4.3.1).

6.2 Reduction of Computational Domain for Wigner-Seitz Grains.

While the variational principles derived in §6.1 can be readily used to solve the corresponding boundary value problems for any periodic cell geometry on the microscale, the computation is greatly simplified for the Wigner-Seitz grains in the sense that certain symmetry relations of the solution among the sectors enable the computational domain to be reduced to a small fraction of the cell. We shall show this by cutting out one sector and establishing the same variational principles for that sector with implied boundary conditions.

In the solid phase, only ϕ_i^{xx} and ϕ_i^{xy} need to be solved (cf.(5.1.1)). Suppose that sector $A(x > 0, y > 0, z > 0)$ of Fig. 5.1 has been cut out of the cell. Let us denote the new boundaries at $x = 0$, $y = 0$ and $z = 0$ by S_x^-, S_y^- and S_z^- respectively. Also let the solid portion at $x = 1/2$, $y = 1/2$ and $z = 1/2$ (previously called Γ_s) be S_x^+, S_y^+ and S_z^+.

Inspection of the loading condition for ϕ_i^{xx} (Fig. C.2a) on the interface Γ readily shows that $\phi_x^{xx} = 0$, $\partial\phi_y^{xx}/\partial y = \partial\phi_y^{xx}/\partial z = 0$ and $\partial\phi_z^{xx}/\partial x = 0$ on $S_x^{\pm}$. Similarly we have $\partial\phi_y^{xx}/\partial y = 0$, $\phi_y^{xx} = 0$, $\partial\phi_z^{xx}/\partial y = 0$ on $S_y^{\pm}$ and $\partial\phi_x^{xx}/\partial z = \partial\phi_y^{xx}/\partial z = 0$, $\phi_z^{xx} = 0$ on $S_z^{\pm}$. Accordingly the boundary value problem ϕ_i^{xx} must satisfy in sector A becomes

$$
\begin{aligned}
\frac{\partial}{\partial x_i}\sigma_{ij}(\phi^{xx}) &= 0 && x > 0, y > 0, z > 0 \\
\overline{T}_j &= -a^*_{ijxx}N_i^s && \text{on } \Gamma \\
\phi_x^{xx} = \sigma_{xy}(\phi^{xx}) = \sigma_{xz}(\phi^{xx}) &= 0 && \text{on } S_x^{\pm} \\
\sigma_{xy}(\phi^{xx}) = \phi_y^{xx} = \sigma_{xz}(\phi^{xx}) &= 0 && \text{on } S_y^{\pm} \\
\sigma_{xz}(\phi^{xx}) = \sigma_{yz}(\phi^{xx}) = \phi_z^{xx} &= 0 && \text{on } S_z^{\pm}
\end{aligned}
\qquad (6.2.1a-e)
$$

Equations (6.2.1c-e) are the implied boundary conditions obtained from the symmetry of cell geometry about $x = 0$, $y = 0$ and $z = 0$.

Likewise, from Fig. C.2(d) in Appendix C, we have for the same sector that $\partial\phi_z^{xy}/\partial x = 0$ and $\phi_y^{xy} = \phi_z^{xy} = 0$ on $S_x^{\pm}$. Consideration of sectors A and D and A and E in Fig.4 gives $\phi_z^{xy} = \phi_x^{xy} = 0$, $\partial\phi_y^{xy}/\partial y = 0$ on $S_y^{\pm}$ and $\partial\phi_z^{xy}/\partial z = \partial\phi_y^{xy}/\partial z = 0$ on $S_z^{\pm}$. Thus ϕ_i^{xy} in sector A must satisfy

$$\begin{aligned}
\frac{\partial}{\partial x_i}\sigma_{ij}(\phi^{xy}) &= 0 && x>0, y>0, z>0 \\
\overline{T}_j &= -a^*_{ijxy}N_i^s && \text{on} \quad \Gamma \\
\sigma_{xx}(\phi^{xy}) = \phi_y^{xy} = \phi_x^{xy} &= 0 && \text{on} \quad S_x^{\pm} \\
\phi_x^{xy} = \sigma_{yy}(\phi^{xy}) = \phi_z^{xy} &= 0 && \text{on} \quad S_y^{\pm} \\
\sigma_{xz}(\phi^{xy}) = \sigma_{yz}(\phi^{xy}) = \phi_z^{xy} &= 0 && \text{on} \quad S_z^{\pm}
\end{aligned} \qquad (6.2.2a-e)$$

Derivation of the variational principles follows precisely the same procedure as in §6.1. It is obvious from (6.1.2) that we need to consider the integration on Γ which is now composed of $S_x^{\pm}$, $S_y^{\pm}$ and $S_z^{\pm}$. On the surface S_x^-, the integral for ϕ_i^{xx} becomes

$$\begin{aligned}
&\int_{S_\infty^-} a^*_{ijpq}e_{pq}(\phi^{xx})\delta\phi_j^{xx}N_i^s\,dS = -\int_{S_\infty^-}\sigma_{xj}(\phi^{xx})\delta\phi_j^{xx}\,dS \\
&= -\int_{S_\infty^-}\left[\sigma_{xx}(\phi^{xx})\delta\phi_x^{xx} + \sigma_{xy}(\phi^{xx})\delta\phi_y^{xx} + \sigma_{xz}(\phi^{xx})\delta\phi_z^{xx}\right]dS
\end{aligned} \qquad (6.2.3)$$

which vanishes because $\delta\phi_x^{xx} = \sigma_{xy} = \sigma_{xz} = 0$ from (6.2.1c). On the surface S_x^+, it only changes sign. Similarly on $S_y^{\pm}$, we have after using (6.2.1d and e)

$$\begin{aligned}
\int_{S_y^{\pm}} a^*_{ijpq}e_{pq}(\phi^{xx})\delta\phi_j^{xx}N_i^s\,dS &= \pm\int_{S_y^{\pm}}\left(\sigma_{yx}\delta\phi_x^{xx} + \sigma_{yy}\delta\phi_y^{xx} + \sigma_{yz}\delta\phi_z^{xx}\right)dS = 0 \\
\int_{S_z^{\pm}} a^*_{ijpq}e_{pq}(\phi^{xx})\delta\phi_j^{xx}N_i^s\,dS &= \pm\int_{S_z^{\pm}}\left(\sigma_{zx}\delta\phi_x^{xx} + \sigma_{zy}\delta\phi_y^{xx} + \sigma_{zz}\delta\phi_z^{xx}\right)dS = 0
\end{aligned} \qquad (6.5.16)$$

in which $\pm$ represents the sign of the unit outward normal vector. Therefore the integrals on $S_x^{\pm}$, $S_y^{\pm}$ and $S_z^{\pm}$ vanish and, in the same manner, we can readily show for ϕ_i^{xy} that the integral on Γ in (6.1.2) vanishes.

In the fluid phase, we first note, in view of the linearity of (6.1.7a and b), that the driving external pressure gradient δ_{ij} of (6.1.7b) can always be decomposed into x, y and z components. Accordingly it suffices to consider one of them,e.g. $j = x$.

It readily follows from Fig. C.5(a) and (b) that the implied boundary conditions on $S_x^{\pm}$, $S_y^{\pm}$ and $S_z^{\pm}$ for sector $A(X>0, Y>0, Z>0)$ are summarized as

$$\begin{aligned} \frac{\partial k_{xx}}{\partial x} = k_{yx} = k_{zx} &= 0 \quad \text{on} \quad S_x^{\pm} \\ \frac{\partial k_{xx}}{\partial y} = k_{yx} = \frac{\partial k_{xz}}{\partial y} &= 0 \quad \text{on} \quad S_y^{\pm} \\ \frac{\partial k_{xx}}{\partial z} = \frac{\partial k_{yx}}{\partial z} = k_{zx} &= 0 \quad \text{on} \quad S_z^{\pm} \end{aligned} \tag{6.2.5}$$

The surface integrals on Γ_f in (6.1.8) for $j = x$ now become

$$\begin{aligned} &\int_{\Gamma_f} \left[(\delta k_{ix}) \frac{\partial k_{ix}}{\partial x_n} N_n^f - k_{ix} (\delta S_x) N_i^f \right] dS \\ &= \pm \int_{S_x^{\pm}} \left[(\delta k_{xx}) \frac{\partial k_{xx}}{\partial x} + (\delta k_{yx}) \frac{\partial k_{yx}}{\partial x} + (\delta k_{zx}) \frac{\partial k_{zx}}{\partial x} \right] dS - \int_{S_x^{\pm}} k_{xx} (\delta S_x) N_x^f dS \\ &\pm \int_{S_y^{\pm}} \left[(\delta k_{xx}) \frac{\partial k_{xx}}{\partial y} + (\delta k_{yx}) \frac{\partial k_{yx}}{\partial y} + (\delta k_{zx}) \frac{\partial k_{zx}}{\partial y} \right] dS - \int_{S_y^{\pm}} k_{yx} (\delta S_x) N_y^f dS \\ &\pm \int_{S_z^{\pm}} \left[(\delta k_{xx}) \frac{\partial k_{xx}}{\partial z} + (\delta k_{yx}) \frac{\partial k_{yx}}{\partial z} + (\delta k_{zx}) \frac{\partial k_{zx}}{\partial z} \right] dS - \int_{S_z^{\pm}} k_{zx} (\delta S_x) N_z^f dS \end{aligned} \tag{6.2.6}$$

The first integrals on $S_x^{\pm}$, $S_y^{\pm}$ and $S_z^{\pm}$ vanish due to the implied boundary conditions (6.2.5) whereas those involving δS_x vanish because of the Ω-periodicity condition (6.1.7d). So the surface integrals on Γ_f make no contribution to J_f and the functional (6.1.10) is valid for the flow field in the fluid region of sector A. In implementing the minimization of J_f, only the essential boundary conditions of (6.2.5) need to be incorporated.

The heat transfer in sector A can be similarly solved by minimizing the functional J_h of (6.1.12) with the implied boundary conditions $A_x^{f,e} = 0$ on $S_x^{\pm}$, $A_y^{f,e} = 0$ on $S_y^{\pm}$ and $A_z^{f,e} = 0$ on $S_z^{\pm}$. The actual computation has been carried out with the variational principle for the convection diffusion problem of Part B and the reduction of computational domain for heat transfer will be examined later.

6.3 Finite Element Approximations.

Finite elements with linear shape functions are used to represent the functionals J_e, J_f and J_h in terms of the unknowns at discrete nodal points. The unknown

quantities ϕ_i^{mn}, k_{ij} and $A_i^{f,e}$ are expressed by the product of shape function matrix and their values at discrete nodes so that spatial variation is accounted for by the shape function. By using this representation of the unknowns in the functionals and taking the first variation (Appendix E), the following algebraic equations are obtained.

In the solid phase, we have for both ϕ_i^{xx} and ϕ_i^{xy}

$$\mathbf{K}_\phi \mathbf{q}(\phi) = \mathbf{Q}_\phi \tag{6.3.1}$$

where

$$\mathbf{K}_\phi = \sum_{n=1}^{M} \frac{1}{2} \int_{\Omega_n} (\mathbf{DN})^T \mathbf{E}(\mathbf{DN}) d\Omega$$

$$\mathbf{Q}_\phi = \sum_{n=1}^{M} \int_{\partial\Omega_n} \mathbf{T} dS \tag{6.3.2a-c}$$

$\mathbf{q}(\phi)$ is the nodal unknown vector

in which M is the total number of elements and $\mathbf{N}$ is the shape function matrix. Also $\mathbf{D}$ and $\mathbf{E}$ are the matrix forms for strain operator and elastic coefficients and $\mathbf{T}$ is the traction force vector on Γ (Appendix E). The differences between ϕ_i^{xx} and ϕ_i^{xy} are in the traction force vector $\mathbf{Q}_\phi$ and the implied essential boundary conditions as stated in (6.2.1) and (6.2.2).

In the fluid phase, following the similar procedure, it can be shown that (6.1.9) and (6.1.10) yield

$$\mathbf{K}_k \mathbf{q}(k) + \mathbf{K}_S \mathbf{q}(S) = \mathbf{F}$$

$$\mathbf{K}_S \mathbf{q}(k) = 0 \tag{6.3.3a,b}$$

where

$$\mathbf{K}_k = \sum_{n=1}^{M} \int_{\Omega_n} \left[\frac{\partial \mathbf{N}}{\partial x_k}^T\right] \left[\frac{\partial \mathbf{N}}{\partial x_k}\right] d\Omega$$

$$\mathbf{K}_S = -\sum_{n=1}^{M} \int_{\Omega_n} \mathbf{N}^T \left[\frac{\partial \mathbf{N}}{\partial x_k}\right] d\Omega \tag{6.3.4a-c}$$

$$\mathbf{F} = \sum_{n=1}^{M} \int_{\Omega_n} \mathbf{I}\mathbf{N} d\Omega$$

and $\mathbf{q}(k)$ and $\mathbf{q}(S)$ are nodal unknown vectors for k and S in (6.1.7). In real computations, the essential boundary conditions in (6.2.5) should be imposed.

For the heat diffusion, (6.1.11) and (6.1.12) also give

$$\mathbf{A}_f \mathbf{q}_f + \mathbf{A}_s \mathbf{q}_s = \mathbf{f}_f + \mathbf{f}_s \tag{6.3.5}$$

where

$$\mathbf{A}_f = 2 \sum_{n=1}^{M_f} \int_{\Omega_n} \left[\frac{\partial \mathbf{N}}{\partial x_k}^T\right] \left[\frac{\partial \mathbf{N}}{\partial x_k}\right] d\Omega$$

$$\mathbf{A}_s = \sum_{n=1}^{M_s} \int_{\Omega_n} \left[\frac{\partial \mathbf{N}}{\partial x_k}^T\right] \left[\frac{\partial \mathbf{N}}{\partial x_k}\right] d\Omega \tag{6.3.6a-d}$$

$$\mathbf{f}_f = -\sum_{n=1}^{M_f} \int_{\Omega_n} \nabla \cdot \mathbf{N} d\Omega$$

$$\mathbf{f}_s = -\sum_{n=1}^{M_s} \int_{\Omega_n} \nabla \cdot \mathbf{N} d\Omega$$

in which M_f and M_s are the total numbers of elements in Ω_f and Ω_s of sector A.

By solving the algebraic equations (6.3.1),(6.3.3) and (6.3.5), we obtain the values of ϕ_i^{mn}, k_{ij} and $A_i^{f,s}$ at each node. These solutions are then used to calculate the macroscale coefficients.

6.4 Numerical Results and Discussions.

By using the variational principles obtained in §6.1 the macroscale coefficients were calculated for the Wigner-Seitz grains. The numerical results are presented and discussed in the order of elastic coefficients and the permeability. The calculation of permeability for the Wigner-Seitz grains has been carried out by Sun and Mei(1993) and their results are cited here. The macroscale thermal conductivity will be discussed in Part B.

6.4.1 The Computational Domain for Wigner-Seitz Grains.

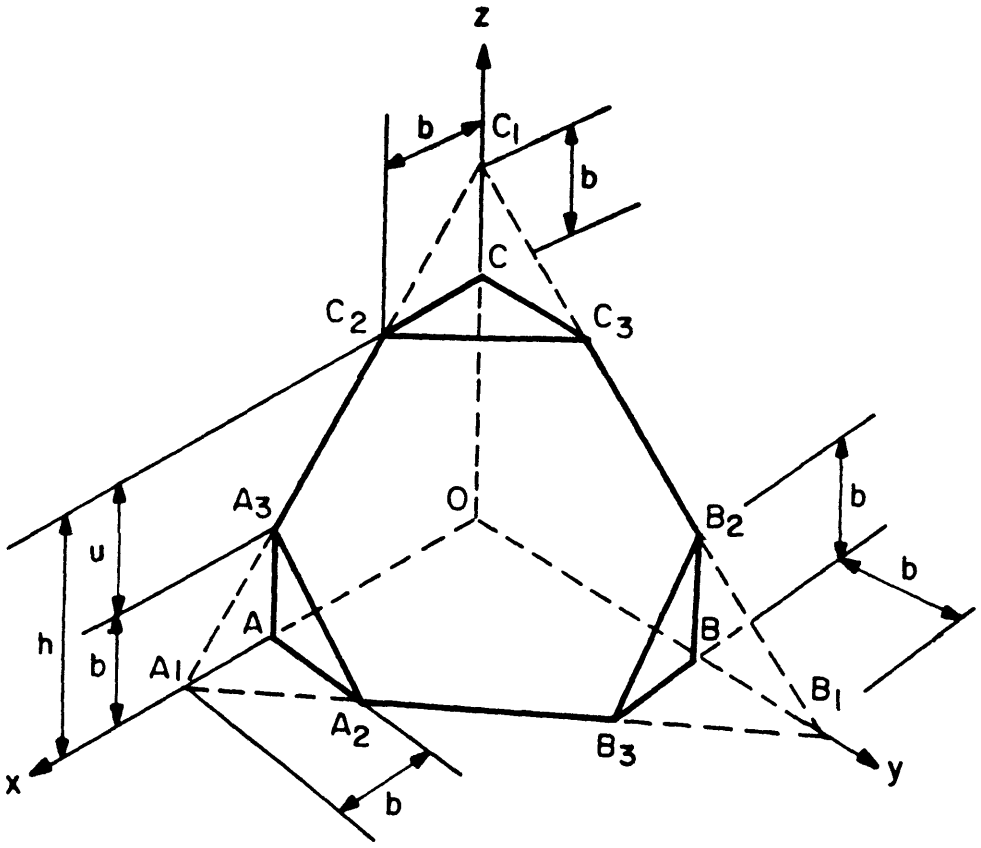

b	u	b/h	n'
1	4	1/5	0.716
1	2	1/3	0.623
1	1	1/2	0.500
2	1	2/3	0.377
3	1	3/4	0.284

Fig. 6.1 The computational domain for Wigner-Seitz grain and the porosity values for several ratios of b/h.

As shown in §6.2, only 1/8-th of the Wigner-Seitz cell is needed to solve the microscale boundary value problems. The solid phase of sector $A(x > 0, y > 0, z > 0)$ is depicted in Fig. 6.1.

Let the volume of the extended tetrahedron $OA_1B_1C_1$ be V_o and that of $AA_1A_2A_3$ (also $BB_1B_2B_3$ and $CC_1C_2C_3$) be v which are given by

$$V_o = \frac{1}{6}(h+b)^3, \qquad v = \frac{1}{6}b^3 \tag{6.4.1}$$

The volume of the solid phase V_s of Fig. 6.1 is then $V_s = V_o - 3v$ and thus the porosity n' is given by

$$n' = 1 - \frac{V_s}{h^3} = 1 - \frac{1}{6}\left[\left(1+\frac{b}{h}\right)^3 - 3\left(\frac{b}{h}\right)^3\right] \tag{6.4.2}$$

The porosity varies continuously, covering fairly wide range of values, between the two limiting cases $n'_{max} = 5/6 = 0.833$ when $b/h \to 0$ and $n'_{min} = 1/6 = 0.167$ when $b/h \to 1$. Some typical values of porosity are listed in Fig. 6.1.

6.4.2 The Elastic Coefficients.

The elastic moduli of the medium are given by (C.36) of Appendix C as

$$\begin{aligned} a_I &= a'_{xxxx} = (1-n')a^*_{xxxx} + \langle \sigma_{xx}(\phi^{xx}) \rangle \\ a_{II} &= a'_{xxyy} = (1-n')a^*_{xxyy} + \langle \sigma_{yy}(\phi^{xx}) \rangle \\ a_{III} &= a'_{xyxy} = (1-n')a^*_{xyxy} + \langle \sigma_{xy}(\phi^{xy}) \rangle \end{aligned} \tag{6.4.3}$$

where a^*_{xxxx}, a^*_{xxyy} and a^*_{xyxy} are related to the Possion's ratio ν by(cf.(4.1.17) and (4.1.18))

$$\begin{aligned} a^*_{xxxx} &= \frac{1-\nu}{(1+\nu)(1-2\nu)}, \quad a^*_{xxyy} = \frac{\nu}{(1+\nu)(1-2\nu)} \\ a^*_{xyxy} &= \frac{1}{2}(a^*_{xxxx} - a^*_{xxyy}) = \frac{1}{2(1+\nu)} \end{aligned} \tag{6.4.4}$$

A common value of $\nu = 0.3$ has been used in computations.

The porosity values used are those shown in Fig. 6.1,e.g. n'=0.284, 0.377, 0.5, 0.623 and 0.716. The computational domain of 1/8-th of Wigner-Seitz grain has been discretized with uniform spacing along x,y and z-axes. A sample of the

numbers of nodes and elements is shown in Table 6.1 for the case of n'=0.5. Computed values of $< \sigma_{xx}(\phi^{xx}) >$, $< \sigma_{yy}(\phi^{xx}) >$ and $< \sigma_{xy}(\phi^{xy}) >$ for different meshes and their converging trends are summarized in Table 6.2. Numbers on top of each column denote the number of equal intervals along each axis,e.g. between O and A along x-axis and so on. From the calculated values for four progressively smaller mesh sizes, polynomial extrapolation has been used to obtain the values corresponding to zero mesh size. As a measure of convergence with decreasing mesh size and accuracy of extrapolation, an error (the last column in Table 6.2) is defined by

$$e = \frac{\langle \sigma_{ij}(\phi^{mn}) \rangle_\Delta - \langle \sigma_{ij}(\phi^{mn}) \rangle_o}{\langle \sigma_{ij}(\phi^{mn}) \rangle_\Delta} \tag{6.4.5}$$

where $\langle \sigma_{ij}(\phi^{mn}) \rangle_\Delta$ is for the finest mesh and $\langle \sigma_{ij}(\phi^{mn}) \rangle_o$ is the extrapolated one for zero mesh. Specifically the cubic spline has been used for the extrapolation except the case of porosity 0.284 for which quadratic extrapolation was used instead. The extrapolation error is less than or around 1 % and the convergence is satisfactory.

The extrapolated values of average stress are plotted against porosity in Fig. 6.2. We also show the stress averages over the solid phase volume only in Fig. 6.3. The porosity dependence is clearly seen in Fig. 6.3,e.g. the magnitude increases with porosity. This is due to the variation of the interface area(Γ) and the volume of the solid phase(Ω_s) with porosity. As porosity increases from small to large values(Fig. 6.1), the area of the interface increases whereas the solid volume decreases so that both the net traction force on Γ and volume density of stress increase. It is also seen from Fig. 6.3 that the magnitude of compressional stress $\langle \sigma_{xx}(\phi^{xx}) \rangle / (1 - n')$ is greater than $\langle \sigma_{yy}(\phi^{xx}) \rangle / (1 - n')$ due to larger x-component of traction than y-component on the interface in Fig. C.2(a). Although the solid phase volume averages show monotonic trend with porosity, the unit cell averages in Fig. 6.2 are not so because the fluid phase volume is also included in averaging.

Computed elastic moduli a_I, a_{II} and a_{III} are plotted as a function of porosity in Fig. 6.4. They decrease with porosity since the volumetric portion of solid matrix which resists externally imposed loading also decreases. It is noted that

except for small porosity values the shear modulus a_{III} is slightly greater than a_{II}. Interestingly this feature is found in the elastic constants of cubic crystals such as Na, diamond, Si and NaCl(Cottrell, 1964). For the convenience of reference, some typical data are reproduced in Table 6.3. We caution that the crystal structure in these material is on the much smaller atomic scale.

The elastic anisotropy factor μ_o/μ_1 is defined by the relation

$$\frac{\mu_o}{\mu_1} = \frac{a_{III}}{(a_I - a_{II})/2} \tag{6.4.6}$$

where $\mu_1 = (a_I - a_{II})/2$ is the shear modulus a'_{xyxy} measured in the coordiante system obtained after rotation of the initial one about one of the symmetry axes by 45 degrees. Recall that $\mu_1 = a_{III}$ for isotropic medium and the anisotropy factor is then unity. Thus the ratio μ_o/μ_1 is a measure of the degree of anisotropy of elastic medium with cubic symmetry. The anisotropy factor for the Wigner-Seitz grains is also shown in Fig. 6.4. It decreases with porosity and exhibits a tendency of approaching unity as porosity decreases. It will go to unity, in the limit of $n' = 0$, because there is no fluid and the entire space in the Wigner-Seitz cell is occupied by the isotropic solid. But as porosity increases, the degree of anisotropy becomes larger and the ratio μ_o/μ_1 deviates further from unity. We also note that the anisotropy factor is less than unity which implies that the medium is more rigid to shear loading in the rotated axes by 45 degrees than in the original coordinate system of symmetry and this property is more pronounced for larger porosity values. As a possible analogy on the atomic scale we note that the majority of cubic crystals possess μ_o/μ_1 greater than unity (see Table 6.3). However some sodium chlorides such as NaCl and KCl whose crystal structures are simple cubic as the Wigner-Seitz grain have the elastic anisotropy factor less than unity(Cottrell, 1964).

The pressure coefficient $\alpha' = \gamma'$, the thermal modulus β'_t, and other elastic coefficients β'_c and ζ'_c of the consolidation equation are calculated from the elastic

moduli a_I, a_{II} and a_{III} by using

$$\begin{aligned}
\alpha' =&\gamma' = 1 - \frac{(a_I + 2a_{II})}{(3\lambda^* + 2\mu^*)}, \qquad \beta'_t = \beta^* \frac{(a_I + 2a_{II})}{(3\lambda^* + 2\mu^*)} \\
\beta'_c =&\frac{3}{3\lambda^* + 2\mu^*} \left[1 - n' - \frac{a_I + 2a_{II}}{3\lambda^* + 2\mu^*}\right], \qquad \zeta'_c = -\beta^* \beta'_c
\end{aligned} \tag{6.4.7}$$

where the Lame constants are given by(cf.(4.1.17) and (4.1.18))

$$\lambda^* = \frac{\nu}{(1+\nu)(1-2\nu)}, \quad \mu^* = \frac{1}{2(1+\nu)} \tag{6.4.8}$$

They are plotted in Fig. 6.5 against porosity. The first term in α' is from the microscale independent pore pressure whereas the second term is the result of the interaction between the solid and fluid phases on the interface. In the limiting case of $n' \to 0$, the fluid phase diminishes and the medium becomes pure solid which is isotropic. The coefficients a_I and a_{II} then reduce to $a^*_{xxxx} = \lambda^* + 2\mu^*$ and $a^*_{xxyy} = \lambda^*$ and α' becomes zero. On the other hand, if the porosity goes to unity, a_I and a_{II} becomes zero and α' approaches the hydrostatic value of unity. Over the intermediate range of porosity, it increases monotonically with porosity. The thermal modulus β'_t obviously decreases as porosity increases. For the chosen value of $\nu = 0.3$, we have $\beta^* = 3\lambda^* + 2\mu^* = 1/(1-2\nu) = 2.5$ and β'_t will approach to 2.5 and 0 respectively as porosity goes to zero and unity.

For the pressure coefficient β'_c of the consolidation equation, by the same reasoning, it is readily seen from (6.4.7) that the coefficient becomes zero for both $n' \to 0$ and $n' \to 1$. Similarly does the coefficient ζ'_c. It has been shown in §4.1 that $\beta'_c > 0$ and $\zeta'_c < 0$ and their variations with porosity are shown in Fig. 6.5. It is finally noted that, in view of the relation $\zeta'_c = -\beta^* \beta'_c$ and $\beta^* = 1/(1-2\nu) > 1$ that the effect of time variation of temperature is always greater than that of pressure when the porous medium is composed of periodic Wigner-Seitz grains on the microscale.

6.4.3 Permeability.

The permeability of the Wigner-Seitz grains is isotropic(cf.(5.2.1)). Sun and Mei(1993) have computed the permeability in 1/8-th of the microcell by using the

variational principle of §6.2. They used quadratic shape functions in the finite elements so that there are total 10 nodes in a tetrahedral element because additional nodes are introduced at the midpoints of each side. The porosity value ranges from 0.252 to 0.979 which also include suspended grains (n'=0.879 - 0.979) that are not in contact. The results and comparison with others by Sun and Mei are breifly discussed here.

In Fig. 6.6, their computed hydraulic conductivity is compared with the empirical formula of Kozeny and Carman (Carman, 1937). Due to irregularity of size and shape, the scattering of measured data used in fitting to Kozeny-Carman formila lies between 10 to 20 percent. The cureves of data scatter are also shown in Fig. 6.6. The numerical results show good agreement over the practical range of porosities $0.37 \sim 0.68$. Their numerical results have also been compared with those calculated for various packing of uniform spheres by Zick and Homsy(1980). The results by Sun and Mei fall a little below due to the difference in grain shape.

The velocity field in the pore space of the Wigner-Seitz grains is later used in the calculation of dispersion tensor in Part B.

mesh type	number of nodes in $0< x <0.5$	total number of nodes	total number of elements
1	4	72	160
2	8	395	1280
3	12	1162	4320
4	16	2565	10240

Table 6.1 Numbers of nodes and elements for four types of meshes(n'=0.5).

$n' = .284$	5	10	15	extrapol.	error(%)
$< \sigma_{xx}(\phi^{xx}) >$	-.296700	-.326894	-.335614	-.339564	1.1
$< \sigma_{yy}(\phi^{xx}) >$	-.201172	-.215381	-.219189	-.220895	.78
$< \sigma_{xy}(\phi^{xy}) >$	-8.5890d-02	-9.5894d-02	-9.8461d-02	-9.9627d-02	1.2

$n' = .377$	3	6	12	18	extrapol.	error(%)
$< \sigma_{xx}(\phi^{xx}) >$	-.296844	-.348941	-.369403	-.375504	-.379617	1.1
$< \sigma_{yy}(\phi^{xx}) >$	-.204723	-.229299	-.237279	-.239707	-.241363	.68
$< \sigma_{xx}(\phi^{xx}) >$	-8.7962d-02	-.105967	-.112368	-.113992	-.114736	.65

$n' = .5$	4	8	12	16	extrapol.	error(%)
$< \sigma_{xx}(\phi^{xx}) >$	-.336849	-.363525	-.371183	-.374744	-.377810	.81
$< \sigma_{yy}(\phi^{xx}) >$	-.2181054	-.227164	-.229702	-.230892	-.231918	.44
$< \sigma_{xy}(\phi^{xy}) >$	-.106595	-.115353	-.117558	-.118496	-.119290	.66

$n' = .623$	6	12	18	21	extrapol.	error(%)
$< \sigma_{xx}(\phi^{xx}) >$	-.321622	-.333752	-.337286	-.338240	-.340141	.56
$< \sigma_{yy}(\phi^{xx}) >$	-.192119	-.195149	-.196013	-.196245	-.196706	.23
$< \sigma_{xy}(\phi^{xy}) >$	-.104855	-.107257	-.108276	-.109151	-.109609	.42

$n' = .716$	5	10	15	20	extrapol.	error(%)
$< \sigma_{xx}(\phi^{xx}) >$	-.273767	-.286585	-.290213	-.291889	-.293331	.49
$< \sigma_{yy}(\phi^{xx}) >$	-.154298	-.156439	-.157000	-.157252	-.157468	.14
$< \sigma_{xy}(\phi^{xy}) >$	-8.8944d-02	-9.2259d-02	-9.3094d-02	-9.3451d-02	-9.3753d-02	.32

Table 6.2 Computed values of stresses, their convergence and the extrapolation.

Elastic Constants of Cubic Crystals (10^{12} dyn cm^{-2})

Substance	Structure	c_{11}	c_{12}	c_{44}	μ_0/μ_1
Na	b.c.c.	0·055	0·042	0·049	7·5
K	b.c.c.	0·046	0·037	0·026	5·7
Fe	b.c.c.	2·37	1·41	1·16	2·4
W	b.c.c.	5·01	1·98	1·51	1·0
Al	f.c.c.	1·08	0·62	0·28	1·2
Cu	f.c.c.	1·684	1·214	0·754	3·2
Ni	f.c.c.	2·50	1·60	1·185	2·6
Pb	f.c.c.	0·48	0·41	0·14	4·0
Diamond	diamond	9·2	3·9	4·3	1·6
Si	diamond	1·66	0·64	0·79	1·55
Ge	diamond	1·29	0·48	0·67	1·7
NaCl	NaCl	0·486	0·127	0·128	0·7
NaBr	NaCl	0·33	0·13	0·13	1·3
KCl	NaCl	0·40	0·062	0·062	0·36
KBr	NaCl	0·35	0·058	0·050	0·33
KI	NaCl	0·27	0·043	0·042	0·36
LiF	NaCl	1·19	0·54	0·53	1·6

Table 6.3 Elastic constants of cubic crystals (after Cottrell (1964)).

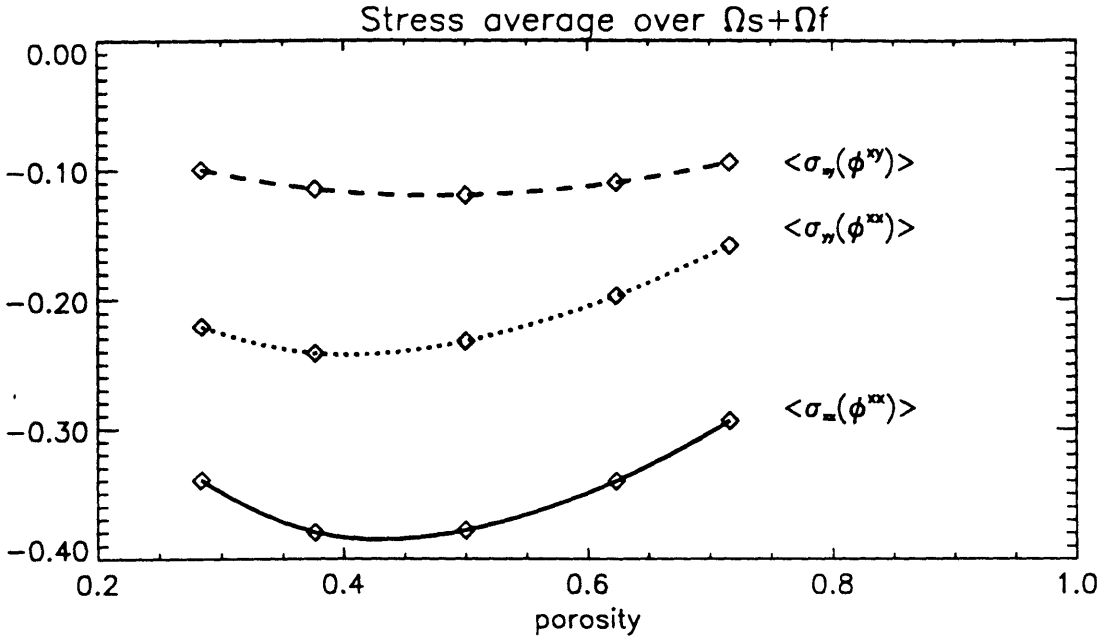

Fig. 6.2 The unit cell volume average of the solid stresses.

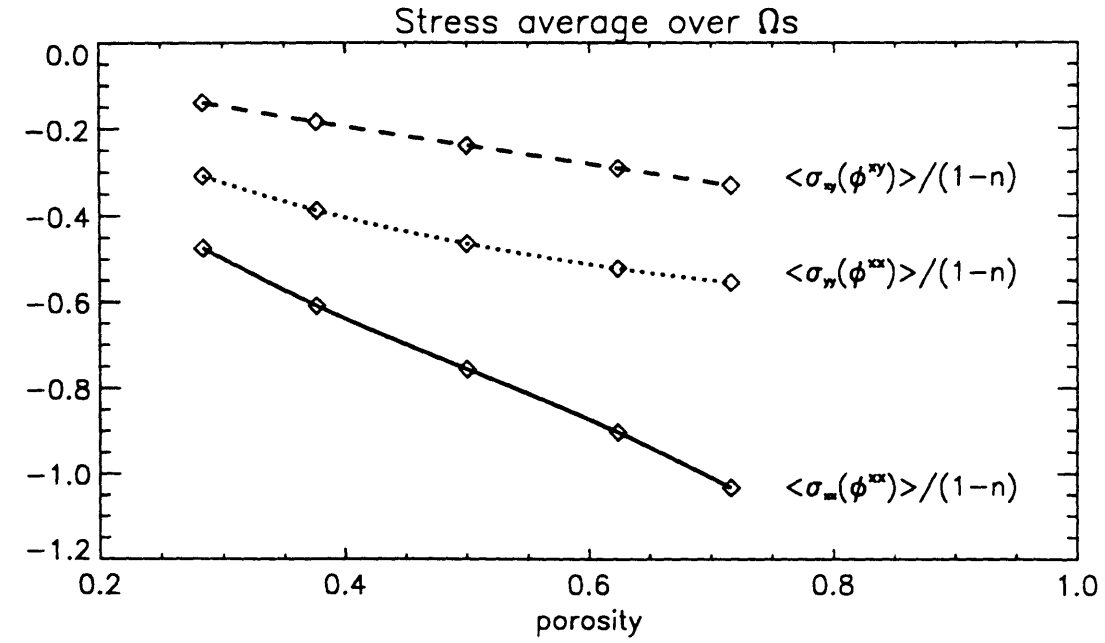

Fig. 6.3 The average of solid stresses over the solid phase volume Ω_s.

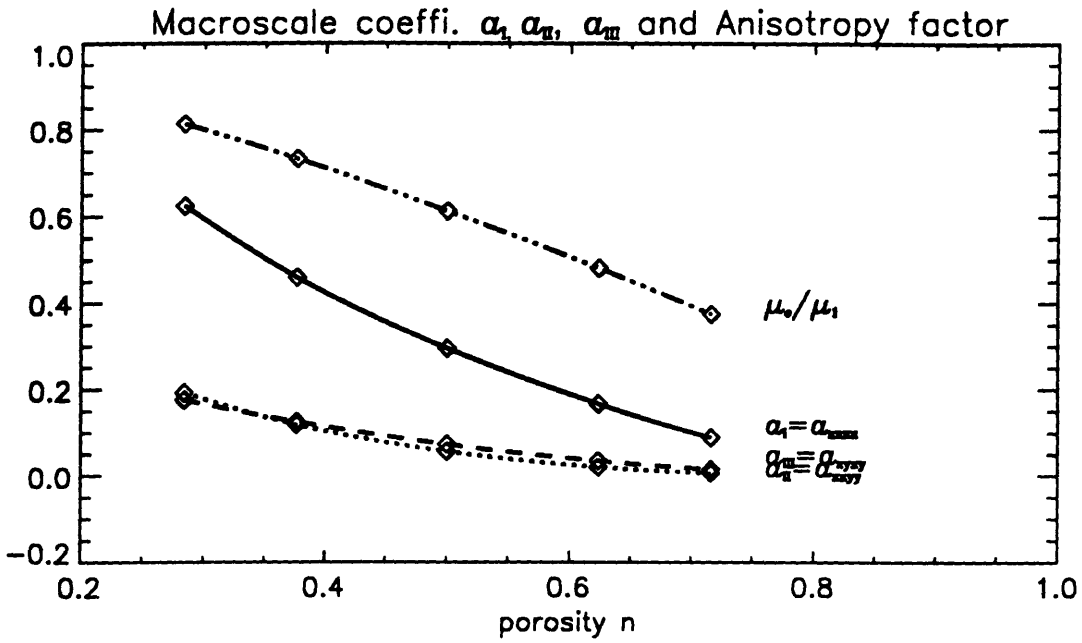

Fig. 6.4 The macroscale elastic coefficients a_I, a_{II}, a_{III} and the anisotropy factor μ_o/μ_1.

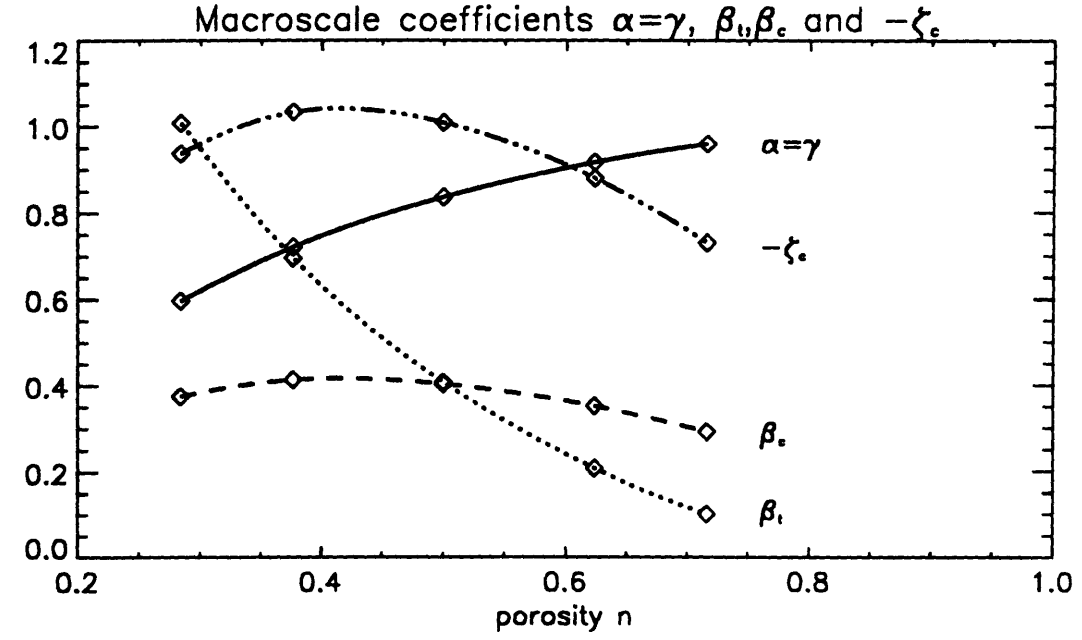

Fig. 6.5 The macroscale coefficients $\alpha' = \gamma'$, β_i', β_c' and $-\zeta_i'$.

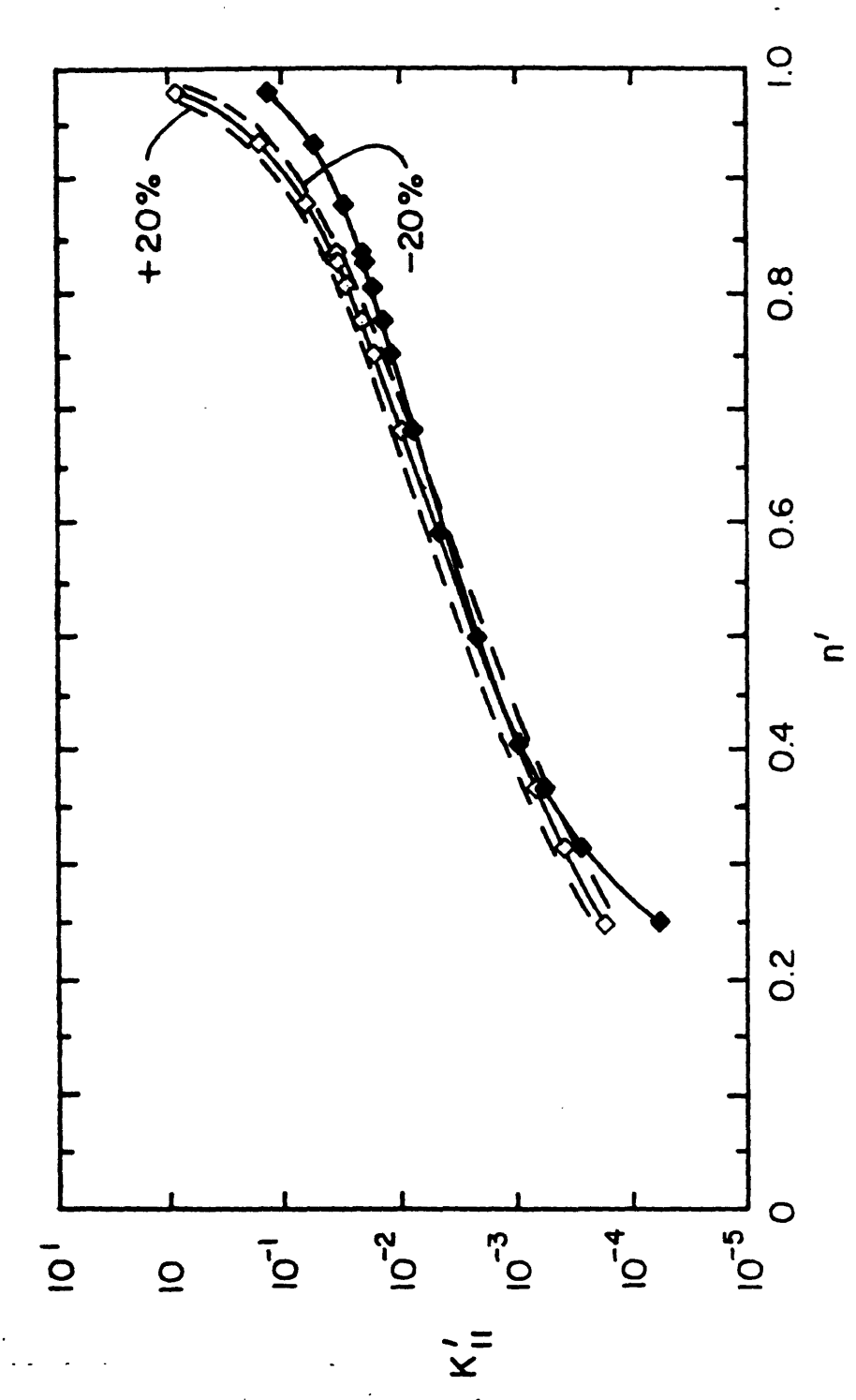

Fig. 6.6 Computed permeability for Wigner-Seitz grains (Sun and Mei, 1993) in black diamond and the comparison with the empirical Kozeny-Carman formula in open diamond.

7. Thermoconsolidation due to Pumping in a Porous Layer.

The general theory of thermoconsolidation is now applied to a soil layer at the bottom of which the pore fluid is extracted either uniformly or through a small sink. It is first shown that ranges of the dimensionless parameters estimated from the reported values at some geothermal fields agree fairly well with the range assumed earlier. In addition, classical research on the instability of fluid motion in a rigid porous layer with initial temperature gradient are recalled in terms of the critical Rayleigh number. After a brief explanation of the numerical scheme based on finite differences, the macroscale coefficients calculated in §6 are used to investigate the effects of varying permeability and pumping rate. Numerical results are presented for both one-dimensional and two-dimensional cases.

7.1 Background.

Before applying the thermoconsolidation theory to geothermal reservoirs from which hot fluid is extracted, some field examples are discussed and the typical values of the Peclét and Rayleigh numbers are estimated. Then studies on flow instability in porous layers with vertical temperature gradient are reviewed which can be used as guidelines in choosing the dimensionless parameters.

7.1.1 Examples of Liquid-Dominated Geothremal Reservoirs.

The geothremal fields at Wairakei, New Zealand and Cerro Prieto, Mexico are typical examples of liquid-dominated geothremal reservoirs. In these areas, almost all of the fluid withdrawn has been replenished by recharge (Narasimhan and Goyal, 1984) and the production rates were about $O(10^{10}$ kg/yr)=$O(10^{-3}m^3/s)$ (Stilwell et al(1975), Bixley(1984) and Goyal et al(1981)).

At the Wairakei where the vertical subsidence was as high as 4.5m over the period 1964 - 1975(Stilwell et al,1975), the thickness of the Waiora formation composed mainly of pumice sandstone and breccia varies rapidly from 400m in the western section to 750m in the eastern section and the area of main production was about $2\,\mathrm{km}^2$(Bixley,1984). Taking the thermal diffusivity α_f of $O(10^{-7}\,\mathrm{m}^2/\mathrm{s})$ and

the thickness of the reservoir $h = O(10^2 m)$, it follows that the macroscale Peclét number $Pe^* = Qh/\alpha_f = O(10^{-1}-10)$ where Q is the fluid removal rate per unit area estimated above. The temperature variation Θ across the reservoir depth is $60°C$ or larger(Bolton,1970). If the thermal expansion coefficient $\beta_T = O(10^{-4}1/°C)$ typical of water and the hydraulic conductivity $K = O(10^{-7} - 10^{-9}\,\mathrm{m/s})$ are used, the Rayleigh number $Ra = K\beta_T\Theta h/\alpha_f$ may be estimated to be in the range $O(10^{-1} - 10)$. These estimates lie in the range consistent with the assumptions made earlier as $Pe = O(\epsilon)$,e.g. $Pe^* = Pe/\epsilon = O(1)$, and $Ra = O(1)$. Several values chosen from these ranges will be later used in the computations. Reported values of pressure drop P' at the Wairakei vary in the range $300 \sim 350$ psi from eastern to western sections(Bolton,1970; Stilwell et al,1975). The relative magnitude of P', when compared with the elastic modulus $\mathcal{D}$=$O(10^7 - 10^{10} N/m^2)$ for sand and rock, is thus estimated to be $P'/\mathcal{D} = O(10^{-4} - 10^{-1})$ which is very small and is consistent with our assumption $P'/\mathcal{D} = O(\epsilon)$.

The shape, the formation and the composition of the cited geothermal reservoirs are of course very complicated. In this chapter, an idealized situation of a single layer of porous medium is considered and the general theory will be specialized to one-dimensional and two-dimensional pumping of hot water from the bottom of reservoir.

7.1.2 Instability of Fluid Motion in a Layer of Porous Medium with Vertical Temperature Gradient.

When a horizontal layer of saturated rigid porous medium is subject to a vertical temperature gradient, the stability of fluid motion breaks down and a steady convective motion can develop if the Rayleigh number reaches critical values. In this section, some previous works on the stability of fluid motion are briefly reviewed for both the case of zero mean flow through the medium and the case of uniform vertical through flow. Comprehensive reviews on convection in porous media can be found in the book by Nield and Bejan(1992).

Lapwood(1948) and Horton and Rogers(1945) have analyzed the linear stability in the case of initially stagnant pore fluid and obtained the critical Rayleigh numbers beyond which small disturbances lose stability and cellular convective motions develop in the medium. Let us consider a horizontal porous layer with thickness h in which the lower and upper bounding surfaces are kept at constant temperatures. The initial temperature varies linearly across the depth and decreases vertically upwards by Θ. It is assumed that the fluid velocity and the perturbations of temperature, density and pressure are small. By solving coupled eigenvalue problems for the dimensionless perturbations of the vertical component of fluid velocity and the temperature, it can be shown (Appendix G) that the critical Rayleigh number R_c for marginal stability,e.g. zero time growth rate, is given as follows. If both boundaries are impermeable, R_c is

$$R_c = 4\pi^2 \simeq 40 \tag{7.1.1}$$

where R_c is defined by

$$R_c = \frac{K\beta_T \Theta h}{\alpha_m} \tag{7.1.2}$$

with $\alpha_m = \bar{m}'/(\rho C_p)_f$ being the thermal diffusivity of the medium defined in terms of the heat capacity of fluid. On the other hand, if the pressure on the upper boundary at $z = h$ is constant, it becomes(Lapwood, 1948)

$$R_c = 27.1 \tag{7.1.3}$$

For various combinations of boundary conditions at $z = 0$ and $z = h$ including insulated(to temperature perturbation) boundaries, Nield(1968) has computed critical values of R_c and the most unstable horizontal wave number and has observed that both decrease as the boundary conditions are changed to those of constant pressure or constant heat flux.

When there is uniform through flow, the eigenvalue problem for temperature perturbation (7.1.2) is modified to include the convection term which is signified by the Peclét number

$$P = Uh/\alpha_m \tag{7.1.4}$$

where U is the velocity of the uniform through flow(see Appendix F). Note that for non-zero through flow the steady state temperature gradient is not constant due to convection as will be shown in the case of one-dimensional thermoconsolidation later in §7.4. When the boundaries are impermeable to velocity perturbations, Homsy and Sherwood(1976) have calculated the critical Rayleigh number R_c as function of the Peclét number P by using both linear theory for infinitesimal disturbances and the energy theory for finite amplitude motions. Later by including the constant pressure boundary condition and allowing combinations with impermeable boundary, Jones and Persichetti(1986) have calculated R_c by using linear theory for four types of boundary conditions. Their results are reproduced in Fig.7.1 in which Homsy and Sherwood's results are shown in squares for impermeable boundaries by linear theory and in dashed curves for the energy theory. So, in the case of impermeable boundaries, the flow is definitely unstable above the curve with squares and definitely stable below the dashed curve. Lapwood criteria (7.1.1) and (7.1.3) are also shown for $P = 0$. A positive Peclét number means that the vertical through flow is upward. It is noted that, as P increases, the R_c curves merge into two which are distinguished by the boundary condition toward which the flow is directed. At the same time, R_c increases with P. As pointed out by Homsy and Sherwood, this is due to the thermal boundary layer near the upper boundary across which most of the temperature variation occurs. This has the effect of decreasing the effective Rayleigh number through the decrease of h in (7.1.2) and therefore tends to stabilize the fluid motion.

These studies on the stability will serve as a guide in selecting the Rayleigh number for calculating thermoconsolidation in a porous deformable layer.

7.2 Normalized Governing Equations and Boundary Conditions.

The thermoconsolidation problem is described for two-dimensional situation. The one-dimensional version is given simply by extending the pumping uniformly all over the bottom.

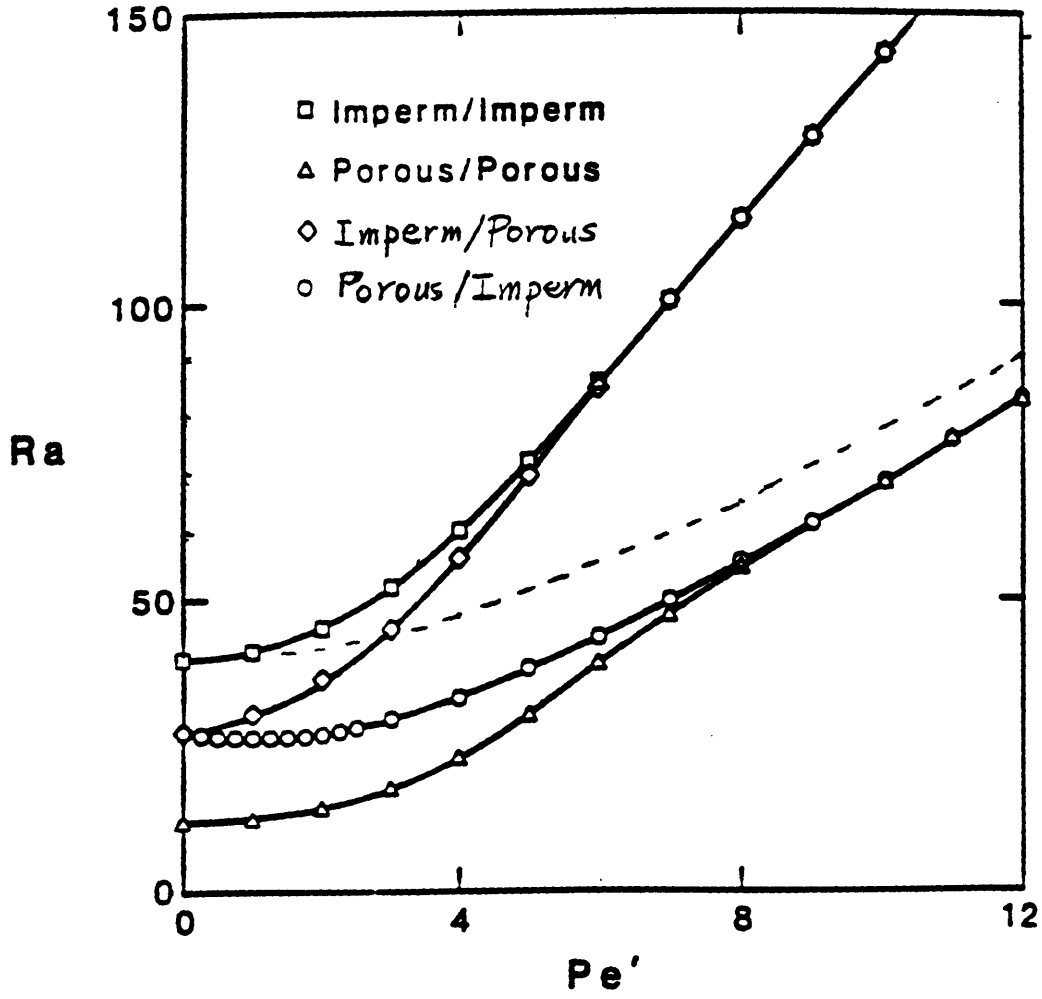

Fig. 7.1 The critical Rayleigh numbers by linear stability theory for combinations of upper/lower boundary conditions (after Jones and Persichetti, 1986). The dashed curve is by the energy stability theory for impermeable/impermeable boundary conditions (after Homsy and Sherwood, 1976).

Consider a single layer of saturated porous medium with thickness h shown in Fig.7.2 in which the initial temperature before pumping starts is linear in z with $T = T_1$ at $z = 0$ and $T = T_2 (> T_1)$ at $z = h$. It is supported by a rigid impermeable bedrock at constant temperature. At the upper boundary($z = h$), it is assumed that the pressure and the temperature are kept at the initial values so that the variations are maintained to be zero. This is roughly the case in Wairakei and Cerro Prieto. It is also assumed that the stress variations at $z = h$ are zero.

Suppose that the pore fluid is withdrawn at the rate of U per unit length in x through a narrow sink located at the bottom. Taking U as the normalization scale for seepage velocity, the pore pressure is scaled by $P = UH/\tilde{k}$ from Darcy's law (3.7.10). The solid displacement is then estimated by balancing the strain and pore pressure in the equilibrium equation (3.7.8) to be $V = O(Ph/\mathcal{D})$ where $\mathcal{D}$ is the scale of the elastic modulus of the medium. The medium temperature variation from initial state will be at most $O(\Theta = T_2 - T_1)$. The heat diffusion time $T_d = h^2/\alpha_f$ is chosen for the time scale since the consolidation time T_c is usually less than T_d. Spatial coordinates are normalized by the layer thickness h. These scales are summarized below.

$$\langle u \rangle = U, \quad P = \frac{Uh}{\tilde{k}}, \quad V = \frac{Ph}{\mathcal{D}}, \quad \Theta = T_2 - T_1, \quad T_d = \frac{h^2}{\alpha_f}, \quad x, z = h \qquad (7.2.1)$$

These order of magnitude estimates and those for the material coefficients summarized in §3.7 are used in the following sections to normalize the governing equations and the boundary conditions.

7.2.1 Normalized Governing Equations.

The governing equations in dimensionless variables have been deduced already in §3. Two-dimensional forms which will be used in the numerical computation are given here. In the two-dimensional porous medium of Fig.7.2, the solid displacement along and the derivatives in y direction vanish.

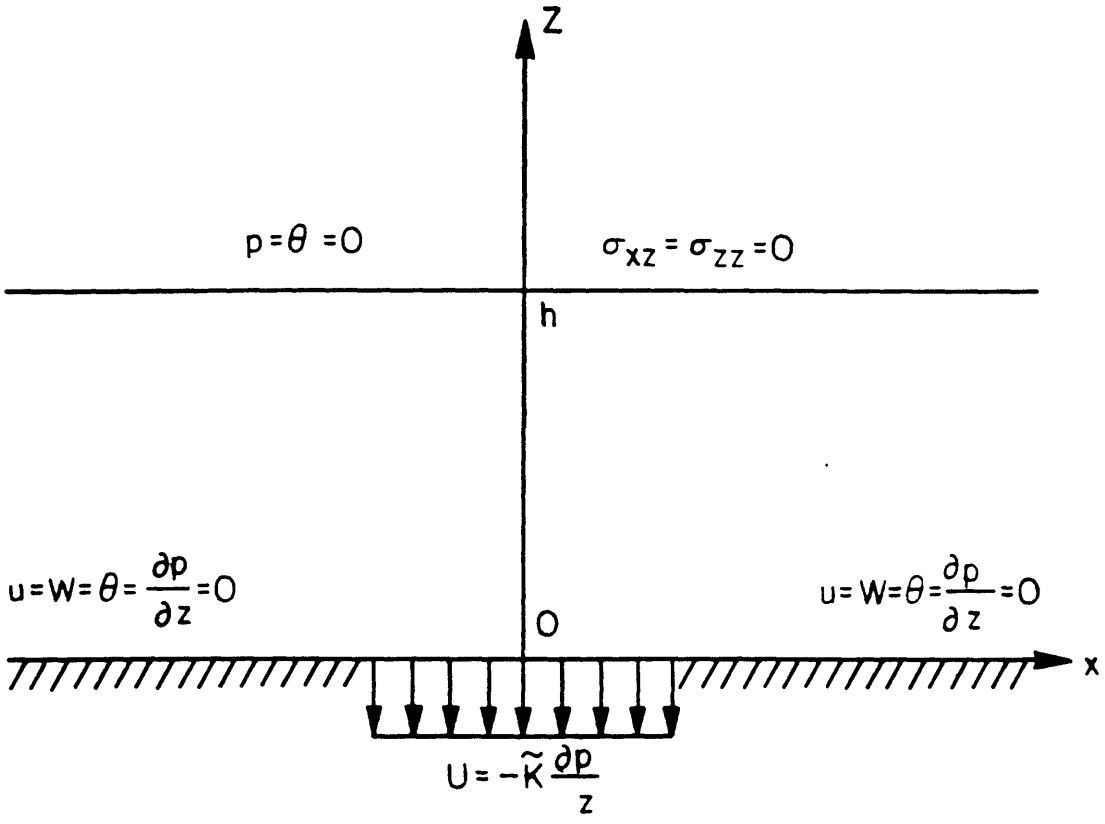

Fig. 7.2 A poroelastic layer subject to pumping rate U per unit length through a small sink at the bottom.

The equilibrium equation (3.7.8) is normalized according to (7.2.1).

$$\begin{aligned} \frac{\partial \sigma_{xx}}{\partial x} + \frac{\partial \sigma_{xz}}{\partial z} &= 0 \\ \frac{\partial \sigma_{xz}}{\partial x} + \frac{\partial \sigma_{zz}}{\partial z} &= -n' \frac{Ra}{Pe^*} \theta \end{aligned} \tag{7.2.2}$$

where (3.7.3) has been used. The stresses are given by Hooke's law for plane strain as

$$\begin{aligned} \sigma_{xx} &= a_I \frac{\partial u}{\partial x} + a_{II} \frac{\partial w}{\partial z} - \alpha' p - b\beta_t' \theta \\ \sigma_{xz} &= a_{III} \left(\frac{\partial u}{\partial z} + \frac{\partial w}{\partial x} \right) \\ \sigma_{zz} &= a_I \frac{\partial w}{\partial z} + a_{II} \frac{\partial u}{\partial x} - \alpha' p - b\beta_t' \theta \end{aligned} \tag{7.2.3}$$

in which u, w, p and θ are the displacement components in x and z directions, the excessive pore pressure and the temperature variation respectively. The parameter b is the scale ratio of thermal stress to the pore pressure and is given by

$$b = \frac{B\Theta}{P} = \frac{\tilde{k}B}{h} \frac{\Theta}{U} \tag{7.2.4}$$

where B is the scale of the thermal modulus. The dimensionless parameters Ra and Pe^* are the Rayleigh and Peclét numbers respectively given by

$$Ra = \frac{\tilde{k}\rho_f g \beta_T h \Theta}{\alpha_f}, \qquad Pe^* = \frac{Uh}{\alpha_f} \tag{7.2.5}$$

where the permeability $\tilde{k}$ is related to the hydraulic conductivity K by $\tilde{k} = K/\rho_f g$. Note that the Peclét number Pe^* is based on the macroscale length h.

Darcy's law (3.7.10) and the consolidation equation (3.7.11) are normalized as

$$\begin{aligned} \langle u \rangle_x - n' \left(\frac{T_c}{T_d} \right) \frac{\partial u}{\partial t} &= - \frac{\partial p}{\partial x} \\ \langle u \rangle_z - n' \left(\frac{T_c}{T_d} \right) \frac{\partial w}{\partial t} &= - \left(\frac{\partial p}{\partial z} - \frac{Ra}{Pe^*} \theta \right) \end{aligned} \tag{7.2.6}$$

and

$$\begin{aligned} &\frac{\partial^2 p}{\partial x^2} + \frac{\partial}{\partial z} \left(\frac{\partial p}{\partial z} - \frac{Ra}{Pe^*} \theta \right) \\ &\quad = \left[\gamma' \frac{\partial}{\partial t} \left(\frac{\partial u}{\partial x} + \frac{\partial w}{\partial z} \right) + \beta_c' \frac{\partial p}{\partial t} + b\zeta_c' \frac{\partial \theta}{\partial t} \right] \left(\frac{T_c}{T_d} \right) \end{aligned} \tag{7.2.7}$$

where $T_c/T_d = \rho_f g \alpha_f / \mathcal{D} K$ is the ratio of the consolidation time to heat diffusion time.

Similarly the dimensionless nonlinear heat equation (3.7.13) becomes

$$\overline{\rho C_p}\frac{\partial \theta}{\partial t} + Pe^* \left[U_x \frac{\partial \theta}{\partial x} + U_z \left(\frac{\partial \theta}{\partial z} - 1 \right) \right] = m' \left(\frac{\partial^2 \theta}{\partial x^2} + \frac{\partial^2 \theta}{\partial z^2} \right) \tag{7.2.8}$$

where

$$\begin{aligned} U_x =& \langle u \rangle_x + (\rho C_p)_r (1 - n') \left(\frac{T_c}{T_d} \right) \frac{\partial u}{\partial t} + [(\rho C_p)_r - 1] \left(\frac{T_c}{T_d} \right) \frac{\partial u}{\partial t} \left\langle \frac{\partial A_x^s}{\partial x} \right\rangle \\ U_z =& \langle u \rangle_z + (\rho C_p)_r (1 - n') \left(\frac{T_c}{T_d} \right) \frac{\partial w}{\partial t} + [(\rho C_p)_r - 1] \left(\frac{T_c}{T_d} \right) \frac{\partial w}{\partial t} \left\langle \frac{\partial A_z^s}{\partial z} \right\rangle \end{aligned} \tag{7.2.9}$$

are the convection velocity components of heat transport in x and z directions.

7.2.2 The Boundary Conditions.

Owing to the symmetry about $x = 0$, the computational domain is reduced to the half-infinite strip $x > 0$ and $0 < z < 1$.

On the lower boundary $z = 0$, the solid displacements and the temperature variation are zero:

$$u = w = \theta = 0 \qquad \text{at} \quad z = 0 \tag{7.2.10}$$

Since the sink through which the pore fluid is extracted is confined to $0 < x < a$ (Fig.7.2), it follows from (7.2.6) and (7.2.10) that

$$\frac{\partial p}{\partial z} = \begin{cases} 1 & 0 < x < a, z = 0 \\ 0 & x > a, \quad z = 0 \end{cases} \tag{7.2.11}$$

The boundary conditions on the upper surface are imposed on the instantaneous location where the excessive pore pressure, the temperature variation and the traction forces are zero. After expansion about the initial location $z = 1$ and linearization, we have

$$\begin{aligned} p =& \theta = 0 \\ \sigma_{zz} =& a_I \frac{\partial w}{\partial z} + a_{II} \frac{\partial u}{\partial x} = 0 \qquad \text{at } z = 1 \\ \sigma_{xz} =& a_{III} \left(\frac{\partial u}{\partial z} + \frac{\partial w}{\partial x} \right) = 0 \end{aligned} \tag{7.2.12a - c}$$

in which (7.2.12a) has been used in the traction boundary conditions(cf.(7.2.3)).

At the vertical boundary $x = 0$, we have due to symmetry,

$$u = \frac{\partial w}{\partial x} = \frac{\partial p}{\partial x} = \frac{\partial \theta}{\partial x} = 0 \tag{7.2.13}$$

At infinity the disturbances vanish so that

$$u = w = p = \theta = 0 \qquad \text{as} \quad x \to \infty \tag{7.2.14}$$

As initial condition, we also impose

$$u = w = p = \theta = 0 \qquad t = 0 \tag{7.2.15}$$

The initial boundary value problem (7.2.2),(7.2.7),(7.2.8),(7.2.10)-(7.2.15) is now solved numerically in the following sections. As has been mentioned in §3, the governing equations (7.2.2),(7.2.7) and (7.2.8) are all coupled and should be solved together. Especially the convection part in (7.2.8) involves nonlinear couplings among u, w, p and θ.

7.3 Numerical Scheme.

Finite differences are used to solve the initial boundary value problem defined in §7.2. The horizontal extent of the computational domain is truncated at large but finite value of x_N large enough to ensure that the numerical results are not affected by further increase in x_N. Horizontal variations are expected to be large near the sink and small at large x. To achieve numerical efficiency the horizontal coordinate is transformed by introducing a logarithmic coordinate

$$\xi = \ln(x + 1) \tag{7.3.1}$$

so that the region $0 < x < x_N$ is mapped onto $0 < \xi < \ln(x_N + 1)$ and uniform mesh in ξ corresponds to nonuniform mesh in x which grows logarithmically as x increases. The spatial derivatives in x direction then become

$$\frac{\partial}{\partial x} \to e^{-\xi} \frac{\partial}{\partial \xi}, \qquad \frac{\partial^2}{\partial x^2} \to e^{-2\xi} \left(\frac{\partial^2}{\partial \xi^2} - \frac{\partial}{\partial \xi} \right) \tag{7.3.2}$$

Along the z direction uniform meshes are used.

The computation at each time step requires iterations for two reasons. First the convection in (7.2.8) is composed of nonlinearly coupled terms among the unknowns(cf.(7.2.6) and (7.2.9)). Second the traction-free boundary conditions (7.2.12b and c) involve both u and w neither of which is not known a priori at $z = 1$. On the other hand, the buoyancy in the z component of Darcy velocity (7.2.6) makes the convection part strongly nonlinear for finite values of Ra due to the presence of $Ra\theta\partial\theta/\partial z$ in (7.2.8). In order to avoid too large number of iterations, the medidum temperature is rescaled as

$$\theta' = Ra\theta \tag{7.3.3}$$

The governing equations are now written for u, w, p and θ' in ξ and z coordinates. The equilibrium equation (7.2.2) becomes, after using (7.2.3), as

$$\begin{aligned} &a_I e^{-\xi}\left(\frac{\partial^2 u}{\partial \xi^2} - \frac{\partial u}{\partial \xi}\right) + a_{III}e^{\xi}\frac{\partial^2 u}{\partial z^2} + (a_{II} + a_{III})\frac{\partial^2 w}{\partial \xi \partial z} - \alpha'\frac{\partial p}{\partial \xi} - \frac{b}{Ra}\beta_t'\frac{\partial \theta'}{\partial \xi} = 0 \\ &(a_{II} + a_{III})e^{-\xi}\frac{\partial^2 u}{\partial \xi \partial z} + a_{III}e^{-2\xi}\left(\frac{\partial^2 w}{\partial \xi^2} - \frac{\partial w}{\partial \xi}\right) + a_I\frac{\partial^2 w}{\partial z^2} \\ &\quad - \alpha'\frac{\partial p}{\partial z} - \frac{b}{Ra}\beta_t'\frac{\partial \theta'}{\partial z} = -\frac{n'}{Pe^*}\theta' \end{aligned} \tag{7.3.4}$$

The consolidation equation (7.2.7) also becomes

$$\begin{aligned} &e^{-2\xi}\left(\frac{\partial^2 p}{\partial \xi^2} - \frac{\partial p}{\partial \xi}\right) + \frac{\partial}{\partial z}\left(\frac{\partial p}{\partial z} - \frac{\theta'}{Pe^*}\right) \\ &\qquad = \left[\gamma'\left(e^{-\xi}\frac{\partial^2 u}{\partial \xi \partial t} + \frac{\partial^2 w}{\partial z \partial t}\right) + \beta_c'\frac{\partial p}{\partial t} + \frac{b}{Ra}\zeta_c'\frac{\partial \theta'}{\partial t}\right]\left(\frac{T_c}{T_d}\right) \end{aligned} \tag{7.3.5}$$

The heat transport equation (7.2.8) is written as

$$\begin{aligned} &\overline{\rho C_p}\frac{\partial \theta'}{\partial t} + \left[-Pe^* e^{-\xi}\frac{\partial p}{\partial \xi} + Pe^*\left(\frac{T_c}{T_d}\right)f_z\frac{\partial u}{\partial t}\right]e^{-\xi}\frac{\partial \theta'}{\partial \xi} \\ &\qquad + \left[-Pe^*\frac{\partial p}{\partial z} + Pe^*\left(\frac{T_c}{T_d}\right)f_z\frac{\partial w}{\partial t} + \theta'\right]\left(\frac{\partial \theta'}{\partial z} - Ra\right) \\ &\qquad = m'\left[e^{-2\xi}\left(\frac{\partial^2 \theta'}{\partial \xi^2} - \frac{\partial \theta'}{\partial \xi}\right) + \frac{\partial^2 \theta'}{\partial z^2}\right] \end{aligned} \tag{7.3.6}$$

where

$$f_x = (\rho C_p)_r + ((\rho C_p)_r - 1)\left(\left\langle \frac{\partial A_x^s}{\partial x} \right\rangle - n'\right)$$
$$f_z = (\rho C_p)_r + ((\rho C_p)_r - 1)\left(\left\langle \frac{\partial A_z^s}{\partial z} \right\rangle - n'\right) \tag{7.3.7}$$

in which (7.2.6) and (7.2.9) have been used in the convection. The boundary conditions are not repeated here. It only requires the use of (7.3.2).

Centered difference for spatial derivatives and implicit scheme for time marching have been used in the finite difference form of the governing equations and boundary conditions. Detailed derivations are documented in Appendix G and only computational procedures are described here.

Suppose that computations have been completed upto n-th time step. Advancing to $(n+1)$-th time step is performed as follows.

(i) Take n-th time step results for $f^n (f = u, w, p, \theta')$ as the trial values for the first iteration and solve (7.3.4)-(7.3.6) for ${}^1f^{n+1} (f = u, w, p, \theta')$ where the superscript on the left shoulder denotes the iteration count.

(ii) Use ${}^1f^{n+1}$ in the convection velocity of (7.3.6) and the traction boundary conditions (7.2.12) to calculate ${}^2f^{n+1}$.

(iii) Repeat steps (i) and (ii) until the difference in the solution values of two consecutive iterations becomes negligibly small,e.g.

$$|{}^{k+1}f^{n+1} - {}^kf^{n+1}|/|{}^kf^{n+1}| < \delta \tag{7.3.8}$$

The computation for $(n+1)$-th time step is now complete and ready to move to the next time step. In real computations, $\delta = 10^{-6}$ has been used.

It is noted that, in the transport processes, use of centered difference in the convection term can cause the appearance of oscillatory behavior as wiggles in numerical results(aliasing) which can be avoided by restricting the grid Peclét number $Pe_g = V\Delta/\alpha$ to be less than 2 (Roache(1977) and Pinder and Gray(1977)) where V and α are the convection velocity and thermal diffusivity of the medium and Δ

is the grid spacing. The values of Pe^* which signifies the convection term were less than 10 and $\alpha \sim 1$ and $\Delta < 0.1$ for which the grid Peclét number is always less than one.

7.4 The Macroscale Coefficients and Dimensionless Parameters.

The coefficients computed for the Wigner-Seitz grains in §6 will be used as the macroscale coefficients. The porosity is chosen to be $n' = 0.377$ which is in the range of common values.

The elastic coefficients are from Figs. 6.4 and 6.5 and are given as

$$\begin{aligned} a_I &= 0.4597 \qquad a_{II} = 0.1183 \qquad a_{III} = 0.1251 \\ \alpha' &= \gamma' = 0.7251 \qquad \beta_i' = 0.6962 \\ \beta_c' &= 0.4140 \qquad \zeta_c' = -1.035 \end{aligned} \tag{7.4.1}$$

The mass heat capacity of minerals which constitute porous medium lies usually in the range of 0.19 to 0.22 Cal/kg°C (Jumikis, 1977) from which the value C_p=0.2 Cal/kg°C has been chosen. The dry density of rock materials is typically $\rho = 2.2 \times 10^3 kg/m^3$. Those values for water around 100 °C are $\rho = 9.6 \times 10^2 kg/m^3$ and $C_p = 4.2 \times 10^3$ J/kg°C (de Marsily, 1986). Combining these values we obtain

$$(\rho C_p)_r = \frac{(\rho C_p)_s}{(\rho C_p)_f} = 0.561, \qquad \overline{\rho C_p} = n' + (\rho C_p)_r (1 - n') = 0.726 \tag{7.4.2}$$

The thermal conductivity of geological materials varies from 0.21 Cal/m h °C for clays to 1.4 Cal/m h °C for sandstones (Jumikis, 1977). An intermediate value of $M_s = 0.80$ Cal/m h °C =0.92 W/m °C is chosen. The thermal conductivity ratio $M_r = M_s/M_f$ then becomes, by using $M_f = 0.67$ W/m °C for water, $M_r = 1.37$. The macroscale thermal conductivity m' normalized by M_f (cf.(3.4.15b)) requires the solution $A^{f,s}$ of the microscale heat conduction problem (3.4.7). It is given by

$$m' = n' + M_r(1 - n') + \left\langle \frac{\partial A_x^f}{\partial x} \right\rangle + M_r \left\langle \frac{\partial A_x^s}{\partial x} \right\rangle \tag{7.4.3}$$

By making use of the variational principle of §6, A^f and A^s have been obtained for the Wigner-Seitz cell with $n' = 0.377$ (i.e. $b/h = 2/3$ in Fig. 6.1). The calculated

values of the bracketed terms in (7.4.3) were obtained as, for three progressively smaller meshes, as

$$\left\langle \frac{\partial A_x^f}{\partial x} \right\rangle = 2.4048 \times 10^{-2}(6), \quad 2.4718 \times 10^{-2}(9), \quad 2.51219 \times 10^{-2}(18)$$
$$M_r \left\langle \frac{\partial A_x^s}{\partial x} \right\rangle = -3.0534 \times 10^{-2}(6), \quad -3.13819 \times 10^{-2}(9), \quad -3.18816 \times 10^{-2}(18) \tag{7.4.4}$$

where the numbers in parentheses denote the intervals between $0 < x < 0.5$ of Fig. 6.1. The extrapolated values corresponding to zero mesh size are $\langle \partial A_x^f/\partial x \rangle = 2.52 \times 10^{-2}$ and $M_r \langle \partial A_x^s/\partial x \rangle = -3.22 \times 10^{-2}$. It then follows that

$$m' = 1.22 \qquad \text{and} \qquad \langle \partial A_x^s/\partial x \rangle = -2.33 \times 10^{-2} \tag{7.4.5}$$

The latter is needed in the convection velocity of heat transport(cf.(7.2.9)).

There are four dimensionless parameters, Ra, Pe^*, the ratio of thermal stress to pore pressure b and the time scale ratio T_c/T_d. While the temperature difference Θ across the depth h and other coefficients such as β_T and α_f are not expected to vary significantly, the pumping rate U and the hydraulic conductivity $K = \tilde{k}\rho_f g$ may do. The dependence of the parameters on U and K is seen from (7.2.4) and (7.2.5) as

$$Pe^* \propto U, \quad Ra \propto K, \quad b \propto \frac{K}{U}, \quad \frac{T_c}{T_d} \propto \frac{1}{K} \tag{7.4.6}$$

We shall choose $Pe^* = Ra = b = T_c/T_d = 1$ as the reference state and vary the parameters according to (7.4.6) to examine mainly the effect of medium permeability and the pumping rate on the thermoconsolidation in a porous layer.

At the initial state, it is assumed that there is no natural convection due to the temperature gradient. As has been mentioned in §7.1, the pore fluid is unstable to disturbances if the Rayleigh number R defined in (7.1.2) is larger than R_c. In the present case, the bottom at $z = 0$ is impermeable to velocity fluctuations and the pressure at $z = 1$ is constant. The critical Rayleigh number is $R_c = 27.1$ for zero

Peclét number and increases with Peclét number. From the relation between Ra and R_c of (7.1.2)

$$Ra = \frac{K\beta_T \Theta h}{\alpha_f} = \frac{K\beta_T \Theta h}{\alpha_m} \frac{\tilde{m}'}{M_f} = m' R_c \tag{7.4.7}$$

the critical Rayleigh number Ra_c for the onset of convection in the layer then becomes

$$Ra_c = 33 \tag{7.4.8}$$

in view of (7.4.5). Therefore we restrict Ra to be less than this value to ensure no free convection for either stagnant fluid or through flow.

The following two case of parameter variations from the reference state will be considered.

Case(i)	Pe^*	Ra	b	T_c/T_d
	1	1	1	1
	1	10	10	0.1
	1	20	20	0.05
	1	30	30	0.0333

(7.4.9)

Case(ii)	Pe^*	Ra	b	T_c/T_d
	0.1	10	100	0.1
	5	10	2	0.1
	10	10	1	0.1

(7.4.10)

In Case (i), the pumping rate U is fixed and the hydraulic conductivity K is increased. This corresponds, as readily seen in the Darcy's law, to the decrease in the pore pressure P(cf.(7.2.1)). According to (7.4.6), b increases whereas T_c/T_d decreases. In Case (ii), the Rayleigh number is fixed at 10,e.g. the medium is relatively porous and permeable as compared to the reference state. With K fixed, the pumping rate U is allowed to vary so that Pe^* ranges from 0.1 to 10 to see the effect of pumping rate variation. The time scale ratio T_c/T_d is fixed but b decreases.

7.5 One-dimensional Thermoconsolidation due to Uniform Pumping at the Bottom.

As the first application of the thermoconsolidation theory, we consider one-dimensional thermoconsolidation in a single layer of porous medium at the bottom of which the fluid is extracted at uniform rate. The main objectives of the study of

one-dimensional problem are two-fold. It provides a reliable check of the numerical scheme with analytic solution in the case of rigid medium and more importantly the implications from the one-dimensional results help understand the two-dimensional thermoconsolidation to be discussed later in §7.6. The actual computation has been carried out by using the numerical scheme for two-dimensional problem of §7.3. The dimensionless governing equations and boundary conditions are those listed in §7.2 after setting $w = 0$ and omitting the x derivatives except the boundary conditions (7.2.14) at $x = \infty$ which are changed to the same form as (7.2.13) to ensure one-dimensionality. The governing equations are

$$\frac{\partial}{\partial z}\left(a_I \frac{\partial w}{\partial z} - \alpha' p - b\beta_i' \theta\right) = -n' \frac{Ra}{Pe^*}\theta \tag{7.5.1}$$

$$\langle u \rangle_z - n' \left(\frac{T_c}{T_d}\right) \frac{\partial w}{\partial t} = -\left(\frac{\partial p}{\partial z} - \frac{Ra}{Pe^*}\theta\right) \tag{7.5.2}$$

$$\frac{\partial}{\partial z}\left(\frac{\partial p}{\partial z} - \frac{Ra}{Pe^*}\theta\right) = \left[\gamma' \frac{\partial^2 w}{\partial z \partial t} + \beta_c' \frac{\partial p}{\partial t} + b\zeta_c' \frac{\partial \theta}{\partial t}\right] \left(\frac{T_c}{T_d}\right) \tag{7.5.3}$$

$$\overline{\rho C_p} \frac{\partial \theta}{\partial t} + U\left(\frac{\partial \theta}{\partial z} - 1\right) = m' \frac{\partial^2 \theta}{\partial z^2} \tag{7.5.4}$$

where

$$U = -Pe^* \frac{\partial p}{\partial z} + Ra\theta + Pe^* \left(\frac{T_c}{T_d}\right) \frac{\partial w}{\partial t} \left[(\rho C_p)_r + ((\rho C_p)_r - 1)\left(\left\langle \frac{\partial A_z^s}{\partial z} \right\rangle - n'\right)\right] \tag{7.5.5}$$

The initial and boundary conditions are

$$w = \theta = p = 0, \qquad \text{at} \quad t = 0 \tag{7.5.6}$$

$$w = \theta = 0, \quad \frac{\partial p}{\partial z} = 1 \qquad \text{at} \quad z = 0 \tag{7.5.7}$$

$$p = \theta = 0, \quad \frac{\partial w}{\partial z} = 0 \qquad \text{at} \quad z = 1 \tag{7.5.8}$$

7.5.1 The Limiting Case of Rigid Porous Medium.

In order to provide a check on the numerical scheme, we consider the case of rigid medium for which analytical solutions exist.

A rigid medium is a limiting case when the elastic modulus $\mathcal{D}$ is infinite. The time scale ratio then becomes

$$T_c/T_d = \rho_f g \alpha_f / \mathcal{D} K \to 0 \tag{7.5.9}$$

After using the boundary conditions (7.5.7) and (7.5.8), the consolidation equation (7.5.3) then simply yields

$$\langle u \rangle_z = -\left(\frac{\partial p}{\partial z} - \frac{Ra}{Pe^*} \theta \right) = -1 \qquad 0 < z < 1 \tag{7.5.10}$$

If we invoke (7.5.9) and (7.5.10) in (7.5.5), the convection velocity reduces to $U_z = \langle u \rangle_z = -1$. Accordingly the heat equation (7.5.4) becomes

$$\overline{\rho C_p} \frac{\partial \theta}{\partial t} - Pe^* \left(\frac{\partial \theta}{\partial z} - 1 \right) = m' \frac{\partial^2 \theta}{\partial z^2} \tag{7.5.11}$$

The constant term Pe^* is the result of the static geothermal gradient. The initial boundary value problem has the followiwng analytic solution (Appendix H)

$$\begin{aligned} \theta =& z - \frac{1 - \exp\left(-\frac{Pe^*}{m'} z\right)}{1 - \exp\left(-\frac{Pe^*}{m'}\right)} \\ & - \frac{2Pe^*}{m'} \exp\left(-\frac{Pe^*}{2m'} z\right) \sum_{n=1}^{\infty} \frac{(-1)^n n\pi \exp\left[-\left(\frac{Pe^{*2}}{4m'} + m' n^2 \pi^2\right) t / \overline{\rho C_p}\right]}{\left[n^2\pi^2 + \left(\frac{Pe^*}{2m'}\right)^2\right]^2} \\ & \times \left[\exp\left(\frac{Pe^*}{2m'}\right) \sin n\pi z - \sin n\pi (z-1) \right] \end{aligned} \tag{7.5.12}$$

The first time independent part is the steady state response when uniform heat source of intensity $-Pe^*$ is distrubuted in the medium while the boundaries are held at zero temperature. It is noted that the effect of the convection term is in the increase of the time factor as compared with pure diffusion case so that the steady state will be reached much faster. Recall that θ is the departure of the medium temperature from the initial state. Since the dimensionless initial temperature gradient is -1, the total temperature gradient at the steady state becomes

$$\frac{\partial}{\partial z}\left(\theta + \overline{T}\right) = -\frac{Pe^*}{m'} \frac{\exp\left(-\frac{Pe^*}{m'}\right) z}{1 - \exp\left(-\frac{Pe^*}{m'}\right)} \tag{7.5.13}$$

This is the initial temperature gradient used in the stability of fluid motion when there is a vertical through flow in the medium(cf.(G.20) of Appendix G) and is not uniform in z as mentioned earlier.

As a sample calculation, we have chosen the values of $Ra = b = 1$, $Pe^* = 5$ and $T_c/T_d = 0$. The numerical results for θ and the analytic solution (7.5.12) are plotted together at three different depths in Fig.7.3. The discrepancy is less than 1% and the agreement is satisfactory. It is seen that the temperature reaches its steady state very quickly due to convection as explained above.

We note again that the computation has been performed by using the finite difference scheme for two-dimensional problem summarized in §7.3 and Fig.7.3 demonstrates the validity of the numerical scheme.

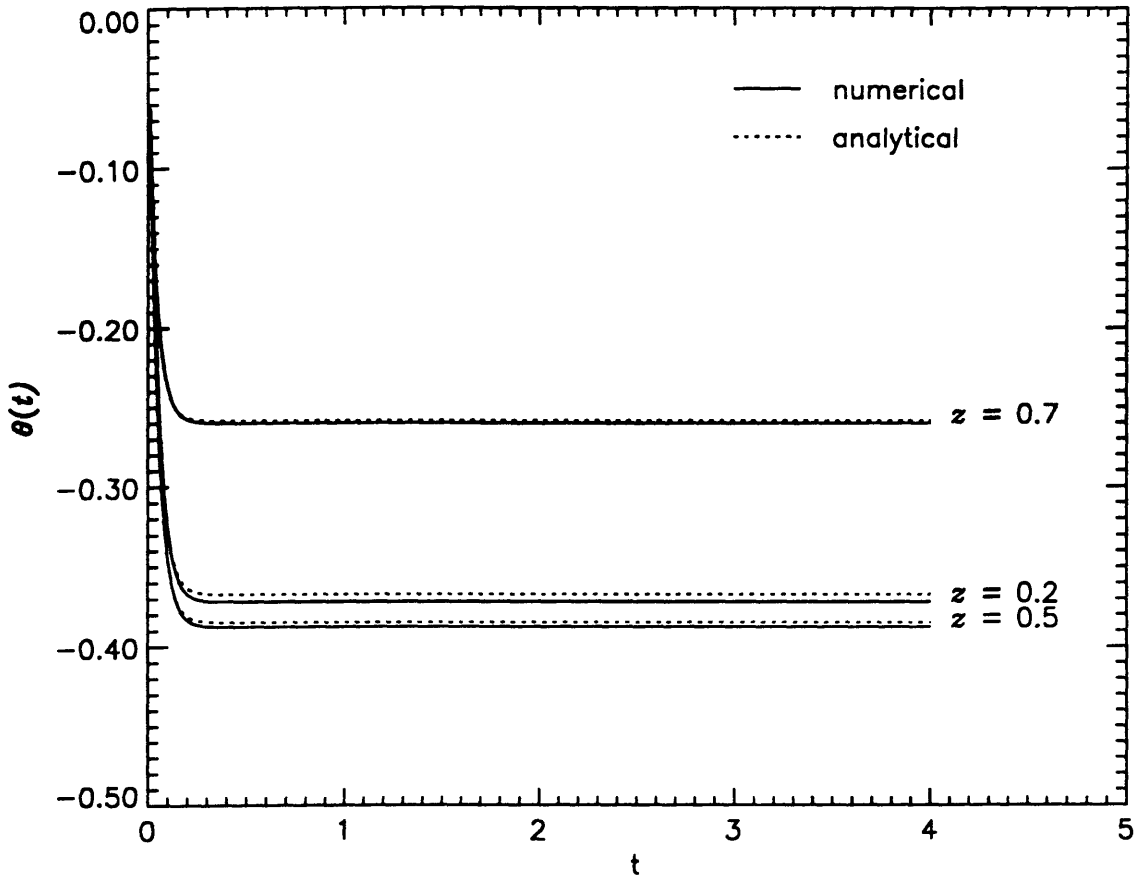

Fig. 7.3 Comparison of the numerical and analytical solutions of temperature for rigid medium with $Ra = 1$ and $Pe^* = 5$.

7.5.2 Numerical Results and Discussions.

The numerical results for one-dimensional thermoconsolidation are presented and discussed. After discussing the steady state, attention will be focused on the following

(a) Thermal effects on the pore pressure and medium deformatiopn.

(b) Nonlinear coupling among the solid displacement, pore pressure and temperature.

The former will be discussed by comparing the responses in the medium with those of isothermal consolidation. The nonlinear coupling effects are dominant during the transient period via heat convection and will be compared with the rigid medium for $Ra = 30$.

The steady state is first examined and then the numerical results for Cases (i) and (ii) of §7.4 are discussed. Comparisons with isothermal consolidation and the case of rigid medium are also made.

Steady State. At the steady state the time derivatives vanish and the solutions are obtained by integrating (7.5.1), (7.5.3) and (7.5.5) subject to the boundary conditions (7.5.7) and (7.5.8). The temperature θ approaches to the steady state form of (7.5.12) which is

$$\theta(z) = z - \frac{1 - \exp\left(-\frac{Pe^*}{m'}z\right)}{1 - \exp\left(-\frac{Pe^*}{m'}\right)} \tag{7.5.14}$$

The consolidation equation similarly gives

$$\begin{aligned} p(z) =& z - 1 + \frac{Ra}{Pe^*}\int_1^z \theta dz \\ =& z - 1 + \frac{Ra}{Pe^*}\left[\frac{1}{2}(z^2-1) + \frac{z-1}{e^{-Pe^*/m'}-1} + \frac{m'}{Pe^*}\frac{e^{-Pe^*z/m'} - e^{-Pe^*/m'}}{e^{-Pe^*/m'}-1}\right] \end{aligned} \tag{7.5.15}$$

The steady vertical displacement then becomes

$$\begin{aligned} w(z) =& \frac{\alpha'}{a_I}\int_o^z p dz + \frac{b\beta_t'}{a_I}\int_o^z \theta dz + \frac{n'}{a_I}\frac{Ra}{Pe^*}\int_o^z dz\int_1^z \theta d\xi \\ =& \frac{\alpha'}{a_I}\left(\frac{z^2}{2} - z\right) + \frac{1}{a_I}(\alpha' - n')\frac{Ra}{Pe^*}\int_o^z dz\int_1^z \theta d\xi + \frac{b\beta_t'}{a_I}\int_o^z \theta dz \end{aligned} \tag{7.5.16}$$

In the case of isothermal consolidation, $\theta = 0$ and $Ra = b = 0$ and they reduce to

$$\theta = 0, \quad p_{iso}(z) = z - 1, \quad w_{iso}(z) = \frac{\alpha'}{a_I}\left(\frac{z^2}{2} - z\right) \tag{7.5.17}$$

so that the excessive pore pressure and the medium deformation are linear and quadratic in z respectively.

The steady state temperature depends only on the Peclét number Pe^* and not Ra. It follows from (7.5.14) that

$$\frac{\partial\theta}{\partial z} = 1 + \frac{Pe^*}{m'}\frac{e^{-Pe^* z/m'}}{e^{-Pe^*/m'} - 1}, \quad \frac{\partial^2\theta}{\partial z^2} = -\left(\frac{Pe^*}{m'}\right)^2 \frac{e^{-Pe^* z/m'}}{e^{-Pe^*/m'} - 1} \tag{7.5.18}$$

Since $\theta(0) = \theta(1) = 0$ and $\partial\theta/\partial z(z = 0) < 0$, $\partial^2\theta/\partial z^2 > 0$, the temperature variation from the initial state is always negative in the medium. This is intuitively true because the initial temperature decreases with z and the downward flow has the effect of moving relatively cold fluid to warmer region. It is clearly seen that θ is strongly affected by Pe^* in (7.5.14). In accordance with temperature variation, the difference in the pressure between the thermoconsolidation and the isothermal consolidation, which is the last part in brackets in (7.5.15), is always positive. If the Rayleigh number is large, it may overwhelm $p_{iso}(z)$ and the pressure even becomes positive as will be shown later. Physically this thermal effect on the pressure is due to the buoyancy that fluid experiences which is produced by the relative cooling as compared to the initial state thereby produces sinking of fluid when the pumping rate at the bottom remains the same.

The solid displacement is affected by thermal changes through not only the buoyancy but also thermal stress. The second term in (7.5.16) represents the buoyancy effects on the displacement. This contribution is from the buoyancy effects in

both the fluid through the pressure and the solid skeleton through the body force. It depends on the sign of the coefficient $(\alpha' - n')$. Since the integral expression $\int_o^z dz \int_1^z \theta d\xi$ is positive, it is positive if $\alpha' > n'$ and negative if $\alpha' < n'$. Specifically in the present case, we have $\alpha' > n'$ and the net effect is the decrease of the vertical compaction as compared to the isothermal case. Recall that buoyancy is the consequence of small density variation due to temperature change in the fluid. In the present case, θ is negative and the fluid contracts. This creates positive fluid pressure in the medium relative to the isothermal case i.e., less pressure drop, thereby causing relative expansion of the porous medium. This effect is accounted for by the coefficient α'. On the other hand, the slight increase in fluid density, the second part denoted with $-n'$, induces downward buoyant force in the porous medium and thus increase in the body force which implies more compaction. All together in the present case, the buoyancy effects due to negative θ tend to decrease the vertival compaction in the medium. The thermal stress effect, the last term in (7.5.16), is obvious. Negative θ causes thermal contraction of the solid skeleton and thus contributes more compaction to the soil layer. We also note that $\int_1^z \theta d\xi$ is positive maximum near the bottom $z = 0$ whereas the magnitude of $\int_o^z \theta dz$ is minimum there. Therefore, when the buoyancy effect which is signified by the ratio Ra/Pe^* is strong, the vertical displacement in thermoconsolidation can be less in the lower part and more in the upper part than the isothermal case.

Transient Evolution of Reference State. Results for the reference state of $Pe^* = Ra = b = T_c/T_d = 1$ are plotted against time at different depths in Fig.7.4. Vertical variations at discrete times are shown in Fig.7.5. Also shown are those for the isothermal consolidation with the same pumping rate in dotted curves. At $t = 0$ the pumping starts at the uniform rate of $Pe^* = 1$. This causes the pressure to decreases at the bottom. For small time the pressure is confined to near the lower surface. Since the consolidation equation (7.5.3) is a diffusion equation for p, the negative pore pressure then gradually diffuses upwards and finally becomes nearly linear in z as shown in Fig.7.5. Time variation of p in Fig.7.4 is mild and follows quite similar pattern for the isothermal case. The pressure drop is less in thermoconsolidation

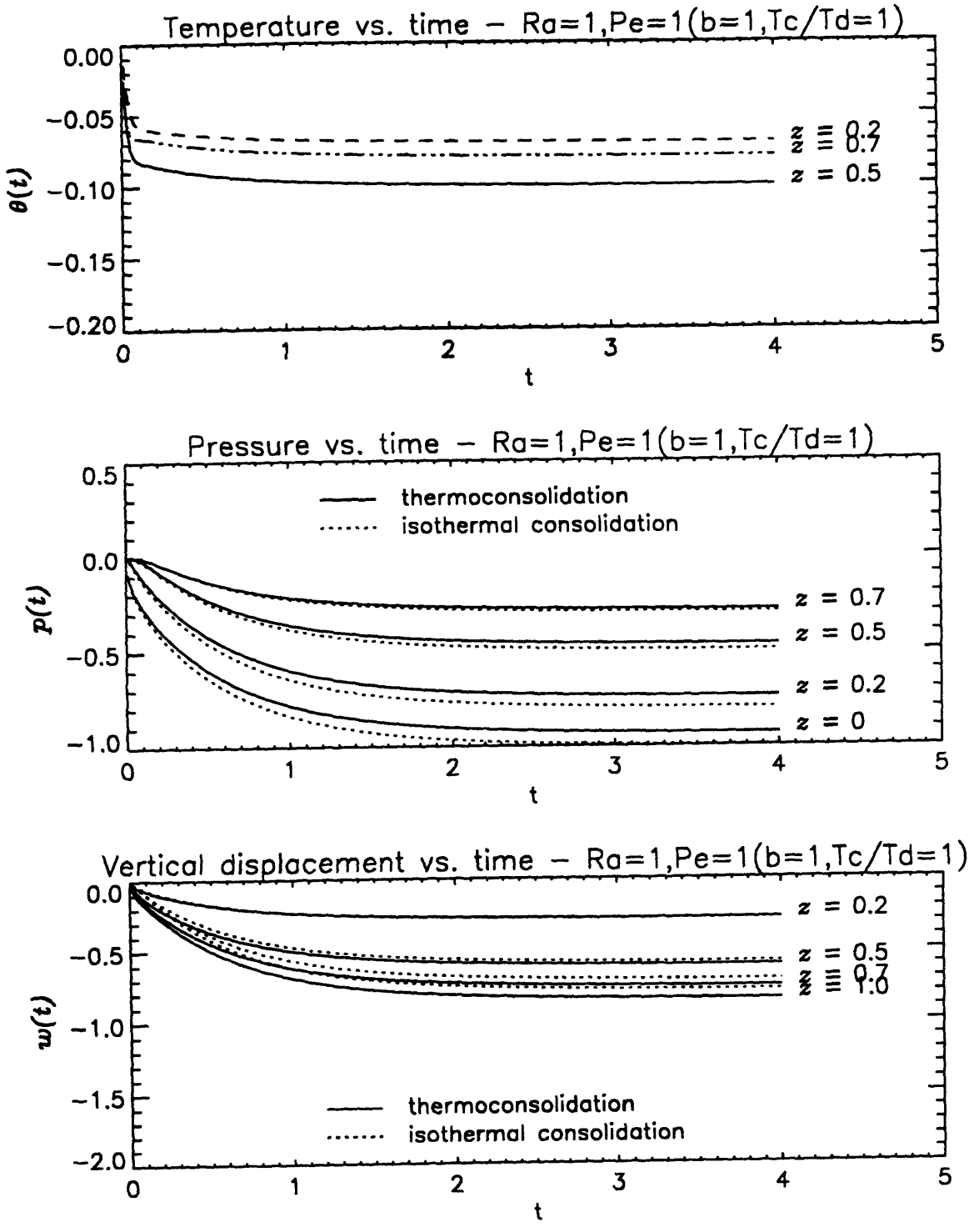

Fig. 7.4 Time variations of the temperature θ, pressure p and vertical displacement w at different depths for the reference state with $Ra = 1$, $Pe^* = 1$, $b = 1$ and $T_c/T_d = 1$.

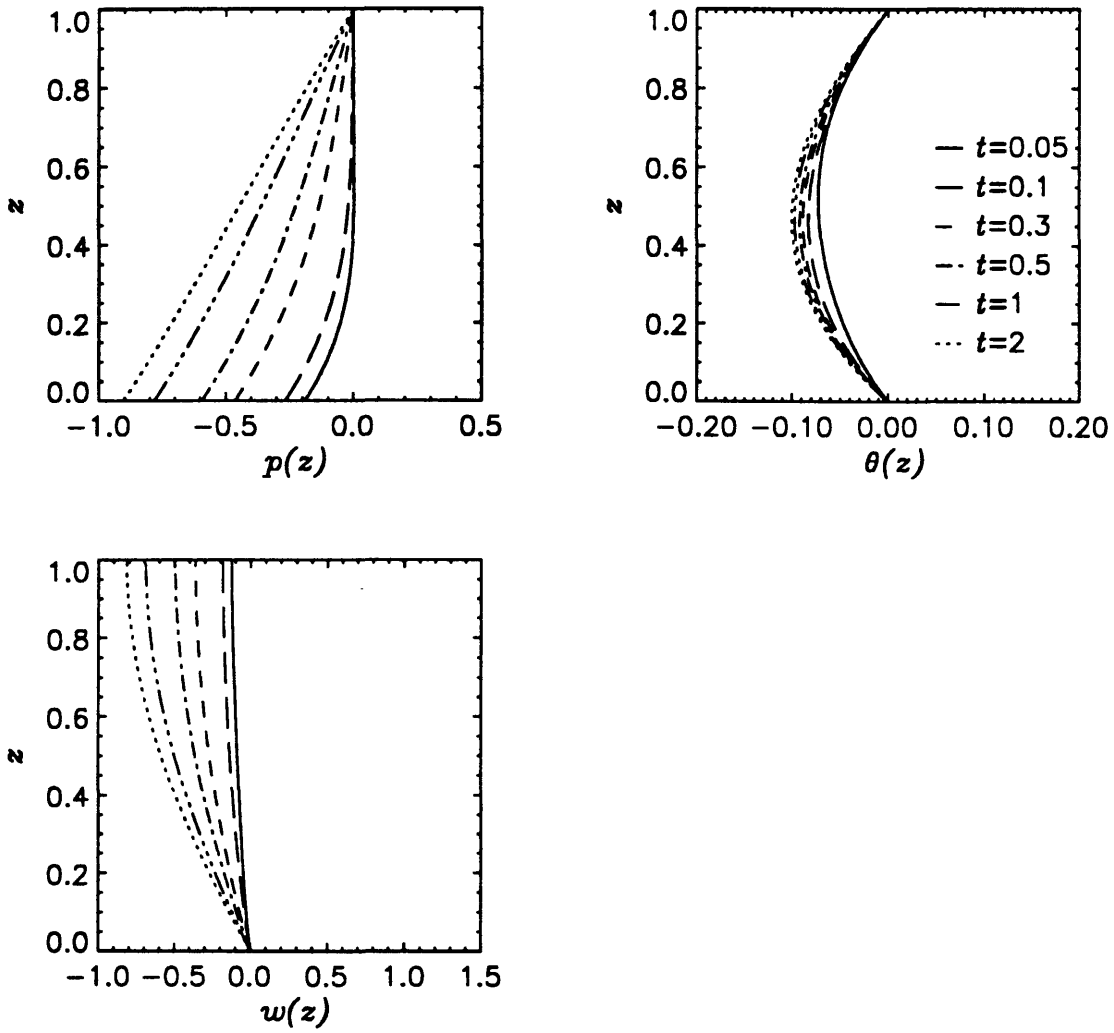

Fig. 7.5 Depth variations of p, θ and w at discrete times for the reference state.

for the reason explained above in the analysis of steady state. The temperature variation with time is entirely different. It drops very quickly in the early time and then slowly approaches the steady state. The impulsive change over $0 < t < 0.1$ is due to the time varying source term U in (7.5.4). This is essentially the effect of convection (by both fluid and solid) due to pumping. The value of U is large negative for small time due to the enhanced convection by downward solid velocity and approaches to -1 as t increases. The slow variation which comes after the early stage is by the mild variation of $\partial p/\partial z$ and $\partial w/\partial t$. As t becomes large, θ goes to -0.07, -0.1, -0.08 respectively at $z = 0.2, 0.5, 0.7$, i.e. the steady state values from (7.5.14) with $m' = 1.22$ of (7.4.5). Because of the fixed temperature at $z = 0$ and 1, the maximum departure θ occurs at an intermediate depth. For the reference state ($Pe^* = 1$), we find from (7.5.18) after setting $\partial\theta/\partial z = 0$, the location of peak is at $z = 0.466$ which is shown in the vertical variation of θ in Fig.7.5. We note that, for the present case of mild pumping rate, the temperature deviation is only 10% of the initial temperature difference across the depth. The vertical displacement also varies mildly but because of the accumulated effect of thermal stress the magnitude of w becomes greater as z increases.

We now examine the effects of varying the parameters $Ra(K)$ and $Pe^*(U)$ according to Cases (i) and (ii) of §7.4.

Case (i). Keeping the pumping rate at the same value $Pe^* = 1$, the Rayleigh number is increased to 10, 20 and 30 from the reference state as summarized in (7.4.9). In addition to the comparison of the thermoconsolidation with the isothermal consolidation, the effects of the nonlinear coupling among p, w and θ are discussed by comparing with rigid medium for the case of $Ra = 30$. Since the medium becomes more and more permeable, the pressure diffuses more easily through the medidum. Accordingly Ra and the thermal stress to pore pressure ratio b increase by the same amount but the time scale ratio decreases(cf.(7.4.6)). Significantly increased buoyancy effects are expected to prevail.

The results for $Ra = b = 10$ and $T_c/T_d = 0.1$ are shown in Figs. 7.6 and 7.7 for temporal and vertical variations respectively. We first note that time variations in Fig.7.6 are much faster for both thermoconsolidation and isothermal case due to the decrease in T_c. As a result, the steady state is reached quickly after $t = 0.1$,i.e. the convection velocity U of (7.5.5) becomes -1, the same value as for the rigid medium.

The governing equations are nonlinearly coupled via the convection velocity U and such coupling effect will be most pronounced before U reaches its steady state value, that is over the interval $0 < t < 0.1$. For the heat equation, that effect is in the increased convection as compared to the reference state and $\theta(t)$ remains constant after $t = 0.1$. The steady state θ is the same as in the reference state because it only depends on one parameter Pe^*. The pressure variation is very different. At the early time it decreases in response to the pumping. But, as the buoyancy effect promptly dominates, the decreasing trend is weakened and the pressure reaches its steady state value quickly. Note that, although θ is only -0.1, the Rayleigh number is large and the product is nearly -1. The difference between thermoconsolidation and isothermal case is quite substantial. Because of this increased buoyancy, the pressure gradient in the mid-depth region (Fig.7.7) is small implying that the downward seepage flow is dominantly from the sinking of cool fluid. The vertical displacement also reflects increased effects of buoyancy and thermal stress explained earlier. At $z = 0.2$, it is less than the isothermal consolidation. But the subsidence at $z = 1$ is almost as twice large due mostly to thermal contraction of the matrix.

In Figs. 7.8 and 7.9, plots are made for $Ra = b = 20$ and $T_c/T_d = 0.05$. The nonlinear effects are now more pronounced for small time so that both θ and w bounce back after $t = 0.1$. Note that the pressure even becomes positive in the lower half region of the layer due to strong buoyancy effect. Its vertical variation in Fig.7.9 is in reverse trend to the reference state except at $z = 0$ and $z = 1$ where $\partial p/\partial z$ is maintained at unity to be consistent with the uniform pumping. The vertical

displacement is clearly less than the isothermal case in the lower region ($z < 0.2$) due to the increased buoyancy ($Ra/Pe^* = 20$) and increases sharply with z, as shown in Fig.7.9, because of the increased thermal stress effect($b = 20$). The subsidence at the top is more than twice as large as the isothermal case. We particularly note the swelling of the medium, which is the consequence of nonlinear coupling which is overwhelmed soon by buoyancy. This will be explained for $Ra = 30$ in connection with θ and p.

Finally, Ra and b are further increased to 30 and $T_c/T_d = 0.0333$. More prevailing effects of buoyancy and thermal stress are observed in Fig.7.10 and 7.11. In order to show the nonlinear coupling effects, computation has also been performed for rigid medium for which the consolidation equation and the heat transport are decoupled as shown in §7.5.1. The results θ and p for rigid medium are shown in Fig. 7.10. Notice that, due to increased heat convection, θ and p develop more quickly. They overshoot beyond and bounce back to the steady state. The vertical displacement reaches its maximum values and then swelling follows as the nonlinear coupling effect dies out. In the rigid medium, the convection velocity is constant $U = -1$ as mentioned in §7.5.1 and there is no coupled effect in the heat equation (7.5.11) but the pressure is coupled in linear fashion to the temperature via buoyancy in the consolidation equation. They approach smoothly to steady state. The difference in the pressure and vertical displacement between thermoconsolidation and isothermal case are similar to those with $Ra = 20$. The settlement at the top is more than three times larger than the isothermal case.

It has been shown in Case (i) that, as the Rayleigh number increases for fixed pumping rate, the pore pressure and medium deformation are strongly affected by the buoyancy and the thermal stress. The pressure can develop to positive levels due to buoyancy and the deformation increases considerably due to thermal stress effect. Moreover, as the consequence of nonlinear coupling among the pressure, vertical displacement and temperature, the medium swells up after rapid compaction in the early time.

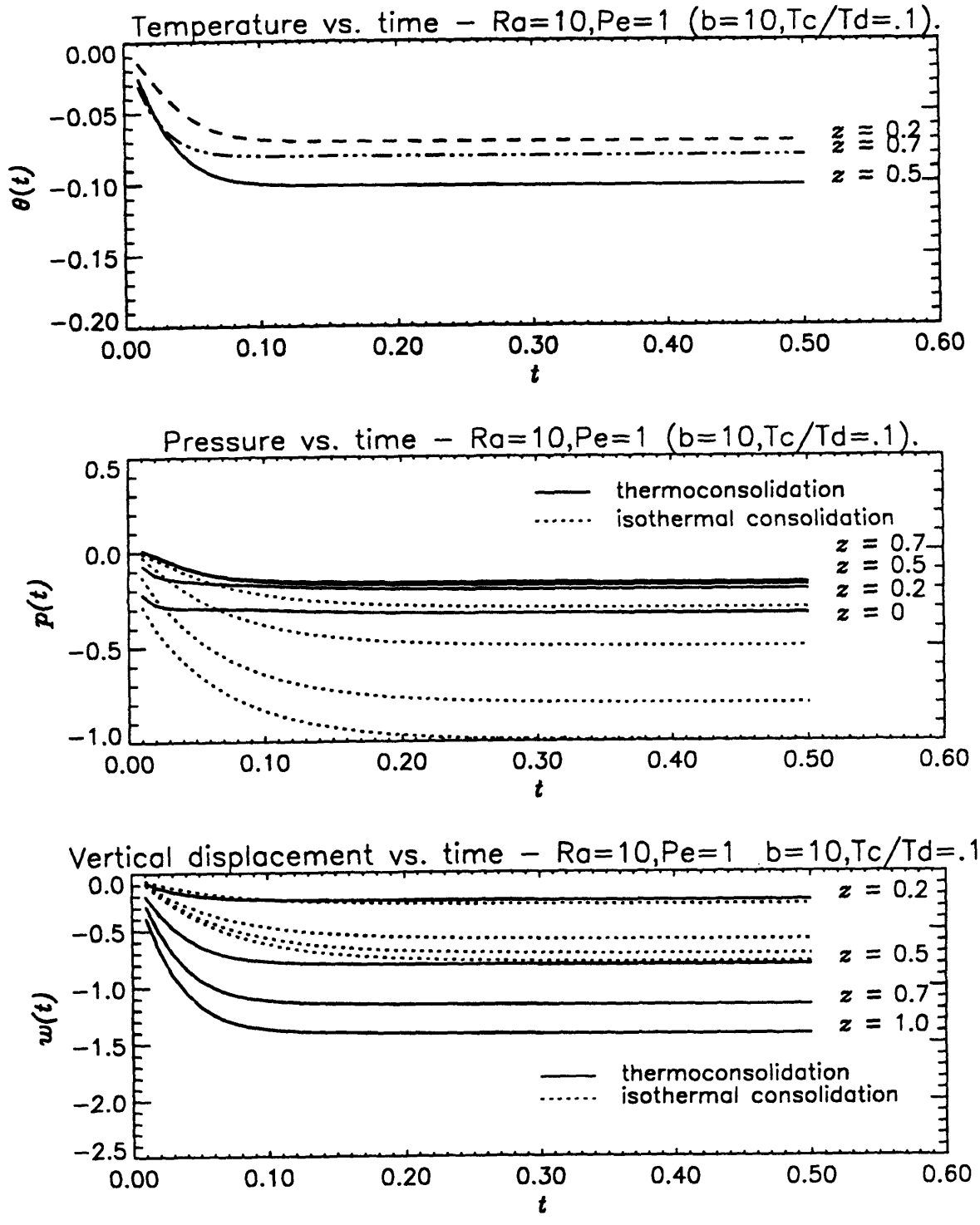

Fig. 7.6 Time variations of the temperature θ, pressure p and vertical displacement w at different depths with $Ra = 10$, $Pe^* = 1$, $b = 10$ and $T_c/T_d = 0.1$.

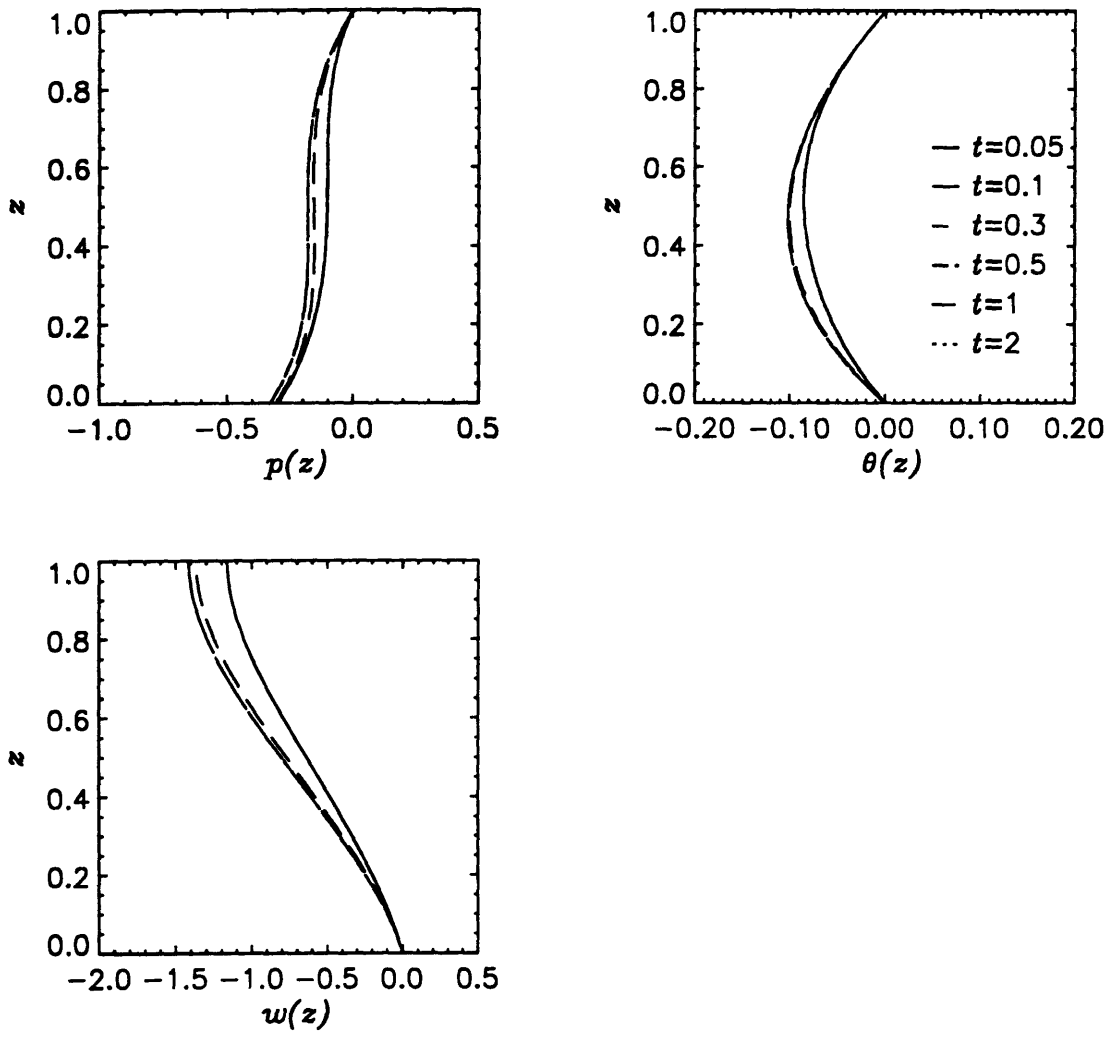

Fig. 7.7 Depth variations of p, θ and w at discrete times for with $Ra = 10$, $Pe^* = 1$, $b = 10$ and $T_c/T_d = 0.1$.

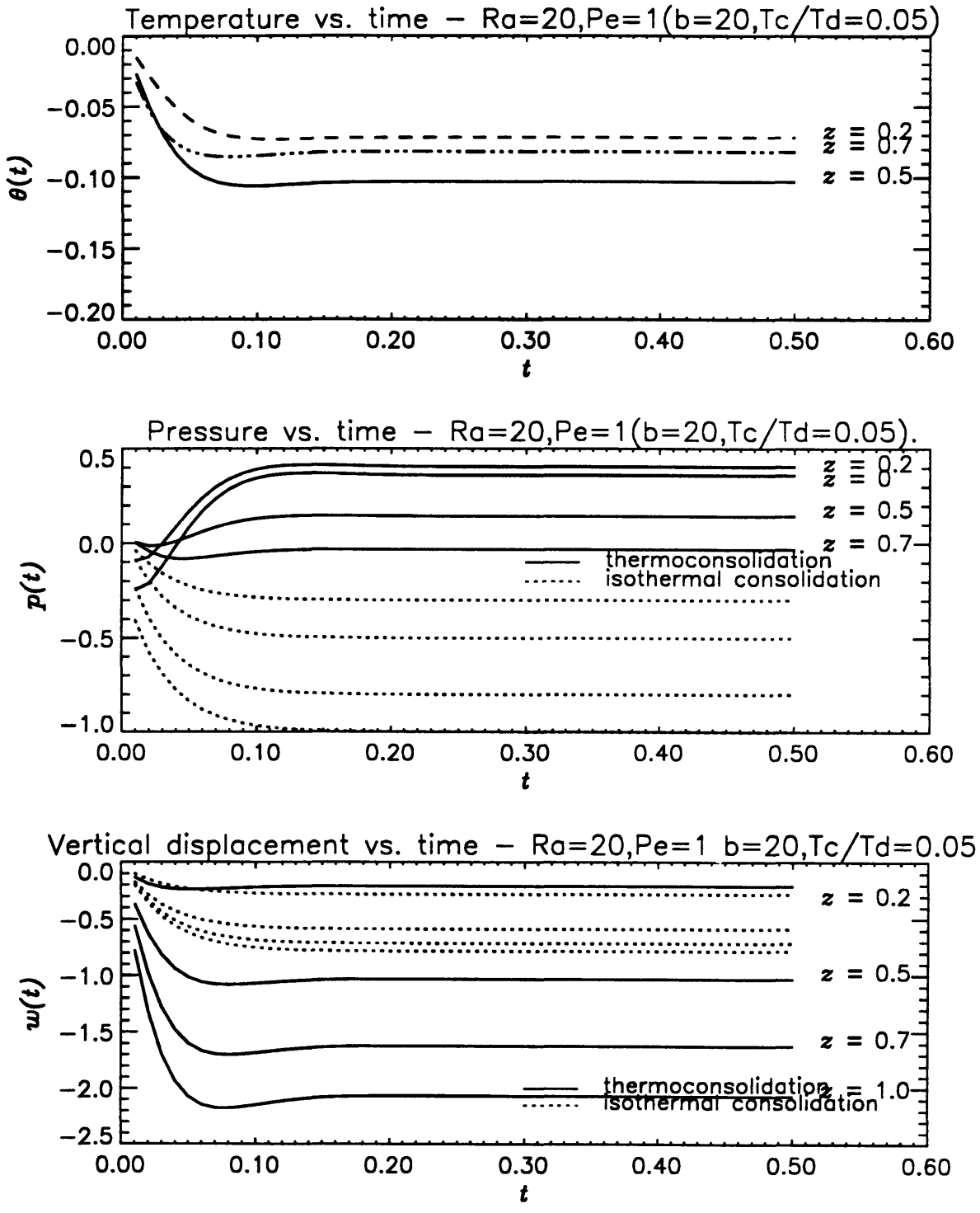

Fig. 7.8 Time variations of the temperature θ, pressure p and vertical displacement w at different depths with $Ra = 20$, $Pe^* = 1$, $b = 20$ and $T_c/T_d = 0.05$.

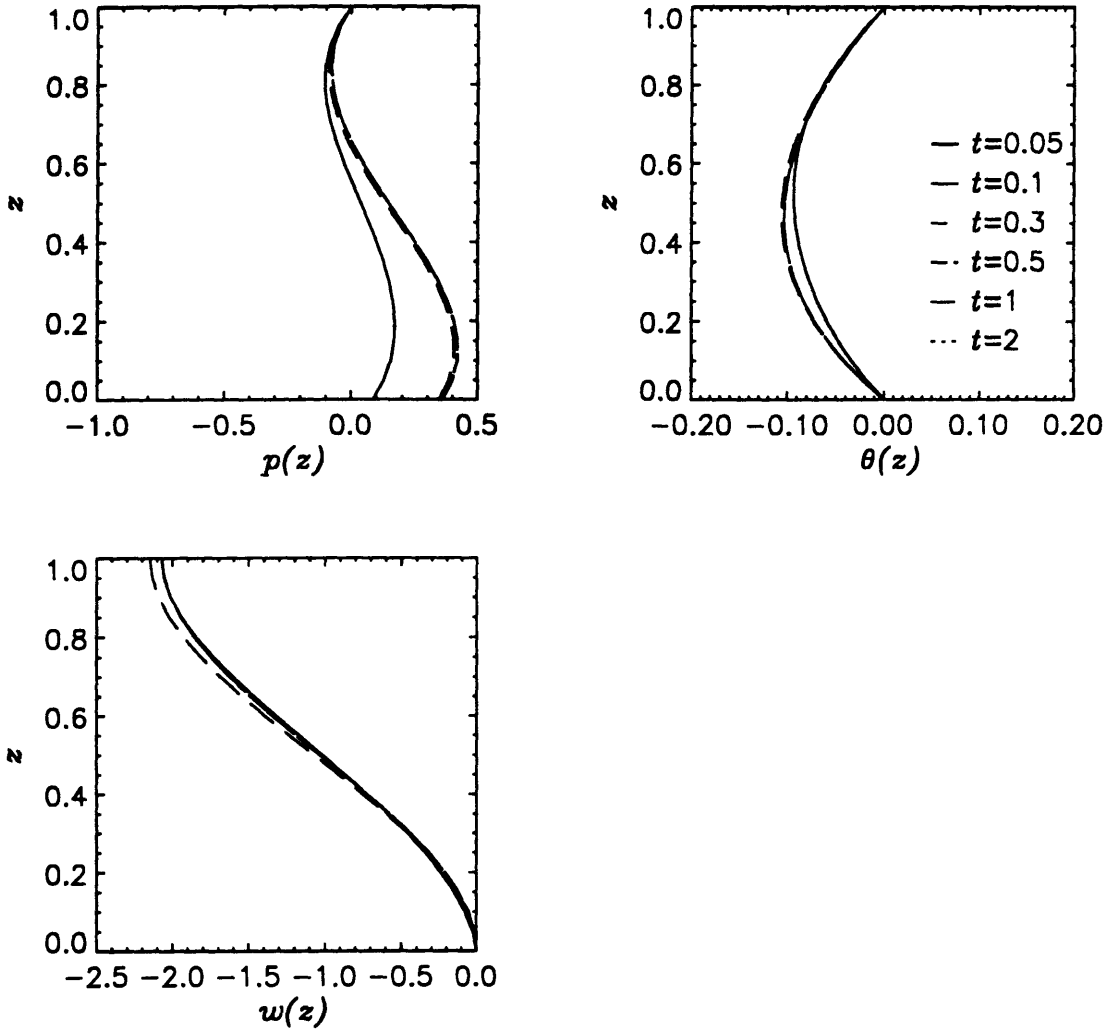

Fig. 7.9 Depth variations of p, θ and w at discrete times for with $Ra = 20$, $Pe^* = 1$, $b = 20$ and $T_c/T_d = 0.05$.

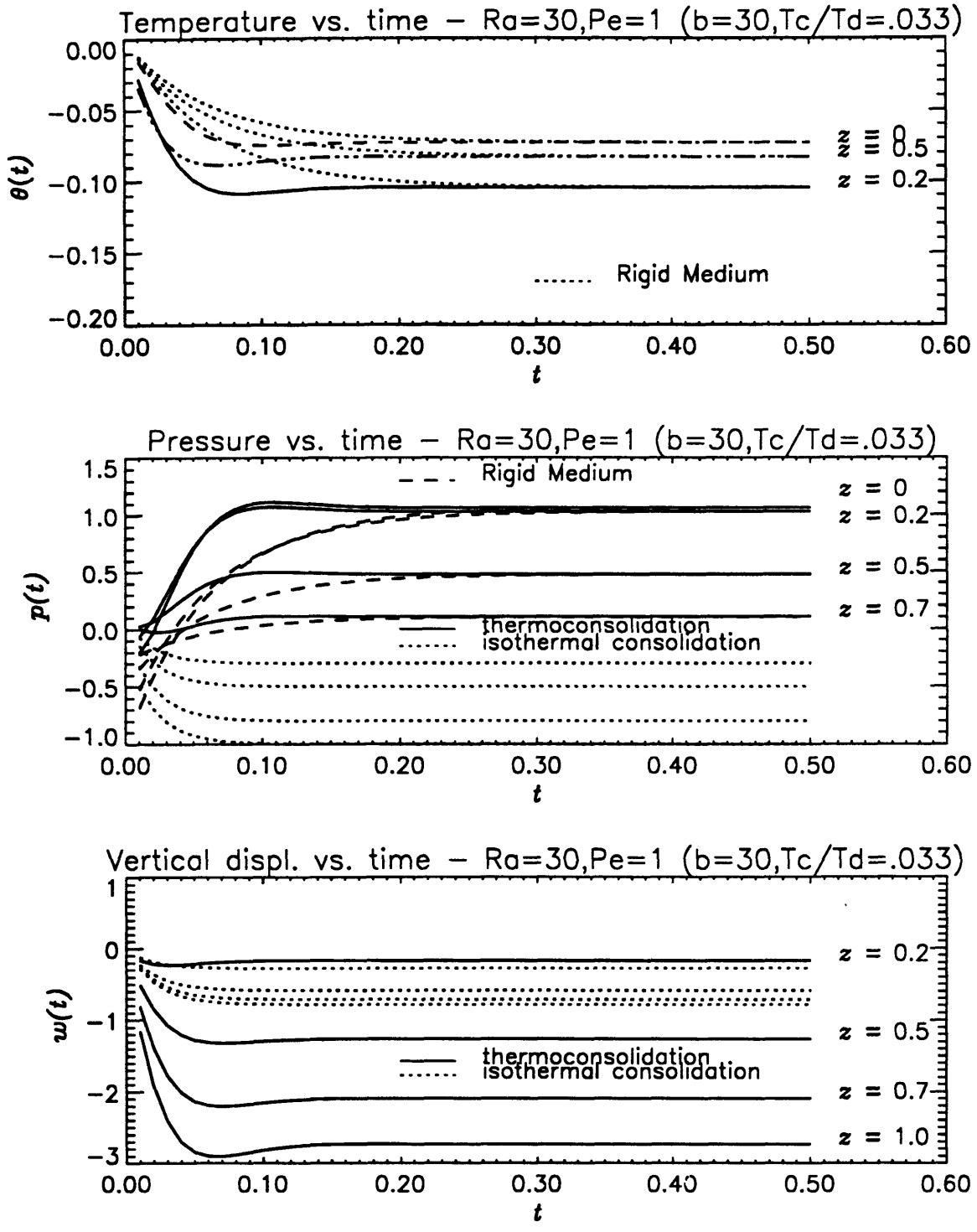

Fig. 7.10 Time variations of the temperature θ, pressure p and vertical displacement w at different depths with $Ra = 30$, $Pe^* = 1$, $b = 30$ and $T_c/T_d = 0.0333$.

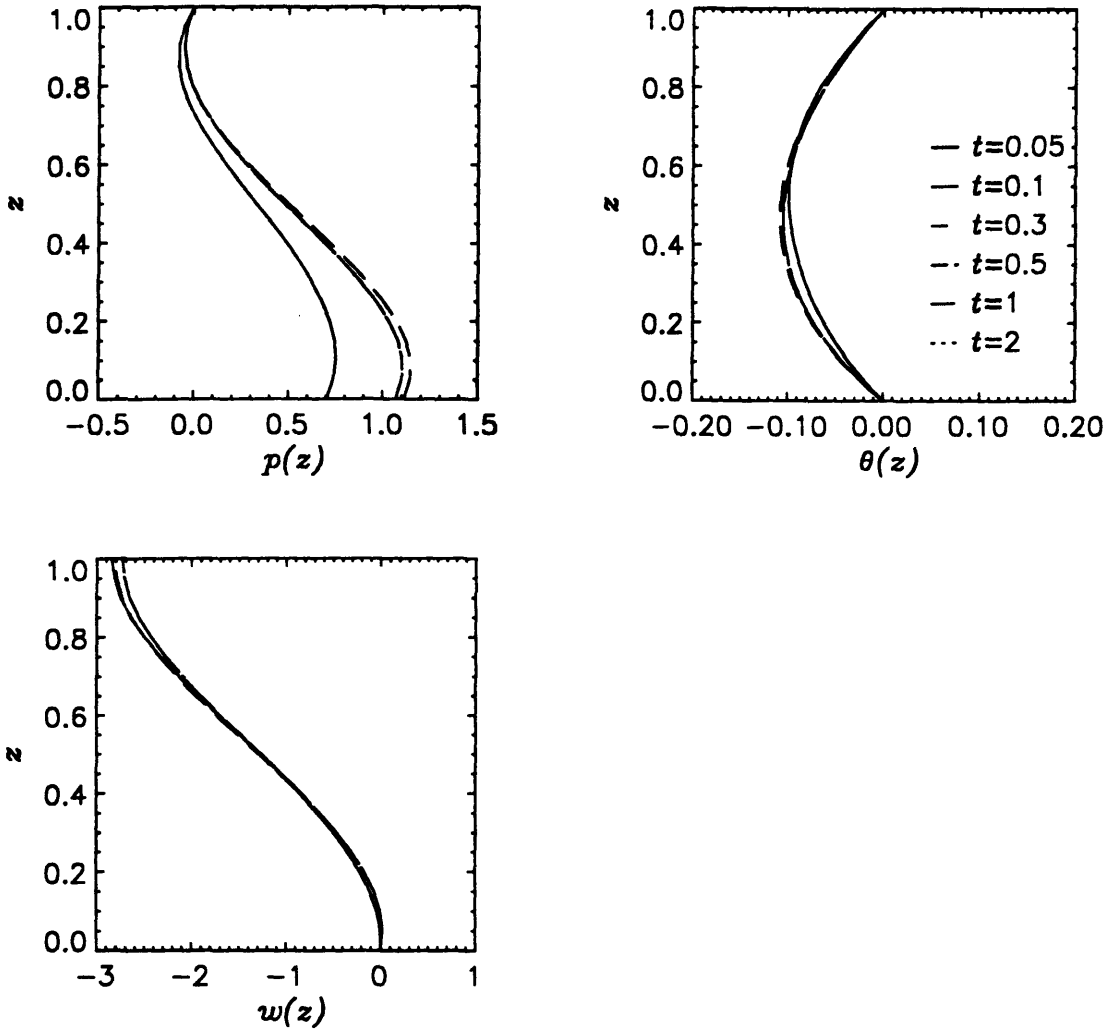

Fig. 7.11 Depth variations of p, θ and w at discrete times for with $Ra = 30$, $Pe^* = 1$, $b = 30$ and $T_c/T_d = 0.0333$.

Case (ii). The hydraulic conductivity is now held fixed and the pumping rate (U) is changed according to (7.4.10). In order to have appreciable buoyancy effect, the Rayleigh number is fixed at the value $Ra = 10$ increased from the reference state.

The case of $Pe^* = 0.1$ and $b = 100$ is plotted in Fig.7.12 for time variations. Since the Peclét number is small, the temperature variation is small too(cf.(7.5.14)). But the ratio Ra/Pe^*100 which signifies the buoyancy in the consolidation eqautiopn (7.5.2) is large and it is shown that the pressure distribution strongly reflects the buoyancy. As in Case (i), the vertical displacement shows the buoyancy and thermal stress effects in the lower and upper regions respectively.

When Pe^* is increased to 5, Fig.7.13, the temperature variation also increases to the level of about 40% of the initial temperature difference. In response to the increase in Pe^*, the peak of θ moves downward from the central region. Due to the decrease in Ra/Pe^*, the reduced buoyancy effects are observed and a tendency of approaching to isothermal case is shown. Since b is decreased while Pe^* is increased, terms $b\beta_t'\theta$ and $n'Ra/Pe^*\theta$ do not change much as $|\theta|$ increases. Thus $w(t)$ variation is not very different from that for $Pe^* = 0.1$ except that the buoyancy effect on w is reduced so that the vertical compaction is greater than the isothermal case throughout the depth.

In Fig.7.14, the Peclét number is increased to 10. In addition to larger temperature variation (60% of the initial difference), the peak has moved down further. From (7.5.18), the location is calulated to be at $z = 0.26$ so that $\partial\theta/\partial z$ is very steep in the region close to the bottom. Although the two cases $Pe^* = 5$ and $Pe^* = 10$ show similar responses, the actual physical variations are larger for larger Peclét number because of the normalization in (7.2.1).

In summary, the primary effect of increasing Pe^* is therefore the increase in temperature deviation. But the effects of buoyancy on the pressure and the vertical displacement are relatively reduced as Pe^* increases. The pressure variation stays on the negative side and the compaction is affected mostly by thermal stress.

Therefore, increased Pe^* tend to decrease both the buoyancy effect and the nonlinear coupling effect in the medium response.

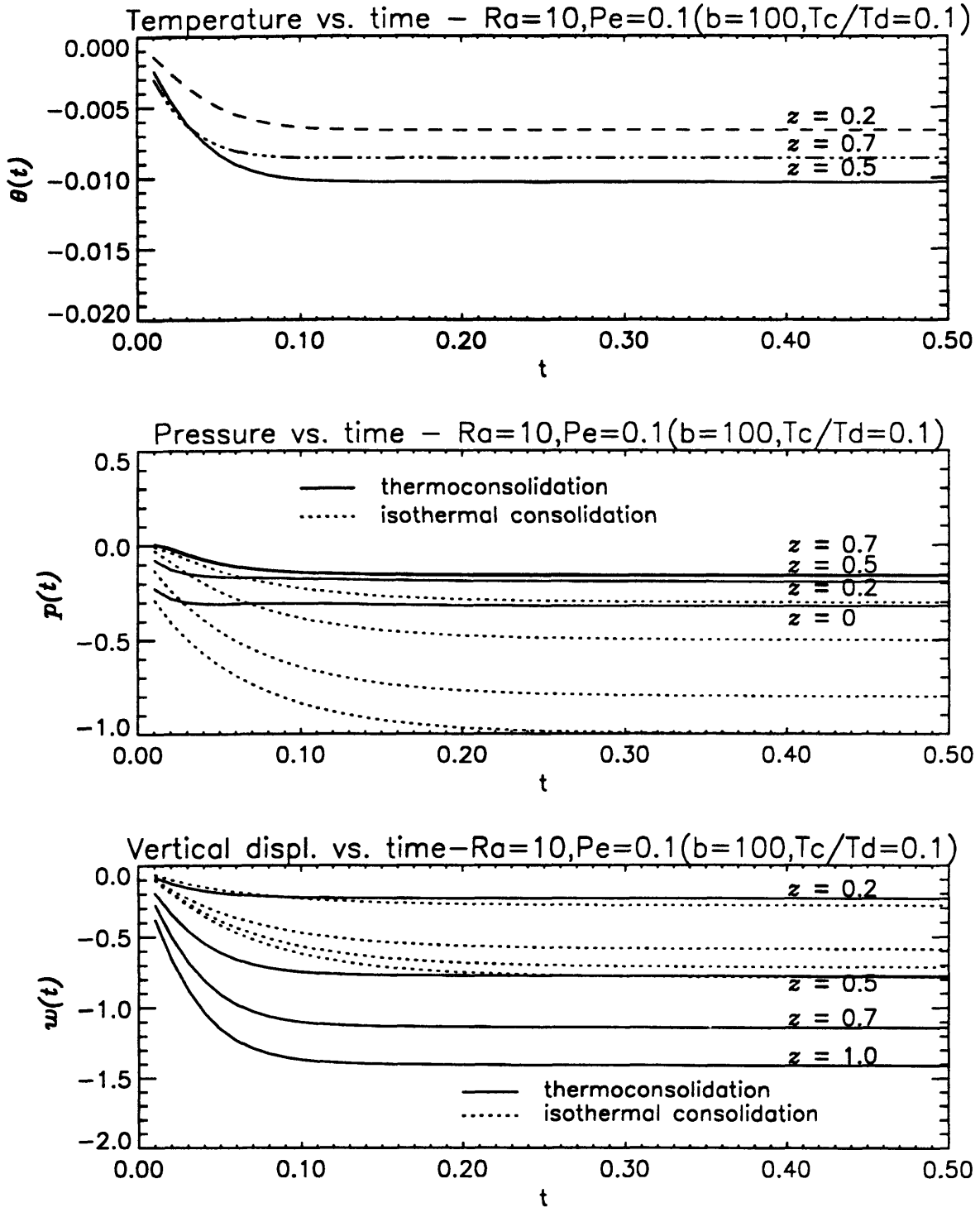

Fig. 7.12 Time variations of the temperature θ, pressure p and vertical displacement w at different depths with $Ra = 10$, $Pe^* = 0.1$, $b = 100$ and $T_c/T_d = 0.1$.

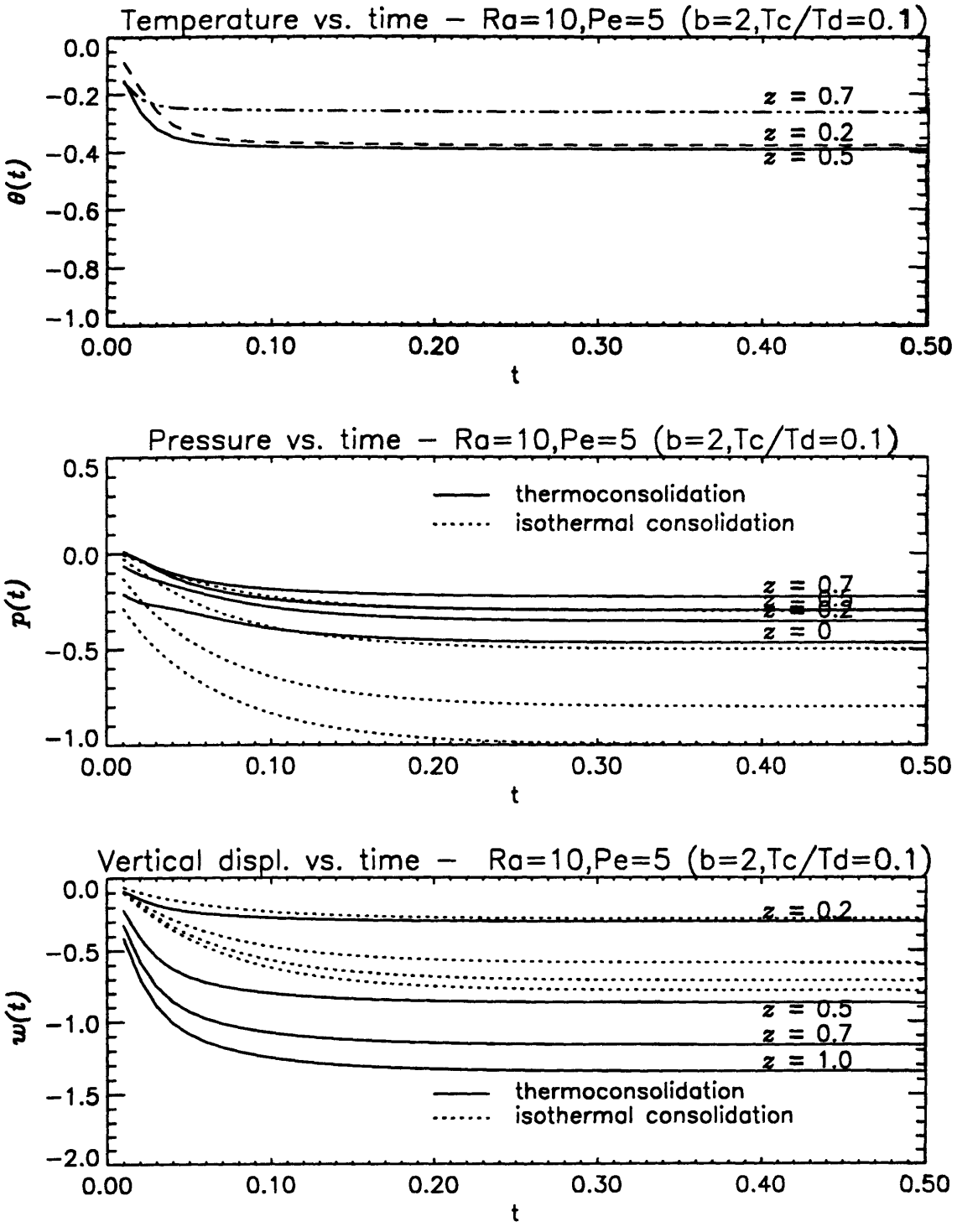

Fig. 7.13 Time variations of the temperature θ, pressure p and vertical displacement w at different depths with $Ra = 10$, $Pe^* = 5$, $b = 2$ and $T_c/T_d = 0.1$.

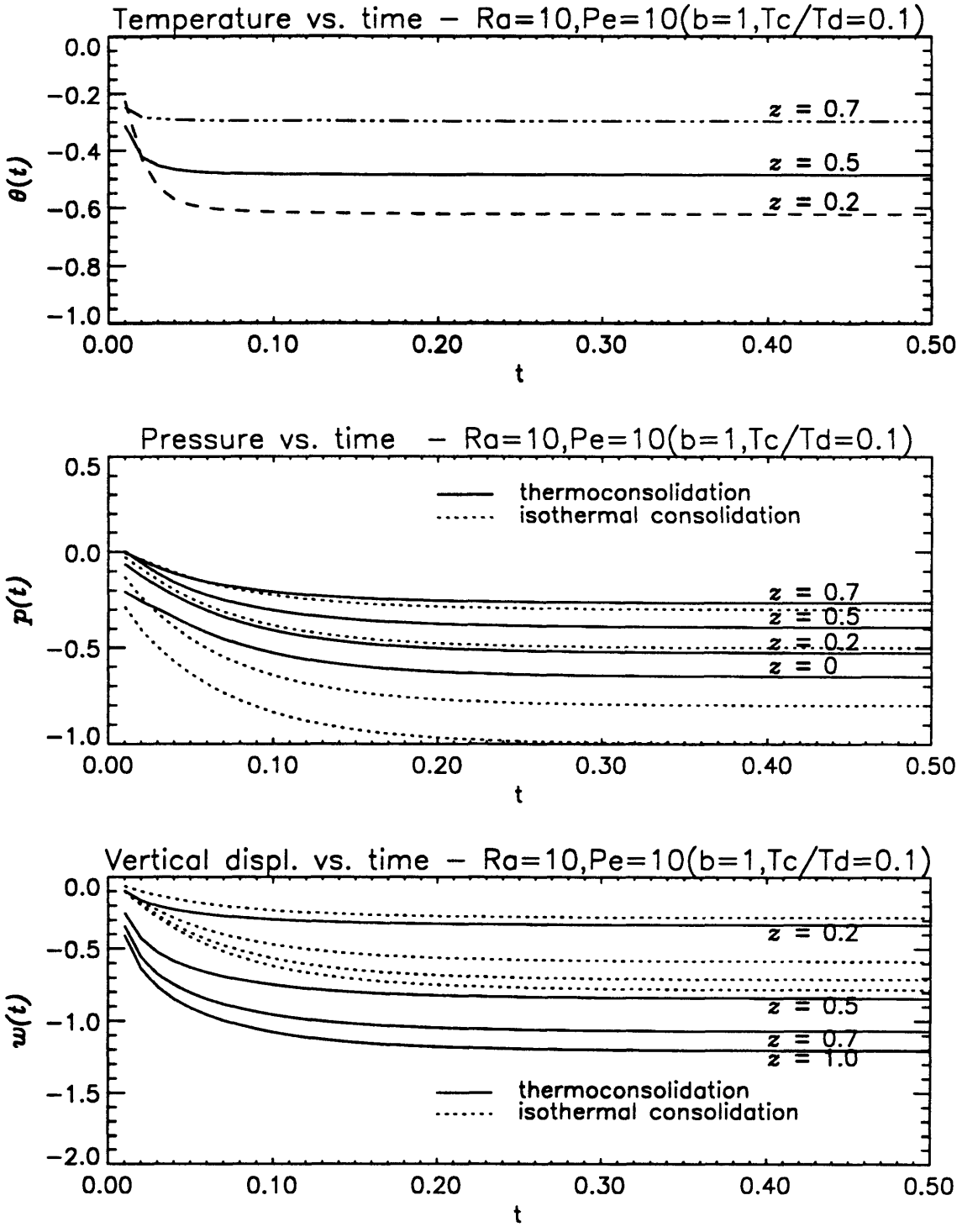

Fig. 7.14 Time variations of the temperature θ, pressure p and vertical displacement w at different depths with $Ra = 10$, $Pe^* = 10$, $b = 1$ and $T_c/T_d = 0.1$.

7.6 Two-dimensional Thermoconsolidation due to Pumping from a Narrow Sink at the Bottom.

The computed results for two-dimensional consolidation (Fig.7.2) are presented. As in the one-dimensional case of §7.5, the reference state ($Ra = Pe^* = b = T_c/T_d = 1$) is first considered. Then the numerical results for Case (i) in which the hydraulic conductivity K is varied with fixed pumping rate are discussed. In Case (ii), the effects of varying the pumping rate with K fixed are examined for one Ra value selected from Case (i). It is shown that, in the two-dimensional case, the critical Rayleigh number is less than the one-dimensional case due to nonlinear coupling through heat convection so that the cellular convection occurs at Rayleigh numbers lower than the value in (7.4.8). The governing equations and the boundary conditions have been summarized in §7.2.

7.6.1 Effects of Spatial Discretization.

In order to check that the numerical scheme gives sufficiently convergent results as the spatial discretization becomes smaller, several test runs have been made. The dimensionless parameters were chosen to be $Pe^* = 1$, $Ra = 5$, $b = 5$ and $T_c/T_d = 0.2$

In Fig.7.15(a) the horizontal variation of $\theta(x, z = 0.5)$, $p(x, z = 0)$ and $w(x, z = 1)$ at discrete times are shown for two different vertical spacings $\Delta z = 0.1$ and $\Delta z = 0.05$. The horizontal extent is $\xi_N = 2$ in the logarithmic coordinate of (7.3.1) which is equivalent to $x_N = 6.4$. The difference is negligibly small. Similarly, the effect of decreasing $\Delta\xi$ has been tested for $\Delta\xi = 0.05$ and $\Delta\xi = 0.04286$ with $x_N = 4.5$ and the results are shown in Fig.7.15(b) for the same variables. Again the difference is small. Also, to examine the effect of truncating the infinite horizontal extent at finite value of x_N, the two values of $x_N = 4.5$ and $x_N = 6.4$ were used with $\Delta z = 0.1$ and $\Delta\xi = 0.05$(Fig.7.15(c)). It is seen that $x_N = 4.5$ is large enough to replace the infinite horizontal domain and ensure satisfactory convergence.

Based on these test results, $\Delta\xi = 0.05$, $\Delta z = 0.1$ and $x_N = 4.5$ will be used in the subsequent calculations.

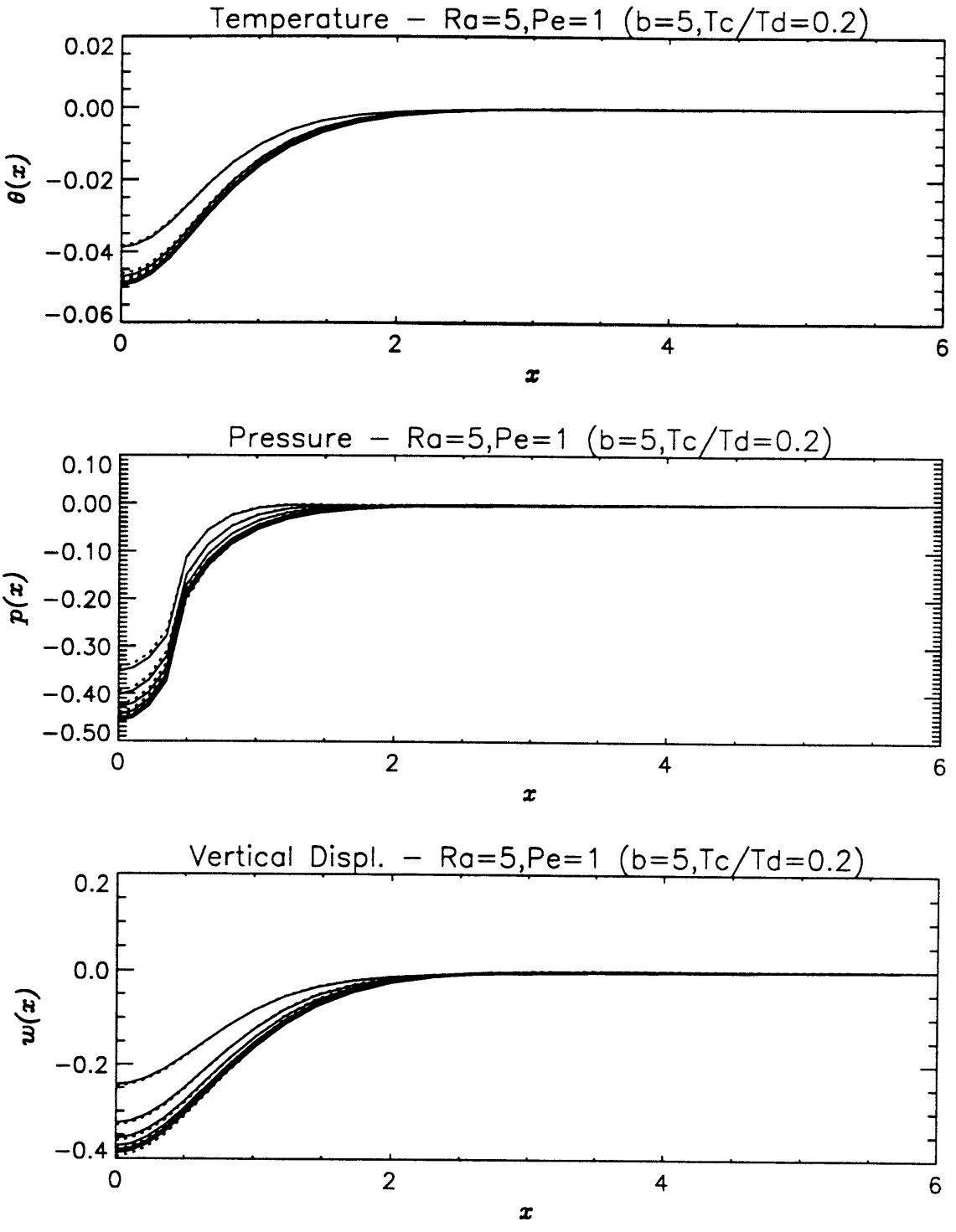

Fig. 7.15(a) Comparison of numerical solutions for $\Delta z = 0.1$ (solid line) and $\Delta z = 0.05$ (dotted line) with $\Delta\xi = 0.1$ and $x_N = 6.4$. The parameters are $Ra = 5$, $Pe^* = 1$, $b = 5$ and $T_c/T_d = 0.2$.

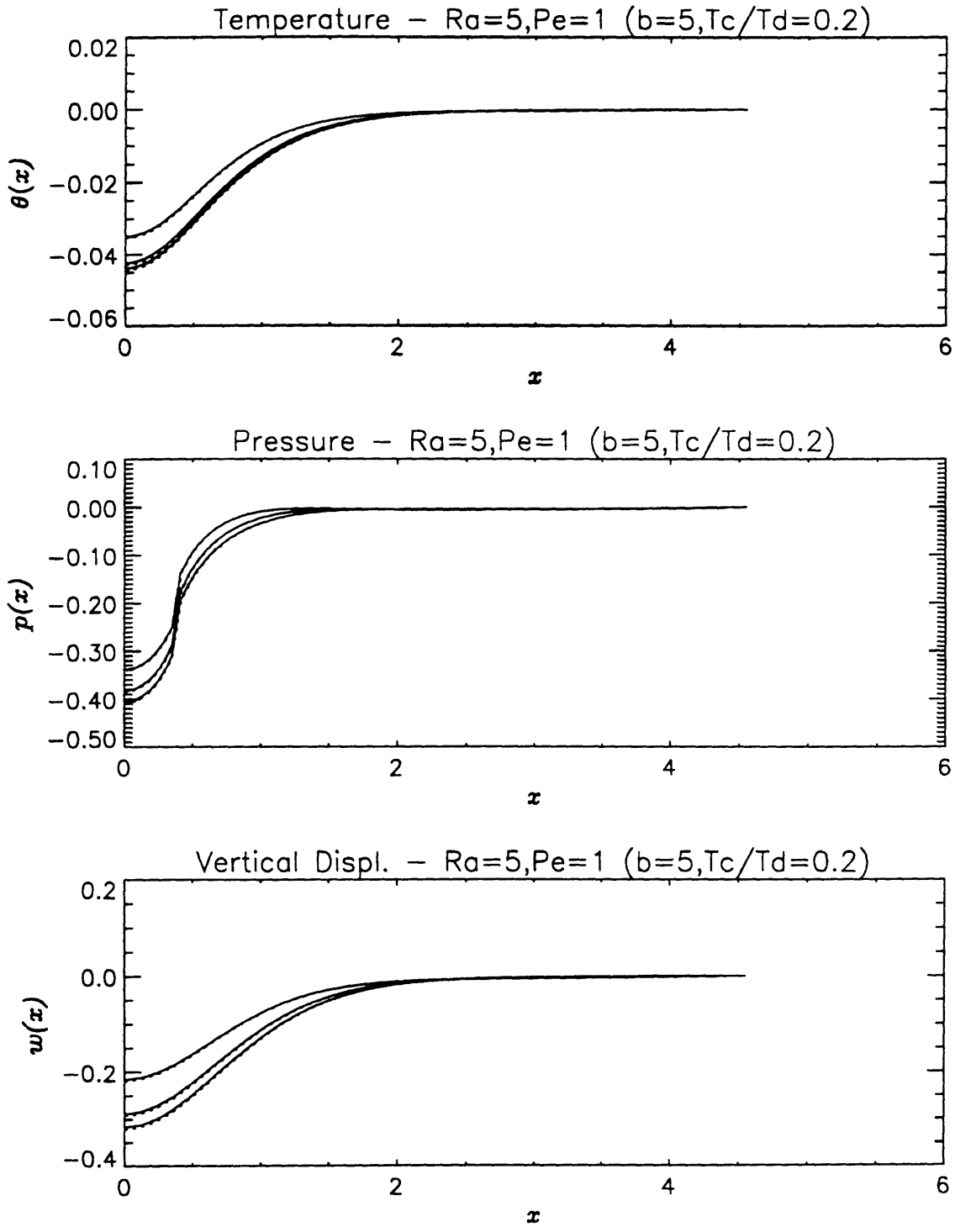

Fig. 7.15(b) Comparison of numerical solutions for $\Delta\xi = 0.0429$ (solid line) and $\Delta\xi = 0.05$ (dotted line) with $\Delta z = 0.1$ and $x_N = 4.5$. For parameters see the caption of Fig. 7.15(a).

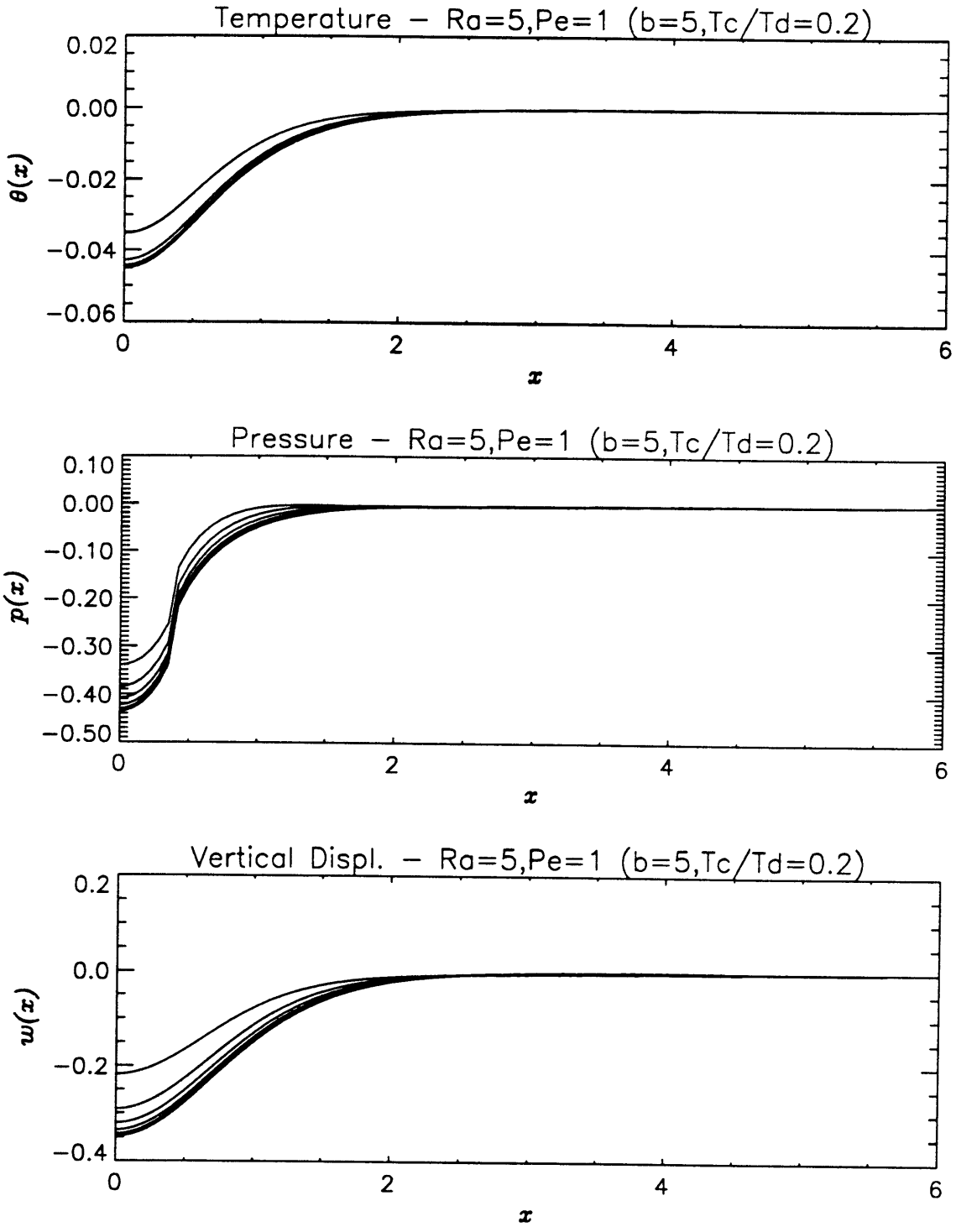

Fig. 7.15(c) Comparison of numerical solutions for $x_N = 6.4$ (solid line) and $x_N = 4.5$ (dotted line) with $\Delta\xi = 0.05$ and $\Delta z = 0.1$ For parameters see the caption of Fig. 7.15(a).

7.6.2 Numerical Results and Discussions.

The numerical results are discussed in the order of the reference state, Case (i) and Case (ii).

7.6.2.1 The Reference State.

For $Pe^* = Ra = b = T_c/T_d = 1$, the numerical results for the pore pressure $p(x,z)$, the temperature $\theta(x,z)$ and the vertical and horizontal displacements $w(x,z)$ and $u(x,z)$ are shown in contour plots for $t = 0.01, 0.1, 0.3, 0.5$ and 1 in Fig.7.16(a)-(d). The horizontal distance for the figures is cut at $x = 2$. The half width of the sink at the bottom($z = 0$) is $x = 0.3$. In the early time, the negative pore pressure produced by the uniform extraction of fluid through the sink is confined to the very vicinity of the sink. As time increases, the pressure diffuses in both vertical and horizontal directions in the xz plane. The maximum pressure drop is about half of the one-dimensional case (cf. Fig.7.4) and occurs at $x = 0$ due to symmetry. Similarly the temperature variation is the largest at $x = 0$ and decreases as x increases. The vertical location of the peak is about at the mid-depth. The vertical displacement thus reaches its maximum at the plane $x = 0$ and decreases with x, but the horizontal displacement is zero at $x = 0$ and becomes maximum at some distance from the symmetry plane and at the top surface (Fig.7.16 (c) and (d)). The magnitude of the horizontal displacement is at most one-third of vertical displacement.

In Fig.7.17, the spatial distribution of the Darcy velocity $\langle u \rangle - n' \partial v/\partial t$ is shown for $t = 0.01, 0.1$ and 1. As it should be, the Darcy velocity is noticeable only just above the sink at $t = 0.01$ and the distribution spreads out as t increases. Consequently the recharge at $z = 1$ is over much larger distance along x and the recharge velocity is very small as compared with the pumping at the sink. From this we infer that the heat convection is mainly vertical in the near field above the sink as in the one-dimensional case and horizontal in the outer region. The vertical and time variations are similar to the one-dimensional case with decreasing magnitude as x increases. In Fig.7.18(a) and (b), the horizontal variation of w and u at $z = 1$

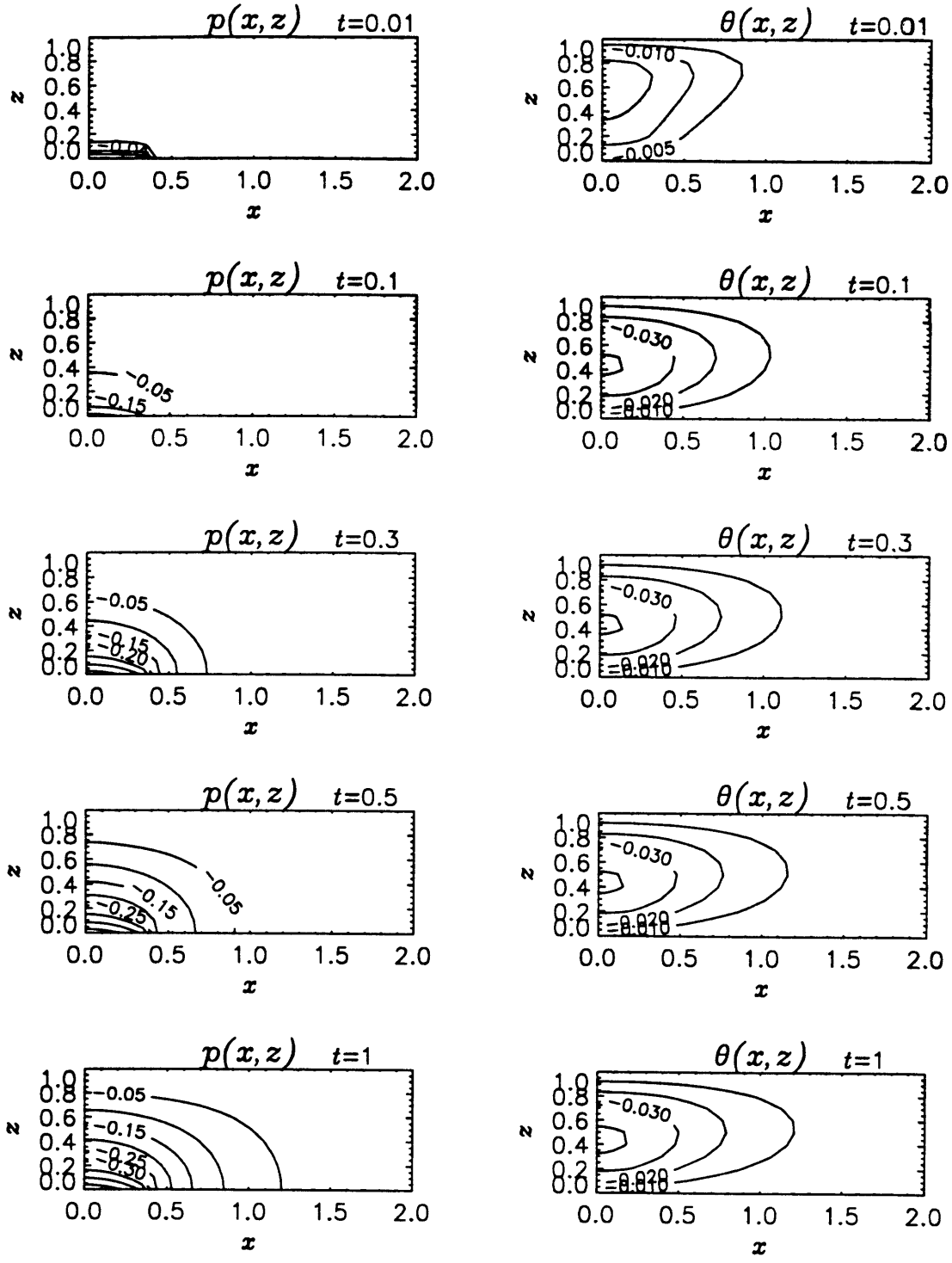

Fig. 7.16 Contour plots of (a) $p(x,z)$, (b) $\theta(x,z)$, (c) $w(x,z)$, and (d) $u(x,z)$ at discrete times for the reference state with $Ra = 1$, $Pe^* = 1$, $b = 1$ and $T_c/T_d = 1$.

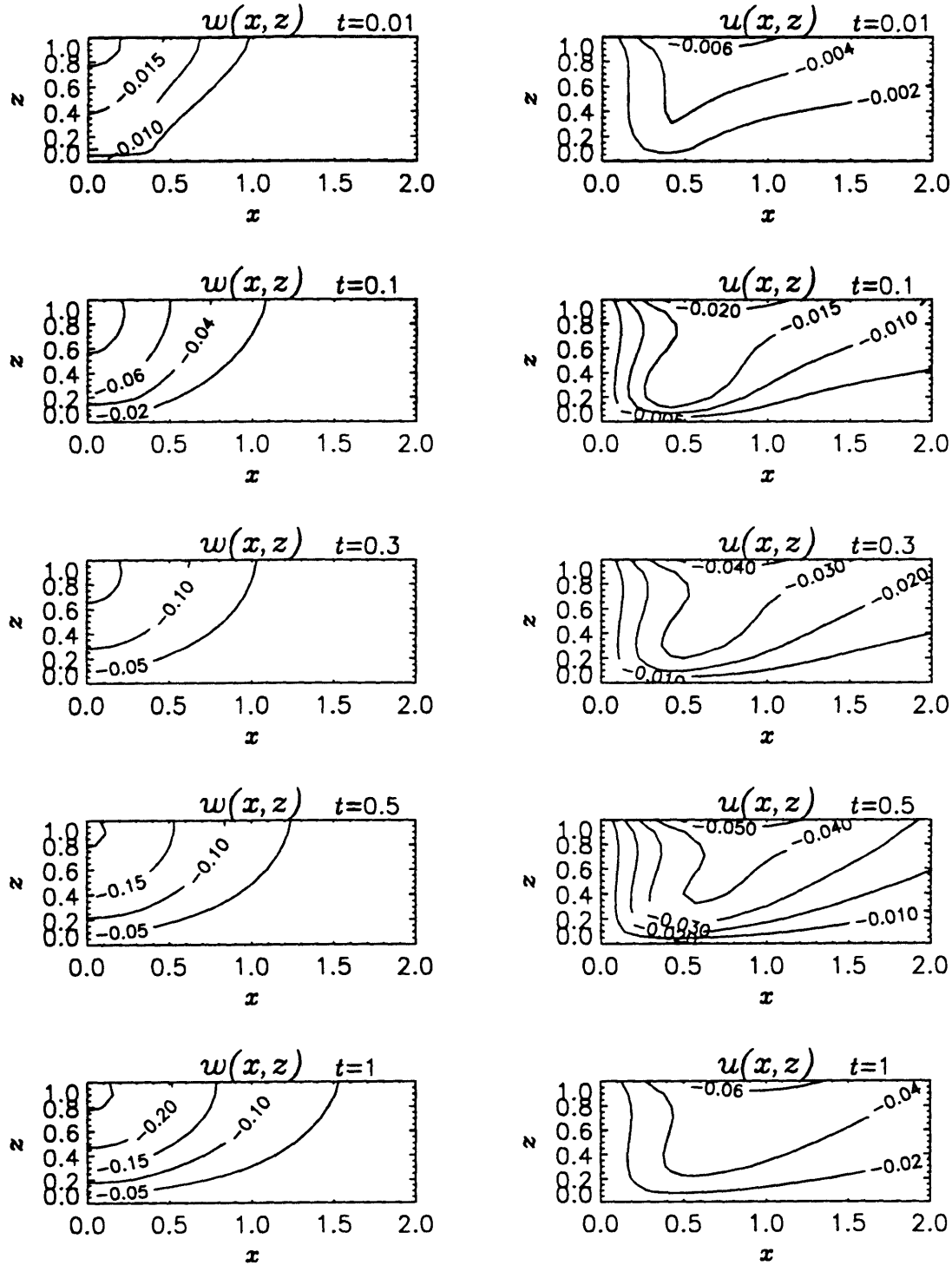

Fig. 7.16 (continued.)

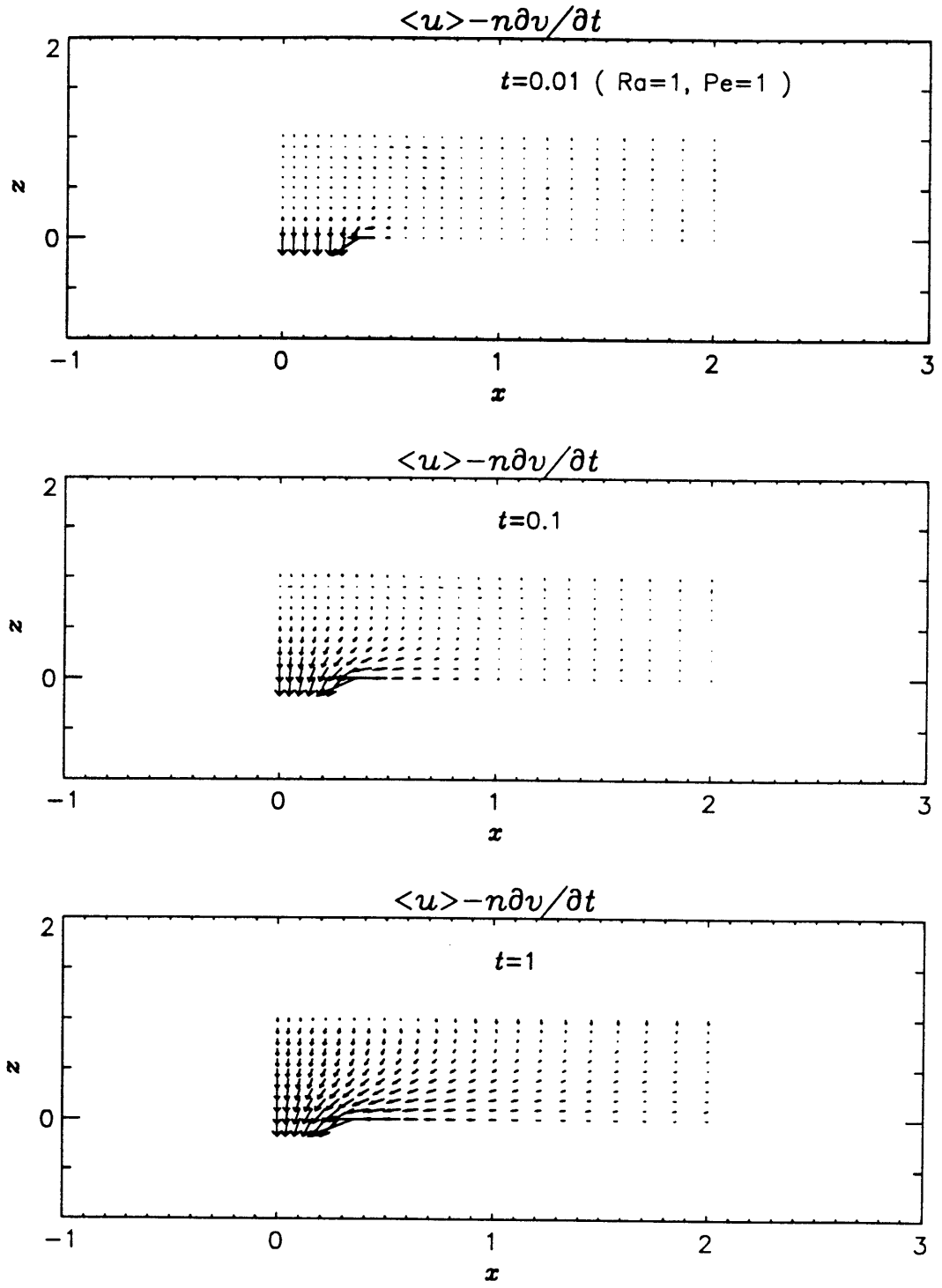

Fig. 7.17 Vector plot of Darcy velocity $\langle u \rangle - n'\partial v/\partial t$ at t=0.01, 0.1 and 1 for the reference state.

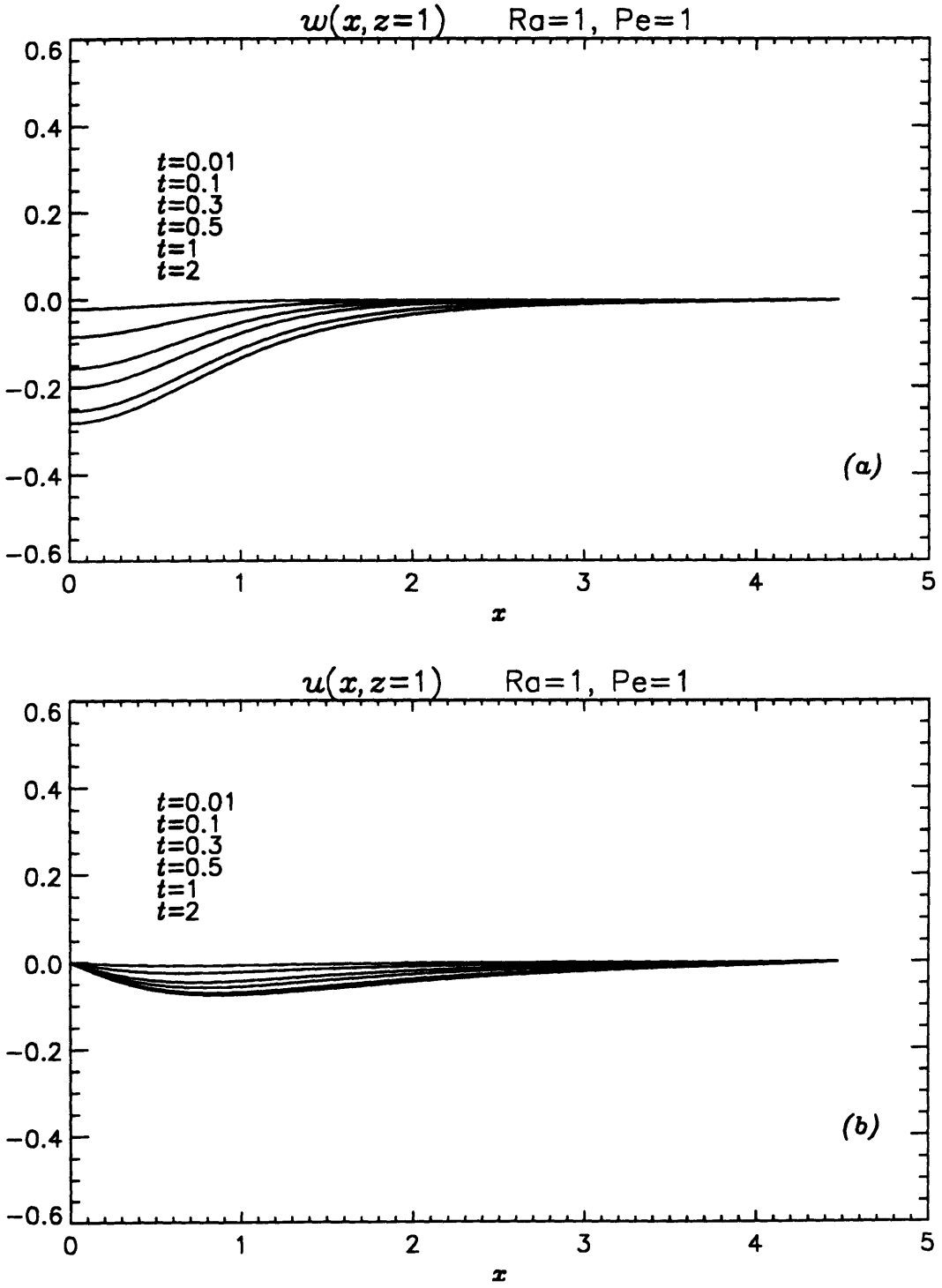

Fig. 7.18 Horizontal variation of (a) $w(x, z = 1)$ and (b) $u(x, z = 1)$ at discrete times for the reference state.

and discrete times are shown. The development of two-dimensional compaction bowl is clearly demonstrated.

7.6.2.2 Case (i) : The Effects of Ra with Fixed Pe^*.

The Rayleigh number is increased, as before, to 10, 20 and 30 while the Peclét number is fixed.

$\underline{Ra=10,\ Pe^* = 1}$ The results for $Ra = 10$ are shown in Fig.7.19(a) - (d) for p, θ, w and u. Due to the decrease in T_c/T_d, time variations are faster than the reference state. Recall from the analysis of one-dimensional thermoconsolidation that the buoyancy effect resulted in the decrease of the magnitude of pressure drop. This is also shown for two-dimensional case in Fig.7.19(a) and the magnitude is only one half of the reference state. The temperature distribution is similar to the reference state but the magnitude of fully-developed variation is larger, unlike in the one-dimensional case. This is due to the increased heat convection with large Rayleigh number in the buoyancy term in two-dimensional situation. In the one-dimensional case, it was determined only by the Peclét number. In accordance with increased effect of thermal stress, the vertical and horizontal displacements become larger. The horizontal equilibrium equation in (7.2.2) is affected by only the pore pressure and thermal stress not by buoyancy and therefore the increase in the horizontal displacement is greater than that in the vertical one as compared to the reference state everywhere in the soil layer. From Figs. 7.16 (c) and (d) and 7.19 (c) and (d), it is seen that the maximum of u has increased by a factor of 3 whereas it is about twice for w. The horizontal variations of w and u at $z = 1$ are plotted in Fig.7.20 (a) and (b). The increases in the depth of the compaction bowl and the magnitude of u from the reference state are clearly seen due to increased thermal stress effect.

The patterns of seepage flow and thermoconsolidation become very different from the previous cases if the Rayleigh number is further increased.

$\underline{Ra=20,\ Pe^* = 1}$ The pressure and temperature distributions for $Ra = 20$ are shown in Fig.7.21 (a) and (b). At $t = 0.01$, the spatial variations of p and θ are

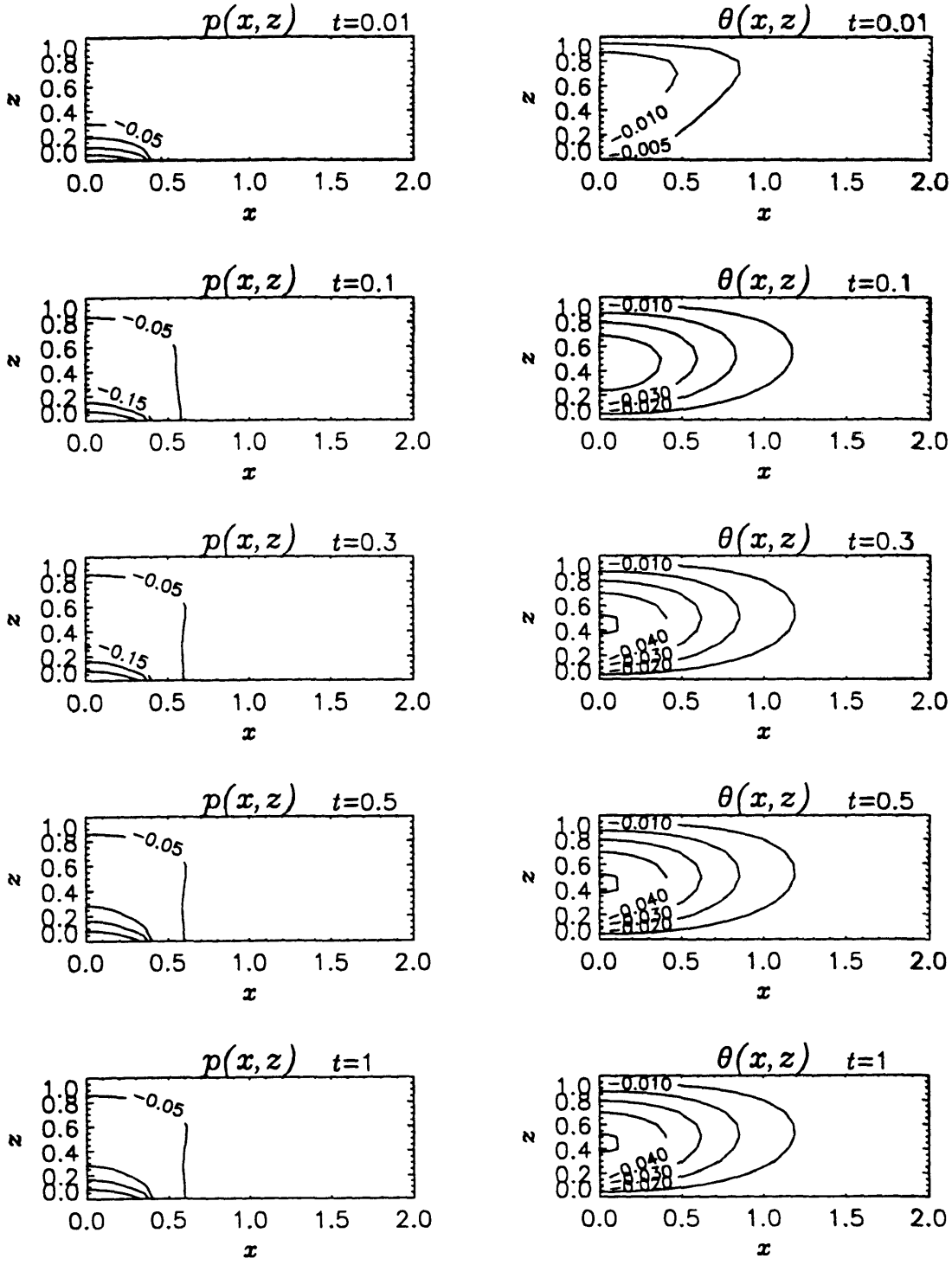

Fig. 7.19 Contour plots of (a) $p(x,z)$, (b) $\theta(x,z)$, (c) $w(x,z)$, and (d) $u(x,z)$ at discrete times for $Ra = 10$, $Pe^* = 1$, $b = 10$ and $T_c/T_d = 0.1$.

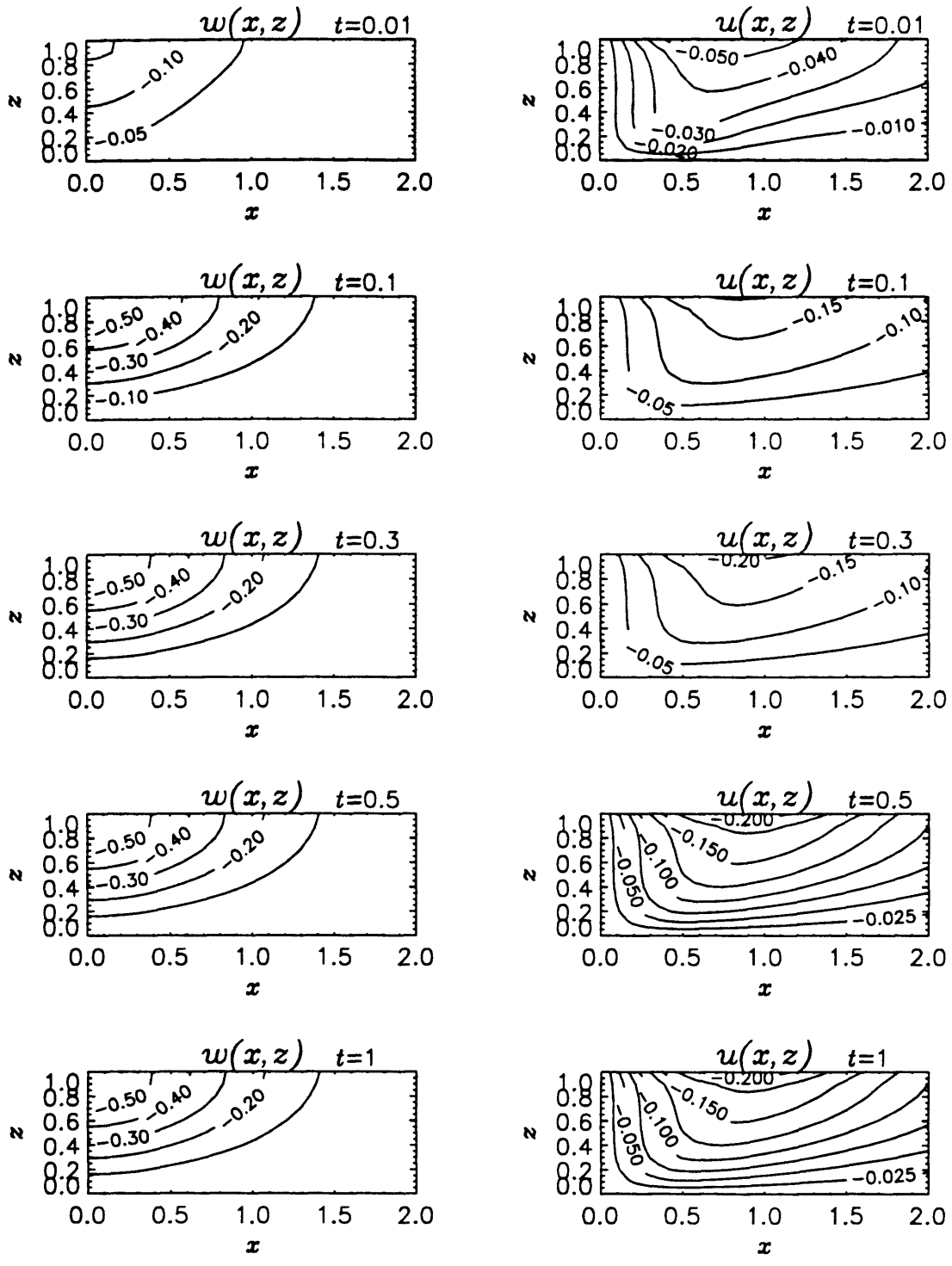

Fig. 7.19 (continued.)

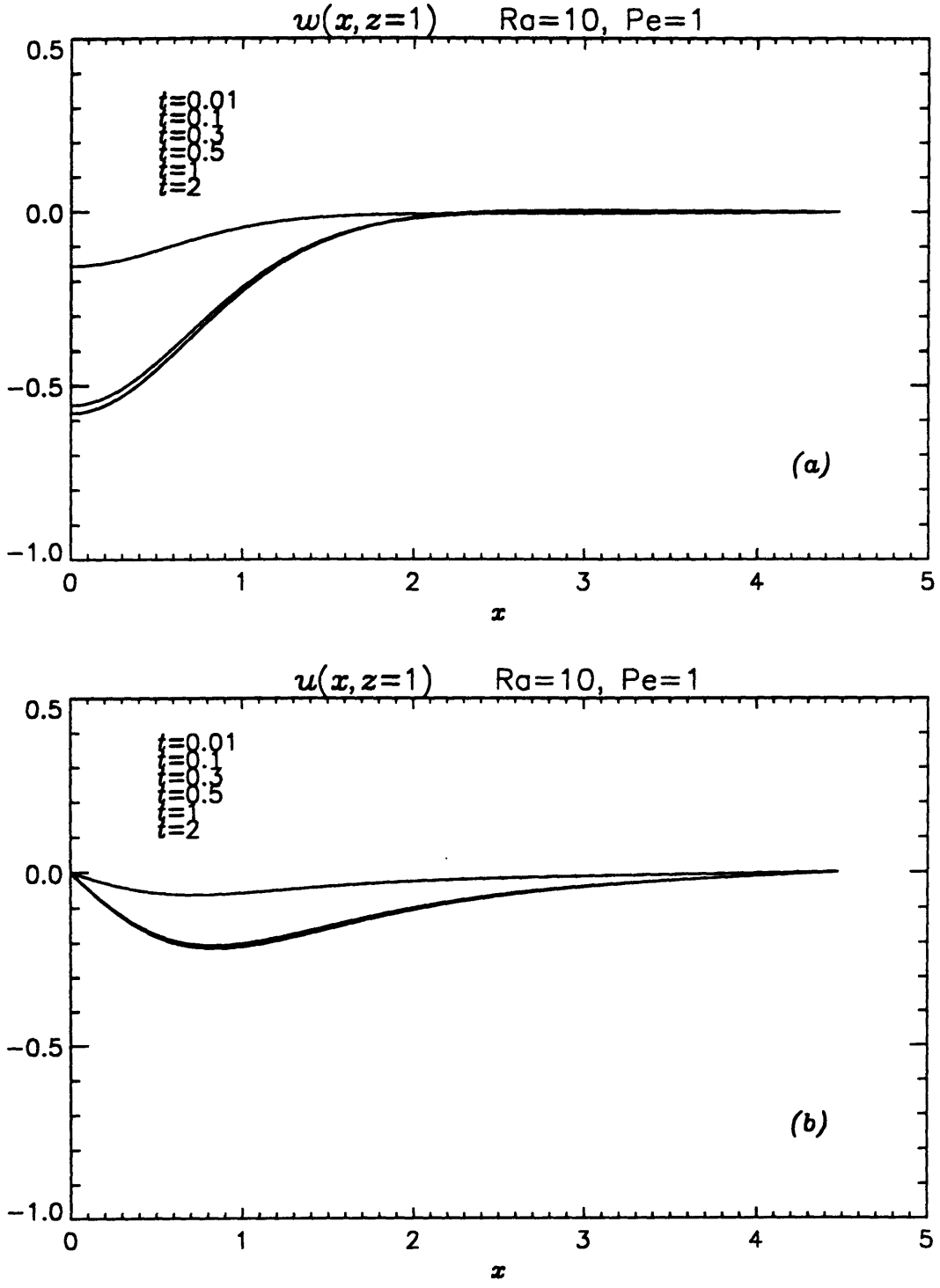

Fig. 7.20 Horizontal variation of (a) $w(x, z = 1)$ and (b) $u(x, z = 1)$ at discrete times for $Ra = 10$, $Pe^* = 1$, $b = 10$ and $T_c/T_d = 0.1$.

similar to the case with smaller Ra except that, in the region around $x = 1$ and $x = 2$ respectively near the bottom, positive pressure and temperature are being produced. This indicates that the seepage flow is beginning to lose stability and disturbances are being created. This process continues until steady state patterns are established at $x = 0.5$. At the centerline $x = 0$, it is dominantly one-dimensional and very much like Fig.7.9. The pressure is positive maximum at $x = 0.6$ on the bottom and decreases radially in the xz plane. The horizontal component of seepage velocity is determined by the negative of pressure gradient(cf.(7.2.6)) and Fig.7.21 (a) shows that $\langle u \rangle_x$ directs to the right in the region outside $x = 0.6$ below $z = 0.5$ unlike in the region $x < 0.6$ where it points to the left. The temperature is negative in the region $x < 1.4$ and positive outside $x = 1.4$ which shows that the vertical component of Darcy velocity due to buoyancy is downward for $x < 1.4$ and upward for $x > 1.4$. Since $\partial p/\partial z$ is negligibly small outside $x = 1.4$, the vertical flow thus becomes upwards. The corresponding seepage velocity distribution is shown in Fig.7.22 in which cellular convective motion is clearly demonstrated and swirls around the center at $x = 1.1$ and $z = 0.7$. It is also shown in the same figure that the flow pattern in the central region near $x = 0$ is like the one through a converging conduit from $z = 1$ to $z = 0$ due to the rotating motion in the cell. As a result, the recharge rate at the top surface near $x = 0$ is greatly increased as compared to the cases without convection cells. We note that, in the region beyond $x = 1$, the pore fluid never flows toward the sink and is affected only by the instability thus forming a rotational pattern.

We recall from (7.4.8) that, in the case of vertical through flow, the critical Rayleigh number Ra_c is 33 or larger. At the initial state before pumping starts, there were no convective motions because $Ra = 20 < Ra_c = 33$. The results discussed above show that, in the case of two-dimensional problem with finite amplitude motions, the flow becomes unstable at a lower $Ra_c(< 20)$ and thus convection cells develop. This is due to the nonlinearly coupled heat convection term in (7.2.8) which increases the interaction of the convection velocity with the initial temperature gradient.

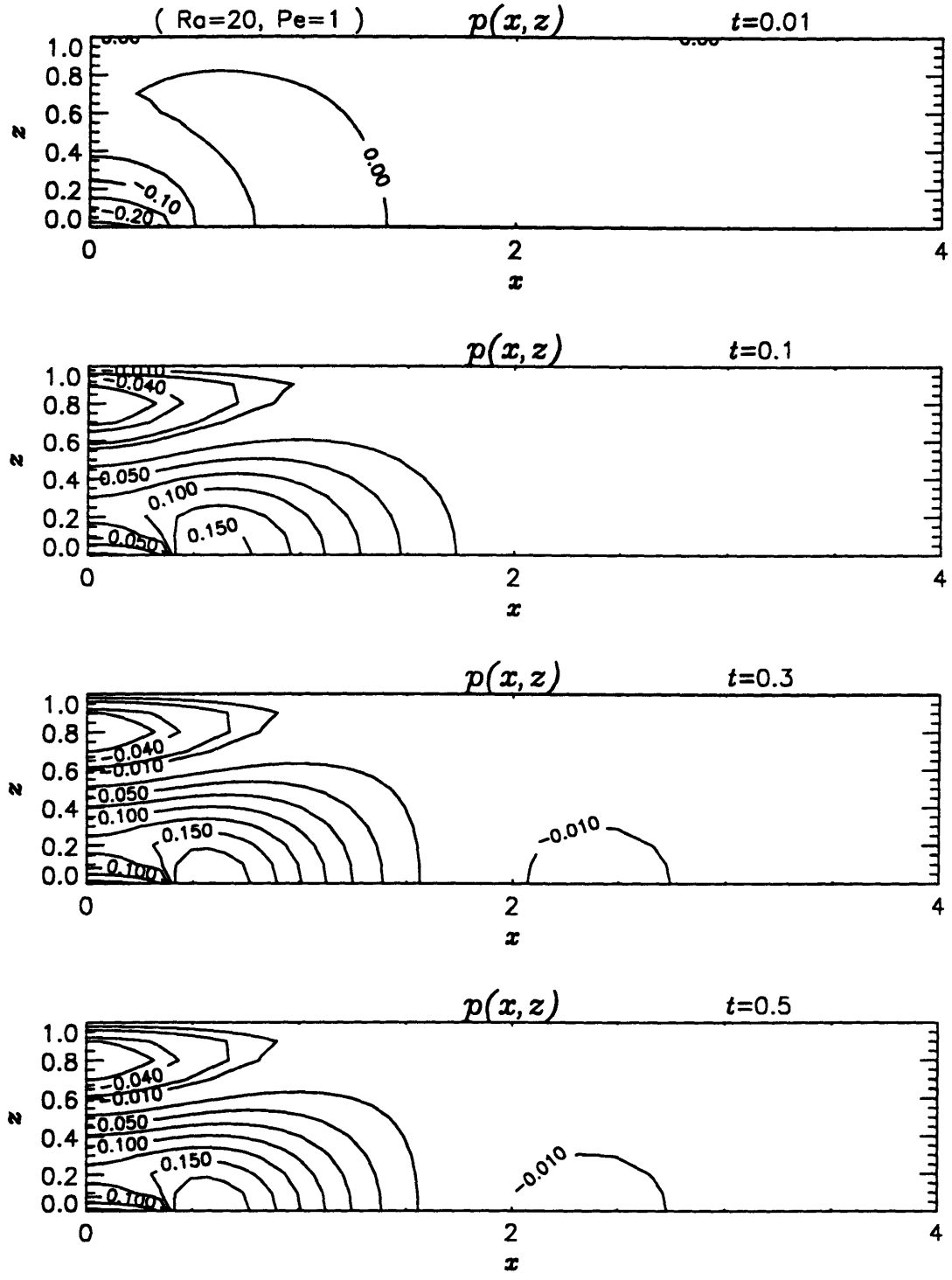

Fig. 7.21(a) Contour plot of the pressure distribution $p(x,z)$ at discrete times for $Ra = 20$, $Pe^* = 1$, $b = 20$ and $T_c/T_d = 0.05$.

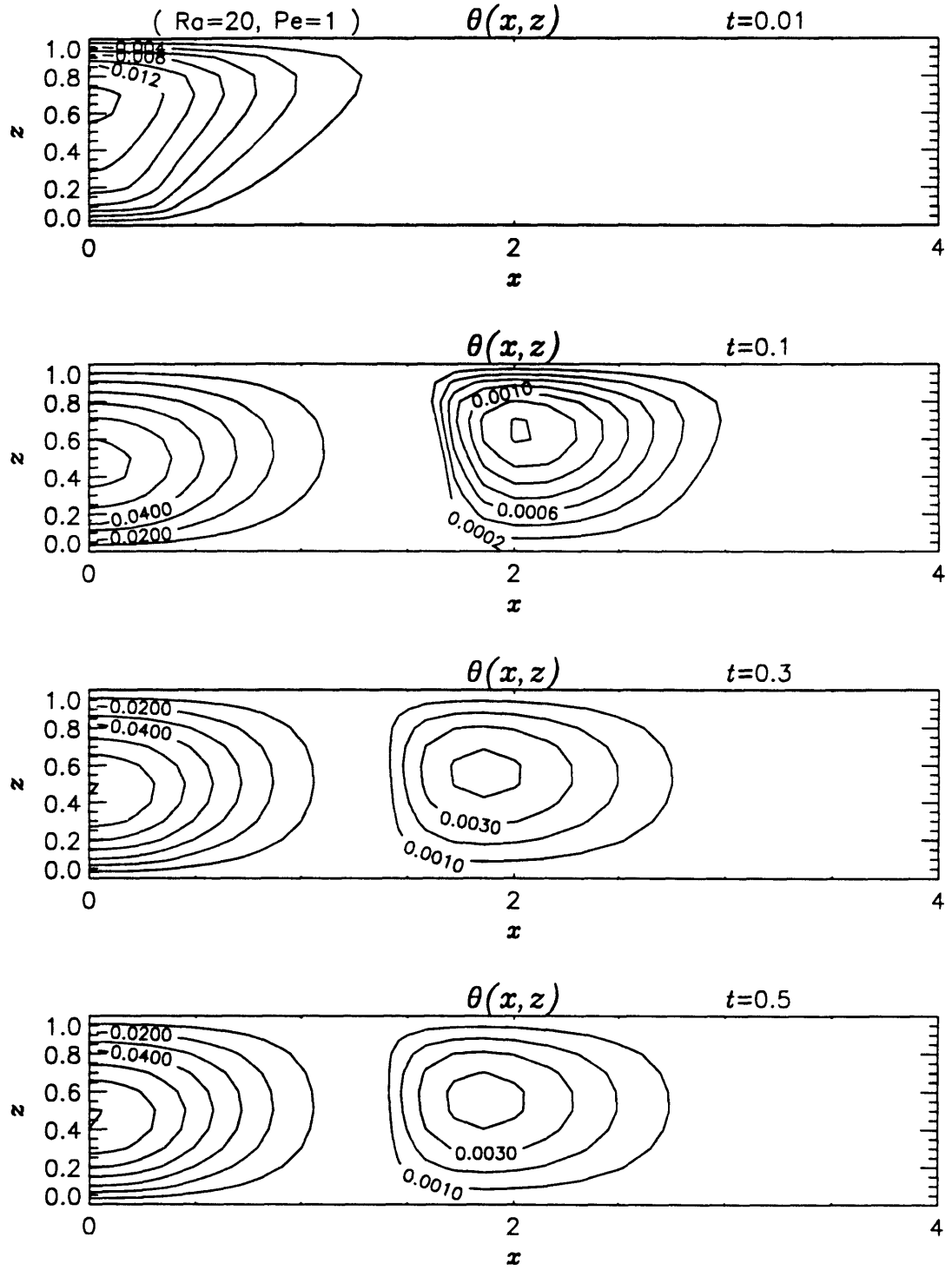

Fig. 7.21(b) Contour plot of the temperature distribution $\theta(x, z)$ at discrete times for $Ra = 20$, $Pe^* = 1$, $b = 20$ and $T_c/T_d = 0.05$.

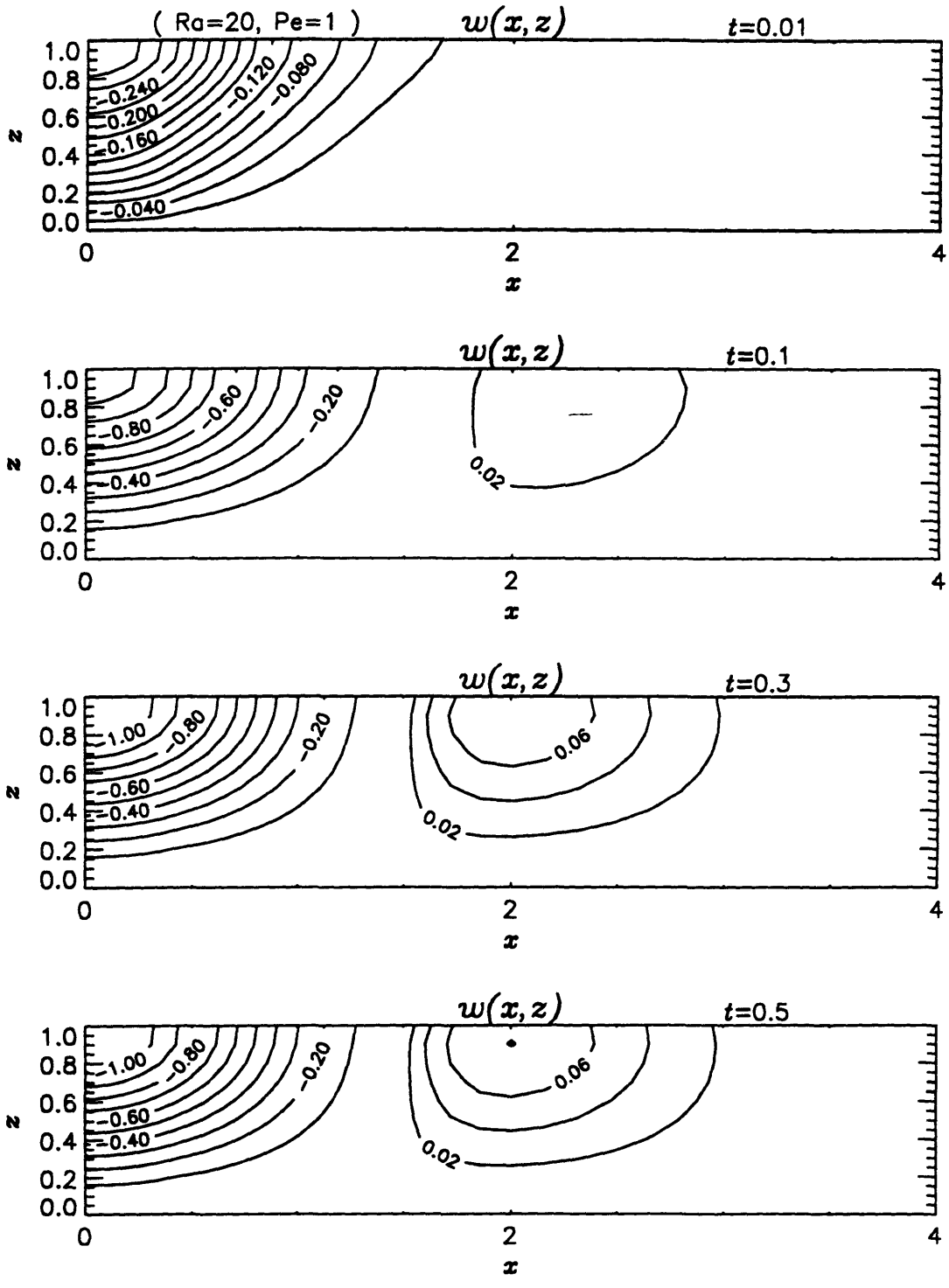

Fig. 7.21(c) Contour plot of the vertical displacement $w(x,z)$ at discrete times for $Ra = 20$, $Pe^* = 1$, $b = 20$ and $T_c/T_d = 0.05$.

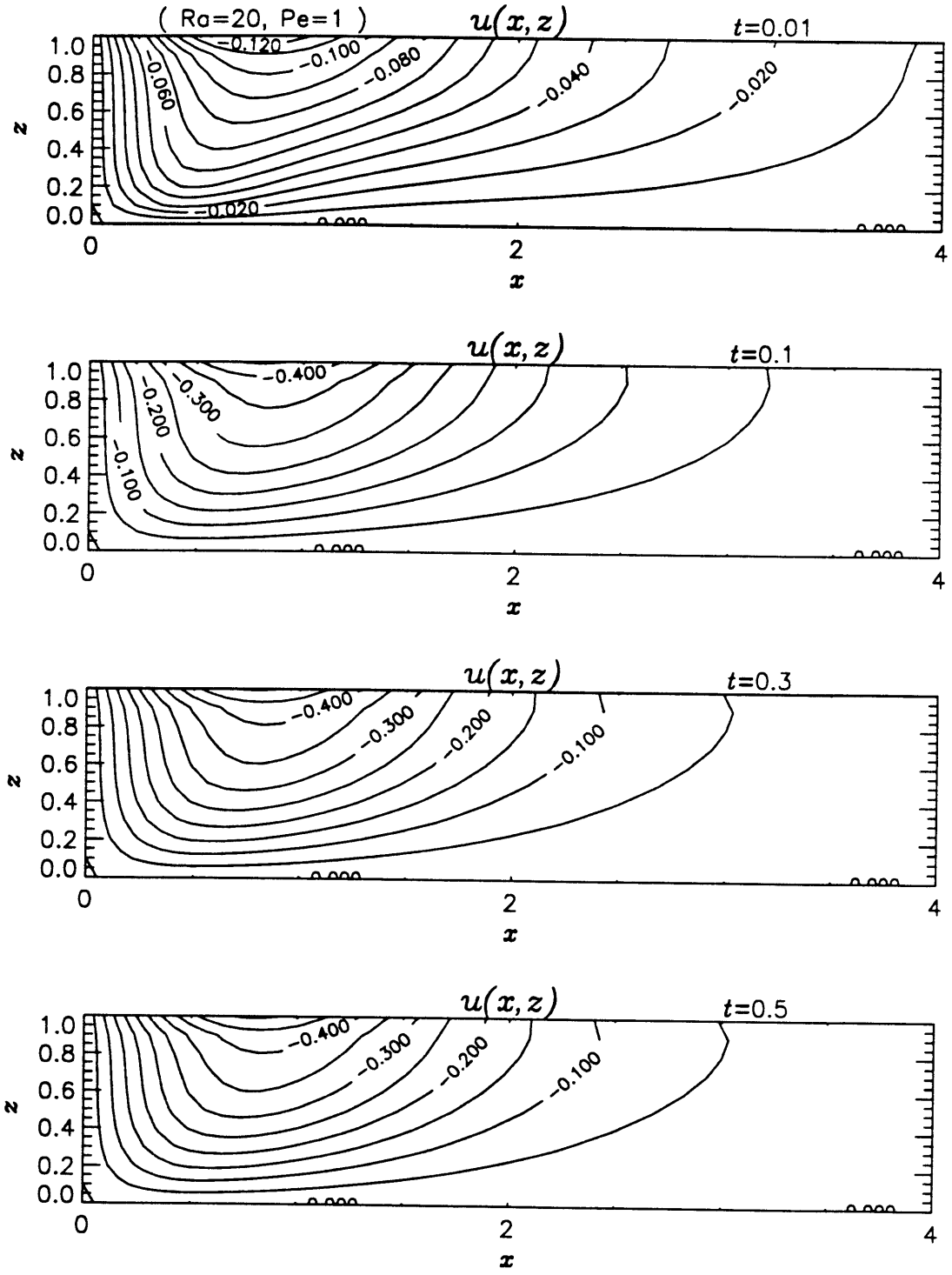

Fig. 7.21(d) Contour plot of the horizontal displacement $u(x, z)$ at discrete times for $Ra = 20$, $Pe^* = 1$, $b = 20$ and $T_c/T_d = 0.05$.

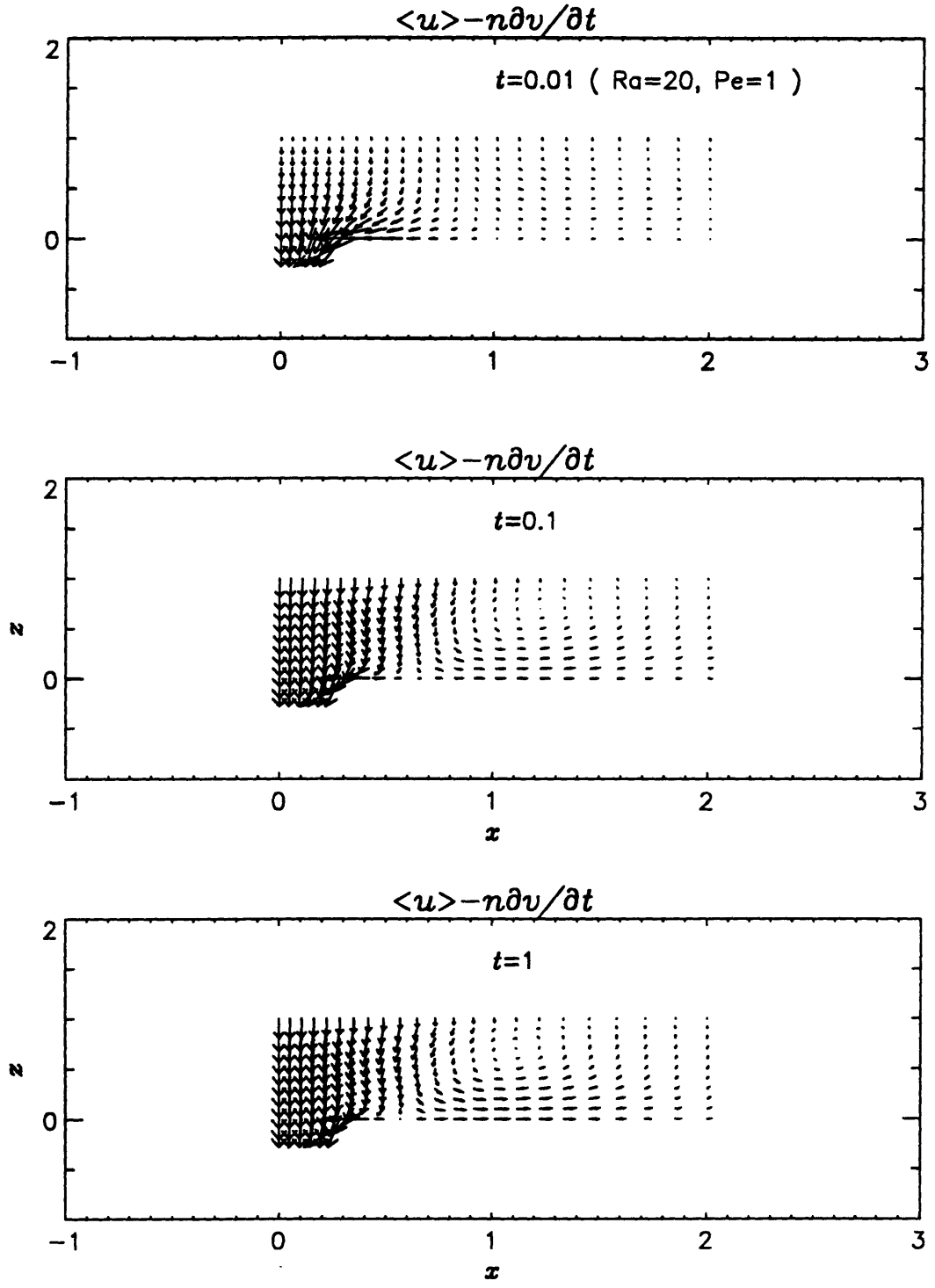

Fig. 7.22 Vector plot of Darcy velocity $\langle u \rangle - n' \partial v / \partial t$ at t=0.01, 0.1 and 1 for $Ra = 20$, $Pe^* = 1$, $b = 20$ and $T_c/T_d = 0.05$.

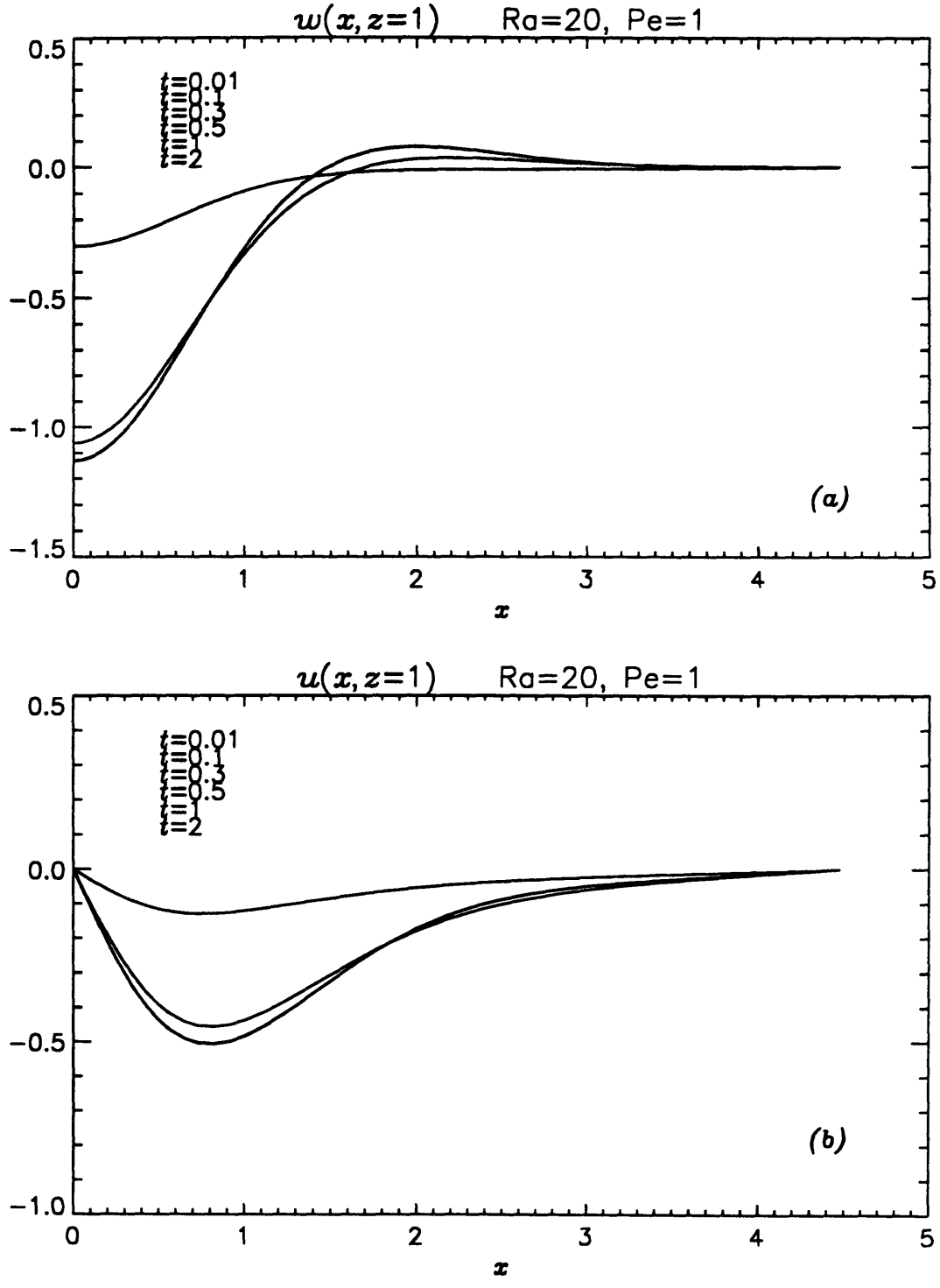

Fig. 7.23 Horizontal variation of (a) $w(x, z = 1)$ and (b) $u(x, z = 1)$ at discrete times for $Ra = 20$, $Pe^* = 1$, $b = 20$ and $T_c/T_d = 0.05$.

The vertical and horizontal displacements are shown in Fig.7.21(c) and (d). The one-dimensional resemblance is observed in the center region above $x = 0$. As shown in Fig.7.21(a), the pressure is noticeably large only in the inner region $x < 1.5$ and diminishes quickly as x increases. This implies that outside $x = 1.5$ the thermal stress dominantes the medium deformation. Fig.7.21(c) shows that the vertical displacement distribution is quite similar to the one-dimensional case when $x < 1.4$ but, in the outside region where θ is positive, the medium expands and thus causes the top surface at $z = 1$ to swell up. The snap-shot distribution of w and u in Fig.7.23 shows that trend.

$\underline{Ra=30,\ Pe^* = 1}$ When Rayleigh number is further increased to 30, which is still less than $Ra_c = 33$ to ensure no free convection in the initial state, the buoyancy effect and thus the nonlinear coupling effect becomes more pronounced.

The pore pressure and temperature distributions at discrete times are shown in Fig. 7.24 (a) and (b). As observed in the one-dimensional case, the pressure becomes more positive in the central region and the magnitude of pressure drop (negative in $1.2 < x < 2.5$) also increases substantially as compared to the case of $Ra = 20$. The temperature variation, unlike the one-dimensional case, is considerably affected by Ra in two-dimensions. In the region $x < 1$, the magnitude of θ is doubled from $Ra = 20$ case and even further, in the region $1 < x < 2.4$, it is 10 times larger. The buoyancy effect has thus been greatly increased. We also note that the dividing contours between positive and negative regions for p and θ have moved toward the symmetry plane. It has moved from $x = 1.8$ to $x = 1.2$ for the pressure and from $x = 1.4$ to $x = 1$ for the temperature. This readily means that the region affected by cellular convective motion is increased toward $x = 0$. This trend is shown in the arrow plot of Darcy velocities in Fig.7.25 so that the conduit analogy near $x = 0$ is now converging and then diverging flow path as z decreases from 1 to 0. Thus the downward velocity reaches maximum at the mid-depth and decreases as approaching to the sink. Due to increased nonlinear coupling, a pair of counter-rotating cells is clearly shown and there is another pair in the region $x < 0$.

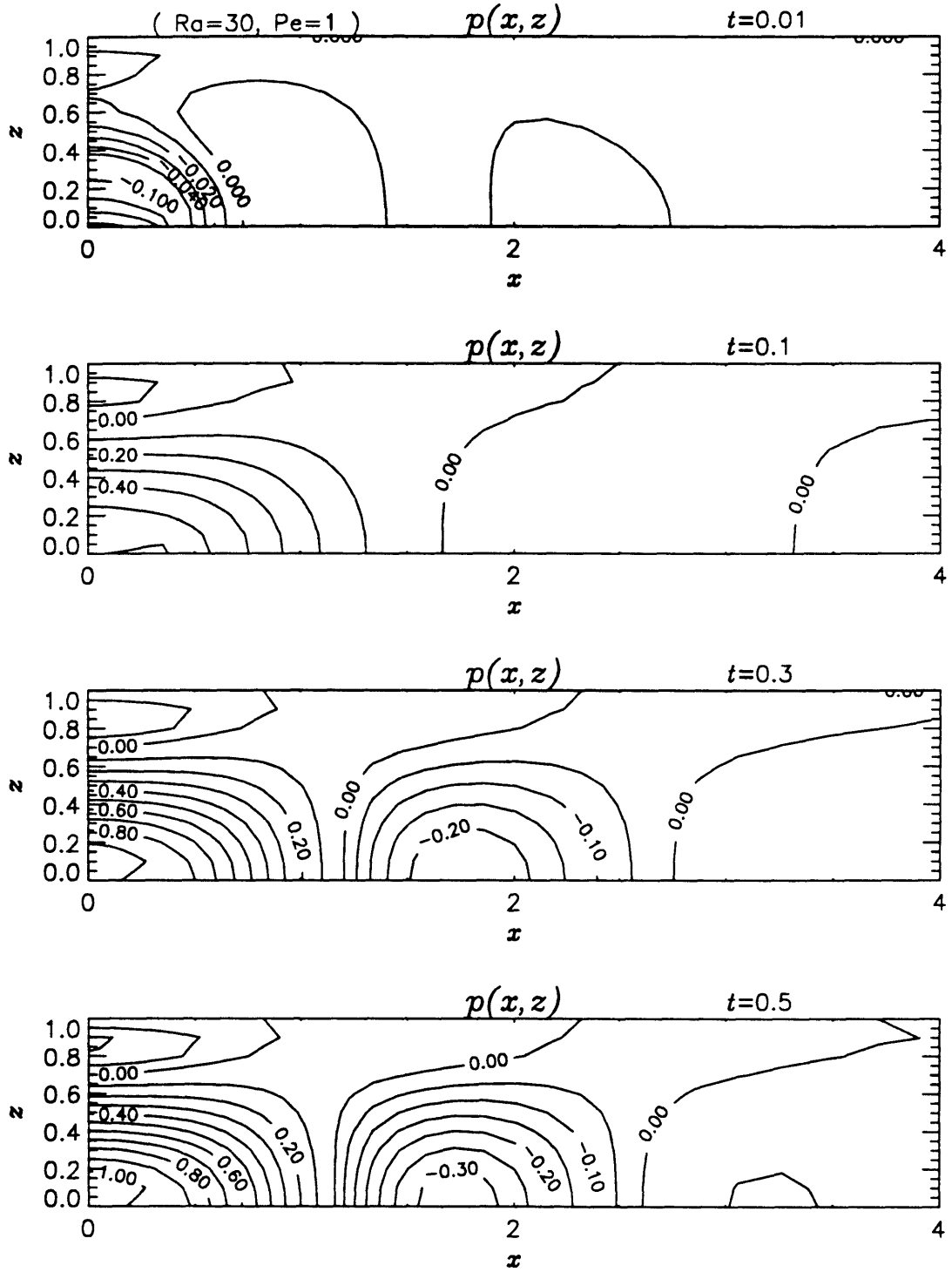

Fig. 7.24(a) Contour plot of the pressure distribution $p(x, z)$ at discrete times for $Ra = 30$, $Pe^* = 1$, $b = 30$ and $T_c/T_d = 0.0333$.

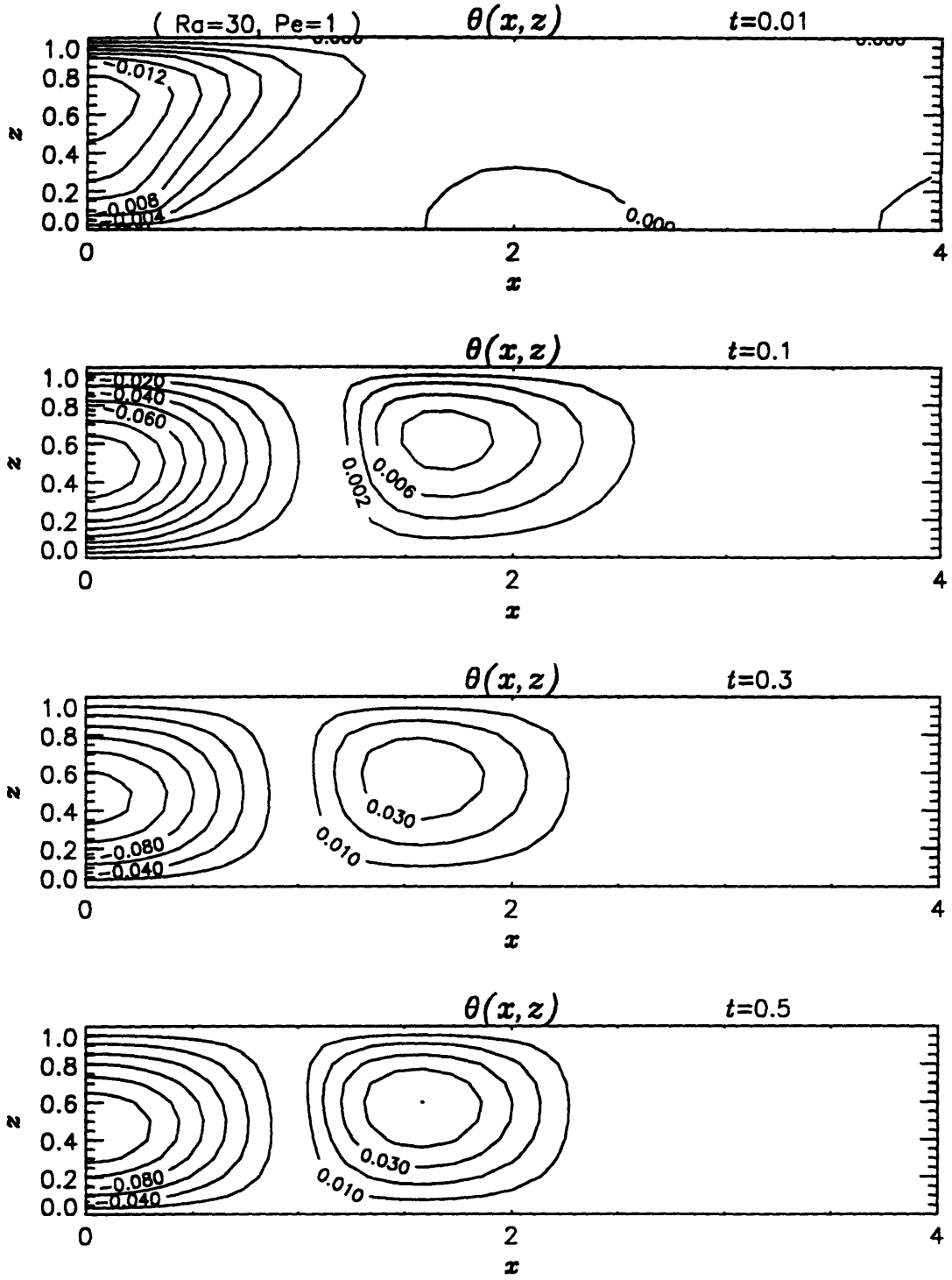

Fig. 7.24(b) Contour plot of the temperature distribution $\theta(x, z)$ at discrete times for $Ra = 30$, $Pe^* = 1$, $b = 30$ and $T_c/T_d = 0.0333$.

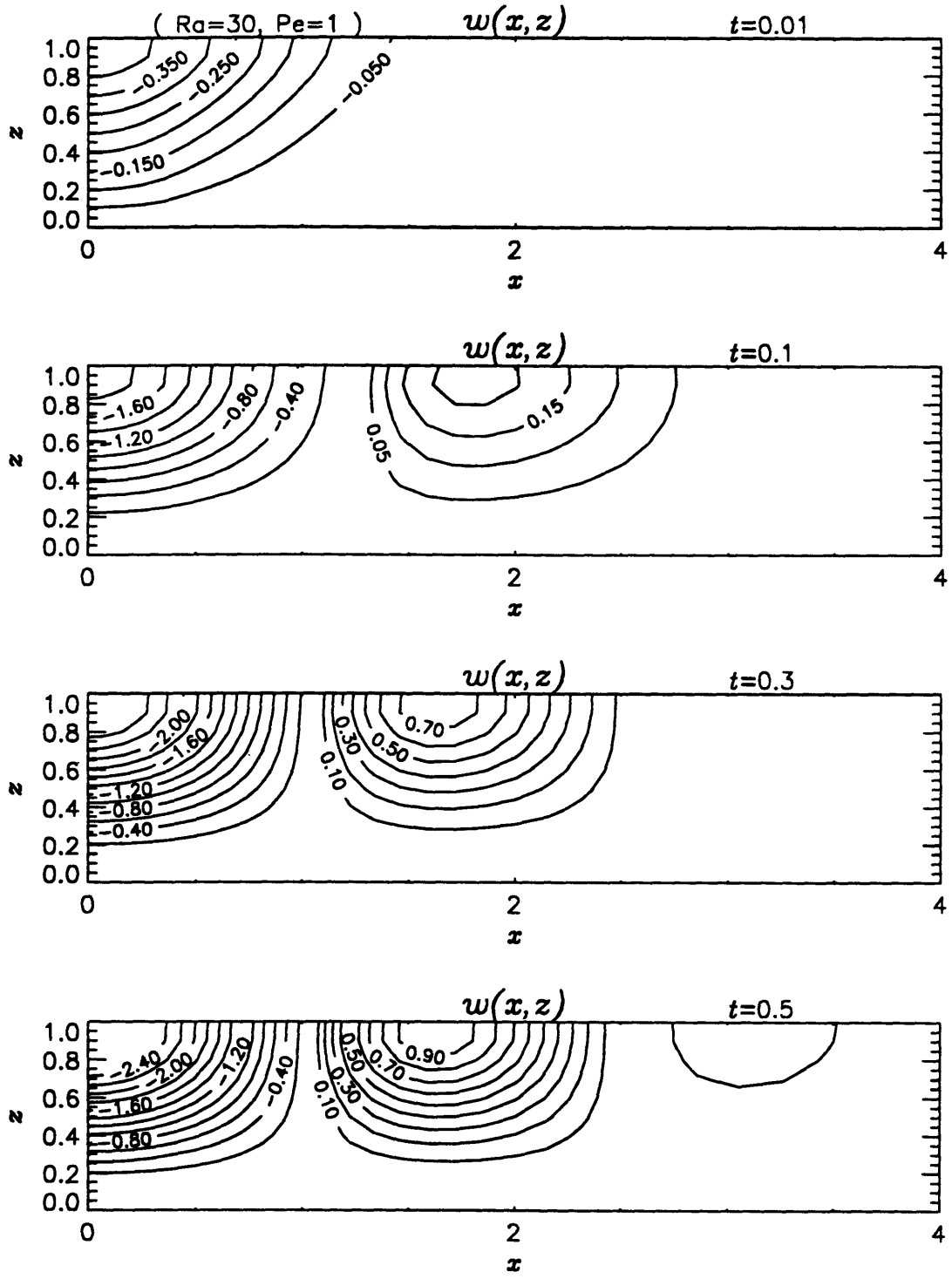

Fig. 7.24(c) Contour plot of the vertical displacement $w(x,z)$ at discrete times for $Ra = 30$, $Pe^* = 1$, $b = 30$ and $T_c/T_d = 0.0333$.

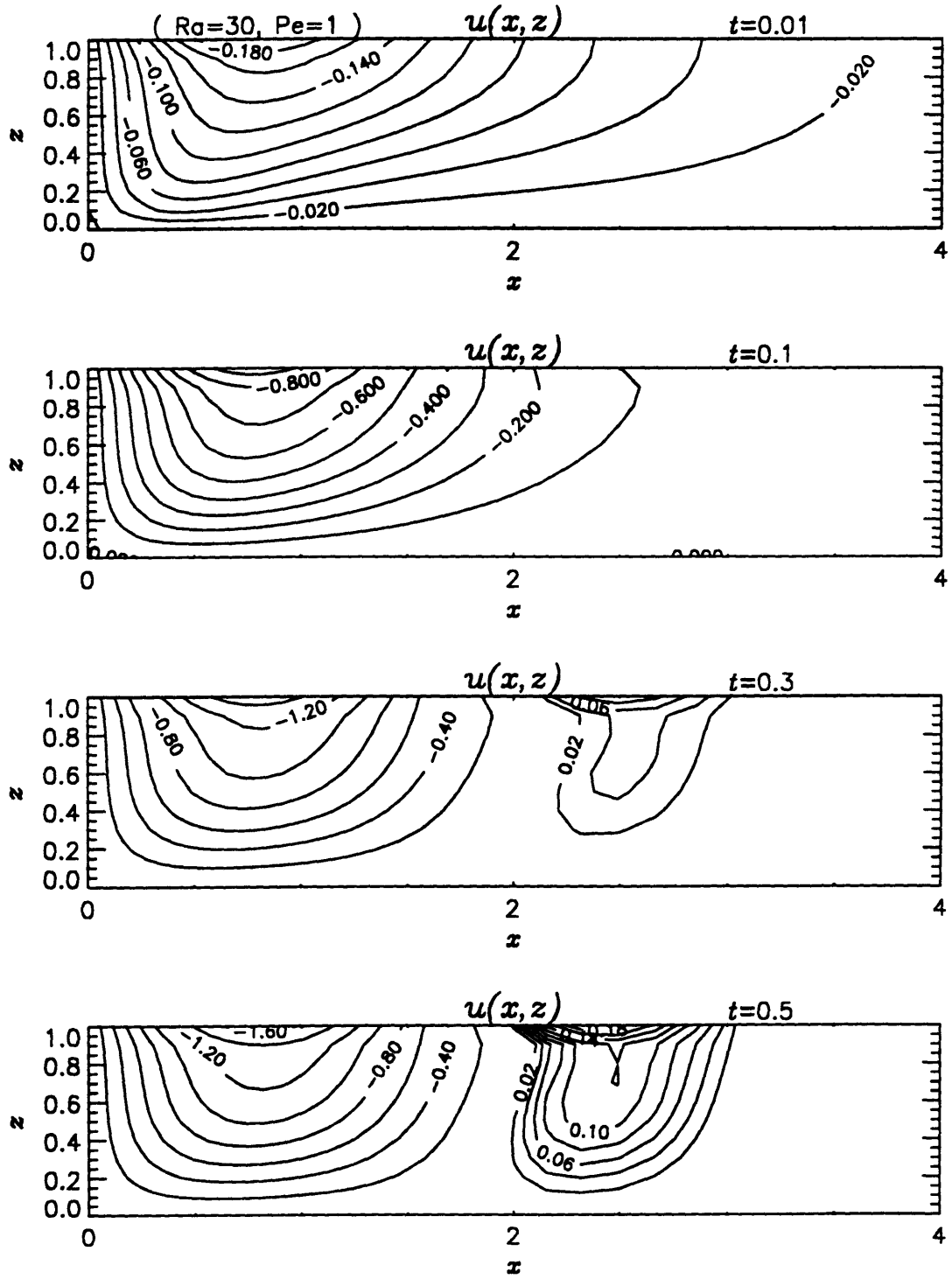

Fig. 7.24(d) Contour plot of the horizontal displacement $u(x,z)$ at discrete times for $Ra = 30$, $Pe^* = 1$, $b = 30$ and $T_c/T_d = 0.0333$.

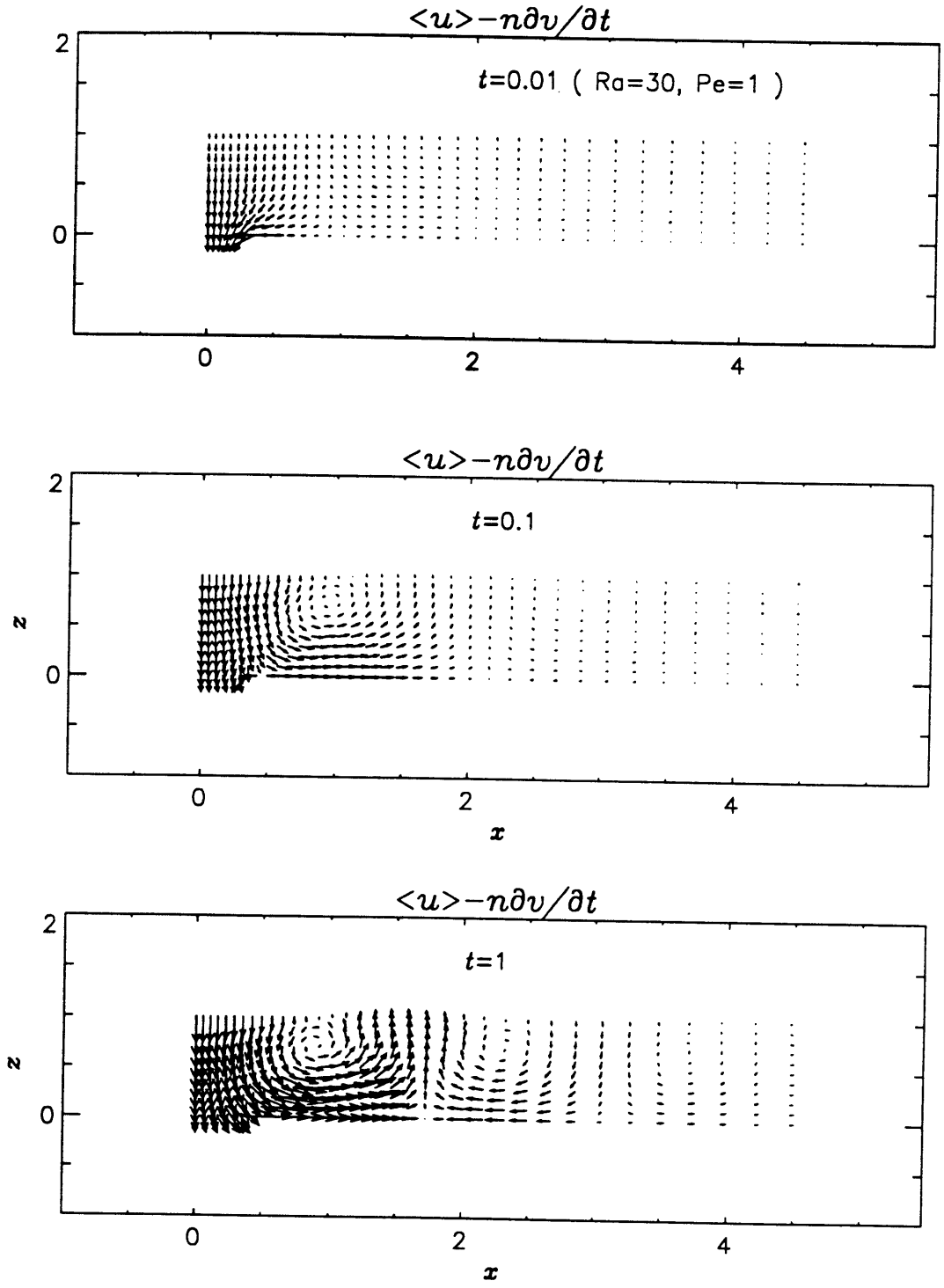

Fig. 7.25 Vector plot of Darcy velocity $\langle u \rangle - n' \partial v / \partial t$ at t=0.01, 0.1 and 1 for $Ra = 30$, $Pe^* = 1$, $b = 30$ and $T_c/T_d = 0.0333$.

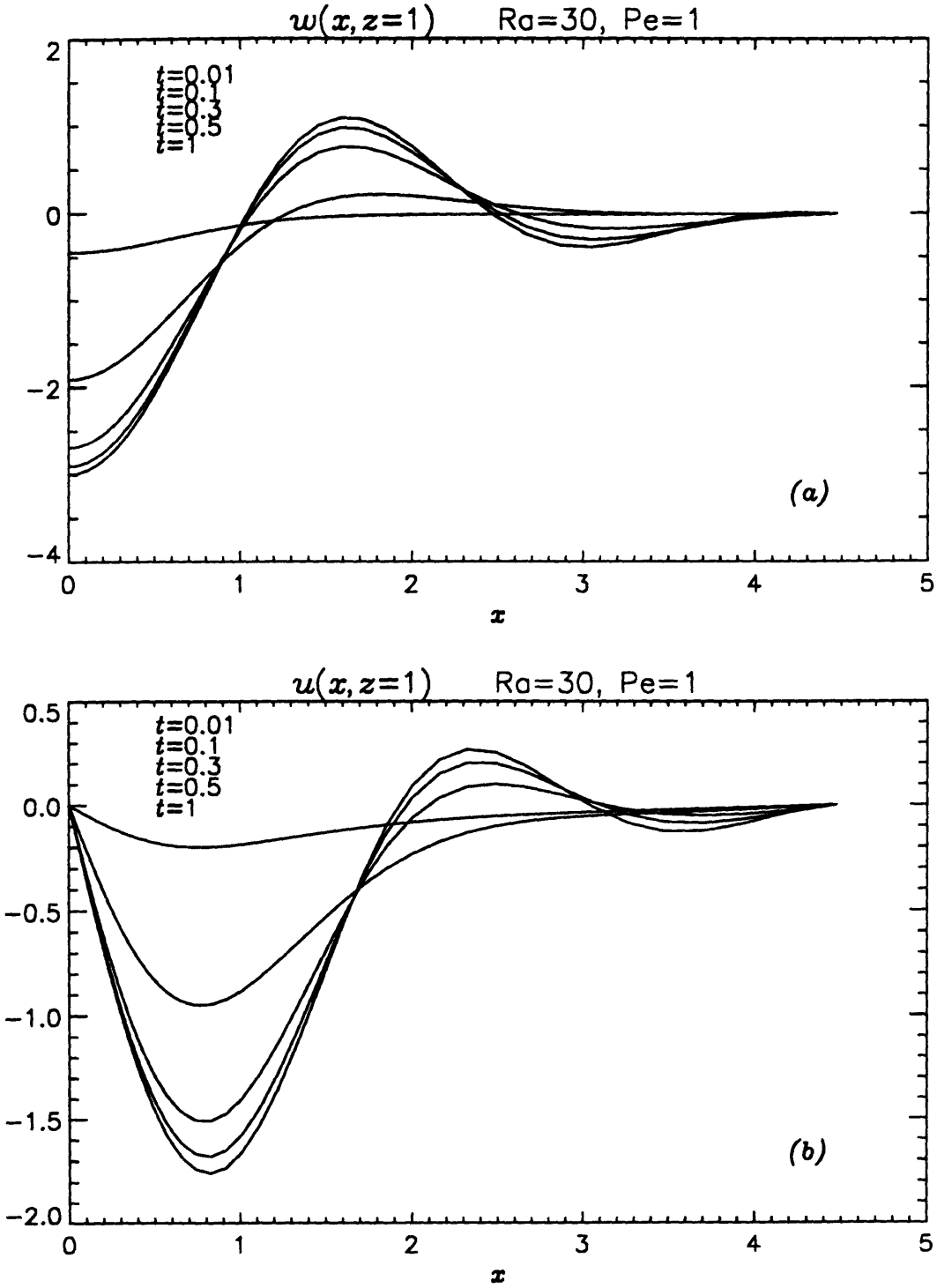

Fig. 7.26 Horizontal variation of (a) $w(x, z = 1)$ and (b) $u(x, z = 1)$ at discrete times for $Ra = 30$, $Pe^* = 1$, $b = 30$ and $T_c/T_d = 0.0333$.

The spatial variations of displacements w and u in the soil layer are shown in Fig.7.24 (c) and (d). The sinking and swelling pattern with increasing x is more pronounced than the case of $Ra = 20$. Because of larger temperature variations, the horizontal displacement now varies from negative values(inward movement) in the region $x < 2$ to positive values(outward movement) outside and thus the soil layer experiences horizontal compression and tension alternatingly in those regions. The horizontal variations of w and u are shown in Fig.7.26. As mentioned earlier, near the top surface the thermal stress effect dominates and it is shown that the depth of the compaction bowl and the height of swelling are twice and 10 times larger respectively than those for $Ra = 20$. If we reflect Fig.7.26 over the plane $x = 0$, the deformed shape on the top surface is in wavy pattern with decreasing amplitude as the distance from $x = 0$ increases.

7.6.2.3 Case (ii) : The Effects of Pe^* with Ra Fixed.

In order to examine the effects of varying pumping rate for fixed permeability, the Peclét number may be changed for each Rayleigh number considered in Case (i). Based on the observations in the one-dimensional case, we can easily infer that the differences due to varying Pe^* in terms of dimensionless variables are minor with Rayleigh numbers less than 20 for which cellular convection does not occur. Also the discussions for the case with $Ra = 20$ are similar to those for $Ra = 30$. Therefore we shall restrict our attention to the following case in which convective motions are more pronounced.

Case(ii)	$RaPe^*$	Pe^*	b	T_c/T_d
	30	0.1	300	0.0333
	30	1	30	0.0333
	30	10	3	0.0333

in which the middle case of $Pe^* = 1$ has been discussed in Case (i).

The pore pressure development for $Pe^* = 0.1$ and $Pe^* = 10$ are plotted in contours in Fig.7.27 (a) and (b) respectively. For $Pe^* = 1$ see Fig.7.20 (a). Similarly the temperature variations are shown in Fig.7.28 (a) and (b) (see Fig.7.20 (b) for $Pe^* = 1$). We first note, as in the one-dimensional case, that the magnitude of

temperature variation is roughly in the trend of being proportional to the Peclét number which implies that the buoyancy term $Ra/Pe^*\theta$ does not change noticeably as Pe^* varies from 0.1 to 1 and then to 10 as can be estimated from Fig.7.28. Although the peak moves downward as the pumping rate increases in the central region, it stays at the mid-depth in the neighboring cells with no regard to Pe^*. Recall that the cellular convective motions are due to the instability of disturbances relative to the steady state. Therefore the temperature distribution ($\theta > 0$) in the outer region where uniform pumping induced variations are small should be almost insensitive to Pe^* and Fig.7.28 (a) and (b) show the same pattern of temperature distribution. However the location of the positive temperature region depends on the size of pumping dominated region. It is seen in Fig.7.28(b) that the region fro $\theta > 0$ appears beyond $x = 2$ because of increased Peclét number. The pressure distribution for $Pe^* = 0.1$ is nearly the same as that for $Pe^* = 1$. As Pe^* is further increased to 10 in Fig.7.27(b), the pressure in the central region near $x = 0$ becomes negative, since the buoyancy effect on the pressure decreases for intensive pumping. As a result the region of $p > 0$ is now expanded outward to the right. The expansion of pumping dominated region with increasinf Pe^* is shown in Fig.7.29 where the seepage velocity distribution at steady state has been made in arrow plots for $Pe^* = 0.1, 1$ and 10. Note that not only the convective cells are moved to the right but also the velocity of rotational motion is greatly reduced for larger Peclét number.

The distributions of dimensionless vertical displacement w are similar for different Peclét numbers and, as expected, the compaction bowl at the top surface becomes larger for increased Peclét number. The dimensionless horizontal displacement u is quite the same since the horizontal equilibrium equation does not depend on the buoyancy. The plots of w and u for spatial variations are not shown here. Instead the displacements at the top surface $z = 1$ for steady state are plotted in Fig.7.30 for $Pe^* = 0.1$ and 1 for which the pumping rate is mild, the wavy shape is clearly shown but as Pe^* is incrased to 10,i.e. the region affected by buoyancy in terms of positive temperature variation is moved outward, the swelling

becomes much less than compaction. Similarly the horizontal movement at the top surface becomes inwards only for $Pe^* = 10$. Since for fixed K increase of $Pe^* = Uh/\alpha_f$ means increase of the pressure scale P and thus the displacement scale V (cf.(7.2.1)),the displacements in physical units corresponding to the curves in Fig.7.30 increase with Pe^*.

In summary for two-dimensional case, the increase of the Rayleigh number has the effect of destabilizing the fluid motion in the medium due to nonlinear coupling through heat convection and rotational convection occurs at Rayleigh numbers lower than that for one-dimensional case. On the other hand, the Peclét number tends to decrease the effects due to Rayleigh number.

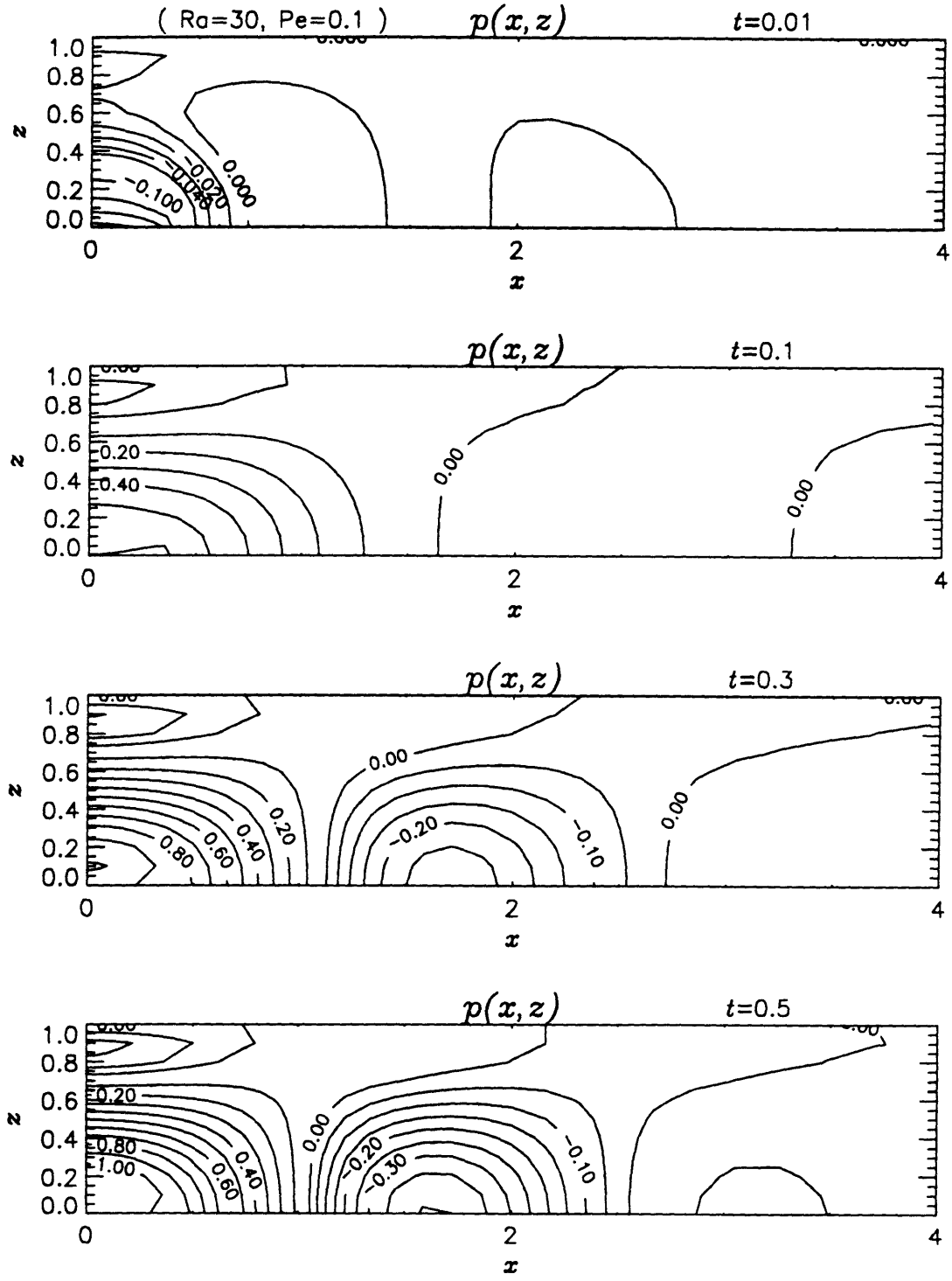

Fig. 7.27(a) Contour plot of the pressure distribution $p(x,z)$ at discrete times for $Ra = 30$, $Pe^* = 0.1$, $b = 300$ and $T_c/T_d = 0.0333$.

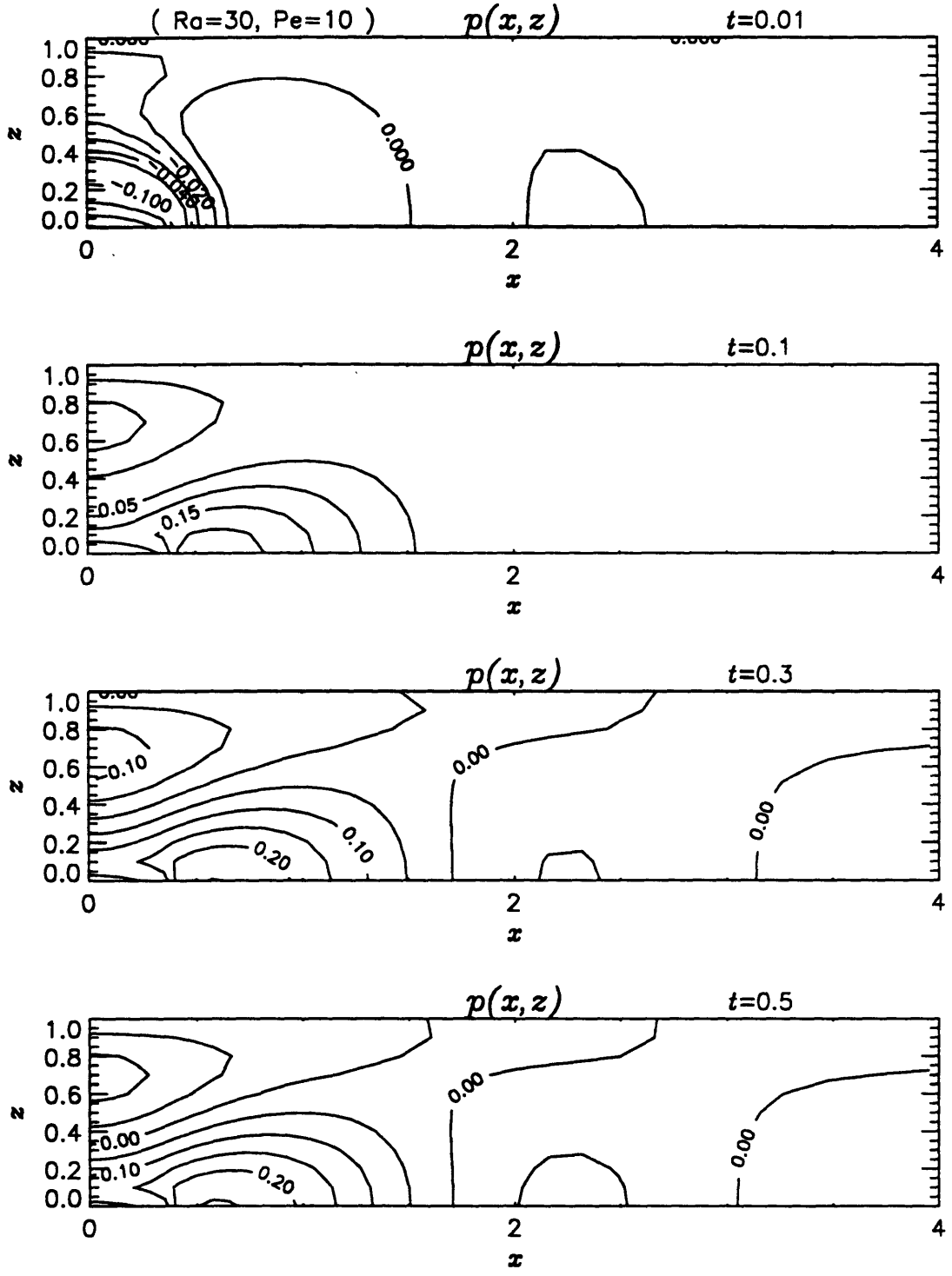

Fig. 7.27(b) Contour plot of the pressure distribution $p(x, z)$ at discrete times for $Ra = 30$, $Pe^* = 10$, $b = 3$ and $T_c/T_d = 0.0333$.

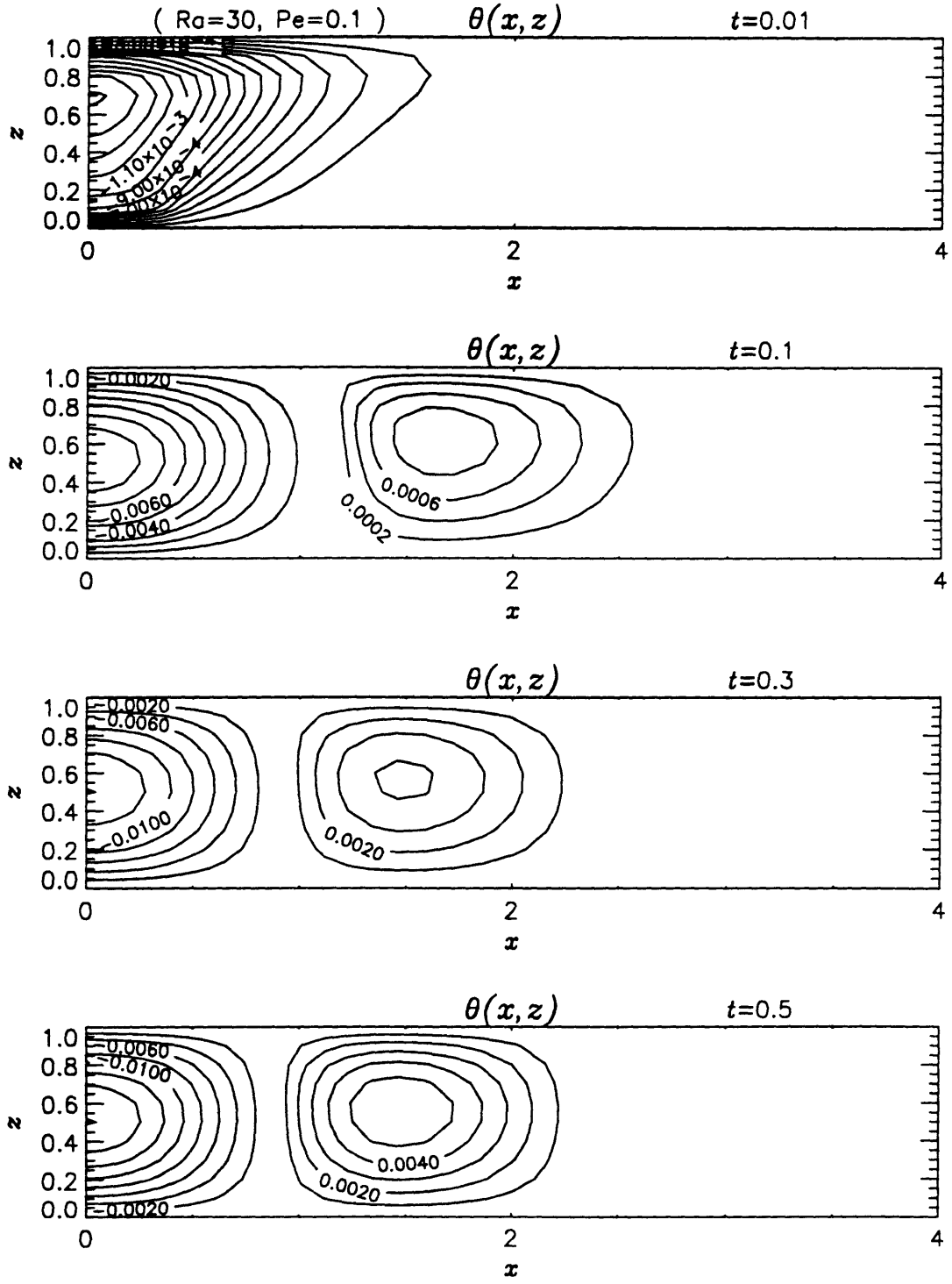

Fig. 7.28(a) Contour plot of the temperature distribution $\theta(x, z)$ at discrete times for $Ra = 30$, $Pe^* = 0.1$, $b = 300$ and $T_c/T_d = 0.0333$.

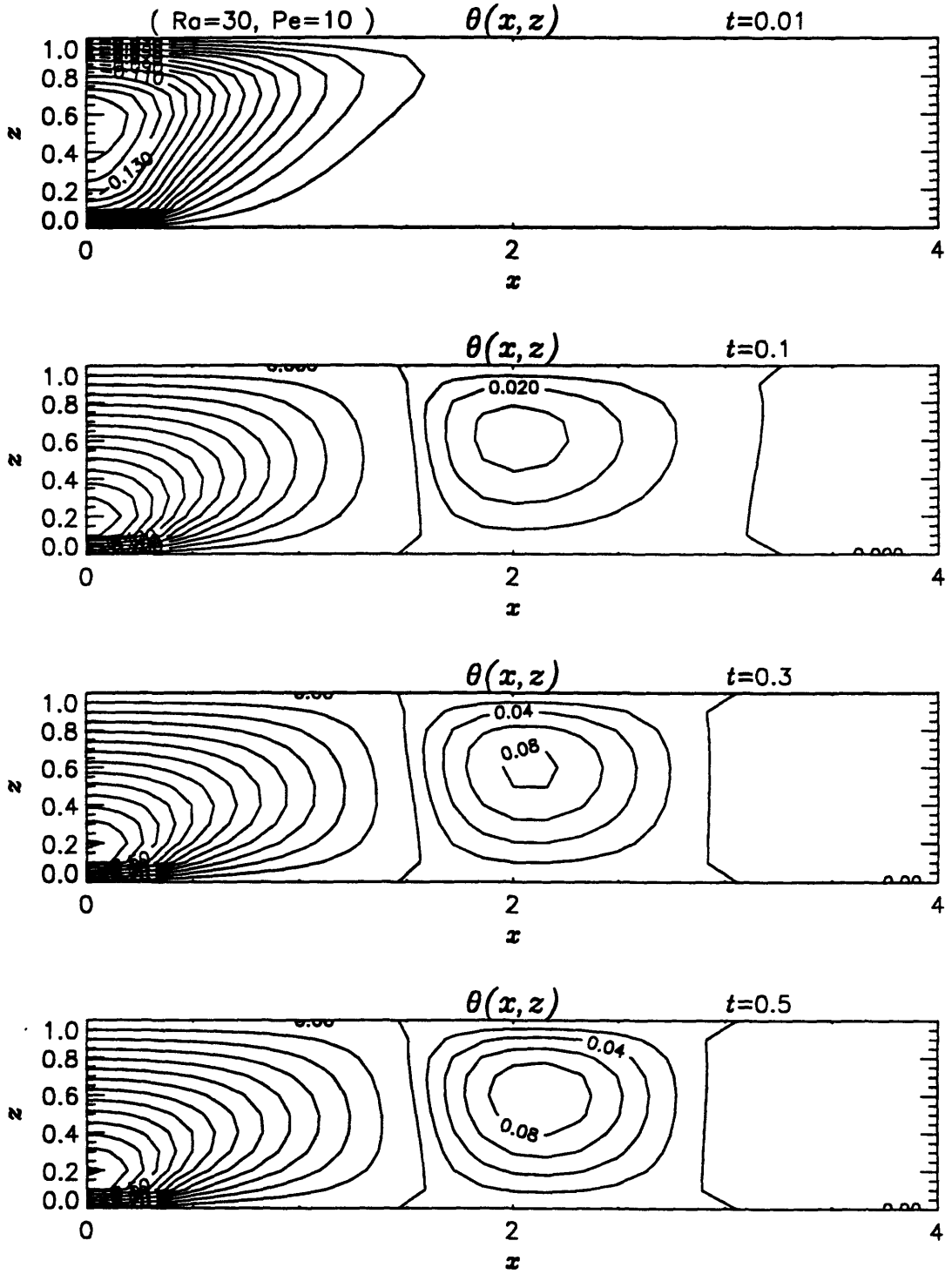

Fig. 7.28(b) Contour plot of the temperature distribution $\theta(x, z)$ at discrete times for $Ra = 30$, $Pe^* = 10$, $b = 3$ and $T_c/T_d = 0.0333$.

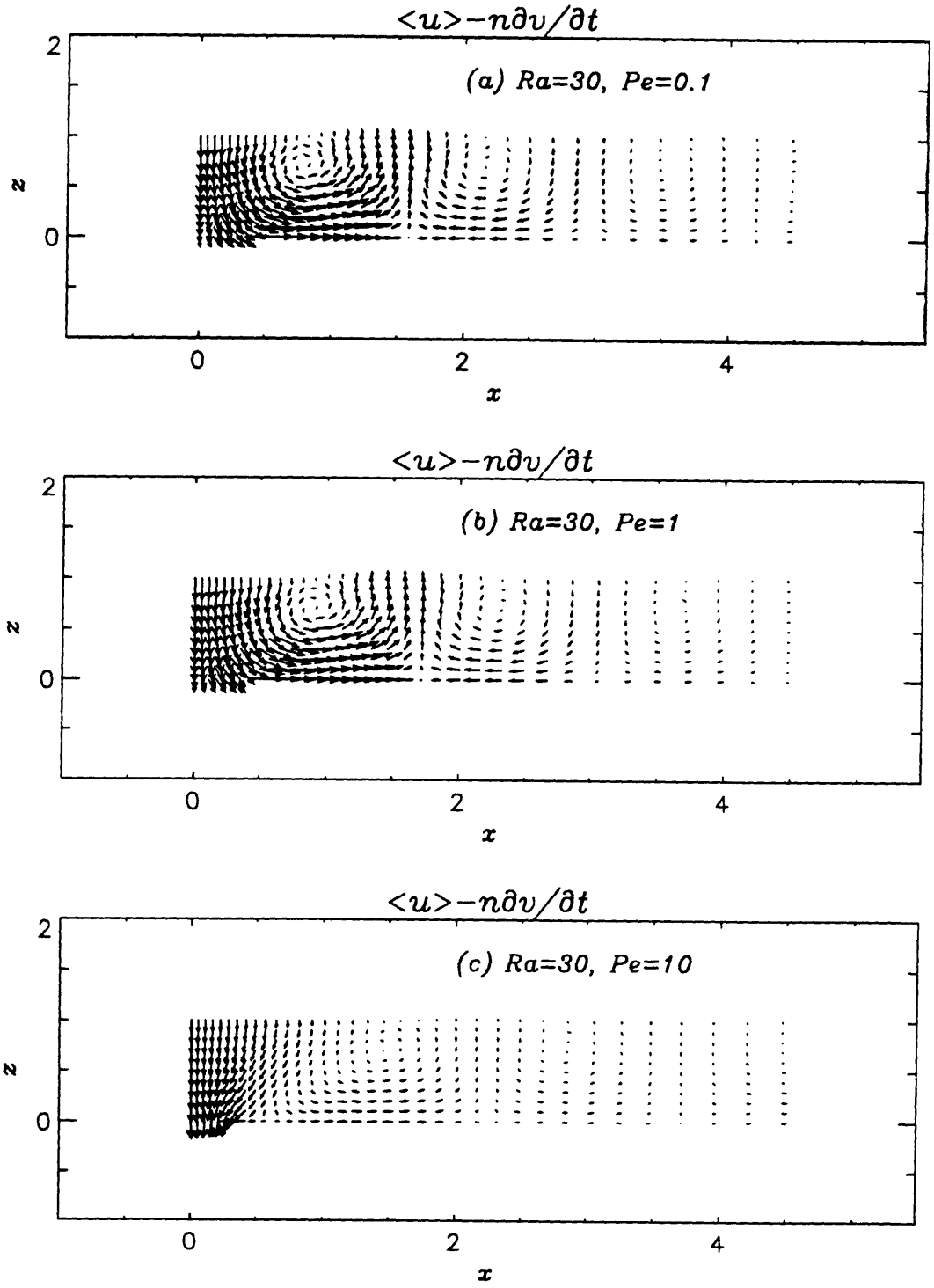

Fig. 7.29 Vector plot of Darcy velocity $\langle u \rangle - n' \partial v / \partial t$ at steady state fro (a) $Ra = 30$, $Pe^* = 0.1$; (b) $Ra = 30$, $Pe^* = 1$ and (c) $Ra = 30$, $Pe^* = 10$.

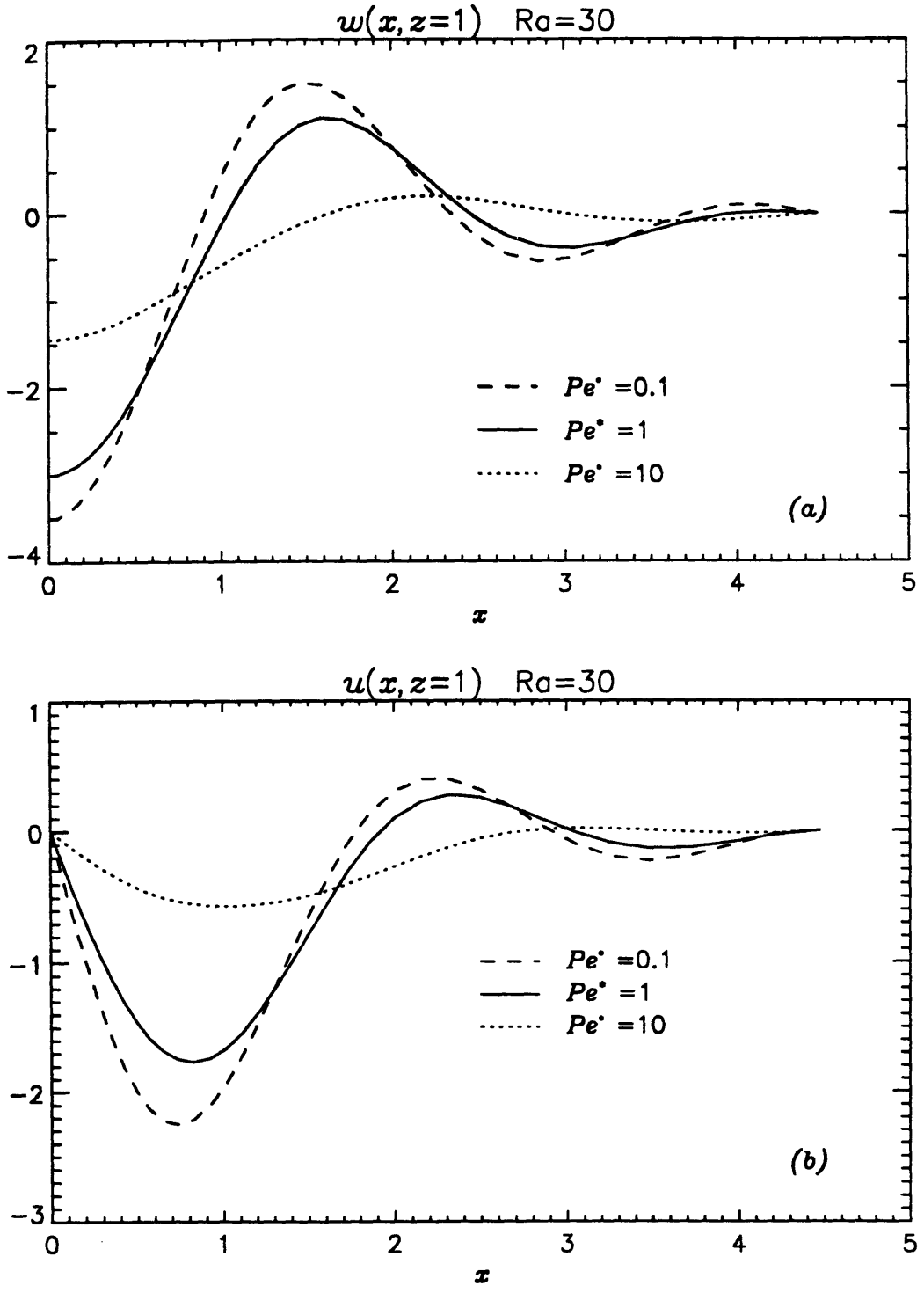

Fig. 7.30 Horizontal variation of (a) $w(x, z = 1)$ and (b) $u(x, z = 1)$ at steady state for Pe^*=0.1, 1 and 10 with $Ra = 30$.

8. Conclusions

We have investigated the thermoconsolidation in two scale porous media. By using the theory of homogenization which assumes disparity of length scales and periodicity of medium structure and material coefficients on the microscale, the macroscale governing equations have been deduced without making empirical assumptions. By allowing the medium deformation to be comparable to typical grain size, it has been shown that the governing equations are in general nonlinearly coupled due to nonlinear boundary conditions on the fluid-solid interfaces. Therefore Biot's linear theory of consolidation is theoretically justified only if the solid displacement much smaller than the grain size. However, when the microcell geometry has three planes of symmetry, those nonlinear terms steming from the nonlinear interfaces boundary conditions vanish. These limitations have not been brought out in previous works on the consolidation of porous media (Auriault and Sanchez-Palencia, 1977; Burridge and Keller, 1983) where infinitesimal strain is simply assumed to justify the use of Hooke's law.

For a cubic array of Wigner-Seitz grains, it has been shown by using the symmetry properties of the solutions of the canonical cell boundary value problems that the elastic coefficients reduce to three independent coefficients, implying that the porous medium possesses cubic symmetry. This kind of symmetry is well known in crystal structures (Cottrell, 1964). Here, the cubic symmetry of the elastic property of the porous medium composed of Wigner-Seitz grains has been established by utilizing the symmetry relations of the elastostatic problems defined in a microcell. We may find an analogy in crystal structures where such relation is obtained by comparing the array of particles about the planes of symmetry in a lattice structure. Similarly it has been shown that the pressure coefficient and thermal modulus in Hooke's law, and the permeability and the thermal conductivity are isotropic in a cubic array of Wigner-Seitz grains. The above symmetry properties can readily be extended to be true for cubic arrays of other grains such as spheres.

We have also calculated the macroscale coefficients by solving the microcell boundary value problems numerically for the cubic array of Wigner-Seitz grains. The minimization of the variational principles derived from the boundary value problems has been done by employing finite element approximations. Several porosity values were chosen by varying the length ratio in the cell geometry. The numerical results have shown that the elastic coefficients and thermal modulus decrease with increasing porosity whereas the pressure coefficient decreases with porosity. Also it was shown that the coefficients of time derivatives of the pressure and temperature in the consolidation equation reach maximum values at intermediate porosity and decrease as the porosity goes to unity and to zero.

The macroscale equations have been applied to thermoconsolidation in a porous layer due to pumping of the pore fluid. Both one-dimensional case of uniform pumping at the lower boundary and two-dimensional case in which pore fluid is extracted through a small sink located at the bottom of the layer have been considered.

In the one-dimensional case, the effects of buoyancy induced by thermal disturbances are the decreases in the pore pressure and the vertical compaction. For sufficiently large Rayleigh number, the pressure perturbation even becomes positive. The thermal stress significantly increases the vertical compaction of the layer. The steady state temperature distribution depends only on the Peclét number. It was shown that the nonlinear coupling due to Rayleigh number tends to accelerate the development of pressure, temperature and compaction. For large Rayleigh number, they overshoot beyond and approach to the steady state values. On the other hand, the Peclét number tends to decrease the nonlinear coupling by Rayleigh number and the buoyancy effects.

In the two-dimensional case, it is first shown that, for large Rayleigh number, cellular convection occurs. If the Rayleigh number increases, the intensity of convective motion increases and the size of the cell in the central region near the source decreases. The peak values of the pressure, temperature and displacement increase with Rayleigh number. For large Rayleigh number, wavy pattern of deformation on

the top surface is developed. The Peclét number has stabilizing effects so that as the Peclét number increases, the convective motion becomes weak and the cellular convection region moves away from the central region.

Chapter II. Thermoconsolidation in Three-scale Porous Media

1. Introduction

A three-scale porous medium is characterized by the existence of three disparate length scales, the microscale ℓ, the mesoscale ℓ' and the macroscale ℓ''. It is assumed that $\ell/\ell' \ll 1$ and $\ell'/\ell'' \ll 1$. In Chapter 1, the homogenization theory has been applied to a two scale (ℓ, ℓ') medium to deduce the governing equations on the ℓ' scale. The ℓ' scale which has been previously called the macroscale is now named the mesoscale in three-scale medium. Starting from the mesoscale governing equations, the homogenization procedure is applied to deduce the governing equations on the macroscale ℓ''. The porous medium is assumed to be periodic on the mesoscale so that the medium is composed of periodic arrays of Ω'-cells with periodic length ℓ'. The material coefficients are also assumed to be Ω'-periodic.

2. The Governing Equations and Normalization.

The two relevant spatial scales are now the mesoscale ℓ' and the macroscale ℓ'' with $\ell'/\ell'' = \epsilon \ll 1$. We note that the scale ratio ϵ is used only between the mesoscale and the macroscale and is not necessarily equal to that between the micro- and mesoscales. Before the basic governing equations on the mesoscale are presented, some order estimates are first made. The governing equations are normalized accordingly. Other dimensionless parameters are also examined.

2.1 Order Estimates.

We consider the flow driven by a pressure difference P'' over the macroscale ℓ'' . The velocity scale U' is then given by the anticipated Darcy's law as

$$U' = \tilde{k}\frac{P''}{\ell''} \tag{2.1.1}$$

where $\tilde{k}$ is the permeability of the medium. From the scale relation $\ell' = \epsilon\ell''$ it follows that the pressure drop P' over the mesoscale ℓ' is $\epsilon P''$. We then have from (2.16) of Ch.1, after using $\tilde{k} = O(\ell^2/\mu)$, that

$$U = \frac{P'\ell^2}{\mu\ell'} = \frac{\ell^2}{\mu}\frac{P''}{\ell''} = \tilde{k}\frac{P''}{\ell''} = U' \tag{2.1.2}$$

which must be true in view of fluid mass conservation. It is stressed that Darcy's law applies only when the Reynolds number $Re = U\ell^2/\nu$ is very small($\leq O(\epsilon)$).

Let us now consider stress balance in the medium. From Hooke's law (3.3.16) of Chapter 1 which is legitimate only for infinitesimal strain we have

$$\frac{\tilde{\alpha}P''}{\tilde{a} : e(v)} \sim \frac{\tilde{\alpha}P''}{\tilde{a}\delta'} \sim \frac{P''}{\mathcal{D}\delta'} = O(1) \tag{2.1.3}$$

where $\mathcal{D}$ and δ' are the orders of magnitude of the elastic modulus and the strain in the medium. Use has been made of the fact that the pressure coefficient $\tilde{\alpha}$ is dimensionless and is $O(1)$. We shall assume that

$$\delta' \sim \frac{P''}{\mathcal{D}} = O(\epsilon) \ll 1 \tag{2.1.4}$$

so that the global strain of the medium is very small,e.g. if $\Delta V''$ is the scale of the medium deformation on the macroscale ℓ'', $\delta' = \Delta V''/\ell'' = O(\epsilon)$ which means that the displacement of the medium is very small as compared to the macroscale length ℓ'' i.e.,

$$\Delta V'' = O\left(\frac{P''}{\mathcal{D}}\ell''\right) = O(\epsilon\ell'') = O(\ell') \tag{2.1.5}$$

If we let P' and ΔV be the scales of pressure drop and the medium deformation across the mesoscale ℓ', it follows from (2.1.4) that

$$\frac{P'}{\mathcal{D}} = \frac{\epsilon P''}{\mathcal{D}} = O(\epsilon^2) \quad ; \quad \Delta V = O(\epsilon^2\ell') \tag{2.1.6}$$

This implies that the solid displacement over the mesoscale is much less than the microcell size as long as $\epsilon^2 \ll \ell/\ell'$. Recall that the two scale analysis was carried out with the assumption that $P'/\mathcal{D} = O(\ell/\ell')$. The scale of the medium stiffness $\mathcal{D}$ does not change much from scale to scale. Equation (2.1.6) then shows that the medium deformation over the mesoscale in the lower two scale (ℓ, ℓ') medium are much less than that of the previous two scale analysis.

The time scales are T_c' for consolidation, T_d' for diffusion and T_v' for convection which are given by

$$T_c' = \frac{\rho_f g \ell''^2}{\mathcal{D}K}, \quad T_d' = \frac{\ell''^2}{\alpha_f}, \quad T_v' = \frac{\ell''}{U'} \tag{2.1.7}$$

Their ratios are

$$\frac{T_c'}{T_d'} = \frac{\rho_f g \alpha_f}{\mathcal{D}K} \quad \text{and} \quad \frac{T_v'}{T_d'} = \frac{\ell'}{\ell''}\frac{\alpha_f}{U'\ell'} = O\left(\frac{\epsilon}{Pe'}\right) \tag{2.1.8a,b}$$

where Pe' is the Peclét number which signifies the relative importance of heat convection to heat diffusion based on the mesoscale length ℓ', and is defined as

$$Pe' = \frac{U'\ell'}{\alpha_f} \tag{2.1.9}$$

For thermoconsolidation, we shall assume that the Peclét number is very small. $Pe' = O(\epsilon) \ll 1$. In view of (2.1.2), the lower scale Peclét number Pe used in Ch.1 is related to Pe' of (2.1.9) by

$$Pe = \frac{U\ell}{\alpha_f} = \frac{U'\ell'}{\alpha_f}\frac{\ell}{\ell'} = \frac{\ell}{\ell'}Pe' \tag{2.1.10}$$

In order to allow the wide range of variation of the time scale ratio T_c'/T_d', it is assumed that $T_c' \sim T_d'$. Thus

$$Pe' = O(\epsilon) \quad , \quad T_c' \simeq T_d' \simeq T_v' \tag{2.1.11}$$

In our previous twp-scale analysis involving the microscale and the mesoscale , (2.1.6) shows that the departure of the solid-fluid interface is much smaller than the microcell size and the balance between fluid and solid stresses becomes $P'/\mathcal{D} \ll O(\epsilon)$. Consequently the nonlinearly coupled terms except the convection of heat in the mesoscale governing equations become negligibly small, and may be omitted at the outset. Those governing equations without the nonlinear coupling terms will be used in the following sections for order estimates and normalization.

2.2 Normalized Governing Equations.

On mesoscale, there is no such distinction as fluid and solid phases and the medium is continuous and inhomogeneous on the mesoscale level.

We first recall the governing equations from §3 of Ch.1 after dropping nonlinear coupling terms. The quasi-static equilibrium equation is

$$\nabla \cdot \sigma = \nabla \cdot \left[\tilde{a} : e(v) - \tilde{\alpha} p - \tilde{\beta}_t \theta \right] = -\rho_f g \beta_T n' \theta \mathbf{e}_z \tag{2.2.1}$$

in which θ is the temperature variation form the initial state. The thermoconsolidation equation reads

$$\nabla \cdot [\tilde{k} \cdot (\nabla p - \rho_f g \beta_T \theta \mathbf{e}_z)] = (\nabla n') \cdot \frac{\partial v}{\partial t} + \tilde{\gamma} : e\left(\frac{\partial v}{\partial t}\right) + \tilde{\beta}_c \frac{\partial p}{\partial t} + \tilde{\zeta}_c \frac{\partial \theta}{\partial t} \tag{2.2.2}$$

and the heat transport equation reads

$$\overline{\rho C_p} \frac{\partial T}{\partial t} + (\rho C_p)_f \overline{U} \cdot \nabla T = \nabla \cdot (\tilde{m} \cdot \nabla T) \tag{2.2.3}$$

in which T denotes the total temperature including the initial temperature and

$$\overline{U} = \langle u \rangle - \frac{\partial v}{\partial t} \cdot \langle \nabla \tilde{A}^s \rangle + \frac{(\rho C_p)_s}{(\rho C_p)_f} \frac{\partial v}{\partial t} \cdot \left((1 - n') I + \langle \nabla \tilde{A}^s \rangle \right) \tag{2.2.4}$$

is the effective velocity of heat convection. The flow of pore fluid through the porous medium is given by Darcy's law

$$\langle u\rangle - n'\frac{\partial v}{\partial t} = -\tilde{k}\cdot(\nabla p - \rho_f g\beta_T\theta \mathbf{e}_z) \tag{2.2.5}$$

The effective mesoscale coefficients in (2.2.1) to (2.2.5) have been given in §5. For the purpose of normalization we only summarize the orders of magnitude of those coefficients here.

$$\begin{array}{llll} \tilde{a}\sim\mathcal{D}, & \tilde{\alpha}\sim 1, & \tilde{\beta}_t\sim B & \\ \tilde{k}\sim\frac{\ell^2}{\mu}, & \tilde{\gamma}\sim 1, & \tilde{\beta}_c\sim 1/\mathcal{D}, & \tilde{\zeta}_c\sim B/\mathcal{D} \\ \langle\nabla\tilde{A}^e\rangle\sim 1, & \tilde{m}\sim M_f & & \end{array} \tag{2.2.6}$$

where B is the scale of thermal modulus. By using the scale estimates of §2.1, the unknown variables are normalized as follows:

$$\begin{aligned} x &= \ell' x^*, \quad t = Tt^* \\ \langle u\rangle &= U'\langle u\rangle^* = \tilde{k}\frac{P''}{\ell''}\langle u\rangle^* \\ v &= V'' v^* = \ell' v^* \\ \theta &= \Theta''\theta^*, \quad T = \Theta'' T^* \\ \sigma &= \mathcal{D}\sigma^* \end{aligned} \tag{2.2.7}$$

in which variables with the superscript symbol '*' are dimensionless. The temperature difference Θ'' is over the macroscale ℓ'' and is related to the variation Θ' over the mesoscale ℓ' by the relation $\Theta''\sim\Theta'/\epsilon$.

Substituting (2.2.6) and (2.2.7) into (2.2.1),(2.2.2),(2.2.3) and (2.2.5), we obtain

$$\nabla^*\cdot\sigma^* = -\epsilon^3\frac{Ra'}{Pe'}\theta^*\mathbf{e}_z \tag{2.2.8}$$

$$\sigma^* = a^* : e^*(v^*) - \left[\frac{P''}{\mathcal{D}}\right]\alpha^* p^* - \left[\frac{B\Theta''}{\mathcal{D}}\right]\beta_t^*\theta^* \tag{2.2.9}$$

$$\epsilon\langle u\rangle^* - \epsilon\left[\frac{V''}{U'T}\right]n'\frac{\partial v^*}{\partial t^*} = -k^*\cdot\left(\nabla^* p^* - \epsilon^2\frac{Ra'}{Pe'}\theta^*\mathbf{e}_z\right) \tag{2.2.10}$$

$$\begin{aligned} \nabla^*\cdot\left[k^*\cdot\left(\nabla^* p^* - \epsilon^2\frac{Ra'}{Pe'}\theta^*\mathbf{e}_z\right)\right] &= \epsilon\left[\frac{V''}{U'T}\right]\left((\nabla^* n')\cdot\frac{\partial v^*}{\partial t^*} + \gamma^* : e^*\left(\frac{\partial v^*}{\partial t^*}\right)\right) \\ &\quad + \left[\frac{\epsilon\ell'}{UT}\right]\left(\epsilon\beta_c^*\frac{\partial p^*}{\partial t^*} + \left[\frac{B\Theta''}{\mathcal{D}}\right]\zeta_c^*\frac{\partial\theta^*}{\partial t^*}\right) \end{aligned} \tag{2.2.11}$$

$$\begin{aligned} &\left[\frac{\ell'^2}{\alpha_f T}\right]\overline{\rho C_p}^*\frac{\partial T^*}{\partial t^*} + Pe'\left\{\langle u\rangle^* + \left[\frac{V''}{U'T}\right]\frac{\partial v^*}{\partial t^*}\cdot r^*\right\}\cdot\nabla^* T^* \\ &\qquad = \nabla^*\cdot(m^*\cdot\nabla^* T^*) \end{aligned} \tag{2.2.12}$$

where

$$r^* = -\langle \nabla \tilde{A}^s \rangle^* + \frac{(\rho C_p)_s}{(\rho C_p)_f} \left[(1-n')I + \langle \nabla \tilde{A}^s \rangle^* \right] \tag{2.2.13}$$

The dimensionless parameter Ra' is the Rayleigh number defined for the macroscale length ℓ'':

$$Ra' = \frac{K\beta_T \Theta'' \ell''}{\alpha_f} \tag{2.2.14}$$

It has been shown in §2 that the thermal modulus B is such that

$$B \sim \alpha \mathcal{D} \tag{2.2.15}$$

in which α is the linear coefficient of thermal expansion. Since the thermal stress must be balanced by the strain term in Hooke's law (2.2.9), the multiplying factor in thermal stress of (2.2.9) is estimated as

$$\frac{B\Theta''}{\mathcal{D}} \sim \alpha \Theta'' = O(\epsilon) \tag{2.2.16}$$

As has been mentioned earlier, three time scales are all comparable and it is anticipated that this will lead to thermoconsolidation with convection of heat contributed by both flow and solid deformation. Only one time scale is used.

We examine first the ratio of solid velocity to seepage velocity. Using T'_d for T and $V'' = O(\ell')$ we get

$$\frac{V''}{U'T} = O\left(\frac{\ell'}{\tilde{k}\frac{P''}{\ell''}\frac{\rho_f g \ell''^2}{\mathcal{D}K}} \frac{T'_c}{T'_d} \right) = O\left(\frac{K}{\tilde{k}\rho_f g} \frac{\mathcal{D}}{P''} \frac{\ell'}{\ell''} \frac{T'_c}{T'_d} \right) = O\left(\frac{\mathcal{D}}{P''} \epsilon \frac{T'_c}{T'_d} \right) = O(1) \tag{2.2.17}$$

where $\tilde{k} = K/\rho_f g$ and (2.1.2) were used. Therefore heat convection due to flow and solid deformation are equally important in (2.2.12). Suppose that the initial temperature difference of $O(\Theta'')$ across ℓ'' is too small to induce natural convection. Guided by the criterion for the onset of natural convection in porous media for a simple case(Lapwood, 1948) that $Ra' = 4\pi^2 \sim 40$, we impose the following restriction on Ra'

$$Ra' \leq O(1) \tag{2.2.18}$$

As a check for practical relevance, we choose the following values $\beta_T = O(10^{-4\circ}C^{-1})$ and $\alpha_f = O(10^{-7}m^2/s)$ which are typical of water and allowing $\Theta'' \leq O(10^{2\circ})$ and $\ell'' \leq O(10^2 m)$. Then for a less permeable medium with $K = O(10^{-7}m/s)$ from Table 2.1 of Chapter 1, we indeed have $Ra' = O(1)$.

The multiplying factor of the local derivative in (2.2.12) becomes, upon using $T = T'_c \sim T'_d$

$$\frac{\ell'^2}{\alpha_f T'_c} = \frac{\ell'^2}{\alpha_f T'_d}\frac{T'_d}{T'_c} \simeq \left(\frac{\ell'}{\ell''}\right)^2 \frac{T'_d}{T'_c} = O(\epsilon^2) \tag{2.2.19}$$

Note that the temporal changes of temperatures θ and T in the consolidation equation (2.2.11) and the heat equation (2.2.12) are equally scaled as $O(\epsilon^2)$ which confirms that p and θ evolve over a comparable time scale as implied by $T'_c \sim T'_d$.

3. The Macroscale Governing Equations.

Starting from the normalized governing equations on the mesoscale of §2, the governing equations and constitutive relations on the macroscale are deduced. In §3.1, the multiple scale perturbation expansions are introduced and the governing equations at successive orders of ϵ are obtained. Then in §3.2 and §3.3, the macroscale governing equations for the deformation, flow and heat transport are derived. Certain canonical cell boundary value problems are obtained. Their solutions take account of the mesoscale heterogeneity and are essential in the calculation of the macroscale coefficients. Finally in §3.4, a limiting case of highly permeable medium with $T_c/T_d \ll 1$ is discussed and the governing equations are presented in physical variables in §3.5.

3.1 Multiple-Scale Expansions and Perturbation Equations

If (2.2.16) to (2.2.31) are substituted into (2.2.8) to (2.2.12), we have

$$\nabla^* \cdot \sigma^* = -\epsilon^2 n' \frac{Ra'}{\hat{P}e'} \theta \mathbf{e}_z \tag{3.1.1}$$

$$\sigma^* = a^* : e^*(v^*) - \epsilon \alpha^* p^* - \epsilon \beta_t^* \theta^* \tag{3.1.2}$$

$$\epsilon \langle u \rangle^* - \epsilon n' \frac{\partial v^*}{\partial t^*} = -k^* \cdot \left(\nabla^* p^* - \epsilon \frac{Ra'}{\hat{P}e'} \theta^* \mathbf{e}_z \right) \tag{3.1.3}$$

$$\begin{aligned} \nabla^* \cdot \left[k^* \cdot \left(\nabla^* p^* - \epsilon \frac{Ra'}{\hat{P}e'} \theta^* \mathbf{e}_z \right) \right] =& \epsilon (\nabla^* n') \cdot \frac{\partial v^*}{\partial t^*} + \epsilon \gamma^* : e^* \left(\frac{\partial v^*}{\partial t^*} \right) \\ &+ \epsilon^2 \beta_c^* \frac{\partial p^*}{\partial t^*} + \epsilon^2 \zeta_c^* \frac{\partial \theta^*}{\partial t^*} \end{aligned} \tag{3.1.4}$$

$$\epsilon^2 \overline{\rho C_p}^* \frac{\partial T^*}{\partial t^*} + \hat{P}e' \epsilon \left[\langle u \rangle^* + \frac{\partial v^*}{\partial t^*} \cdot r^* \right] \cdot \nabla^* T^* = \nabla^* \cdot (m^* \cdot \nabla^* T^*) \tag{3.1.5}$$

where

$$\hat{P}e' = Pe'/\epsilon = O(1) \tag{3.1.6}$$

and r^* was given in (2.2.13). The coefficients are supposed to have been calculated for a given cell geometry at the microscale and are assumed to be Ω'-periodic.

Assuming a periodic structure on the mesoscale, we divide the medium into periodic mesoscale cells of length ℓ'. The variables are assumed to be Ω'-periodic.

Introducing the multiple-scale vectors in space

$$x', \quad x'' = \epsilon x' \tag{3.1.7}$$

which represent the meso-and macroscales respectively, the differential operators are accordingly expanded as

$$\begin{aligned} \nabla^* &= \nabla' + \epsilon \nabla'' \\ e^*(\cdot) &= e'(\cdot) + \epsilon e''(\cdot) \end{aligned} \tag{3.1.8a,b}$$

We also introduce the expansion in perturbation series

$$f^* = f^{(0)} + \epsilon f^{(1)} + \epsilon^2 f^{(2)} + \dots \tag{3.1.9}$$

for

$$f^* = \langle u \rangle^*, v^*, p^* \quad \text{and} \quad \theta^* \tag{3.1.10}$$

where all the perturbation quantities depend on x', x'' and t^* and are Ω'-periodic, but

$$\sigma^* = \sigma^{(-1)} + \epsilon \sigma^{(0)} + \epsilon^2 \sigma^{(1)} + \cdots \tag{3.1.11}$$

for the stress in view of (2.1.4).

3.1.1 Equilibrium, Darcy's law and Consolidation Equations.

In the equilibrium equation (3.1.1), we expand Hooke's law after substituting (3.1.9) for v^* and (3.1.8b) for strain tensors to obtain

$$\begin{aligned} \sigma^* = a^* : e'(v^{(0)}) + \epsilon a^* : \left[e''(v^{(0)}) + e'(v^{(1)}) \right] \\ + \epsilon^2 a^* : \left[e''(v^{(1)}) + e'(v^{(2)}) \right] + \cdots \end{aligned} \tag{3.1.12}$$

From (3.1.11) it follows that

$$\begin{aligned} \sigma^{(-1)} &= a^* : e'(v^{(0)}) \\ \sigma^{(0)} &= a^* : [e''(v^{(0)}) + e'(v^{(1)})] - \alpha^* p^{(0)} - \beta_t^* \theta^{(0)} \\ \sigma^{(1)} &= a^* : [e''(v^{(1)}) + e'(v^{(2)})] - \alpha^* p^{(1)} - \beta^* \theta^{(1)} \end{aligned} \tag{3.1.13a-c}$$

Substituting (3.1.13) into (3.1.1), it immediately follows that

$$v^{(0)} = v^{(0)}(x'', t^*) \tag{3.1.14}$$

Therefore the leading order solid displacement does not depend on the mesoscale and is of $O(\ell')$. The medium strain is then $\delta' = v/\ell'' = O(\epsilon)$ which is consistent with (2.1.4).

At subsequent orders of ϵ, it follows from (3.1.1) that

$$\begin{array}{ll} O(\epsilon) & \nabla' \cdot \sigma^{(0)} = 0 \\ O(\epsilon^2) & \nabla'' \cdot \sigma^{(0)} + \nabla' \cdot \sigma^{(1)} = -n' \frac{Ra'}{\hat{P}e'} \theta \end{array} \tag{3.1.15a,b}$$

It is seen that the expansion of the equilibrium equation resembles completely that for the micro-meso scale case.

The Darcy's law (3.1.3), which is the momentum equation, is similarly expanded :

$$\begin{array}{ll} O(1) & 0 = -k^* \cdot \nabla' p^{(0)} \\ O(\epsilon) & \langle u \rangle^{(0)} - n' \frac{\partial v^{(1)}}{\partial t^*} = -k^* \cdot \left[\left(\nabla'' p^{(0)} + \nabla' p^{(1)} - \frac{Ra'}{\hat{P}e'} \theta^{(0)} \mathbf{e}_z \right) \right] \end{array} \tag{3.1.16a,b}$$

It follows immediately from (3.1.16a) that

$$p^{(0)} = p^{(0)}(x'', t^*) \tag{3.1.17}$$

which shows that the leading order pressure does not depend on x'.

The consolidation equation (3.1.4) becomes

$$\begin{aligned} O(1) \quad & \nabla' \cdot \left(k^* \cdot \nabla' p^{(0)} \right) = 0 \\ O(\epsilon) \quad & \nabla' \cdot \left[k^* \cdot \left(\nabla'' p^{(0)} + \nabla' p^{(1)} - \frac{Ra'}{\hat{P}e'} \theta^{(0)} \mathbf{e}_z \right) \right] + \nabla'' \cdot \left(k^* \cdot \nabla' p^{(0)} \right) \\ & \qquad = (\nabla' n') \cdot \frac{\partial v^{(0)}}{\partial t^*} + \gamma^* : e' \left(\frac{\partial v^{(0)}}{\partial t^*} \right) \\ O(\epsilon^2) \quad & \nabla'' \cdot \left[k^* \cdot \left(\nabla'' p^{(0)} + \nabla' p^{(1)} - \frac{Ra'}{\hat{P}e'} \theta^{(0)} \mathbf{e}_z \right) \right] \\ & \qquad + \nabla' \cdot \left[k^* \cdot \left(\nabla'' p^{(1)} + \nabla' p^{(2)} - \frac{Ra'}{\hat{P}e'} \theta^{(1)} \mathbf{e}_z \right) \right] \\ & \qquad = (\nabla'' n') \cdot \frac{\partial v^{(0)}}{\partial t^*} + (\nabla' n') \cdot \frac{\partial v^{(1)}}{\partial t^*} \\ & \qquad + \gamma^* : \left[e'' \left(\frac{\partial v^{(0)}}{\partial t^*} \right) + e' \left(\frac{\partial v^{(1)}}{\partial t^*} \right) \right] + \beta^* \frac{\partial p^{(0)}}{\partial t^*} + \zeta^* \frac{\partial \theta^{(0)}}{\partial t^*} \end{aligned} \tag{3.1.18a-c}$$

in which (3.1.18a) is automatically satisfied by (3.1.17).

3.1.2 The Heat Transport Equation.

Expanding (3.1.5) according to (3.1.8) and (3.1.9), we obtain

$$
\begin{aligned}
O(1) \quad & 0 = \nabla' \cdot \left(m^* \cdot \nabla' T^{(0)} \right) \\
O(\epsilon) \quad & \hat{P}e' \left(\langle u \rangle^{(0)} + \frac{\partial v^{(0)}}{\partial t^*} \cdot r^* \right) \cdot \nabla' T^{(0)} \\
& \qquad = \nabla' \cdot \left[m^* \cdot \left(\nabla'' T^{(0)} + \nabla' T^{(1)} \right) \right] + \nabla'' \cdot \left(m^* \cdot \nabla' T^{(0)} \right) \\
O(\epsilon^2) \quad & \overline{\rho C_p}^* \frac{\partial T^{(0)}}{\partial t^*} + \hat{P}e' \left(\langle u \rangle^{(0)} + \frac{\partial v^{(0)}}{\partial t^*} \cdot r^* \right) \cdot \left(\nabla'' T^{(0)} + \nabla' T^{(1)} \right) \\
& + \hat{P}e' \left(\langle u \rangle^{(1)} + \frac{\partial v^{(1)}}{\partial t^*} \cdot r^* \right) \cdot \nabla' T^{(0)} = \nabla'' \cdot \left[m^* \cdot \left(\nabla'' T^{(0)} + \nabla' T^{(1)} \right) \right] \\
& \qquad + \nabla' \cdot \left[m^* \cdot \left(\nabla'' T^{(1)} + \nabla' T^{(2)} \right) \right]
\end{aligned}
\tag{3.1.19a - c}
$$

Since the thermal conductivity m^* is positive define, it readily follows from (3.1.19a) that

$$
T^{(0)} = T^{(0)}(x'', t^*) \tag{3.1.20}
$$

after imposing the Ω'-periodicity condition. Thus the leading order temperature is independent of the mesoscale. If we decompose the total temperature into the initial temperature $\overline{T}^{(0)}$ and the variation $\theta^{(0)}$, (3.1.20) shows that

$$
\overline{T}^{(0)} = \overline{T}^{(0)}(x'', t^*), \quad \theta^{(0)} = \theta^{(0)}(x'', t^*) \tag{3.1.21}
$$

since $\overline{T}^{(0)}$ is also governed by the same diffusion equation (3.1.19a).

3.2 The Macroscale Equations for Deformation and Flow.

Deformation of the Medium

In the Ω'-cell, the deformation of the medium is governed by (3.1.15a) which is written

$$
\nabla' \cdot \sigma^{(0)} = \nabla' \cdot \left[a^* : [e''(v^{(0)}) + e'(v^{(1)})] - \alpha^* p^{(0)} - \beta_t^* \theta^{(0)} \right] = 0 \tag{3.2.1}
$$

after using (3.1.13b). We also impose that

$$\sigma^{(0)} \quad \text{is } \Omega'\text{-periodic.} \tag{3.2.2}$$

In view of (3.1.14), (3.1.17) and (3.1.21) and linearity, we assume that

$$v^{(1)} = \phi' : e''(v^{(0)}) - \eta' p^{(0)} - \zeta' \theta^{(0)} \tag{3.2.3}$$

where ϕ' is a third order tensor and η' and ζ' are vectors. They are fuctions of x' and x'' and are assumed to be Ω'-periodic. Variables $v^{(0)}$, $p^{(0)}$ and $\theta^{(0)}$ are yet to be determined.

Substitution of (3.2.3) into (3.2.1) and (3.2.2) gives the following mesoscale cell boundary value problems.

$$\begin{aligned} &\nabla' \cdot [a^* : e'(\phi')] + \nabla' \cdot (a^* \cdot II) = 0 \\ &\nabla' \cdot [a^* : e'(\eta')] + (\nabla' \cdot \alpha^*) = 0 \qquad \text{in } \Omega' \\ &\nabla' \cdot [a^* : e'(\zeta')] + (\nabla' \cdot \beta_i^*) = 0 \end{aligned} \tag{3.2.4a-c}$$

and

$$\phi', \eta', \zeta' \quad \text{are } \Omega'\text{-periodic.} \tag{3.2.4d}$$

They are elastostatic problems in the Ω'-cell with distributed body force produced by the heterogeneities in the elastic properties on the mesoscale. By using positive definiteness of strain energy, it is straightforward to show that ϕ', η', ζ' in (3.2.4a-d) are unique upto a mesoscale independent constant. For uniqueness, we further require that

$$\langle \phi' \rangle_{\Omega'} = \langle \eta' \rangle_{\Omega'} = \langle \zeta' \rangle_{\Omega'} = 0 \tag{3.2.4e}$$

where the angle-brackets denote the Ω'-average

$$\langle f \rangle_{\Omega'} = \frac{1}{\Omega'} \int_{\Omega'} f d\Omega' \tag{3.2.5}$$

The canonical boundary value problems (3.2.4) can be solved for a specified distribution of mesoscale heterogeneity in the Ω'-cell.

We now take the Ω'-average of (3.1.15b) and use Gauss theorem and Ω'-periodicity to obtain

$$\nabla'' \cdot \langle \sigma^{(0)} \rangle = -n'' \frac{Ra'}{\hat{P}e'} \theta^{(0)} \mathbf{e}_z \tag{3.2.6}$$

which is the macroscale equilibrium equation. Note the existence of body force which originates from the buoyancy effects in the pore fluid on the microscale. Upon substituting (3.1.13c) and (3.2.3) into (3.2.6) the macroscale Hooke's law becomes

$$\langle \sigma^{(0)} \rangle = a'' : e''(v^{(0)}) - \alpha'' p^{(0)} - \beta_t'' \theta^{(0)} \tag{3.2.7}$$

where

$$\begin{aligned} a'' &= \langle a^* : [II + e'(\phi')] \rangle_{\Omega'} \\ \alpha'' &= \langle \alpha^* \rangle_{\Omega'} + \langle a^* : e'(\eta') \rangle_{\Omega'} \\ \beta_t'' &= \langle \beta^* \rangle_{\Omega'} + \langle a^* : e'(\zeta') \rangle_{\Omega'} \end{aligned} \tag{3.2.8a-c}$$

are the macroscale elastic coefficient, the pressure coefficient and the thermal modulus respectively. Note its complete resemblance to Hooke's law on the mesoscale. The first terms in (3.2.8) are simply the volume averages of the coefficients over the mesocale. The second terms are the effects of mesoscale heterogeneities on the macroscale effective elastic coefficients.

Flow

After invoking (3.1.14) and (3.1.17), the consolidation equation (3.1.18b) becomes

$$\nabla' \cdot \left[k^* \cdot \left(\nabla'' p^{(0)} + \nabla' p^{(1)} - \frac{Ra'}{\hat{P}e'} \theta^{(0)} \mathbf{e}_z \right) - n' \frac{\partial v^{(0)}}{\partial t^*} \right] = 0 \tag{3.2.9}$$

where $\gamma^* = n'I - \langle e(\phi) : I \rangle$ (cf.(3.3.?) of Ch. 1) has been used to move the solid velocity term $n' \partial v^{(0)} / \partial t^*$ to the left-hand side of (3.1.18b). Equation (3.2.9) suggests the following form for $p^{(1)}$.

$$p^{(1)} = S' \cdot \left(\nabla'' p^{(0)} - \frac{Ra'}{\hat{P}e'} \theta^{(0)} \mathbf{e}_z \right) - W' \cdot \frac{\partial v^{(0)}}{\partial t^*} \tag{3.2.10}$$

in which $S'(x', x'')$ and $W'(x', x'')$ are Ω'-periodic vectors. They must satisfy the following boundary value problems which are obtained after substituting (3.2.10) into (3.2.9).

$$\nabla' \cdot [k^* \cdot (I + \nabla' S')] = 0 \qquad \text{in } \Omega'$$
$$\nabla' \cdot (k^* \cdot \nabla' W' + n' I) = 0 \qquad \text{in } \Omega' \qquad (3.2.11a, b)$$

$$S' \quad \text{and} \quad W' \quad \text{are } \Omega'\text{-periodic.} \qquad (3.2.11c)$$

$$\langle S' \rangle = \langle W' \rangle = 0 \qquad (3.2.11d)$$

where (3.2.11d) is imposed for uniqueness. These are steady seepage flow problems for S' and W' with distributed sources due to heterogeneities in the permeability k' and porosity n' on the mesoscale ℓ'.

At the next order $O(\epsilon^2)$, (3.1.18c) becomes, after using (3.2.3) and (3.2.10), as

$$\begin{aligned}
&\nabla'' \cdot \left\{ k^* \cdot \left[\nabla'' p^{(0)} + \nabla' \left(S' \cdot \left(\nabla'' p^{(0)} - \frac{Ra'}{\hat{P} e'} \theta^{(0)} \mathbf{e}_z \right) - W' \cdot \frac{\partial v^{(0)}}{\partial t^*} \right) \right] \right\} \\
&- \frac{Ra'}{\hat{P} e'} \nabla'' \cdot \left(k^* \cdot \theta^{(0)} \mathbf{e}_z \right) + \nabla' \cdot \left[k^* \cdot \left(\nabla'' p^{(1)} + \nabla' p^{(2)} - \frac{Ra'}{\hat{P} e'} \theta^{(1)} \mathbf{e}_z \right) \right] \\
&= \nabla' \cdot \left(n' \frac{\partial v^{(1)}}{\partial t^*} \right) + (\gamma^* - n' I) : e' \left[\phi' : e'' \left(\frac{\partial v^{(0)}}{\partial t^*} \right) - \eta' \frac{\partial p^{(0)}}{\partial t^*} - \zeta' \frac{\partial \theta^{(0)}}{\partial t^*} \right] \\
&+ (\nabla'' n') \cdot \frac{\partial v^{(0)}}{\partial t^*} + \gamma^* : e'' \left(\frac{\partial v^{(0)}}{\partial t^*} \right) + \beta^* \frac{\partial p^{(0)}}{\partial t^*} + \zeta^* \frac{\partial \theta^{(0)}}{\partial t^*}
\end{aligned} \qquad (3.2.12)$$

Integrating (3.2.12) over Ω'-cell and using Gauss theorm and Ω'-periodicity, we obtain

$$\begin{aligned}
&\nabla'' \cdot \left[k'' \cdot \left(\nabla'' p^{(0)} - \frac{Ra'}{\hat{P} e'} \theta^{(0)} \mathbf{e}_z \right) \right] = [\nabla'' \cdot (n'' I + \delta_c'')] \cdot \frac{\partial v^{(0)}}{\partial t^*} \\
&+ \gamma'' : e'' \left(\frac{\partial v^{(0)}}{\partial t^*} \right) + \delta_c'' : \nabla'' \left(\frac{\partial v^{(0)}}{\partial t^*} \right) + \beta_c'' \frac{\partial p^{(0)}}{\partial t^*} + \zeta_c'' \frac{\partial \theta^{(0)}}{\partial t^*}
\end{aligned} \qquad (3.2.13)$$

where

$$\begin{aligned}
k'' &= \langle k^* \cdot (I + \nabla' S') \rangle \\
\gamma'' &= \langle \gamma^* + (\gamma^* - n' I) : e'(\phi') \rangle = n'' I - \langle \langle e(\phi) : I \rangle^* : (II + e'(\phi')) \rangle \\
\beta_c'' &= \langle \beta_c^* - (\gamma^* - n' I) : e'(\eta') \rangle = \langle \langle e(\eta) : I \rangle + \langle e(\phi) : I \rangle^* : e'(\eta') \rangle \\
\zeta_c'' &= \langle \zeta_c^* - (\gamma^* - n' I) : e'(\zeta') \rangle = \langle \langle e(\zeta) : I \rangle^* + \langle e(\phi) : I \rangle^* : e'(\zeta') \rangle \\
\delta_c'' &= \langle k^* \cdot \nabla' W' \rangle
\end{aligned} \qquad (3.2.14a - e)$$

in which the mesoscale coefficients $\gamma^* = n'I - \langle e(\phi) : I\rangle^*$, $\beta_c^* = \langle\langle e(\eta) : I\rangle^*$ and $\zeta_c^* = \langle\langle e(\zeta) : I\rangle^*$ from §3 of Ch.1 have been used. The coefficient k'' is the macroscale permeability and $\gamma'', \beta_c'', \zeta_c''$ and δ_c'' are the coefficients related to the elastic properties of the medium. The macroscale thermoconsolidation equation (3.2.13) includes again two thermal effects : one is the effect of buoyancy on the flow and the other is the deformation of the medium on the right-hand side denoted by ζ_c''.

After integration over Ω'-cell, the Darcy's law readily follows from (3.1.16b)

$$\langle\langle u\rangle^{(0)}\rangle - n''\frac{\partial v^{(0)}}{\partial t^*} = -k'' \cdot \left(\nabla'' p^{(0)} - \frac{Ra'}{\hat{P}e'}\theta^{(0)}\mathbf{e}_z\right) \qquad (3.2.15)$$

in which k'' has been given by (3.2.14a).

So far the macroscale governing equations for deformation of and flow through porous medium have been obtained. Note that, if the medium is homogeneous at the mesoscale level, the forcing terms in (3.2.4) and (3.2.11) diminish and the mesoscale unknown variables introduced above all vanish. Therefore, any difference in the meso-and macroscale coefficients is the outcome of the mesoscale heterogeneities. This is different from the heterogeneities on the microscale level which were only due to the existence of different phases such as fluid and solid.

3.3 The Macroscale Heat Transport Equation.

As in the deformation and flow, another mesoscale boundary value problem is defined whose solution reflects the effects of mesoscale heterogeneity in thermal conductivity on the thermal properties of the medium at the macroscale.

It has been shown in (3.1.20) that the leading order temperatures do not depend on the mesoscale. At the next order $O(\epsilon)$, (3.1.19b),(3.1.20) and Ω'-periodicity give

$$\begin{aligned} \nabla' \cdot \left[m^* \cdot \left(\nabla'' T^{(0)} + \nabla' T^{(1)}\right)\right] = 0 \qquad & \text{in } \Omega' \\ T^{(1)} \text{ is } \Omega'\text{-periodic} \qquad & \text{on } \partial\Omega' \end{aligned} \qquad (3.3.1a,b)$$

which is again a steady conduction problem. Both the initial temperature $\overline{T}^{(1)}$ and the deviation from it $\theta^{(1)}$ are governed by the same equation. Equation (3.3.1a) then suggests

$$\theta^{(1)} = A' \cdot \nabla'' \theta^{(0)} \quad ; \quad \overline{T}^{(1)} = A' \cdot \nabla'' \overline{T}^{(0)} \tag{3.3.2}$$

where $A'(x', x'')$ is Ω'-periodic vector and must satisfy

$$\begin{aligned} \nabla' \cdot [m^* \cdot (I + \nabla' A')] &= 0 \qquad \text{in } \Omega' \\ A' \quad \text{is } \Omega'\text{-periodic} &\qquad \text{on } \partial\Omega' \\ \langle A' \rangle_{\Omega'} &= 0 \end{aligned} \tag{3.3.3a-c}$$

the last of which is imposed for the uniqueness of A'. It is a steady conduction problem with source distribution inside the cell which reflects the heterogeneity of the medium in thermal conductivity m' on the mesoscale.

Finally at $O(\epsilon^2)$, we have from (3.1.19c) after using (3.1.20)

$$\begin{aligned} &\overline{\rho C_p}^* \frac{\partial T^{(0)}}{\partial t^*} + \hat{P}e' \left(\langle u \rangle^{(0)} + \frac{\partial v^{(1)}}{\partial t^*} \cdot r^* \right) \cdot \left(\nabla'' T^{(0)} + \nabla' T^{(1)} \right) \\ &= \nabla'' \cdot \left[m^* \cdot \left(\nabla'' T^{(0)} + \nabla' T^{(1)} \right) \right] + \nabla' \cdot \left[m^* \cdot \left(\nabla'' T^{(1)} + \nabla' T^{(2)} \right) \right] \qquad \text{in } \Omega' \end{aligned} \tag{3.3.4}$$

Substituting (3.3.2) into (3.3.4), integrating over Ω'-cell and decomposing the total temperature into the initial and deviation parts, we finally obtain

$$\begin{aligned} \langle \overline{\rho C_p}^* \rangle \frac{\partial \theta^{(0)}}{\partial t^*} + \hat{P}e' \left[\langle \langle u \rangle^{(0)} \cdot (I + \nabla' A') \rangle + \frac{\partial v^{(0)}}{\partial t^*} \cdot \langle r^* \qquad \cdot (I + \nabla' A') \rangle \right] \\ \cdot \left(\nabla'' \theta^{(0)} + \nabla'' \overline{T}^{(0)} \right) = \nabla'' \cdot \left[m'' \cdot \nabla'' \theta^{(0)} \right] \end{aligned} \tag{3.3.5}$$

where

$$m'' = \langle m^* \cdot (I + \nabla' A') \rangle \tag{3.3.6}$$

is the macroscale thermal conductivity. Equation (3.3.5) governs the transport of heat at the macroscale. Even though the convection of heat at the mesoscale is very small, i.e. $Pe' = O(\epsilon)$, it is equally important as diffusion at the macroscale due to different proportionality of time scales T'_v and T'_d to the length(cf.(2.1.7)). Again, if the medium has homogeneous thermal conductivity on the mesoscale, $A' = 0$ and

m'' reduces to m' obtained previously from the two scale analysis for the micro- and mesoscales. It should be stressed that the heat equation (3.3.5) is nonlinearly coupled to the pressure and solid movement through the convection term.

The macroscale governing equations (3.2.6), (3.2.13), (3.2.15) and (3.3.5) are fully coupled in that each of them involve $v^{(0)}$, $\langle u\rangle^{(0)}$ and $\theta^{(0)}$ and should be solved together. This feature is the same as in the two scale case. Under some special conditions, further reductions can be made (see §3.5 of two scale problem).

3.4 A Special Case of Small T_c' ; $T_c'/T_d' = O(\epsilon^2)$.

As explained in the two scale case, highly permeable medium such as sand is very often characterized by small ratio of T_c'/T_d' typically of $O(\epsilon^2)$. In such case, T_c' is of negligible interest whereas T_v' and T_d' are still comparable. The ratio of the medium velocity to seepage flow velocity then becomes, upon using T_v' or T_d' for T in (2.2.17),

$$\frac{V}{UT_c'} = \frac{V}{UT_c'}\frac{T_c'}{T_d'} = O(\epsilon^2) \tag{3.4.1}$$

As a result terms due to solid movement in (2.2.10) to (2.2.12) become very small. Therefore we readily have

$$\nabla''\cdot\left[a'' : e''(v^{(0)}) - \alpha'' p^{(0)} - \beta_t'' \theta^{(0)}\right] = -n''\frac{Ra'}{\hat{P}e'}\theta^{(0)}\mathbf{e}_z \tag{3.4.2}$$

$$\langle\langle u\rangle^{(0)}\rangle = -k''\cdot\left(\nabla'' p^{(0)} - \frac{Ra'}{\hat{P}e'}\theta^{(0)}\mathbf{e}_z\right) \tag{3.4.3}$$

$$\nabla''\cdot\left[k''\cdot\left(\nabla'' p^{(0)} - \frac{Ra'}{\hat{P}e'}\theta^{(0)}\mathbf{e}_z\right)\right] = 0 \tag{3.4.4}$$

$$\langle\overline{\rho C_p}^{*}\rangle\frac{\partial\theta^{(0)}}{\partial t^*} + \hat{P}e'\langle\langle u\rangle^{(0)}\cdot\left(\nabla''\theta^{(0)} + \nabla''\overline{T}^{(0)}\right) = \nabla''\cdot\left[m''\cdot\nabla''\theta^{(0)}\right] \tag{3.4.5}$$

As in the case of two scale medium, only the flow and heat transport are nonlinearly coupled through buoyancy. The medium deformation is determined afterwards from the pore pressure and temperature.

3.5 The Macroscale Governing Equations in Physical Variables.

If we reall the normalization scales (2.2.6) and (2.2.7), the governing equations in physical variables become as follows.

$$\nabla \cdot [\tilde{a} : e(v) - \tilde{\alpha} p - \tilde{\beta}_t \theta] = -n'' \rho_f g \beta_T \theta \mathbf{e}_z \tag{3.5.1}$$

$$\begin{aligned} \nabla \cdot [\tilde{k} \cdot (\nabla p - \rho_f g \beta_T \theta \mathbf{e}_z)] &= \left[\nabla \cdot (n'' + \tilde{\delta}_c)\right] \cdot \frac{\partial v}{\partial t} + \tilde{\gamma} : e\left(\frac{\partial v}{\partial t}\right) + \tilde{\beta}_c \frac{\partial p}{\partial t} \\ &+ \tilde{\zeta}_c \frac{\partial \theta}{\partial t} + \tilde{\delta}_c : \nabla\left(\frac{\partial v}{\partial t}\right) \end{aligned} \tag{3.5.2}$$

$$\langle\langle u \rangle\rangle - n' \frac{\partial v}{\partial t} = -\tilde{k} \cdot (\nabla p - \rho_f g \beta_T \theta \mathbf{e}_z) \tag{3.5.3}$$

$$\begin{aligned} \overline{\overline{\rho C_p}} \frac{\partial \theta}{\partial t} + (\rho C_p)_f \left[\langle u \rangle \cdot (I + \nabla' \tilde{A}') + \frac{\partial v}{\partial t} \cdot \langle \tilde{r} \cdot (I + \nabla' \tilde{A}') \rangle\right] \cdot (\nabla \overline{T} + \nabla \theta) \\ = \nabla \cdot (\tilde{m}'' \cdot \nabla \theta) \end{aligned} \tag{3.5.4}$$

where the overhead symbol ($\tilde{}$) has been used to denote dimensional coefficients and

$$\begin{aligned} \overline{\overline{\rho C_p}} &= \langle \overline{\rho C_p} \rangle = \langle (\rho C_p)_f n' + (\rho C_p)_s (1 - n') \rangle \\ \tilde{r} &= -(\rho C_p)_f \langle \nabla \tilde{A}^s \rangle + (\rho C_p)_s \left[(1 - n') I + \langle \nabla \tilde{A}^s \rangle\right] \end{aligned} \tag{3.5.5}$$

Note that all coefficients reflect the influence of heterogeneities both on the microscale due to the presence of different phases(solid and fluid) and on the mesoscale by composition of heterogeneous media.

4. Properties of Macroscale Coefficients.

As in the case of two scale medium, there exist certain properties of the macroscale coefficients. For the isothermal case, Mei and Auriault(1989) studied the consolidation of three scale media and extended the two scale results by Auriault and Sanchez -Palencia (1977). They established certain constraints on α'', γ'' and β_c''. Specifically they showed the symmetry and posotive definiteness of the permeability k''.

We now extend Mei and Auriault(1989) (from here on refered to as M&A) to thermoconsoilidation. From (3.2.4a-e) the boundary value problems for ϕ', η' and ζ' may be written in indicial form as

$$\frac{\partial}{\partial x_i'}\left[a'_{ijpq}\left(\delta_{pm}\delta_{qn}+e'_{pq}(\phi'^{mn})\right)\right]=0 \qquad \text{in} \quad \Omega'$$

$$\frac{\partial}{\partial x_i'}\left[a'_{ijpq}e'_{pq}(\eta')+\alpha'_{ij}\right]=0 \qquad \text{in} \quad \Omega' \qquad (4.1a-c)$$

$$\frac{\partial}{\partial x_i'}\left[a'_{ijpq}e'_{pq}(\zeta')+(\beta'_t)_{ij}\right]=0 \qquad \text{in} \quad \Omega'$$

$$\phi', \quad \eta' \quad \text{and} \quad \zeta' \quad \text{are} \quad \Omega'-\text{periodic} \qquad (4.1d)$$

and

$$\langle\phi'\rangle=\langle\eta'\rangle=\langle\zeta'\rangle=0 \qquad (4.1e)$$

M&A have shown by using (4.1a and b) that

$$\langle a' : e'(\eta')\rangle=\langle\alpha' : e'(\phi')\rangle \qquad (4.2)$$

$$\langle\alpha' : e'(\eta')\rangle<0 \qquad (4.3)$$

We now extend it to find similar relationships between ϕ' and ζ' and η' and ζ'. If we multiply (4.1a) by ζ' and integrate over Ω'-cell, it follows after using Gauss theorem and Ω'-periodicity that

$$\int_{\Omega'} a'_{ijpq}\delta_{pm}\delta_{qn}e'_{ij}(\zeta')d\Omega'+\int_{\Omega'} a'_{ijpq}e'_{pq}(\phi'^{mn})e'_{ij}(\zeta')d\Omega'=0 \qquad (4.4)$$

Also by multiplying (4.1c) by ϕ'^{mn} and integrate over Ω'-cell, we get

$$\int_{\Omega'} a'_{ijpq} e'_{pq}(\phi'^{mn}) e'_{ij}(\zeta') d\Omega' + \int_{\Omega'} (\beta'_t)_{ij} e'_{ij}(\phi'^{mn}) d\Omega' = 0 \tag{4.5}$$

Subtracting (4.5) from (4.4) and making use of the symmetry relation $a'_{ijmn} = a'_{mnij}$, we obtain

$$\langle a' : e'(\zeta') \rangle = \langle \beta'_t : e'(\phi') \rangle \tag{4.6}$$

Following the same procedure for (4.1b) and (4.1c) it is readily seen that

$$\langle \beta'_t : e'(\eta') \rangle = \langle \alpha' : e'(\zeta') \rangle \tag{4.7}$$

On the other hand, upon multiplying (4.1c) by ζ' and recalling that a'_{ijkl} is positive definite,

$$\langle \beta'_t : e'(\zeta') \rangle < 0 \tag{4.8}$$

In view of (4.2) and (4.6), the coefficients α'' and β''_t of (3.2.8) now become

$$\alpha'' = \langle \alpha' + a' : e'(\eta') \rangle = \langle \alpha' + \alpha' : e'(\phi') \rangle = \langle \alpha' : [II + e'(\phi')] \rangle \tag{4.9}$$

$$\beta''_t = \langle \beta'_t + a' : e'(\zeta') \rangle = \langle \beta'_t + \beta'_t : e'(\phi') \rangle = \langle \beta'_t : [II + e'(\phi')] \rangle \tag{4.10}$$

so that the thermal modulus in Hooke's law (3.2.7) is also determined in terms of ϕ' only.

In the consolidation equation (3.2.13), M&A obtained

$$\gamma'' = \alpha'' - \langle n' e'(\phi') : I \rangle = \alpha'' - \langle n' \nabla' \cdot \phi' \rangle \tag{4.11}$$

which reduces to γ' of two scale medium if n' is uniform on the mesoscale. Also it has been shown that

$$\beta''_c = \langle \beta'_c - \alpha' : e'(\eta') + n' e'(\eta') : I \rangle \tag{4.12}$$

from (3.2.14c) after using the relation $\gamma' = \alpha'$ on the mesoscale. After using (4.3) and the property $\beta'_c > 0$ (cf.(4.28) of Ch.1), it futher becomes

$$\beta''_c - \langle n' e'(\eta') : I \rangle > 0 \tag{4.13}$$

Similar relation is now found for the coefficient ζ_c'' of (3.2.14d) which may be written as

$$\zeta_c'' = \langle \zeta_c' - (\alpha' - n'I) : e'(\zeta') \rangle \tag{4.14}$$

Assuming that the solid phase of the microscale grains is isotropic, it follows from (4.25) and (4.26) of Ch.1 that

$$\alpha' = I - \beta_t'/3K^* \tag{4.15}$$

where K^* is the bulk modulus of the solid phase. Combining (4.14) and (4.15) we get

$$\zeta_c'' = \langle \zeta_c' \rangle + \langle \beta_t' : e'(\zeta')/3K^* \rangle - \langle (1 - n')e'(\zeta') : I \rangle \tag{4.16}$$

which shows after using (4.8) and $\langle \zeta_c' \rangle < 0$ that

$$\zeta_c'' + \langle (1 - n')e'(\zeta') : I \rangle < 0 \tag{4.17}$$

We now examine the flow problem. Equation (3.2.11) is rewritten in indicial form as

$$\begin{aligned} &\frac{\partial}{\partial x_n'}\left[k_{n\ell}'\left(\delta_{\ell j} + \frac{\partial S_j'}{\partial x_\ell'}\right)\right] = 0 \\ &\frac{\partial}{\partial x_n'}\left[k_{n\ell}'\frac{\partial W_j'}{\partial x_\ell'} + n'\delta_{nj}\right] = 0 \qquad (4.18a-d) \\ &S' \quad \text{and} \quad W' \quad \text{are} \quad \Omega' - \text{periodic.} \end{aligned}$$

$$\langle S' \rangle = \langle W' \rangle = 0$$

Multiply (4.18a) by W_i' and integrate over Ω'-cell to get

$$\left\langle k_{jn}'\frac{\partial W_i'}{\partial x_n'} \right\rangle = -\left\langle k_{mn}'\frac{\partial W_i'}{\partial x_m'}\frac{\partial S_j'}{\partial x_n'} \right\rangle \tag{4.19}$$

Likewise after multiplying (4.18b) by S_i' and integrating over Ω'-cell, we get

$$\left\langle n'\frac{\partial S_i'}{\partial x_j'} \right\rangle = -\left\langle k_{mn}'\frac{\partial W_j'}{\partial x_m'}\frac{\partial S_i'}{\partial x_n'} \right\rangle \tag{4.20}$$

Taking the transpose of (4.19) and adding to (4.20) we get

$$\left\langle k_{in}'\frac{\partial W_j'}{\partial x_n'} \right\rangle = \left\langle n'\frac{\partial S_i'}{\partial x_j'} \right\rangle$$

or

$$\langle k' \cdot \nabla' W' \rangle = \langle n' \nabla' S' \rangle^T \tag{4.21}$$

The coefficient δ_c'' of (3.2.14e) then becomes

$$\delta_c'' = \langle n' \nabla' S' \rangle^T \tag{4.22}$$

Therefore, the boundary value problem for W' needs not be solved unless the mesoscale variation of pressure $p^{(1)}$ due to solid movement is required.

The symmetry and positive definiteness of k'' of (3.2.14a) have been shown by M&A which can be readily extended to the case including buoyancy by following the same procedure as §4 in Ch. 1 since the boundary value problem for S' (cf.(3.2.11a)) is unchanged.

In the heat transport, the positive definiteness of the macroscale thermal conductivity m'' follows by the same reasoning as in two-scale case. We only give an alternate form for m'' here.

Rewriting (3.3.3a) in indicial form we have

$$\frac{\partial}{\partial x_n'} \left[m_{nk}' \left(\delta_{kj} + \frac{\partial A_j'}{\partial x_k'} \right) \right] = 0 \tag{4.23}$$

Multiplying (4.23) by A_i', integrating over Ω'-cell and using Gauss theorem and Ω'-periodicity, we get

$$\left\langle m_{jn}' \frac{\partial A_i'}{\partial x_n'} \right\rangle = - \left\langle m_{nk}' \frac{\partial A_i'}{\partial x_n'} \frac{\partial A_j'}{\partial x_k'} \right\rangle \tag{4.24}$$

If (4.24) is used in (3.3.6) together with the symmetry relation $m_{nk}' = m_{kn}'$, there follows

$$m_{ij}'' = \left\langle m_{in}' \left(\delta_{nj} + \frac{\partial A_j'}{\partial x_n'} \right) \right\rangle = \left\langle m_{nk}' \left(\delta_{ni} \delta_{kj} - \frac{\partial A_i'}{\partial x_k'} \frac{\partial A_j'}{\partial x_n'} \right) \right\rangle \tag{4.25}$$

which shows that

$$m_{ij}' = m_{ji}' \tag{4.26}$$

The macroscale coefficients a'', α'', β_i'' and γ'' are thus determined after solving for ϕ' in given mesoscale cell, but β_c'' and ζ_c'' of (4.12) and (4.14) require η' and ζ' unlike in two scale sace in which only ϕ was required when the microscale grains are of homogeneous and isotropic solid.

5. A Periodically Stratified Porous Medium.

The general theory developed in §3 is now applied to derive explicitly the effective constitutive coefficients for the governing equations at the macroscale from the mesoscale coefficients and the mesoscale cell boundary value problems. The mesoscale coefficients are assumed to have been found for a given microcell geometry.

On the mesoscale ℓ' the medium is assumed to be stratified along x_3'-axis, while it is homogeneous in $x_1'x_2'$-plane i.e., uniform material coefficients in $x_1'x_2'$-plane. The medium is periodically stratified in x_3' direction so that after a period of ℓ' in the x_3'-axis the pattern of stratification is repeated (see Fig. 5.1). The lateral dimension is assumed to be infinite so that the mesoscale cell is an infinite stratum with thickness of ℓ' along x_3'-axis.

The cell boundary value problems defined on the scale ℓ' will be solved analytically for a medium like Fig. 5.1 and then the macroscale coefficients are determined.

5.1 The Elastic Coefficients.

We start with those elastic coefficients treated in Ch.1 which possess the property of cubic symmetry. Modifications to allow general anisotropy on the mesoscale are minor and are not pursued here.

It has been shown for a cubic array of Wigner-Seitz grains that there are only three distinct constants in $a'_{ijk\ell}$ which has the following symmetry properties.

$$a'_{ijk\ell} = a'_{jik\ell} = a'_{ij\ell k} = a'_{k\ell ij} \tag{5.1.1}$$

They are specifically

$$\begin{aligned} a_I &= a'_{xxxx} = a'_{yyyy} = a'_{zzzz} \\ a_{II} &= a'_{xxyy} = a'_{yyzz} = a'_{zzxx} \\ a_{III} &= a'_{xyxy} = a'_{yzyz} = a'_{zxzx} \end{aligned} \tag{5.1.2a-c}$$

and all other $a'_{ijk\ell}$ are zero.

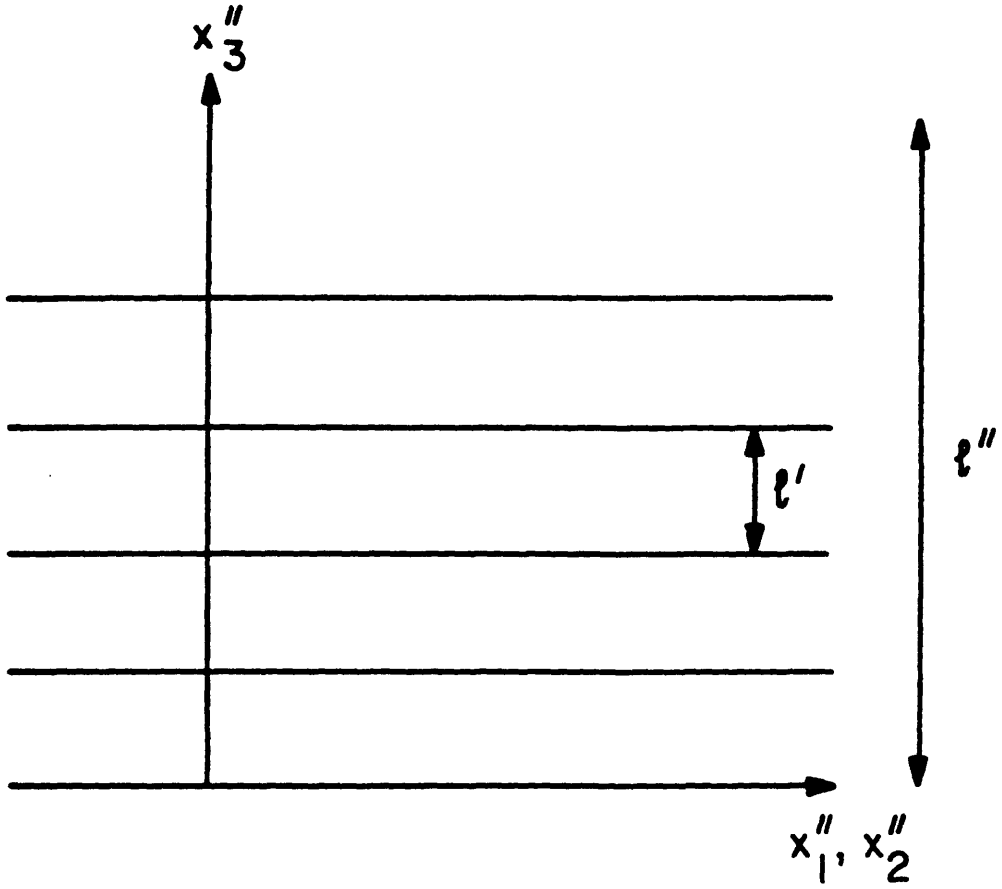

Fig. 5.1 A periodically stratified layers on the mesoscale. The periodic length is ℓ' in x_3'-direction.

We first solve for $\phi_i^{'jk}$. From (3.2.4a,d and e)

$$\frac{\partial}{\partial x_i'}\left[a_{ijk\ell}'e_{k\ell}'(\phi^{'mn}) + a_{ijmn}'\right] = 0 \qquad \text{in } \Omega'$$
$$\phi_i^{'mn} \quad \text{is} \quad \Omega' - \text{periodic} \qquad (5.1.3a-c)$$
$$\langle \phi_i^{'mn} \rangle = 0$$

The boundary value problem (5.1.3a-c) is a elastostatic problem with body force. If a_{ijmn}' is uniform in the mesoscale cell Ω', there is no body force and it can be readily shown that $\phi^{'mn}$ is at most mesoscale-independent constant, by using positive definiteness of $a_{ijk\ell}'$, which must be zero because of (5.1.3c). Again the variations of $v^{(1)}$ on the scale ℓ' is the consequence of heterogeneities on the mesoscale. Without loss of generality we set $p^{(0)} = \theta^{(0)} = 0$ in (3.2.3). It follows after using $e_{jk}''(v^{(0)}) = e_{kj}''(v^{(0)})$ that

$$v_i^{(1)}(x', x'', t^*) = \phi_i^{jk} e_{jk}''(v^{(0)}) = \phi_i^{kj} e_{kj}''(v^{(0)}) = \phi_i^{kj} e_{jk}''(v^{(0)})$$

Therefore, even if the number of $\phi_i^{'jk}$ components is 3^3=27, only the following 18 components remain

$$\phi_i^{'jk} \quad \text{for} \quad i = x, y, z \quad \text{and} \quad jk = xx, yy, zz, xy, yz, zx \qquad (5.1.4)$$

These are now determined from (5.1.3) in terms of the mesoscale coefficients in (5.1.2a-c).

Since the medium property varies in x_3'-direction only, (5.1.3a) becomes one - dimensional :

$$\frac{\partial}{\partial z'}\left(a_{zjz\ell}'\frac{\partial \phi_\ell^{'mn}}{\partial z'} + a_{zjmn}'\right) = 0 \qquad \text{in } \Omega' \qquad (5.1.5)$$

where

$$\begin{aligned} a_{ijk\ell}'e_{k\ell}' &= a_{ijk\ell}'\frac{1}{2}\left(\frac{\partial \phi_\ell^{'mn}}{\partial x_k'} + \frac{\partial \phi_k^{'mn}}{\partial x_\ell'}\right) \\ &= a_{ijk\ell}'\left[\frac{1}{2}\left(\frac{\partial \phi_\ell^{'mn}}{\partial x_k'} + \frac{\partial \phi_k^{'mn}}{\partial x_\ell'}\right) + \frac{1}{2}\left(\frac{\partial \phi_\ell^{'mn}}{\partial x_k'} - \frac{\partial \phi_k^{'mn}}{\partial x_\ell'}\right)\right] \\ &= a_{ijk\ell}'\frac{\partial \phi_\ell^{'mn}}{\partial x_k'} \end{aligned}$$

has been used because the product of $a'_{ijk\ell}$ and the anti-symmetric rotation tensor $\omega'_{k\ell} = \frac{1}{2}(\partial\phi'^{mn}_{\ell}/\partial x'_k - \partial\phi'^{mn}_{k}/\partial x'_\ell)$ is zero. After integration (5.1.5) becomes

$$a'_{zjz\ell}\frac{\partial\phi'^{mn}_{\ell}}{\partial z'} + a'_{zjmn} = C_1 \tag{5.1.6}$$

where C_1 is a mesoscale independent constant which may vary with x''. Note that (5.1.6) satisfies the continuity of stress, beacuse at the interface between any two layers the left-hand side is the stress component $\sigma^{(0)}_{zj}$(cf.(3.2.3)) due to deformation only.

Consider the case $j = x$ in (5.1.6). Since $a'_{zxzx} = a_{III}$ is the only nonvanishing coefficint for $a'_{zjz\ell}$, (5.1.6) becomes

$$\frac{\partial\phi'^{mn}_{x}}{\partial z'} = \frac{C_1 - a'_{zxmn}}{a_{III}} \tag{5.1.7}$$

If $mn = xx$, we have after integration with z'

$$\phi'^{xx}_{x} = C_1\int_0^{z'}\frac{dz'}{a_{III}} + \phi'^{xx}_{x}(z' = 0) \tag{5.1.8}$$

At $z' = \ell'$, it becomes

$$\phi'^{xx}_{x}(z' = \ell') = C_1\int_0^{\ell'}\frac{dz'}{a_{III}} + \phi'^{xx}_{x}(z' = 0)$$

Imposing the periodicity condition (5.1.3b) i.e., $\phi'^{xx}_{x}(z' = 0) = \phi'^{xx}_{x}(z' = \ell')$, we get $C_1 = 0$. Substitute this into (5.1.8) and use (5.1.3c):

$$\langle\phi'^{xx}_{x}\rangle = \frac{1}{\ell'}\int_0^{\ell'}\phi'^{xx}_{x}dz' = \phi'^{xx}_{x}(z' = 0) = 0$$

Hence

$$\phi'^{xx}_{x} = 0 \tag{5.1.9}$$

Recall that this is due to the vanishing of a'_{zxmn} for $mn = xx$ in (5.1.6). Similarly we have

$$\phi'^{xx}_{x} = \phi'^{xz}_{x} = \phi'^{xy}_{x} = \phi'^{yz}_{x} = 0 \tag{5.1.10}$$

If $mn = zx$ in (5.1.7), it becomes

$$\frac{\partial \phi_x^{\prime zx}}{\partial z'} = \frac{C_1}{a_{III}} - 1 \tag{5.1.11}$$

Integrating (5.1.11) from 0 to z', we have

$$\phi_x^{\prime zx} = C_1 \int_0^{z'} \frac{dz'}{a_{III}} - z' + \phi_x^{\prime zx}(z' = 0)$$

The constant C_1 is determined from (5.1.3b) as

$$C_1 = \frac{\ell'}{\int_0^{\ell'} \frac{dz'}{a_{III}}}$$

So (5.1.11) becomes

$$\frac{\partial \phi_x^{\prime zx}}{\partial z'} = \frac{\ell'}{a_{III} \int_0^{\ell'} \frac{dz'}{a_{III}}} - 1 = \frac{1}{a_{III} \langle \frac{1}{a_{III}} \rangle} - 1 \tag{5.1.12}$$

Note that derivatives of $\phi_i^{\prime jk}$ are required to derive the macroscale elastic coefficients, not $\phi_i^{\prime jk}$ itself(cf.(3.2.8)).

By precisely the same procedure, it can be shown for the case $j = y'$ in (5.1.6) that

$$\begin{aligned} &\phi_y^{\prime xx} = \phi_y^{\prime yy} = \phi_y^{\prime zz} = \phi_y^{\prime xy} = \phi_y^{\prime yz} = 0 \\ &\frac{\partial \phi_y^{\prime yz}}{\partial z'} = \frac{\partial \phi_x^{\prime zx}}{\partial z'} = \frac{\ell'}{a_{III} \int_0^{\ell'} \frac{dz'}{a_{III}}} - 1 = \frac{1}{a_{III} \langle \frac{1}{a_{III}} \rangle} - 1 \end{aligned} \tag{5.1.13a,b}$$

Also for $j = z'$, we readily obtain

$$\begin{aligned} &\phi_z^{\prime xy} = \phi_z^{\prime yz} = \phi_z^{\prime zx} = 0 \\ &\frac{\partial \phi_z^{\prime xx}}{\partial z'} = \frac{\partial \phi_z^{\prime yy}}{\partial z'} = \frac{1}{a_I} \left(\frac{\int_0^{\ell'} \frac{a_{II}}{a_I} dz'}{\int_0^{\ell'} \frac{1}{a_I} dz'} - a_{II} \right) = \frac{\left\langle \frac{a_{II}}{a_I} \right\rangle}{a_I \left\langle \frac{1}{a_I} \right\rangle} - \frac{a_{II}}{a_I} \\ &\frac{\partial \phi_z^{\prime zz}}{\partial z'} = \frac{\ell'}{a_I \int_0^{\ell'} \frac{dz'}{a_I}} - 1 = \frac{1}{a_I \left\langle \frac{1}{a_I} \right\rangle} - 1 \end{aligned} \tag{5.1.14a-c}$$

Next we solve for η' in (3.2.4b). After keeping z'-derivatives only, it is written

$$\begin{aligned} &\frac{\partial}{\partial z'} \left(a'_{zjzq} \frac{\partial \eta'_q}{\partial z'} + \alpha'_{zj} \right) = 0 \qquad \text{in } \Omega' \\ &\eta'_q \quad \text{is} \quad \Omega' - \text{periodic} \\ &\langle \eta'_q \rangle = 0 \end{aligned} \tag{5.1.15a-c}$$

This is again one-dimensional elastostatic problem with body force the distribution of which takes account of the mesoscale heterogeneities in α'_{zj}. For the Wigner-Seitz grains α'_{ij} is isotropic i.e.,

$$\alpha'_{ij} = \alpha' \delta_{ij} \quad ; \quad \alpha' = \alpha'_{xx} = \alpha'_{yy} = \alpha'_{zz} \tag{5.1.16}$$

If (5.1.2) and (5.1.16) are used in (5.1.15a-c), we get

$$\begin{aligned} \eta'_x &= \eta'_y = 0 \\ \frac{\partial \eta'_z}{\partial z'} &= \frac{\int_0^{\ell'} \frac{\alpha'}{a_I} dz'}{a_I \int_0^{\ell'} \frac{1}{a_I} dz'} - \frac{\alpha'}{a_I} \end{aligned} \tag{5.1.17}$$

The boundary value problem for ζ', (3.2.4c), is the same as (5.1.15) except that α'_{zj} is replaced by $(\beta'_t)_{zj}$. Since β'_t is also isotropic, it follows from (5.1.17) that

$$\begin{aligned} \zeta'_x &= \zeta'_y = 0 \\ \frac{\partial \zeta'_z}{\partial z'} &= \frac{\int_0^{\ell'} \frac{\beta'}{a_I} dz'}{a_I \int_0^{\ell'} \frac{1}{a_I} dz'} - \frac{\beta'}{a_I} \end{aligned} \tag{5.1.18}$$

The elastic coefficients can now be found in terms of the nonvanishing derivatives (5.1.12), (5.1.13), (5.1.14), (5.1.17) and (5.1.18).

5.1.1 Coefficients $a''_{ijk\ell}$, α''_{ij} and $(\beta''_t)_{ij}$.

By keeping only z'-derivatives of ϕ' in (3.2.8), the elastic coefficients $a''_{ijk\ell}$ are written as

$$a''_{ijk\ell} = \left\langle a'_{ijk\ell} + a'_{ijzn} \frac{\partial \phi'^{k\ell}_n}{\partial z'} \right\rangle \tag{5.1.19}$$

which gives after using (5.1.2)

$$\begin{aligned} a''_{xxzz} &= a''_{yyyy} = \left\langle a_I + a_{II} \frac{\partial \phi'^{zz}_z}{\partial z'} \right\rangle \\ a''_{xzxz} &= \left\langle a_I + a_I \frac{\partial \phi'^{zz}_z}{\partial z'} \right\rangle \\ a''_{xxyy} &= \left\langle a_{II} + a_{II} \frac{\partial \phi'^{yy}_z}{\partial z'} \right\rangle \\ a''_{yyzz} &= a''_{zxzx} = \left\langle a_{II} + a_{II} \frac{\partial \phi'^{zz}_z}{\partial z'} \right\rangle \\ a''_{xyxy} &= \langle a_{III} \rangle \\ a''_{yxyx} &= a''_{zxzx} = \left\langle a_{III} + a_{III} \frac{\partial \phi'^{zz}_z}{\partial z'} \right\rangle \end{aligned} \tag{5.1.20a-f}$$

There are six independent coefficients in $a''_{ijk\ell}$. A medium with six distinct coefficients as (5.1.20) is said to have tetragonal symmetry(Love, 1944;Lekhnitskii, 1963). It is not surprising that, under the assumption of homogeneous material property in $x'_1x'_2$-plane, the effective coefficients do not reduce to that for transverse isotropy. This is due to the microcell structure of cubic Wigner-Seitz grains which have been shown to possess cubic symmetry. If the medium is isotropic on ℓ'-scale, the mesoscale coefficients a_I, a_{II} and a_{III} are related by

$$a_I - a_{II} = 2a_{III} \tag{5.1.21}$$

After using (5.1.14b), the coefficients a''_{xxxx}, a''_{xxyy} and a''_{xyxy} are combined to yield

$$a''_{xxxx} - a''_{xxyy} = 2a''_{xyxy} \tag{5.1.22}$$

Then the total number of independent coefficients in (5.1.19) is five and the medium is transversely isotropic. M& A have assumed transverse isotropy at the scale ℓ' and derived $a''_{ijk\ell}$ which are also transversely isotropic.

The coefficients α''_{ij} and $(\beta''_t)_{ij}$ in (3.2.8) similarly become as follows, by using (5.1.9) and (5.1.10),

$$\begin{aligned} \alpha''_{ij} &= \langle \alpha' : [II + e'(\phi')] \rangle = \left\langle \alpha'_{ij} + \alpha'_{zq} \frac{\partial \phi'^{ij}_q}{\partial z'} \right\rangle \\ (\beta''_t)_{ij} &= \langle \beta'_t : [II + e'(\phi')] \rangle = \left\langle (\beta'_t)_{ij} + (\beta'_t)_{zq} \frac{\partial \phi'^{ij}_q}{\partial z'} \right\rangle \end{aligned} \tag{5.1.23a,b}$$

from which we have

$$\begin{aligned} &\alpha''_{xx} = \alpha''_{yy} = \left\langle \alpha' \left(1 + \frac{\partial \phi'^{xz}_z}{\partial z'} \right) \right\rangle, \quad \alpha''_{zz} = \left\langle \alpha' \left(1 + \frac{\partial \phi'^{zz}_z}{\partial z'} \right) \right\rangle \\ &\alpha''_{ij} = 0 \quad (i \neq j) \\ &(\beta''_t)_{xx} = (\beta''_t)_{yy} = \left\langle \beta'_t \left(1 + \frac{\partial \phi'^{xz}_z}{\partial z'} \right) \right\rangle, \quad (\beta''_t)_{zz} = \left\langle \beta'_t \left(1 + \frac{\partial \phi'^{zz}_z}{\partial z'} \right) \right\rangle \\ &(\beta''_t)_{ij} = 0 \quad (i \neq j) \end{aligned} \tag{5.1.24}$$

They are again diagonal as in two scale medium but anisotropic because of the stratification in x'_3-direction.

5.1.2 Coefficients γ''_{ij}, β''_c, ζ''_c.

These coefficients are determined in terms of ϕ', η' and ζ' from the elastostatic problems. From (5.1.11) γ'' becomes for a medium stratified in x'_3-axis

$$\gamma'' = \alpha'' - \langle n' \nabla' \cdot \phi' \rangle$$

from which we obtain

$$\begin{aligned} \gamma''_{xx} &= \gamma''_{yy} = \alpha''_{xx} - \left\langle n' \frac{\partial \phi'^{xx}_x}{\partial z'} \right\rangle \\ \gamma''_{zz} &= \alpha''_{zz} - \left\langle n' \frac{\partial \phi'^{zz}_z}{\partial z'} \right\rangle \\ \gamma''_{ij} &= 0 \quad (i \neq j) \end{aligned} \tag{5.1.25}$$

From (5.1.12) the coefficients β''_c similarly becomes

$$\begin{aligned} \beta''_c &= \langle \beta'_c - \alpha' : e'(\eta') + n' e'(\eta') : I \rangle \\ &= \left\langle \beta'_c - \alpha' \frac{\partial \eta'_z}{\partial z'} + n' \frac{\eta'_z}{\partial z'} \right\rangle \\ &= \left\langle \beta'_c + (n' - \alpha') \frac{\partial \eta'_z}{\partial z'} \right\rangle \end{aligned} \tag{5.1.26}$$

Also from (5.1.14), the coefficients ζ''_c becomes

$$\zeta''_c = \left\langle \zeta'_c + (\alpha' - n') \frac{\partial \zeta'_z}{\partial z'} \right\rangle \tag{5.1.27}$$

The remaining coefficients k'' and δ'' of the consolidation equation (3.2.13) will be determined in the next section after solving the flow equation (3.2.11).

So far the coefficients related to the elastic properties of the medium, a'', α'', β''_t, γ'', β''_c and ζ''_c, have been derived in terms of ϕ', η' and ζ'. They involve derivatives of these functions. If the stratification pattern in Ω'-cell is known, obtaining the explicit expressions of those coefficients is only a matter of quadrature. Later a special case of two different uniform layers will be considered.

5.2 Coefficients k'' and δ''.

We first recall that the permeability k' at the mesoscale ℓ' is isotropic,e.g.

$$\begin{aligned} k'_{xx} &= k'_{yy} = k'_{zz} = k' \\ k'_{ij} &= 0 \quad (i \neq j) \end{aligned} \tag{5.2.1}$$

In horizontally stratified medium of Fig. 1, (3.2.11) takes the following form.

$$\begin{aligned} &\frac{\partial}{\partial z'}\left(k'_{zj} + k'_{zz}\frac{\partial S'_j}{\partial z'}\right) = 0 \\ &S'_j \quad \text{is } \Omega'\text{-periodic} \\ &\langle S'_j \rangle = 0 \end{aligned} \tag{5.2.2a-c}$$

since only z'-derivatives remain. Integration of (5.2.2a) in z' yields

$$k'_{zz}\frac{\partial S'_j}{\partial z'} + k'_{zj} = C_1 \qquad \text{in } \Omega'. \tag{5.2.3}$$

where C_1 is a constant which is independent of x'. Equation (5.2.3) satisfies the condition of normal flux continuity at any interface between two neighboring layers in the Ω'-cell. If $j = x$ or $j = y$, it readily follows from (5.2.3) that

$$\frac{\partial S'_x}{\partial z'} = \frac{\partial S'_y}{\partial z'} = 0 \tag{5.2.4a}$$

after imposing the conditions (5.2.2b and c). For the case $j = z$, by using (5.2.1), (5.2.3) becomes

$$\frac{\partial S'_z}{\partial z'} = \frac{C_1}{k'} - 1$$

The constant C_1 is determined after integrating once more and using (5.2.2b and c). It then follows that

$$\frac{\partial S'_z}{\partial z'} = \frac{\ell'}{k' \int_0^{\ell'} \frac{dz'}{k'}} - 1 = \frac{1}{k' \left\langle \frac{1}{k'} \right\rangle} - 1 \tag{5.2.4b}$$

The permeability k'' of (3.2.14a) now becomes, by using (5.2.1) and (5.2.4), as

$$\begin{aligned} k''_{xx} &= k''_{yy} = \langle k' \rangle \\ k''_{zz} &= \left\langle k'\left(1 + \frac{\partial S'_z}{\partial z'}\right)\right\rangle = \frac{1}{\left\langle \frac{1}{k'} \right\rangle} \\ k''_{ij} &= 0 \quad (i \neq j) \end{aligned} \tag{5.2.5}$$

which is now anisotropic due to the stratification in vertical direction of Fig. 1. The permeability in the horizontal plane is the arithmetic mean over the length ℓ' whereas, in the direction normal to the stratification, it is the harmonic mean value as is well known.

Similarly the coefficient δ_c'' of (3.2.14e) reduces, after using (5.1.19), to

$$\begin{aligned} \delta_{zz}'' &= \left\langle n' \frac{\partial S_z'}{\partial z'} \right\rangle \\ \delta_{ij}'' &= 0 \qquad \text{otherwise} \end{aligned} \tag{5.2.6}$$

so that only one coefficient remains.

Equation (5.2.4b) is sifficient for the calculation of the macroscale permeability k''. However, we further find $S_z'(z')$ for later use in thermal dispersion in Part B. Integrating (5.2.4b), we have

$$S_z'(z') - S_z'(0) = k_{zz}'' \int_0^{z'} \frac{dz'}{k'} - z' \tag{5.2.7}$$

Another integration from 0 to ℓ' gives after using (5.2.2c)

$$\begin{aligned} S_z'(0) &= \frac{\ell'}{2} - \frac{k_{zz}''}{\ell'} \int_0^{\ell'} dz' \int_0^{z'} \frac{d\xi}{k'(\xi)} \\ &= \frac{\ell'}{2} - \frac{k_{zz}''}{\ell'} \left[z' \int_0^{z'} \frac{d\xi}{k'(\xi)} \Big|_{z'=0}^{z'=\ell'} - \int_0^{\ell'} dz' \frac{z'}{k'(z')} \right] = k_{zz}'' \left\langle \frac{z'}{k'(z')} \right\rangle - \frac{\ell'}{2} \end{aligned} \tag{5.2.8}$$

Equation (5.2.7) then becomes

$$S_z'(z') = k_{zz}'' \int_0^{z'} \frac{dz'}{k'} + k_{zz}'' \left\langle \frac{z'}{k'(z')} \right\rangle - z' - \frac{\ell'}{2} \tag{5.2.9}$$

5.3 Thermal Conductivity Tensor m_{ij}''.

The macroscale thermal conductivity tensor m_{ij}'' is now derived in terms of thermal conductivity m' on the mesoscale ℓ' from the boundary valus problem (3.3.3) and (4.25). We first rcall that m' is isotropic tensor,e.g.

$$\begin{aligned} m_{xx}' &= m_{yy}' = m_{zz}' = m' \\ m_{ij}' &= 0 \quad (i \neq j) \end{aligned} \tag{5.3.1}$$

From (3.3.3), for vertically varying medium on the ℓ' scale, the boundary value problem for A' becomes

$$\begin{aligned} &\frac{\partial}{\partial z'}\left(m'_{zj}+m'_{zz}\frac{\partial A'_j}{\partial z'}\right)=0 \qquad \text{in } \Omega'. \\ &A'_j \quad \text{is } \Omega'\text{-periodic} \\ &\langle A'_j\rangle = 0 \end{aligned} \tag{5.3.2a-c}$$

It is precisely the same as the flow equation (5.2.2) and we readily obtain

$$\begin{aligned} &\frac{\partial A'_x}{\partial z'}=\frac{\partial A'_y}{\partial z'}=0 \\ &\frac{\partial A'_z}{\partial z'}=\frac{\ell'}{m'\int_0^{\ell'}\frac{dz'}{m'}}-1=\frac{1}{m'\left\langle\frac{1}{m'}\right\rangle}-1 \end{aligned} \tag{5.3.3a-c}$$

It automatically satisfies the continuity of normal heat flux at any interface inside the Ω'-cell. If m' is discontinuous at a certain point in Ω', the diffusive heat flux $m'\partial A'_z/\partial z'$ has a jump of strength equal to the change in thermal conductivity m' which is balanced by the heat source $\partial m'_{zz}/\partial z'$ in (5.3.2a). From (3.3.6) we then have

$$m''_{ij}=\left\langle m'\delta_{ij}+m'\delta_{iz}\frac{\partial A'_j}{\partial z'}\right\rangle \tag{5.3.4}$$

Upon using (5.3.3), (5.3.4) yields

$$\begin{aligned} &m''_{xx}=m''_{yy}=\langle m'\rangle \\ &m''_{zz}=\left\langle m'\left(1+\frac{\partial A'_z}{\partial z'}\right)\right\rangle=\frac{1}{\left\langle\frac{1}{m'}\right\rangle} \\ &m''_{ij}=0 \quad (i\neq j) \end{aligned} \tag{5.3.5}$$

Again the thermal conductivity is the arithmetic mean in the horizontal plane and the harmonic mean along z'-direction.

6. A Periodic Stratum with Piecewise Constant Properties

The derivations in §5 are applicable to any type of porous medium with periodic variation along the vertival direction,i.e. sinusoidally varying medium or a medium with arbitrary number of layers in the periodic length of ℓ' on the mesoscale. They are specialized to a periodic medium with two layers which are discontinuous in the mesoscale material coefficients at the interface. It is assumed that in each layer the medium is homogeneous so that all the coefficients in a layer are constant.

Consider a periodic medium composed of two different layers as shown in Fig. 6.1. The coefficients in the lower layer ($0 < z' < (1-s)\ell'$) are denoted with a superscript symbol $()^-$ and those in the upper layer ($(1-s)\ell' < z' < \ell'$) with another symbol $()^+$. They are discontinuous at the interface $z' = (1-s)\ell'$, but physical quantities such as displacement, stress, flow and heat flux are continuous as has been shown in §5. Explicit forms of the macroscale coefficients are now obtained for the simple strata of Fig. 6.1 in terms of the coefficients at the scale ℓ'.

6.1 The Elastic Coefficients.

In order to calculate $a''_{ijk\ell}$, it is necessary to calculate $\langle a_i^{-1}\rangle^{-1}$ for $i = I, II, III$ and $\langle a_{II}/a_I\rangle$.

$$\begin{aligned}\langle a_i^{-1}\rangle^{-1} &= \left(\frac{1}{\ell'}\int_o^{\ell'}\frac{1}{a_i}dz'\right)^{-1} = \left[\frac{1}{\ell'}\left(\int_o^{(1-s)\ell'}\frac{dz'}{a_i}+\int_{(1-s)\ell'}^{\ell'}\frac{dz'}{a_i}\right)\right]^{-1} \\ &= \left[\frac{(1-s)}{a_i^-}+\frac{s}{a_i^+}\right]^{-1} = \frac{a_i^+a_i^-}{Q_i} \qquad (i=I,II,III)\end{aligned} \tag{6.1.1}$$

where

$$Q_i = (1-s)a_i^+ + sa_i^- \qquad (i=I,II,III) \tag{6.1.2}$$

Similarly

$$\left\langle\frac{a_{II}}{a_I}\right\rangle = \frac{a_{II}^-}{a_I^-}(1-s)+\frac{a_{II}^+}{a_I^+}s = \frac{1}{a_I^+a_I^-}\left[a_I^+a_{II}^-(1-s)+a_I^-a_{II}^+s\right] \tag{6.1.3}$$

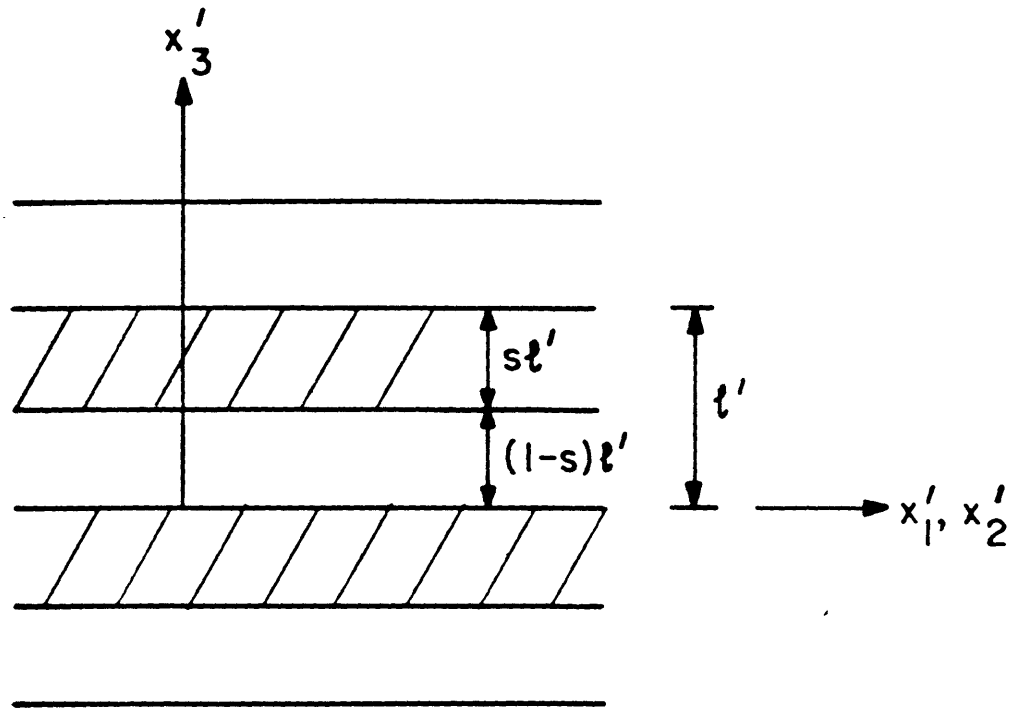

Fig. 6.1 A periodic medium with two layers on the mesoscale ℓ'.

The coefficients are then calculated from (5.1.20a-f) by using (6.1.2) and (6.1.3). From (5.1.14b) we have

$$\begin{aligned}\frac{\partial \phi'^{xx}_z}{\partial z'} = \frac{\partial \phi'^{yy}_z}{\partial z'} &= \frac{1}{a_I}\langle a_i^{-1}\rangle^{-1}\left\langle \frac{a_{II}}{a_I}\right\rangle - \frac{a_{II}}{a_I} \\ &= \frac{a_I^+ a_{II}^-(1-s) + a_I^- a_{II}^+ s}{Q_I}\begin{Bmatrix}\frac{1}{a_I^-}\\ \frac{1}{a_I^+}\end{Bmatrix} - \begin{Bmatrix}\frac{a_{II}^-}{a_I^-}\\ \frac{a_{II}^+}{a_I^+}\end{Bmatrix} \\ &= \frac{[\![a_{II}]\!]}{Q_I}\begin{Bmatrix} s & 0<z'<(1-s)\ell' \\ s-1 & (1-s)\ell'<z'<\ell'\end{Bmatrix}\end{aligned} \tag{6.1.4}$$

where

$$[\![a_{II}]\!] = a_{II}^+ - a_{II}^- \tag{6.1.5}$$

is the increase in a_{II} when crossing the interface from the lower to the upper layers. Then (5.1.20a) becomes

$$\begin{aligned}a''_{xxxx} = a''_{yyyy} &= \langle a_I\rangle + \frac{[\![a_{II}]\!]}{Q_I}\left\langle \begin{Bmatrix} sa_{II}^- & 0<z'<(1-s)\ell' \\ (s-1)a_{II}^+ & (1-s)\ell'<z'<\ell'\end{Bmatrix}\right\rangle \\ &= a_I^-(1-s) + a_I^+ s + \frac{[\![a_{II}]\!]^2 s(s-1)}{Q_I}\end{aligned} \tag{6.1.6a}$$

In the same manner, we also obtain

$$\begin{aligned}a''_{zzzz} &= \langle a_I\rangle + \left\langle\left(\frac{\langle a_i^{-1}\rangle^{-1}}{a_I} - 1\right)\right\rangle = \langle a_I^{-1}\rangle^{-1} = \frac{a_I^+ a_I^-}{Q_I} \\ a''_{zzyy} &= \langle a_{II}\rangle + \left\langle a_{II}\frac{\partial \phi'^{yy}_z}{\partial z'}\right\rangle = a_{II}^-(1-s) + a_{II}^+ s + \frac{[\![a_{II}]\!]^2 s(s-1)}{Q_I} \\ a''_{yyzz} = a''_{zzxx} &= \langle a_{II}\rangle + \left\langle \frac{a_{II}}{a_I}\right\rangle\langle a_I^{-1}\rangle^{-1} - \langle a_{II}\rangle = \frac{1}{Q_I}\left[a_I^+ a_{II}^-(1-s) + a_I^- a_{II}^+ s\right] \\ a''_{zyzy} &= \langle a_{III}\rangle = (1-s)a_{III}^- + sa_{III}^+ \\ a''_{yzyz} = a''_{zxzx} &= \langle a_{III}\rangle + \langle a_{III}^{-1}\rangle^{-1} - \langle a_{III}\rangle = \frac{a_{III}^+ a_{III}^-}{Q_{III}}\end{aligned} \tag{6.1.6b-f}$$

As mentioned earlier, material with six different elastic coefficients as above is said to have tetragonal symmetry (Cottrell,1964; Lekhnitskii,1963). For the same two layer model but transversely isotropic medium at ℓ' scale Mei and Auriault(1989) have calculated elastic coefficients similar to (6.1.6). There are only five independent coefficients in transversely isotropic medium.

The coefficients α''_{ij} are calculated by (5.1.24) as

$$\begin{aligned}
\alpha''_{xx} &= \alpha''_{yy} = \langle\alpha'\rangle + \left\langle \alpha' \frac{\partial \phi'^{xx}_{z}}{\partial z'} \right\rangle = \langle\alpha'\rangle + \frac{[\![a_{II}]\!]}{Q_I} \left\langle \begin{Bmatrix} \alpha'^{-} s \\ \alpha'^{+}(s-1) \end{Bmatrix} \right\rangle \\
&= \langle\alpha'\rangle + [\![a_{II}]\!][\![\alpha']\!] s(s-1)/Q_I \\
\alpha''_{zz} &= \langle\alpha'\rangle + \left\langle \alpha' \frac{\partial \phi'^{zz}_{z}}{\partial z'} \right\rangle = \langle\alpha'\rangle + \frac{[\![a_I]\!]}{Q_I} \left\langle \begin{Bmatrix} \alpha'^{-} s \\ \alpha'^{+}(1-s) \end{Bmatrix} \right\rangle \\
&= \langle\alpha'\rangle + [\![a_I]\!][\![\alpha']\!] s(s-1)/Q_I
\end{aligned} \tag{6.1.7a,b}$$

where

$$[\![\alpha']\!] = \alpha'^{+} - \alpha'^{-}$$

Likewise the coefficients $(\beta''_t)_{ij}$ are

$$\begin{aligned}
(\beta''_t)_{xx} &= (\beta''_t)_{yy} = \langle\beta'_t\rangle + [\![\beta'_t]\!][\![a_{II}]\!] s(s-1)/Q_I \\
(\beta''_t)_{zz} &= \langle\beta'_t\rangle + [\![\beta'_t]\!][\![a_I]\!] s(s-1)/Q_I
\end{aligned} \tag{6.1.8}$$

All other coefficients of α'' and β''_t are zero.

The elastic coefficients γ''_{ij}, $(\beta''_c)_{ij}$ and $(\zeta''_c)_{ij}$ are similarly determined as follows. From (5.1.25)

$$\begin{aligned}
\gamma''_{xx} &= \gamma''_{yy} = \alpha''_{xx} - \left\langle n' \frac{\partial \phi'^{xx}_{z}}{\partial z'} \right\rangle = \alpha''_{xx} - \frac{[\![a_{II}]\!]}{Q_I} \left\langle \begin{Bmatrix} n'^{-} s \\ n'^{+}(1-s) \end{Bmatrix} \right\rangle \\
&= \alpha''_{xx} + ([\![\alpha']\!] - [\![n']\!])\,[\![a_{II}]\!] s(s-1)/Q_I \\
\gamma''_{zz} &= \alpha''_{zz} + ([\![\alpha']\!] - [\![n']\!])\,[\![a_I]\!] s(s-1)/Q_I
\end{aligned} \tag{6.1.9}$$

Also, from (5.1.17) and (5.1.18) after some manipulation, we get

$$\begin{aligned}
\frac{\partial \eta'_z}{\partial z'} &= \frac{\langle a_I^{-1}\rangle^{-1}}{a_I} \left\langle \frac{\alpha'}{a_I} \right\rangle - \frac{\alpha'}{a_I} = \frac{1}{Q_I a_I} \left[a_I^{+} \alpha'^{-}(1-s) + a_I^{-} \alpha'^{+} s \right] - \frac{\alpha'}{a_I} \\
&= \frac{[\![\alpha']\!]}{Q_I} \begin{Bmatrix} s \\ s-1 \end{Bmatrix} \qquad \begin{matrix} 0 < z' < (1-s)\ell' \\ (1-s)\ell' < z' < \ell' \end{matrix} \\
\frac{\partial \zeta'_z}{\partial z'} &= \frac{\langle a_I^{-1}\rangle^{-1}}{a_I} \left\langle \frac{\beta'_t}{a_I} \right\rangle - \frac{\beta'_t}{a_I} = \frac{[\![\beta'_t]\!]}{Q_I} \begin{Bmatrix} s \\ s-1 \end{Bmatrix} \qquad \begin{matrix} 0 < z' < (1-s)\ell' \\ (1-s)\ell' < z' < \ell' \end{matrix}
\end{aligned} \tag{6.1.10}$$

It then follows from (5.1.26) and (5.1.27) that

$$\begin{aligned}
\beta''_c &= \langle\beta'_c\rangle + \left\langle (n' - \alpha'_{zz}) \frac{\partial \eta'_z}{\partial z'} \right\rangle \\
&= \langle\beta'_c\rangle + ([\![n']\!] - [\![\alpha']\!])\,[\![\alpha']\!] s(s-1)/Q_I \\
\zeta''_c &= \langle\zeta'_c\rangle + ([\![n']\!] - [\![\alpha']\!])\,[\![\beta'_t]\!] s(s-1)/Q_I
\end{aligned} \tag{6.1.11}$$

The macroscale coefficients related to the elastic properties of the medium have been expressed in terms of mesoscale coefficients and porosity for two layer periodic medium.

6.2 The Coefficients k''_{ij} and δ''_{ij}.

The permeability k'' of (5.2.5) simply becomes for the two-layered medium of Fig. 2

$$\begin{aligned} k''_{xx} &= k''_{yy} = k'^{-}(1-s) + k'^{+}s \\ k''_{zz} &= \left\langle k'^{-1} \right\rangle^{-1} = \frac{k'^{+}k'^{-}}{R} \end{aligned} \tag{6.2.1}$$

where

$$R = (1-s)k'^{+} + sk'^{-} \tag{6.2.2}$$

From (5.2.4b) and (5.2.5) we obtain

$$\begin{aligned} \delta''_{zz} &= \left\langle n' \frac{\partial S'_z}{\partial z'} \right\rangle = \left\langle k'^{-1} \right\rangle \left\langle \frac{n'}{k'} \right\rangle - n'' \\ &= \frac{k'^{+}k'^{-}}{R} \left[\frac{n'^{-}}{k'^{-}}(1-s) + \frac{n'^{+}}{k'^{+}}s \right] - n'' = \frac{n'^{-}k'^{+}(1-s) + n'^{+}k'^{-}s}{R} - n'' \end{aligned} \tag{6.2.3}$$

The coefficients in consolidation equation are now all determined. We move to heat transport.

6.3 Thermal Conductivity m''_{ij}.

The macroscale thermal conductivity m''_{ij} appears to be precisely the same form as permeability k''_{ij} and we replace k'^{+} and k'^{-} in (6.2.1) and (6.2.2) by m'^{+} and m'^{-}. We then have

$$\begin{aligned} m''_{xx} &= m''_{yy} = m'^{-}(1-s) + m'^{+}s \\ m''_{zz} &= \left\langle m'^{-1} \right\rangle^{-1} = \frac{m'^{+}m'^{-}}{M} \end{aligned} \tag{6.3.1}$$

where

$$M = (1-s)m'^{+} + sm'^{-} \tag{6.3.2}$$

6.4 Quantitative Effects of Mesoscale Heterogeneities on the Macroscale Coefficients.

For the porous medium with two alternating layers on the mesoscale, we examine the effects of heterogeneities on the macroscale coefficients. Our attention is particularly focused on the contrast of the scales of mesoscale coefficients between the layers.

We recall that the dimensionless mesoscale coefficients presented in Ch.1, which were called the macroscale coefficients, have been normalized by the order of magnitude on the mesoscale. Likewise, in the present meso-and macroscale analysis, the scales of the physical coefficients on the macroscale are used in normalization. Thus the relative order of magnitude in each layer on the mesoscale predominantly detemines the dimensionless coefficients. If we let, for example, the elastic moduli on the mesoscale be $\mathcal{D}$, the elastic coefficients in physical units in the lower and upper layers are $\tilde{a}_I^- = (\mathcal{D}a_I)^-$ and $\tilde{a}_I^+ = (\mathcal{D}a_I)^+$ where a_I is of $O(1)$ and is dimensionless. We assume that the difference in a_I between two layers is negligible. The depth average is $\langle \tilde{a}_I^- \rangle = (1-s)(\mathcal{D}a_I)^- + s(\mathcal{D}a_I)^+$. Normalizing by $\langle \tilde{a}_I^- \rangle$ we get

$$\begin{aligned} a_I^- &= \frac{\tilde{a}_I^-}{\langle \tilde{a}_I^- \rangle} = \frac{(\mathcal{D}a_I)^-}{(1-s)(\mathcal{D}a_I)^- + s(\mathcal{D}a_I)^+} \\ a_I^+ &= \frac{\tilde{a}_I^+}{\langle \tilde{a}_I^- \rangle} = \frac{(\mathcal{D}a_I)^+}{(1-s)(\mathcal{D}a_I)^- + s(\mathcal{D}a_I)^+} \end{aligned} \tag{6.4.1}$$

from which it follows that

$$\begin{aligned} &\frac{\mathcal{D}^+}{\mathcal{D}^-} \ll 1 \quad ; \quad a_I^- \simeq \frac{1}{1-s}, \quad a_I^+ \ll 1 \quad ; \quad \frac{a_I^+}{a_I^-} \ll 1 \\ &\frac{\mathcal{D}^+}{\mathcal{D}^-} \gg 1 \quad ; \quad a_I^- \ll 1, \quad a_I^+ \simeq \frac{1}{s} \quad ; \quad \frac{a_I^+}{a_I^-} \gg 1 \end{aligned} \tag{6.4.2}$$

Therefore, the ratio of the normalized coefficients a_I^+/a_I^- is a direct measure of the contrast in elastic modulus between layers i.e., the heterogeneity in the elastic property. Similarly the degree of heterogeneities in the permeability and thermal conductivity will be measured by the ratios k^+/k^- and m^+/m^-. The difference in the porosity is assumed to be small and ignored.

In view of these, the macroscale coefficients of the previous section are further normalized by their depth averages as follows.

The elastic coefficients :

$$\begin{aligned}
\frac{a''_{xxxx}}{\langle a_I\rangle} &= 1-\left(\frac{a_{II}^-}{a_I^-}\right)^2\frac{\left(1-\frac{a_{II}^+}{a_{II}^-}\right)^2 s(1-s)}{A_I B_I}, \qquad \frac{a''_{zzzz}}{\langle a_I\rangle} = \frac{\frac{a_I^+}{a_I^-}}{A_I B_I} \\
\frac{a''_{xxyy}}{\langle a_{II}\rangle} &= 1-\left(\frac{a_{II}^-}{a_I^-}\right)\frac{\left(1-\frac{a_{II}^+}{a_{II}^-}\right)^2 s(1-s)}{A_{II} B_I}, \qquad \frac{a''_{yyzz}}{\langle a_{II}\rangle} = \frac{(1-s)\frac{a_I^+}{a_I^-}+s\frac{a_{II}^+}{a_{II}^-}}{A_{II}B_I} \\
\frac{a''_{xyxy}}{\langle a_{III}\rangle} &= 1, \qquad \frac{a''_{yzyz}}{\langle a_{III}\rangle} = \frac{\frac{a_{III}^+}{a_{III}^-}}{A_{III}B_{III}}
\end{aligned} \tag{6.4.3}$$

where

$$A_i = (1-s)+s\frac{a_i^+}{a_i^-}, \qquad B_i = s+(1-s)\frac{a_i^+}{a_i^-} \quad (i=I,II,III) \tag{6.4.4}$$

The pressure coefficients and thermal modulus :

$$\begin{aligned}
\frac{\alpha''_{xx}}{\langle\alpha'\rangle} &= 1-\frac{a_{II}^-}{a_I^-}\frac{\left(\frac{a_{II}^+}{a_{II}^-}-1\right)\left(\frac{\alpha^+}{\alpha^-}-1\right)s(1-s)}{A_\alpha B_I} \\
\frac{\alpha''_{zz}}{\langle\alpha'\rangle} &= 1-\frac{\left(\frac{a_I^+}{a_I^-}-1\right)\left(\frac{\alpha^+}{\alpha^-}-1\right)s(1-s)}{A_\alpha B_I} \\
\frac{(\beta''_t)_{xx}}{\langle\beta'_t\rangle} &= 1-\frac{a_{II}^-}{a_I^-}\frac{\left(\frac{a_{II}^+}{a_{II}^-}-1\right)\left(\frac{\beta_t^+}{\beta_t^-}-1\right)s(1-s)}{A_{\beta_t} B_I} \\
\frac{(\beta''_t)_{zz}}{\langle\beta'_t\rangle} &= 1-\frac{\left(\frac{a_I^+}{a_I^-}-1\right)\left(\frac{\beta_t^+}{\beta_t^-}-1\right)s(1-s)}{A_{\beta_t} B_I}
\end{aligned} \tag{6.4.5}$$

where

$$A_\alpha = (1-s)+s\frac{\alpha^+}{\alpha^-}, \qquad A_{\beta_t} = (1-s)+s\frac{\beta_t^+}{\beta_t^-} \tag{6.4.6}$$

The coefficients in the consolidation equation are

$$\begin{aligned}
\frac{\gamma''_{xx}}{\langle\gamma'\rangle} &= 2\frac{\alpha''_{xx}}{\langle\alpha'\rangle}-1, \quad \frac{\gamma''_{zz}}{\langle\gamma'\rangle} = 2\frac{\alpha''_{zz}}{\langle\alpha'\rangle}-1 \\
\frac{\beta''_c}{\langle\beta'_c\rangle} &= 1+\frac{\alpha^{-2}}{\beta_c^+ a_I^-}\frac{\left(\frac{\alpha^+}{\alpha^-}-1\right)^2 s(1-s)}{A_{\beta_c} B_I} \\
\frac{\zeta''_c}{\langle\zeta'_c\rangle} &= 1+\frac{\beta_t^-\alpha^-}{\beta_c^- a_I^-}\frac{\left(\frac{\alpha^+}{\alpha^-}-1\right)\left(\frac{\beta_t^+}{\beta_t^-}-1\right)s(1-s)}{\left[(1-s)+s\frac{\zeta_c^+}{\zeta_c^-}\right]B_I}
\end{aligned} \tag{6.4.7}$$

where

$$A_{\beta_c} = (1-s)\frac{\beta_c^-}{\beta_c^+} + s \tag{6.4.8}$$

The permeability and thermal conductivity are

$$\begin{aligned} \frac{k''_{xx}}{\langle k' \rangle} &= 1, \qquad \frac{k''_{zz}}{\langle k' \rangle} = \frac{\left(\frac{k^+}{k^-}\right)}{\left[(1-s)+s\frac{k^+}{k^-}\right]\left[s+(1-s)\frac{k^+}{k^-}\right]} \\ \frac{m''_{xx}}{\langle m' \rangle} &= 1, \qquad \frac{m''_{zz}}{\langle m' \rangle} = \frac{\left(\frac{m^+}{m^-}\right)}{\left[(1-s)+s\frac{m^+}{m^-}\right]\left[s+(1-s)\frac{m^+}{m^-}\right]} \end{aligned} \tag{6.4.9}$$

From §3 of Ch.1, we recall that, in physical coefficients,

$$\begin{aligned} &a_{I,II,III} = O(\mathcal{D}), \quad \alpha' = O(1), \quad \beta'_t = O(\alpha\mathcal{D}) \\ &\gamma' = O(1), \quad \beta'_c = O\left(\frac{1}{\mathcal{D}}\right), \quad \zeta'_c = O(\alpha) \end{aligned} \tag{6.4.9a}$$

where α is the linear coefficient of thermal expansion for soild. Because of the inverse proportionality of β'_c to $\mathcal{D}$, the ratio of β'_c in (6.4.8) between layers has been chosen as β_c^-/β_c^+ to be in consistent trend as a_i^+/a_i^-. Then the multiplying factor $\alpha^{-2}/\beta_c^+ a_I^-$ in β''_c is a constant of $O(1)$ because α^-(or α^+)=$O(1)$ is dimensionless and is expected not to be affected noticeably by the scale of elastic modulus. For convenience it is regarded as unity in the subsequent calculations. Similarly the linear expansion coefficient is nearly constant regardless of the elastic property of the medium (see e.g., Jumikis, 1977) and the factor $\beta_t^-/\beta_c^- a_I^-$ in ζ''_c is also taken to be unity.

The behavior of the macroscale coefficients when the ratios $\mathcal{D}^+/\mathcal{D}^-$, k^+/k^- and m^+/m^- are varied is examined. The depth fraction of the upper layer is fixed at $s = 0.5$ so that the two layers are of equal thickness.

Elactic Coefficients a''_{ijkl} and Thermal Modulus $(\beta''_t)_{ij}$: As shown in (6.4.2), another measure of the degree of heterogeneity $\mathcal{D}^+/\mathcal{D}^-$ is $a_i^+/a_i^-(i = I, II, III)$. The ratio is allowed to change over a fairly wide range of values. The main objective is to

examine the effects of the contrast in $\mathcal{D}$. We thus assume that the three coefficients a_I, a_{II} and a_{III} vary only according to $\mathcal{D}$. The ratio will be denoted by a_r.

$$a_r = \frac{a_I^+}{a_I^-} = \frac{a_{II}^+}{a_{II}^-} = \frac{a_{III}^+}{a_{III}^-} \tag{6.4.10}$$

It then follows from (6.4.3) that

$$\frac{a''_{xzxz}}{\langle a_I \rangle} = \frac{a''_{yyzz}}{\langle a_{II} \rangle} = \frac{a''_{yzyz}}{\langle a_{III} \rangle} \tag{6.4.11}$$

On the other hand, it has been shown for the same rigidity $\mathcal{D}$ that the ratio a_{II}^-/a_I^- in a layer varies considerably from very small to finite value of about 0.3. Three values of a_{II}^-/a_I^- have chosen as 0.01, 0.1 and 0.3.

The variations of the elastic coefficients and thermal modulus are plotted against a_r in Fig. 6.2(a) and (b). They are symmetric about $a_r = 1$ because the macroscale behavior of the medium is immaterial to the alternating pattern of the layers. From (6.4.3) we have

$$\frac{a''_{xxxx}}{\langle a_I \rangle} \simeq 1 - \left(\frac{a_{II}^-}{a_I^-}\right)^2, \quad \frac{a''_{xxyy}}{\langle a_{II} \rangle} \simeq 1 - \frac{a_{II}^-}{a_I^-}, \quad \frac{a''_{xzxz}}{\langle a_I \rangle} \simeq 0 \qquad \text{for} \quad a_r \ll 1, a_r \gg 1 \tag{6.4.12}$$

Thus as the degree of heterogeneity increases, a''_{xzxz} is quickly reduced whereas others vary mildly of which a''_{xxxx} is almost insensitive to a_r as shown in Fig. 6.2(a). Equation (6.4.12) also shows that

$$\begin{aligned} a''_{xxxx} &\simeq \langle a_I \rangle - \left(\frac{a_{II}^-}{a_I^-}\right)^2 \begin{Bmatrix} a_I^-(1-s) & a_r \ll 1 \\ a_I^+ s & a_r \gg 1 \end{Bmatrix} \\ a''_{xxyy} &\simeq \left(1 - \frac{a_{II}^-}{a_I^-}\right) \begin{Bmatrix} a_{II}^-(1-s) & a_r \ll 1 \\ a_{II}^+ s & a_r \gg 1 \end{Bmatrix} \end{aligned} \tag{6.4.13}$$

The coefficient a''_{xxxx} approaches to its depth average plus some correction which is affected predominantly by the hard layer beacause external load is sustained mostly by the more rigid part of the medium. Similarly a''_{xxyy} is determined by the hard layer. But the medium, with soft layers periodically sandwiched between hard layers, can not resist to the loading imposed in the direction normal to the layers and therefore a''_{xzxz} decreases greatly with increasing or decreasing a_r. Coefficients

a''_{yyzz} and a''_{yzyz} follow the same curve as a''_{zzzz}(cf.(6.4.11)). The thermal moduli $(\beta''_t)_{xx}$ and $(\beta''_t)_{zz}$ vary in the same manner as for a''_{xxyy} and a''_{zzzz} respectively as shown in Fig. 6.2(b) because of the same reason.

Other Elastic Coefficients : The rest of the elastic coefficients are shown in Fig. 6.3(a) and (b) also for three values of a^-_{II}/a^-_I. Since the pressure coefficient α' in Hooke's law is dimensionless, it does not vary much from layer to layer and two values of the ratio $\alpha_r = \alpha^+/\alpha_-$ have been chosen as 0.5 and 2 respectively in Fig. 6.3(a) and (b). As shown in (6.4.5) and (6.4.7), the ratio α_r determines the variation of the coefficients with a_r. The curves are not symmetric about $a_r = 1$. We note from (6.4.5) and (6.4.7) that their variations with a_r are dependent upon the ratio α^+/α^-. It readily follows that

$$
\begin{aligned}
\alpha''_{xx} &\simeq \langle\alpha'\rangle - \frac{a^-_{II}}{a^-_I}\left\{\begin{matrix}(\alpha^- - \alpha^+)(1-s) & a_r \ll 1\\ (\alpha^+ - \alpha^-)s & a_r \gg 1\end{matrix}\right\}\\
\alpha''_{zz} &\simeq \langle\alpha'\rangle - \left\{\begin{matrix}(\alpha^- - \alpha^+)(1-s) & a_r \ll 1\\ (\alpha^+ - \alpha^-)s & a_r \gg 1\end{matrix}\right\}\\
\beta''_c &\simeq \langle\beta'_c\rangle + (\alpha^+ - \alpha^-)^2\left\{\begin{matrix}(1-s)/a^-_I & a_r \ll 1\\ s/a^+_I & a_r \gg 1\end{matrix}\right\}\\
\zeta''_c &\simeq \langle\zeta'_c\rangle + \left\{\begin{matrix}(\alpha^- - \alpha^+)(1-s)\beta^-_t/a^-_I & a_r \ll 1\\ (\alpha^+ - \alpha^-)s\beta^+_t/a^+_I & a_r \ll 1\end{matrix}\right\}
\end{aligned}
\qquad (6.4.14)
$$

The pressure coefficient thus approaches to the depth average $\langle\alpha'\rangle$ subtracted by the difference in α' of hard layer from that of the soft layer. The coefficient α'' is the stress generated by the pore presssure change and thus the hard layer is more responsible for the stress induced. Since α''_{zz} is independent of the ratio a^-_{II}/a^-_I (cf.(6.4.5)), its curves are all equal in Fig. 6.3(a) and (b). The pressure coefficient β''_c in the consolidation equation means the rate of fluid influx to the porous medium due to the pore pressure change. So if the medium is soft more fluid can be absorbed into the medium by pressure increase and vice versa as is evidenced by the scale proportionality of β'_c in (6.4.9a). This is reflected in the depth average $\langle\beta'_c\rangle = (1-s)\beta^-_c + s\beta^+_c$. But the correction to the average is controlled by the hard layer which behaves as a barrier and has the tendency of preventing the influx as in (6.4.14). Similarly the temperature coefficient ζ''_c bears the meaning of mass

influx due to temperature change. If temperature variation is positive, the porous matrix expands and the fluid in the pores is squeezed out. A behavior similar to β_c'' is observed in Fig. 6.3. The variations are mild as compared to Fig. 6.2.

The variations shown so far in Figs. 6.2 and 6.3 are based on the normalization by the depth average of each indivisual coefficient and it should be noted that the average values themselves change with the ratio a_r.

Permeability and Thermal Conductivity :

Since the permeability and thermal conductivity are of the same form in (6.4.9), we only discuss the permeability.

While the permeability in the horizontal direction is always unity, the vertical permeability $k_{zz}''/\langle k' \rangle$ strongly depends on the permeability contrast between layers. It is readily seen from (6.4.9) that $k_{zz}''/\langle k' \rangle$ is symmetric in the ratio k^+/k^- about $k^+/k^- = 1$. Let the ratio be denoted by k_r :

$$k_r = \frac{k^+}{k^-} \tag{6.4.15}$$

It follows then from (6.4.9) and $\langle k' \rangle = (1-s)k^- + sk^+$ that

$$k_{zz}'' \simeq \left\{ \begin{matrix} k^+/(1-s)s & k_r \ll 1 \\ k^-/(1-s)s & k_r \gg 1 \end{matrix} \right\} \tag{6.4.16}$$

When the permeability contrast is large, the effective vertical permeability is thus predominantly controlled by that of the less permeable layer. The dependence of $k_{zz}''/\langle k' \rangle$ on k_r is the same as that of a_{zzzz}'' on a_r shown in Fig. 6.2 and the figure is not produced separately here.

The above discussion is equally valid for the thermal conductivity.

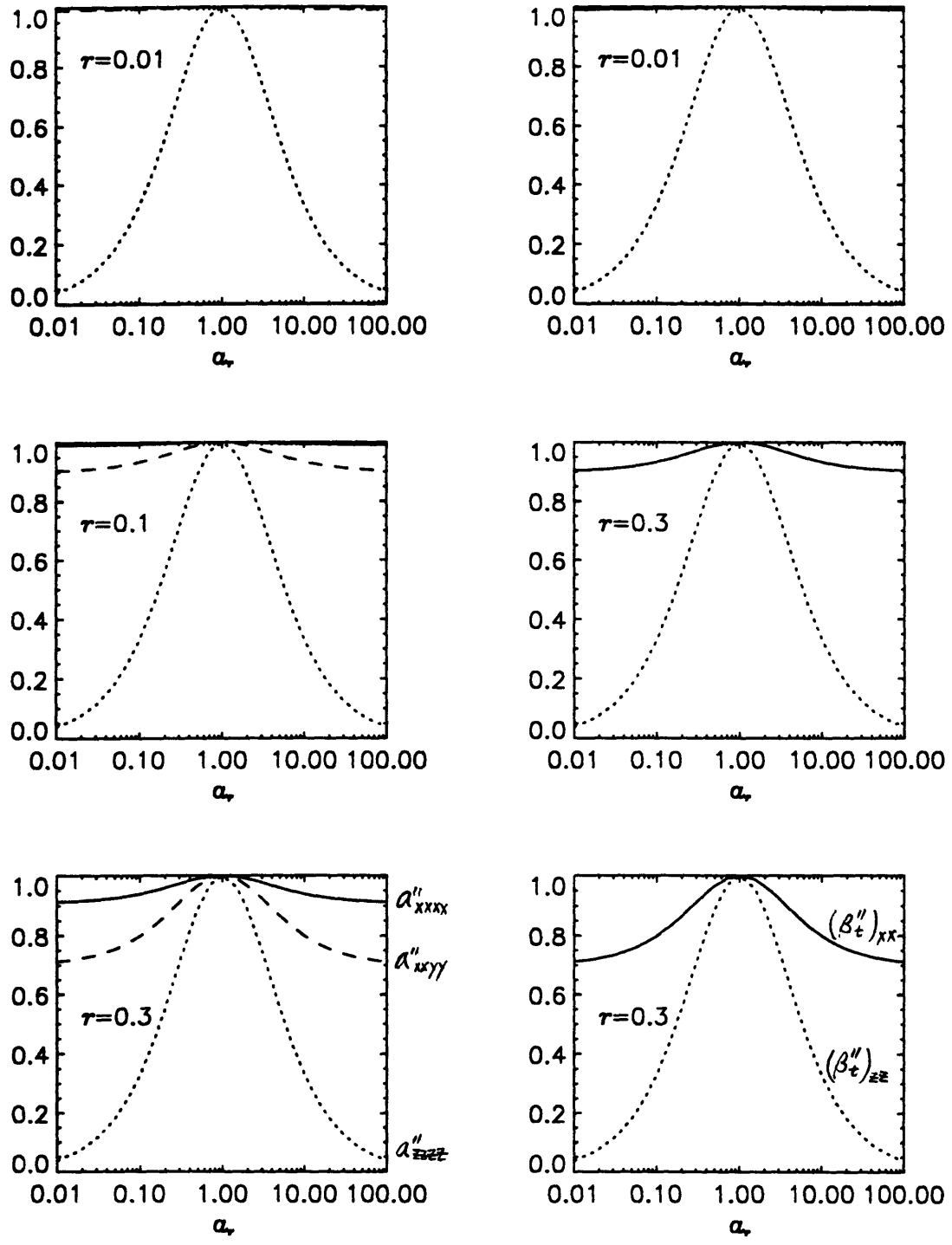

Fig. 6.2 The elastic coefficients a''_{zzzz}, a''_{zzyy} and a''_{zzzz} and thermal moduli $(\beta'')_{zz}$ and $(\beta'')_{zz}$. The symbol r denotes a_{II}^{-}/a_{I}^{-}.

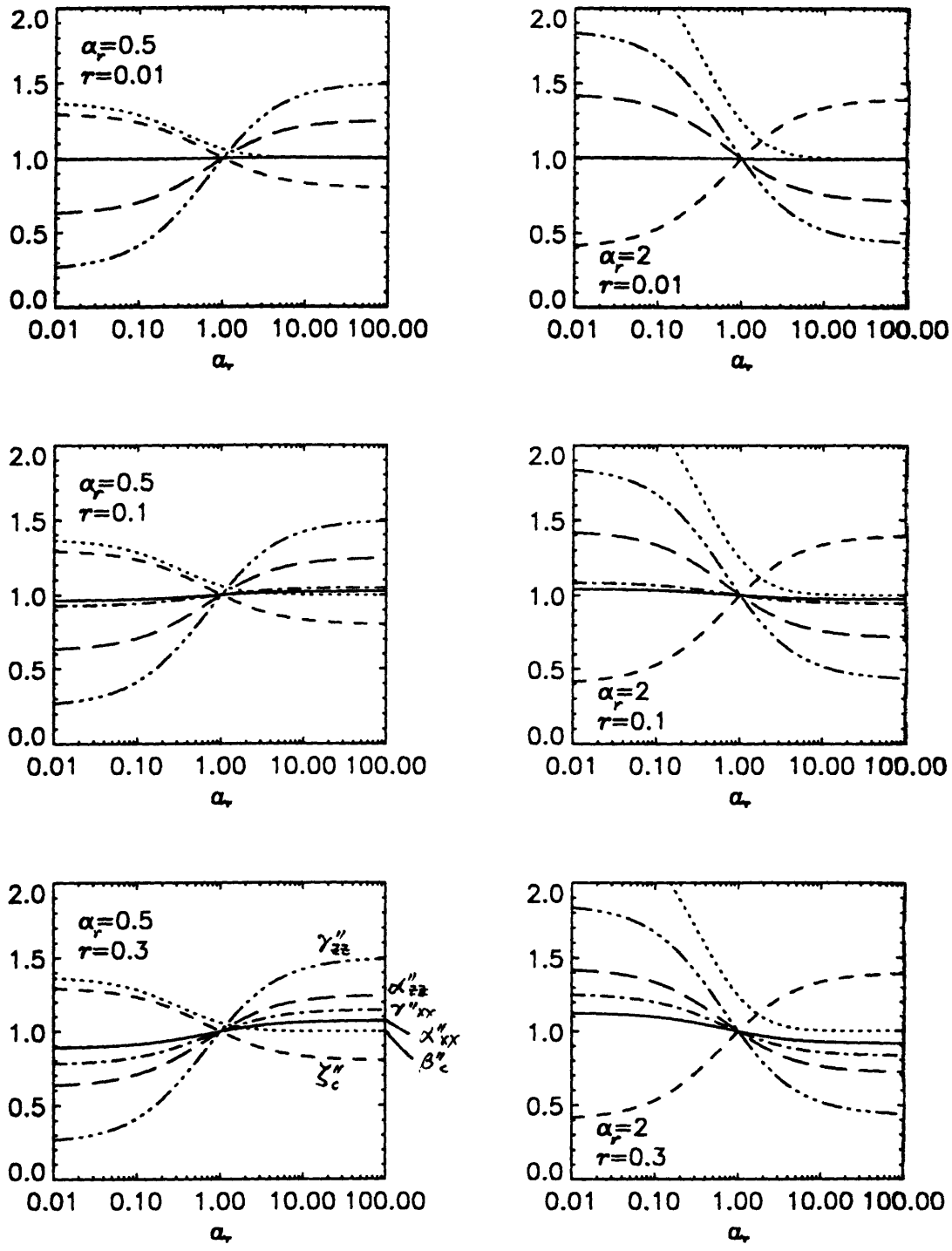

Fig. 6.3 The coefficients α''_{xx}, α''_{zz}, γ''_{xx}, γ''_{zz}, β''_c and ζ''_c for different values of α_r and $r = a_{II}^{-}/a_{I}^{-}$.

7. Concluding Remarks

For three scale porous medium characterized by the existence of the microscale ℓ, the mesoscale ℓ' and the macroscale ℓ'', the governing equations for thermoconsolidation on the macroscale have been deduced starting from the mesoscale governing equations. The macroscale governing equations are of the same form as those on the mesoscale. Several mesoscale cell boundary value problems are defined whose solutions depend on the mesoscale variation of the material coefficients. Therefore if the mesoscale coefficients are uniform, the macroscale governing equations and constitutive coefficients identically reduce to those on the mesoscale.

The macroscale coefficients have been calculated for a medium with two alternating layers on the mesoscale. The effects of the contrast of the mesoscale coefficients have been examined. For horizontally layered medium, the macroscale coefficients are obviously anisotropic. In general, due to the layered structure, the coefficients in the direction normal to the layering are more sensitive to the contrast of the mesoscale coefficients.

While the macroscale elastic coefficients and the thermal modulus depend on the ratio of elastic properties between layers, the pressure coefficient α''_{ij} and the coefficients γ'', β''_c and ζ''_c in the consolidation equation depend not only on the elastic properties but also on the pore pressure coefficientα' on the mesoscale, because they reflect the variations in the pore fluid due to the interaction between solid and fluid phases.

GENERAL SUMMARY AND CONCLUSIONS

We have investigated the thermoconsolidation in poroelastic media, in Chapter I for two scale media and in Chapter II for three scale media by using the theory of homogenization. Two key assumptions are made in the homogenization theory. One is the existence of disparate length scales. The other is the periodicity of the medium structure and material coefficients at all scales but the largest one. The multiple-scale perturbation analysis is then readily used to deduce the governing equations and the constitutive coefficients on the macroscale without empirical assumptions. During the analysis, certain microscale and mesoscale cell boundary value problems are defined whose solutions are necessary to calculate the macroscale coefficients.

In Chapter I, first the macroscale governing equations are deduced by starting from the basic governing equations for the fluid and solid phases on the microscale. The microscale Peclét number is assumed to be small as $O(\epsilon)$, where $\epsilon = \ell/\ell' \ll 1$ with ℓ and ℓ' being the microscale and the macroscale. Accordingly heat convection is negligibly small on the microscale, but is comparable to heat diffusion on the macroscale. The Rayleigh number is assumed to be finite.

It is shown that, when the medium deformation is comparable to typical grain size, the governing equations are in general nonlinearly coupled due to nonlinear boundary conditions on the fluid-solid interfaces. For isothermal consolidation the linear theory of consolidation due to Biot(1941) is the most widely used tool in practice. It is obtained on the phenomenological basis. Our results show that the applicability of Biot's theory should be limited to the cases of solid displacement much smaller than the grain size. However, as shown in §5 of Ch. I and Appendix D, those nonlinear terms which originate from the nonlinear interface boundary conditions vanish identically for special class of microcell geometries with three orthogonal planes of symmetry. In such case, use of Biot's theory is justified. This kind of distinction has not been made before in the previous works on the application of the homogenization theory to consolidation in porous media (Auriault and Sanchez-Palencia, 1977; Burridge and Keller, 1983; Mei and Auriault, 1989).

Infinitesimal strain is merely assumed to allow the use of Hooke's law. Our theory cautions that care should be taken in the applications.

In addition to its capability of deducing the macroscale governing equations theoretically, there is another advantage in the use of homogenization theory although the medium is restricted to periodic micro-structures. Once the macroscale problem is solved, the variations on the lower scale are readily determined in terms of the solutions of the microcell boundary value problems. This is particularly advantageous when one is concerned about local processes which may lead to unwanted breakdown or failure. The earlier theories (Schiffman, 1971; Brownell et al 1977; Derski and Kowalski, 1979; Bear and Corapcioglu, 1981) are based on the volume averaged variables and lack in this capability.

Properties of the macroscale coefficients are also examined. For isothermal consolidation, Auriault and Sanchez-Palencia(1977) have established certain constraints on the elastic coefficients. By assuming elastic isotropy, they show that the pressure coefficient β_c' in the consolidation equation (cf. (4.1.28) in Ch. I) is positive and that the coefficient γ' for solid dilation rate is equal to the pressure coefficient α' in Hooke's law. This implies that it is only necessary to solve some elastostatic problems in the solid phase of a microcell to detemine the macroscale coefficients. These constraints are extended to thermoconsolidation in this study. We proved that the temperature coefficient ζ_c' in the consolidation equation is negative. Alternatively the heuristic reason is as follows. The coefficient ζ_c' is the rate of pore fluid influx due to temperature change in the solid phase. If the temperature increases, the solid expands relative to the initial position of the interface and thus tends to squeeze pore fluid out of the microcell. Thus ζ_c' must be negative. It is also shown that the thermal modulus $(\beta_i')_{ij}$ in Hooke's law is given in terms of the elastic coefficient tensor $a'_{ijk\ell}$. Therfore, in thermoconsolidation too, all the coefficients in the equilibrium and consolidation equations are determined in terms of the solutions of a few elastostatice problems in the microcell (cf. ϕ_k^{ij} in §4 in Ch. I).

Calculation of the macroscale coefficients is performed for a cubic array of Wiger-Seitz grains (which have three planes of symmetry) by solving the microcell boundary value problems numerically. As far as we are aware, no previous calulations of the coefficients in the consolidation theory exist. By examining the symmetry properties of the elastostatic problems defined in the microcell, we first show that the elastic coefficient tensor $a'_{ijk\ell}$ reduces to only three distinct coefficients (cubic symmetry). This type of symmetry is well known in crystal structures and anisotropic elasticity (Love, 1944; Lekhnitskii, 1963; Cottrell, 1964) where the symmetry relations are derived by examining the material symmetry or particle arrays in a lattice. However, we establish the cubic symmetry property for Wiger-Seitz grains by making explicit use of the symmetry relations for the solutions inside the microcell. We also show for the same geometry that the following coefficients are isotropic : the pressure coefficient α'_{ij}, thermal modulus $(\beta'_t)_{ij}$, the coefficient γ'_{ij} and the thermal conductivity m'_{ij}.

As application of the macroscale equations, pumping of hot fluid from geothermal reservoirs with initial vertical temperature gradient is considered.

In the case of one-dimensional pumping from the lower boundary, the buoyancy effects are the decreases in the pore pressure and vertical compaction whereas the thermal stress (due to cooling) tends to increase vertical compaction. However, in the early transient stage for sufficiently large Rayleigh number but still less than the critical value of Lapwood, the pore pressure, temperature and vertical displacement develop much faster due to nonlinear coupling. The upper surface undergoes compaction then followed by finite swelling. In the two-dimensional pumping through a small sink at the bottom, it is shown that cellular cenvective motions occur for Rayleigh numbers smaller than the critical value of Lapwood. This shows that the critical Rayleigh number for two-domensional pumping is smaller than that for one-dimensional case of uniform through flow. As a result, the deformation on the upper surface of reservoir becomes wavy.

In the previous studies on geothermal reservoirs, the primary emphasis has been either on the areal distribution of the pressure and temperature in the liquid system or on the two-phase (liquid and vapor) system (Mercer et al, 1975; Garg et al 1975; Faust and Mercer, 1979a,b; Mercer and Faust, 1979). In areal models, the effect of Rayleigh number which leads to the development of convection cells is discarded. Lippman et al (1976) considered Rayleigh numbers greater than Lapwood's critical value 40 so that there already exist convective motions at the initial state. They only consider minor temperature changes due to injection and pumping schemes. Little attention is focused on the medium deformation. In all these, the role of Rayleigh number is not examined in two- or three-dimensions. We have specifically shown, in two-dimensional case, that the critical Rayleigh number is at least as low as 20. The direct consequence, as mentioned above, is the wavy pattern of deformation on the upper surface.

As has been mentioned earlier, a geothermal field of particular interests is Wairakei site in New Zealand. The recorded ground subsidence in the production area was as high as $4.5m$ over the period 1964 - 1974 (Stilwell et al, 1975). Also, the measurement of horizontal movement of ground surface has shown $0.8m$ at a location. But it is not clear whether that is the maximum horizontal movement which occurred at Wairakei because the observation has been made at some construction sites. Our calculations for two-dimensional situation show that the horizontal displacement ranges from one-third to one half of the vertical displacement on the reservoir surface. This is roughly consistent with the field observations at the Wairakei.

In Chapter II, thermoconsolidation in three-scale medium is considered. A three-scale medium is characterized by the existence of three disparate length scales, the microscale ℓ, the mesoscale ℓ' and the macroscale ℓ'' for which $\ell/\ell' \ll 1$ and $\ell'/\ell'' \ll 1$. By extending the homogenization procedure to ℓ' and ℓ'' scales, the macroscale governing equations and effective coefficients are deduced. In principle, the macroscale governing equations take the same form as those on the mesoscale.

The theory is applied to derive the macroscale coefficients for a medium with two alternating layers on the mesoscale. It is shown that the coefficients in the direction normal to the layers is more sensitive to the contrast of the mesoscale coeficients between layers.

Based on the present study, it is hoped that future research will be pursued in the following directions.

The microcell studied in this work is a single grain model with three planes of symmetry. Because of the crystalline structure of the medium, the elastic coefficient tensor is always anisotropic. In our particular choice, it possesses cubic symmetry. Future extensions can be viewed in two ways. First, in nature, particles are often arranged in fairly disordered manner in many instances, studies of multi-grain microcells are needed. Although the numerical tasks are expected to be difficult, it will be useful in assessing the effects of irregular size with homogenization theory. Secondly and more importantly, even for single-grain microcells, calculation of the macroscale coefficients for cell geometries without symmetry is needed. As we have seen earlier, the governing equations are nonlinear in general and the validity of Biot's theory is severely limited. Studies with nonsymmetric cell geometry will definitely help understand the differences between the nonlinear theory and Biot's linear theory.

For three-scale medium we have considered layered medium only. However, in many natural porous media, inclusions in the form of lenses and beds are frequently encountered (Poland, 1984). Very often those inclusions are ignored. In this regard, application of the theory to medium with various inclusions should be very useful in approaching toward realistic problems.

Finally, on the application to geothermal reservoirs, study of three-dimensional pumping situation would be very promising. Examples are a single well pumping and extraction of hot fluid from a small sink in which cases flow is radially converging. Also pumping from multiple-sink is easily attacked. It is anticipated that only numerical difficulties matter in view of large storage and efficient handling of

solution procedure. All of the field examples are indeed three-dimensional. It is well known in the study of three-dimensional flow instability in porous layer that the convective motions develop in hexagonal cells (Combarnous and Bories, 1975). Examination of the development of pore pressure and temperature should be challenging. More interestingly, the deformation on the reservoir surface is expected to be fully three-dimensional in view of the hexagonal convection cells.

REFERENCES

Auriault, J.-L., Borne, L. and Chambron, R. (1985), Dynamique des composites élastiques peériodique, Arch. Mech., 37:269-284.

Auriault, J.-L. and Sanchez-Palencia, E. (1977), Etude du comportment macroscopique d'un milieu poreux sature deformable, J. de Mecanique, 16(4):575-603.

Bakhbalov, N. and Panasenko, G. (1989), Homogenization: Averaging Processes in Periodic Media, Kluwer Academic Pub.

Bear, J. and Corapcioglu, M.Y. (1981a), Mathematical model for regional land subsidence due to pumping, 1. Integrated aquifer subsidence equations based on vertical displacement only, Water Resources Research, 17(4):937-946.

Bear, J. and Corapcioglu, M.Y. (1981b), Mathematical model for regional land subsidence due to pumping, 1. Integrated aquifer subsidence equations for vertical and horizontal displacements, Water Resources Research, 17(4):947-958.

Bear, J. and Corapcioglu, M.Y. (1981c), A mathematical model for consolidation in a thermoelastic aquifer due to hot water injection or pumping, Water Resources Research, 17(3):723-736.

Bensoussan, A., Lions, J.L. and Papanicolaou, G. (1978), Asymptotic Analysis for Periodic Structures, North-Holland Pub., Amsterdam.

Biot, M.A. (1941), General theory of three-dimensional consolidation, J. Appl. Phys., 12:155-165.

Bixley, P.F. (1984), Case history No. 9.9; the Wairakei geothermal field, New Zealand, in Poland(1984), 233-240.

Bolton, R.S. (1970), The behavior of the Wairakei geothermal foeld during exploration, U.N. Symp. on the Development and Utilization of Geothermal resources, Pisa, 1426-1439.

Booker, J.R. and Savvidou, C. (1985), Consolidation around a point heat source, Int. J. Num. Analy. Meth. Geomech., 9:173-184.

Brownell, D.H., Garg, S.K. and Pritchett, J.W. (1977), Governing equations for geothermal reservoirs, Water Resources Research, 13(6):929-934.

Burridge, R. and Keller, J.B. (1983), Poroelasticity equations derived from microstructures, J. Acous. Soc. Am., 70:1140-1146.

Cheng, P. (1978), Heat transfer in geothermal systems, Adv. in Heat Transfer, 14:1-105.

Cheng, P. and Minkowycz, W.J. (1977), Free convection about a vertical flat plate embedded in a porous medium with application to heat transfer from a dike, J. Geophy. Res., 82(14):2040-2044.

Combarnous, M.A. and Bories, S.A. (1975), Hydrothermal convection in a saturated porous medium, Adv. Hydroscience, 10:232-307.

Cooper, H.H. (1966), The equation of groundwater flow in fixed and deforming coordinates, J. Geophy. Res., 71:4785-4790.

Corapcioglu, M.Y. and Bear, J. (1983), A mathematical model for regional land subsidence due to pumping, 3. Integrated equations for a phreatic aquifer, Water Resources Research, 19(4):895-908.

Cottrell, A.H. (1964), The Mechanical Properties of Matter, John Wiley and Sons.

de Marsily, G. (1986), Quantitative hydrogeology, Academic Press.

Derski, W. and Kowalski, S.J. (1979), Equatiopns of linear thermoconsolidation, Arch. Mech., 31(3):303-316.

Domenico, P.A. and Schwartz,F.W. (1990), Physical and Chemical Hydrogeology, John Wiley and Sons.

Donaldson, I.G. and Grant, M.A. (1981), Heat extraction from geothermal reservoirs, in Rybach, L. and Muffler, L.J.P.(eds.), (1981), 145-179.

Ene, M.I. and Polisevski, D. (1987), Thermal Flow in Porous Media, D. Reidel Pub. Co.

Ene, M.I. and Sanchez-Palencia, E. (1975), Equations et phenomenes de surface pour l'coulement dan un modele de milieu poreux, J. Mecan., 14:73-108.

Ene, M.I. and Sanchez-Palencia, E. (1981), Some thermal problems in flow through a periodic model of porous media, Int J. Engng Sci., 19(1):117-127.

Ene, M.I. and Sanchez-Palencia, E. (1982), On thermal equation fro flow in porous media., Int J. Engng Sci., 20(5), 623-630.

Fallou, S.N., Mei, C.C. and Lee, C.K. (1992), Subsidence due to pumping fron a layered soil - Aperturbation theory, Int J. Num. Analy. Meth. Geomech., 16:157-187.

Faust, C.R. and Mercer, J.W. (1979a), Geothermal reservoir simulation, 1. Mathematical models for liquid- and vapor-dominated hydrothermal systems, Water Resources Research, 15(1):23-30.

Faust, C.R. and Mercer, J.W. (1979a), Geothermal reservoir simulation, 2. Numerical solution techniques for liquid- and vapor-dominated hydrothermal systems, Water Resources Research, 15(1):31-46.

Franklin, J.A. and Dusseault, M.B. (1989), Rock Engineering, McGraw-Hill.

Frind, O.E. (1983), Exact aquitard response functions for multiple aquifer mechanics, in Pinder, G.(ed.), Flow Through Porous Media, Computational Mechanics Pub., 86-91.

Frosch, R.A. (1977), Disposing of high-level radioactive waste, Oceanus, 20(1):4-17.

Gambolati, G.A. (1973a), Equation for one-dimensional vertical flow of groundwater, 1. The rigorous theory, Water Resources Research, 9:1022-1028

Gambolati, G.A. (1973b), Equation for one-dimensional vertical flow of groundwater, 2. Valiodity range of the diffusion equation, Water Resources Research, 9:1385-1395.

Gambolati, G.A. and Freeze, R.A. (1973), Mathematical simulation of the subsidence of Venice, 1. Theory, Water Resources Research, 9(3):721-733.

Gambolati, G.A., Gatto P. Freeze, R.A. (1974), Mathematical simulation of the subsidence of Venice, 2. ,Water Resources Research, 10:563-577.

Gambolati, G.A., Sartoretto, F. and Uniana, F. (186), A conjugate gradient finite element model of flow for large multiaquifer systems, Water Resources Research, 22(7):1033-1015.

Garg, S.K., Pritchett, J.W. and Brownell, D.H. (1975), Transport of mas and energy in porous media, Proc. 2nd U.N. Symp. on the Development and use of Geothermal Resources, San Francisco, 1975: Washington, D.C., U.S. Goverment Printing Office, v. 3, 1651-1656.

Garg, S.K. and Pritchett, J.W. (1984a), Pressure transient analysis for hot water geothermal wells, in Groundwater Hydraulics, Rosenshein, J. and Bennett, G.D¿ (eds.), 242-255.

Garg, S.K. and Pritchett, J.W. (1984b), Pressure transient analysis for two-phase geothermal wells: some numerical results, Water Resources Research, 20(7):963-970.

Gibson, R.E., England, G.L. and Hussey, M.J.L. (1967), The theory of one- dimensional consolidation of saturated clays, I. Finite non-linear consolidation of thin homogeneius layers, Geotechnique, 17:261-271.

Gibson, R.E., Schiffman, R.L. and Cargill, K.W. (1981), The theory of one- dimensional consolidation of saturated clays, II, Finite non- linear consolidation of thick homogeneius layers, Can. Geotech. J., 18:280-293.

Goyal,K.P., Miller,C.W., Lippmannn, M.J. and Von der Haar, S.P. (1981), Analysis of Cerro Prieto production data, Proc. 3rd Symp. on Cerro Prieto Geothermal Field, Baja California, Mexico.

Hantush, M.S. (1960), Modification of the theory of leaky aquifers, J. Geophy. Res., 65(11):3713-3725.

Hantush, M.S. and Jacob, C.E. (1955a), Nonsteady radial flow in an infinite leaky aquifer, Trans. Am. Geophy. Union, 36, 95-100.

Hantush, M.S. and Jacob, C.E. (1955b), Steady three-dimensional flow to a well in a two-layered quifer, Trans. Am. Geophy. Union, 36, 286-292.

Helm, D.C. (1975), One-dimensional simulation of aquifer system compaction near Pixley, California, 1. Constant parameters, Water Resources Research, 11(3):465-478.

Helm, D.C. (1976), One-dimensional simulation of aquifer system compaction near Pixley, California, 2. Stress-dependent parameters, Water Resources Research, 12(3):375-391.

Herrera, I and Figueroa, G.E. (1969), A correspondence principle for the theory of leaky aquifers, Water Resources Research, 5(4):900-904.

Hollister, C.D. (1977), The seabed option, Oceanus, 20(1):18-25.

Homsy, C.W. and Sherwood, A.E. (1976), Convective instabilities in porous media with through flow, AIChE J., 22(1):168-174.

Horton, C.W. and Rogers, F.T. (1945), Convection current in a porous medium, J. Appl. Phys., 16:367-370.

Jones, M.C. and Persichetti, J.M. (1986), Convective instabilities in packed beds with throughflow, AIChE J., 32(9):1555-1557.

Jumikis, A.R. (1983), Rock Mechanics.

Keller, G.V. (1984), Geothermal exploration in the western United States, in Geophysics and Geothermal Areas: State of the Art and Future Development, Rapolla, A. and Keller, G.V.(eds.), Colorado School of Mines, 265-305.

Kurashige, M. (1989), A thermoelastic theory of fluid-filled porous materials, Int. J. Solids and Structures, 25(9):1039-1052.

Lapwood, E.R. (1948), Convection of a fluid in a porous medium, Proc. Camb. Phil. Soc., 44:508-521.

Lee, C.K., Fallou, S.N. and Mei, C.C. (1992), Subsidence due to pumping fron a soil stratum with a soft aquitard, Phil. Trans. Roy. Soc. Lond., a339, 193-230.

Lekhnitskii, S.G. (1963), Theory of elasticity of an anisotropic elastic body, San Francisco, Holden-Day.

Levy, T. (1979), Propagation of waves in fluid-saturated porous elastic solid, Int. J. Engng. Sci., 17, 1005-1014.

Lippmann, M.J., Narasimhan, T.N. and Witherspoon, P.A. (1976), Numerical simulation of reservoir compaction in liquid dominated geothermal systems, Proc. 2nd Symp. Land Sunsidence.

Lofgren, B.E. (1978), Monitoring crustal deformation in the Geysers-Clear lake geothermal area, California, U.S.G.S. Open File Rep. 78-597, 99pp.

Love,A.E.H. (1944), A Treatise on the Mathematical Theory of Elasticity, Dover.

Lunis, B.C. and Lienan, P.J. (1988), Status and trends of geothermal direct use projects in the United States, Trans. Geotherm, Resources Council, 12:15-19.

McNabb, A. (1965), On convection in a porous medium, in Proc. 2nd Australian Conf Hydraulics and Fluid Mech, Univ Auckland, New Zealand, C161-171.

McTigue, D.F. (1986), Thermoelastic response of fluid-saturated porous rocks, J Geophy. res., 91(B9):9533-9542.

Mei, C.C. (1985), Gravity effects in the consolidation of a soft soil, J Engng. Mech. Div., ASCE, 111(8):1038-1047.

Mei, C.C. and Auriault, J.-L. (1989), Mechanics of heterogeneous porous media with several spatial scales, Proc. Roy. soc. Jondon, A426:391-423.

Mei, C.C. and Tyvand, P.A. (1988), Thermal consolidation of thick and soft soil layer, J. Engng. Mech. Div., ASCE, 114(6):990-1010.

Mercer, J.W. and Faust, C.R. (1979), Geothermal reservoir simulation, 3. Application of liquid- and vapor-dominated hydrothermal modeling techniques to Warakei, New Zealand, Water Resources Research, 15(3):653-671.

Mercer, J.W. et al (1982), Review of simulation techniques for aquifer thermal energy storage(ATES), Adv. in Hydrosci., 13:2-120.

Mercer, J.W., Pinder, G.F. and Donaldson, I.G. (1975), A Galerkin-finite element analysis of the hydrothermal system at Wairakei, New Zealand, J. Geophys. Res., 80(17):2608-2621.

Minkowycz, W.J. and Cheng, P. (1976), Frww convection about a vertical cylinder embedded in a porous medium, Int J. Heat Mass Transfer, 19:805-813.

Narasimhan, T.N. and Goyal, K.P.(1984), Subsidence due to geothermal fluid withdrawal, Rev. Engng. Geol., VI, 35-66.

Neuman, S.P. and Witherspoon, T.N. (1969), Theory of flow in a confined aquifer system, Water Resources Research, 5(4):803-816.

Neuman, S.P., Preller, C. and Witherspoon, T.N. (1982), Adaptive explicit-implicit quasi three-dimensional finite element model of flow and subsidence in multiaquifer system, Water Resources Research, 18(5):1551-1561.

Nield, D.A. (1968), Onset of thermohaline convection in a porous medium, Water Resources Research, 11:553-560.

Nield, D.A. and Bejan, a. (1992), Convection in Porous Media, Springer-Verlag, 408pp.

Pinder, G.F. and Gray, W.G. (1977), Finite Element Simulations in Surface and Subsurace Hydrology, Academic Press.

Poland, J.F. (ed.) (1984), Guidebook to Studies of Land Subsidence due to Groundwater Withdrawal, UNESCO Studies and Reports in Hydrology 40, 323pp.

Poland, J.F. and Davis, G.H. (1969), Land Subsidencedue to Withdrawal of Fluids, Rev. Eng. Geol., 2:187-269.

Rana, R., Horne, R.N. and Cheng, P. (1979), Natural convection in a multilayered geothermal reservoir, J. Heat Transfer, ASME, 101:411-416.

Roache, P.J. (1977), Computational Fluid Dynamics, Hermosa Publishers.

Sanchez-Palencia, E. (1974), Compartement local et macroscopique d'un type de milieu physiques heterogenes, Int J. engng Sci., 12:331-351

Sanchez- Palencia, E. (1980), Non- homogeneous Media and Vibration Theory, Springer- Verlag.

Savvidou, C. and Booker, J.R. (1989), Consolidation around a heat source buried deep in a porous thermoelastic medium with anisotropic flow properties, Int J. Num. analy. Meth. Geomech., 13:75-90.

Schiffman, R.L. (1971), A thermoelastic theory of consolidation, in Environmental and Geophysical Heat Transfer, ASCE, 78-84.

Silva, A.J. (1977), Physical processes in deep-sea clays, Oceanus, 20(1):31-40.

Small, J.C. and Booker, J.C. (1986), The behavior of layered soil or rock containing a decaying heat source, Int J. Num. analy. Meth. Geomech., 10:501-519.

Sokolnikoff,I.S. (1956), Mathematical Theory of Elasticity, McGraw-Hill Book Co.

Stilwell, W.B., Hall, W.K. and Tawhai, J.(1975), Ground movement in New Zealand geothermal fields, in Proc. 2nd U.N. Symp. Development and Use of Geothermal Resources, San Francisco, CA, U.S.A., 1427-1434.

Verruijt, A. (1969), Elastic storage of aquifers, in Flow Through Porous Media, de Wist, J.M.(ed.), 331-376.

Waltham, A.C. (1989), Ground Subsidencedue, Blackie.

Wooding, R.A. (1963), Convection in a saturated medium at large Rayleigh number or Peclet number, J. Fluid Mech., 15(4):527-544.

Yih, C.S. (1865), Dynamics of Nonhomogeneous Fluids, McMillan.

Zelwer, R. and Grannell, R.B. (1982), Correlation between precision gravity and subsidence measurement at Cerro Prieto, Proc. 4th Symp. Cerro Prieto Geothermal Field, Baja California, Mexico.

Zick, A.A. and Homsy, G.M. (1980), Stokes flow through periodic array of Spheres, J. Fluid Mech., 115:13-26.

Figure Captions and Tables

Chapter I

Fig. 5.1 A Wigner-seitz microcell. The interiot of the soccer ball shape is fluid and the rest is solid. The mean flow is shown in the x-direction.

Fig. 6.1 The computational domain for Wigner-Seitz grain and the porosity values for several ratios of b/h.

Fig. 6.2 The unit cell volume average of the solid stresses.

Fig. 6.3 The average of solid stresses over the solid phase volume Ω_s.

Fig. 6.4 The macroscale elastic coefficients a_I, a_{II}, a_{III} and the anisotropy factor μ_o/μ_1.

Fig. 6.5 The macroscale coefficients $\alpha' = \gamma'$, β_t', β_c' and $-\zeta_t'$.

Fig. 6.6 Computed permeability for Wigner-Seitz grains (Sun and Mei, 1993) in black diamond and the comparison with the empirical Kozeny-Carman formula in open diamond.

Fig. 7.1 The critical Rayleigh numbers by linear stability theory for combinations of upper/lower boundary conditions (after Jones and Persichetti, 1986). The dashed curve is by the energy stability theory for impermeable/impermeable boundary conditions (after Homsy and Sherwood, 1976).

Fig. 7.2 A poroelastic layer subject to pumping rate U per unit length through a small sink at the bottom.

Fig. 7.3 Comparison of the numerical and analytical solutions of temperature for rigid medium with $Ra = 1$ and $Pe^* = 5$.

Fig. 7.4 Time variations of the temperature θ, pressure p and vertical displacement w at different depths for the reference state with $Ra = 1$, $Pe^* = 1$, $b = 1$ and $T_c/T_d = 1$.

Fig. 7.5 Depth variations of p, θ and w at discrete times for the reference state.

Fig. 7.6 Time variations of the temperature θ, pressure p and vertical displacement w at different depths with $Ra = 10$, $Pe^* = 1$, $b = 10$ and $T_c/T_d = 0.1$.

Fig. 7.7 Depth variations of p, θ and w at discrete times for with $Ra = 10$, $Pe^* = 1$, $b = 10$ and $T_c/T_d = 0.1$.

Fig. 7.8 Time variations of the temperature θ, pressure p and vertical displacement w at different depths with $Ra = 20$, $Pe^* = 1$, $b = 20$ and $T_c/T_d = 0.05$.

Fig. 7.9 Depth variations of p, θ and w at discrete times for with $Ra = 20$, $Pe^* = 1$, $b = 20$ and $T_c/T_d = 0.05$.

Fig. 7.10 Time variations of the temperature θ, pressure p and vertical displacement w at different depths with $Ra = 30$, $Pe^* = 1$, $b = 30$ and $T_c/T_d = 0.0333$.

Fig. 7.11 Depth variations of p, θ and w at discrete times for with $Ra = 30$, $Pe^* = 1$, $b = 30$ and $T_c/T_d = 0.0333$.

Fig. 7.12 Time variations of the temperature θ, pressure p and vertical displacement w at different depths with $Ra = 10$, $Pe^* = 0.1$, $b = 100$ and $T_c/T_d = 0.1$.

Fig. 7.13 Time variations of the temperature θ, pressure p and vertical displacement w at different depths with $Ra = 10$, $Pe^* = 5$, $b = 2$ and $T_c/T_d = 0.1$.

Fig. 7.14 Time variations of the temperature θ, pressure p and vertical displacement w at different depths with $Ra = 10$, $Pe^* = 10$, $b = 1$ and $T_c/T_d = 0.1$.

Fig. 7.15(a) Comparison of numerical solutions for $\Delta z = 0.1$ (solid line) and $\Delta z = 0.05$ (dotted line) with $\Delta\xi = 0.1$ and $x_N = 6.4$. The parameters are $Ra = 5$, $Pe^* = 1$, $b = 5$ and $T_c/T_d = 0.2$.

Fig. 7.15(b) Comparison of numerical solutions for $\Delta\xi = 0.0429$ (solid line) and $\Delta\xi = 0.05$ (dotted line) with $\Delta z = 0.1$ and $x_N = 4.5$. For parameters see the caption of Fig. 7.15(a).

Fig. 7.15(c) Comparison of numerical solutions for $x_N = 6.4$ (solid line) and $x_N = 4.5$ (dotted line) with $\Delta\xi = 0.05$ and $\Delta z = 0.1$ For parameters see the caption of Fig. 7.15(a).

Fig. 7.16 Contour plots of (a) $p(x,z)$, (b) $\theta(x,z)$, (c) $w(x,z)$, and (d) $u(x,z)$ at discrete times for the reference state with $Ra = 1$, $Pe^* = 1$, $b = 1$ and $T_c/T_d = 1$.

Fig. 7.17 Vector plot of Darcy velocity $\langle u \rangle - n'\partial v/\partial t$ at t=0.01, 0.1 and 1 for the reference state.

Fig. 7.18 Horizontal variation of (a) $w(x, z = 1)$ and (b) $u(x, z = 1)$ at discrete times for the reference state.

Fig. 7.19 Contour plots of (a) $p(x,z)$, (b) $\theta(x,z)$, (c) $w(x,z)$, and (d) $u(x,z)$ at discrete times for $Ra = 10$, $Pe^* = 1$, $b = 10$ and $T_c/T_d = 0.1$.

Fig. 7.20 Horizontal variation of (a) $w(x, z = 1)$ and (b) $u(x, z = 1)$ at discrete times for $Ra = 10$, $Pe^* = 1$, $b = 10$ and $T_c/T_d = 0.1$.

Fig. 7.21(a) Contour plot of the pressure distribution $p(x,z)$ at discrete times for $Ra = 20$, $Pe^* = 1$, $b = 20$ and $T_c/T_d = 0.05$.

Fig. 7.21(b) Contour plot of the temperature distribution $\theta(x,z)$ at discrete times for $Ra = 20$, $Pe^* = 1$, $b = 20$ and $T_c/T_d = 0.05$.

Fig. 7.21(c) Contour plot of the vertical displacement $w(x,z)$ at discrete times for $Ra = 20$, $Pe^* = 1$, $b = 20$ and $T_c/T_d = 0.05$.

Fig. 7.21(d) Contour plot of the horizontal displacement $u(x,z)$ at discrete times for $Ra = 20$, $Pe^* = 1$, $b = 20$ and $T_c/T_d = 0.05$.

Fig. 7.22 Vector plot of Darcy velocity $\langle u \rangle - n' \partial v/\partial t$ at t=0.01, 0.1 and 1 for $Ra = 20$, $Pe^* = 1$, $b = 20$ and $T_c/T_d = 0.05$.

Fig. 7.23 Horizontal variation of (a) $w(x, z = 1)$ and (b) $u(x, z = 1)$ at discrete times for $Ra = 20$, $Pe^* = 1$, $b = 20$ and $T_c/T_d = 0.05$.

Fig. 7.24(a) Contour plot of the pressure distribution $p(x,z)$ at discrete times for $Ra = 30$, $Pe^* = 1$, $b = 30$ and $T_c/T_d = 0.0333$.

Fig. 7.24(b) Contour plot of the temperature distribution $\theta(x,z)$ at discrete times for $Ra = 30$, $Pe^* = 1$, $b = 30$ and $T_c/T_d = 0.0333$.

Fig. 7.24(c) Contour plot of the vertical displacement $w(x,z)$ at discrete times for $Ra = 30$, $Pe^* = 1$, $b = 30$ and $T_c/T_d = 0.0333$.

Fig. 7.24(d) Contour plot of the horizontal displacement $u(x,z)$ at discrete times for $Ra = 30$, $Pe^* = 1$, $b = 30$ and $T_c/T_d = 0.0333$.

Fig. 7.25 Vector plot of Darcy velocity $\langle u \rangle - n' \partial v/\partial t$ at t=0.01, 0.1 and 1 for $Ra = 30$, $Pe^* = 1$, $b = 30$ and $T_c/T_d = 0.0333$.

Fig. 7.26 Horizontal variation of (a) $w(x, z = 1)$ and (b) $u(x, z = 1)$ at discrete times for $Ra = 30$, $Pe^* = 1$, $b = 30$ and $T_c/T_d = 0.0333$.

Fig. 7.27(a) Contour plot of the pressure distribution $p(x,z)$ at discrete times for $Ra = 30$, $Pe^* = 0.1$, $b = 300$ and $T_c/T_d = 0.0333$.

Fig. 7.27(b) Contour plot of the pressure distribution $p(x,z)$ at discrete times for $Ra = 30$, $Pe^* = 10$, $b = 3$ and $T_c/T_d = 0.0333$.

Fig. 7.28(a) Contour plot of the temperature distribution $\theta(x,z)$ at discrete times for $Ra = 30$, $Pe^* = 0.1$, $b = 300$ and $T_c/T_d = 0.0333$.

Fig. 7.28(b) Contour plot of the temperature distribution $\theta(x,z)$ at discrete times for $Ra = 30$, $Pe^* = 10$, $b = 3$ and $T_c/T_d = 0.0333$.

Fig. 7.29 Vector plot of Darcy velocity $\langle u \rangle - n' \partial v / \partial t$ at steady state fro (a) $Ra = 30$, $Pe^* = 0.1$; (b) $Ra = 30$, $Pe^* = 1$ and (c) $Ra = 30$, $Pe^* = 10$.

Fig. 7.30 Horizontal variation of (a) $w(x, z = 1)$ and (b) $u(x, z = 1)$ at steady state for Pe^*=0.1, 1 and 10 with $Ra = 30$.

Chapter II

Fig. 5.1 A periodically stratified layers on the mesoscale. The periodic length is ℓ' in x_3'-direction.

Fig. 6.1 A periodic medium with two layers on the mesoscale ℓ'.

Fig. 6.2 The elastic coefficients a''_{xxxx}, a''_{xxyy} and a''_{zzzz} and thermal moduli $(\beta'')_{xx}$ and $(\beta'')_{zz}$.

Fig. 6.3 The coefficients α''_{xx}, α''_{zz}, γ''_{xx}, γ''_{zz}, β''_c and ζ''_c.

Appendices

Fig. C.1 A Wigner-Seitz microcell with three planes of symmetry. THe region inside the solid-lined shape is the solid phase.

Fig. C.2 The boundary value problems defined by (C.2a-d) and the schematic of the traction forces on the interface.

Fig. C.3 A rotational coordinate transformation from (x, y, z) to (x_A, y_A, z_A).

Fig. C.4 Another coordinate transformation from (x, y, z) to (x_B, y_B, z_B).

Fig. C.5 (a) The fluid region in the microcell defined in XYZ-coordinates and typical velocity components at points symmetric about $X = 0$, $Y = 0$ and $Z = 0$ planes, and (b) the symmetry relations for K_{iz} $(i = x, y, z)$ in sectors A, D, E and H.

Fig. C.6 Fluid velocity components in symmetric sectors (a) k_{iy} due to $\partial p^{(0)} / \partial Y'$ and (b) k_{iz} due to $\partial p^{(0)} / \partial Z'$.

Fig. C.7 The heat flux boundary condition on the interface with distributed heat source of strength $(M_r m^s - m^f) N_\ell^f$.

Fig. C.8 The distribution of heat source on the interface for (a) A_x^f and A_x^s, (b) A_y^f and A_y^s, and (c) A_z^f and A_z^s.

Fig. D.1 The symmetry relations for ϕ_i^{xx}, its derivatives and the stresses at the points located symmetrically about the planes $y = 0$ and $z = 0$. The superscripts 'xx' have been omitted.

Fig. D.2 The symmetry relations for ϕ_i^{xy} its derivatives and the stresses at the points located symmetrically about the planes $y = 0$ and $z = 0$. The superscripts 'xy' have been omitted.

Tables

Chapter I

Table 2.1 Typical values of $\mathcal{D}$ and K for some common soils.

Table 6.1 Numbers of nodes and elements for four types of meshes(n'=0.5).

Table 6.2 Computed values of stresses, their convergence and the extrapolation.

Table 6.3 Elastic constants of cubic crystals (after Cottrell (1964)).

Appendix A. A Posteriori Check of the Omitted Terms.

In the beginning(§2), several unimportant terms were neglected from the outset to simplify the equations. We now justify the omission by comparing those terms to the most dominant terms in the governing equations. For later reference in Part III where thermal dispersion is important, we also make some remarks on the case with $Pe = O(1)$.

Conservation of mass in the fluid which accounts density variation reads

$$\frac{1}{\rho_f}\frac{\partial \rho_f}{\partial t} + \frac{1}{\rho_f} u \cdot \nabla \rho_f + \nabla \cdot u = 0 \qquad (A.1)$$

In order to incorporate density change due to pressure variation, we use the more general equation of state for the pore fluid so that (2.4) is written

$$\frac{\rho_f - \rho_o(z)}{\rho_f} \simeq \frac{\rho_f - \rho_o(z)}{\rho_o(z)} = -\beta_T \theta_f + \beta_p p \qquad (A.2)$$

where β_T and β_p are the thermal expansion coefficient and the compressibility of fluid. Typically $\beta_T = O(10^{-4\circ} C^{-1})$ and $\beta_p = O(10^{-10} m^2/N)$. Substituting (A.2) into (A.1) we obtain

$$\left(-\beta_T \frac{\partial \theta_f}{\partial t} + \beta_p \frac{\partial p}{\partial t}\right) + u \cdot (-\beta_T \nabla \theta_f + \beta_p \nabla p) + \nabla \cdot u = 0 \qquad (A.3)$$

by using the scales estimated in §2.1.

Comparing to the last term, the importance of the first term is

$$\beta_T \frac{\partial \theta_f}{\partial t} / \nabla \cdot u \sim \frac{\beta_T \Theta' \ell}{U T_v} = \beta_T \Theta' \frac{\ell}{\ell'} = \epsilon \beta_T \Theta'$$

The density change due to temperature variation is small and was already assumed to be $\beta_T \Theta' \leq O(\epsilon)$, therefore

$$\beta_T \frac{\partial \theta_f}{\partial t} / \nabla \cdot u = O(\epsilon^2) \qquad (A.4)$$

Similarly the importance of the second term is estimated by using $P' = O(\epsilon \mathcal{D})$ and $\mathcal{D} < O(10^{10} N/m^2)$,

$$\beta_p \frac{\partial p}{\partial t} / \nabla \cdot u \sim \frac{\beta_p P' \ell}{U T_v} = \epsilon \beta_p P' = \epsilon^2 \beta_p \mathcal{D} < O(\epsilon^2) \qquad (A.5)$$

while the third and fourth terms are simply

$$u \cdot (-\beta_T \nabla \theta_f + \beta_p \nabla p)/\nabla \cdot u \sim \beta_T \Theta' + \beta_p P' < O(\epsilon) \qquad (A.6)$$

Substituting (A.4), (A.5) and (A.6) into (A.3), the law of mass conservation may be written in dimensionless variables as

$$\epsilon u^* \cdot (-\nabla^* \theta_f^* + \nabla^* p^*) + \nabla^* \cdot u^* = O(\epsilon^2) \qquad (A.7)$$

Recall that $p^{(0)}$ and $\theta_f^{(0)}$ are independent of the microscale, so (A.7) becomes

$$\nabla^* \cdot u^* = O(\epsilon^2) \qquad (A.8)$$

Thus use of (2.1.1) is legitimate within the accuracy of $O(\epsilon)$ only (cf.(3.22a and b)).

The full momentum equation for fluid is

$$\rho_f \left(\frac{\partial u}{\partial t} + u \cdot \nabla u \right) = -\nabla p + \mu \nabla^2 u + \rho_f \beta_T \theta_f \mathbf{e}_z - \rho_f \beta_p p g \mathbf{e}_z + \frac{1}{3} \mu \nabla (\nabla \cdot u) \quad (A.9)$$

The last two terms are the buoyancy induced by density change due to pressure variation and the fluid stress due to compression. Consider the following ratios.

$$\frac{\rho_f \beta_p p g}{\nabla p} \sim \frac{\rho_f \beta_p P' g}{P'/\ell} = \rho_f \beta_p g \ell < O(\epsilon^3) \qquad (A.10)$$

where $\rho_f = 10^3 (kg/m^3)$, $g = 10 (m/s^2)$ and $\ell = O(10^{-3} m)$ have been used. Also, by using (2.1.17),

$$\frac{\frac{1}{3}\mu \nabla (\nabla \cdot u)}{\nabla p} \sim \frac{\mu U/\ell^2}{P'/\ell} = \frac{\mu U}{P' \ell} = \frac{\ell}{\ell'} = O(\epsilon^3) \qquad (A.11)$$

where the last equality follows after using (A.8). Therefore terms omitted in (2.1.2) are at most $O(\epsilon^3)$ and do not appear.

The full energy equation for fluid is

$$(\rho C_p)_f \left(\frac{\partial \theta_f}{\partial t} + u \cdot \nabla \theta_f \right) = \nabla \cdot (m_f \cdot \nabla \theta_f) + \beta_T T_f \left(\frac{\partial p}{\partial t} + u \cdot \nabla p \right) + \mu \Phi \quad (A.12)$$

where T_f is the absolute temperature and

$$\begin{aligned}\Phi =& 2\left[\left(\frac{\partial u}{\partial x}\right)^2+\left(\frac{\partial v}{\partial y}\right)^2+\left(\frac{\partial w}{\partial z}\right)^2\right] \\ &+\left(\frac{\partial v}{\partial x}+\frac{\partial u}{\partial y}\right)^2+\left(\frac{\partial w}{\partial y}+\frac{\partial v}{\partial z}\right)^2+\left(\frac{\partial u}{\partial z}+\frac{\partial w}{\partial x}\right)^2-\frac{2}{3}(\nabla\cdot u)^2\end{aligned} \tag{A.13}$$

is the rate of energy dissipation. The second term on the right-hand side of (A.12) is the compressional work. We examine these terms. For $Pe = O(\epsilon)$ we have $T_v = T_d$ (cf.(2.2.2)). So by using $T_d = \ell'^2/\alpha_f$

$$\begin{aligned}\frac{\beta_T T_f \frac{\partial p}{\partial t}}{\nabla\cdot(m_f\cdot\nabla\theta_f)} &\sim \frac{\ell^2\beta_T T_f P'}{T_d M_f \Theta'} = \frac{\beta_T T_f P'\ell^2}{\ell'^2(\rho C_p)_f\Theta'} = \epsilon^2\frac{\beta_T T_f P'}{(\rho C_p)_f\Theta'} \\ &= \epsilon^2\frac{P'}{\mathcal{D}}\frac{\beta_T T_f\mathcal{D}}{(\rho C_p)_f\Theta'} = O(\epsilon^4)\end{aligned} \tag{A.14}$$

where $P'/\mathcal{D} = O(\epsilon)$, $C_p = O(10^3 m^2/s^{2\circ}K)$, $T_f = O(10^{3\circ}K)$, $\mathcal{D} = O(10^7 - 10^8 N/m^2)$ and $\Theta' \le O(10^{2\circ}C)$ were used. On the other hand, the ratio of the convective term to the local term in pressure work is

$$\frac{u\cdot\nabla p}{\frac{\partial p}{\partial t}} \sim \frac{UT_v}{\ell} = \frac{U}{\ell}\frac{\ell'}{U} = O(\epsilon^{-1}) \tag{A.15}$$

and it follows from (A.14) and (A.15) that

$$\frac{\beta_T T_f u\cdot\nabla p}{\nabla\cdot(m_f\cdot\nabla\theta_f)} = O(\epsilon^4) \tag{A.16}$$

The ratio of viscous dissipation to heat diffusion is

$$\begin{aligned}\frac{\mu\Phi}{\nabla\cdot(m_f\cdot\nabla\theta_f)} &\sim \frac{\mu U^2}{\ell^2}\frac{\ell^2}{M_f\Theta'} = \frac{P'}{\ell'}\frac{U\ell^2}{M_f\Theta'} = \frac{\ell}{\ell'}\frac{U\ell}{\alpha_f}\frac{P'}{(\rho C_p)_f\Theta'} \\ &= \epsilon Pe\frac{\epsilon^2\mathcal{D}}{(\rho C_p)_f\Theta'} = O(\epsilon^3)\end{aligned} \tag{A.17}$$

for $\mathcal{D} = O(10^8 m^2/N)$. It is thus shown from (A.14), (A.15), (A.16) and (A.17) that the omitted terms in the fluid equation are at most $O(\epsilon^3)$ or less.

In conclusion, all the omitted terms are negligibly small and do not affect the results obtained in §3.

Remarks for the case of $Pe = O(1)$ and $T_c/T_d = O(\epsilon^2)$

As will be shown in Part B, if Pe is increased to $O(1)$ for highly porous medium,e.g. $T_c/T_d = O(\epsilon^2)$, the effect of weak inertia comes into effect in the momentum conservation at $O(\epsilon^2)$. Equation (A.11) shows that the omitted terms are still negligible. Also the ratios in (A.14) and (A.16) become as

$$\frac{\beta_T T_f \frac{\partial p}{\partial t}}{\nabla \cdot (m_f \cdot \nabla \theta_f)} = O(\epsilon^3) \qquad (A.18)$$

$$\frac{\beta_T T_f u \cdot \nabla p}{\nabla \cdot (m_f \cdot \nabla \theta_f)} = O(\epsilon^3) \qquad (A.19)$$

Since the energy equation is considered only upto $O(\epsilon^2)$, the effects of pressure work and the viscous dissipation are negligibly small.

Appendix B Compliance Coefficient Tensor $b_{\alpha\beta kh}$.

Hooke's law in dimensionless form reads

$$\sigma^*_{ij} = a^*_{ij\ell m} e_{\ell m} \tag{B.1}$$

where $e_{\ell m}$ is the strain tensor and $a^*_{ij\ell m}$ posesses the symmetry property

$$a^*_{ij\ell m} = a^*_{ji\ell m} = a^*_{ijm\ell} = a^*_{\ell mij} \tag{B.2}$$

Equation (B.1) may be written

$$e_{\ell m} = b_{\ell mij}\sigma^*_{ij} \tag{B.3}$$

where $b_{\ell mij}$ is the compliance tensor.

Multiply (B.1) by $b_{\alpha\beta ij}$ to get

$$b_{\alpha\beta ij}\sigma^*_{ij} = b_{\alpha\beta ij}a^*_{ij\ell m}e_{\ell m} \tag{B.4}$$

For (B.4) to be of the form (B.3), we should have

$$b_{\alpha\beta ij}a^*_{ij\ell m}e_{\ell m} = e_{\alpha\beta} \tag{B.5}$$

which implies

$$b_{\alpha\beta ij}a^*_{ij\ell m} = \delta_{\alpha\ell}\delta_{\beta m} \tag{B.6}$$

Also, since $e_{\alpha\beta} = e_{\beta\alpha}$, (B.5) can be written

$$b_{\alpha\beta ij}a^*_{ij\ell m}e_{\ell m} = e_{\beta\alpha}$$

which gives

$$b_{\alpha\beta ij}a^*_{ij\ell m} = \delta_{\alpha m}\delta_{\beta\ell} \tag{B.7}$$

Adding (B.6) and (B.7), we obtain

$$b_{\alpha\beta ij}a^*_{ij\ell m} = \frac{1}{2}(\delta_{\alpha\ell}\delta_{\beta m} + \delta_{\alpha m}\delta_{\beta\ell})$$

or using $a^*_{ij\ell m} = a^*_{\ell mij}$

$$a^*_{ijkh} b_{\alpha\beta kh} = \frac{1}{2}(\delta_{\alpha i}\delta_{\beta j} + \delta_{\alpha j}\delta_{\beta i}) \qquad (B.8)$$

which is (4.1.20). The relation holds for general anisotropic material which has the symmetry property (B.2).

As a special case, if the material is isotropic, a^*_{ijtr} can be written as

$$a^*_{ijtr} = \lambda^* \delta_{ij}\delta_{tr} + \mu^*(\delta_{it}\delta_{jr} + \delta_{ir}\delta_{jt}) \qquad (B.9)$$

Thus

$$a^*_{ijkh} b_{\alpha\beta kh} = \lambda^* \delta_{ij} b_{\alpha\beta rr} + \mu^*(b_{\alpha\beta ij} + b_{\alpha\beta ji}) = \lambda^* \delta_{ij} b_{\alpha\beta rr} + 2\mu^* b_{\alpha\beta ij} \qquad (B.10)$$

Combining (B.8) and (B.10)

$$\lambda^* \delta_{ij} b_{\alpha\beta rr} + 2\mu^* b_{\alpha\beta ij} = \frac{1}{2}(\delta_{\alpha i}\delta_{\beta j} + \delta_{\alpha j}\delta_{\beta i})$$

If a contraction is made by setting $i = j$, we obtain

$$b_{\alpha\beta rr} = \frac{\delta_{\alpha\beta}}{3\lambda^* + 2\mu^*} \qquad (B.11)$$

Appendix C. Symmetry of Constitutive Coefficients for Cubic Array of Wigner-Seitz Grains.

In this Appendix, the reduction of the macroscale constitutive coefficients for the Wigner-Seitz microcell of Fig. 5.1 is shown by making use of symmetry properties of the solutions of the microcell boundary value problems. For convenience, Fig. 5.1 is reproduced in Fig. C.1.

C.1 A Model of Microcell Geometry.

As a specific model of microcell, we consider the Wigner-Seitz cell depicted in Fig C.1. It satisfies the condition of Ω-periodicity so that the curve dividing fluid and solid phases on the negative x-face is repeated after a period of length ℓ on the positive x-face and similarly on y- and z-faces. The three planes of symmetry are $x = 0$, $y = 0$ and $z = 0$.

The solid phase is assumed to be homogeneous and isotropic. The elastic coefficients $a^*_{ijk\ell}$ of solid then contain only two independent constants as shown in (4.1.17). Under isothermal condition, the dimensionless stress-strain relation via Hooke's law is

$$\begin{Bmatrix} \sigma^*_{xx} \\ \sigma^*_{yy} \\ \sigma^*_{zz} \\ \sigma^*_{xy} \\ \sigma^*_{yz} \\ \sigma^*_{zx} \end{Bmatrix} = \begin{bmatrix} a^*_{xxxx} & a^*_{xxyy} & a^*_{xxzz} & 0 & 0 & 0 \\ & a^*_{yyyy} & a^*_{yyzz} & 0 & 0 & 0 \\ & & a^*_{zzzz} & 0 & 0 & 0 \\ & & & 2a^*_{xyxy} & 0 & 0 \\ & \text{sym.} & & & 2a^*_{yzyz} & 0 \\ & & & & & 2a^*_{zxzx} \end{bmatrix} \begin{Bmatrix} e_{xx} \\ e_{yy} \\ e_{zz} \\ e_{xy} \\ e_{yz} \\ e_{zx} \end{Bmatrix} \qquad (C.1)$$

with the coefficients given by (4.1.18).

C.2 Elastic Coefficients.

Because of (4.1.24) nad (4.1.25) it is only necessary to consider the boundary value problem for ϕ^{jk}_i.

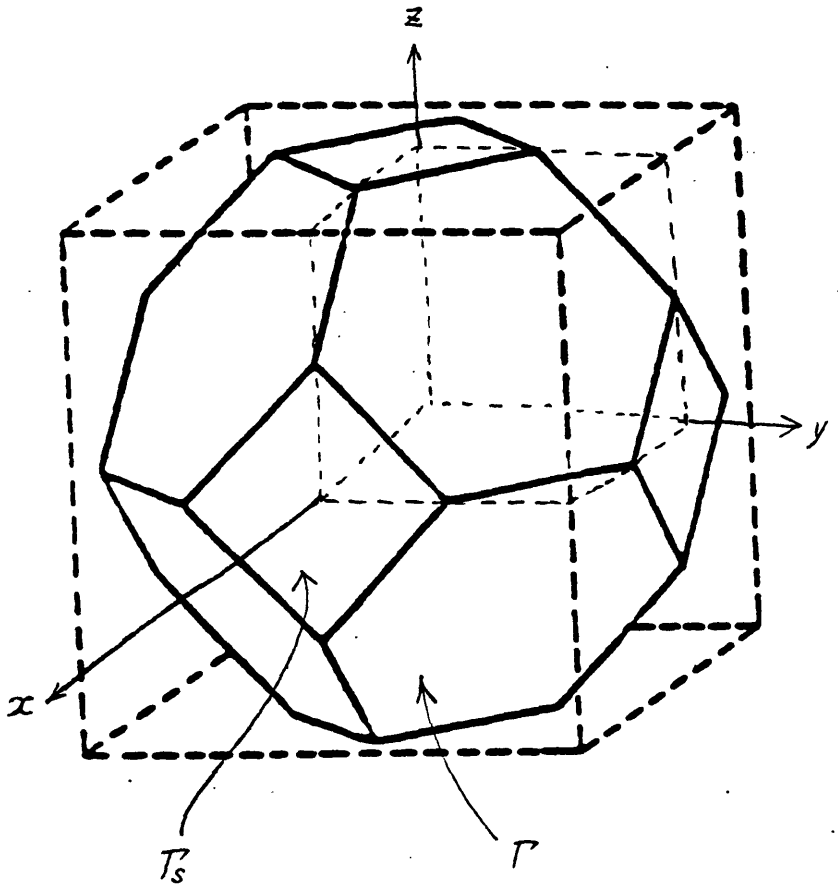

Fig. C.1 A Wigner-Seitz microcell with three planes of symmetry. The region inside the solid-lined shape is the solid phase.

For homogeneous and isotropic solid, equations (4.1.7a), (4.1.8a) and (4.1.9a and b) become

$$\begin{aligned} \frac{\partial}{\partial x_i}[a^*_{ijpq}e_{pq}(\phi^{mn})] &= 0 \qquad && \text{in} \quad \Omega_s \\ a^*_{ijpq}(\delta_{pm}\delta_{qn} + e_{pq}(\phi^{mn}))N^s_i &= 0 \qquad && \text{on} \quad \Gamma(0) \\ \phi^{mn} \quad \text{is} \quad \Omega-\text{periodic} \qquad && \text{on} \quad \Gamma_s \\ \langle\phi^{mn}\rangle &= 0 \end{aligned} \qquad (C.2a-d)$$

The boundary Γ_s is the solid phase part of the cell boundary $\partial\Omega$ of the microcell($\Omega = \Omega_f U \Omega_s$) so that across Γ_s the solid phase Ω_s is extended to the neighboring cell(Fig C.1).

It is readily seen that ϕ^{mn} is a solution of elastistatic problem for a grain acted on by prescribed surface traction on the interface $\Gamma(0)$. The Ω-periodicity condition gives constraints on ϕ^{mn}_j as well as associated strains and stresses on Γ_s. The boundary value problem (C.2a-c) has unique solution up to a microscale independent constant which can be ignored by absorbing it into $v^{(0)}$(cf.(3.1.13)) because it corresponds to rigid body motion.

By definition, we have(cf.(3.3.3))

$$\begin{aligned} v^{(1)}_i(x,x',t^*) &= \phi^{jk}_i e'_{jk}(v^{(0)}) - \eta_i p^{(0)} - \zeta_i\theta^{(0)} \\ &= \phi^{kj}_i e'_{kj}(v^{(0)}) - \eta_i p^{(0)} - \zeta_i\theta^{(0)} = \phi^{kj}_i e'_{jk}(v^{(0)}) - \eta_i p^{(0)} - \zeta_i\theta^{(0)} \end{aligned}$$

due to symmetry $e'_{jk} = e'_{kj}$, which depends only on the macroscale coordinates x', it follows that ϕ^{jk}_i are symmetric with respect to the interchange of j and k. Hence there are six different vectors in ϕ^{jk}_i,e.g.

$$\{\phi^{xx}_i\}, \{\phi^{yy}_i\}, \{\phi^{zz}_i\}, \{\phi^{xy}_i\}, \{\phi^{yz}_i\} \quad \text{and} \quad \{\phi^{zx}_i\}$$

where $i = x, y, z$. The boundary value problem for these vector quantities are summarized in Fig C.2 in which spheres are used instead of Wigner-Seitz grains for graphical clarity. For computations the whole sphere is divided into 8 equal sectors which are specified as $A(x > 0, y > 0)$, $B(x < 0, y > 0)$, $C(x < 0, y < 0)$

(a) ϕ_ℓ^{xx}

$$\frac{\partial}{\partial x_i}\sigma_{ij}(\phi_\ell^{xx}) = 0 \quad \text{in} \quad \Omega_e$$

$$\overline{T}_j = -a^*_{ijxx}N_i \quad \text{on} \quad \Gamma$$

$$\overline{T}_x = -a^*_{xxxx}N_x = -\frac{1-\nu}{(1+\nu)(1-2\nu)}N_x$$

$$\overline{T}_y = -a^*_{yyxx}N_x = -\frac{\nu}{(1+\nu)(1-2\nu)}N_y$$

$$\overline{T}_z = -a^*_{zzxx}N_x = -\frac{\nu}{(1+\nu)(1-2\nu)}N_z$$

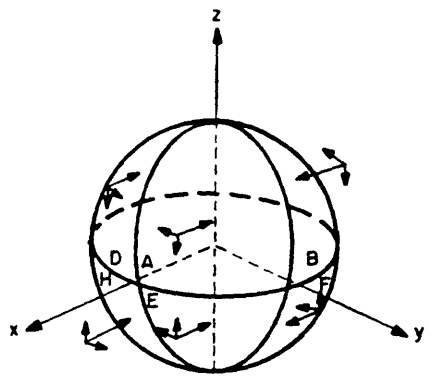

(b) ϕ_ℓ^{yy}

$$\frac{\partial}{\partial x_i}\sigma_{ij}(\phi_\ell^{yy}) = 0 \quad \text{in} \quad \Omega_e$$

$$\overline{T}_j = -a^*_{ijyy}N_i \quad \text{on} \quad \Gamma$$

$$\overline{T}_x = -a^*_{xxyy}N_x = -\frac{\nu}{(1+\nu)(1-2\nu)}N_x$$

$$\overline{T}_y = -a^*_{yyyy}N_x = -\frac{1-\nu}{(1+\nu)(1-2\nu)}N_y$$

$$\overline{T}_z = -a^*_{zzyy}N_x = -\frac{\nu}{(1+\nu)(1-2\nu)}N_z$$

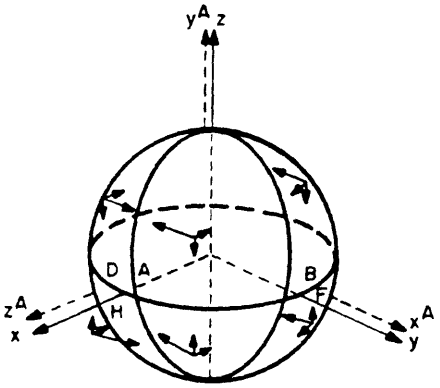

(c) ϕ_ℓ^{zz}

$$\frac{\partial}{\partial x_i}\sigma_{ij}(\phi_\ell^{zz}) = 0 \quad \text{in} \quad \Omega_e$$

$$\overline{T}_j = -a^*_{ijzz}N_i \quad \text{on} \quad \Gamma$$

$$\overline{T}_x = -a^*_{xxzz}N_x = -\frac{\nu}{(1+\nu)(1-2\nu)}N_x$$

$$\overline{T}_y = -a^*_{yyzz}N_x = -\frac{\nu}{(1+\nu)(1-2\nu)}N_y$$

$$\overline{T}_z = -a^*_{zzzz}N_x = -\frac{1-\nu}{(1+\nu)(1-2\nu)}N_z$$

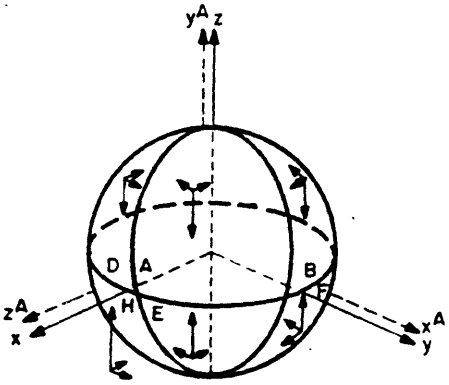

Fig. C.2 The boundary value problems defined by (C.2a-d) and the schematic of the traction forces on the interface.

(d) ϕ_ℓ^{xy}

$\frac{\partial}{\partial x_i}\sigma_{ij}(\phi_\ell^{xy}) = 0 \quad \text{in} \quad \Omega_s$

$\overline{T}_j = -a^*_{ijxy}N_i \quad \text{on} \quad \Gamma$

$\overline{T}_x = -a^*_{yxxy}N_x = -\frac{1}{2(1+\nu)}N_y$

$\overline{T}_y = -a^*_{xyxy}N_x = -\frac{1}{2(1+\nu)}N_x$

$\overline{T}_z = 0$

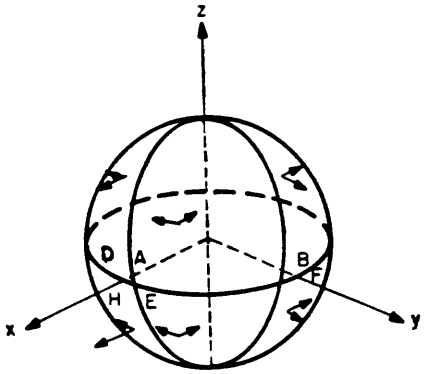

(e) ϕ_ℓ^{yz}

$\frac{\partial}{\partial x_i}\sigma_{ij}(\phi_\ell^{yz}) = 0 \quad \text{in} \quad \Omega_s$

$\overline{T}_j = -a^*_{ijyz}N_i \quad \text{on} \quad \Gamma$

$\overline{T}_x = 0$

$\overline{T}_y = -a^*_{zyyz}N_z = -\frac{1}{2(1+\nu)}N_z$

$\overline{T}_z = -a^*_{yzyz}N_z = -\frac{1}{2(1+\nu)}N_y$

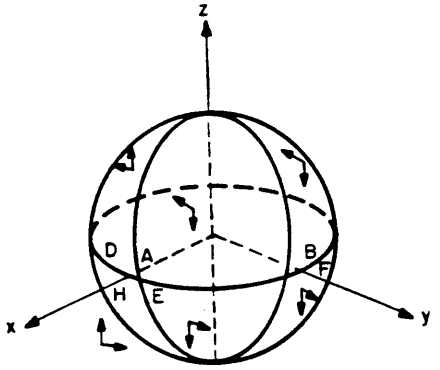

(f) ϕ_ℓ^{zz}

$\frac{\partial}{\partial x_i}\sigma_{ij}(\phi_\ell^{zz}) = 0 \quad \text{in} \quad \Omega_s$

$\overline{T}_j = -a^*_{ijzz}N_i \quad \text{on} \quad \Gamma$

$\overline{T}_x = -a^*_{xzzz}N_z = -\frac{1}{2(1+\nu)}N_z$

$\overline{T}_y = 0$

$\overline{T}_z = -a^*_{zzzz}N_z = -\frac{1}{2(1+\nu)}N_z$

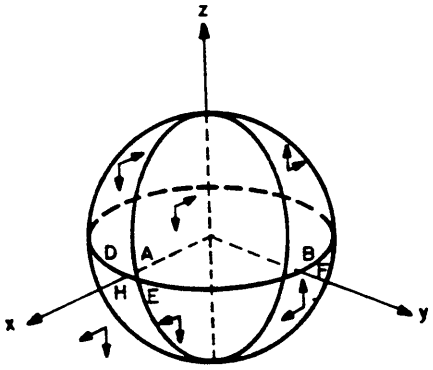

Fig. C.2 (Continued.)

and $D(x > 0, y < 0)$ in the upper hemisphere ($z < 0$) and $E(x < 0, y > 0)$, $F(x < 0, y > 0)$, $G(x < 0, y < 0)$ and $H(x > 0, y < 0)$ in the lower hemisphere ($z < 0$). The loading condition (C.2b) at some typical points on the interface $\Gamma(0)$ is sketched in Fig C.2.

C.2.1 Coefficients a'_{ijmn}.

By using the symmetry properties of ϕ_j^{mn}, the elastic coefficients a'_{ijmn} are shown to have cubic symmetry and to be describable by only three distinct coefficients.

From (4.1.3a) we have for homogeneous and isotropic grains

$$a'_{ijmn} = (1 - n')a^*_{ijmn} + \langle \sigma_{ij}(\phi^{mn}) \rangle \tag{C.3}$$

where

$$\begin{aligned} \langle \sigma_{ij}(\phi^{mn}) \rangle &= a^*_{ijpq} \langle e_{pq}(\phi^{mn}) \rangle \\ &= a^*_{ijpq} \frac{1}{2} \left\langle \frac{\partial \phi_q^{mn}}{\partial x_p} + \frac{\partial \phi_p^{mn}}{\partial x_q} \right\rangle \end{aligned} \tag{C.4}$$

is the stress due to deformation ϕ_j^{mn} inside Ω_s and $e_{pq}(\phi^{mn})$ is the strain tensor.

In the study of crystalline structures(Love(1944), Lekhnitskii(1963)), the cubic symmetry is the consequence of having three planes of symmetry and also 90-degree rotational symmetry about the three axes. We shall first exploit the rotational symmetry to reduce 21 coefficients of a'_{ijmn} to 7 constants and then the three planes of symmetry to further reduce to 3 constants.

Let us consider a coordinate transformation from (x, y, z) to (x^A, y^A, z^A), as shown in Fig C.3. The transformation matrix from (x, y, z) to (x^A, y^A, z^A) is then given by

$$A_{ij} = \mathbf{e}_i \cdot \mathbf{e}_j^A = \begin{bmatrix} 0 & 0 & 1 \\ 1 & 0 & 0 \\ 0 & 1 & 0 \end{bmatrix} \tag{C.5}$$

The unit vectors $\mathbf{e}_i$ and $\mathbf{e}_j^A$ are along x_i-axis and x_j^A-axis$(i, j = 1, 2, 3)$ respectively. The new axis system $x^A y^A z^A$ is obtained by rotating first the xyz frame 90 degrees counterclockwise about the z-axis and then about the y-axis in the same manner.

Notice that x^A, y^A and z^A axes are the result of 90 degree rotation of x, y and z axes about the three axes z, x and y respectively. Therefore the properties associated with three axes of rotational symmetry can be found by the use of the transformation in Fig C.3.

The tensor quantity in (C.4) defined in xyz-frame, when expressed by variables in $x^Ay^Az^A$ frame, should obey the law of transformation

$$\begin{aligned}\sigma_{ij}(\phi^{mn}) &= a^*_{ijk\ell}\frac{1}{2}\left(\frac{\partial\phi^{mn}_\ell}{\partial x_k}+\frac{\partial\phi^{mn}_k}{\partial x_\ell}\right)\\ &= A_{ie}A_{jf}A_{kg}A_{\ell h}a^{*A}_{efgh}A_{ka}A_{\ell b}A_{mc}A_{nd}\frac{1}{2}\left(\frac{\partial\psi^{cd}_b}{\partial x^A_a}+\frac{\partial\psi^{cd}_a}{\partial x^A_b}\right)\\ &= A_{ie}A_{jf}A_{mc}A_{nd}(A^T_{gk}A_{ka})(A^T_{h\ell}A_{\ell b})a^*_{efgh}\frac{1}{2}\left(\frac{\partial\psi^{cd}_b}{\partial x^A_a}+\frac{\partial\psi^{cd}_a}{\partial x^A_b}\right)\\ &= A_{ie}A_{jf}A_{mc}A_{nd}a^*_{efgh}\frac{1}{2}\left(\frac{\partial\psi^{cd}_h}{\partial x^A_g}+\frac{\partial\psi^{cd}_g}{\partial x^A_h}\right)\end{aligned} \tag{C.6}$$

where the property of transformation matrix

$$A^T_{gk}A_{ka}=A^{-1}_{gk}A_{ka}=\delta_{ga} \tag{C.7}$$

has been used. In (C.6), ψ^{cd}_h is the displacement component along x^A_h direction corresponding to the macroscopic strain tensor $e'_{cd}=(\partial v^{(1)}_d/\partial x^{A'}{}_c+\partial v^{(1)}_c/\partial x^{A'}{}_d)/2$, when the deformation field ϕ^{mn}_ℓ defined in xyz-frame is viewed from $x^Ay^Az^A$-frame. The elastic coefficient a^{*A}_{efgh} has been replaced by a^*_{efgh} because of the isotropy of the solid phase. In view of this, the symmetry property of a'_{ijmn} in (C.3) is determined by that of $\langle\sigma_{ij}(\phi^{mn})\rangle$, which we now examine for the special form of A_{ij} given by (C.5).

The symmetry relations (4.1.5a and b) reduce 36 coefficients to 21 which may be summarized conveniently in the following matrix form.

$$a'_{ijmn}=\begin{bmatrix} a'_{xxxx} & a'_{xxyy} & a'_{xxzz} & 2a'_{xxzy} & 2a'_{xxyz} & 2a'_{xxxz}\\ & a'_{yyyy} & a'_{yyzz} & 2a'_{yyzy} & 2a'_{yyyz} & 2a'_{yyxz}\\ \text{sym.} & & a'_{zzzz} & 2a'_{zzzy} & 2a'_{zzyz} & 2a'_{zzxz}\\ & & & 2a'_{zyzy} & 2a'_{zyyz} & 2a'_{zyxz}\\ \text{one-half of} & & & & 2a'_{yzyz} & 2a'_{yzxz}\\ \text{upper right} & & & & & 2a'_{zxxz}\end{bmatrix} \tag{C.8}$$

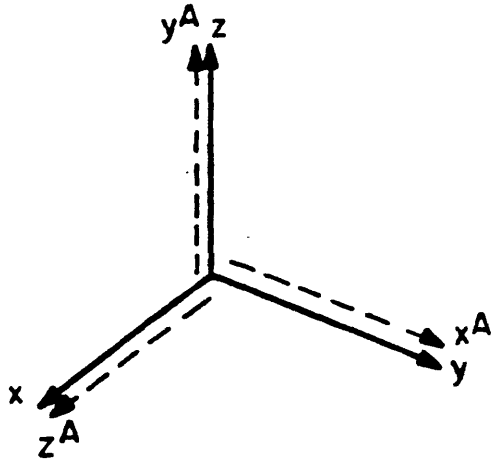

Fig. C.3 A rotational coordinate transformation from (x, y, z) to (x^A, y^A, z^A).

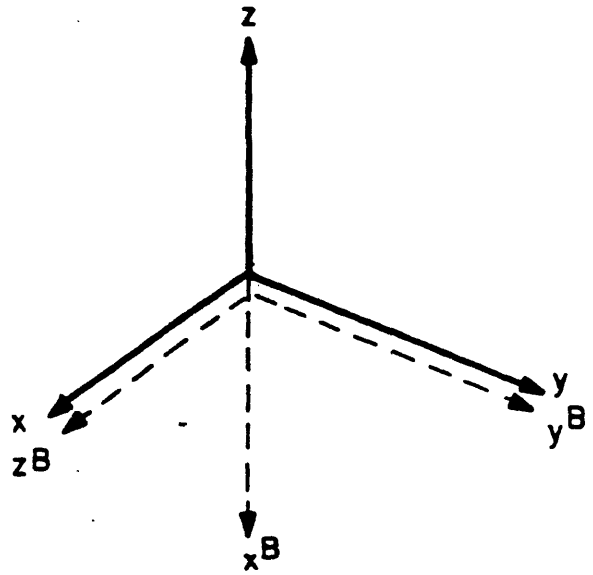

Fig. C.4 Another coordinate transformation from (x, y, z) to (x^B, y^B, z^B).

Consider the coefficients in the upper left part of (C.8). If $i = j = m = n = y$, it follows from (C.6), (C.5) and the transformation matrix A_{ij} in Fig C.3, that

$$\sigma_{yy}(\phi^{yy}) = a^*_{xxgh}\frac{1}{2}\left(\frac{\partial\psi^{xx}_h}{\partial x^A_g} + \frac{\partial\psi^{xx}_g}{\partial x^A_h}\right) \qquad (C.9)$$

The loading condition for ϕ^{yy} in Fig C.2(b), when viewed from the $x^Ay^Az^A$ coordinates (drawn with broken lines in Fig C.2(b)), is identical to that for ϕ^{xx} in Fig C.2(a). Then the displacement components ψ^{xx}_j resulting from the loading in Fig C.2(b) in $x^Ay^Az^A$ coordinates must be equal to ϕ^{xx}_j of Fig C.2(a). Therefore equation (C.9) becomes

$$\sigma_{yy}(\phi^{yy}) = a^*_{xxgh}\frac{1}{2}\left(\frac{\partial\phi^{xx}_h}{\partial x_g} + \frac{\partial\phi^{xx}_g}{\partial x_h}\right) = \sigma_{xx}(\phi^{xx}) \qquad (C.10)$$

If $i = j = m = n = z$ is chosen in (C.6), we have

$$\sigma_{zz}(\phi^{zz}) = a^*_{yygh}\frac{1}{2}\left(\frac{\partial\psi^{yy}_h}{\partial x^A_g} + \frac{\partial\psi^{yy}_g}{\partial x^A_h}\right)$$

It is again readily observed that the displacement ψ^{yy}_j under the loading in Fig C.2(c) when viewed from $x^Ay^Az^A$ coordinates is the same as ϕ^{yy}_j of Fig C.2(b). Thus

$$\sigma_{zz}(\phi^{zz}) = \sigma_{yy}(\phi^{yy}) \qquad (C.11)$$

Combining (C.10) and (C.11)

$$\sigma_{xx}(\phi^{xx}) = \sigma_{yy}(\phi^{yy}) = \sigma_{zz}(\phi^{zz}) \qquad (C.12)$$

so that the diagonal elements in the upper left of (C.10) are identical.

On the other hand, if $i = j = x$ and $m = n = z$ in (C.6), it follows that

$$\sigma_{xx}(\phi^{zz}) = a^*_{xxgh}e_{gh}(\psi^{yy}) = a^*_{xxgh}e_{gh}(\phi^{yy}) = \sigma_{zz}(\phi^{yy}) = \sigma_{yy}(\phi^{zz}) \qquad (C.13)$$

Similarly, for $i = j = x$ and $m = n = y$, we have

$$\sigma_{xx}(\phi^{yy}) = a^*_{xxgh}e_{gh}(\psi^{xx}) = \sigma_{zz}(\phi^{xx}) = \sigma_{xx}(\phi^{zz}) \qquad (C.14)$$

From (C.13) and (C.14), we obtain

$$\sigma_{xx}(\phi^{yy}) = \sigma_{yy}(\phi^{zz}) = \sigma_{zz}(\phi^{zz}) \qquad (C.15)$$

which shows that the off-diagonal terms in the upper left of (C.8) are equal.

We now consider the elements in the lower right of (C.8). For $i = x$, $j = y$, $m = x$, and $n = y$, (C.6) gives

$$\sigma_{xy}(\phi^{xy}) = a^*_{xxgh} e_{gh}(\psi^{xx}) = a^*_{xxgh} e_{gh}(\phi^{xx}) = \sigma_{xx}(\phi^{xx}) \qquad (C.16)$$

Also, for $i = x$, $j = z$, $m = x$, and $n = z$, we have

$$\sigma_{xz}(\phi^{xz}) = a^*_{xygh} e_{gh}(\psi^{xy}) = a^*_{xygh} e_{gh}(\phi^{xy}) = \sigma_{yz}(\phi^{yz}) \qquad (C.17)$$

If $(ijmn)$ are further chosen as $(xyyz)$ and $(zxxy)$, (C.6) becomes

$$\begin{aligned} \sigma_{xy}(\phi^{yz}) &= a^*_{xxgh} e_{gh}(\psi^{xy}) = a^*_{xxgh} e_{gh}(\phi^{xy}) = \sigma_{xx}(\phi^{xy}) \\ \sigma_{xx}(\phi^{xy}) &= a^*_{yxgh} e_{gh}(\psi^{xx}) = a^*_{yxgh} e_{gh}(\phi^{xx}) = \sigma_{yx}(\phi^{xx}) \end{aligned} \qquad (C.18)$$

Combining (C.16) and (C.18)

$$\begin{aligned} \sigma_{xy}(\phi^{xy}) &= \sigma_{yx}(\phi^{yx}) = \sigma_{xx}(\phi^{xx}) \\ \sigma_{xy}(\phi^{yx}) &= \sigma_{yx}(\phi^{xx}) = \sigma_{xx}(\phi^{xy}) \end{aligned} \qquad (C.19)$$

so that the lower part of (C.8) reduces to two constants, diagonal and off-diagonal ones.

As the final use of the transformation matrix A_{ij} of (C.5), consider the elements in the upper right part of (C.8). Replacement of ψ by ϕ in the following lines comes, the same as above, from the inspection of displacement components ψ in the $x^A y^A z^A$-coordinates and the comparison of them with ϕ in the xyz-coordinates.

$(ijmn)$	
$xxxy$	$\sigma_{xx}(\phi^{xy}) = a^*_{xxgh} e_{gh}(\phi^{xx}) = \sigma_{xx}(\phi^{xx})$
$zzzx$	$\sigma_{xx}(\phi^{xx}) = a^*_{yygh} e_{gh}(\phi^{yx}) = \sigma_{yy}(\phi^{yx})$
$xxyz$	$\sigma_{xx}(\phi^{yx}) = a^*_{xxgh} e_{gh}(\phi^{xy}) = \sigma_{xx}(\phi^{xy})$
$zzxy$	$\sigma_{xx}(\phi^{xy}) = a^*_{yygh} e_{gh}(\phi^{xx}) = \sigma_{yy}(\phi^{xx})$
$xxzx$	$\sigma_{xx}(\phi^{xx}) = a^*_{xxgh} e_{gh}(\phi^{yx}) = \sigma_{xx}(\phi^{yx})$
$zzyz$	$\sigma_{xx}(\phi^{yx}) = a^*_{yygh} e_{gh}(\phi^{xy}) = \sigma_{yy}(\phi^{xy})$

from which the relationships among the elements in the upper right of (C.8) follow as

$$\begin{aligned}
\sigma_{zz}(\phi^{xy}) &= \sigma_{yy}(\phi^{yz}) = \sigma_{zz}(\phi^{xz}) \\
\sigma_{zz}(\phi^{yz}) &= \sigma_{yy}(\phi^{xz}) = \sigma_{zz}(\phi^{xy}) \\
\sigma_{zz}(\phi^{xz}) &= \sigma_{yy}(\phi^{xy}) = \sigma_{zz}(\phi^{yz})
\end{aligned} \tag{C.20}$$

In view of (C.12), (C.15), (C.19) and (C.20), it follows from (C.3) that there are only the following seven coefficients.

$$\begin{aligned}
&a'_{xxxx} = a'_{yyyy} = a'_{zzzz}, \quad a'_{xxyy} = a'_{yyzz} = a'_{zzxx}, \quad a'_{xyxy} = a'_{yzyz} = a'_{zxzx}, \\
&a'_{xyyx} = a'_{yzzx} = a'_{zxxy}, \quad a'_{xxxy} = a'_{yyyz} = a'_{zzzx}, \quad a'_{xxyz} = a'_{yyzx} = a'_{zzxy}, \\
&a'_{xxzx} = a'_{yyzy} = a'_{zzyz}
\end{aligned} \tag{C.21a-g}$$

So far only the rotational symmetry has been used to establish the relations in (C.21). In order to exploit the sign and symmetry properties about planes of symmetry, we consider another coordinate transformation shown in Fig. C.4. The transformation matrix is then given by

$$B_{ij} = \mathbf{e}_i \cdot \mathbf{e}^B_j = \begin{bmatrix} 0 & 0 & 1 \\ 0 & 1 & 0 \\ -1 & 0 & 0 \end{bmatrix} \tag{C.22}$$

We apply (C.22) to the coefficients in (C.21d-g). In the following, the use of different symbol ψ for displacement component in the transformed frame is omitted. In the procedure leading to (C.21), by inspection of ψ in the transformed frame and comparison with those in the initial frame, the equivalence has been shown. It should be noted that the equivalence is strictly the consequence of the geometric symmetry of the cell in a cube. From a'_{xyyz} we have

$$a'_{xyyz} = B_{xi}B_{yj}B_{yp}B_{zq}a'_{ijpq} = -a'_{zyyz} = -a'_{xyyz}$$

so that

$$a'_{xyyz} = 0 \tag{C.23}$$

Similarly, after using (C.21g), we have from (C.21e)

$$\begin{aligned} a'_{zzzy} &= a'_{zzzy} = a'_{zzzz} \\ a'_{yyyz} &= -a'_{yyyz} = a'_{zzzz} \end{aligned} \tag{C.24}$$

Thus

$$a'_{zzzy} = a'_{yyyz} = 0 \tag{C.25}$$

Also, it follows from (C.21f) that

$$a'_{zzyz} = -a'_{zzyz} = -a'_{zyzz} \tag{C.26}$$

Therefore the coefficients in the last four groups of (C.21d-g) all vanish.

$$\begin{aligned} a'_{zyyz} = a'_{yzzz} = a'_{zzzy} = 0 \\ a'_{zzzy} = a'_{yyyz} = a'_{zzzz} = 0 \\ a'_{zzyz} = a'_{yyzz} = a'_{zzzy} = 0 \\ a'_{zzzz} = a'_{yyzy} = a'_{zzyz} = 0 \end{aligned} \tag{C.27}$$

From (C.21), (C.23), (C.25) and (C.27) it follows finally that only three coefficients remain out of 21 a'_{ijkl} for microcell geometries which have three orthogonal planes of symmetry. Accorddingly the coefficient matrix (C.8) may be written as

$$a'_{ijmn} = \begin{bmatrix} a_I & a_{II} & a_{II} & & & \\ a_{II} & a_I & a_{II} & & 0 & \\ a_{II} & a_{II} & a_I & & & \\ & & & 2a_{III} & & \\ & 0 & & & 2a_{III} & \\ & & & & & 2a_{III} \end{bmatrix} \tag{C.28}$$

where

$$\begin{aligned} a_I &= a'_{zzzz} = a'_{yyyy} = a'_{zzzz} \\ a_{II} &= a'_{zzyy} = a'_{yyzz} = a'_{zzzz} \\ a_{III} &= a'_{zyzy} = a'_{yzyz} = a'_{zzzz} \end{aligned} \tag{C.29}$$

Material which has the elastic coefficients as (C.28) with three distinct constants is said to possess cubic symmetry property(Love(1944), Lekhnitskii(1963)). If further

the relation $(a_I - a_{II}) = 2a_{III}$ holds, the material is called isotropic and there are only two independent coefficients.

C.2.2 Coefficients α'_{ij} and $(\beta'_t)_{ij}$

The coefficients α'_{ij} and $(\beta'_t)_{ij}$ are now expressed in terms of a'_{ijmn} by examining all subscripts i and j.

From (4.1.24) we have

$$\alpha'_{ij} = \delta_{ij} - \frac{a'_{pqij}\delta_{pq}}{3\lambda^* + 2\mu^*} = \delta_{ij} - \frac{a'_{pqij}}{3\lambda^* + 2\mu^*} \qquad (C.30)$$

If $i = j = x$,

$$\begin{aligned}\alpha'_{xx} &= 1 - \frac{a'_{ppxx}}{3\lambda^* + 2\mu^*} = 1 - \frac{1}{3\lambda^* + 2\mu^*}(a'_{xxxx} + a'_{yyxx} + a'_{zzxx}) \\ &= 1 - \frac{a_I + 2a_{II}}{3\lambda^* + 2\mu^*}\end{aligned}$$

Similarly, if $i = j = y$ or $i = j = z$,

$$\alpha'_{yy} = 1 - \frac{a'_{ppyy}}{3\lambda^* + 2\mu^*} = 1 - \frac{a_I + 2a_{II}}{3\lambda^* + 2\mu^*}$$

$$\alpha'_{zz} = 1 - \frac{a'_{ppzz}}{3\lambda^* + 2\mu^*} = 1 - \frac{a_I + 2a_{II}}{3\lambda^* + 2\mu^*}$$

Off-diagonal terms are as follows. If $i = x$ and $j = y$,

$$\alpha'_{xy} = -\frac{a'_{ppxy}}{3\lambda^* + 2\mu^*} = 0$$

since $a'_{xxxy} = a'_{yyxy} = a'_{zzxy} = 0$(cf.(C.27)). For $i = x$, $j = z$ and $i = y$, $j = z$ we also have

$$\alpha'_{xz} = -\frac{a'_{ppxz}}{3\lambda^* + 2\mu^*} = 0, \qquad \alpha'_{yz} = -\frac{a'_{ppyz}}{3\lambda^* + 2\mu^*} = 0$$

Combining all these we obtain

$$\alpha'_{ij} = \alpha' \begin{bmatrix} 1 & 0 & 0 \\ 0 & 1 & 0 \\ 0 & 0 & 1 \end{bmatrix} \qquad (C.31)$$

where

$$\alpha' = 1 - (a_I + 2a_{II})/(3\lambda^* + 2\mu^*) \qquad (C.32)$$

The thermal modulus (4.1.25) is written

$$(\beta'_t)_{ij} = \beta^* \frac{a'_{ppij}}{3\lambda^* + 2\mu^*} \tag{C.33}$$

On comparison of (C.33) with (C.30), we readily obtain

$$(\beta'_t)_{ij} = \beta'_t \begin{bmatrix} 1 & 0 & 0 \\ 0 & 1 & 0 \\ 0 & 0 & 1 \end{bmatrix} \tag{C.34}$$

where

$$\beta'_t = \beta^*(a_I + 2a_{II})/(3\lambda^* + 2\mu^*) \tag{C.35}$$

It is shown again(for cubic symmetry) that, if a_I and a_{II} are determined, α'_{ij} and $(\beta'_t)_{ij}$ are given by (C.32) and (C.35) without solving the cell problems fro η and ζ in (4.1.7) to (4.1.9). The total number of independent coefficients in the governing equations (4.1.1) to (4.1.3) is therefore the following three:

$$\begin{aligned} a_I &= a'_{xxxx} = (1-n')a^*_{xxxx} + \langle \sigma_{xx}(\phi^{xx}) \rangle \\ a_{II} &= a'_{xxyy} = (1-n')a^*_{xxyy} + \langle \sigma_{yy}(\phi^{xx}) \rangle \\ a_{III} &= a'_{xyxy} = (1-n')a^*_{xyxy} + \langle \sigma_{xy}(\phi^{xy}) \rangle \end{aligned} \tag{C.36}$$

In view of this, it is only necessary to solve the problems for ϕ_j^{xx} and ϕ_j^{xy} of Fig C.2(a) and (b). Finally we remark that both α'_{ij} and $(\beta'_t)_{ij}$ are diagonal with same constant and therefore are isotropic.

C.2.3 Coefficients γ'_{ij}, β'_c and ζ'_c

Obviously, from (4.1.26) and (C.31), γ' becomes

$$\gamma'_{ij} = \alpha' \delta_{ij} = \alpha' \begin{bmatrix} 1 & 0 & 0 \\ 0 & 1 & 0 \\ 0 & 0 & 1 \end{bmatrix} \tag{C.37}$$

and is issotropic. Since a'_{ppjj} in (4.1.27) is the sum of the elements in the upper left corner of (C.28),e.g.

$$a'_{ppjj} = 3(a_I + a_{II})$$

it follows from (4.1.27) and (4.1.28) that

$$\beta_c' = \frac{3}{3\lambda^* + 2\mu^*}\left[1 - n' - \frac{a_I + 2a_{II}}{3\lambda^* + 2\mu^*}\right] > 0 \qquad (C.38)$$

and from (4.1.31) and (4.1.32) that

$$\zeta_c' = -\beta^*\beta_c' = -\frac{3\beta^*}{3\lambda^* + 2\mu^*}\left[1 - n' - \frac{a_I + 2a_{II}}{3\lambda^* + 2\mu^*}\right] < 0 \qquad (C.39)$$

The coefficients γ_{ij}', β_c' and ζ_c' also have been expressed in terms of only a_I and a_{II}.

C.3 Permeability k_{ij}' (Symmetry and Isotropy).

Before examining the symmetry properties of k_{ij}, we note that k_{ij} is the fluid velocity along x_i-direction inside a microcell when the externally imposed macroscale pressure gradient is in x_j'-direction. Hence the second index j may be regarded as given. For an arbitrary direction of $\nabla' p^{(0)}$, the resultant velocity field k_{ij} can be determined in view of linearity of the Stokes problem (3.3.20a-d), by linearly superposing the velocity components due to each j-th component of $\nabla' p^{(0)}$.

The symmetry properties of k_{ij} in the fluid phase can be obtained as follows. As an example, $k_{iz}(i = x, y, z)$ only will be examined. Extensions to k_{iy} and k_{iz} are straightforward.

We first show that the geometry of the fluid phase in the microcell is identical to that of the solid phase. Consider the cube defined by $0 < x < 0.5\ell$, $0 < y < 0.5\ell$ and $0 < z < 0.5\ell$ in Fig C.1. The geometry of the fluid region in that cube is the same as the solid phase in the cube defined by $-0.5\ell < x < 0$, $-0.5\ell < y < 0$ and $-0.5\ell < z < 0$ in Fig C.1. This is also true in y and z directions. If we define new Cartesian coordinates $X = x - \frac{\ell}{2}$, $Y = y - \frac{\ell}{2}$ and $Z = z - \frac{\ell}{2}$, the new Ω-cell defined by $-\frac{\ell}{2} < X < \frac{\ell}{2}$, $-\frac{\ell}{2} < Y < \frac{\ell}{2}$, and $-\frac{\ell}{2} < Z < \frac{\ell}{2}$ is identical to that shown in Fig C.1 except that the inside of the solidlined shape of Fig C.1 is now occupied by fluid. So the coordinates x, y, z in Fig C.1 can be replaced by X, Y, Z and the flow field driven by an external pressure gradient in X-direction can be analyzed by looking at the inside of the new cell geometry (Fig C.5).

From (3.3.19a) we have for $\partial p^{(0)}/\partial X'$, after omitting the buoyancy,

$$u_d^{(0)}{}_i = -k_{ix}\frac{\partial p^{(0)}}{\partial X'} \qquad (C.40)$$

The same symbols A through H are used to denote the sectors in Fig C.5(a). Since the sectors $A(X > 0, Y > 0, Z > 0)$ and $D(X > 0, Y < 0, Z > 0)$ are symmetric about the plane $Y = 0$, the fluid velocities at any two points located symmetrically about $Y = 0$ (i.e. P_1 and P_2 in Fig C.5(a)) must be related by

$$k_{xx}|_{P_1} = k_{xx}|_{P_2}, \quad k_{yx}|_{P_1} = -k_{yx}|_{P_2}, \quad k_{zx}|_{P_1} = k_{zx}|_{P_2} \qquad (C.41)$$

which are shown by arrows parallel to X, Y and Z at P_1 and P_2. Similarly at points P_1 and P_3 in sectors A and E $(X > 0, Y > 0, Z < 0)$ because of the geometric symmetry about $Z = 0$ plane, it follows that

$$k_{xx}|_{P_1} = k_{xx}|_{P_3}, \quad k_{yx}|_{P_1} = k_{yx}|_{P_3}, \quad k_{zx}|_{P_1} = -k_{zx}|_{P_3} \qquad (C.42)$$

as shown in Fig C.5(a). Similar relations among other sectors are also shown in Fig C.5(a). The sign relations are summarized in Fig C.5(b) for sectors A, D, E and H.

Employing the same symmetry arguments, the velocity fields k_{iy} and k_{iz} indeuced by $\partial p^{(0)}/\partial Y'$ and $\partial p^{(0)}/\partial Z'$ respectively can be related among sectors. These are summarized schematically in Fig C.6 (a) and (b) using arrows.

Consider the rotational coordinate transformation of Fig C.3 again. Using the transformation matrix of (C.5) the permeability in xyz-frame is related to k_{ij}^A in $x^A y^A z^A$-frame by

$$k_{ij} = A_{ip}A_{jq}k_{pq}^A \qquad (C.43)$$

If $i = j = x$, (C.43) becomes

$$k_{xx} = A_{xp}A_{xq}k_{xx}^A$$

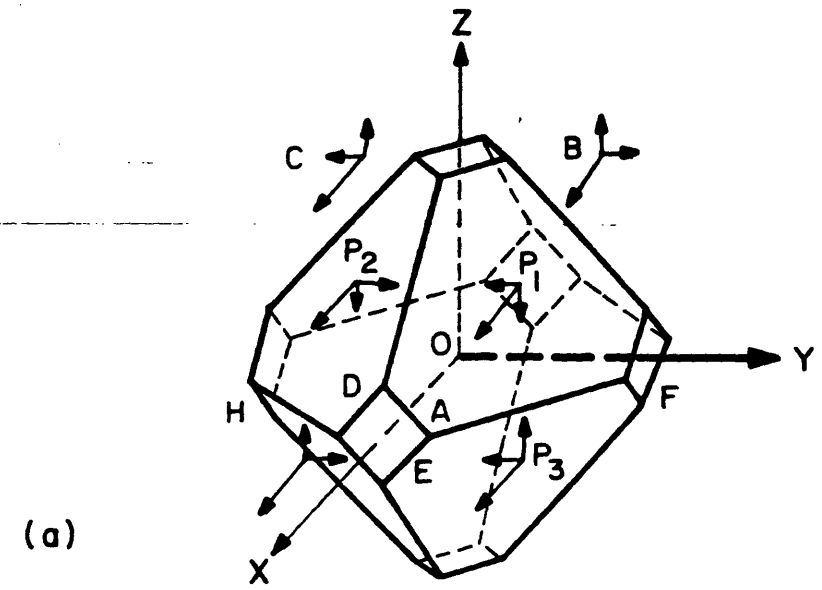

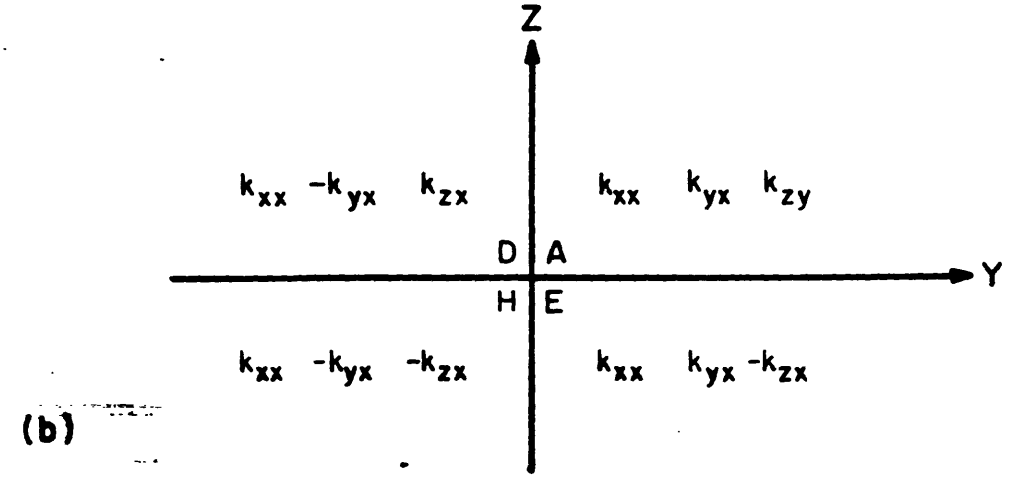

Fig. C.5 (a) The fluid region in the microcell defined in XYZ-coordinates and typical velocity components at points symmetric about $X = 0$, $Y = 0$ and $Z = 0$ planes, and (b) the symmetry relations for K_{iz} $(i = x, y, z)$ in sectors A, D, E and H.

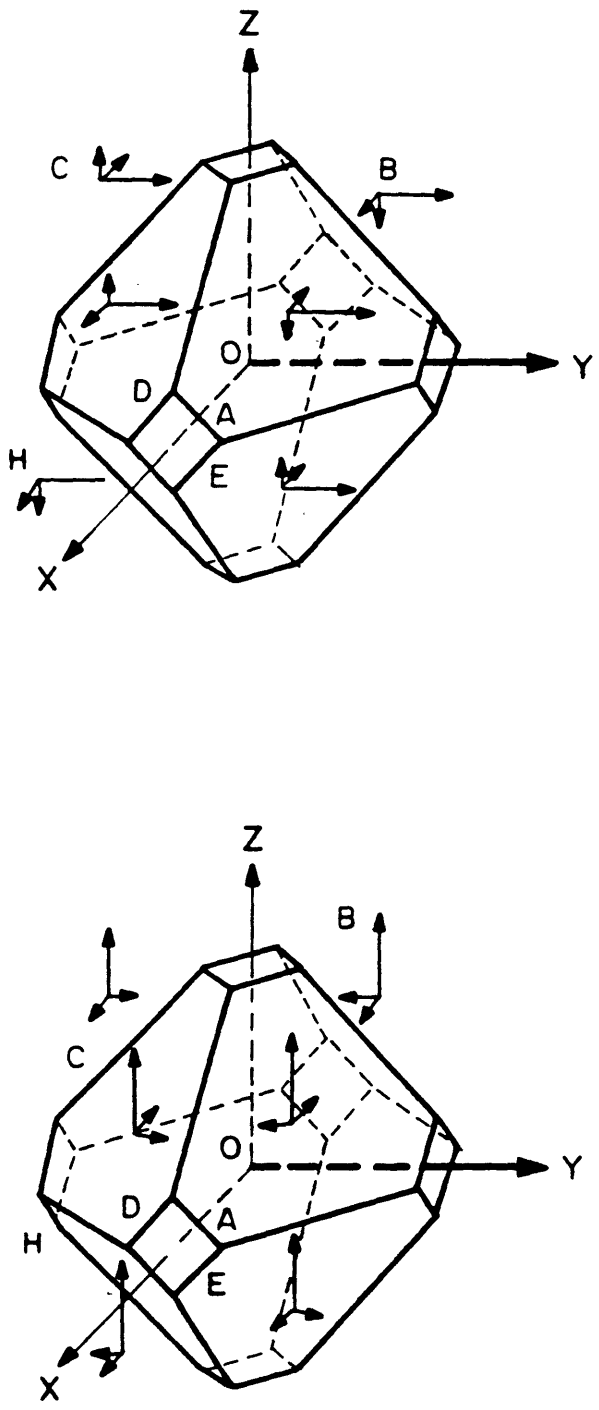

Fig. C.6 Fluid velocity components in symmetric sectors (a) k_{iy} due to $\partial p^{(0)}/\partial Y'$ and (b) k_{iz} due to $\partial p^{(0)}/\partial Z'$.

Since the flow field of Fig C.5(a) driven by $\partial p^{(0)}/\partial X'$ is, when viewed from $x^A y^A z^A$-frame, identical to that of Fig C.6(b) driven by $\partial p^{(0)}/\partial Z'$, we have $k^A_{xz} = k_{zz}$. Thus

$$\langle k_{xx} \rangle = \langle k_{zz} \rangle \tag{C.44}$$

Similarly, if $i = j = y$, (C.43) gives

$$\langle k_{yy} \rangle = A_{yp} A_{yq} \langle k^A_{pq} \rangle = \langle k_{zz} \rangle \tag{C.45}$$

On the other hand, if $i = y$, $j = x$ and $i = z$, $j = x$, we obtain

$$\begin{aligned} \langle k_{yx} \rangle &= A_{yp} A_{xq} \langle k^A_{pq} \rangle = \langle k^A_{xz} \rangle = \langle k_{zz} \rangle \\ \langle k_{zx} \rangle &= A_{zp} A_{xq} \langle k^A_{pq} \rangle = \langle k^A_{yz} \rangle = \langle k_{yz} \rangle \end{aligned} \tag{C.46}$$

But it is seen in Fig C.5(b) that k_{yz} cancels between sectors A and D and E and H and k_{zz} cancels between sectors A and E and D and H. Therefore

$$\langle k_{yx} \rangle = \langle k_{yz} \rangle = \langle k_{zz} \rangle \tag{C.47}$$

and the permeability tensor is finally reduced to the following isotropic form

$$k'_{ij} = k' \begin{bmatrix} 1 & 0 & 0 \\ 0 & 1 & 0 \\ 0 & 0 & 1 \end{bmatrix} \qquad k' = \langle k_{xx} \rangle = \langle k_{yy} \rangle = \langle k_{zz} \rangle = 0 \tag{C.48}$$

for the special cell geometry chosen which has three orthogonal planes of symmetry.

C.4 Thermal Conductivity m'_{ij} (Symmetry and Isotropy).

For homogeneous and isotropic fluid and solid $(m_f)_{ij} = m_f \delta_{ij}$ and $(m_s)_{ij} = m_s \delta_{ij}$. Then (4.3.1a-d) become

$$\begin{aligned} 0 &= m^*_f \frac{\partial^2 A^f_\ell}{\partial x_i \partial x_j} \qquad \text{in} \quad \Omega_f \\ 0 &= M_r m^*_s \frac{\partial^2 A^s_\ell}{\partial x_i \partial x_j} \qquad \text{in} \quad \Omega_s \\ A^f_\ell &= A^s_\ell \qquad \text{on} \quad \Gamma(0) \\ \left(m^*_f \frac{\partial A^f_\ell}{\partial x_i} - M_r m^*_s \frac{\partial A^s_\ell}{\partial x_i} \right) N_i &= (M_r m^*_s - m^*_f) N_\ell \qquad \text{on} \quad \Gamma(0) \end{aligned} \tag{C.49a - d}$$

The boundary condition (C.49d) may be written as

$$m_f^* \frac{\partial A_\ell^f}{\partial x_i} N_i^f + M_r m_s^* \frac{\partial A_\ell^s}{\partial x_i} N_i^s = (M_r m_s^* - m_f^*) N_\ell^f \qquad (C.50)$$

where N_i^f and N_i^s are the outward unit normal vectors on $\Gamma(0)$ from the fluid and solid phases respectively. Equation (C.50) states that there is a known distribution of heat source on $\Gamma(0)$(see Fig. C.7).

The distribution of heat source on the interface is shown in Fig. C.8(a)-(c) for $\ell = x, y, z$ at some typical points on $\Gamma(0)$ in the sectors. The sign of distributed heat source on $\Gamma(0)$ is determined by that of N_ℓ^f on the right-hand side of (C.50), assuming that the multiplying factor $(M_r m_s^* - m_f^*)$ is positive, the distribution is denoted in accordance with N_ℓ^f on the interface. For graphical cconvenience, the sphere is used again. The designation of sectors A for solid and fluid are the corresponding phase portions inside the small cube bounded by $0 < x < 1/2$, $0 < y < 1/2$ and $0 < z < 1/2$.

We rewrite m'_{ij} in (3.4.15b) for isotropic grains. after using the Gauss theorem and Ω-periodicity,

$$\begin{aligned} m'_{ij} &= \langle (m_f^*)_{il} \left(\delta_{\ell j} + \frac{\partial A_j^f}{\partial x_\ell} \right) \rangle + M_r \langle (m_s^*)_{il} \left(\delta_{\ell j} + \frac{\partial A_j^s}{\partial x_\ell} \right) \rangle \\ &= (n' m_f^* + (1 - n') M_r m_s^*) \delta_{ij} + \frac{1}{\Omega} \left(m_f^* \int_{\Omega_f} \frac{\partial A_j^f}{\partial x_i} d\Omega + M_r m_s^* \int_{\Omega_f} \frac{\partial A_j^s}{\partial x_i} d\Omega \right) \\ &= \overline{m} \delta_{ij} + \frac{1}{\Omega} \left(m_f^* \int_{\Gamma(0)} A_j^f N_i^f + M_r m_s^* \int_{\Gamma(0)} A_j^s N_i^s dS \right) \end{aligned} \qquad (C.51)$$

where

$$\overline{m} = n' m_f^* + (1 - n') M_r m_s^* \qquad (C.52)$$

The rotational coordinate transformation of Fig. C.3 is used again here. Denoting variables defined in $x^A y^A z^A$-frame with superscript 'A', (C.51) becomes

$$m'_{ij} = \overline{m} A_{ip} A_{jq} \delta_{pq} + A_{ip} A_{jq} \frac{1}{\Omega} \left[m_f^* \int_{\Gamma(0)} (A_q^f N_p^f)^A dS + M_r m_s^* \int_{\Gamma(0)} (A_q^s N_p^s)^A dS \right] \qquad (C.53)$$

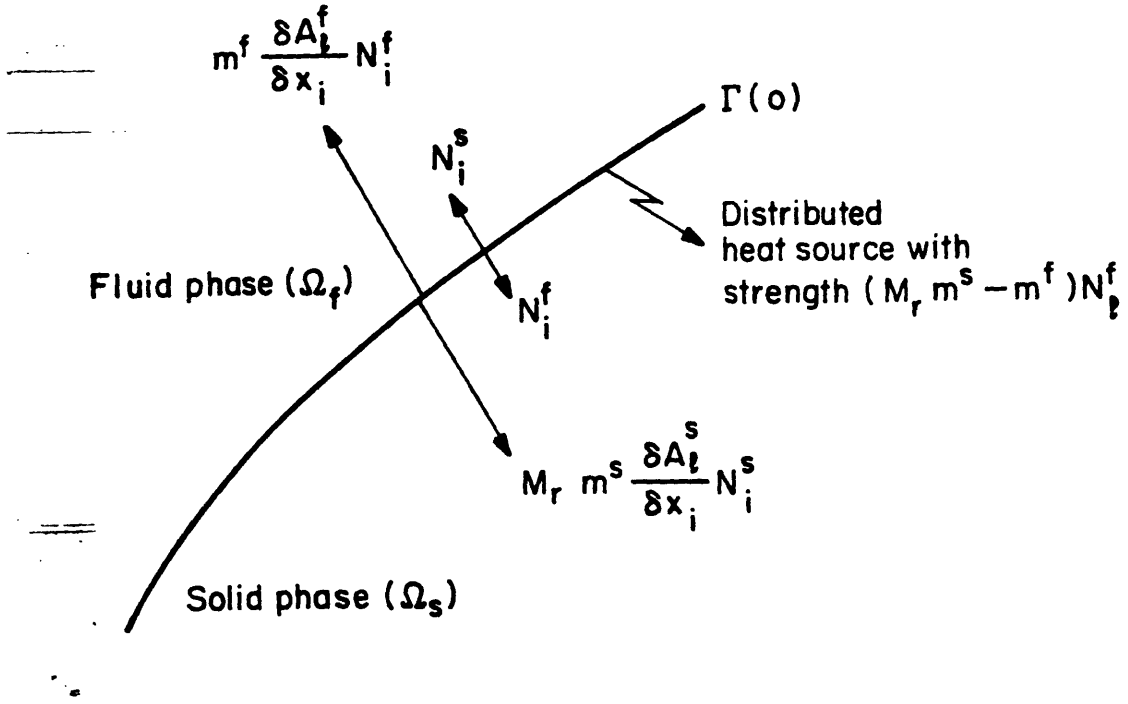

Fig. C.7 The heat flux boundary condition on the interface with distributed heat source of strength $(M_r m^s - m^f)N_\ell^f$.

If $i = j = y$, (C.53) gives, after using A_{ij} (C.5),

$$m'_{yy} = \overline{m} + \frac{1}{\Omega}\left[m_f^* \int_{\Gamma(0)} (A_x^f N_x^f)^A dS + M_r m_s^* \int_{\Gamma(0)} (A_x^s N_x^s)^A dS\right] \qquad (C.54)$$

From Fig. C.8(b) it is seen that the heat source distribution on $\Gamma(0)$, when viewed from $x^A y^A z^A$-frame, is identical to that for A_x^f and A_x^s of Fig. C.8(a) and thus (C.54) gives

$$m'_{yy} = m'_{xx}$$

Similarly, if $i = j = z$ is chosen, it readily follows from (C.53) that

$$m'_{zz} = m'_{xx}$$

Therefoer we have

$$m'_{xx} = m'_{yy} = m'_{zz} \qquad (C.55)$$

On the other hand, if $i = x$, $j = y$ and $i = y$, $j = z$ are chosen, it can be shown by the same reasoning that

$$m'_{xy} = m'_{yz} = m'_{xx} \qquad (C.56)$$

The symmetric thermal conductivity tensor m'_{ij} is thus reduced to two distinct components.

In order to make use of reflectional symmetry among the sectors, we use the transformation matrix (C.22). Note that the direct application of the transformation matrix is valid because of hte cubic symmetry of the cell geometry. It readily follows that

$$m'_{xx} = B'_{xa} B'_{xb} m'_{ab} = -m'_{xx} = -m'_{xx} \qquad (C.57)$$

Thus the coefficients in (C.56) vanish.

Combining (C.55), (C.56) and (C.57) we finally obtain the following isotropic effective thermal conductivity tensor for a cell geometry with three planes of symmetry

$$m'_{ij} = m' \begin{bmatrix} 1 & 0 & 0 \\ 0 & 1 & 0 \\ 0 & 0 & 1 \end{bmatrix} \qquad (C.58)$$

where

$$m' = m'_{xx} = m'_{yy} = m'_{zz} = \overline{m} + \frac{1}{\Omega}\left(m_f^* \int_{\Gamma(0)} A_x^f N_x^f dS + M_r m_s^* \int_{\Gamma(0)} A_x^s N_x^s dS\right) \tag{C.59}$$

Thus it is only necessary to solve for only one component of $A_\ell^f(\ell = x, y, z)$ and $A_\ell^s(\ell = x, y, z)$ to determine the thermal conductivity tensor.

(a) A_x^f

$$m^f \frac{\partial A_x^f}{\partial x_i} N_i^f + M_r m^s \frac{\partial A_x^s}{\partial x_i} N_i^s = (M_r m^s - m^f) N_x^f$$

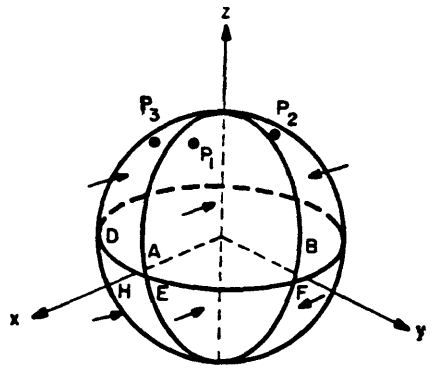

(b) A_y^f

$$m^f \frac{\partial A_y^f}{\partial x_i} N_i^f + M_r m^s \frac{\partial A_y^s}{\partial x_i} N_i^s = (M_r m^s - m^f) N_y^f$$

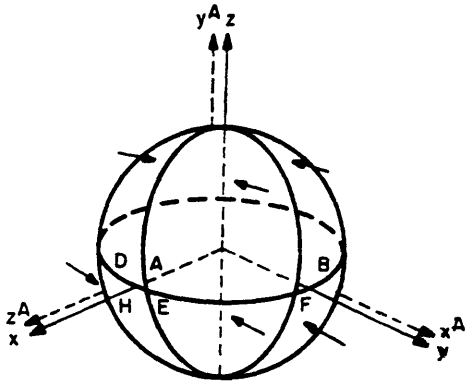

(c) A_z^f

$$m^f \frac{\partial A_z^f}{\partial x_i} N_i^f + M_r m^s \frac{\partial A_z^s}{\partial x_i} N_i^s = (M_r m^s - m^f) N_z^f$$

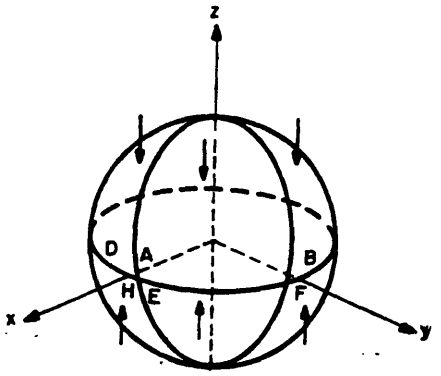

Fig. C.8 The distribution of heat source on the interface for (a) A_x^f and A_x^s, (b) A_y^f and A_y^s, and (c) A_z^f and A_z^s.

Appendix D. Vanishing of Nonlinear Terms for Microcells with Three Planes of Symmetry

In this appendix, the vanishing of the coefficients of the nonlinearly coupled terms is shown for a cubic microcell with three planes of symmetry. Specifically we show the vanishing of F'_{jmngh} in the equilibrium equation, J'_{jmn} in the consolidation equation and S'_{mnk} in the heat transport equation by making use of coordinate transformations introduced in Appendix C. Other coefficients are simpler in that they are related to vector functions η and ζ. Vanishing of those coefficients can be shown as a special form of F'_{jmngh}, J'_{jmn} and S'_{mnk}. It is noted that the inspection of the solutions in the rotated frame and comparison with those in the original unrotated frame are possible because of the special cubic symmetry of the cell geometry.

D.1 Vanishing of F'_{jmngh}

From (3.1.13a) after using (3.3.5a), the coefficient F'_{jmngh} becomes

$$F_j^{mngh} = \frac{1}{\Omega}\int_\Gamma a_{ijpq}\left(\delta_{pm}\delta_{qn} + e_{pq}(\phi^{mn})\right)\frac{\partial \phi_k^{gh}}{\partial x_i}N_k^s dS \qquad (D.1.1)$$

where for the purpose of convenience the prime has been omitted and the last four indices have been placed in the upper right corner. The indices mn and gh are those of the macroscale strain $e'(v^{(0)})$. Because of the symmetry property $e'_{ij}(v^{(0)}) = e'_{ji}(v^{(0)})$, there are only six combinations in mn and gh respectively. Therefore, in the most general case, F_j^{mngh} has 108 coefficients. We arrange the coefficients into several groups.

Group 1. F_j^{mmnn} (no summation over m or n) in which 'mm' and 'nn' can take any one from (xx, yy, zz). There are 27 coefficients.

Group 2. F_j^{mmgh} and F_j^{ghmm} (no summation over m). The subscripts 'mm' takes one of (xx, yy, zz) and the subscripts 'gh' takes one of (xy, yz, zx). There are 54 coefficients.

Group 3. F_j^{mnmn} (no summation over m or n). The subscripts 'mn' are chosen from (xy, yz, zx). There are 9 coefficients.

Group 4. F_j^{mngh}. The subscripts 'mn' and 'gh' are from (xy, yz, zx) but different so that there are 18 coefficients.

Vanishing of F_j^{mmnn} in Group 1.

We shall employ the coordinate transformations considered in Appendix C. The transformation matrices are given by

$$A_{ij} = \mathbf{e}_i \cdot \mathbf{e}_j^A = \begin{bmatrix} 0 & 0 & 1 \\ 1 & 0 & 0 \\ 0 & 1 & 0 \end{bmatrix} \quad ; \quad B_{ij} = \mathbf{e}_i \cdot \mathbf{e}_j^B = \begin{bmatrix} 0 & 0 & 1 \\ 0 & 1 & 0 \\ -1 & 0 & 0 \end{bmatrix} \qquad (D.1.2a,b)$$

Let us rewrite (D.1.1) in terms of the variables defined in the rotated (x^A, y^A, z^a) frame as follows.

$$\begin{aligned} F_j^{mmnn} &= A_{jb}A_{mc}A_{md}A_{ng}A_{nh}\frac{1}{\Omega}\int_\Gamma \bar{a}_{ibcd}\frac{\partial \bar{\phi}_k^{gh}}{\partial x_i^A}\bar{N}_k^s dS \\ &+ A_{jb}A_{mc}A_{md}A_{ng}A_{nh}\frac{1}{\Omega}\int_\Gamma \bar{a}_{ibpq}\bar{e}_{pq}(\bar{\phi}^{cd})\frac{\partial \bar{\phi}_k^{gh}}{\partial x_i^A}\bar{N}_k^s dS \end{aligned} \qquad (D.1.3)$$

where quantities with overhead bar are defined in the rotated frame. If we choose $mm = xx$ and $nn = xx$ in (D.1.3) and use (D.1.2a), (D.1.3) becomes

$$F_j^{xxxx} = A_{jb}\frac{1}{\Omega}\int_\Gamma \left(a_{ibzz}\frac{\partial \bar{\phi}_k^{zz}}{\partial x_i^A} + a_{ibpq}\bar{e}_{pq}(\bar{\phi}^{zz})\frac{\partial \bar{\phi}_k^{gh}}{\partial x_i^A}\right)\bar{N}_k^s dS \qquad (D.1.4)$$

The overhead bar of the elastic coefficients has been dropped since the coefficients are invariant under any coordinate transformation for isotropic solid. As has been shown in Appendix C, the displacement $\bar{\phi}_k^{zz}$, which is ϕ_k^{zz} when viewed from (x^A, y^A, z^A) frame in Fig. C.2(a), is identical to ϕ_k^{zz} in Fig. C.2(c). Thus (D.1.4) readily becomes

$$F_j^{xxxx} = A_{jb}F_b^{zzzz} \qquad (D.1.5)$$

from which we have

$$F_x^{xxxx} = F_z^{zzzz}, \quad F_y^{xxxx} = F_x^{zzzz}, \quad F_z^{xxxx} = F_y^{zzzz} \qquad (D.1.6)$$

If $mm = yy$ and $nn = yy$ in (D.1.3), there follows similarly that

$$F_x^{yyyy} = F_z^{zzzz}, \quad F_y^{yyyy} = F_x^{zzzz}, \quad F_z^{yyyy} = F_y^{zzzz} \qquad (D.1.7)$$

Combinig (D.1.6) and (D.1.7), we have

$$\begin{aligned} F_x^{zzzz} &= F_y^{yyyy} = F_z^{zzzz} \\ F_y^{zzzz} &= F_z^{yyyy} = F_x^{zzzz} \\ F_z^{zzzz} &= F_x^{yyyy} = F_y^{zzzz} \end{aligned} \qquad (D.1.8a-c)$$

Following the same procedure for $mm \neq nn$, we also obtain

$$\begin{aligned} F_x^{zzyy} &= F_z^{zzzz} = F_y^{yyzz} \\ F_y^{zzyy} &= F_x^{zzzz} = F_z^{yyzz} \\ F_z^{zzyy} &= F_y^{zzzz} = F_x^{yyzz} \end{aligned} \qquad (D.1.9a-c)$$

and

$$\begin{aligned} F_x^{yyzz} &= F_z^{zzzz} = F_y^{zzyy} \\ F_y^{yyzz} &= F_x^{zzzz} = F_z^{zzyy} \\ F_z^{yyzz} &= F_y^{zzzz} = F_x^{zzyy} \end{aligned} \qquad (D.1.10a-c)$$

Therefore 27 coefficients in Group 1 have been reduced to 9 coefficients by using the transformation A_{ij} of (D.1.2a).

We now use the transformation B_{ij} of (D.1.2b). The procedure is the same. After using B_{ij}, (D.1.3) becomes

$$\begin{aligned} F_j^{mmnn} = {} & B_{jb}B_{mc}B_{md}B_{ng}B_{nh}\frac{1}{\Omega}\int_\Gamma \bar{a}_{ibcd}\frac{\partial \bar{\phi}_k^{gh}}{\partial x_i^A}\bar{N}_k^s dS \\ & + B_{jb}B_{mc}B_{md}B_{ng}B_{nh}\frac{1}{\Omega}\int_\Gamma \bar{a}_{ibpq}\bar{e}_{pq}(\bar{\phi}^{cd})\frac{\partial \bar{\phi}_k^{gh}}{\partial x_i^A}\bar{N}_k^s dS \end{aligned} \qquad (D.1.11)$$

If we apply (D.1.11) with (D.1.2b) to some coefficients in (D.1.8), there follows that

$$F_y^{zzzz} = F_y^{zzzz}, \quad F_z^{zzzz} = -F_x^{zzzz}, \quad F_z^{zzzz} = -F_x^{zzzz} \qquad (D.1.12)$$

Comparing (D.1.12) with (D.1.8), we have

$$F_i^{zzzz} = 0 \qquad (i = x, y, z) \qquad (D.1.13)$$

Similarly, use of (D.1.11) in (D.1.9) and (D.1.10) gives

$$F_z^{zzyy} = F_z^{zzyy}, \quad F_y^{zzyy} = F_y^{zzyy}, \quad F_z^{zzyy} = -F_z^{zzyy} \qquad (D.1.14)$$

$$F_z^{zzzz} = -F_z^{zzzz}, \quad F_z^{zzzz} = F_z^{zzzz}, \quad F_y^{zzzz} = F_y^{zzzz} \qquad (D.1.15)$$

Comparing (D.1.14) with (D.1.9) and (D.1.10), we get

$$F_z^{zzyy} = F_y^{yyzz}, \quad F_y^{zzyy} = F_z^{yyzz}, \quad F_z^{zzyy} = -F_z^{yyzz} \qquad (D.1.16)$$

Also comparing (D.1.15) with (D.1.9) and (D.1.10), we have

$$F_z^{zzyy} = -F_y^{yyzz}, \quad F_y^{zzyy} = -F_z^{yyzz}, \quad F_z^{zzyy} = F_z^{yyzz} \qquad (D.1.17)$$

Equations (D.1.16) and (D.1.17) show that all coefficients in (D.1.9) and (D.1.10) vanish,e.g.

$$F_i^{zzyy} = F_i^{yyzz} = F_i^{zzzz} = F_i^{yyzz} = F_i^{zzyy} = F_i^{yyzz} = 0 \qquad (D.1.18)$$

Therefore all of the 27 coefficients in Group 1 vanish identically.

Vanishing of F_j^{mmgh} in Group 2.

The coefficients in Group 2 are as follows.

$$\begin{array}{lll} F_j^{zzzy}, & F_j^{zzyz}, & F_j^{zzzz} \\ F_j^{yyzy}, & F_j^{yyyz}, & F_j^{yyzz} \\ F_j^{zzzy}, & F_j^{zzyz}, & F_j^{zzzz} \end{array} \qquad (D.1.19)$$

In (D.1.19) there are 27 coefficients. If the first and second indices and the third and fourth indices are switched, there are another set of 27 coefficients. It suffices to show the vanishing of the coefficients in (D.1.19).

For transformation A_{ij}, (D.1.3) is written for Group 2 as

$$F_j^{mmgh} = A_{jb}A_{mc}A_{md}A_{gr}A_{hs}F_b^{cdrs} \qquad (D.1.20)$$

Let us apply (D.1.20) to the coefficients in (D.1.19). After using A_{ij} of (D.1.2a), we obtain the following relations.

$$\begin{aligned} &F_x^{zzzy} = F_z^{zzzx}, \quad F_y^{zzzy} = F_x^{zzzx}, \quad F_z^{zzzy} = F_y^{zzzx} \\ &F_x^{zzyz} = F_z^{zzzy}, \quad F_y^{zzyz} = F_x^{zzzy}, \quad F_z^{zzyz} = F_y^{zzzy} \\ &F_x^{zzxz} = F_z^{zzyz}, \quad F_y^{zzxz} = F_x^{zzyz}, \quad F_z^{zzxz} = F_y^{zzyz} \end{aligned} \tag{D.1.21}$$

and

$$\begin{aligned} &F_x^{yyzy} = F_z^{zzzx}, \quad F_y^{yyzy} = F_x^{zzzx}, \quad F_z^{yyzy} = F_y^{zzzx} \\ &F_x^{yyyz} = F_z^{zzzy}, \quad F_y^{yyyz} = F_x^{zzzy}, \quad F_z^{yyyz} = F_y^{zzzy} \\ &F_x^{yyzz} = F_z^{zzyz}, \quad F_y^{yyzz} = F_x^{zzyz}, \quad F_z^{yyzz} = F_y^{zzyz} \end{aligned} \tag{D.1.22}$$

Combining (D.1.21) and (D.1.22), we have

$$\begin{aligned} &F_x^{zzzy} = F_y^{yyyz} = F_z^{zzzx} \\ &F_y^{zzzy} = F_z^{yyyz} = F_x^{zzzx} \\ &F_z^{zzzy} = F_x^{yyyz} = F_y^{zzzx} \end{aligned} \tag{D.1.23a-c}$$

$$\begin{aligned} &F_x^{zzyz} = F_y^{yyzz} = F_z^{zzzy} \\ &F_y^{zzyz} = F_z^{yyzz} = F_x^{zzzy} \\ &F_z^{zzyz} = F_x^{yyzz} = F_y^{zzzy} \end{aligned} \tag{D.1.24a-c}$$

$$\begin{aligned} &F_x^{zzxz} = F_y^{yyzy} = F_z^{zzyz} \\ &F_y^{zzxz} = F_z^{yyzy} = F_x^{zzyz} \\ &F_z^{zzxz} = F_x^{yyzy} = F_y^{zzyz} \end{aligned} \tag{D.1.25a-c}$$

Under the transformation B_{ij}, the coefficient becomes

$$F_j^{mmgh} = B_{jb}B_{mc}B_{md}B_{gr}B_{hs}F_b^{cdrs} \tag{D.1.26}$$

Applying (D.1.26) to some of the coefficients in (D.1.24), we get

$$\begin{aligned} &F_x^{zzyz} = -F_z^{zzzy}, \quad F_x^{zzyz} = -F_x^{zzyz} \\ &F_y^{zzyz} = -F_y^{zzzy}, \quad F_y^{zzyz} = -F_z^{zzyz} \\ &F_z^{zzyz} = F_z^{zzzy}, \quad F_z^{zzyz} = F_y^{zzyz} \end{aligned} \tag{D.1.27}$$

where the relations (D.1.24a-c) have been used. Thus we have

$$F_x^{zzyz} = F_y^{zzyz} = F_z^{zzyz} = 0 \qquad (D.1.28)$$

and the coefficient in (D.1.24) vanish. Similarly if we apply (D.1.26) to (D.1.23) and (D.1.25), we obtain

$$\begin{aligned} &F_x^{zzzy} = F_z^{zzyz}, \quad F_x^{zzzy} = F_x^{zzzz} \\ &F_y^{zzzy} = F_y^{zzyz}, \quad F_y^{zzzy} = F_z^{zzzz} \qquad (D.1.29a-c) \\ &F_z^{zzzy} = -F_x^{zzyz}, \quad F_z^{zzzy} = -F_y^{zzzz} \end{aligned}$$

$$\begin{aligned} &F_x^{zzzz} = -F_z^{zzzz}, \quad F_x^{zzzz} = -F_x^{zzzy} \\ &F_y^{zzzz} = -F_y^{zzzz}, \quad F_y^{zzzz} = -F_z^{zzzy} \qquad (D.1.30a-c) \\ &F_z^{zzzz} = F_x^{zzzz}, \quad F_z^{zzzz} = F_y^{zzzy} \end{aligned}$$

$$\begin{aligned} &F_x^{zzyz} = -F_z^{zzzy}, \quad F_y^{zzzz} = -F_z^{zzzy} \\ &F_y^{zzyz} = -F_y^{zzzy}, \quad F_z^{zzzz} = -F_y^{zzzy} \qquad (D.1.31a-c) \\ &F_z^{zzyz} = F_x^{zzzy}, \quad F_x^{zzzz} = F_x^{zzzy} \end{aligned}$$

It then follows from (D.1.29a) and (D.1.30a) and (D.1.29b) and (D.1.31b) that

$$F_x^{zzzy} = F_y^{zzzy} = F_x^{zzzz} = F_z^{zzzz} = 0 \qquad (D.1.32)$$

By using (D.1.28) and (D.1.32) in (D.1.23) to (D.1.25), there remains only one coefficient

$$F_z^{zzzy}(= F_x^{yyyz} = F_y^{zzzz}) = F_y^{zzzz}(= F_z^{yyzy} = F_x^{zzyz}) \qquad (D.1.33)$$

The vanishing of F_z^{zzzy} will be shown by using symmetry and sign relations of the solutions of the elastostatic problems of Fig. C.2 among the sectors.

We first show the symmetry relations of ϕ_i^{zz} and the associated stresses in Fig. D.1 among the sectors A, D and E. It is readily obtained from Fig. C.2(a).

Likewise from Fig. C.(d), the symmetry relations of ϕ_i^{xy} and the associated stresses are summarized in Fig. D.3. From (D.1.1) the coefficient F_z^{xxzy} is written as

$$\begin{aligned}
F_z^{xxzy} =& \frac{1}{\Omega}\int_\Gamma a_{zzzz}\frac{\partial \phi_k^{xy}}{\partial z}N_k^s dS + \frac{1}{\Omega}\int_\Gamma \sigma_{iz}(\phi^{xx})\frac{\partial \phi_k^{xy}}{\partial x_i}N_k^s dS \\
=& \frac{1}{\Omega}\int_\Gamma a_{zzzz}\left(\frac{\partial \phi_x^{xy}}{\partial z}N_x^s + \frac{\partial \phi_y^{xy}}{\partial z}N_y^s + \frac{\partial \phi_z^{xy}}{\partial z}N_z^s\right) dS \\
&+ \frac{1}{\Omega}\int_\Gamma \left[\sigma_{zz}(\phi^{xx})\frac{\partial \phi_x^{xy}}{\partial x} + \sigma_{yz}(\phi^{xx})\frac{\partial \phi_x^{xy}}{\partial y} + \sigma_{zz}(\phi^{xx})\frac{\partial \phi_x^{xy}}{\partial z}\right] N_x^s \quad (D.1.38) \\
&+ \frac{1}{\Omega}\int_\Gamma \left[\sigma_{zz}(\phi^{xx})\frac{\partial \phi_y^{xy}}{\partial x} + \sigma_{yz}(\phi^{xx})\frac{\partial \phi_y^{xy}}{\partial y} + \sigma_{zz}(\phi^{xx})\frac{\partial \phi_y^{xy}}{\partial z}\right] N_y^s \\
&+ \frac{1}{\Omega}\int_\Gamma \left[\sigma_{zz}(\phi^{xx})\frac{\partial \phi_z^{xy}}{\partial x} + \sigma_{yz}(\phi^{xx})\frac{\partial \phi_z^{xy}}{\partial y} + \sigma_{zz}(\phi^{xx})\frac{\partial \phi_z^{xy}}{\partial z}\right] N_z^s
\end{aligned}$$

From Fig. D.1 and D.2, it is shown that the first three lines in (D.1.38) cancel out between sectors A and D and the last line similarly cancels out between sectors A and E. Clearly the same kind of cancellation occurs in other sectors. So the coefficient F_z^{xxzy} vanishes. Therefore all the coefficients in Group 2 vanish identically.

The vanishing of the coefficients in Groups 3 and 4 can be shown in the same manner and is omitted here.

D.2 Vanishing of J'_{jmn}

From (3.3.26) the coefficient J'_{jmn} becomes

$$J_j^{mn} = \frac{1}{\Omega}\int_\Gamma \frac{\partial k_{ij}}{\partial x_k}\phi_k^{mn}N_i dS \qquad (D.2.1)$$

where the second and third indices have been placed in the upper right corner. Since $mn = \{xx, yy, zz, xy, yz, zx\}$, there are 18 coefficients in (D.2.1). We consider first the case with $m = n$ and apply the transformation relations as follows.

$$J_j^{mn} = A_{jb}A_{mc}A_{md}J_b^{cd} \qquad (D.2.2)$$

For $mm = xx$, after using (D.1.2a), we have

$$J_x^{xx} = J_z^{zz} \quad , \quad J_y^{xx} = J_x^{zz} \quad , \quad J_z^{xx} = J_y^{zz} \qquad (D.2.3)$$

Also for $mm = yy$,

$$J_x^{yy} = J_z^{zz} \quad , \quad J_y^{yy} = J_x^{zz} \quad , \quad J_z^{yy} = J_y^{zz} \tag{D.2.4}$$

Combining (D.2.3) and (D.2.4),

$$\begin{aligned} J_x^{zz} &= J_z^{zz} = J_y^{yy} \\ J_y^{zz} &= J_x^{zz} = J_z^{yy} \\ J_z^{zz} &= J_y^{zz} = J_x^{yy} \end{aligned} \tag{D.2.5a-c}$$

Similarly if we apply the transformation (D.1.2b), we get

$$J_j^{mn} = B_{jb} B_{mc} B_{md} J_b^{cd} \tag{D.2.6}$$

from which we obtain

$$\begin{aligned} J_x^{zz} = J_z^{zz} \quad , \quad J_y^{zz} = J_y^{zz} \quad , \quad J_z^{zz} = -J_x^{zz} \\ J_x^{zz} = J_z^{zz} \quad , \quad J_y^{zz} = J_y^{zz} \quad , \quad J_z^{zz} = -J_x^{zz} \end{aligned} \tag{D.2.7a,b}$$

From (D.2.5a and b) and (D.2.7a), we have

$$J_y^{zz} = J_z^{zz} \quad , \quad J_z^{zz} = -J_y^{zz} \tag{D.2.8}$$

Also from (D.2.7b) and (D.2.5)

$$J_x^{zz} = -J_x^{zz} \tag{D.2.9}$$

Thus the coefficients in (D.2.5) all vanish.

For the coefficients with $m \neq n$, the coordinate transformation is used in the same manner. After using the transformation matrix A_{ij} in (D.1.2a), we get

$$\begin{aligned} J_x^{zy} = J_z^{zz} \quad , \quad J_y^{zy} = J_x^{zz} \quad , \quad J_z^{zy} = J_y^{zz} \\ J_x^{yz} = J_z^{zy} \quad , \quad J_y^{yz} = J_x^{zy} \quad , \quad J_z^{yz} = J_y^{zy} \end{aligned}$$

which gives

$$\begin{aligned} J_x^{zy} &= J_z^{zz} = J_y^{yz} \\ J_y^{zy} &= J_x^{zz} = J_z^{yz} \\ J_z^{zy} &= J_y^{zz} = J_x^{yz} \end{aligned} \tag{D.2.10}$$

Similarly after using the transformation matrix B_{ij} of (D.1.2b), we have

$$J_y^{xy} = J_y^{yz} \quad , \quad J_z^{xy} = -J_z^{yz}$$
$$J_x^{yz} = -J_x^{xy} \quad , \quad J_y^{yz} = -J_y^{xy} \qquad (D.2.11a,b)$$

It then follows from (D.2.10) and (D.2.11) that the coefficients in (D.2.10) vanish. Therefore all of the 18 coefficients in J_j^{mn} vanish.

D.3 Vanishing of S'_{mnk}

From (3.4.13) for isotropic thermal conductivities on the microscale, the coefficient S'_{mnk} becomes

$$S_k^{mn} = \frac{1}{\Omega}\left[m^f \int_\Gamma \phi_j^{mn} \frac{\partial}{\partial x_j}\left(\frac{\partial A_k^f}{\partial x_i}\right) N_i dS - M_r m^s \int_\Gamma \phi_j^{mn} \frac{\partial}{\partial x_j}\left(\frac{\partial A_k^s}{\partial x_i}\right) N_i dS\right] \qquad (D.3.1)$$

Equation (D.3.1) is of the form (D.2.1),e.g. the indices mn are from ϕ_j^{mn} and the other index is for the component of the microscale varying vector $A_k^{f,s}$. Therefore by complete analogy, the same procedure as in §D.2 proves the vanishing of the coefficients S_k^{mn} It is omitted here.

In Appendix D, the vanishing of some typical coefficients of the nonlinearly coupled terms in the macroscale governing equations has been shown for a cubic microcell geometry with three planes of symmetry. We note that the vanishing of the coefficients is strictly the consequence of the symmetry of the cell geometry.

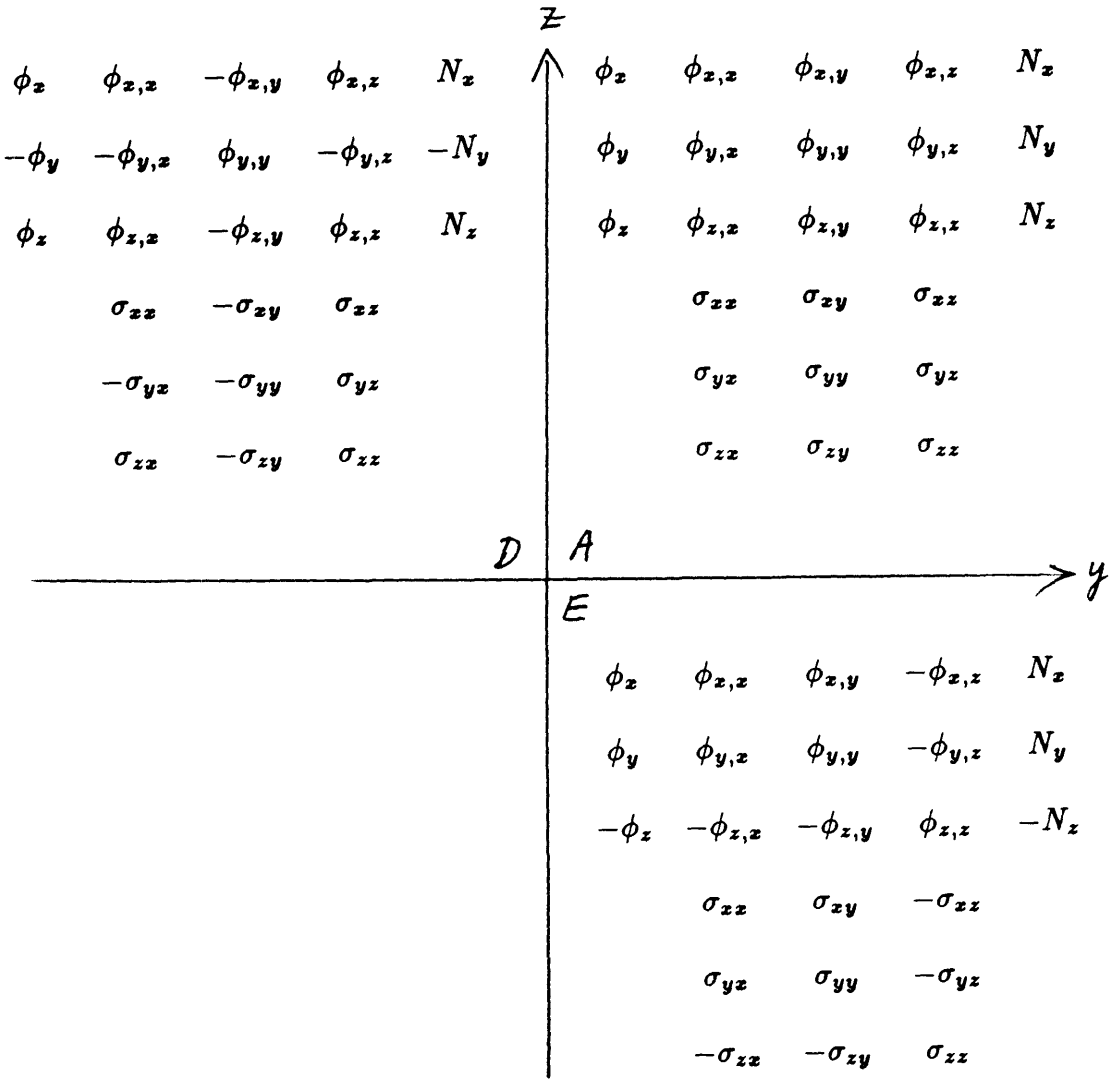

Fig. D.1 The symmetry relations for ϕ_i^{xx}, its derivatives and the stresses at the points located symmetrically about the planes $y = 0$ and $z = 0$. The superscripts 'xx' have been omitted.

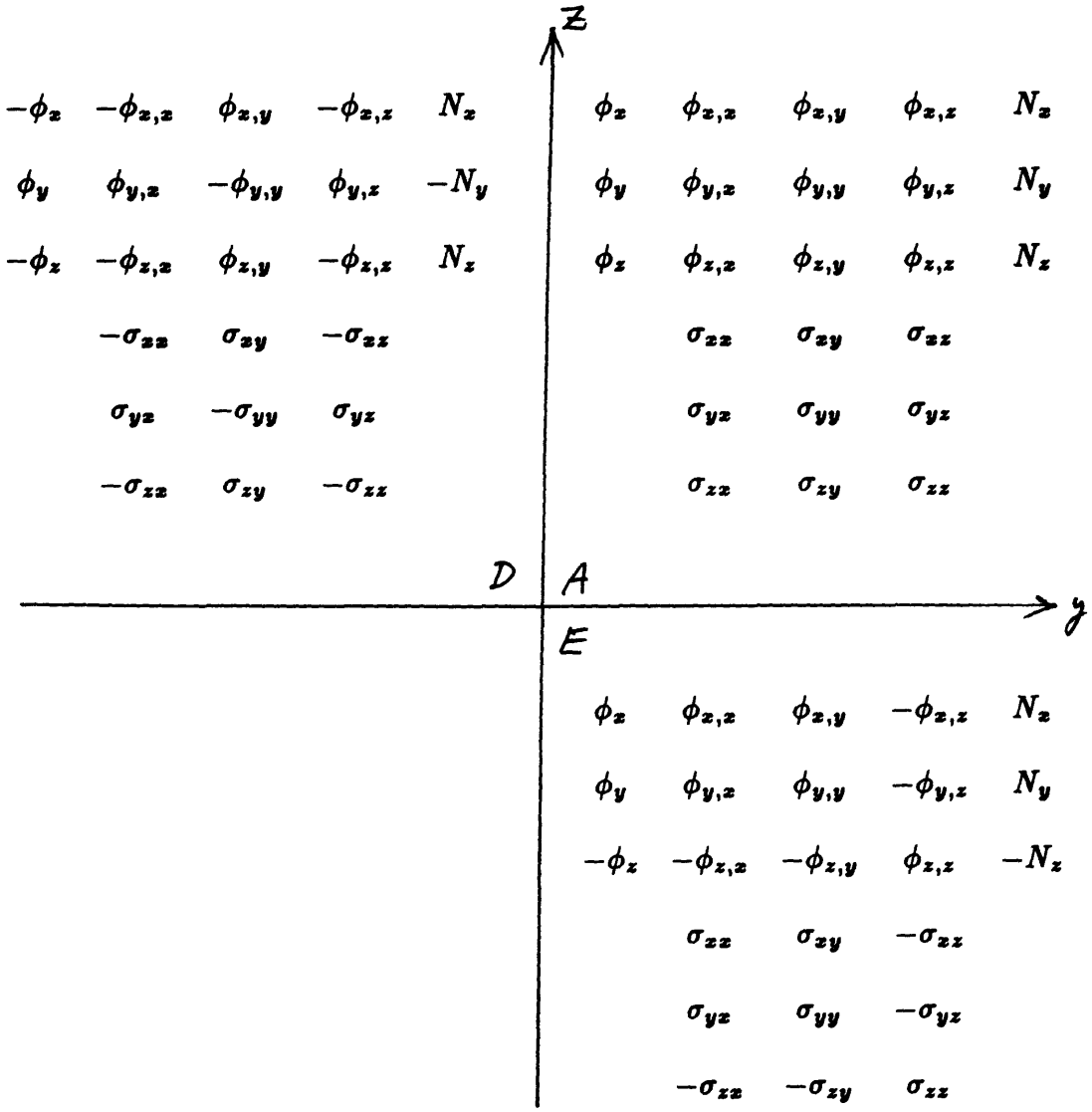

Fig. D.2 The symmetry relations for ϕ_i^{xy} its derivatives and the stresses at the points located symmetrically about the planes $y = 0$ and $z = 0$. The superscripts 'xy' have been omitted.

Appendix E. Finite Element Approximation for J_s.

It is customary in the finite element approximation of elasticity problems to use vectorial form of strains and stresses. The strains are written as

$$\epsilon = \begin{Bmatrix} e_{xx} \\ e_{yy} \\ e_{zz} \\ 2e_{xy} \\ 2e_{yz} \\ 2e_{zx} \end{Bmatrix} = \mathbf{D}\phi = \mathbf{D} \begin{Bmatrix} \phi_x \\ \phi_y \\ \phi_z \end{Bmatrix} \tag{E.1}$$

where

$$\mathbf{D} = \begin{bmatrix} \frac{\partial}{\partial x} & 0 & 0 \\ 0 & \frac{\partial}{\partial y} & 0 \\ 0 & 0 & \frac{\partial}{\partial z} \\ \frac{\partial}{\partial y} & \frac{\partial}{\partial x} & 0 \\ 0 & \frac{\partial}{\partial z} & \frac{\partial}{\partial y} \\ \frac{\partial}{\partial z} & 0 & \frac{\partial}{\partial x} \end{bmatrix} \tag{E.2}$$

The stress-strain relation then becomes

$$\sigma = \mathbf{E}\epsilon \tag{E.3}$$

where $\mathbf{E}$ is the elastic coefficient matrix so that

$$\sigma = \begin{Bmatrix} \sigma_{xx} \\ \sigma_{yy} \\ \sigma_{zz} \\ \sigma_{xy} \\ 2\sigma_{yz} \\ 2\sigma_{zx} \end{Bmatrix} \quad \text{and} \quad \mathbf{E} = \begin{bmatrix} E_{11} & E_{12} & E_{12} & 0 & 0 & 0 \\ & E_{11} & E_{12} & 0 & 0 & 0 \\ & & E_{11} & 0 & 0 & 0 \\ & & & E_{44} & 0 & 0 \\ & \text{sym.} & & & E_{44} & 0 \\ & & & & & E_{44} \end{bmatrix} \tag{E.4}$$

where

$$E_{11} = \frac{1-\nu}{(1+\nu)(1-2\nu)}, \quad E_{12} = \frac{\nu}{(1+\nu)(1-2\nu)}, \quad E_{44} = \frac{1}{2(1+\nu)} \tag{E.5}$$

Substituting (E.1) into (E.3), the stress is expressed in terms of the displacement component vector as

$$\sigma = (\mathbf{ED})\,\phi \tag{E.6}$$

The solid region will be discretized by linear tetrahedra. The use of higher order shape functions only requires minor changes in the shape function. In a linear

tetrahedron, there are four local nodes 1,2,3 and 4. The nodes are numbered in such a way that, when viewed from node 4, the nodes 1, 2 and 3 are arranged counterclockwise. The natural coordinates are defined by

$$\xi_1 = \frac{V_{234P}}{V}, \quad \xi_2 = \frac{V_{341P}}{V}, \quad \xi_3 = \frac{V_{124P}}{V}, \quad \xi_4 = \frac{V_{123P}}{V} \tag{E.7}$$

where V is the volume of tetrahedron so that they are constrained by the relation

$$\xi_1 + \xi_2 + \xi_3 + \xi_4 = 1 \tag{E.8}$$

They are also called the volume coordinates.

In the following, we shall use isoparametric formulation,e.g. both the spatial coordinates and the unknowns are represented by the same shape functions which depend on the natural coordinates of (E.7).

If we let the shape functions be

$$N_1 = \xi_1, \quad N_2 = \xi_2, \quad N_3 = \xi_3, \quad N_4 = \xi_4 = 1 - (\xi_1 + \xi_2 + \xi_3) \tag{E.9}$$

so that N_i is unity at node i and decreases linearly as P in Fig. E.1 moves away from node i becoming zero at nodes $j \neq i$, vector quantity ϕ is approximated in the linear tetrahedron by

$$\phi = \begin{Bmatrix} \phi_x \\ \phi_y \\ \phi_z \end{Bmatrix} = \mathbf{Nq} \tag{E.10}$$

where the shape function matrix $\mathbf{N}$ and nodal unknown vector $\mathbf{q}$ are respectively given by

$$\mathbf{N} = \begin{bmatrix} N_1 & 0 & 0 & N_2 & 0 & 0 & N_3 & 0 & 0 & N_4 & 0 & 0 \\ 0 & N_1 & 0 & 0 & N_2 & 0 & 0 & N_3 & 0 & 0 & N_4 & 0 \\ 0 & 0 & N_1 & 0 & 0 & N_2 & 0 & 0 & N_3 & 0 & 0 & N_4 \end{bmatrix} \tag{E.11}$$

and

$$\mathbf{q} = [\phi_x^1 \quad \phi_y^1 \quad \phi_z^1 \quad \phi_x^2 \quad \phi_y^2 \quad \phi_z^2 \quad \phi_x^3 \quad \phi_y^3 \quad \phi_z^3 \quad \phi_x^4 \quad \phi_y^4 \quad \phi_z^4]^T \tag{E.12}$$

The superscript i in (E.12) denotes the local node number. The total degrees of freedom in a linear tetrahedral element are then 12.

The derivatives in the global coordinates x_i and in the natural coordinates ξ_i are related by, for a scalar function f,

$$\nabla_\xi f = [J]\nabla_x f = \frac{\partial(x,y,z)}{\partial(\xi_1,\xi_2,\xi_3)}\nabla_x f \tag{E.13}$$

or

$$\nabla_x f = [J]^{-1}\nabla_\xi f = \frac{\text{Cof.(J)}}{|J|}\nabla_\xi f = \frac{1}{|J|}f'_{,\xi} \tag{E.14}$$

where $[J]$ is the Jacobian matrix and Cof is the cofactor. If we substitute (E.10) into (E.1) and (E.6), it follows that

$$\begin{aligned} \epsilon &= \mathbf{D}\phi = \frac{1}{|J|}(\mathbf{DN})'\,\phi \\ \sigma &= \mathbf{E}\epsilon = \frac{1}{|J|}\mathbf{E}\,(\mathbf{DN})'\,\phi \end{aligned} \tag{E.15}$$

where $(\mathbf{DN})'$ is the matrix given by

$(\mathbf{DN})' =$ matrix

$$\begin{matrix} N'_{1,1} & 0 & 0 & N'_{2,1} & 0 & 0 & N'_{3,1} & 0 & 0 & N'_{4,1} & 0 & 0 \\ 0 & N'_{1,2} & 0 & 0 & N'_{2,2} & 0 & 0 & N'_{3,2} & 0 & 0 & N'_{4,2} & 0 \\ 0 & 0 & N'_{1,3} & 0 & 0 & N'_{2,3} & 0 & 0 & N'_{3,3} & 0 & 0 & N'_{4,3} \\ N'_{1,2} & N'_{1,1} & 0 & N'_{2,2} & N'_{2,1} & 0 & N'_{3,2} & N'_{3,1} & 0 & N'_{4,2} & N'_{4,1} & 0 \\ 0 & N'_{1,3} & N'_{1,2} & 0 & N'_{2,3} & N'_{2,2} & 0 & N'_{3,3} & N'_{3,2} & 0 & N'_{4,3} & N'_{4,2} \\ N'_{1,3} & 0 & N'_{1,1} & N'_{2,3} & 0 & N'_{2,1} & N'_{3,3} & 0 & N'_{3,1} & N'_{4,3} & 0 & N'_{4,1} \end{matrix} \tag{E.16}$$

in which $N'_{i,j} = \partial N_i/\partial\xi_j$ is calculated by (E.14).

The functional J_s in (6.1.6) for a single element then becomes

$$\begin{aligned} (J_s)_n &= \int_{\Omega_n} \frac{1}{2}\mathbf{e}_n^T\sigma_n d\Omega - \int_{\Gamma_n}\phi_n^T\mathbf{T}_n dS \\ &= \int_{\Omega_n}\frac{1}{2}\frac{1}{|J|}\left[(\mathbf{DN})'_n\,\phi_n\right]^T\mathbf{E}\frac{1}{|J|}\left[(\mathbf{DN})'_n\,\phi_n\right]|J|d\Omega_\xi - \int_{\Gamma_n}(\mathbf{N}\phi_n)_n^T\mathbf{T}_n dS \end{aligned} \tag{E.17}$$

where $d\Omega_\xi = d\xi_1 d\xi_2 d\xi_3$. If (E.17) is summed over the elements, we get

$$J_s = \sum_{n=1}^{M}(J_s)_n = \sum_{n=1}^{M}\left(\phi_n^T\mathbf{k}_n\phi_n - \phi_n^T\mathbf{Q}_n\right) \tag{E.18}$$

where

$$\mathbf{k}_n = \int_{\Omega_n} (\mathbf{DN})'^T_n \mathbf{E} (\mathbf{DN})'_n \frac{1}{|J|_n} d\xi_1 d\xi_2 d\xi_3$$
$$\mathbf{Q}_n = \int_{\Gamma_n} \mathbf{N}^T \mathbf{T}_n dS \qquad (E.19)$$

are the element stiffness matrix and the traction force vector(on Γ) respectively.

Finally by taking the variation of (E.18), we obtain

$$\mathbf{K}_\phi \mathbf{q}(\phi) = \mathbf{Q}_\phi \qquad (E.20)$$

which is (6.3.1) and $\mathbf{K}_\phi$, $\mathbf{q}_\phi$ and $\mathbf{Q}_\phi$ are given in (6.3.2). It is a system of algebraic equations for the nodal degrees of freedom $\phi^i_{x_j}$ for $x_j = x, y, z$ and $i = 1, 2, \cdots, N_t$, where N_t is the total number of nodes.

Appendix F. Lapwood Theory of Linear Stability in a Horizontal Porous Layer with Vertical Temperature Gradient.

For convenience of reference we outline Lapwood theory here. At the initial state, the pore fluid is at rest and the temperature $\overline{T}(z)$ is linear in z. But in the case of through flow which will be mentioned at the end, $\partial\overline{T}(z)/\partial z$ varies with z.

It is assumed that the heat capacity, permeability and thermal conductivity are constant and the disturbances are small. For rigid medium, the consolidation equation (3.7.11) reduces to

$$\nabla \cdot \mathbf{u} = 0 \tag{F.1}$$

where the fluid velocity is given by

$$\mathbf{u} = -\tilde{k}\left(\nabla p - \rho_f g \beta_T \theta \mathbf{e}_z\right) \tag{F.2}$$

Similarly the heat equation (3.7.13) becomes

$$\overline{\rho C_p}\frac{\partial \theta}{\partial t} + (\rho C_p)_f \langle \mathbf{u} \rangle \cdot \left(\nabla\theta + \nabla\overline{T}\right) = \tilde{m}' \nabla^2 \theta \tag{F.3}$$

We choose the following normalization scales

$$x, y, z \sim h, \quad t \sim h^2/\kappa_m, \quad \mathbf{u} \sim \kappa_m/h, \quad p \sim \kappa_m/\tilde{k}, \quad \theta \sim \Theta \tag{F.4}$$

in which

$$\kappa_m = \tilde{m}'/\overline{\rho C_p} \tag{F.5}$$

is the thermal diffusivity based on the thermal conductivity and the heat capacity of the medium and h and Θ are the depth and temperature difference across the depth respectively.

If (F.4) is used and the first order terms are retained in (F.1) - (F.3), it follows in dimensionless variables that

$$\nabla \cdot \mathbf{u} = 0 \tag{F.6}$$

$$\mathbf{u} = (u, v, w) = -\left(\nabla p - Ra\theta \mathbf{e}_z\right) \tag{F.7}$$

$$\frac{\partial \theta}{\partial t} + \frac{1}{\overline{\rho C_p}^*} w \frac{\partial \overline{T}}{\partial z} = \nabla^2 \theta \tag{F.8}$$

where Ra is the Rayleigh number $Ra = \rho_f g \tilde{k} \beta_T \Theta h / \kappa_m$ and $\partial \overline{T} / \partial z$ and $\overline{\rho C_p}^* = \overline{\rho C_p} / (\rho C_p)_f$ are the initial temperature gradient(which is actually -1) and the medium heat capacity normalized by that of the fluid.

We now use the following identity from vector calculus

$$\nabla \times (\nabla \times \mathbf{f}) = \nabla(\nabla \cdot \mathbf{f}) - \nabla^2 \mathbf{f} \qquad (F.9)$$

where $\mathbf{f}$ is any vector quantity. With the help of (F.6) and (F.9) and the fact that the curl of a gradient is zero, it follows from the z-component of (F.7) that

$$\nabla^2 w = R \nabla_2^2 \theta \qquad (F.10)$$

where $\nabla_2^2 = \partial^2/\partial x^2 + \partial^2/\partial y^2$ is the Laplacian in the xy plane. Assume for the perturbation quantities w and θ

$$\begin{aligned} w &= \Gamma(z) e^{i\ell x + imy} e^{nt} \\ \theta &= Z(z) e^{i\ell x + imy} e^{nt} \end{aligned} \qquad (F.11)$$

Substituting (F.11) into (F.10) and (F.8), we obtain

$$\left(-\ell^2 - m^2 + \frac{\partial^2}{\partial z^2}\right) \Gamma(z) = Ra \left(-\ell^2 - m^2\right) Z(z) \qquad (F.12)$$

$$-nZ(z) + \frac{1}{\overline{\rho C_p}^*} \frac{\partial \overline{T}}{\partial z} \Gamma(z) = \left(-\ell^2 - m^2 + \frac{\partial^2}{\partial z^2}\right) Z(z) \qquad (F.13)$$

We shall only examine marginal stability and set $n = 0$, corresponding to disturbances which neither die down nor grow exponentially.

If the boundaries at $z = 0$ and $z = 1$ are impermeable and isothermal, we impose

$$\Gamma = Z = 0 \qquad \text{at} \quad z = 0, 1 \qquad (F.14)$$

These are satisfied by

$$Z(z) = A \sin s\pi z \qquad (F.15)$$

Substituting (F.15) into (F.12) and (F.13) and combining them, we get the eigenvalue condition

$$\frac{Ra}{\overline{\rho C_p}^*} = \frac{(\alpha^2 + s^2\pi^2)^2}{\alpha^2} \qquad (F.16)$$

where $\alpha^2 = \ell^2 + m^2$ (cf.(F.11)) and α is the wave number in the horizontal direction. The minimum value of Ra occurrs when $s = 1$ and $\alpha = \pi$:

$$\frac{R_c}{\overline{\rho C_p}^*} = 4\pi^2 \qquad (F.17)$$

If $m = \pi$ or $\ell = \pi$, the wavelength of a pair of counter-rotating cells(one wavelength) becomes 2 and the height to width ratio of a cell is one. The axes of convection rolls are then parallel to either x or y axis. If $\ell = m$ so that $\alpha^2 = (\alpha_x^2 + \alpha_y^2)$ with $\alpha_x = \alpha_y$, the convection cells are square in plan form and the width of a cell in a cross-section parallel to x or y axis is $\sqrt{2}$, since $2\alpha_x^2 = \pi^2$ which shows that the half wavelength is $\pi/\alpha_x = \sqrt{2}$(Lapwood, 1948). It is also possible to have hexagonal cell shape when θ is written, for the same wave number $\alpha = \pi$, as

$$\theta = A \sin\frac{\pi z}{h}\left[\cos\alpha x + 2\cos\frac{\alpha x}{2}\cos\frac{\sqrt{3}\alpha y}{2}\right]$$

for which sidelength of the hexagon to depth ratio is 1.33(Combarnous and Bories, 1975).

Other boundary conditions lead to different eigenvalue conditions. When the pressure on the upper boundary is constant and the temperature is still constant at $z = 0$ and $z = 1$, we have from the Darcy's law (F.7) that

$$\begin{aligned} Z &= \Gamma = 0 \qquad \text{at} \quad z = 0 \\ Z &= d\Gamma/dz = 0 \qquad \text{at} \quad z = 1 \end{aligned} \qquad (F.18)$$

the second of which is obtained after using the continuity equation (F.6) at $z = 1$ which implies, since $p = 0$, $\partial u/\partial x = \partial v/\partial y = 0$ and thus $\partial w/\partial z = 0$. In this case (F.12) and (F.13) can be solved graphically and the corresponding critical Rayleigh number is (Lapwood, 1948)

$$\frac{R}{\overline{\rho C_p}^*} = 27.1 \qquad (F.19)$$

Assuming $\ell = m$, Lapwood obtains the width in a cross-section in xz plane to be given by 1.91 which means the horizontal wave number is reduced as compared to the case of impermeable boundaries.

If there exists uniform vertical through flow in the medium, (F.13) becomes

$$-nZ(z) + \frac{1}{\overline{\rho C_p}^*}\frac{\partial \overline{T}}{\partial z}\Gamma(z) = \left[\left(-\ell^2 - m^2 + \frac{\partial^2}{\partial z^2}\right) - P\frac{\partial}{\partial z}\right] Z(z) \qquad (F.20)$$

where $P = Uh/\kappa_m$ is the Peclet number for the uniform through flow. The results are discussed in the main text(§7.1).

Appendix G. Finite Difference Equations for Thermoconsolidation.

Finite difference forms of the governing equations and boundary conditions are derived here. For a scalar variable f its spatial derivatives are approximated by using centered difference for which the truncation error is $O(\Delta^2)$ where Δ is grid spacing. Let $f_{i,j}$ be the value of f at node (i,j) which is located at $\xi = (i-1)\Delta\xi$ and $z = (j-1)\Delta z$. The derivatives then become

$$\begin{aligned}\left(\frac{\partial f}{\partial \xi}\right)_{i,j} &= \frac{1}{2\Delta\xi}\left(f_{i+1,j} - f_{i-1,j}\right) + O(\Delta\xi^2) \\ \left(\frac{\partial^2 f}{\partial \xi^2}\right)_{i,j} &= \frac{1}{\Delta\xi^2}\left(f_{i+1,j} - 2f_{i,j} + f_{i-1,j}\right) + O(\Delta\xi^2)\end{aligned} \tag{G.1}$$

in which the error terms are the consistency of the finite difference approximations and are from the truncation of Taylor expansion of f. For z derivatives one simply replaces $\Delta\xi$,i and j by Δz,j and i. Similarly the cross derivatives are approximated by

$$\begin{aligned}\left(\frac{\partial^2 f}{\partial \xi \partial z}\right)_{i,j} &= \frac{1}{4\Delta\xi\Delta z}\left(f_{i+1,j+1} - f_{i-1,j+1} - f_{i+1,j-1} + f_{i-1,j-1}\right) \\ &\quad + O(\Delta\xi^2, \Delta z^2, \Delta\xi\Delta z)\end{aligned} \tag{G.2}$$

If we substitute (G.1) and (G.2) into the x-component of the equilibrium equation (6.3.4), multiply by $(\Delta\xi)^2$ and collect temrs at the same nodes, it follows that

$$\begin{aligned}&e^{-\xi_i} XU12 u^{n+1}_{i-1,j} + XW11 w^{n+1}_{i-1,j-1} + XW13 w^{n+1}_{i-1,j+1} \\ &\qquad + XP12 p^{n+1}_{i-1,j} + XT12 \theta'^{n+1}_{i-1,j} \\ &+e^{\xi_i} XU21 u^{n+1}_{i,j-1} + \left(-2e^{-\xi_i} - e^{\xi_i} XU22\right) u^{n+1}_{i,j} + e^{\xi_i} XU23 u^{n+1}_{i,j+1} \\ &+e^{-\xi_i} XU32 u^{n+1}_{i+1,j} + XW31 w^{n+1}_{i+1,j-1} + XW33 w^{n+1}_{i+1,j+1} \\ &\qquad + XP32 p^{n+1}_{i+1,j} + XT32 \theta'^{n+1}_{i+1,j} = 0\end{aligned} \tag{G.3}$$

in which the iteration count k has been omitted. The variable ξ_i is the coordinate of i-th node in ξ direction. The coefficients in (G.3) are given by

$$\begin{aligned}&XU12 = 1 + \frac{\Delta\xi}{2}, \quad XW11 = -XW13 = -XW31 = XW33 = \frac{a_{II} + a_{III}}{a_I}\frac{\Delta\xi}{4\Delta z} \\ &XP12 = -XP32 = \frac{\alpha'}{a_I}\frac{\Delta\xi}{2}, \quad XT12 = -XT32 = \frac{b}{Ra}\frac{\beta'_i}{a_I}\frac{\Delta\xi}{2} \\ &XU21 = \frac{1}{2}XU22 = XU23 = \frac{a_{III}}{a_I}\frac{(\Delta\xi)^2}{(\Delta z)^2}, \quad XU32 = 1 - \frac{\Delta\xi}{2}\end{aligned} \tag{G.4}$$

Following the same procedure it is readily obtained for the z-component that

$$
\begin{aligned}
&ZU11u^{n+1}_{i-1,j-1} + ZU13u^{n+1}_{i-1,j+1} + e^{-\xi_i} ZW12w^{n+1}_{i-1,j} \\
&+e^{\xi_i} ZW21w^{n+1}_{i,j-1} + \left(-e^{\xi_i} ZW22 - 2e^{-\xi_i}\frac{a_{III}}{a_I}\right) w^{n+1}_{i,j} + e^{\xi_i} ZW23w^{n+1}_{i,j+1} \\
&+ e^{\xi_i}\left(ZP21p^{n+1}_{i,j-1} + ZP23p^{n+1}_{i,j+1} + ZT21\theta'^{n+1}_{i,j-1} + ZT22\theta'^{n+1}_{i,j} + ZT23\theta'^{n+1}_{i,j+1}\right) \\
&+ZU31u^{n+1}_{i+1,j-1} + ZU33u^{n+1}_{i+1,j+1} + e^{-\xi_i} ZW32w^{n+1}_{i+1,j} = 0
\end{aligned}
\tag{G.5}
$$

where

$$
\begin{aligned}
&ZU11 = -ZU13 = -ZU31 = ZU33 = XW11, \quad ZW12 = \frac{a_{III}}{a_I}\left(1 + \frac{\Delta\xi}{2}\right) \\
&ZW21 = \frac{1}{2}ZW22 = ZW23 = \frac{(\Delta\xi)^2}{(\Delta z)^2} \\
&ZP21 = -ZP23 = \frac{\alpha'}{a_I}\frac{(\Delta\xi)^{2\,\prime}}{2\Delta z} \quad ZT21 = -ZT23 = \frac{b}{Ra}\frac{\beta'_i}{a_I}\frac{(\Delta\xi)^2}{2\Delta z} \\
&ZT22 = -(\Delta\xi)^2\frac{n'}{Pe^*}, \quad ZW32 = \frac{a_{III}}{a_I}\left(1 - \frac{\Delta\xi}{2}\right)
\end{aligned}
\tag{G.6}
$$

The consolidation equation (7.3.5) is of transient form and the pore pressure is the major unknown. Employing the implicit scheme it may be written as

$$
\beta'_c\left(\frac{T_c}{T_d}\right)\frac{{}^k p^{n+1}_{i,j} - p^n_{i,j}}{\Delta t} = {}^k R^{n+1}_{i,j} + O(\Delta t) \tag{G.7}
$$

where ${}^k R^{n+1}_{i,j}$ is the rest of (7.3.5) at the current time step $(n+1)$ and iteration number k and is given by

$$
\begin{aligned}
{}^k R^{n+1}_{i,j} &= e^{-2\xi_i}\left[{}^k\left(\frac{\partial^2 p}{\partial\xi^2}\right)^{n+1}_{i,j} - {}^k\left(\frac{\partial p}{\partial\xi}\right)^{n+1}_{i,j}\right] + {}^k\left(\frac{\partial^2 p}{\partial z^2}\right)^{n+1}_{i,j} - \frac{1}{Pe^*}{}^k\left(\frac{\partial\theta'}{\partial z}\right)^{n+1}_{i,j} \\
&- \left(\frac{T_c}{T_d}\right)\left\{\gamma'\left[{}^k\left(\frac{\partial^2 u}{\partial\xi\partial t}\right)^{n+1}_{i,j} e^{-\xi_i} + {}^k\left(\frac{\partial^2 w}{\partial z\partial t}\right)^{n+1}_{i,j}\right] + \zeta'_c\frac{b}{Ra}{}^k\left(\frac{\partial\theta'}{\partial t}\right)^{n+1}_{i,j}\right\}
\end{aligned}
\tag{G.8}
$$

The consistency of (G.7) is $O(\Delta t)$. In the actual computations, $\Delta t = 0.002$ and $\Delta\xi = \Delta z \leq O(10^{-1})$ have been used. Accordingly both of the consistencies $O(\Delta\xi^2, \Delta z^2, \Delta\xi\Delta z)$ and $O(\Delta t)$ are comparable at $O(10^{-3})$. In order to keep the

truncation error of ${}^kR_{i,j}^{n+1}$ at the second order, the derivatives in it were written as with a truncation error of $O(\Delta t^2)$

$$
\begin{aligned}
{}^k\left(\frac{\partial\theta'}{\partial t}\right)_{i,j}^{n+1} &= \frac{1}{2\Delta t}\left(3^k\theta'^{n+1}_{i,j} - 4\theta'^{n}_{i,j} + \theta'^{n-1}_{i,j}\right) \\
{}^k\left(\frac{\partial^2 u}{\partial\xi\partial t}\right)_{i,j}^{n+1} &= \frac{1}{4\Delta\xi\Delta t}\left(3^k u^{n+1}_{i+1,j} - 4u^{n}_{i+1,j} + u^{n-1}_{i+1,j}\right) \\
&\quad - \frac{1}{4\Delta\xi\Delta t}\left(3^k u^{n+1}_{i-1,j} - 4u^{n}_{i-1,j} + u^{n-1}_{i-1,j}\right)
\end{aligned}
\qquad (G.9)
$$

Substituting (G.8) and (G.9) into (G.7), multiplying by $e^{2\xi_i}(\Delta\xi)^2$ and rearranging, we obtain

$$
\begin{aligned}
&e^{\xi_i}CU12u^{n+1}_{i-1,j} + CP12p^{n+1}_{i-1,j} + e^{2\xi_i}CW21w^{n+1}_{i,j-1} + e^{2\xi_i}CW23w^{n+1}_{i,j+1} \\
&+e^{2\xi_i}CP21p^{n+1}_{i,j-1}(-2 - e^{2\xi_i}CP22)p^{n+1}_{i,j} + e^{2\xi_i}CP23p^{n+1}_{i,j+1} + e^{2\xi_i}CT21\theta'^{n+1}_{i,j-1} \\
&+e^{2\xi_i}CT22\theta'^{n+1}_{i,j} + e^{2\xi_i}CT23\theta'^{n+1}_{i,j+1} + e^{\xi_i}CU32u^{n+1}_{i+1,j} + CP32p^{n+1}_{i+1,j} \\
&= -\left(\frac{T_c}{T_d}\right)\beta'_c e^{2\xi_i}\frac{(\Delta\xi)^2}{\Delta t}p^n_{i,j} \\
&\quad + \left(\frac{T_c}{T_d}\right)\gamma' e^{\xi_i}\frac{\Delta\xi}{4\Delta t}\left(-4u^n_{i+1,j} + u^{n-1}_{i+1,j} + 4u^n_{i-1,j} - u^{n-1}_{i-1,j}\right) \\
&\quad + \left(\frac{T_c}{T_d}\right)\gamma' e^{2\xi_i}\frac{(\Delta\xi)^2}{4\Delta z\Delta t}\left(-4w^n_{i+1,j} + w^{n-1}_{i+1,j} + 4w^n_{i-1,j} - w^{n-1}_{i-1,j}\right) \\
&\quad + \left(\frac{T_c}{T_d}\right)\frac{b}{Ra}\zeta'_c e^{2\xi_i}\frac{(\Delta\xi)^2}{2\Delta t}\left(-4\theta'^{n}_{i,j} + \theta'^{n-1}_{i,j}\right)
\end{aligned}
\qquad (G.10)
$$

where

$$
\begin{aligned}
&CP12 = 1 + \frac{\Delta\xi}{2}, \quad CU12 = -CU32 = \left(\frac{T_c}{T_d}\right)\gamma'\frac{3\Delta\xi}{4\Delta t}, \quad CP21 = CP23 = \frac{(\Delta\xi)^2}{(\Delta z)^2} \\
&CP22 = 2\frac{(\Delta\xi)^2}{(\Delta z)^2} + \left(\frac{T_c}{T_d}\right)\beta'_c\frac{(\Delta\xi)^2}{2\Delta t}, \quad CW21 = -CW23 = \left(\frac{T_c}{T_d}\right)\gamma'\frac{3(\Delta\xi)^2}{4\Delta z\Delta t} \\
&CT21 = -CT23 = \frac{1}{Pe^*}\frac{(\Delta\xi)^2}{2\Delta z}, CT22 = -\left(\frac{T_c}{T_d}\right)\frac{b}{Ra}\zeta'_c\frac{3(\Delta\xi)^2}{2\Delta t}, CP32 = 1 - \frac{\Delta\xi}{2}
\end{aligned}
\qquad (G.11)
$$

The heat equation (7.3.6) is similarly written by using the implicit scheme as

$$
\frac{}{\rho C_p}\frac{{}^k\theta'^{n+1}_{i,j} - \theta'^{n}_{i,j}}{\Delta t} = {}^kS^{n+1}_{i,j} + O(\Delta t) \qquad (G.12)
$$

where the right-hand side is given, by combining (7.3.6) and (7.3.7), as

$$
\begin{aligned}
{}^{k}S_{i,j}^{n+1} = m' e^{-2\xi_i} \left[{}^{k}\left(\frac{\partial^2 \theta'}{\partial \xi^2}\right)_{i,j}^{n+1} - {}^{k}\left(\frac{\partial \theta'}{\partial \xi}\right)_{i,j}^{n+1} \right] + m'^{k}\left(\frac{\partial^2 \theta'}{\partial z^2}\right)_{i,j}^{n+1} \\
+ \left[Pe^* e^{-\xi_i {}^{k-1}}\left(\frac{\partial p}{\partial \xi}\right)_{i,j}^{n+1} - Pe^*\left(\frac{T_c}{T_d}\right) f_z{}^{k-1}\left(\frac{\partial u}{\partial t}\right)_{i,j}^{n+1} \right] e^{-\xi_i {}^{k}}\left(\frac{\partial \theta'}{\partial \xi}\right)_{i,j}^{n+1} \\
+ \left[Pe^{*k-1}\left(\frac{\partial p}{\partial z}\right)_{i,j}^{n+1} - Pe^*\left(\frac{T_c}{T_d}\right) f_z{}^{k-1}\left(\frac{\partial w}{\partial t}\right)_{i,j}^{n+1} - {}^{k-1}\theta'^{n+1}_{i,j} \right] \\
\times \left[{}^{k}\left(\frac{\partial \theta'}{\partial z}\right)_{i,j}^{n+1} - Ra \right]
\end{aligned}
\tag{G.13}
$$

Notice that the convection velocity terms are calculated by using the previous iteration values $(k-1)$. As in the consolidation equation all derivatives in (G.13) are approximated by finite difference forms with second order accuracy. Substituting appropriate finite difference formulas from (G.1) and (G.9) into (G.13), the final form becomes, after some algebra,

$$
\begin{aligned}
&(e^{-2\xi_i} T12 + CVX)\theta'^{n+1}_{i-1,j} + (e^{-2\xi_i} T32 - CVX)\theta'^{n+1}_{i+1,j} \\
&+(1 + CVZ)\theta'^{n+1}_{i,j-1} + \left(-2e^{-2\xi_i}\frac{(\Delta z)^2}{(\Delta \xi)^2} + T22\right)\theta'^{n+1}_{i,j} + (1 - CVZ)\theta'^{n+1}_{i,j+1} \\
&= -\frac{\overline{\rho C_p}}{m'}\frac{(\Delta z)^2}{\Delta t}\theta'^{n}_{i,j} - 2\Delta z Ra CVZ
\end{aligned}
\tag{G.14}
$$

where the nodal variables on the left-hand side are for the current iteration step k and

$$
\begin{aligned}
&T12 = \frac{(\Delta z)^2}{(\Delta \xi)^2} + \frac{2\Delta z}{2\Delta \xi}, \quad T22 = -2 - \frac{\overline{\rho C_p}}{m'}\frac{(\Delta z)^2}{\Delta t}, \quad T32 = \frac{(\Delta z)^2}{(\Delta \xi)^2} - \frac{(\Delta z)^2}{2\Delta \xi} \\
&CVX = e^{\xi_i} TF1\left(3^{k-1}u^{n+1}_{i,j} - 4u^{n}_{i,j} + u^{n-1}_{i,j}\right) - e^{-2\xi_i} TF2\left({}^{k-1}p^{n}_{i+1,j} - {}^{k-1}p^{n}_{i-1,j}\right) \\
&CVZ = TF3\left(3^{k-1}w^{n+1}_{i,j} - 4w^{n}_{i,j} + w^{n-1}_{i,j}\right) \\
&\quad - TF4\left({}^{k-1}p^{n}_{i,j+1} - {}^{k-1}p^{n}_{i,j-1}\right) + TF5\,{}^{k-1}\theta'^{n+1}_{i,j}
\end{aligned}
\tag{G.15}
$$

in which the coefficients in CVX and CVZ are given by

$$
\begin{aligned}
&TF1 = \frac{Pe^*}{m'}\left(\frac{T_c}{T_d}\right)\frac{(\Delta z)^2}{4\Delta \xi \Delta t} f_z, \quad TF2 = \frac{Pe^*}{m'}\frac{(\Delta z)^2}{4(\Delta \xi)^2}, \quad TF3 = \frac{Pe^*}{m'}\left(\frac{T_c}{T_d}\right)\frac{\Delta z}{4\Delta t} f_z \\
&TF4 = \frac{1}{4}\frac{Pe^*}{m'}, \quad TF5 = \frac{1}{m'}\frac{\Delta z}{2}
\end{aligned}
\tag{G.16}
$$

The finite difference equations (G.3),(G.5),(G.10) and (G.14) are those used in numerical computation of thermoconsolidation in §7.

Finite difference forms of the boundary conditions in §7.2.2 are simple. The stress boundary conditions (7.2.12) are further discussed here. They are in (ξ, z) coordinates

$$\begin{aligned} \sigma_{zz} =& a_I \frac{\partial w}{\partial z} + a_{II} e^{-\xi_i} \frac{\partial u}{\partial \xi} = 0 \qquad \text{at } z = 1 \\ \sigma_{xz} =& a_{III} \left(\frac{\partial u}{\partial z} + e^{-\xi_i} \frac{\partial w}{\partial \xi} \right) = 0 \end{aligned} \tag{G.17a,b}$$

which can be regarded as the Neumann boundary conditions for w and u respectively at $z = 1$. Therefore we approximate (G.17) in finite difference form as, with M being the node along z axis at $z = 1$,

$$\begin{aligned} {}^k w_{i,M}^{n+1} =& \frac{4}{3} {}^k w_{i,M-1}^{n+1} - \frac{1}{3} {}^k w_{i,M-2}^{n+1} - \frac{a_{II}}{a_I} e^{-\xi_i} \frac{\Delta z}{3\Delta \xi} \left({}^{k-1} u_{i+1,M}^{n+1} - {}^{k-1} u_{i-1,M}^{n+1} \right) \\ & + O(\Delta \xi^2, \Delta z^2) \\ {}^k u_{i,M}^{n+1} =& \frac{4}{3} {}^k u_{i,M-1}^{n+1} - \frac{1}{3} {}^k u_{i,M-2}^{n+1} - e^{-\xi_i} \frac{\Delta z}{3\Delta \xi} \left({}^{k-1} w_{i+1,M}^{n+1} - {}^{k-1} w_{i-1,M}^{n+1} \right) \\ & + O(\Delta \xi^2, \Delta z^2) \end{aligned} \tag{G.18}$$

where the second terms in (G.17) have been written in terms of the values from the previous iteration step. When the convergence is good enough, (G.16) is identically satisfied within the truncation error. Other boundary conditions are as follows.

$$\begin{aligned} {}^k u_{i,1}^{n+1} =& {}^k w_{i,1}^{n+1} = {}^k \theta'^{n+1}_{i,1} = 0 \qquad \text{at} \quad z = 0 \\ {}^k p_{i,1}^{n+1} =& \frac{4}{3} {}^k p_{i,2}^{n+1} - \frac{1}{3} {}^k p_{i,3}^{n+1} + p_o \qquad \text{at} \quad z = 0 \end{aligned} \tag{G.19}$$

where $p_o = 0$ for $x > a$ and $p_o = 2\Delta z/3$ for $0 < x < a$. Also from (6.2.12a) we have

$${}^k p_{i,M}^{n+1} = {}^k \theta'^{n+1}_{i,M} = 0 \qquad \text{at} \quad z = 0 \tag{G.20}$$

At the symmetry boundary ($z = 0$), (6.2.13) becomes

$${}^k f_{1,j}^{n+1} = \frac{4}{3} {}^k f_{2,j}^{n+1} - \frac{1}{3} {}^k f_{3,j}^{n+1} \qquad \text{for} \quad f = w, p, \theta' \tag{G.21}$$

Finally (7.2.14) becomes at $\xi = \xi_N$

$${}^k f_{N,j}^{n+1} = 0 \qquad \text{for} \quad f = u, w, p, \theta' \tag{G.22}$$

Equations (G.17)-(G.22) complete the finite difference approximations of the boundary conditions and must be incorporated into the earlier governing equations.

Appendix H. Analytic Solution for Rigid Medium.

The analytic solution for the one- dimensional convection diffusion in a rigid medium is obtained by using the Laplace transform. If we let

$$a = \frac{\overline{\rho C_p}}{m'}, \qquad P = \frac{Pe^*}{m'} \tag{H.1}$$

equation (7.5.3) becomes

$$a\frac{\partial \theta}{\partial t} - P\left(\frac{\partial \theta}{\partial z} - 1\right) = \frac{\partial^2 \theta}{\partial z^2} \qquad 0 < z < 1 \tag{H.2}$$

The initial and boundary conditions are

$$\theta = 0 \qquad t = 0 \tag{H.3}$$

$$\theta = 0 \qquad z = 0, 1 \tag{H.4}$$

In order to remove the convection term, we introduce a new variable $q(z,t)$ given by

$$\theta(z,t) = z + e^{-Pz/2} q(z,t) \tag{H.5}$$

Substituting (H.5) into (H.2) - (H.4), we get

$$\begin{aligned} a\frac{\partial q}{\partial t} &= -\frac{P^2}{4}q + \frac{\partial^2 q}{\partial z^2} && 0 < z < 1 \\ q &= -ze^{Pz/2} && t = 0 \\ q &= 0 && z = 0 \\ q &= -e^{P/2} && z = 1 \end{aligned} \tag{H.6a - d}$$

The decay term is further removed by another change of variable

$$q(z,t) = e^{-P^2 t/4a} r(z,t) \tag{H.7}$$

The initial boundary value problem (H.6) then becomes

$$\begin{aligned} a\frac{\partial r}{\partial t} &= \frac{\partial^2 r}{\partial z^2} && 0 < z < 1 \\ r &= -ze^{Pz/2} && t = 0 \\ r &= 0 && z = 0 \\ r &= -e^{P/2} e^{P^2 t/4a} && z = 1 \end{aligned} \tag{H.8a - d}$$

It is now a pure diffusion problem with initial temperature distribution $r(z,0) = -ze^{Pz/2}$. The temperature remains zero at $z = 0$ but grows exponentially with time at $z = 1$.

The Laplace transform of a function $g(z,t)$ is defined by

$$\bar{g}(z,s) = \mathcal{L}\{g(z,t)\} = \int_o^\infty g(z,t)e^{-st}dt \qquad (H.9)$$

where s is a positive number for which the integral exists. It has the following property

$$\mathcal{L}\left\{\frac{\partial g}{\partial t}\right\} = s\bar{g} - g(z,0) \qquad (H.10)$$

Let us take the Laplace transform of (H.8a-d) and use (H.10). We then have the following ordinary differential equation

$$\begin{aligned} \frac{d^2\bar{r}}{dz^2} - as\bar{r} &= aze^{Pz/2} \qquad 0 < z < 1 \\ \bar{r} &= 0 \qquad z = 0 \\ \bar{r} &= -e^{P/2}\frac{1}{s - P^2/4a} \qquad z = 1 \end{aligned} \qquad (H.11a-c)$$

Since a and s are positive, the homogeneous solution $\bar{r}_h$ of (H.11a) is

$$\bar{r}_h = C_1 \sinh cz + C_2 \cosh cz \qquad (H.12)$$

where

$$c = \sqrt{as} \qquad (H.13)$$

and C_1 and C_2 are constants to be determined later from the boundary conditions. The particular solution $\bar{r}_p$ is obtained by integrating

$$(D + c)(D - c)\bar{r}_p = e^{-cz}\frac{d}{dz}\left[e^{cz}(D - c)\bar{r}_p\right] = f(z) \qquad (H.14)$$

where

$$D = \frac{d}{dz}, \qquad f(z) = aze^{Pz/2} \qquad (H.15)$$

Integrating (H.14) with respect to z once, we get

$$(D - c)\bar{r}_p = e^{cz}\frac{d}{dz}\left(e^{-cz}\bar{r}_p\right) = e^{-cz}\int_o^z f(\xi)e^{c\xi}d\xi \qquad (H.16)$$

Another integration yields

$$\bar{r}_p = -\frac{1}{2c}\left[\int_o^z f(\xi)e^{c(\xi-z)}d\xi - \int_o^z f(\xi)e^{-c(\xi-z)}d\xi\right] \qquad (H.17)$$

Substituting (H.15) into (H.17) and carrying out the integrations, we obtain

$$\bar{r}_p = a\left[\frac{z}{P^2/4-c^2} - \frac{P}{(P^2/4-c^2)^2}\right]e^{Pz/2} - \frac{a}{2c}\left[\frac{e^{-cz}}{\left(\frac{P}{2}+c\right)^2} - \frac{e^{cz}}{\left(\frac{P}{2}-c\right)^2}\right] \qquad (H.18)$$

The general solution then becomes

$$\bar{r} = \bar{r}_h + \bar{r}_p \qquad (H.19)$$

which must satisfy the boundary conditions (H.11b and c). It is easily seen that $\bar{r}_p(z=0)$ vanishes. Thus from (H.11b) we have

$$\bar{r}(0) = \bar{r}_h(0) + \bar{r}_p(0) = C_2 = 0 \qquad (H.20)$$

Also it follows from (H.11c) after suing (H.20) that

$$C_1 = \frac{a}{(as-P^2/4)^2\sinh c}\left[Pe^{P/2} - P\cosh c - \frac{(as+P^2/4)}{(as-P^2/4)^2}\frac{1}{c}\sinh c\right] \qquad (H.21)$$

If we substitute (H.20) and (H.21) into (H.12) and then (H.12) and (H.18) into (H.19), it finally becomes after using (H.13) that

$$\begin{aligned}\bar{r}(z,s) =& \frac{aP}{(as-P^2/4)^2\sinh\sqrt{as}}\left[e^{P/2}\sinh\sqrt{as}z - \sinh\sqrt{as}(z-1)\right] \\ & - a\left[\frac{z}{as-P^2/4} + \frac{P}{(as-P^2/4)^2}\right]e^{Pz/2}\end{aligned} \qquad (H.22)$$

We now take the inverse Laplace transform of (H.22) to obtain $r(z,t)$. The inverse transform is defined by

$$g(z,t) = \mathcal{L}^{-1}\{\bar{g}(z,s)\} = \frac{1}{2\pi i}\int_{\gamma-i\infty}^{\gamma+i\infty}\bar{g}(z,s)e^{st}ds \qquad (H.23)$$

where $i = \sqrt{-1}$ and γ is large enough to have all the singularities of $\bar{g}(z,s)$ on the left of the line $(\gamma - i\infty, \gamma + i\infty)$. The second part of (H.22) is readily transformed by using Laplace transform table. The inverse transform of (H.22) then becomes

$$r(z,t) = aPe^{P/2}\mathcal{L}^{-1}\left\{\frac{1}{(as-P^2/4)^2}\frac{\sinh\sqrt{as}z}{\sinh\sqrt{as}}\right\} - aP\mathcal{L}^{-1}\left\{\frac{1}{(as-P^2/4)^2}\frac{\sinh\sqrt{as}(z-1)}{\sinh\sqrt{as}}\right\} - e^{Pz/2}(z+Pt)e^{P^2t/4a} \tag{H.24}$$

We only need to consider the first term in (H.24), which is written by using (H.23) as

$$\mathcal{L}^{-1}\left\{\frac{1}{(as-P^2/4)^2}\frac{\sinh\sqrt{as}z}{\sinh\sqrt{as}}\right\} = \frac{1}{2\pi i}\int_{\gamma-i\infty}^{\gamma+i\infty}\frac{1}{(as-P^2/4)^2}\frac{\sinh\sqrt{as}z}{\sinh\sqrt{as}}e^{st}ds \tag{H.25}$$

The integrand has a second order pole at $s = P^2/4a$. When s goes to zero, the hyperbolic functions are expanded as

$$\frac{\sinh\sqrt{as}z}{\sinh\sqrt{as}} = \frac{\sqrt{as}z + \frac{1}{6}(\sqrt{as}z)^3 + \cdots}{\sqrt{as} + \frac{1}{6}(\sqrt{as})^3 + \cdots} = \frac{z + \frac{1}{6}asz^3 + \cdots}{1 + \frac{1}{6}as + \cdots} \tag{H.26}$$

Although the arguments of the hyperbolic functions are double-valued at $s = 0$, the ratio of (H.26) is single-valued and $s = 0$ is not a branch point. The denominator $\sinh\sqrt{as}$ has infinite number of simple poles at the points where it vanishes. The corresponding points satisfy the relation

$$\sqrt{as_n} = in\pi \quad ; \quad s_n = -\frac{1}{a}n^2\pi^2 \quad (n \neq 0) \tag{H.27}$$

Equation (H.25) then becomes after using the residue theorem

$$\mathcal{L}^{-1}\left\{\frac{1}{(as-P^2/4)^2}\frac{\sinh\sqrt{as}z}{\sinh\sqrt{as}}\right\} = \text{Res}\left(s = \frac{P^2}{4a}\right) + \sum_{n=1}^{\infty}\text{Res}\left(s_n = -\frac{1}{a}n^2\pi^2\right) \tag{H.28}$$

The residues are determined as follows. If we let the integrand of (H.25) be denoted by I,

$$\begin{aligned}\text{Res}\left(s=\frac{P^2}{4a}\right) &= \lim_{s\to P^2/4a}\frac{d}{ds}\left[\left(s-\frac{P^2}{4a}\right)^2 I\right] = \lim_{s\to P^2/4a}\frac{d}{ds}\left(\frac{\sinh\sqrt{as}ze^{st}}{a^2\sinh\sqrt{as}}\right)\\ &= \frac{1}{aP}\left(\frac{z\cosh\frac{P}{2}z}{\sinh\frac{P}{2}}-\frac{\cosh\frac{P}{2}\sinh\frac{P}{2}z}{\sinh^2\frac{P}{2}}\right)e^{P^2t/4a}+\frac{\sinh\frac{P}{2}z}{a^2\sinh\frac{P}{2}}te^{P^2t/4a}\end{aligned} \tag{H.29}$$

We also have after expansion about $s=s_n$

$$\begin{aligned}\text{Res}\left(s_n=-\frac{1}{a}n^2\pi^2\right) &= \lim_{s\to s_n}\frac{(s-s_n)\sinh\sqrt{as}z}{\left(as-\frac{P^2}{4}\right)^2\sinh\sqrt{as}}e^{st}\\ &= \frac{\sinh in\pi z}{\left(n^2\pi^2+\frac{P^2}{4}\right)^2\cosh in\pi}\frac{2in\pi}{a}e^{-n^2\pi^2t/a}\\ &= -\frac{2}{a}\frac{(-1)^n n\pi\sin n\pi z}{\left(n^2\pi^2+\frac{P^2}{4}\right)^2}e^{-n^2\pi^2t/a}\end{aligned} \tag{H.30}$$

Therefore (H.28) becomes after substituting (H.29) and (H.30)

$$\begin{aligned}\mathcal{L}^{-1}\left\{\frac{1}{(as-P^2/4)^2}\frac{\sinh\sqrt{as}z}{\sinh\sqrt{as}}\right\} &= \frac{1}{aP}\left(\frac{z\cosh\frac{P}{2}z}{\sinh\frac{P}{2}}--\frac{\cosh\frac{P}{2}\sinh\frac{P}{2}z}{\sinh^2\frac{P}{2}}\right)e^{P^2t/4a}\\ &+\frac{\sinh\frac{P}{2}z}{a^2\sinh\frac{P}{2}}te^{P^2t/4a}-\frac{2}{a}\sum_{n=1}^{\infty}\frac{(-1)^n n\pi\sin n\pi z}{\left(n^2\pi^2+\frac{P^2}{4}\right)^2}e^{-n^2\pi^2t/a}\end{aligned} \tag{H.31}$$

The second term in (H.24) is the same form as (H.31) except that z is replaced by $z-1$.

If we use (H.30) and (H.31) in (H.24), there follows after some algebra that

$$\begin{aligned}r(z,t) = &-e^{P/2}e^{P^2t/4a}\frac{\sinh Pz/2}{\sinh^2 Pz/2}\\ &-2P\sum_{n=1}^{\infty}\frac{(-1)^n n\pi e^{-n^2\pi^2t/a}}{(n^2\pi^2+P^2/4)^2}\left[e^{Pz/2}\sin n\pi z-\sin n\pi(z-1)\right]\end{aligned} \tag{H.32}$$

Finally, by using (H.5) and (H.7), we obtain

$$\begin{aligned}\theta(z,t) =& z + e^{-Pz/2}e^{-P^2t/4a}r(z,t)\\ =& z - \frac{1-e^{-Pz}}{1-e^{-P}}\\ & - 2Pe^{-Pz/2}\sum_{n=1}^{\infty}\frac{(-1)^n n\pi e^{-n^2\pi^2 t/a}}{\left(n^2\pi^2+P^2/4\right)^2}\left[e^{P/2}\sin n\pi z - \sin n\pi(z-1)\right]\end{aligned} \tag{H.33}$$

which becomes (7.5.5) if (H.1) is used.

PART B. THERMAL DISPERSION IN POROELASTIC MEDIA

NOTATIONS

a	elastic coefficient tensor of rank four $a_{ijk\ell}$ in solid or $Pe'\langle u\rangle_z$ (cf.(4.1.19) in Chapter II)
a_I	elastic coefficient a'_{zzzz} in a medium with cubic symmetry
a_{II}	elastic coefficient a'_{zzyy} in a medium with cubic symmetry
a_{III}	elastic coefficient a'_{zyzy} in a medium with cubic symmetry
a_1, a_2	macrosale elastic coefficients(a''_{zzzz}, a''_{zzzz})
a_4, a_6	macrosale elastic coefficients(a''_{zzzz}, a''_{zzzz})
a'	elastic coefficient tensor of rank four $a'_{ijk\ell}$ of porous medium on the ℓ' scale
a''	elastic coefficient tensor of rank four $a''_{ijk\ell}$ of porous medium on the ℓ'' scale
$\bar{a}$	average heat capacity of porous medium on the ℓ' scale
A_{ij}	coordinate transformation matrix in the horizontal $x'y'$ plane (cf. (4.1.13) in Chapter II)
$\mathbf{A}$	shape function matrix for finite elements
b	1-1/$\bar{a}$
B	scale of thermal modulus
B'	vector coefficient function for $\theta^{(1)}$ (cf. (3.3.9) in Chapter II)
$\bar{B}'$	vector coefficient function B' for mean flow in $\bar{x}'\bar{z}'$ plane
$B^{f,s}$	vector function for $\theta^{(1)}_{f,s}$
B_{jk}, B'_{jk}	second order tensor coefficients (cf. (3.3.3) in Chapter I)
c	ratio of body force to buoyancy in a porous layer
$C'_z(z')$	$=B'_z(z') - A'_z(z')$
$C_i^{f,s}$	vector function ($=B_i^{f,s} + x_i$)
C_p	specific heat
C_{ij}	coordinate transformation matrix (cf. (4.2.4) in Chapter I)
$\mathbf{C}_f, \mathbf{C}_s$	coefficient matrices for $\mathbf{q}_f$ and $\mathbf{q}_s$ in finite element equation for convection-diffusion equation
$\mathbf{C}_\lambda$	coefficient matrix for Lagrange multiplier
D_I	$=D_{zz}$ for mean flow along symmetry axis of microcell
D_{II}	$=D_{yy} = D_{zz}$ for mean flow along symmetry axis of microcell
D_L	longitudinal dispersion coefficient
D_T	transverse dispersion coefficient

D'_{ij} macroscale dispersion tensor on the ℓ' scale

D''_{ij} macroscale dispersion tensor on the ℓ'' scale

D^s_{ij} symmetric dispersion tensor

D^u_{ij} anti-symmetric dispersion tensor

$\bar{D}^s_{ij}$ symmetric dispersion tensor for mean flow in $\bar{x}'\bar{z}'$ plane

$\bar{D}^u_{ij}$ anti-symmetric dispersion tensor for mean flow in $\bar{x}'\bar{z}'$ plane

e extrapolation error in numerical results

$e_{ij}(B^{f,s}) = \frac{1}{2}\left(\frac{\partial B_j^{f,s}}{\partial x_i} + \frac{\partial B_i^{f,s}}{\partial x_j}\right)$

$\mathbf{e}_i$ unit vector in i-th direction

$\mathbf{e}_i^C$ unit vector in i-th direction in x^C frame

E Young's modulus

E scalar coefficient (cf. (3.3.3) in Chapter I)

E'_j vector coefficient (cf. (3.4.4) in Chapter II)

$E'_{i\ell}$ second order tensor coefficient (cf. (3.4.12) in Chapter II)

F_i vector coefficient (cf. (3.3.3) in Chapter I)

F'_{ij} second order tensor coefficient (cf. (3.4.4) in Chapter II)

$F'_{ij\ell}$ third order tensor coefficient (cf. (3.4.12) in Chapter II)

$\mathbf{f}_f, \mathbf{f}_s$ forcing vectors in finite element equation
for convection-diffusion equation

$\mathbf{F}_f, \mathbf{F}_s$ coefficient matrices for $\mathbf{q}_f$ and $\mathbf{q}_s$ in finite element equation
for convection-diffusion equation

g gravitational acceleration

$G(z','xi)$ Green's function for B'_x, B'_y and B'_z

G'_{ij} second order tensor coefficient (cf. (3.4.4) in Chapter II)

$G'_{ij\ell}$ third order tensor coefficient (cf. (3.4.12) in Chapter II)

h thickness of porous layer

I identity tensor

I_j $= \langle \overline{\rho C_p} B'_j \rangle$ (cf. (5.4.1) in Chapter II)

$I_{ij}^{f,s}$ $= \frac{\partial B_i^{f,s}}{\partial x_k \partial x_k} \frac{\partial B_j^{f,s}}{\partial x_k \partial x_k}$

J functional for convection-diffusion equation in microcell

J_j $= \nabla''_i \cdot (m^u_{ij} + D^u_{ij})$ (cf. (5.4.8) in Chapter II)

k_r anisotropy ratio of permeability ($= k''_{xx}/k''_{zz}$)

$\hat{k}_{ij}$ $= k_{ij} - k'_{ij}$

k' permeability tensor k'_{ij} on the ℓ' scale

k'' permeability tensor k''_{ij} on the ℓ'' scale

K	hydraulic conductivity of porous medium or bulk modulus of solid
K_{ij}, K'_{ij}	second order tensor coefficients (cf. (3.3.3) in Chapter I)
ℓ	microscale length
ℓ'	macroscale length in two-scale medium or mesoscale length in three-scale medium
ℓ''	macroscale length in three-scale medium
L_{ijk}, L'_{ijk}	third order tensor coefficients (cf. (3.3.3) in Chapter I)
$\overline{m}$	microcell average of thermal conductivity
$m_{f,s}$	thermal conductivity of fluid(f) or soild(s)
m'	thermal conductivity of porous medium on the ℓ' scale
$\langle m' \rangle$	average of m' over mesoscale cell
m''	thermal conductivity of porous medium on the ℓ'' scale
M	diffusivity of solute
$M_{f,s}$	scale of thermal conductivity of fluid(f) or soild(s)
M_r	M_s/M_f
n'	porosity on the mesoscale ℓ'
n''	porosity on the macroscale ℓ''
N	unit normal vector
$N^{f,s}$	outward unit normal vector from fluid(f) or soild(s)
N_o	unit normal vector on the initial fluid-solid interface
O	order symbol
p	dynamic pressure variation
$p(z')$	integrating factor for the Green's function $G(z', \xi)$
$\bar{p}^{(1)}, \bar{p}^{(2)}$	microcell averages of $p^{(1)}, p^{(2)}$
P'	scale of pressure drop over the length ℓ'
P''	scale of pressure drop over the length ℓ''
Pe	microscale Peclét number
Pe_m	local Peclét number in porous mediu
$\overline{Pe}_f$	Peclét number of uniform flow in porous medium layer based on α_f (cf. (6.1.18) in Chapter II)
$\overline{Pe}_m$	Peclét number of uniform flow in porous medium layer based on α_m (cf. (6.1.21) in Chapter II)
Pe'	mesoscale Peclét number
Pr	Prandtl number
$\mathbf{q}$	nodal unknown vectorin finite element equation for convection-diffusion equation

$r(\xi)$ forcing function for B'_x

$\hat{r}(\xi)$ $=r(\xi)/Pe'\langle\langle u\rangle_x\rangle$

R_c critical Rayleigh number for a porous medium layer

Ra mesoscale Rayleigh number

Ra' macroscale Rayleigh number

$\hat{Ra}'$ $\epsilon Ra'$

Re Reynolds number $(=U\ell/\nu)$

$\hat{Re}$ Re/ϵ

$s(\xi)$ forcing function for B'_y

$s, (1-s)$ thickness of layers

S vector coefficient (cf. (3.2.2) in Chapter I)

S_i heat source in the equation for B_i^s (cf. (5.1.2) in Chapter I)

S' vector coefficient (cf. (3.2.4) in Chapter II)

S_j, S'_j vector coefficient (cf. (3.3.3) in Chapter I)

t time

$t(\xi)$ forcing function for B'_x

$\hat{t}(\xi)$ $=t(\xi)/Pe'\langle u\rangle_x$

$t_d = t'$ slow time sale of heat diffusion over ℓ''

t_v fast time sale of heat convection over ℓ'

T_c consoildation time scale over ℓ' scale

T'_c consoildation time scale over ℓ'' scale

T_d heat diffusion time scale over ℓ' scale

T'_d heat diffusion time scale over ℓ'' scale

T_v heat convection time scale over ℓ' scale

T'_v heat convection time scale over ℓ'' scale

u fluid velocity vector

$\tilde{u}^{(0)}$ fluid velocity fluctuation about weighted mean
(cf. (3.4.9) in Chapter I)

$\hat{u}^{(0)}$ fluid velocity fluctuation about the mean (cf. (3.4.19) in Chapter I)

$\langle u\rangle$ seepage velocity vector on the ℓ' scale

$\widetilde{\langle u\rangle}^{(0)}$ seepage velocity fluctuation about weighted mean
(cf. (3.3.8) in Chapter II)

$\langle\hat{u}\rangle^{(0)}$ seepage velocity fluctuation about about the mean
(cf. (3.3.20) in Chapter II)

$\langle\breve{u}\rangle$ seepage velocity added to the mean (cf. (3.3.34) in Chapter II)

$\langle\langle u\rangle\rangle$ seepage velocity vector on the ℓ'' scale

U	scale of fluid velocity on the microscale ℓ
	or uniform seepage velocity in a porous layer
U'	scale of seepage velocity on the ℓ' scale
v	solid displacement
V_e	effective heat convection velocity (cf. (4.3.1) in Chapter II)
V_x, V_z	heat convection velocity in the moving frame
V'	scale of solid displacement over ℓ' scale
V''	scale of solid displacement over ℓ'' scale
x	microscale vector coordinates
x'	mesoscale vector coordinates
x''	macroscale vector coordinates
x'	mesoscale vector coordinates
$\bar{x}'$	mesoscale vector coordinates for which $\langle u \rangle$ is in $\bar{x}'\bar{z}'$ plane
x''	macroscale vector coordinates
x, y, z	Cartesian coordinates
x^C, y^C, z^C	rotated Cartesian coordinates
$\{Y\}$	(cf. (3.3.4) in Chapter I)
α	linear expansion coefficient of solid
α'	pressure coefficient tensor of porous medium in Hookes's law
	(cf. (3.3.15) in Chapter I)
α''	pressure coefficient tensor of porous medium in Hookes's law
	(cf. (3.2.8) in Chapter II)
$\alpha_{f,s}$	thermal diffusivity of fluid(f) or soild(s)
α_m	thermal diffusivity of porous medium
β	thermal modulus of solid
β_T	thermal expansion coefficient of fluid
β_i'	thermal modulus tensor of porous medium in Hookes's law
	(cf. (3.3.15) in Chapter I)
β_i''	thermal modulus tensor of porous medium in Hookes's law
	(cf. (3.2.8) in Chapter II)
Γ	fluid-solid interface
$\Gamma(0)$	initial position of fluid-solid interface
$\Gamma_{f,s}$	fluid(f) or soild(s) part on the periodic boundary
δ	scale of solid strain over ℓ' scale
δ'	scale of solid strain over ℓ'' scale

δ_{ij}	Kronecker delta
ϵ	scale ratio (ℓ/ℓ' or ℓ'/ℓ'')
θ	medium temperature
	or meridianal angle measured from z' axis on the mesoscale
$\theta_{f,s}$	temperature variation in the fluid(f) or soild(s)
Θ'	scale of temperature variation over ℓ'
Θ''	scale of temperature variation over ℓ''
λ_i	i-th component of unit vector in the mean flow direction
	(cf.(4.2.10) in Chapter I) or
	Lagrange multiplier in the functional J (cf.(5.1.5) in Chapter I)
μ	Lamé constant for solid or absolute viscosity of fluid
ν	kinematic viscosity of fluid or Poisson's ratio for solid
ξ	moving coordinate (cf. (6.1.1) in Chapter II)
$\rho_{f,s}$	density of fluid(f) or soild(s)
$(\rho C_p)_r$	$(\rho C_p)_s/\rho C_p)_f$
$\overline{\rho C_p}$	mesoscale heat capacity of porous medium
$\sigma_{f,s}$	stress in fluid(f) or soild(s)
σ_T	total stress($=\sigma_f$ in Ω_f) or ($=\sigma_s$ in Ω_s)
ϕ	azimuthal angle in $x'z'$ plane on the ℓ' scale (cf. 4.1.13) in Chapter II)
ψ	stream function
Ω	periodic cell on the microscale
Ω'	periodic cell on the mesoscale
$\Omega_{f,s}$	fluid(f) or soild(s) region in a microcell
$\mathcal{D}$	scale of the elastic modulus of solid
$e(\cdot)$	microscale strain operator
$e'(\cdot)$	macroscale strain operator(2-scale) or mesoscale strain operator(3-scale)
$e''(\cdot)$	macroscale strain operator(3-scale)
$(\cdot)^{(n)}$	n-th order term in perturbation series
$(\cdot)^T$	transpose
:	second order contraction
$(\cdot)^*$	normalized quantity
$(\cdot)^{\pm}$	variables in the upper(+) or lower(-) layer
$\tilde{(\cdot)}$	coefficients in physical units
$\langle\cdot\rangle$	unit cell volume average
$[\![\cdot]\!]$	difference of between layers ($=(\cdot)^+ - (\cdot)^-$)

∇	microscale gradient operator
∇'	macroscale gradient operator(2-scale)
	or mesoscale gradient operator(3-scale)
	in the moving frame
∇''	macroscale gradient operator(3-scale)

INTRODUCTION

LITERATURE REVIEW

Dispersion in porous media is of wide-ranging importance in many areas of engineering disciplines,e.g. mechanical, chemical and environmental. The applications are very broad including geothermal energy exploration, nuclear waste repository, packed bed chromatography, nuclear reactors etc. Many other examples are listed in the books by Kaviany(1991) and Brenner and Edwards (1993). We review some literature on this subject with primary emphasis on the thermal dispersion in porous media.

Idealized Models on the Microscale

One class of theoretical models, pertaining to solute dispersion in a porous medium as continuum, is the random capillary network approach (de Jong, 1958; Saffman, 1959,1960; Haring and Greenkorn, 1970). In these models, the porous medium is assumed to be composed of a large number of randomly oriented straight tubes with statistical isotropy. The flow is represented by the mean velocity over the cross-section (except in Saffman in which parabolic velocity profile is used.) The main purpose of the models is to understand the relationships among the characteristics of idealized pores, the mean flow through porous medium and dispersion. Predicted longitudinal dispersion coefficient is proportional to the Peclét number P_ℓ in de Jong and Haring and Greenkorn and is proportional to $P_\ell \ln P_\ell$ in Saffman where P_ℓ is defined in terms of the tubelength ℓ.

There has been also the volume averaging approach (Whitaker, 1967; Slattery, 1972 ; Carbonel and Whitaker, 1983 ; see also Bear and Bachmat, 1990). In this approach, the basic governing equations on the microscopic level are averaged over the representative elementary volume whose dimension is assumed to be much larger than the pore scale length. The transport equation on the macroscale level after volume averaging contains a set of unknowns which can only be determined by experiments. The method itself does not possess predictive capability (Carbonel and

Whitaker, 1983). For thermal dispersion Hsu and Cheng (1990) used the method of volume averaging and obtained thermal dispersion tensor which is proportional to P^2 and P for low and high Reynolds number regimes, where $P = Ud_p/\alpha_f$ is the Peclét number with U, d_p and α_f being the mean flow velocity, particle diameter and thermal diffusivity of the fluid. Drag forces based on hydrodynamics for a single sphere are used for closure modeling. Therefore the dispersion tensor is only relevant to dilute array of spheres. Again certain coefficients must be determined from experiments.

For spatially periodic three-dimensional porous medium, Brenner(1980) has deduced the dispersion tensor for solute by extending the Taylor-Aris moment method for dispersion in circular tubes. It is based on the Brownian motion theory of a particle in flow through intersticial pore space. The porous medium in a periodic length in space is called the unit cell. Once the unit cell geometry is known, the dispersion tensor is determined by solving the cell problem which is a convection-diffusion equation with distributed sources. No ad hoc assumptions are introduced and the dispersion tensor is obtained theoretically. Extensions and applications to adsorption, periodic capillary networks and reaction have followed (Brenner and Adler, 1982; Adler and Brenner, 1984; Dungan at al, 1990). Motivated by this Carbonel and Whitaker (1983) considered the volume averaging method for spatially periodic structure and obtained the same cell boundary value problem as Brenner's.

By allowing the heat diffusion in the solid particles, Koch et al (1989) have deduced approximate analytical dispersion tensor in spatially periodic media. Assuming dilute suspension of particles, the velocity field is approximated as that due to a point force. Also, in their development, the heat convection velocity is asumed to be equal to that of the uniform mean flow. Thus the interactions among particles are ignored and the no-slip boundary condition on the particle surface is not satisfied. Their results show explicitly for a cubic array of spheres that the longitudinal dispersion coefficient D_L grows as P^2 at high Peclét numbers but the transverse dispersion coefficient D_T remains almost the same as the diffusion coefficient as

P increases. Interestingly they find that the dispersion coefficients reach constant limits for mean flow directions not parallel to the lattice vectors in two dimensional array of cylinders.

The key step in determining the dispersion tensor for spatially periodic media is to solve the unit cell boundary value problem. Some numerical results are available. Calculation of dispersion tensor for two-dimensional array of cylinders has been carried out by Eidsath et al (1983) for several arrays of cylinders. Results are presented only for D_L. Edwards et al (1989) have computed D_L and D_T for circular cylinders in square and staggered arrays. On the other hand, Salles et al (1993) carries out compuations for a variety of models of periodic media including cubic array of spheres. In all of these, D_L shows consistently P^2 behavior whereas Eidsath et al (1983) obatains $P^{1.7}$ trend. The P^2 trend is consistent with the experimental results for cubic array of spheres by Gunn and Pryce(1969).

Koch and Brady (1985) modeled the microstructure of a porous medium as randomly distributed spheres in that the averaging is taken over an ensemble of realizations of the bed. Their analysis is based on the assumption that the medium is dilute and the disturbances are basically induced by a single particle. They consider several mechanisms which contribute to dispersion. In the low Peclét number regime, by considering convection and diffusion, D_L and D_T are shown to be proportional to P^2. Purely mechanical dispersion with diffusion neglected for high P yields $D_L \propto P$ and $D_T = 0$. However by including particle interactions D_T becomes proportional to $(1-n)^{1/2}P$ where n is the porosity. The effect of hold up of solute in particles creates $D_L \propto P^2$ and $D_T = 0$ for high P because the solute held in and released from the solid particle gives rise to diffusion on the macroscale transport. Also non-mechanical dispersion due to bounadry layer near the paticle surface gives another contribution $D_L \propto nP\ln P$, which is the same as Saffman's (1960) for randomly oriented capillaries. Combining all these and noting that the theory is essentially valid for dilute particles $(1-n \ll 1)$, they become $D_L \propto P$ and $D_T \propto (1-n)^{1/2}P$ at high Peclét number regime. Comparison with data compiled

by Fried and Combarnous (1971) shows good agreement. It is noteworthy that inclusion of the effects of particle interactions gives D_T behavior which grows with Peclét number.

On the other hand, the theory of homogenization has been applied to dispersion through porous media (Rubinstein and Mauri, 1986; Mei, 1991, 1992). The theory assumes (i) the existence of two disparate length scales and (ii) the periodicity of the micro-structure of medium and the material coefficients. By using the multiple-scale analysis not only the macroscale governing equations and coefficients are deduced but also the macroscale inhomogeneities are incorporated easily. The unit cell boundary value problem defined on the microscale are identical to that obtained in Brenner(1980). Mei(1991) points out that the dispersion tensor is in general not symmetric and the anti-symmetric part contributes to the convection velocity. Similar arguments have been made by Koch and Brady(1987) who obtained expressions for the Eulerian and Lagrangian dispersion tensors by using ensemble averaging and multiple-scale analysis. The latter is symmetric whereas the former is in principle not symmetric and is affected by specific microstructure. It is noted again that their theory is for dilute medium which was necessary for closure scheme.

Natural Porous Media

Dispersion in natural porous media on geological scale of $O(1 - 10^4 m)$ which is much larger than the pore scale of $O(10^{-5} - 10^{-2} m)$ is of interest in most hydrologic applications (Gelhar, 1993). The majority of environmental issues related to dispersion belong to the same category. There exists a vast literature on the large scale dispersion. One popular approach to the field scale macrodispersion in subsurface hydrology is to use stochastic analysis. The subject is well summarized in the books by Dagan(1989) and Gelhar(1993). In the stochastic approach, one begins with the empirical Darcy's law and the law of dispersion measured from laboratory samples. The variables such as the specific discharge, the pressure and the solute concentration are represented by random field (Gelhar and Axness, 1983). Also the

permeability is assumed to be a random process which reflects hydraulic characteristics of the medium. These random processes are expressed as the sum of mean and zero-mean perturbation quantities which are assumed to be small. Typically the random processes are assumed to be statistically homogeneous (stationary) and ergodic. Under these assumptions, the covariance functions depend only on the separation and the ensemble averages are replaced by the averages over a single realization. It is shown (Gelhar and Axness, 1983; Dagan, 1984) that the longitudinal macrodispersivity is proportional to the variance and correlation scale of the natural logarithm of hydraulic conductivity. It should be noted that the above assumptions are satisfied only when the mean quantities vary slowly in space and the region in which transport occurs is much larger than the correlation scale of the covariance of the log permeability. The stochastic approach is based on empirical relations at the starting point so that certain coefficients must be determined by experiments. Even if spatial distributions of quantities are measured by sampling and medium characteristics are estimated, there exists certain level of uncertainty which can can be expressed only by a range of confidence interval since explicit microscale variatins are not taken into account. Also under the assumption of stationarity, the macroscale heterogeneities cannot be incorporated.

Field confirmation of stochastic theories demands comprehensive measurements which are not often available. It is known that the field scale dispersivities are several orders of magnitude larger than those on the laboratory scale (see e.g., Gelhar, 1986). Gelhar et al (1992) have compiled dispersivity observations from 59 different field sites. They conclude that, with no regard to reliability, the longitudinal macrodispersivity shows clear trend of systematic increase with scale and recommend to use dispersivity values in the lower half of the range at any given scale. It should be noted however that even the reliable dispersivity data are scattered over a range of at least an order of magnitude meaning variability from site to site. They just serve as suggestive information.

In many situations porous formations appear to be stratified. Whether the assumption of perfect stratification is justified depends of course on the size of the domain. Gelhar and Axness (1983) are of the opinion that very extreme stratification (e.g., continuous lenses 1 km long) is required for the Taylor dispersion mechanism to be controlling in the field.

For its mathematical simplicity, considerable work has been done along this line. Gelhar et al (1979) considered perfectly stratified medium in that the hydraulic conductivity variation is allowed only in the vertical direction. A stochastic analysis of the Taylor dispersion has been performed by assuming that the hydraulic conductivity is a statistically homogeneous(stationary) one-dimensional random field. They note that the hydraulic conductivity spectra should approach zero at small wave number (hole-type spectra). In the case of finite energy at small wave number, the dispersion coefficient grows and constant dispersion coefficient is never attained. The results show that the transport process becomes Fickian for large time. They also note that, since the asymptotic approach is slow, significant non-Fickian transport occurrs early in the process. Matheron and de Marsily(1980) also considered the transport in stratified porous medium and examined the effects of non-zero vertical component of the mean flow. They showed that, however small the vertical component is, the longitudinal dispersion coefficient always reaches a finite asymptotic values. The same kind of behavior has been obtained by Gupta and Bhattacharya (1986) who assumed periodically stratified media. On the other hand, Güven et al(1984) and Güven and Moltz(1986) have calculated the longitudinal dispersion coefficient by using the method of moment for several specified hydraulic conductivity profiles. For the special case of sinusoidally varying hydraulic conductivity in the vertical direction, the results by Güven and Moltz(1986) are identical to those by Gupta and Bhattacharya (1986). Also comparison with the results by using the stochastic approach of Gelhar et al show that both approach asymptotically to identical values for large time. Sensitive variations with the vertical component of the mean velocity are also observed.

While most works on the field scale dispersion are related to dispersion due to heterogeneities in permeability, the effects of density and viscosity variations on the macroscale dispersivity are considered by employing the stochastic approach of Gelhar and Axness (1983) in Welty and Gelhar (1991). The natural logarithms of density and viscosity are treated as stationary three-dimensional random field. One-dimensional vertical mean flow of miscible fluids is chosen to obtain the longitudinal dispersivity A_L, but the three-dimensional variability of the medium is still contained by allowing A_L to be three-dimensional over the wave number domain. The dispersivity depends not only on the covariance and correlation scale of the log permeability as in tracer case, but also on the concentration gradient, geometric means of density, viscosity and log permeability, and mean specific discharge. This implies that the dispersivity A_L is coupled to the transport on the macroscale. It has a resemblance, in view of coupling to the macroscale proceses, to thermal dispersion with important buoyancy on the macroscale which is studies in Chapter II where nonlinear coupling of dispersion tensor to macroscale heat transport is shown. In stable case, A_L increases in early time and then decreases exponentially to asymptotic limit whereas, in unstable case, A_L grows exponentially with displacement distance. However the assumption of one-dimensional mean concentration gradient and mean flow is too restrictive in that dispersion phenomenon is almost always multi-dimensional. The transverse dispersivity and its difference from the longitudinal one should be examined together. This is particulary so in that the dispersivities are coupled to the macroscale problem.

SCOPE OF THE PRESENT WORK

Given the complexity of the natural phenomena, every theory focuses on part of the issues and bypasses other part that it cannot deal with effectively. All theories tend to contain assumptions which cannot be confirmed in details, but their virtues can only be judged by either their ability to predict certain gross features or the scientific insight they help reveal. The method of homogenization has the virtue

of permitting the most thorough and consistent theory but is limited to a very special class of microstructure which is more common in manufactured materials than natural geological media. As has been mentioned earlier, theories which start with empirical relations cannot take the effects of microscael variations on the macroscale processes into account explicitly. Even in the random capillary model of Saffman (1959), certain properties should be determined by measurements. Similarly the model of randomly distributed spherical particles (Koch and Brady, 1985) is valid for dilute suspensions that are not appealing. On the other hand, with the assumption of periodic structures on the lower scales, it canonot be overemphasized that the homogenization theory proves to be a rigorous tool to systematically provide the macroscale governing equations and coefficients starting from the mocroscale of pore size. Also the macroscael heterogeneities are readily incorporated by employing the multiple-scales.

In this part, we investigate thermal dispersion in deformable periodic porous media by using the theory of homogenization. The issue of medium characterization is not treated here. Instead we shall focus our attention on the thermomechanics and dispersion in spatially periodic porous media.

In Chapter I, two-scale medium is considered. The medium is assumed to be relatively highly permeable and hard. The Peclét number and Rayleigh number are assumed to be finite. Under these assumptions, the soild deformation is decoupled from the flow and heat transport in that the pore pressure and the medium temperature affect the deformation but not vice versa. By multiple-scale perturbation analysis, the macroscale governing equations and consgtitutive coefficients are deduced. Because of hard porous medium, Darcy's law takes the form for rigid media. The consolidation and heat transport equations are nonlinearly coupled via the first order convection velocity. For moderate Rayleigh number the buoyancy effect is small and appears at the first order seepage velocity. However it can affect heat convection over large time scale of heat diffusion and makes the flow and heat transport nonlinearly coupled.

A canonical microcell boundary value problem is defined which must be solved for a given cell geometry to calculate the macroscale dispersion tensor. Other microcell boundary value problems are the same as those treated in Part A for themoconsolidation. For a special three-dimensional microcell geometry of Wigner-Seitz grains, the dispersion tensors for solute and heat are computed numerically by using a variational principle for a mean flow along a symmetry axis. By using symmetry relations of the solution for such special flow direction, it is shown that there are only two non-vanishing independent dispersion coefficients, the longitudinal D_L and the transverse D_T. They are isotropic in the plane normal to the flow direction. Computed D_L and D_T are compared with the numerical results by Salles et al(1993) and the experimental results by Gunn and Pryce(1969), both for cubic array of spheres. The behavior of Pe^2 for D_L is confirmed and D_T also follows the similar trend. In particular for the special flow direction, the increasing trend of D_T with Pe is demonstrated for the first time for spatially periodic media. This has not been shown previously in the approximate analytical theory for dilute periodic suspensions (Koch et al, 1989) and the numerical results for periodic cylinders (Eidsath et al, 1983; Edwards et al, 1989) and cubic array of spheres (Salles et al, 1993). It should be pointed out that in natural granular media numerous experiments and theories based on random capillary network or particles show that D_T increases with Pe although the growth is the first power of Pe.

In Chapter II, thermal dispersion in three-scale deformable porous media is studied by extending the two-scale analysis of Ch. I. The larger scale which was called the macroscale is now the mesoscale. The macroscale is much larger than the mesoscale. The mesoscale Peclét number is assumed to be finite, but the Rayleigh number is allowed to be large. Due to the increase of Rayleigh number as compared to the two-scale medium, the buoyancy becomes important in Darcy's law i.e., the temperature affects the seepage flow which in turn modifies the dispersion tensor. This implies that thermal dispersion in porous media is a nonlinearly coupled process among the flow, temperature and dispersion. The medium deformation is determined from the equilibrium equation.

The mesoscale cell boundary value problem is a convection-diffusion equation with distributed sources due to the inhomogeneities of the medium property on the mesoscale. It is shown that the macroscale dispersion tensor is composed of not only those due to heterogeneity of permeability but also those due to spatially varying heat capacity of the medium. This is analogous to the stochastic theory of macrodispersion for spatially varying concentration distribution coefficient K_d in solid phase by Garabedian et al (1988) in which an additive term due to random field of K_d uncorrelated to log permeability appears. The mesoscale cell boundary value problem is nonlinearly coupled to the heat transport on the macroscale. For periodically stratified medium, the cell problem becomes one-dimensional and can be solved analytically for a given seepage velocity field. For general periodic stratification, the problem is solved in terms of the Green's function and the symmetric and anti-symmetric dispersion tensors are explicitly obtained. They obey the tensor transformation rule in the horizontal plane. For the special case of two alternating layers on the mesoscale, the dispersion tensors are examined. It is demonstrated that the longitudinal dispersion coefficient grows with Pe'^2, where Pe' is the mesoscale Peclét number, when the mean flow is perfectly in plane with layers, but reaches finite asymptotic values for non-zero vertical component of the mean flow, as shown in the previous works (Matheron and de Marsily, 1980; Gupta and Bhattacharya, 1986; Güven and Moltz, 1986). When the permeability variation only is allowed, the off-diagonal coefficients in the symmetric dispersion tensor and the anti-symmetric tensor vanish. However for thermal dispersion, in which not only the permeability but also the heat capacity and thermal conductivity are inhomogenous, they are non-zero.

The general theory is applied to thermal dispersion of a thermal cloud in layered porous media with uniform longitudinal seepage flow. The Rayleigh number tends to increase the disturbances in flow and temperature and thus variation of the dispersion coefficients, but the Peclét number tends to weaken the effects of Rayleigh number. For sufficiently large Rayleigh number the thermal cloud rises across the layer before the medium temperature spreads out due to dispersion.

Chapter I. THERMAL DISPERSION IN TWO-SCALE POROELASTIC MEDIA

1. Introduction

A two scale porous medium is characterized by the existence of two disparate length scales, the microscale ℓ and the macroscale ℓ'. The scale ratio $\epsilon = \ell/\ell'$ is assumed to be very small. The structure of the porous medium is assumed to be periodic on the microscale with periodic length ℓ. It is also assumed that the variables and material propertiers are periodic over the microscale.

The microscale Peclét number $Pe = U\ell/\alpha_f$, where U and α_f are the fluid velocity and the thermal diffusivity of fluid, is assumed to be $O(1)$. It is shown that the heat transport is dominated by convection over the convection time scale. For much longer time scale of heat diffusion, dispersion which is convection-enhanced diffusion on the macroscale and convection due to weak inertia in the fluid momentum equation become important. Hence the flow and heat ransport are nonlinearly coupled. By solving numerically the canonical microcell boundary value problem, which is a convection diffusion equation with distributed sources, for a cubic array of Wigner-Seitz grains dispersion coefficients are calculated.

2. The Governing Equations and Boundary Conditions

On the microscale the basic governing equations and boundary conditions are the same as those in Part A for thermoconsolidation. In the present case of thermal dispersion in poroelastic media, the Pecét number is allowed to be finite and is asssumed to be $O(1)$.

2.1 The Governing Equations, Boundary Conditions and Order Estimates

We start from the governing equations on the microscale listed in §2 of Ch. I in Part A. At the initial state, it is assumed that the porous medium is isothermal.

In the fluid phase, the governing equations are the conservation laws of mass

$$\nabla \cdot u = 0 \quad \text{in} \quad \Omega_f \tag{2.1.1}$$

momentum

$$\rho_f \left(\frac{\partial u}{\partial t} + u \cdot \nabla u \right) = -\nabla p + \mu \nabla^2 u + \rho_f g \beta_T \theta_f \mathbf{e}_z \quad \text{in} \quad \Omega_f \tag{2.1.2}$$

and energy

$$(\rho C_p)_f \left(\frac{\partial \theta_f}{\partial t} + u \cdot \nabla \theta_f \right) = \nabla \cdot (m_f \cdot \nabla \theta_f) \quad \text{in} \quad \Omega_f \tag{2.1.3}$$

where u, p and θ are the velocity, dynamic pressure and temperature variation from the initial state and the subscript f denotes the fluid phase. Also, ρ, C_p and m denote the density, specific heat and thermal conductivity, respectively. The last term in (2.1.2) is the body force induced by buoyancy obtained after making use of Boussinesq

In the solid phase, we have the *quasi*-static equilibrium

$$\nabla \cdot \sigma_s = 0 \quad \text{in} \quad \Omega_s \tag{2.1.4}$$

for sufficiently slow motion. The energy balance is governed by

$$(\rho C_p)_s \left(\frac{\partial \theta_s}{\partial t} + \frac{dv}{dt} \cdot \nabla \theta_s \right) = \nabla \cdot (m_s \cdot \nabla \theta_s) \quad \text{in} \quad \Omega_s \tag{2.1.5}$$

where σ_s is the solid stress, dv/dt is the velocity of solid phase, The subscript s stands for the solid phase. Assuming linear elastic deformation, the solid stress σ_s is related to v via Hooke's law

$$\sigma_s = a : e(v) - \beta\theta_s \cdot I \tag{2.1.6}$$

where a is the elastic coefficient tensor of rank four and β is the thermal modulus tensor of rank two. The symbol I denotes the identity tensor. Also $e(\cdot)$ is the linear strain operator

On the instantaneous interface $\Gamma(t)$ between the fluid and solid, the following boundary conditions are imposed: the kinematic boundary condition :

$$u = \frac{dv}{dt} \qquad \text{on} \quad \Gamma(t) \tag{2.1.7}$$

and the dynamical condition :

$$\sigma_s \cdot N = \sigma_f \cdot N \qquad \text{on} \quad \Gamma(t) \tag{2.1.8}$$

where N is the unit normal vector on Γ pointing from the fluid into the solid. For heat transfer we also impose temperature continuity :

$$\theta_f = \theta_s \tag{2.1.9}$$

and heat flux continuity :

$$(m_f \cdot \nabla\theta_f) \cdot N = (m_s \cdot \nabla\theta_s) \cdot N \tag{2.1.10}$$

The fluid stress σ_f in (2.1.8) is defined as

$$\sigma_f = -pI + 2\mu e(u) \tag{2.1.11}$$

Consider the flow through pores of micro-length scale ℓ driven by a pressure drop P' over the macroscale ℓ'. We impose the basic assumptions that the length

ratio $\epsilon = \ell/\ell' \ll 1$ is very small. For sufficiently slow motion, the fluid velocity is scaled by balancing the pressure gradient and the viscous stress,e.g.

$$U = \frac{P'\ell^2}{\mu\ell'} \tag{2.1.12}$$

We assume that the Reynolds number is very small.

$$Re = \frac{U\ell}{\nu} \leq O(\epsilon) \tag{2.1.13}$$

The relevant time scales are the consolidation time T_c, the convection time T_v and the diffusion time

$$T_c = \frac{\rho_f g \ell'^2}{\mathcal{D}K}, \quad T_v = \frac{\ell'}{U}, \quad T_d = \frac{\ell'^2}{\alpha_f} \tag{2.1.14}$$

where $\mathcal{D}$ and $K = O\left(g\ell^2/\nu\right)$ are the elastic modulus and the hydraulic conductivity of the medium respectively and $\alpha_f = m_f/(\rho C_p)_f$ is the thermal diffusivity of the fluid. From (2.1.14) it follows that

$$\frac{T_c}{T_d} = \frac{\rho_f g \alpha_f}{\mathcal{D}K} \quad \text{and} \quad \frac{T_v}{T_d} = \frac{\ell}{\ell'}\frac{\alpha_f}{U\ell} = \frac{\epsilon}{Pe} \tag{2.1.15}$$

where

$$Pe = Re \cdot Pr = \frac{U\ell}{\nu}\frac{\nu}{\alpha_f} = \frac{U\ell}{\alpha_f} \tag{2.1.16}$$

is the Peclét number defined by the microscale and $Pr = \nu/\alpha_f$ is the Prandtl number.

The Peclét number is a measure of the relative importance of heat convection to diffusion. The Prandtl number of fluid varies widely from low to large numbers ; it is $O(1)$ for water and is greater than $O(10^3)$ for some oils (Lienhard, 1984; Kays and Crawford, 1980; Eckert and Drake, 1987). For generality we shall assume that $Pr = O(1/\epsilon)$. It then follows from (2.1.13), (2.1.15) and (2.1.16) that

$$Pr = O(1/\epsilon) \quad ; \quad Pe = O(1) \quad ; \quad T_v/T_d = O(\epsilon) \tag{2.1.17}$$

It is anticipated that the transport of heat on the macroscale is dominated by convection which is implied by the time scale ratio of (2.1.15). Since dispersion

is more likely to be important in relatively highly permeable medium which is in general also hard (cf. Table 2.1 of Part A), we shall assume that

$$\frac{T_c}{T_d} = O(\epsilon^2) \tag{2.1.18}$$

which is typical of sandy material. Equation (2.1.18) shows that T_c is equivalent to the time scale describing thermal changes over the microscale. Since we are interested in changes which occur over much larger macroscale distances, variations over the shortest time scale will be ignored and T_c is dropped. Consequently two time scales T_v and $T_d = T_v/\epsilon$(cf.(2.23b)) will be used for fast and slow time scales later.

Combining the stress continuity condition (2.1.8) with (2.1.6) and (2.1.11) it is readily seen that

$$\frac{\sigma_f}{\sigma_s} \sim \frac{P'}{a:e(v)} \sim \frac{P'}{\mathcal{D}\delta} = O(1) \quad ; \quad \delta = O\left(\frac{P'}{\mathcal{D}}\right) \tag{2.1.19}$$

Hooke's law (2.1.6) is legitimate only for infinitesimal strain,e.g. $\delta \ll 1$. In Part A on thermoconsolidation, it was assumed that $\delta = O(P'/\mathcal{D}) = O(\epsilon)$. In this Part, the porous medium is assumed to be harder and more permeable so that

$$\frac{P'}{\mathcal{D}} = O(\delta) = O(\epsilon^2) \tag{2.1.20}$$

If we let ΔV be the order of magnitude of medium deformation, (2.1.16) implies that $\Delta V/\ell' = O(\epsilon^2)$ or

$$\Delta V = O(\epsilon\ell) \ll \ell \tag{2.1.21}$$

so that the deformation is much less than the microscale length.

2.2 Normalized Governing Equations and Boundary Conditions

The governing equations and boundary conditions are normalized by using the scale estimates of §2.1. The procedure is quite similar to that in §2.2 of Ch. I

in Part A and is not repeated here. Instead we point out some differences. The normalization is as follows:

$$\begin{aligned} &x = \ell x^*, \quad t = Tt^* \\ &u = Uu^* = \frac{P'\ell^2}{\mu\ell'}u^*, \quad p = P'p^*, \quad \theta_{f,s} = \Theta'\theta^*_{f,s} \\ &\sigma_s = \mathcal{D}\sigma^*_s, \quad \sigma_f = P'\sigma^*_f \quad v = \ell v^* \\ &a = \mathcal{D}a^*, \quad \beta = B\beta^*, \quad m_f = M_f m^*_f, \quad m_s = M_s m^*_s \end{aligned} \tag{2.2.1}$$

in which variables with the superscript * are dimensionless. In view of the time scale difference in (2.1.17), the normalization time scale is chosen as

$$T = T_v \tag{2.2.2}$$

It is noted that the normalization of v and σ_s does not necessarily mean $v = O(\ell)$ (or $e(v) = O(1)$) and $\sigma_s = O(\mathcal{D})$. In fact, it will be shown later that $v = O(\epsilon\ell)$ and $\sigma_s = O(\epsilon^2\mathcal{D})$ so as to be consistent with (2.1.16).

The normalized governing equations are reproduced from §2 in Ch. I of Part A. In the fluid phase, we have

$$\nabla^* \cdot u^* = 0 \qquad \text{in} \quad \Omega_f \tag{2.2.3}$$

$$\left[\frac{\rho_f \ell^2}{\mu T}\epsilon\right]\frac{\partial u^*}{\partial t^*} + \epsilon Re u^* \cdot \nabla^* u^* = -\nabla^* p^* + \epsilon \nabla^{*2} u^* + \left[\frac{\epsilon^2}{Pe} Ra\right]\theta^*_f \mathbf{e}_z \qquad \text{in} \quad \Omega_f \tag{2.2.4}$$

$$\left[\frac{\ell^2}{\alpha_f T}\right]\frac{\partial \theta^*_f}{\partial t^*} + Pe u^* \cdot \nabla^* \theta^*_f = \nabla^* \cdot (m^*_f \cdot \nabla^* \theta^*_f) \qquad \text{in} \quad \Omega_f \tag{2.2.5}$$

where

$$Ra = \frac{g\beta_T \ell^2 \ell' \Theta}{\nu \alpha_f} \tag{2.2.6}$$

Also in the solid phase,

$$\nabla^* \cdot \sigma^*_s = 0 \qquad \text{in} \quad \Omega_s \tag{2.2.7}$$

$$\frac{(\rho C_p)_s}{(\rho C_p)_f}\left(\left[\frac{\ell^2}{\alpha_f T}\right]\frac{\partial \theta^*_s}{\partial t^*} + \left[\frac{V'\ell}{\alpha_f T}\right]\frac{dv^*}{dt^*} \cdot \nabla^* \theta^*_s\right) = \left[\frac{M_s}{M_f}\right]\nabla^* \cdot (m^*_s \cdot \nabla^* \theta^*_s) \qquad \text{in} \quad \Omega_s \tag{2.2.8}$$

Hooke's law is given by

$$\sigma^*_s = a^* : e^*(v^*) - [\alpha\Theta]\beta^*\theta^*_s \qquad \text{in} \quad \Omega_s \tag{2.2.9}$$

It is assumed that the Rayleight number is finite,

$$Ra \leq O(1) \tag{2.2.10}$$

in the buoyancy term. In Hooke's law, thermal stress must be balanced by the strain term. Since the medium strain is such that $\delta = O(\epsilon^2)$ from (2.1.20) and the thermal modulus β is $O(B) = O(\alpha\mathcal{D})$ where α is the linear expansion coefficient , we assume in (2.2.9) that

$$\alpha\Theta' \sim \delta = O(\epsilon^2) \tag{2.2.11}$$

We now estimate other dimensionless factors. As remarked in (2.1.6), $T_c = \epsilon^2 T_d$ is not of interest and there remain

$$T_v, \quad T_d = T_v/\epsilon \tag{2.2.12}$$

The convection velocity ratio V/UT becomes, by using $T = T_v$ and $V = O(\epsilon\ell)$,

$$\frac{V}{UT_v} = \frac{\epsilon\ell}{U\frac{\ell'}{U}} = \epsilon^2 \tag{2.2.13}$$

where, in view of (2.1.21), $v = O\epsilon\ell)$ has been used. It also follows that the multiplying factor in the convection term of (2.2.8) becomes

$$\frac{V\ell}{\alpha_f T} = \frac{U\ell}{\alpha_f}\frac{V}{UT_v} = O(Pe\epsilon^2) \tag{2.2.14}$$

Similarly other dimensionless factors in the local derivatives of fluid momentum, and energy equations of fluid and solid become

$$\frac{\rho_f \ell^2}{\mu T}\epsilon = \frac{\rho_f \ell^2 U}{\mu \ell'}\epsilon = \frac{U\ell}{\nu}\epsilon^2 = O(\epsilon^2 Pe) \tag{2.2.15}$$

$$\frac{\ell^2}{\alpha_f T} = \frac{\ell^2 U}{\alpha_f \ell'} = \frac{U\ell}{\alpha_f}\frac{\ell}{\ell'} = O(\epsilon Pe) \tag{2.2.16}$$

Finally by substituting (2.1.20), (2.2.11)-(2.2.16) into the normalized governing equations (2.2.3)-(2.2.5), (2.2.7)-(2.2.9), we obtain the following governing equations

$$\nabla^* \cdot u^* = 0 \qquad \text{in} \quad \Omega_f \tag{2.2.17}$$

$$\epsilon^3 \frac{\partial u^*}{\partial t^*} + \hat{Re}\epsilon^2 u^* \cdot \nabla^* u^* = -\nabla^* p^* + \epsilon \nabla^{*2} u^* + \epsilon^2 Ra \theta_f^* \mathbf{e}_z \qquad \text{in} \quad \Omega_f \tag{2.2.18}$$

$$Pe\left(\epsilon \frac{\partial \theta_f^*}{\partial t^*} + u^* \cdot \nabla^* \theta_f^*\right) = \nabla^* \cdot \left(m_f^* \cdot \nabla^* \theta_f^*\right) \qquad \text{in} \quad \Omega_f \tag{2.2.19}$$

$$\nabla^* \cdot \sigma_s^* = 0 \qquad \text{in} \quad \Omega_s \tag{2.2.20}$$

$$Pe(\rho C_p)_r \epsilon \left(\frac{\partial \theta^*}{\partial t^*} + \epsilon \frac{dv^*}{dt^*} \cdot \nabla^* \theta^*\right) = M_r \nabla^* \cdot (m_s^* \cdot \nabla^* \theta^*) \qquad \text{in} \quad \Omega_s \tag{2.2.21}$$

where for simplicity the following notations have been used.

$$\hat{Re} = \frac{Re}{\epsilon} = O(1), \quad (\rho C_p)_r = \frac{(\rho C_p)_s}{(\rho C_p)_f}, \quad M_r = \frac{M_s}{M_f} \tag{2.2.22}$$

The stresses in the solid and fluid are scaled as

$$\sigma_s^* = a^* : e^*(v^*) - \epsilon^2 \beta^* \theta_s^* \tag{2.2.23}$$

$$\sigma_f^* = -p^* I + \epsilon e^*(u^*) \tag{2.2.24}$$

Similarly the interface boundary conditions (2.1.7) to (2.1.10) become

$$u^* = \epsilon^2 \frac{dv^*}{dt^*} \qquad \text{on} \quad \Gamma(t) \tag{2.1.25}$$

$$\sigma_s^* \cdot N = \epsilon^2 \sigma_f^* \cdot N \qquad \text{on} \quad \Gamma(t) \tag{2.2.26}$$

$$\theta_f^* = \theta_s^* \qquad \text{on} \quad \Gamma(t) \tag{2.2.27}$$

$$(m_f^* \cdot \nabla^* \theta_f^*) \cdot N = M_r (m_s^* \cdot \nabla^* \theta_s^*) \cdot N \qquad \text{on} \quad \Gamma(t) \tag{2.2.28}$$

Using the above governing equations and boundary conditions, the macroscale governing equations will be deduced in the next section.

3. The Macroscale Governing Equations

The macroscale governing equations are deduced from the normalized governing equations of §2.2. In §3.1 by intoducing the multipe-scale expansions for both spatial coordinates and time, the approximate governing equations and boundary conditions are obtained at each order of small parameter ϵ. In §3.2, the equations which govern the solid and fluid motions on the macroscale are derived. Because of finite microscale Peclét number, the heat transport is dominated by convection over the convection time on the macroscale. Accordingly for much longer time scale of heat diffusion, the heat convection due to first order fluid velocity becomes important. This requires the analysis of weak inertia effect in the fluid momentum equation and will be treated in §3.3 following Mei and Auriault(1991). Finally in §3.4, the macroscale heat transport equation is obtained. A canonical cell problem is defined from which the macroscale dispersion tensor is calculated. It will be shown that the dispersion tensor is composed of not only symmetric part but also anti-symmetric part which in turn modifies the convection velocity. The governing equations in physical variables are presented in §3.5.

3.1 Multiple Scale Expansions and Approximate Equations at Successive Orders of ϵ

We assume a periodic structure on the microscale and divide the medium into periodic micro-cells (Ω-cell). All the variables and material coefficients are assumed to be Ω-periodic.

Introduce the multiple-scale vectors

$$x, \qquad x' = \epsilon x \tag{3.1.1}$$

for spatial coordinates. Also, in view of the disparity in time scales $T_v = \epsilon T_d$ of (2.2.5), we introduce the multiple time scales

$$t = t_v, \qquad t' = t_d = \epsilon t_v \tag{3.1.2}$$

Accordingly, the differential operators become, after expansion,

$$\begin{aligned} \nabla^* &= \nabla + \epsilon\nabla' \\ e^*(\cdot) &= e(\cdot) + \epsilon e'(\cdot) \\ \frac{\partial}{\partial t^*} &= \frac{\partial}{\partial t_v} + \epsilon\frac{\partial}{\partial t_d} \end{aligned} \qquad (3.1.3a-c)$$

Let us introduce the perturbation expansions

$$v^* = v^{(0)} + \epsilon v^{(1)} + \epsilon^2 v^{(2)} + \ldots \qquad (3.1.4)$$

$$\sigma_s^* = \sigma_s^{(-2)} + \epsilon\sigma_s^{(-1)} + \epsilon^2\sigma_s^{(0)} + \ldots \qquad (3.1.5)$$

for the solid displacement and stress. Upon substituting (3.1.2) and (3.1.3) into Hooke's law (2.2.23), we obtain

$$\begin{aligned} \sigma_s^{(-2)} &= a^* : e(v^{(0)}) \\ \sigma_s^{(-1)} &= a^* : [e'(v^{(0)}) + e(v^{(1)})] \\ \sigma_s^{(0)} &= a^* : [e'(v^{(1)}) + e(v^{(2)})] - \beta^*\theta_s^{(0)} \end{aligned} \qquad (3.1.6)$$

It follows immediately from (2.1.2) and (2.2.26) that

$$\sigma_s^{(-2)} = \sigma_s^{(-1)} = 0 \qquad (3.1.7)$$

Obviously the vanishing of $\sigma_s^{(-2)}$ implies that $v^{(0)} = v^{(0)}(x', t, t')$ is independent of the microscale. On the other hand, we have from (2.1.21) and (2.2.1) that $v^* = v/\ell = O(\epsilon)$. In order for (3.1.7) to be consistent with this small strain, it is necessary that

$$v^{(0)} = 0, \quad v^{(1)} = v^{(1)}(x', t, t') \qquad (3.1.8)$$

Since the solid displacement $v = O(\epsilon\ell)$ is very small compared to the size of micro-cell Ω, as implied by (3.1.8), the departure of instantaneous fluid-solid interface $\Gamma(t)$ from its initial position $\Gamma(0)$ is also very small. Thus the interface boundary conditions (2.2.25) to (2.2.28) can be expanded in Taylor series about $\Gamma(0)$ before multiple scale expansions are introduced.

We further introduce the perturbation expansions

$$f^* = f^{(0)} + \epsilon f^{(1)} + \epsilon^2 f^{(2)} + ... \tag{3.1.9}$$

for

$$f = u^*, p^*, \sigma_f^*, \theta_f^* \quad \text{or} \quad \theta_s^* \tag{3.1.10}$$

It then follows from the leading order equation of (2.2.10) that

$$p^{(0)} = p^{(0)}(x', t, t') \tag{3.1.11}$$

so that the leading order pressure does not depend on the microscale coordinate. The equations at higher orders of ϵ give rise to different physical features due to the increased Peclét number.

In the fluid phase, the continuity equation (2.2.17) yields

$$\begin{aligned} O(1) \qquad & \nabla \cdot u^{(0)} = 0 \\ O(\epsilon) \qquad & \nabla' \cdot u^{(0)} + \nabla \cdot u^{(1)} = 0 \end{aligned} \tag{3.1.12a,b}$$

The momentum equation (2.2.18) becomes

$$\begin{aligned} O(1) \qquad & 0 = \nabla p^{(0)} \\ O(\epsilon) \qquad & 0 = -(\nabla' p^{(0)} + \nabla p^{(1)}) + \nabla^2 u^{(0)} = \nabla' \sigma_f^{(0)} + \nabla \sigma_f^{(1)} \\ O(\epsilon^2) \qquad & u^{(0)} \cdot \nabla u^{(0)} = -(\nabla' p^{(1)} + \nabla p^{(2)}) + 2(\nabla \cdot \nabla') u^{(0)} + \nabla^2 u^{(1)} + Ra \theta_f^{(0)} \mathbf{e}_z \\ & \qquad = \nabla' \sigma_f^{(1)} + \nabla \sigma_f^{(2)} + Ra \theta_f^{(0)} \mathbf{e}_z \end{aligned} \tag{3.1.13a-c}$$

in which the fluid stress is given by

$$\begin{aligned} \sigma_f^{(0)} &= -p^{(0)} I \\ \sigma_f^{(1)} &= -p^{(1)} I + 2e(u^{(0)}) \\ \sigma_f^{(2)} &= -p^{(2)} I + 2e'(u^{(0)}) + 2e(u^{(1)}) \end{aligned} \tag{3.1.14a-c}$$

Note that, because of increased Peclét number, bouyancy is negligibly small and appears only at $O(\epsilon^2)$.

The energy equation (2.2.19) becomes

$$
\begin{aligned}
O(1) \qquad & Peu^{(0)} \cdot \nabla\theta_f^{(0)} = \nabla \cdot \left(m_f^* \cdot \nabla\theta_f^{(0)}\right) \\
O(\epsilon) \qquad & Pe\left[\frac{\partial\theta_f^{(0)}}{\partial t_v} + u^{(0)} \cdot \left(\nabla'\theta_f^{(0)} + \nabla\theta_f^{(1)}\right) + u^{(1)} \cdot \nabla\theta_f^{(0)}\right] \\
& \qquad = \nabla' \cdot \left(m_f^* \cdot \nabla\theta_f^{(0)}\right) + \nabla \cdot \left[m_f^* \cdot \left(\nabla'\theta_f^{(0)} + \nabla\theta_f^{(1)}\right)\right] \\
O(\epsilon^2) \qquad & Pe\Big[\frac{\partial\theta_f^{(0)}}{\partial t_d} + \frac{\partial\theta_f^{(1)}}{\partial t_v} + u^{(0)} \cdot \left(\nabla'\theta_f^{(1)} + \nabla\theta_f^{(2)}\right) + u^{(1)} \cdot \left(\nabla'\theta_f^{(0)} + \nabla\theta_f^{(1)}\right) \\
& \qquad + u^{(2)} \cdot \nabla\theta_f^{(0)}\Big] = \nabla' \cdot \left[m_f^* \cdot \left(\nabla'\theta_f^{(0)} + \nabla\theta_f^{(1)}\right)\right] \\
& \qquad + \nabla \cdot \left[m_f^* \cdot \left(\nabla'\theta_f^{(1)} + \nabla\theta_f^{(2)}\right)\right]
\end{aligned}
\tag{3.1.15a - c}
$$

After using (3.1.8a), the energy equation (2.2.21) in the solid phase is similarly expanded as

$$
\begin{aligned}
O(1) \qquad & 0 = M_r \nabla \cdot \left(m_s^* \cdot \nabla\theta_s^{(0)}\right) \\
O(\epsilon) \qquad & (\rho C_p)_r Pe \frac{\partial\theta_s^{(0)}}{\partial t_v} \\
& \qquad = M_r \left\{\nabla' \cdot \left(m_s^* \cdot \nabla\theta_s^{(0)}\right) + \nabla \cdot \left[m_s^* \cdot \left(\nabla'\theta_s^{(0)} + \nabla\theta_s^{(1)}\right)\right]\right\} \\
O(\epsilon^2) \qquad & (\rho C_p)_r Pe \left[\frac{\partial\theta_s^{(0)}}{\partial t_d} + \frac{\partial\theta_s^{(1)}}{\partial t_v} + \frac{dv^{(1)}}{dt_v} \nabla \cdot \theta_s^{(0)}\right] \\
& \qquad = M_r \left\{\nabla' \cdot \left[m_s^* \cdot (\nabla'\theta_s^{(0)} + \nabla\theta_s^{(1)})\right] + \nabla \cdot \left[m_s^* \cdot \left(\nabla'\theta_s^{(1)} + \nabla\theta_s^{(2)}\right)\right]\right\}
\end{aligned}
\tag{3.1.16a - c}
$$

The interface boundary conditions (2.2.25) to (2.2.28) are first expanded in Taylor series about the initial position $\Gamma(0)$ of the interface and then expanded according to (3.1.3), (3.1.5) and (3.1.9). The results are listed here. The kinematic condition (2.2.25) becomes

$$
\begin{aligned}
O(1) \qquad & u_i^{(0)} = 0 \\
O(\epsilon) \qquad & u_i^{(1)} + v_j^{(1)} \frac{\partial u_i^{(0)}}{\partial x_j} = 0
\end{aligned}
\tag{3.1.17a, b}
$$

The dynamical conditions (2.2.26) gives

$$\begin{aligned} 0(1) \qquad & \sigma_s^{(-2)} \cdot N = 0 \\ 0(\epsilon) \qquad & \sigma_s^{(-1)} \cdot N = 0 \\ 0(\epsilon^2) \qquad & \sigma_s^{(0)} \cdot N = \sigma_f^{(0)} \cdot N \\ 0(\epsilon^3) \qquad & (\sigma_s^{(1)} + v^{(1)} \cdot \nabla \sigma_s^{(0)}) \cdot N = (\sigma_f^{(1)} \cdot + v^{(1)} \cdot \nabla \sigma_f^{(0)}) \cdot N \end{aligned} \tag{3.1.18a-c}$$

in which (3.1.18a and b) have already been used to show (3.1.8). In the same manner, the thermal boundary conditions (2.2.27) and (2.2.28) are expanded as

$$\begin{aligned} O(1) \qquad & \theta_f^{(0)} = \theta_s^{(0)} \\ O(\epsilon) \qquad & \theta_f^{(1)} + v^{(1)} \cdot \nabla \theta_f^{(0)} = \theta_s^{(1)} + v^{(1)} \cdot \nabla \theta_s^{(0)} \\ O(\epsilon^2) \qquad & \theta_f^{(2)} + v^{(1)} \cdot (\nabla' \theta_f^{(0)} + \nabla \theta_f^{(1)}) + v^{(2)} \cdot \nabla \theta_f^{(0)} + \frac{1}{2} v^{(1)} v^{(1)} : \theta_f^{(0)} \\ & = \theta_s^{(2)} + v^{(1)} \cdot (\nabla' \theta_s^{(0)} + \nabla \theta_s^{(1)}) + v^{(2)} \cdot \nabla \theta_s^{(0)} + \frac{1}{2} v^{(1)} v^{(1)} : \theta_s^{(0)} \end{aligned} \tag{3.1.19a-c}$$

and

$$\begin{aligned} O(1) \qquad & m_f^* \cdot \nabla \theta_f^{(0)} \cdot N = M_r m_s^* \cdot \nabla \theta_s^{(0)} \\ O(\epsilon) \qquad & m_f^* \cdot \left(\nabla' \theta_f^{(0)} + \nabla \theta_f^{(1)} \right) \cdot N + v_j^{(1)} \frac{\partial}{\partial x_j} \left(m_f^* \cdot \nabla \theta_f^{(0)} \right) \cdot N = \\ & M_r \left\{ m_s^* \cdot \left(\nabla' \theta_s^{(0)} + \nabla \theta_s^{(1)} \right) \cdot N + v_j^{(1)} \frac{\partial}{\partial x_j} \left(m_s^* \cdot \nabla \theta_s^{(0)} \right) \cdot \right\} \end{aligned}$$

$$\begin{aligned} O(\epsilon^2) \quad & m_f^* \cdot \left(\nabla' \theta_f^{(1)} + \nabla \theta_f^{(2)} \right) \cdot N + v_j^{(1)} \frac{\partial}{\partial x_j} \left[m_f^* \cdot \left(\nabla' \theta_f^{(0)} + \nabla \theta_f^{(1)} \right) \right] \cdot N \\ & + v_j^{(2)} \frac{\partial}{\partial x_j} \left(m_f^* \cdot \nabla \theta_f^{(0)} \right) \cdot N = M_r m_s^* \cdot \left(\nabla' \theta_s^{(1)} + \nabla \theta_s^{(2)} \right) \cdot N \\ & + v_j^{(1)} \frac{\partial}{\partial x_j} \left[M_r m_s^* \cdot \left(\nabla' \theta_s^{(0)} + \nabla \theta_s^{(1)} \right) \right] \cdot N + v_j^{(2)} \frac{\partial}{\partial x_j} \left(M_r m_s^* \cdot \nabla \theta_s^{(0)} \right) \cdot N \end{aligned} \tag{3.1.20a-c}$$

3.2 Macroscale Equations for Solid and fluid Motions

The macroscale equilibrium equation and Hooke's law are obtained by following the same procedure as in §3 of Ch. I in Part A. Because of the reduced buoyancy

effect in the fluid momentum equation (3.1.12), the macroscale equilibrium equation does not have buoyancy term. They are reproduced here as

$$\begin{aligned} \nabla' \cdot \langle \sigma_T^{(0)} \rangle &= 0 \\ \langle \sigma_T^{(0)} \rangle &= a' : e'(v^{(1)}) - \alpha' p^{(0)} - \beta_t' \theta^{(0)} \end{aligned} \tag{3.2.1a,b}$$

where a', α' and β_t' are given in (3.3.15a-c) of Ch. I in Part A and the fact that $\theta_s^{(0)} = \theta^{(0)}(x', t_v, t_d)$ (will be shown later) has been used.

In the fluid phase, it may be assumed from (3.1.13b) that

$$\begin{aligned} u^{(0)} &= -k \cdot \nabla' p^{(0)} \\ p^{(1)} - \bar{p}^{(1)} &= S \cdot \nabla' p^{(0)} \end{aligned} \tag{3.2.2a,b}$$

where $k(x, x')$ and $S(x, x')$ must satisfy the Stokes problem defined in §3 of Ch. I in Part A and $\bar{p}^{(1)}$ is independnet of the microscale and is the average of $p^{(1)}$ over the Ω-cell. By taking the Ω-average of (3.2.2a), Darcy's law becomes

$$\langle u^{(0)} \rangle = -k' \cdot \nabla' p^{(0)} \tag{3.2.3}$$

where k' is the permeability tensor given in §3 of Ch. I in Part A. In (3.2.3), as mentioned earlier, the seepage velocity is not affected by buoyancy for finite Peclét number. Also, since the solid velocity is small(cf.(3.1.16)) and $v^{(1)}$ is independent of the microscale, the right-hand side of (3.3.27) of Ch. I in Part A does not appear. Consequently, the consolidation equation reduces to

$$\nabla' \cdot (k' \cdot \nabla' p^{(0)}) = 0 \tag{3.2.4}$$

It is readily seen that the coupling of solid and fluid motions with temperature appears only in the equilibrium equation (3.2.1a). In order to deduce the governing law of macrotransport of heat, we consider the effect of weak inertia in fluid flow (cf. (3.1.13c)) next.

3.3 Effect of Weak Inertia

As shown in Mei (1991b) for a rigid isothermal porous medium, higher order flow velocity associated with weak inertia is in general needed.

The results for deformable medium are similar to those by Mei (1991) and Mei & Auriault (1991) with some additional terms and will be needed later for the mean heat transport equation.

By substituting (3.2.2a and b) into the $O(\epsilon^2)$ momentum equation at $O(\epsilon^2)$ (3.1.13c) and making use of (3.12a) we obtain, in indicial form,

$$k_{mk}\frac{\partial k_{ij}}{\partial x_m}\frac{\partial p^{(0)}}{\partial x'_j}\frac{\partial p^{(0)}}{\partial x'_k}+\frac{\partial S_j}{\partial x'_i}\frac{\partial p^{(0)}}{\partial x'_j}+S_j\delta_{ik}\frac{\partial^2 p^{(0)}}{\partial x'_j\partial x'_k}+\delta_{ij}\frac{\partial \bar{p}^{(1)}}{\partial x'_j}$$

$$+2\left(\frac{\partial^2 k_{ij}}{\partial x_k\partial x'_k}\frac{\partial p^{(0)}}{\partial x'_j}+\frac{\partial k_{ij}}{\partial x_k}\frac{\partial^2 p^{(0)}}{\partial x'_j\partial x'_k}\right)-Ra\delta_{iz}\theta^{(0)}=-\frac{\partial p^{(2)}}{\partial x_i}+\frac{\partial^2}{\partial x_k\partial x_k}u_i^{(1)} \quad (3.3.1)$$

We note that the last term on the left-hand side of (3.3.1) reflects the new effect of buoyancy. Similarly, the continuity equation (3.1.12b) becomes

$$-\frac{\partial k_{ij}}{\partial x'_i}\frac{\partial p^{(0)}}{\partial x'_j}-k_{ij}\delta_{ik}\frac{\partial^2 p^{(0)}}{\partial x'_j\partial x'_k}+\frac{\partial u_i^{(1)}}{\partial x_i}=0 \quad (3.3.2)$$

In view of linearity we assume

$$\begin{Bmatrix} u_i^{(1)} \\ p^{(2)}-\bar{p}^{(2)} \end{Bmatrix}=\begin{bmatrix} -L_{ijk} & -L'_{ijk} & -K'_{ij} & -K_{ij} & -F_i \\ -B_{jk} & -B'_{jk} & -S'_j & -S_j & -E \end{bmatrix}\{Y\} \quad (3.3.3)$$

where

$$\{Y\}=\left[\frac{\partial p^{(0)}}{\partial x'_j}\frac{\partial p^{(0)}}{\partial x'_k},\frac{\partial^2 p^{(0)}}{\partial x'_j\partial x'_k},\frac{\partial p^{(0)}}{\partial x'_j},\frac{\partial \bar{p}^{(1)}}{\partial x'_j},\theta^{(0)}\right]^T \quad (3.3.4)$$

Tensor K_{ij} and vector S_j are the same as those introduced in (3.2.2a and b) and must satisfy the Stokes problem defined in §3 of Ch. I in Part A. It follows from (3.3.1) and (3.3.2) that all other coefficient pairs introduced in (3.23) must satisfy the following momentum equations.

$$\begin{aligned} -k_{mk}\frac{\partial k_{ij}}{\partial x_m} &= -\frac{\partial B_{jk}}{\partial x_i}+\nabla^2 L_{ijk} \\ -S_j\delta_{ik}-2\frac{\partial k_{ij}}{\partial x_k} &= -\frac{\partial B'_{jk}}{\partial x_i}+\nabla^2 L'_{ijk} \\ -\frac{\partial S_j}{\partial x'_i}-2\frac{\partial^2 k_{ij}}{\partial x_m\partial x'_m} &= -\frac{\partial S'_j}{\partial x_i}+\nabla^2 K'_{ij} \\ Ra\delta_{iz} &= -\frac{\partial E}{\partial x_i}+\nabla^2 F_i \end{aligned} \quad (3.3.5)$$

and the mass conservation equations

$$\begin{aligned}
\frac{\partial L_{ij}k}{\partial x_i} &= 0 \\
\frac{\partial L'_{ij}k}{\partial x_i} &= -K_{ij}\delta_{ik} \\
\frac{\partial K'_{ij}}{\partial x_i} &= -\frac{\partial k_{ij}}{\partial x'_i} \\
\frac{\partial F_i}{\partial x_i} &= 0
\end{aligned} \tag{3.3.6}$$

with the boundary conditions

$$L_{ijk} = L'_{ijk} = K'_{ij} = F_i = 0 \quad \text{on} \quad \Gamma$$

and (3.3.7a,b)

$$L_{ijk}, B_{ij}; L'_{ijk}, B'_{ij}; K'_{ij}, S'_j; F_i, E' \quad \text{are} \quad \Omega - \text{periodic}$$

The boundary value problems (3.3.5) to (3.3.7) can be solved numerically for a given cell geometry. Afterwards the Ω-average may be taken to give

$$\begin{pmatrix} \langle u^{(1)} \rangle \\ \langle p^{(2)} \rangle - n\bar{p}^{(2)} \end{pmatrix} = \begin{bmatrix} -\langle L_{ijk} \rangle - \langle L'_{ijk} \rangle & -\langle K'_{ij} \rangle - \langle K_{ij} \rangle - \langle F_i \rangle \\ -\langle B_{jk} \rangle - \langle B'_{jk} \rangle & -\langle S'_j \rangle - \langle S_j \rangle - \langle E \rangle \end{bmatrix} \{ Y \} \tag{3.3.8}$$

of which $\langle u^{(1)} \rangle$ will be needed later.

For an isotropic and homogeneous medium on the macroscale, Mei and Auriault(1991) have shown that the coefficients $\langle L_{ijk} \rangle$, $\langle L'_{ijk} \rangle$ and $\langle K'_{ij} \rangle$ vanish identically. Also since $\langle K_{ij} \rangle$ is the permeability in (3.2.3), $\langle K_{ij} \rangle \partial \bar{p}^{(1)} / \partial x'_j$ can be set to be zero by absorbing $\bar{p}^{(1)}$ into $p^{(0)}$. For the unknown function F_i, we have from (3.3.5) and (3.3.6) that

$$\begin{aligned}
Ra\delta_{iz} = -\frac{\partial E}{\partial x_i} + \frac{\partial^2 F_i}{\partial x_k \partial x_k} \qquad & \text{in} \quad \Omega_f \\
\frac{\partial F_i}{\partial x_i} = 0 \qquad & \text{in} \quad \Omega_f \\
F_i = 0 \qquad & \text{on} \quad \Gamma \\
F_i \quad \text{and} \quad E \quad & \text{are} \quad \Omega\text{periodic}
\end{aligned} \tag{3.3.9}$$

This is Stokes problem (3.3.20) in Ch. I, Part A. Therefore $F_i = k_{iz}$ is equal to the fluid velocity in i-th direction in the microcell when the macroscale pressure gradient is in z direction. In view of the isotropic premeability, we have

$$\langle F_x \rangle = \langle F_y \rangle = 0, \quad \langle F_z \rangle = -Rak' \tag{3.3.10}$$

Accordingly in an isotropic and homogeneous medium

$$\langle u_i^{(1)} \rangle = -Rak'\theta^{(0)}\delta_{iz} \tag{3.3.11}$$

It simply means that the buoyancy effect is important at the first order.

3.4 The Macroscale Heat Transport Equation

3.4.1 The Canonical Cell Problems for Heat Transfer

At $O(1)$, equations (3.1.15a), (3.1.16a), (3.1.19a) and (3.1.20a) give

$$\begin{aligned} Peu^{(0)} \cdot \nabla\theta^{(0)} &= \nabla \cdot (m_f^* \cdot \nabla\theta_f^{(0)}) \quad \text{in} \quad \Omega_f \\ 0 &= M_r \nabla \cdot (m_s^* \cdot \nabla\theta_s^{(0)}) \quad \text{in} \quad \Omega_s \\ \theta_f^{(0)} &= \theta_s^{(0)} \qquad\qquad\qquad \text{on} \quad \Gamma(0) \\ m_f^* \cdot \nabla\theta_f^{(0)} \cdot N &= M_r m_s^* \cdot \nabla\theta_s^{(0)} \cdot N \quad \text{on}\Gamma(0) \end{aligned} \tag{3.4.1a-d}$$

After making use of (3.1.2a), equation (3.4.1a) may be written as

$$Pe\nabla \cdot (u^{(0)}\theta_f^{(0)}) = \nabla \cdot (m_f^* \cdot \nabla\theta_f^{(0)}) \tag{3.4.2}$$

If we multiply (3.4.2) and (3.4.1b) by $\theta_f^{(0)}$ and $\theta_s^{(0)}$, integrate over Ω_f and Ω_s, and use (3.1.17a), (3.4.1c and d), it follows that

$$0 = \int_{\Omega f} m_f^* \cdot \nabla\theta_f^{(0)} \nabla\theta_f^{(0)} d\Omega + \int_{\Omega_s} M_r m_s^* \cdot \nabla\theta_s^{(0)} \nabla\theta_s^{(0)} d\Omega \tag{3.4.3}$$

Since both integrals are positive definite, we have

$$\theta_f^{(0)} = \theta_s^{(0)} = \theta^{(0)}(x', t_v, t_d) \tag{3.4.4}$$

and the leading order temperature of the medium does not depend on the microscale. There is no need to distinguish fluid and solid for the leading order temperature and the subscript will be omitted.

At $O(\epsilon)$, we have from (3.1.15b) (3.1.16b), (3.1.19b) and (3.1.20b), after using (3.4.4),

$$Pe\left[\frac{\partial\theta^{(0)}}{\partial t_v}+u^{(0)}\cdot\nabla'\theta^{(0)}+\nabla\cdot(u^{(0)}\theta_f^{(1)})\right]=\nabla\cdot\left[m_f^*\cdot(\nabla'\theta^{(0)}+\nabla\theta_f^{(1)})\right]\quad\text{in}\quad\Omega_f$$

$$(\rho C_p)_r Pe\frac{\partial\theta^{(0)}}{\partial t_v}=M_r\nabla\cdot\left[m_s^*\cdot\left(\nabla'\theta^{(0)}+\nabla\theta_s^{(1)}\right)\right]\quad\text{in}\quad\Omega_s$$

$$\theta_f^{(1)}=\theta_s^{(1)}\qquad\text{on}\quad\Gamma(0)$$

$$m_f^*\cdot\left(\nabla'\theta^{(0)}+\nabla\theta_f^{(1)}\right)\cdot N=M_r m_s^*\cdot\left(\nabla'\theta^{(0)}+\nabla\theta_s^{(1)}\right)\cdot N\quad\text{on}\quad\Gamma(0)$$

$$(3.4.5a-d)$$

Use has been made of (3.1.2a) to get (3.4.5a). Integrating (3.4.5a) and (3.4.5b) over the Ω-cell and using Gauss theorem, Ω-periodicity, (3.32a) and the boundary conditions (3.4.5c and d), we obtain

$$\bar{a}\frac{\partial\theta^{(0)}}{\partial t_v}+\langle u^{(0)}\rangle\cdot\nabla'\theta^{(0)}=0\tag{3.4.6}$$

where

$$\bar{a}=n'+(1-n')(\rho C_p)_r\tag{3.4.7}$$

is the average heat capacity of the medium. The heat transport over the time scale T_v is therefore governed by convection only.

We now find $\theta_{f,s}^{(1)}$ in terms of the macroscale temperature gradient $\nabla'\theta^{(0)}$. Let us first subtract (3.4.6) times $Pe/\bar{a}$ from (3.4.5a),

$$Pe\left(\tilde{u}^{(0)}\cdot\nabla'\theta^{(0)}+u^{(0)}\cdot\nabla\theta_f^{(1)}\right)=\nabla\cdot\left[m_f^*\cdot(\nabla'\theta^{(0)}+\nabla\theta_f^{(1)})\right]\quad\text{in}\quad\Omega_f\tag{3.4.8}$$

where

$$\tilde{u}^{(0)}=u^{(0)}-\frac{1}{\bar{a}}\langle u^{(0)}\rangle\tag{3.4.9}$$

Let us also subtract (3.4.6) times $Pe(\rho C_p)_r/\bar{a}$ from (3.4.5b)

$$-(\rho C_p)_r Pe\frac{1}{\bar{a}}\langle u^{(0)}\rangle\cdot\nabla'\theta^{(0)}=M_r\nabla\cdot\left[m_s^*(\nabla'\theta^{(0)}+\nabla\theta_s^{(1)})\right]\quad\text{in}\quad\Omega_s\tag{3.4.10}$$

Note that the fluid velocity is determined by solving the consolidation equation (3.2.4) separately for $p^{(0)}$ and using Darcy's law (3.2.2a). Therefore it is a given quantity in the convection-diffusion equations (3.4.8) and (3.4.10). In view of linearity, $\theta_f^{(1)}$ and $\theta_s^{(1)}$ are then assumed to be of the form

$$\begin{aligned} \theta_f^{(1)} &= B^f \cdot \nabla' \theta^{(0)} \quad \text{in} \quad \Omega_f \\ \theta_s^{(1)} &= B^s \cdot \nabla' \theta^{(0)} \quad \text{in} \quad \Omega_s \end{aligned} \tag{3.4.11a,b}$$

The unknown vector functions $B^f(x,x')$ and $B(x,x')$ must satisfy

$$\begin{aligned} Pe\left(\tilde{u}^{(0)} \cdot I + u^{(0)} \cdot \nabla B^f\right) &= \nabla \cdot \left[m_f^* \cdot (I + \nabla B^f)\right] \qquad \text{in} \quad \Omega_f \\ -(\rho C_p)_r Pe \frac{1}{\bar{a}} \langle u^{(0)} \rangle \cdot I &= M_r \nabla \cdot [m_s^* \cdot (I + \nabla B^s)] \quad \text{in} \quad \Omega_s \end{aligned} \tag{3.4.12a,b}$$

which are obtained after substituting (3.4.11a,b) into (3.4.8) and (3.4.10). The interface boundary conditions for B^f and B^s are then given by (3.4.5c and d) as

$$B^f = B^s \qquad \text{on} \quad \Gamma(0) \tag{3.4.12c}$$

$$m_f^* \cdot (I + \nabla B^f) \cdot N = M_r m_s^* \cdot (I + \nabla B^s) \cdot N \quad \text{on} \quad \Gamma(0) \tag{3.4.12d}$$

We also impose for Ω-periodicity

$$B^f \quad \text{and} \quad B^s \quad \text{are} \quad \Omega - \text{periodic} \tag{3.4.12e}$$

and it is further required for uniqueness that

$$\langle B^f \rangle = \langle B^s \rangle = 0 \tag{3.4.12f}$$

The canonical cell problems for B^f and B^s (3.4.12a-f) are now a pair of convection-diffusion problems with distributed source in the fluid phase which is the velocity fluctuation about the mean flow velocity, and with a uniform source in the solid phase. There are source also distributed on the interface(cf.(3.4.12d)). After solving (3.40a-f) for B^f and B^s numerically in a given cell geometry, the microscale fluctuations in temperature $\theta_f^{(1)}$ and $\theta_s^{(1)}$ are given by (3.4.11a and b) in which $\theta^{(0)}$ is yet to be determined.

3.4.2 The Mean Heat Transport Equation

Finally at $O(\epsilon^2)$, we have from (3.1.15c), (3.1.16c), (3.1.19c) and (3.1.20c) after invoking (3.4.4)

$$Pe\left[\frac{\partial\theta^{(0)}}{\partial t_d}+\frac{\partial\theta_f^{(1)}}{\partial t_v}+u^{(0)}\cdot\left(\nabla'\theta_f^{(1)}+\nabla\theta_f^{(2)}\right)+u^{(1)}\cdot\left(\nabla'\theta^{(0)}+\nabla\theta_f^{(1)}\right)\right]$$

$$=\nabla'\cdot\left[m_f^*\cdot\left(\nabla'\theta^{(0)}+\nabla\theta_f^{(1)}\right)\right]+\nabla\cdot\left[m_f^*\cdot\left(\nabla'\theta_f^{(1)}+\nabla\theta_f^{(2)}\right)\right]\qquad\text{in}\quad\Omega_f$$

$$(\rho C_p)_r\,Pe\left(\frac{\partial\theta^{(0)}}{\partial t_d}+\frac{\partial\theta_s^{(1)}}{\partial t_v}\right)$$

$$=M_r\left\{\nabla'\cdot\left[m_s^*\cdot\left(\nabla'\theta^{(0)}+\nabla\theta_s^{(1)}\right)\right]+\nabla\cdot\left[m_s^*\cdot\left(\nabla'\theta_s^{(1)}+\nabla\theta_s^{(2)}\right)\right]\right\}\quad\text{in}\quad\Omega_s$$

$$\theta_f^{(2)}+v_j^{(1)}\left(\frac{\partial\theta_f^{(0)}}{\partial x_j'}+\frac{\partial\theta_f^{(1)}}{\partial x_j}\right)=\theta_s^{(2)}+v_j^{(1)}\left(\frac{\partial\theta_s^{(0)}}{\partial x_j'}+\frac{\partial\theta_s^{(1)}}{\partial x_j}\right)\qquad\text{on}\quad\Gamma(0)$$

$$m_f^*\cdot\left(\nabla'\theta_f^{(1)}+\nabla\theta_f^{(2)}\right)\cdot N+v_j^{(1)}\frac{\partial}{\partial x_j}\left[m_f^*\cdot\left(\nabla'\theta^{(0)}+\nabla\theta_f^{(1)}\right)\right]\cdot N$$

$$=M_r\left\{m_s^*\cdot\left(\nabla'\theta_s^{(1)}+\nabla\theta_s^{(2)}\right)+v_j^{(1)}\frac{\partial}{\partial x_j}\left[m_s^*\cdot\left(\nabla'\theta^{(0)}+\nabla\theta_s^{(1)}\right)\right]\cdot N\right\}\quad\text{on}\quad\Gamma(0)$$

(3.4.13$a-d$)

The convective terms on the left-hand side of (3.4.13a) can be rewritten as

$$u^{(0)}\cdot\left(\nabla'\theta_f^{(1)}+\nabla\theta_f^{(2)}\right)+u^{(1)}\cdot\left(\nabla'\theta^{(0)}+\nabla\theta_f^{(1)}\right)$$

$$=\nabla'\cdot\left(u^{(0)}\theta_f^{(1)}\right)+u^{(1)}\cdot\nabla'\theta^{(0)}+\nabla\cdot\left(u^{(0)}\theta_f^{(2)}\right)+\nabla\cdot\left(u^{(1)}\theta_f^{(1)}\right)$$

$$-\theta_f^{(2)}\nabla\cdot u^{(0)}-\theta_f^{(1)}\left(\nabla'\cdot u^{(0)}+\nabla\cdot u^{(1)}\right)$$

$$=\nabla'\cdot\left(u^{(0)}\theta_f^{(1)}\right)+u^{(1)}\cdot\nabla'\theta^{(0)}+\nabla\cdot\left(u^{(0)}\theta_f^{(2)}\right)+\nabla\cdot\left(u^{(1)}\theta_f^{(1)}\right)\qquad(3.4.14)$$

where (3.1.12a and b) were used.

Upon substituting (3.4.13) into (3.4.12a) and taking the Ω-average of (3.4.13a) and (3.4.13b), we get

$$
\begin{aligned}
&Pe\left[\bar{a}\frac{\partial\theta^{(0)}}{\partial t_d}+\left\langle\frac{\partial\theta_f^{(1)}}{\partial t_v}\right\rangle+(\rho C_p)_r\left\langle\frac{\partial\theta_s^{(1)}}{\partial t_v}\right\rangle\right]\\
&+\nabla'\cdot\left(Pe\langle u^{(0)}\theta_f^{(1)}\rangle\right)+Pe\langle u^{(1)}\rangle\cdot\nabla'\theta^{(0)}\\
&+Pe\left[\frac{1}{\Omega}\int_{\Omega_f}\nabla\cdot\left(u^{(0)}\theta_f^{(2)}\right)d\Omega+\frac{1}{\Omega}\int_{\Omega_f}\nabla\cdot\left(u^{(1)}\theta_f^{(1)}\right)d\Omega\right]=\nabla'\cdot\left(m'\cdot\nabla'\theta^{(0)}\right)\\
&-\frac{1}{\Omega}v_j^{(1)}\int_\Gamma\left\{\frac{\partial}{\partial x_k}\left[(m_f^*)_{k\ell}\left(\frac{\partial\theta^{(0)}}{\partial x'_\ell}+\frac{\partial\theta_f^{(1)}}{\partial x_\ell}\right)\right]\right\}N_j^f\,dS\\
&-\frac{1}{\Omega}v_j^{(1)}\int_\Gamma M_r\left\{\frac{\partial}{\partial x_k}\left[(m_s^*)_{k\ell}\left(\frac{\partial\theta^{(0)}}{\partial x'_\ell}+\frac{\partial\theta_s^{(1)}}{\partial x_\ell}\right)\right]\right\}N_j^s\,dS
\end{aligned}
\tag{3.4.15}
$$

where

$$
m'=\langle m_f^*\cdot(I+\nabla B^f)\rangle+M_r\langle m_s^*\cdot(I+\nabla B^s\rangle \tag{3.4.16}
$$

denotes the macroscale thermal conductivity. In (3.4.14), the surface integrals on the right-hand side of (3.4.15) are obtained after using (3.4.13d). We examine each term in (3.4.15). Because of (3.4.12f) it follows that

$$
\left\langle\frac{\partial\theta_f^{(1)}}{\partial t_v}\right\rangle+(\rho C_p)_r\left\langle\frac{\partial\theta_s^{(1)}}{\partial t_v}\right\rangle=\left(\langle B^f\rangle+(\rho C_p)_r\langle B^s\rangle\right)\frac{\partial}{\partial t_v}\nabla'\theta^{(0)}=0 \tag{3.4.17}
$$

$$
\begin{aligned}
\nabla'\cdot(Pe\langle u^{(0)}\theta_f^{(1)}\rangle)&=\nabla'\cdot\left[Pe\left\langle(\hat{u}^{(0)}+\langle u^{(0)}\rangle)B^f\right\rangle\cdot\nabla'\theta^{(0)}\right]\\
&=\nabla'\cdot\left[Pe\langle\hat{u}^{(0)}B^f\rangle\cdot\nabla'\theta^{(0)}\right]
\end{aligned}
\tag{3.4.18}
$$

where

$$
\hat{u}^{(0)}=u^{(0)}-\langle u^{(0)}\rangle \tag{3.4.19}
$$

is the velocity fluctuation about its mean. After using Gauss theorem, Ω-periodicity and (3.1.17a and b), the volume integrals on the left-hand side of (3.4.15) become

$$\begin{aligned}
&\frac{1}{\Omega}\int_{\Omega_f}\nabla\cdot(u^{(0)}\theta_f^{(2)})d\Omega+\frac{1}{\Omega}\int_{\Omega_f}\nabla\cdot(u^{(1)}\theta_f^{(1)})d\Omega\\
&\quad=-\frac{1}{\Omega}\int_{\Gamma}v_j^{(1)}\frac{\partial u_i^{(0)}}{\partial x_j}\theta_f^{(1)}N_i^f dS=-\frac{1}{\Omega}v_j^{(1)}\int_{\Omega_f}\frac{\partial}{\partial x_i}\left(\frac{\partial u_i^{(0)}}{\partial x_j}\theta_f^{(1)}\right)d\Omega\\
&\quad=-\frac{1}{\Omega}v_j^{(1)}\int_{\Omega_f}\frac{\partial}{\partial x_i}\left[\frac{\partial}{\partial x_j}\left(u_i^{(0)}\theta_f^{(1)}\right)-u_i^{(0)}\frac{\partial\theta_f^{(1)}}{\partial x_j}\right]d\Omega \qquad (3.4.20)\\
&\quad=-\frac{1}{\Omega}v_j^{(1)}\int_{\Omega_f}\left[\frac{\partial}{\partial x_j}\left(u_i^{(0)}\frac{\partial\theta_f^{(1)}}{\partial x_i}\right)-\frac{\partial}{\partial x_i}\left(u_i^{(0)}\frac{\partial\theta_f^{(1}}{\partial x_j}\right)\right]d\Omega\\
&\quad=-\frac{1}{\Omega}v_j^{(1)}\int_{\Gamma}\left(u_i^{(0)}\frac{\partial\theta_f^{(1)}}{\partial x_i}N_j^f-u_i^{(0)}\frac{\partial\theta_f^{(1)}}{\partial x_j}N_i^f\right)dS=0
\end{aligned}$$

After using Gauss theorem and (3.4.5a and b), the surface integrals on the right-hand side of (3.4.15) can be written

$$\begin{aligned}
&-\frac{Pe}{\Omega}v_j^{(1)}\int_{\Omega_f}\frac{\partial}{\partial x_j}\left[\frac{\partial\theta^{(0)}}{\partial t_v}+u_i^{(0)}\left(\frac{\partial\theta^{(0)}}{\partial x_i'}+\frac{\partial\theta_f^{(1)}}{\partial x_i}\right)\right]d\Omega\\
&\qquad+M_r(\rho C_p)_r Pe\int_{\Omega_s}\frac{\partial}{\partial x_j}\left(\frac{\partial\theta^{(0)}}{\partial t_v}\right)d\Omega \qquad (3.4.21)\\
&\qquad=-\frac{Pe}{\Omega}v_j^{(1)}\int_{\Gamma}u_i^{(0)}\left(\frac{\partial\theta^{(0)}}{\partial x_i'}+\frac{\partial\theta_f^{(1)}}{\partial x_i}\right)N_j^f dS=0
\end{aligned}$$

The last integral vanishes because of (3.1.17a).

Substituting (3.4.16), (3.4.17), (3.4.19) and (3.4.20) into (3.4.15) we obtain

$$Pe\left[\bar{a}\frac{\partial\theta^{(0)}}{\partial t_d}+\langle u^{(1)}\rangle\cdot\nabla'\theta^{(0)}\right]=\nabla'\cdot\left[D'\cdot\nabla'\theta^{(0)}\right] \qquad (3.4.22)$$

where

$$D_{ij}'=\langle m_f^*\cdot(I+\nabla B^f)\rangle+M_r\langle m_s^*\cdot(I+\nabla B^s\rangle-Pe\langle\hat{u}_i^{(0)}B_j^f\rangle \qquad (3.4.23)$$

Tensor coefficient D_{ij}' is the macroscale thermal dispersion tensor.

We first note that, over the slow time scale T_d (conduction time), the heat transport is contributed by both convection and diffusion.

The heat transport process is composed not only of molecular diffusion, but also of dispersion. The former includes both the algebraic mean of thermal conductivities and the microscale fluctuations (cf. (3.4.23)). On the other hand, dispersion is induced by convection (represented by $u^{(0)} \cdot \nabla' \theta_f^{(1)}$ in (3.4.13a)) as the consequence of local mixing in a Ω-cell (leading to the last term in (3.4.23)) caused by the velocity fluctuation relative to the mean flow. It is readily seen in (3.4.23) that if the Peclét number is not small dispersion may dominate over molecular diffusion.

The second order tensor D'_{ij} in (3.4.23) is, in general, not symmetric and may be further decomposed into symmetric and anti-symmetric parts.

$$D'_{ij} = m^s_{ij} + m^u_{ij} + D^s_{ij} + D^u_{ij} \tag{3.4.24}$$

where

$$\begin{Bmatrix} m^s_{ij} \\ m^u_{ij} \end{Bmatrix} = \frac{1}{2} \left[\langle (m^*_f)_{ij} \pm (m^*_f)_{ij} \rangle_\Omega + M_r \langle (m^*_s)_{ij} \pm (m^*_s)_{ji} \rangle_\Omega \right] \tag{3.4.25}$$

and

$$\begin{aligned} \begin{Bmatrix} D^s_{ij} \\ D^u_{ij} \end{Bmatrix} &= -\frac{Pe}{2} \left[\langle \hat{u}^{(0)}_i B^f_j \pm \hat{u}^{(0)}_j B^f_i \rangle \right] \\ &+ \frac{1}{2} \left[\left\langle (m^*_f)_{il} \frac{\partial B^f_j}{\partial x_l} \pm (m^*_f)_{jl} \frac{\partial B^f_i}{\partial x_l} \right\rangle_{\Omega_f} + M_r \left\langle (m^*_s)_{il} \frac{\partial B^s_j}{\partial x_l} \pm (m^*_s)_{jl} \frac{\partial B^s_i}{\partial x_l} \right\rangle_{\Omega_s} \right] \end{aligned} \tag{3.4.26}$$

Note that m^s_{ij} and D^s_{ij} are symmetric and m^u_{ij} and D^u_{ij} are anti-symmetric and the microscale fluctuations due to $\theta^{(1)}_{f,s}$ are now included in D^s_{ij} and D^u_{ij}. Coefficients m^s_{ij} and m^u_{ij} are simply the volume averages of the thermal conductivities of the solid and fluid phases.

Combining (3.4.9) and (3.4.19), $\hat{u}^{(0)}$ and $\tilde{u}^{(0)}$ are related by

$$\hat{u}^{(0)} = u^{(0)} - \langle u^{(0)} \rangle = \tilde{u}^{(0)} + \left(\frac{1}{a} - 1 \right) \langle u^{(0)} \rangle \tag{3.4.27}$$

Substituting (3.4.27) into (3.4.26) and invoking (3.4.12f), we have

$$\begin{Bmatrix} D^s_{ij} \\ D^u_{ij} \end{Bmatrix} = -\frac{Pe}{2}\left[\langle \tilde{u}_i^{(0)} B_j^f \pm \tilde{u}_j^{(0)} B_i^f \rangle\right] + \frac{1}{2}\left[\left\langle (m_f^*)_{il}\frac{\partial B_j^f}{\partial x_l} \pm (m_f^*)_{jl}\frac{\partial B_i^f}{\partial x_l}\right\rangle_{\Omega_f} + M_r\left\langle (m_s^*)_{il}\frac{\partial B_j^s}{\partial x_l} \pm (m_s^*)_{jl}\frac{\partial B_i^s}{\partial x_l}\right\rangle_{\Omega_s}\right] \tag{3.4.28}$$

Mei(1991) has further shown for rigid medium that the symmetric dispersion tensor D^s_{ij} can be expressed as

$$\begin{aligned} D^s_{ij} =& \left\langle (m_f^*)_{kl}\frac{\partial B_i^f}{\partial x_k}\frac{\partial B_j^f}{\partial x_l}\right\rangle_{\Omega_f} + M_r\left\langle (m_s^*)_{kl}\frac{\partial B_i^s}{\partial x_k}\frac{\partial B_j^s}{\partial x_l}\right\rangle_{\Omega_s} \\ &+ \left\langle (m_f^*)_{il}\frac{\partial B_j^f}{\partial x_l} + (m_f^*)_{jl}\frac{\partial B_i^f}{\partial x_l}\right\rangle_{\Omega_f} + M_r\left\langle (m_s^*)_{il}\frac{\partial B_j^s}{\partial x_l} + (m_s^*)_{jl}\frac{\partial B_i^s}{\partial x_l}\right\rangle_{\Omega_s} \end{aligned} \tag{3.4.29}$$

by using (3.4.12a,b) and the no slip condition($u^{(0)} = 0$ on $\Gamma(0)$) on the interface. The result is equally applicable for highly permeable medium of the present case because of (3.1.17a). Thus (3.4.29) is valid here.

Substituting (3.4.25) and (3.4.26) into the right-hand side of (3.4.22), we have

$$\begin{aligned} \frac{\partial}{\partial x_i'}\left(D'_{ij}\frac{\partial \theta^{(0)}}{\partial x_j'}\right) =& \frac{\partial}{\partial x_i'}\left[(m^s_{ij} + D^s_{ij})\frac{\partial \theta^{(0)}}{\partial x_j'}\right] \\ &+ \left[\frac{\partial}{\partial x_i'}\left(m^u_{ij} + D^u_{ij}\right)\right]\frac{\partial \theta^{(0)}}{\partial x_j'} + \left(m^u_{ij} + D^u_{ij}\right)\frac{\partial^2 \theta^{(0)}}{\partial x_i' \partial x_j'} \end{aligned} \tag{3.4.30}$$

The last term in (3.4.30) is the product of symmetric and anti-symmetric tensors and vanishes upon summation over the indices. Finally substituting (3.4.30) into (3.4.22) we obtain

$$Pe\overline{a}\frac{\partial \theta^{(0)}}{\partial t_d} + \left[Pe\langle u_j^{(1)}\rangle - \frac{\partial}{\partial x_i'}\left(m^u_{ij} + D^u_{ij}\right)\right]\frac{\partial \theta^{(0)}}{\partial x_j'} = \frac{\partial}{\partial x_i'}\left[(m^s_{ij} + D^s_{ij})\frac{\partial \theta^{(0)}}{\partial x_j'}\right] \tag{3.4.31}$$

In order to find the mean heat transport equation, we multiply (3.4.30) by ϵ and add it to (3.4.6).

$$\begin{aligned} &Pe\overline{a}\left(\frac{\partial}{\partial t_v} + \epsilon\frac{\partial}{\partial t_d}\right)\theta^{(0)} + Pe\left(\langle u_j^{(0)}\rangle + \epsilon\langle u_j^{(1)}\rangle\right)\cdot\frac{\partial \theta^{(0)}}{\partial x_j'} \\ &- \epsilon\left[\frac{\partial}{\partial x_i'}\left(m^u_{ij} + D^u_{ij}\right)\right]\frac{\partial \theta^{(0)}}{\partial x_j'} = \epsilon\frac{\partial}{\partial x_i'}\left[(m^s_{ij} + D^s_{ij})\frac{\partial \theta^{(0)}}{\partial x_j'}\right] \end{aligned} \tag{3.4.32}$$

Recalling the perturbation expansion (3.1.10a) and the multiple time scale (3.1.3c), equation (3.4.32) can be written as

$$Pe\bar{a}\frac{\partial\theta^{(0)}}{\partial t^*} + Pe\langle u_j^*\rangle\frac{\partial\theta^{(0)}}{\partial x_j'} + \epsilon\left[\frac{\partial}{\partial x_i'}\left(m_{ij}^u + D_{ij}^u\right)\right]\frac{\partial\theta^{(0)}}{\partial x_j'} = \epsilon\frac{\partial}{\partial x_i'}\left[\left(m_{ij}^s + D_{ij}^s\right)\frac{\partial\theta^{(0)}}{\partial x_j'}\right] \tag{3.4.33}$$

Equations (3.2.1a) (static equilibrium of solid), (3.2.3) (Darcy's law), (3.2.4) (conservation of fluid mass) and (3.4.33) (conservation of energy) are the governing equations for the consolidation and heat transport in granular porous media when the microscale Peclet number is finite ($Pe = O(1)$).

In this limit, the flow equation and solid deformation are mathematically decoupled. The solution procedure is therefore as follows. The consolidation equation (3.2.4) is first solved for the pressure $p^{(0)}$ in terms of which the seepage velocity $\langle u^{(0)}\rangle$ is given by (3.2.3). Both $p^{(0)}$ and $\langle u^{(0)}\rangle$ are of steady state form. For the calculated velocity field $u^{(0)}$, the microcell boundary value problem (3.4.12a-f) is solved for B^f and B^s from which the dispersion tensors D_{ij}^s and D_{ij}^u of (3.4.28) are determined. For isotropic and homogeneous medium on the macroscale, $\langle u_i^{(1)}\rangle = -Rak'\theta^{(0)}\delta_{iz}$ (cf.(3.3.11)) and the heat transport equation (3.4.33) is then solved for the medium temperature $\theta^{(0)}$ which varies with time. We emphasize that the heat transport equation is nonlinear because of the dependence of $\langle u_i^{(1)}\rangle$ on $\theta^{(0)}$ although it is weak i.e., $O(\epsilon)$.

In view of the steady state form of (3.2.1a) and (3.2.4), the porous medium deforms promptly in response to the quasi-steady pressure field $p^{(0)}$, while the temperature $\theta^{(0)}$ diffuses in a transient manner.

3.4.3 Positive Definiteness of the Dispersion Tensor

The symmetric dispersion tensor is composed of two parts : m_{ij}^s, the volume average of thermal conductivities and D_{ij}^s, the effective diffusion due to convection (cf.(3.4.24)). Following Brenner(1980), it is shown here that the dispersion tensor $(m_{ij}^s + D_{ij}^s)$ is positive definite.

Introduce new variables C_i^f and C_i^s given by

$$C_i^f = B_i^f + x_i, \quad C_i^s = B_i^s + x_i \tag{3.4.34}$$

so that

$$\frac{\partial B_i^f}{\partial x_k} = \frac{\partial C_i^f}{\partial x_k} - \delta_{ik}, \quad \frac{\partial B_i^s}{\partial x_k} = \frac{\partial C_i^s}{\partial x_k} - \delta_{ik} \tag{3.4.35}$$

Substituting (3.4.35) into (3.4.29) we obtain

$$m_{ij}^s + D_{ij}^s = \left\langle (m_f^*)_{k\ell} \frac{\partial C_i^f}{\partial x_k} \frac{\partial C_j^f}{\partial x_\ell} \right\rangle + M_r \left\langle (m_f^*)_{k\ell} \frac{\partial C_i^s}{\partial x_k} \frac{\partial C_j^s}{\partial x_\ell} \right\rangle \tag{3.4.36}$$

If two microscale independent vectors χ_i and χ_j are multiplied to (3.4.36), it follows

$$\chi_i (m_{ij}^s + D_{ij}^s) \chi_j = \left\langle (m_f^*)_{k\ell} \frac{\partial f}{\partial x_k} \frac{\partial f}{\partial x_\ell} \right\rangle + M_r \left\langle (m_s^*)_{k\ell} \frac{\partial g}{\partial x_k} \frac{\partial g}{\partial x_\ell} \right\rangle \tag{3.4.37}$$

where $f = C_i^f \chi_i$ and $g = C_i^s \chi_i$. The quadratic expression on the right-hand side of (3.4.37) is positive since thermal conductivities m_f^* and $m_f^* s$ are positive definite and therefore $(m_{ij}^s + D_{ij}^s)$ is positive definite.

3.5 The Macroscale Governing Equations in Physical Variables

The governing equations deduced in §3.2 are now written in physical variables. Since the equilibrium and consolidation equations are in reduced form of those obtained in thermoconsolidation of Part I, onlt the heat transport equation with dispersion is considered.

By using (2.2.1), the heat transport equation becomes in physical variables

$$\overline{\rho C_p} \frac{\partial \theta}{\partial t} + (\rho C_p)_f \langle u_j \rangle \frac{\partial \theta}{\partial x_j} + \left[\frac{\partial}{\partial x_i} \left(\tilde{m}_{ij}^u + \tilde{D}_{ij}^u \right) \right] \frac{\partial \theta}{\partial x_j} = \frac{\partial}{\partial x_i} \left[\left(\tilde{m}_{ij}^s + \tilde{D}_{ij}^s \right) \frac{\partial}{\partial x_i} \right] \tag{3.5.1}$$

where

$$\left\{ \begin{matrix} \tilde{m}_{ij}^s \\ \tilde{m}_{ij}^u \end{matrix} \right\} = \frac{1}{2} \left[\langle (m_f)_{ij} \rangle \pm \langle (m_f)_{ji} \rangle + \langle (m_s)_{ij} \rangle \pm \langle (m_s)_{ji} \rangle \right] \tag{3.5.2}$$

and

$$\begin{Bmatrix} \tilde{D}^s_{ij} \\ \tilde{D}^u_{ij} \end{Bmatrix} = -\frac{(\rho C_p)_f}{2}\langle \hat{u}_i \tilde{B}^f_j \pm \hat{u}_j \tilde{B}^f_i \rangle + \frac{1}{2}\left[\langle (m_f)_{il} \frac{\partial \tilde{B}^f_j}{\partial x_l} \pm (m_f)_{jl} \frac{\partial \tilde{B}^f_i}{\partial x_l} \rangle + \langle (m_s)_{il} \frac{\partial \tilde{B}^s_j}{\partial x_l} \pm (m_s)_{jl} \frac{\partial \tilde{B}^s_i}{\partial x_l} \rangle \right] \tag{3.5.3}$$

From (3.4.29) the symmetric dispersion tensor can be further written as

$$\begin{aligned} \tilde{D}^s_{ij} = &\left\langle (m_f)_{kl} \frac{\partial \tilde{B}^f_i}{\partial x_k} \frac{\partial \tilde{B}^f_j}{\partial x_l} \right\rangle + \left\langle (m_s)_{kl} \frac{\partial \tilde{B}^s_i}{\partial x_k} \frac{\partial \tilde{B}^s_j}{\partial x_l} \right\rangle \\ &+ \left\langle (m_f)_{il} \frac{\partial \tilde{B}^f_j}{\partial x_l} + (m_f)_{jl} \frac{\partial \tilde{B}^f_i}{\partial x_l} \right\rangle + \left\langle (m_s)_{il} \frac{\partial \tilde{B}^s_j}{\partial x_l} + (m_s)_{jl} \frac{\partial \tilde{B}^s_i}{\partial x_l} \right\rangle \end{aligned} \tag{3.5.4}$$

The equilibrium and consolidation equations are from (3.2.1) and (3.2.4) simply given as

$$\nabla \cdot [\tilde{a} : e(v) - \tilde{\alpha} p - \tilde{\beta}_t \theta] = 0 \tag{3.5.5}$$

$$\nabla \cdot (\tilde{k} \cdot \nabla p) = 0 \tag{3.5.6}$$

from §3.6 of Ch. I in Part A. The coefficients $\tilde{a}$, $\tilde{\alpha}$, $\tilde{\beta}_t$ and $\tilde{k}$ were given there.

4. Dispersion Tensor for a Cubic Array of Wigner-Seitz Grains

The symmetric dispersion tensor $(m^*_{ij} + D^*_{ij})$ of (3.4.24) is examined for a microcell geometry of the Wigner-Seitz grain which has been used to calculate the macroscale coefficients in Part A. The Wigner-Seitz grain has three orthogonal planes of symmetry (see Fig. 4.1). Because of the crystalline structure of the cubic array, the dispersion tensor depends on the mean flow direction. However, it will be shown that, when the mean flow direction coincides with one of the crystallographic axes (coordinate axes in Fig. 4.1), there are only two distinct coefficients which depend on the Peclét number. For the same mean flow direction, the dispersion coefficients in arbitrarily rotated frame can be obtained by tensor tranformation.

4.1 Symmetry Relations in a Wigner-Seitz Grain

For homogeneous and isotropic phases on the microscale $(m^*_f)_{ij} = m^*_f \delta_{ij}$ and $(m^*_s)_{ij} = m^*_s \delta_{ij}$. The effective diffusion coefficients defined by (3.4.24) to (3.4.26) may be written as

$$\begin{aligned} D_{ij} &= m^*_{ij} + D^*_{ij} \\ &= \frac{1}{2}\left\langle m^*_f(\delta_{ij} + \delta_{ji}) + M_r(\delta_{ij} + \delta_{ji})\right\rangle \\ &\quad + m^*_f\left\langle \frac{\partial B^f_i}{\partial x_k}\frac{\partial B^f_j}{\partial x_k}\right\rangle + M_r m^*_s\left\langle \frac{\partial B^s_i}{\partial x_k}\frac{\partial B^s_j}{\partial x_k}\right\rangle \\ &\quad + m^*_f\left\langle \frac{\partial B^f_j}{\partial x_i} + \frac{\partial B^f_i}{\partial x_j}\right\rangle + M_r m^*_s\left\langle \frac{\partial B^s_j}{\partial x_i} + \frac{\partial B^s_i}{\partial x_j}\right\rangle \\ &= \overline{m}\delta_{ij} + m^*_f\langle I^f_{ij}\rangle + M_r m^*_s\langle I^s_{ij}\rangle + 2m^*_f\langle e_{ij}(B^f)\rangle + 2M_r m^*_s\langle e_{ij}(B^s)\rangle \end{aligned} \tag{4.1.1}$$

where

$$\begin{aligned} \overline{m} &= n' m^*_f + M_r(1-n')m^*_s \\ I^f_{ij} &= \frac{\partial B^f_i}{\partial x_k}\frac{\partial B^f_j}{\partial x_k}, \qquad I^s_{ij} = \frac{\partial B^s_i}{\partial x_k}\frac{\partial B^s_j}{\partial x_k} \\ e_{ij}(B^f) &= \frac{1}{2}\left(\frac{\partial B^f_j}{\partial x_i} + \frac{\partial B^f_i}{\partial x_j}\right), \quad e_{ij}(B^s) = \frac{1}{2}\left(\frac{\partial B^s_j}{\partial x_i} + \frac{\partial B^s_i}{\partial x_j}\right) \end{aligned} \tag{4.1.2a-c}$$

with n' being the porosity.

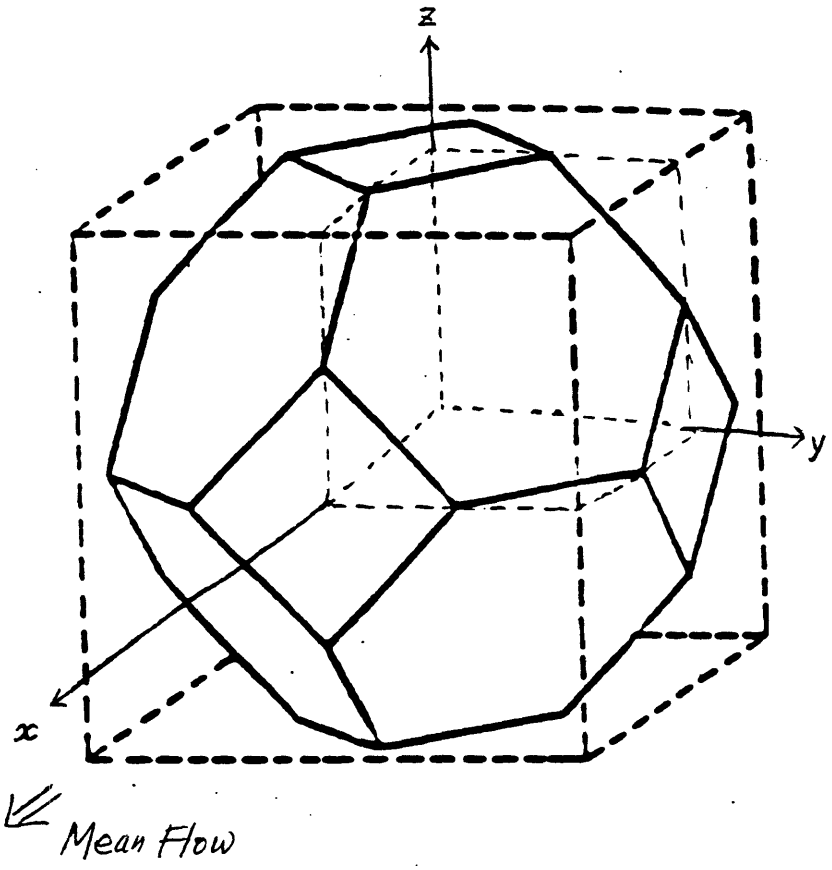

Fig. 4.1 A Wigner-Seitz microcell. The interior of the soccer ball shape is fluid and the rest is solid. The mean flow is shown in the x-direction.

We consider the case when the mean flow is in the x-direction (see Fig. 4.1) and establish symmetry relations for B_i^f and B_i^s among the sectors.

For externally imposed pressure gradient $\nabla' p^{(0)} = (-1, 0, 0)$ the fluid velocity inside the microcell is given by (3.2.2)

$$u_i^{(0)} = k_{ix} \tag{4.1.3}$$

It has been shown in Appendix C in Part A that the fluid phase is of the same shape as the solid grain in the Wigner-seitz grain. The microcell is depicted in Fig. 4.1. The inside of the solid-lined soccer ball shape is the fluid phase and the remainder of the cell is occupied by the solid. In establishing the symmetry relations, the fluid phase is first considered for B_i^f governed by (3.4.12a) and then the solid phase for B_i^s governed by (3.4.12b). The boundary conditions (3.4.12c and d) which involve both B_i^f and B_i^s are also checked for consistency.

As seen in (4.1.3), the fluid velocity inside the microcell is solely determined by k_{ix} whose symmetry relations in sectors A, D, E and H have been summarized in Fig. C.5(b), Part A. For convenient reference it is reproduced in Fig. 4.2(b). In addition, we consider sectors A, B, C and D in the region $z > 0$. It readily follows from Fig. C.5(a), Ch. I, Part A that k_{ix} at those points located symmetrically about the planes $x = 0$ and $y = 0$ are related as shown in Fig. 4.2(a), which is a simpler way of stating the following.

$$\begin{aligned}
&k_{xx}(-x) = k_{xx}(x) \qquad k_{yx}(-x) = -k_{yx}(x) \qquad k_{zx}(-x) = k_{zx}(x) \\
&k_{xx}(-y) = k_{xx}(y) \qquad k_{yx}(-y) = -k_{yx}(y) \qquad k_{zx}(-y) = k_{zx}(y) \\
&k_{xx}(-z) = k_{xx}(z) \qquad k_{yx}(-z) = k_{yx}(z) \qquad k_{zx}(-z) = k_{zx}(z)
\end{aligned}$$

After using (3.4.9) in (3.4.12a), the governing equation for B_j^f becomes

$$Pe\left(\hat{u}_j^{(0)} + b\langle u_j^{(0)}\rangle + u_\ell^{(0)}\frac{\partial B_i^f}{\partial x_\ell}\right) = m_f^* \frac{\partial^2 B_j^f}{\partial x_i \partial x_i} \tag{4.1.4}$$

where

$$b = 1 - \frac{1}{\overline{a}} = 1 - \frac{1}{n' + (1-n')(\rho C_p)_r} = -\frac{(1-n')(\rho C_p)_f}{\overline{\rho C_p}} \tag{4.1.5}$$

with

$$\overline{\rho C_p} = n'(\rho C_p)_f + (1-n')(\rho C_p)_s$$

For $j = x$ (4.1.4) becomes

$$\hat{k}_{xx} + bk' + k_{xx}\frac{\partial B_x^f}{\partial x} + k_{yx}\frac{\partial B_x^f}{\partial y} + k_{zx}\frac{\partial B_x^f}{\partial z} = \frac{m_f^*}{Pe}\left(\frac{\partial^2 B_x^f}{\partial x^2} + \frac{\partial^2 B_x^f}{\partial y^2} + \frac{\partial^2 B_x^f}{\partial z^2}\right) \quad (4.1.6)$$

where

$$\hat{k}_{xx} = k_{xx} - \langle k_{xx}\rangle = k_{xx} - k' \quad (4.1.7)$$

We consider any two points symmetric about $x = 0$ in sectors A and B (or C and D) in Fig. 4.2(a). Since $\hat{k}_{xx}$ and k' are symmetric, so must be other terms in (4.1.6),e.g.

$$\begin{aligned} &k_{xx}\frac{\partial B_x^f}{\partial x},\quad k_{yx}\frac{\partial B_x^f}{\partial y},\quad k_{zx}\frac{\partial B_x^f}{\partial z} && \text{symmetric about } x = 0 \\ &\frac{\partial^2 B_x^f}{\partial x^2},\quad \frac{\partial^2 B_x^f}{\partial y^2},\quad \frac{\partial^2 B_x^f}{\partial z^2} && \text{symmetric about } x = 0 \end{aligned} \quad (4.1.8a,b)$$

Furthermore, in view of the fact that k_{xx} is symmetric about $x = 0$ whereas k_{yx} and k_{zx} are anti-symmetric about $x = 0$, it follows from (4.1.8a) that

$$\begin{aligned} &\frac{\partial B_x^f}{\partial x} && \text{symmetric about } x = 0 \\ &\frac{\partial B_x^f}{\partial y},\quad \frac{\partial B_x^f}{\partial z} && \text{anti-symmetric about } x = 0 \end{aligned} \quad (4.1.9a,b)$$

which imply that

$$\frac{\partial^2 B_x^f}{\partial x^2},\quad \frac{\partial^2 B_x^f}{\partial y^2},\quad \frac{\partial^2 B_x^f}{\partial z^2} \qquad \text{anti-symmetric about } x = 0 \quad (4.1.10)$$

This contradicts (4.1.8b) unless B_x^f is constant which must be zero because of the condition $\langle B_x^f\rangle = 0$. Therefore, for the mean flow in x direction no symmetry relation for B_x^f exists between sectors A and B (and C and D).

We next consider two points symmetric about $y = 0$ in sectors A and D (or E and H) in Fig. 4.2(b). Since $\hat{k}_{xx}$ and k' are symmetric, (4.1.8a and b) should

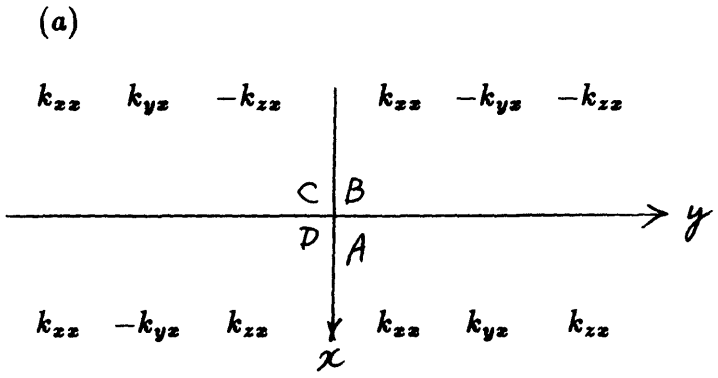

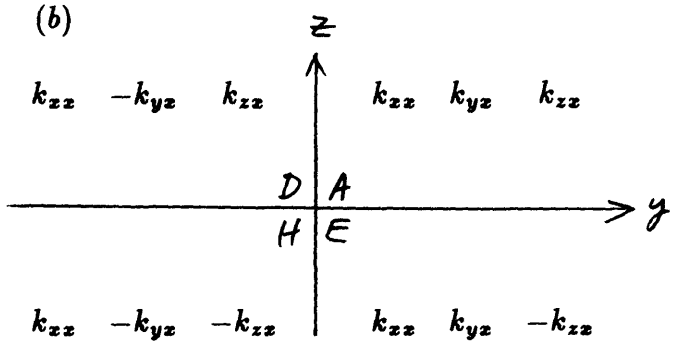

Fig. 4.2 Sign and symmetry relations of the velocity components at points symmetric about the planes $x = 0$, $y = 0$ and $z = 0$ in (a) the region $z > 0$ and (b) the region $x > 0$. Mean flow is in the x-direction.

hold. In Fig. 4.2(b), k_{yz} and k_{zz} are anti-symmetric and symmetric about $y = 0$ respectively and thus we have

$$\begin{array}{ll} \dfrac{\partial B_x^f}{\partial x}, \quad \dfrac{\partial B_x^f}{\partial z} & \text{symmetric about } y = 0 \\ \dfrac{\partial B_x^f}{\partial y} & \text{anti-symmetric about } y = 0 \end{array} \qquad (4.1.11a, b)$$

which is consistent with (4.1.8b). Therefore (4.1.11b) requires for the mean flow in x direction that

$$B_x^f \quad \text{is symmetric about } y = 0 \qquad (4.1.12)$$

For any two points symmetric about $z = 0$ in sectors A and E (or D and H), (4.1.8a and b) still hold since $\hat{k}_{zz}$ and k' are symmetric. Recognizing that k_{yz} and k_{zz} are symmetric and anti-symmetric about $z = 0$, we readily obtain that

$$\begin{array}{ll} \dfrac{\partial B_x^f}{\partial x}, \quad \dfrac{\partial B_x^f}{\partial y} & \text{symmetric about } z = 0 \\ \dfrac{\partial B_x^f}{\partial z} & \text{anti-symmetric about } z = 0 \end{array} \qquad (4.1.13a, b)$$

which also imply (4.1.8b). So

$$B_x^f \quad \text{is symmetric about } z = 0 \qquad (4.1.14)$$

The symmetry relations for B_x^f and its derivatives in sectors A, D, E and H in $x > 0$ region are summarized in the first rows of each sector in Fig. 4.3(a).

If $j = y$ in (4.1.14), it readily follows from Fig. 4.2 that $\langle u_y^{(0)} \rangle = \langle k_{yz} \rangle = \langle k_{zy} \rangle = 0$. We then have from (4.1.4) that

$$\hat{k}_{yz} + k_{zz}\frac{\partial B_y^f}{\partial x} + k_{yz}\frac{\partial B_y^f}{\partial y} + k_{zz}\frac{\partial B_y^f}{\partial z} = \frac{m_f^*}{Pe}\left(\frac{\partial^2 B_y^f}{\partial x^2} + \frac{\partial^2 B_y^f}{\partial y^2} + \frac{\partial^2 B_y^f}{\partial z^2}\right) \qquad (4.1.15)$$

Since there is no symmetry relation for B_x^f about $x = 0$ plane, only the symmetry planes $y = 0$ and $z = 0$ are dealt with (it can be shown by following similar arguments to the case of $j = x$ that no symmetry properties exist for B_y^f between any two sectors symmetric about $x = 0$ either).

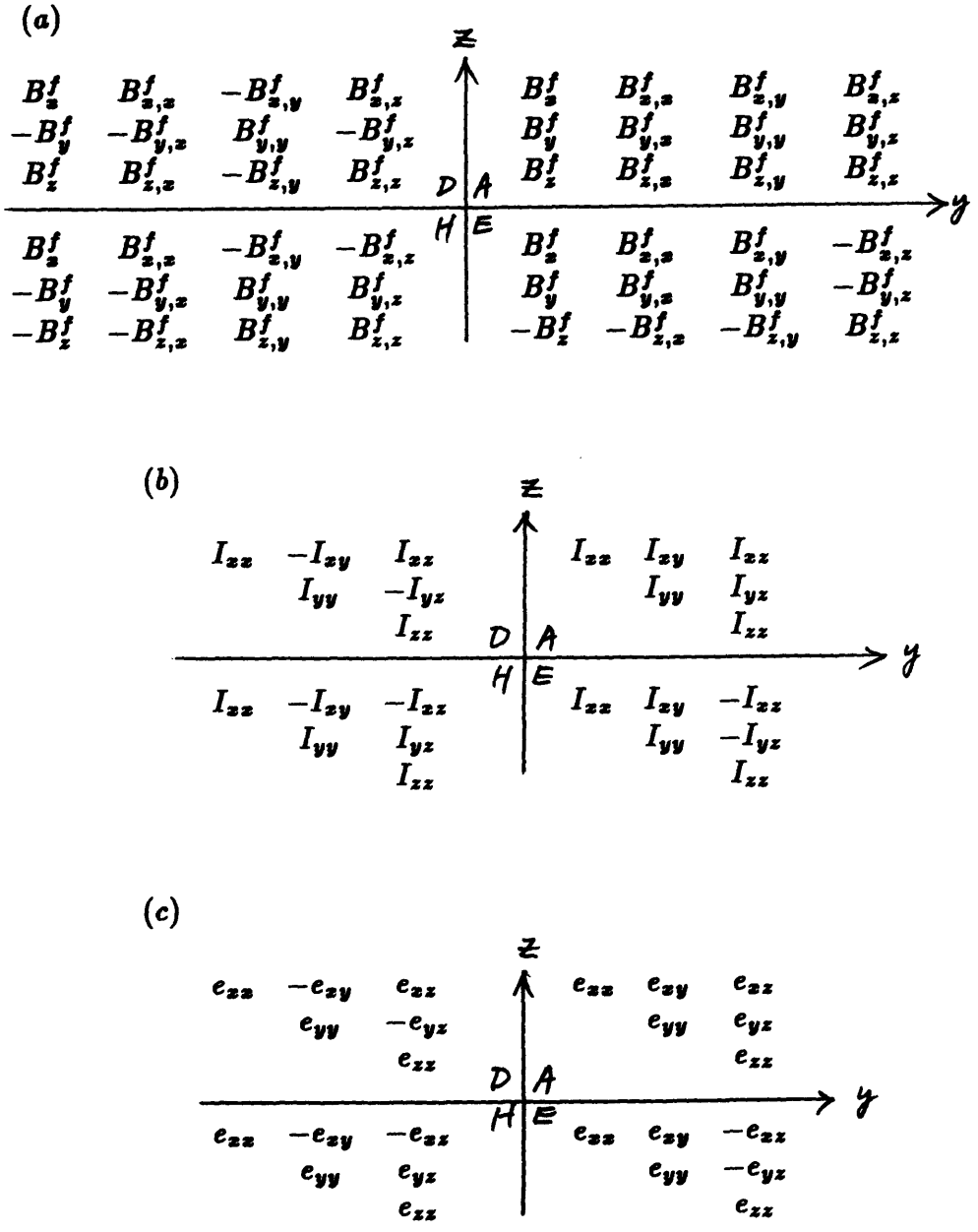

Fig. 4.3 Sign and symmetry properties of B_j^f and related quanties in sectors A, D, E and H when the mean flow is in the x-direction. (a) B_j^f and its derivatives, (b) I_{ij}^f and (c) $e_{ij}(B_j^f)$.

Consider sectors A and D (and E and H) symmetric about $y = 0$ in Fig. 4.2. Because of the anti-symmetric nature of $\hat{k}_{yz}$ all other terms in (4.1.15) are anti-symmetric too,e.g.

$$\begin{aligned} &k_{xz}\frac{\partial B_y^f}{\partial x}, \quad k_{yz}\frac{\partial B_y^f}{\partial y}, \quad k_{zz}\frac{\partial B_y^f}{\partial z} && \text{anti-symmetric about } y = 0 \\ &\frac{\partial^2 B_y^f}{\partial x^2}, \quad \frac{\partial^2 B_y^f}{\partial y^2}, \quad \frac{\partial^2 B_y^f}{\partial z^2} && \text{anti-symmetric about } y = 0 \end{aligned} \qquad (4.1.16a,b)$$

As observed earlier, k_{xx} and k_{zz} are symmetric and k_{yz} is anti-symmetric about $y = 0$ and thus it follows from (4.1.16) that

$$\begin{aligned} &\frac{\partial B_y^f}{\partial x}, \quad \frac{\partial B_y^f}{\partial z} && \text{anti-symmetric about } y = 0 \\ &\frac{\partial B_y^f}{\partial y} && \text{symmetric about } y = 0 \end{aligned} \qquad (4.1.17a,b)$$

which is consistent with (4.1.16b). Therefore

$$B_y^f \quad \text{is symmetric about } z = 0 \qquad (4.1.18)$$

Properties of B_y^f and the derivatives are summarized in the second rows in Fig. 4.3(a).

If $j = z$ in (4.1.4), it becomes

$$\hat{k}_{zz} + k_{xz}\frac{\partial B_z^f}{\partial x} + k_{yz}\frac{\partial B_z^f}{\partial y} + k_{zz}\frac{\partial B_z^f}{\partial z} = \frac{m_f^*}{Pe}\left(\frac{\partial^2 B_z^f}{\partial x^2} + \frac{\partial^2 B_z^f}{\partial y^2} + \frac{\partial^2 B_z^f}{\partial z^2}\right) \qquad (4.1.19)$$

Following the same arguments as before, it can be easily shown that

$$\begin{aligned} &B_z^f \quad \text{is symmetric about } y = 0 \\ &B_z^f \quad \text{is anti-symmetric about } z = 0 \end{aligned} \qquad (4.1.20a,b)$$

which are shown, together with the derivatives, in the third rows in Fig. 4.3(a).

By using the definitions in (4.1.2b and c), the symmetry properties of I_{ij}^f and $e_{ij}(B^f)$ are determined from Fig. 4.3(a) right away and are summarized in Fig. 4.3(b) and (c).

We now move to the solid phase and establish the same kind of symmetry relations for B_j^s by using the governing equation (3.4.12b) and show that B_j^s matches with B_j^f consistently on the interface through the boundary condition (3.4.12d).

Because symmetry is limited to the sectors symmetric about $y = 0$ and $z = 0$, it is sufficient to consider B_j^s in the same sectors and only a cross-section of the cell parallel to yz-plane is shown in Fig. 4.4 in which the hatched areas are the solid phase and the points P_1, P_2, P_3, and P_4 on the interface are symmetric about $y = 0$ and $z = 0$.

After using (4.1.3) in (3.4.12b) and $(m_s^*)_{ij} = m_s^* \delta_{ij}$, we get

$$C\langle k_{jx}\rangle = M_r m_s^* \frac{\partial^2 B_j^s}{\partial x_i \partial x_i} \tag{4.1.21}$$

where

$$C = -(\rho C_p)_r \frac{Pe}{\overline{a}} \tag{4.1.22}$$

is a scalar coefficient and is uniform source distribution in the solid. If $j = x$, (4.1.21) becomes

$$Ck' = M_r m_s^* \left(\frac{\partial^2 B_x^s}{\partial x^2} + \frac{\partial^2 B_x^s}{\partial y^2} + \frac{\partial^2 B_x^s}{\partial z^2} \right) \tag{4.1.23}$$

Since k' is constant, the forcing on the left side is symmetric about both $y = 0$ and $z = 0$. Accordingly each term on the right-hand side of (4.1.23) must be symmetric about both $y = 0$ and $z = 0$. It then follows that

$$B_x^s \quad \text{is symmetric about } y = 0 \text{ and } z = 0 \tag{4.1.24}$$

which is the same as the symmetry property of B_x^f in (4.1.12) and (4.1.14) for in a plane parallel to yz-plane. Therefore the temperature continuity condition (3.4.12c) is automatically satisfied. The symmetry relations for B_y^s and B_z^s follow similarly and are consistent with those for B_y^f and B_z^f. The details are omitted here.

We now examine the heat flux boundary condition (3.4.12d) which reads

$$\begin{aligned} m_f^* \left(N_x + \frac{\partial B_x^f}{\partial x} N_x + \frac{\partial B_x^f}{\partial y} N_y + \frac{\partial B_x^f}{\partial z} N_z \right) \\ = M_r m_s^* \left(N_x + \frac{\partial B_x^s}{\partial x} N_x + \frac{\partial B_x^s}{\partial y} N_y + \frac{\partial B_x^s}{\partial z} N_z \right) \end{aligned} \tag{4.1.25}$$

Consider P_1 and P_2 in Fig. 4.4 which are locatd on the interface symmetrically about $y = 0$. Note that N_x and N_z on $\Gamma(0)$ are symmetric and N_y is anti-symmetric at P_1 and P_2. Also from Fig. 4.3(a), $\partial B_x^f/\partial x$ and $\partial B_x^f/\partial z$ are symmetric and $\partial B_x^f/\partial y$ is anti-symmetric between P_1 and P_2. Consequently the left-hand side of (4.1.25) is symmetric and thus each term on the right-hand side of (4.1.25) must be symmetric, too. This requires that

$$\begin{aligned} &\frac{\partial B_x^s}{\partial x}, \quad \frac{\partial B_x^s}{\partial z} && \text{symmetric at } P_1 \text{ and } P_2 \\ &\qquad\quad \frac{\partial B_x^s}{\partial y} && \text{anti-symmetric at } P_1 \text{ and } P_2 \end{aligned}$$

which is satisfied only if

$$B_x^s \quad \text{is symmetric about } y = 0 \tag{4.1.26a}$$

Similarly for points P_1 and P_3, N_x and N_y are symmetric whereas N_z is anti-symmetric; it follows that

$$\begin{aligned} &\frac{\partial B_x^s}{\partial x}, \quad \frac{\partial B_x^s}{\partial y} && \text{symmetric at } P_1 \text{ and } P_3 \\ &\qquad\quad \frac{\partial B_x^s}{\partial z} && \text{anti-symmetric at } P_1 \text{ and } P_3 \end{aligned}$$

which implies that

$$B_x^s \quad \text{is symmetric about } z = 0 \tag{4.1.26b}$$

Equations (4.1.26a and b) are identical to (4.1.24) which was found by looking at the governing equation for B_x^s (4.1.23) only. Therefore the symmetry relations for B_x^f and B_x^s are implied by both the governing equations and the boundary conditions.

For $i = y$ and $j = z$, a similar procedure readily provides that

$$\begin{aligned} &B_y^s \quad \text{is anti-symmetric about } y = 0 \text{ and symmetric about } z = 0 \\ &B_z^s \quad \text{is symmetric about } y = 0 \text{ and anti-symmetric about } z = 0 \end{aligned} \tag{4.1.27a, b}$$

Note again that the symmetry is consistent with the boundary condition (3.4.12d); the details are omitted.

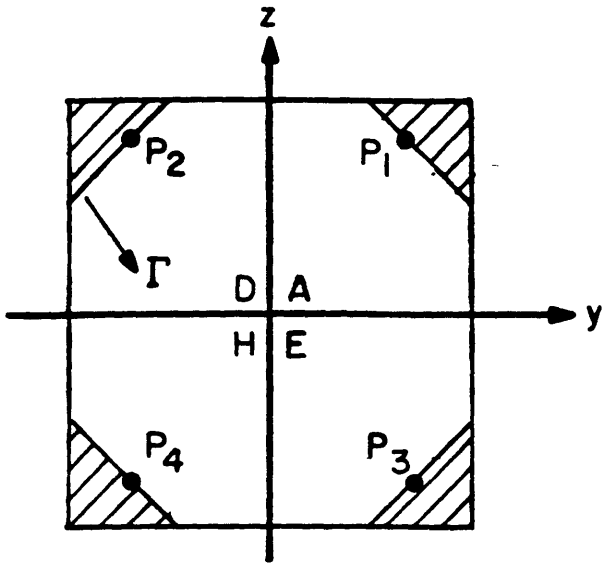

Fig. 4.4 A typical cross-section of the microcell parallel to yz-plane and points on the interface symmetric about $y = 0$ and $z = 0$.

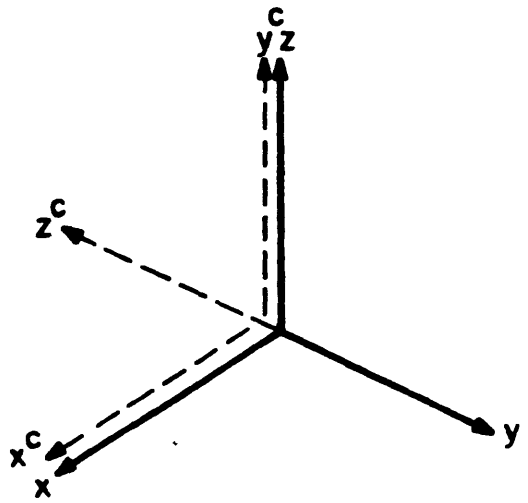

Fig. 4.5 A rotational coordinate transformation by 90 degrees about x-axis counterclockwise.

The symmetry properties of B_j^s between the sectors symmetric about $y = 0$ and $z = 0$ are identical to those of B_j^f and need not be tabulated separately. When necessary, Fig. 4.3 can be used instead.

4.2 The Dispersion Coefficients

Finally let us examine each element of D_{ij} in (4.1.1) by exploiting the relations summarized in Fig. 4.3(a)-(c). Consider the off-diagonal elements first. From (4.1.1) they become

$$\begin{aligned}
D_{xy} = D_{yx} &= m_f^* \langle I_{xy}^f \rangle + M_r m_s^* \langle I_{xy}^s \rangle + 2 \left[m_f^* \langle e_{xy}(B^f) \rangle + M_r m_s^* \langle e_{xy}(B^s) \rangle \right] \\
D_{xz} = D_{zx} &= m_f^* \langle I_{xz}^f \rangle + M_r m_s^* \langle I_{xz}^s \rangle + 2 \left[m_f^* \langle e_{xz}(B^f) \rangle + M_r m_s^* \langle e_{xz}(B^s) \rangle \right] \\
D_{yz} = D_{zy} &= m_f^* \langle I_{yz}^f \rangle + M_r m_s^* \langle I_{yz}^s \rangle + 2 \left[m_f^* \langle e_{yz}(B^f) \rangle + M_r m_s^* \langle e_{yz}(B^s) \rangle \right]
\end{aligned} \qquad (4.2.1a-c)$$

In D_{xy}, the Ω-average of I_{xy}^f,e.g. $\langle I_{xy}^f \rangle$ is zero because I_{xy}^f cancels out between either sectors A and D or sectors E and H in Fig. 4.3. So does $e_{xy}(B^f)$. Certainly $\langle I_{xy}^s \rangle$ and $\langle e_{xy}(B^s) \rangle$ in the solid produce zero net results by the same reasoning. Similar kind of cancellation is seen for D_{xz} and D_{yz} from Fig. 4.3(a)-(c). Therefore, when the mean flow is in x-direction for the microcell of Fig. 4.1, we obtain

$$D_{xy} = D_{yz} = D_{xz} = 0 \qquad (4.2.2)$$

The diagonal terms are written in the same manner from (4.1.1) as

$$\begin{aligned}
D_{xx} &= \overline{m} + m_f^* \langle I_{xx}^f \rangle + M_r m_s^* \langle I_{xx}^s \rangle + 2 \left[m_f^* \langle e_{xx}(B^f) \rangle + M_r m_s^* \langle e_{xx}(B^s) \rangle \right] \\
D_{yy} &= \overline{m} + m_f^* \langle I_{yy}^f \rangle + M_r m_s^* \langle I_{yy}^s \rangle + 2 \left[m_f^* \langle e_{yy}(B^f) \rangle + M_r m_s^* \langle e_{yy}(B^s) \rangle \right] \\
D_{zz} &= \overline{m} + m_f^* \langle I_{zz}^f \rangle + M_r m_s^* \langle I_{zz}^s \rangle + 2 \left[m_f^* \langle e_{zz}(B^f) \rangle + M_r m_s^* \langle e_{zz}(B^s) \rangle \right]
\end{aligned} \qquad (4.2.3a-c)$$

Let us introduce a coordinate transformation shown in Fig. 4.5, which is obtained by rotating xyz-frame 90 degrees counterclockwise about x-axis. The transformation matrix is given by

$$C_{ij} = \mathbf{e}_i \cdot \mathbf{e}_j^G = \begin{bmatrix} 1 & 0 & 0 \\ 0 & 0 & -1 \\ 0 & 1 & 0 \end{bmatrix} \qquad (4.2.4)$$

Using the transformation matrix D_{zz} may be written

$$D_{zz} = \overline{m} + C_{zi}C_{zj}\left\{m_f^*\langle I_{ij}^f\rangle^C + M_r m_s^*\langle I_{ij}^s\rangle^C + 2\left[m_f^*\langle e_{ij}^C(B^f)\rangle + M_r m_s^*\langle e_{ij}^C(B^s)\rangle\right]\right\} \tag{4.2.5}$$

where

$$\langle I_{ij}^{f,s}\rangle^C = \left\langle \frac{\partial B_i^{f,s}}{\partial x_k^C}\frac{\partial B_j^{f,s}}{\partial x_k^C}\right\rangle, \qquad \langle e_{ij}^C(B^{f,s})\rangle = \frac{1}{2}\left\langle \frac{\partial B_j^{f,s}}{\partial x_i^C} + \frac{\partial B_i^{f,s}}{\partial x_j^C}\right\rangle \tag{4.2.6}$$

are all determined in $x^Cy^Cz^C$-frame. The velocity components in Fig. C.5(a) in Appendix A of Part A, when viewed from $x^Cy^Cz^C$-frame, show that 90-degree rotation about x-axis does not alter the velocity distribution. In view of this, (4.2.5) becomes

$$D_{zz} = \overline{m} + m_f^*\langle I_{yy}^f\rangle^C + M_r m_s^*\langle I_{yy}^s\rangle^C + 2\left[m_f^*\langle e_{yy}^C(B^f)\rangle + M_r m_s^*\langle e_{yy}^C(B^s)\rangle\right] = D_{yy} \tag{4.2.7}$$

Recall that (4.2.7) is the outcome of 90-degree rorational symmetry in the distribution of $u_y^{(0)}$ and $u_z^{(0)}$ about x-axis when the mean flow is in the x-direction,e.g. $\langle k_{xx}\rangle = k'$, $\langle k_{yx}\rangle = \langle k_{zx}\rangle = 0$. Obviously D_{xx} is different from D_{yy} or D_{zz} as seen in (4.1.6) in which the source distribution is composed of not only the fluctuating part $\hat{k}_{xx}$ but also steady source represented by bk'.

Combining (4.2.2) and (4.2.7) we finally obtain the effective diffusion coefficients for the mean flow in x-direction as

$$D_{ij} = \begin{bmatrix} D_I & 0 & 0 \\ 0 & D_{II} & 0 \\ 0 & 0 & D_{II} \end{bmatrix} \tag{4.2.8}$$

where

$$\begin{aligned} D_I &= D_{xx} \\ D_{II} &= D_{yy} = D_{zz} \end{aligned} \tag{4.2.9a,b}$$

Equations (4.2.8) and (4.2.9) are equally valid for the mean flow either in y or z direction with appropriate change of the subscripts.

In theories of dispersion of passive solute, the medium is said to be isotropic when dispersion in the medium is charecterized by two coefficients, the longitudinal

and transverse dispersion coefficients, which are constant for any direction of mean flow. For such medium the dispersion tensor can be represented by

$$D_{ij} = \lambda_i \lambda_j D_L + (\delta_{ij} - \lambda_i \lambda_j) D_T \tag{4.2.10}$$

where D_L and D_T are the longitudinal and transverse dispersion coefficients. In (4.2.10) λ_i is the i-th component of the unit vector in the direction of mean flow independent of the microscale coordinates. In isotropic medium, D_L the dispersion coefficient in the direction of mean flow when there is a concentration gradient (or thermal gradient) in the same direction and D_T the dispersion coefficient in any direction normal to the mean flow, are constant with no regard to the mean flow direction.

The dispersion tensor for the present model geometry of the microcell in Fig. 4.1 can be of the form (4.2.8) only when the mean flow direction coincides with one of the coordinate axes. For such flow direction, the dispersion tensor given by (4.2.8) is isotropic for a rotation about the axis of the flow direcion. This is readily seen in (4.2.8) that the lower right 2×2 matrix for y and z axes is isotropic with only one coefficient a_{II}. In this regard, (4.2.8) is transversely isotropic. This does not hold for arbitrary direction of mean flow for the microcell of Fig. 4.1 unless, as noted by Brenner(1980), the flow is along one of the crystallographic axes for periodic media.

5. Numerical Computation of the Dispersion Tensor for Wigner-Seitz Grains

In this section, the dispersion tensor is computed for a cubic array of Wigner-Seitz grains. In order to solve the convection-diffusion equation with distributed source (3.4.12) numerically, a variational principle is derived in §5.1 and the finite element approximation with linear shape function is made in §5.2. After a brief explanation of the convergence with decreasing mesh size in §5.3, the numerical results are discussed in in §5.4 for both passive solute and heat. Comparisons with experimental data and other works are made.

5.1 The Variational Principle.

The thermal properties of the fluid and solid phases are assumed to be isotropic and homogeneous so that the heat capacity and thermal conductivity are constant. For the purpose of convenience the canonical cell problems for B_i^f and B_i^s are rewritten from (3.3.12) in indicial form :

$$
\begin{aligned}
Pe\left(\tilde{u}_i^{(0)} + u_j^{(0)}\frac{\partial B_i^f}{\partial x_j}\right) &= \frac{\partial^2 B_i^f}{\partial x_k \partial x_k} \qquad x_k \in \Omega_f \\
PeS_i &= M_r \frac{\partial^2 B_i^s}{\partial x_k \partial x_k} \qquad x_k \in \Omega_s \\
B_i^f &= B_i^s \qquad x_k \in \Gamma \\
N_i + \frac{\partial B_i^f}{\partial x_k} N_k &= M_r\left(N_i + \frac{\partial B_i^s}{\partial x_k} N_k\right) \qquad x_k \in \Gamma \\
B_i^f \quad &\text{and} \quad B_i^s \quad \text{are } \Omega\text{-periodic} \\
\langle B_i^f \rangle &= \langle B_i^s \rangle = 0
\end{aligned}
\tag{5.1.1a-f}
$$

where

$$
S_i = -\frac{(\rho C_p)_r}{\bar{a}} \langle u^{(0)} \rangle_i \tag{5.1.2}
$$

The pore fluid velocity is determined from the solution of the Stokes problem by (3.3.2a) and is given quantity in (5.1.1) so that its variation is zero, $\delta u_j^{(0)} = 0$. Then

the variations of B_i^f and B_i^s must satisfy

$$
\begin{aligned}
Peu_j^{(0)}\frac{\partial(\delta B_i^f)}{\partial x_j} &= \frac{\partial^2(\delta B_i^f)}{\partial x_k \partial x_k} \qquad x_k \in \Omega_f \\
0 &= M_r \frac{\partial^2(\delta B_i^s)}{\partial x_k \partial x_k} \qquad x_k \in \Omega_s \\
\delta B_i^f &= \delta B_i^s \qquad x_k \in \Gamma \\
\frac{\partial(\delta B_i^f)}{\partial x_k} N_k &= M_r \frac{\partial(\delta B_i^s)}{\partial x_k} N_k \qquad x_k \in \Gamma \\
\delta B_i^f \quad &\text{and} \quad \delta B_i^s \quad \text{are } \Omega\text{-periodic} \\
\langle \delta B_i^f \rangle &= \langle \delta B_i^s \rangle = 0
\end{aligned}
\tag{5.1.3a-f}
$$

To derive the variational principle, we first multiply (5.1.1a) by δB_i^f and (5.1.1b) by δB_i^s, and integrate the sum of these products over the respective phases in the Ω-cell. Similarly, we multiply (5.1.3a) and (5.1.3b) by B_i^f and B_i^s respectively and integrate over the unit cell. We then add the results and make use of the interface boundary conditions and the Ω-periodicity condition. A variational principle can be obtained. The constraint (5.1.1f) is then incorporated by employing the Lagrange multiplier. The result is

$$
\delta J = 0 \tag{5.1.4}
$$

where the functional J is

$$
\begin{aligned}
J = &\int_{\Omega_f} \left[Pe\left(\bar{u}_i^{(0)} B_i^f + u_j^{(0)} B_i^f \frac{\partial B_i^f}{\partial x_j} \right) + \frac{\partial B_i^f}{\partial x_j}\frac{\partial B_i^f}{\partial x_j} + \frac{\partial B_i^f}{\partial x_i} \right] d\Omega \\
&+ \int_{\Omega_s} \left(-PeS_i B_i^s + M_r \frac{\partial B_i^s}{\partial x_k}\frac{\partial B_i^s}{\partial x_k} + M_r \frac{\partial B_i^s}{\partial x_i} \right) d\Omega \\
&+ \lambda_i \left(\int_{\Omega_f} B_i^f d\Omega + \int_{\Omega_s} B_i^s d\Omega \right)
\end{aligned}
\tag{5.1.5}
$$

in which λ_i is the Lagrange multiplier. In the case of dispersion of passive solute, one simply omits the solid part in (5.1.5).

Rather than giving the details of derivation, let us verify that (5.1.1) indeed extremizes the functional J. By taking the first variation of J we get

$$\begin{aligned}\delta J = &\int_{\Omega_f} Pe\left(\tilde{u}_i^{(0)} + u_j^{(0)}\frac{\partial B_i^f}{\partial x_j}\right)\left(\delta B_i^f\right) \\ &+ \int_{\Omega_f}\left[Peu_j^{(0)}\frac{\partial\left(\delta B_i^f\right)}{\partial x_j}B_i^f + 2\frac{\partial B_i^f}{\partial x_j}\delta\left(\frac{\partial B_i^f}{\partial x_j}\right) + \frac{\partial\left(\delta B_i^f\right)}{\partial x_i}\right]d\Omega \\ &+ \int_{\Omega_s} M_r\left[2\frac{\partial B_i^s}{\partial x_j}\delta\left(\frac{\partial B_i^s}{\partial x_j}\right) + \frac{\partial(\delta B_i^s)}{\partial x_i}\right]d\Omega + \int_{\Omega_s} PeS_i\delta B_i^s d\Omega \\ &+ \left(\int_{\Omega_f} B_i^f d\Omega + \int_{\Omega_s} B_i^s d\Omega\right)\delta\lambda_i + \lambda_i\delta\left(\int_{\Omega_f} B_i^f d\Omega + \int_{\Omega_s} B_i^s d\Omega\right)\end{aligned} \tag{5.1.6}$$

The integrand of the second integral in Ω_f can be further written, after using (5.1.3a)

$$\begin{aligned}&Peu_j^{(0)}\frac{\partial\left(\delta B_i^f\right)}{\partial x_j}B_i^f + 2\frac{\partial B_i^f}{\partial x_j}\delta\left(\frac{\partial B_i^f}{\partial x_j}\right) + \frac{\partial\left(\delta B_i^f\right)}{\partial x_i} \\ =&B_i^f\frac{\partial^2\left(\delta B_i^f\right)}{\partial x_j\partial x_j} + 2\frac{\partial B_i^f}{\partial x_j}\delta\left(\frac{\partial B_i^f}{\partial x_j}\right) + \frac{\partial\left(\delta B_i^f\right)}{\partial x_i} \\ =&\frac{\partial}{\partial x_j}\left(B_i^f\frac{\partial\left(\delta B_i^f\right)}{\partial x_j}\right) + \frac{\partial}{\partial x_j}\left(\frac{\partial B_i^f}{\partial x_j}\left(\delta B_i^f\right)\right) - \frac{\partial^2 B_i^f}{\partial x_j\partial x_j}\left(\delta B_i^f\right) + \frac{\partial\left(\delta B_i^f\right)}{\partial x_i}\end{aligned} \tag{5.1.7}$$

Similarly the integrand of the third integral becomes

$$\begin{aligned}&2M_r\frac{\partial B_i^s}{\partial x_j}\delta\left(\frac{\partial B_i^s}{\partial x_j}\right) + M_r\frac{\partial(\delta B_i^s)}{\partial x_i} \\ &\quad= M_r\frac{\partial}{\partial x_j}\left(\frac{\partial B_i^s}{\partial x_j}\delta B_i^s\right) - M_r\frac{\partial^2 B_i^s}{\partial x_j\partial x_j}(\delta B_i^s) \\ &\qquad+ M_r\frac{\partial}{\partial x_j}\left(B_i^s\frac{\partial(\delta B_i^s)}{\partial x_j}\right) - M_rB_i^s\frac{\partial^2(\delta B_i^s)}{\partial x_j\partial x_j} + M_r\frac{\partial(\delta B_i^s)}{\partial x_i} \\ &\quad= -M_r\frac{\partial^2 B_i^s}{\partial x_j\partial x_j}(\delta B_i^s) + M_r\frac{\partial}{\partial x_j}\left(\frac{\partial B_i^s}{\partial x_j}\delta B_i^s + B_i^s\frac{\partial(\delta B_i^s)}{\partial x_j}\right) + M_r\frac{\partial(\delta B_i^s)}{\partial x_i}\end{aligned} \tag{5.1.8}$$

where (5.1.3b) has been used.

Substituting (5.1.7) and (5.1.8) into (5.1.6) and making use of Gauss theorem, we obtain

$$
\begin{aligned}
\delta J = & \int_{\Omega_f} Pe \left(\tilde{u}_i^{(0)} + u_j^{(0)} \frac{\partial B_i^f}{\partial x_j} - \frac{\partial^2 B_i^f}{\partial x_j \partial x_j} \right) \left(\delta B_i^f \right) d\Omega \\
& + \int_{\Omega_s} \left(-PeS_i - M_r \frac{\partial^2 B_i^s}{\partial x_j \partial x_j} \right) \left(\delta B_i^s \right) d\Omega \\
& + \int_{\Gamma} \left[B_i^f \frac{\partial \left(\delta B_i^f \right)}{\partial x_j} - M_r B_i^s \frac{\partial (\delta B_i^s)}{\partial x_j} \right] N_j^f dS \\
& + \int_{\Gamma} \left[\left(\frac{\partial B_i^f}{\partial x_j} N_j^f + N_i^f \right) \delta B_i^f - M_r \left(\frac{\partial B_i^s}{\partial x_j} N_j^f + N_i^f \right) \delta B_i^s \right] dS \qquad (5.1.9) \\
& + \int_{\Gamma_f} \left\{ \left[B_i^f \frac{\partial \left(\delta B_i^f \right)}{\partial x_j} + \frac{\partial B_i^f}{\partial x_j} \left(\delta B_i^f \right) \right] N_j^f + \left(\delta B_i^f \right) N_i^f \right\} dS \\
& + \int_{\Gamma_s} \left\{ M_r \left[B_i^s \frac{\partial (\delta B_i^s)}{\partial x_j} + \frac{\partial B_i^s}{\partial x_j} (\delta B_i^s) \right] N_j^s + M_r (\delta B_i^s) N_i^s \right\} dS \\
& + \left(\int_{\Omega_f} B_i^f d\Omega + \int_{\Omega_s} B_i^s d\Omega \right) \delta \lambda_i + \lambda_i \delta \left(\int_{\Omega_f} B_i^f d\Omega + \int_{\Omega_s} B_i^s d\Omega \right)
\end{aligned}
$$

where Γ_f and Γ_s are the fluid and solid portions respectively on the surface of cubic microcell. The shapes of Γ_f and Γ_s are the same on the opposite faces due to Ω-periodicity. Also N_i^f and N_i^s are the unit normal vectors on the surface pointing outwards from the fluid and solid phases respectively.

The surface integrals on the interface Γ vanish because of the boundary conditions (5.1.1c and d) and (5.1.3c and d). The integral over Γ_f is also zero due to Ω-periodicity and the fact that N_j^f is of opposite sign on Γ_f. Similarly the integral over Γ_s vanishes. Finally, if the zero average condition (5.1.3f) is imposed, the last two integrals in (5.1.9) also vanish. Thus, to extremize the functional J, B_i^f and B_i^s should satisfy the boundary value problem (5.1.1) for arbitrary δB_i^f and δB_i^s. This proves that $\delta J = 0$ is equivalent to solving the boundary value problem (5.1.1).

5.2 Finite Element Approximation

Finite elements are used to represent the functional J in terms of the unknowns B_i^f and B_i^s at discrete nodal points. The first variation with respect to unknowns and the Lagrange multiplier is then taken to obtain algebraic equations for nodal unknowns.

We have used linear tetrahedral element with four local nodes. A vector quantity **M** is approximated in the linear tetrahedron by

$$\mathbf{M} = \begin{Bmatrix} M_x \\ M_y \\ M_z \end{Bmatrix} = \mathbf{A}\mathbf{q} \tag{5.2.1}$$

where

$$\mathbf{A} = \begin{bmatrix} A_1 & 0 & 0 & A_2 & 0 & 0 & A_3 & 0 & 0 & A_4 & 0 & 0 \\ 0 & A_1 & 0 & 0 & A_2 & 0 & 0 & A_3 & 0 & 0 & A_4 & 0 \\ 0 & 0 & A_1 & 0 & 0 & A_2 & 0 & 0 & A_3 & 0 & 0 & A_4 \end{bmatrix} \tag{5.2.2}$$

is the shape function matrix and

$$\mathbf{q} = [\, M_x^1 \quad M_y^1 \quad M_z^1 \quad M_x^2 \quad M_y^2 \quad M_z^2 \quad M_x^3 \quad M_y^3 \quad M_z^3 \quad M_x^4 \quad M_y^4 \quad M_z^4 \,]^T \tag{5.2.3}$$

The superscript i in (5.2.3) denotes the local node number. The representation of (5.2.1) is used for not only $B_i^f = \{B_x^f, B_y^f, B_z^f\}$ and $B_m^s = \{B_x^s, B_y^s, B_z^s\}$ but also the pore fluid velocity $u_m^{(0)} = u_x^{(0)}, u_y^{(0)}, u_z^{(0)}$. The calculation of $u_m^{(0)}$ has already been carried out in Part A where the medium permeability is determined. The details of finite element approximation and the procedure of taking the first variation have been summarized in Appendix C, Part A. We only give the results.

The variational statement (5.1.4) expressed in terms of nodal unknowns and Lagrange multiplier then yields the following algebraic equations.

$$\begin{aligned} \mathbf{C}_f\mathbf{q}_f + \mathbf{C}_s\mathbf{q}_s + \mathbf{C}_\lambda\mathbf{q}_\lambda &= \mathbf{f}_f + \mathbf{f}_s \\ \mathbf{F}_f\mathbf{q}_f + \mathbf{F}_s\mathbf{q}_s &= 0 \end{aligned} \tag{5.2.4a,b}$$

where $\mathbf{q}_f$, $\mathbf{q}_s$ and $\mathbf{q}_\lambda$ stand for $\{B_x^f, B_y^f, B_z^f\}$, $\{B_x^s, B_y^s, B_z^s\}$ and $\{\lambda_x, \lambda_y, \lambda_z\}$ respectively and

$$
\begin{aligned}
\mathbf{C}_f &= \sum_{i=1}^{N_f} \int_{\Omega_i} Pe \left(\tilde{u}_j \mathbf{A}^T \frac{\partial \mathbf{A}}{\partial x_j} + \frac{\partial \mathbf{A}^T}{\partial x_j} \mathbf{A} \tilde{u}_j^T \right) d\Omega \\
&\quad + 2 \sum_{i=1}^{N_f} \int_{\Omega_i} \left[\frac{\partial \mathbf{A}^T}{\partial x_j} \right] \left[\frac{\partial \mathbf{A}}{\partial x_j} \right] d\Omega \\
\mathbf{C}_s &= \sum_{i=1}^{N_s} \int_{\Omega_i} M_r \left[\frac{\partial \mathbf{A}^T}{\partial x_j} \right] \left[\frac{\partial \mathbf{A}}{\partial x_j} \right] d\Omega \\
\mathbf{C}_\lambda &= \sum_{i=1}^{N_f} \int_{\Omega_i} \mathbf{A}^T d\Omega + \sum_{i=1}^{N_s} \int_{\Omega_i} \mathbf{A}^T d\Omega \\
\mathbf{F}_f &= \sum_{i=1}^{N_f} \int_{\Omega_i} \mathbf{A} d\Omega \\
\mathbf{F}_s &= \sum_{i=1}^{N_s} \int_{\Omega_i} \mathbf{A} d\Omega \\
\mathbf{f}_f &= \sum_{i=1}^{N_f} \int_{\Omega_i} \left(-Pe \mathbf{A}^T \mathbf{A} \tilde{\mathbf{u}} + \nabla \cdot \mathbf{A} \right) d\Omega \\
\mathbf{f}_s &= \sum_{i=1}^{N_s} \int_{\Omega_i} M_r \nabla \cdot \mathbf{A} d\Omega
\end{aligned}
\tag{5.2.5}
$$

In (5.2.5), N_f and N_s are the number of tetrahedral elements in Ω_f and Ω_s. Equation (5.2.4a) is the result of taking the variation of J with respect to B_i^f and B_i^s whereas (5.2.4b) is obtained after taking the variation of J with respect to the Lagrange multiplier λ_i. Again for dispersion of passive solute the unknown in the solid phase, $\mathbf{q}_s$, is dropped and (5.2.4a,b) reduce to the one for $\mathbf{q}_f$ and $\mathbf{q}_\lambda$ only.

5.3 Computational Aspects

Before discussing numerical results, we first define the Peclét number and dimensionless dispersion coefficients for passive solute and heat.

For passive solute the Peclét number given in (2.1.16) becomes

$$
Pe = \frac{U\ell}{D} \tag{5.3.1}
$$

where D is the molecular diffusivity of solute and corresponds to thermal diffusivity $\alpha_f = M_f/(\rho C_p)_f$ of fluid. The velocity U is the average of fluid velocity over the entire cell including solid phase. After omitting the solid phase, the symmetric part of dimensionless dispersivity is defined from (3.4.24) as

$$\overline{D}_{jm} = \frac{m^s + D^s_{jm}}{\langle \rho C_p \rangle D} = \frac{m^s + D_{jm}}{n'(\rho C_p)_f D} = 1 + \frac{1}{n'}\left[\left\langle \frac{\partial B^f_m}{\partial x_k}\frac{\partial B^f_j}{\partial x_k}\right\rangle - \left\langle \frac{\partial B^f_m}{\partial x_j} + \frac{\partial B^f_j}{\partial x_m}\right\rangle\right] \tag{5.3.2}$$

since $M_f/(\rho C_p)_f D$ in solute transport. The right-hand side of (5.3.2) is the volume average over Ω_f only.

For heat transport the dimensionless dispersivity is

$$\begin{aligned}\overline{D}_{jm} &= \frac{m^s + D^s_{jm}}{\langle \rho C_p \rangle} \Big/ \frac{M_f}{(\rho C_p)_f} \\ &= \left\{\frac{m^s}{M_f} + \left[\left\langle \frac{\partial B^f_m}{\partial x_k}\frac{\partial B^f_j}{\partial x_k}\right\rangle - \left\langle \frac{\partial B^f_m}{\partial x_j} + \frac{\partial B^f_j}{\partial x_m}\right\rangle\right]\right\} \Big/ \left(n' + \frac{(\rho C_p)_s}{(\rho C_p)_f}(1-n')\right) \\ &\quad + \frac{M_s}{M_f}\left[\left\langle \frac{\partial B^s_m}{\partial x_k}\frac{\partial B^s_j}{\partial x_k}\right\rangle - \left\langle \frac{\partial B^s_m}{\partial x_j} + \frac{\partial B^s_j}{\partial x_m}\right\rangle\right] \Big/ \left(n' + \frac{(\rho C_p)_s}{(\rho C_p)_f}(1-n')\right)\end{aligned} \tag{5.3.3}$$

By solving (5.2.4) for B^f_m and B^s_m and then calculating the volume averages of their derivatives as defined in (5.3.2) and (5.3.3), numerical results for the dispersivities have been obtained for two porosities 0.38 and 0.5. We shall confine ourselves to a uniform mean flow along the positive x-axis($\theta = 0°$). The computational domain is then reduced to one half of the Wigner-Seitz cell in the region $-0.5 < x < 0.5$, $-0.5 < y < 0.5$ and $0 < z < 0.5$ because of the symmetry about the plane z=0. In Table 5.1, we show four different meshes and the numbers of nodes and elements in one half of the unit cell. Sample computational data for porosity $n = 0.38$ are shown for passive solute and heat respectively in Tables 5.2 and 5.3. Polynomial extrapolation has been used from calculated values for four progressively smaller mesh sizes to get values corresponding to zero mesh size. As a measure of convergence with decreasing mesh size and accuracy of extrapolation, an error is defined by

$$e = \frac{\overline{D}_{jm}(\Delta) - \overline{D}_{jm}(0)}{\overline{D}_{jm}(\Delta)} \tag{5.3.4}$$

where $\overline{D}_{jm}(\Delta)$ is the dispersivity value calculated for the finest mesh and $\overline{D}_{jm}(0)$ is the extrapolated value for zero mesh size. For $Pe \leq 100$, the error is less than 2 %. For $Pe = 200$, the error for D_L is 3 to 5 %. The extrapolation error is very small and therefore the convergence is satisfactory. Those values of $\overline{D}_{jm}(0)$ will be used in the plot of dispersion coefficients.

5.4 Numerical Results

We now discuss dispersivities for passive solute and heat.

Passive solute

In the models of dispersion through a random network of capillaries, the dispersion coefficients are independent of the direction of mean flow (Saffman, 1960; de Jong, 1957; Haring and Greenkorn, 1977). Similarly in a porous medium of randomly packed spheres (Koch and Brady, 1985), the dispersion tensor is independent of the direction of mean flow. Because of the crystaline structure of the cubic array, our dispersivity tensor depends on the direction of the global flow. This is a weakness of the periodic model. For mean flow direction along the x axis ($\theta = 0°$) D_{ij} is diagonal with two independent components which are the longitudinal D_L and transverse D_T diffusivities: $D_{11}(\theta = 0) = D_L$ and $D_{22}(\theta = 0) = D_{33}(\theta = 0) = D_T$. For any other flow direction in the xy-plane, there are four independent dispersivity coefficients: $D_{11}, D_{22} \neq D_{33}$, and $D_{12} = D_{21}$ by symmetry and $D_{13} = D_{23} = 0$.

Computed values of longitudinal and transverse dispersivity coefficients D_L and D_T are plotted for Pe upto 300 for D_L and 200 for D_T in Fig. 5.1 for two porosities $n' = 0.38$ and 0.5. The values for $Pe = 300$ are from the results for the finest meshes and curves in the range of $200 < Pe < 300$ are are shown in dotted lines. To conform with experimental literature the Peclét number P in Figs. 5.1(a) and (b) is defined in terms of the mean flow velocity averaged over Ω_f only i.e., $P = \langle u \rangle \ell / n' D = Pe/n'$. In Fig. 5.1(a), the longitudinal dispersivity is also compared with the measured data by Gunn and Pryce(1969) for simple cubic packing of uniform spheres and the calculations by Salles et al(1993) for simple cubic

packing of uniform spheres with $n' = 0.48$, 0.74 and 0.82. The results for $n' = 0.48$ by Koch et al (1989) (based on an approximate analysis for dilute concentration) are also included. All are in qualitative agreement for D_L.

For small Pe where molecular diffusion is dominant, numerical results show that the effective diffusivity defined in (5.3.2) is greater for larger porosity. The reason is that the cross-sectional area through which passive solute can diffuse increases with porosity. It is always less than unity in the diffusion-dominated regime since the presence of solid grains has the effect of reducing the diffusive flux of solute. At the limit of $P = 0$, the effective diffusivity should be close to the effective thermal conductivity for closely packed spheres which has been studied by Sangani and Acrivos(1983) for various kinds of cubic arrays. For closely packed simple cubic array(with a porosity of 0.48) in which spheres are in contact and have zero conductivity, they obtained 0.344 for the effective conductivity. The numerical value for a Wigner-Seitz cell with porosity of 0.5 is 0.359 after multiplying the value 0.718 from Fig. 5.1(a) by porosity to get the unit cell average. Obviously the small difference stems from different geometry. This provides a check for our numerical computation.

For large P, our numerical results D_L for Wigner-Seitz cell, as well as those by Salles et al are consistent with the measurements by Gunn and Pryce that D_L increases with P^2. This trend has been deduced analytically for dilute and periodic spheres by Koch et al(1989) by approximating the flow field in the interstitial space by that of ambient mean flow. In contrast to the case of small Pe, the dependence on the porosity is now reversed, and the dispersivity now increases with decreasing porosity. Heuristically this is because the velocity gradient increases in the pores as porosity decreases and therefore enhances the microscale mixing. The longitudinal dispersion coefficient for Wigner-Seitz cell is also compared in Fig. 5.1(c) and (d) with experimental data for natural granular media (Ebach and White, 1958; Evans and Kenney; 1966; Harleman and Rumer, 1963; Hiby, 1962; Pfannkuch, 1963; Rifai et al, 1956; Simpson, 1962). We first note that D_L for natural granular media

increases as the first power of P. Secondly the experimental results show larger D_L for P upto $O(10^2)$ and smaller D_L for $P > O(10^2)$. The linear increasing behavior with P has been obtained in the models of random network of capillaries (Saffman, 1960; de Jong, 1957; Haring and Greenkorn, 1977) and randomly packed spheres (Koch and Brady, 1985). Our Wigner-Seitz grain model does not show such behavior and rather shows the Taylor dispersion type behavior of being proportional to P^2. The discrepancy seems to stem from the difference in the microscale structure between the single grain Wigner-Seitz cell and natural granular media.

The transverse dispersivity D_T for Wigner-Seitz grain in Fig. 5.1(b) shows the same trend as D_L except that it is less than D_L by roughly two orders of magnitude. The predictions by the dilute concentration theory of Koch et al remain almost constant with Peclét number. This seems to have been caused by the use of average velocity for the convection velocity in (5.1.1a). There are no reliable measurements for D_T for a regular array of spheres. The transverse dispersivity is compared with experimental data for natural granular media in Fig. 5.1(e) and (f) (Blackwell, 1962; Grane and Gardner, 1961; Hiby, 1962; List and Brooks, 1967; Simpson, 1962). Although D_T for natural granular media shows scatter, each individual result exhibits linearly increasing behavior with P as in the case of D_L. The discrepancy between the Wigner-Seitz grain and natural media is again likely due to the different medium structure.

Dispersivity for heat

When the mean flow direction is along the x-axis ($\theta = 0°$), the longitudinal and transverse dispersivities D_L and D_T for heat are plotted for Peclét numbers upto 300 in Fig. 5.2 for two porosity values $n = 0.38$ and $n = 0.5$. In our computation thermal properties of fluid and solid phases are chosen to be equal,e.g. $M_f = M_s$ and $(\rho_f C_P)_f = (\rho_s C_p)_s$.

In the limit $Pe = 0$, both D_L and D_T approach to unity because the medium is homogeneous and there is no distinction between Ω_f and Ω_s for pure diffusion under the condition that thermal conductivities and heat capacities of fluid and

solid are equal. As a check, we have also calculated the effective diffusivities for $M_s/M_f = 2$ with $n = 0.5$ and obtained $D_T = 1.458$. For simple cubic packing of spheres with $n = 0.48$, Sangani and Acrivos(1983)'s calculation gives $D_T = 1.46$ for the same ratio of thermal conductivities. The small discrepancy is again due to different geometries.

In the high Pe region, the dispersivities increase with decreasing porosity as in the case of passive solute (Fig. 5.2). This is again due to increased microscale mixing in the pore space caused by increased velocity gradient for smaller porosity value.

To see the effect of M_s/M_f, we also show D_{ij} in Fig. 5.3 for two porosities ($n' = 0.38, 0.5$) and two ratios, $M_s/M_f = 0$ and 1. At the high Peclét number, the longitudinal dispersivity D_L for $M_s/M_f = 1$ is greater than those for $M_s/M_f = 0$, although the difference is small. This increase is due to heat transfer through the solid phase. When the thermal gradient is in the direction of the mean flow,e.g. D_{xx}, diffusion through the solid phase augments the dispersion in the fluid when $M_s/M_f \neq 0$. But for D_{yy} which is associated with the thermal gradient normal to the flow, transverse dispersion is weakened by the loss of heat into solid. In any case the transfer in solid is by pure diffusion, hence the difference in D_L and D_T between $M_s/M_f = 1$ and $M_s/M_f = 0$ is minor, as shown in Fig. 5.3(a) and (b). We note that the results for $M_s/M_f = 0$ is porosity n' times the dispersivity of the passive solute.

Table 5.1 Numbers of nodes and elements for four types of meshes

mesh type	number of nodes in -0.5< x <0.5	total number of nodes	total number of elements
1	10	3610	14580
2	13	8125	35560
3	16	15376	67500
4	19	26011	116640

Table 5.2 Solute dispersivities for $n = 0.38$

(a) Longitudinal $D_L = D_{xx}$

Pe	mesh 1	mesh 2	mesh 3	mesh 4	$\overline{D}_{xx}(0)$	error $e(\%)$
0.1	.626745	.621665	.618980	.617318	.614402	.475
0.2	.628150	.623086	.620409	.618747	.615825	.474
0.3	.630492	.625457	.622786	.621129	.618218	.471
0.5	.637986	.633042	.630397	.628750	.625851	.463
1.0	.673114	.668597	.666074	.664476	.661640	.429
2.0	.813647	.810818	.808777	.807383	.804823	.318
3.0	1.04794	1.04787	1.04662	1.04556	1.04345	.202
5.0	1.79829	1.80651	1.80774	1.80774	1.80707	.037
10.0	5.32814	5.36460	5.37599	5.38061	5.38647	.109
20.0	19.6622	19.6292	19.6569	19.6747	19.7042	.150
30.0	44.3858	43.5200	43.4871	43.5076	43.5655	.133
50.0	133.062	120.998	119.988	119.852	119.860	6.67e-3
100.0	943.419	511.665	483.864	479.365	474.565	1.01
200.0	-	2954.88	2085.33	1948.10	2006.58	2.91

Table 5.2 (Continued)

(b) Transverse $D_T = D_{yy}$

Pe	mesh 1	mesh 2	mesh 3	mesh 4	$\overline{D}_{yy}(0)$	error $e(\%)$
0.1	.626291	.621203	.618518	.616853	.613928	.476
0.2	.626328	.621240	.618556	.616891	.613965	.477
0.3	.626395	.621304	.618617	.616954	.614036	.475
0.5	.626599	.621506	.618818	.617151	.614222	.477
1.0	.627566	.622454	.619753	.618080	.615143	.477
2.0	.631432	.626249	.623503	.621801	.618812	.483
3.0	.637878	.632572	.629746	.627999	.624937	.490
5.0	.658541	.652813	.649735	.647833	.644502	.517
10.0	.756135	.747865	.743487	.740829	.736223	.626
20.0	1.15913	1.13087	1.11939	1.11319	1.10312	.913
30.0	1.88084	1.77948	1.74916	1.73511	1.71438	1.21
50.0	4.78345	3.94928	3.79271	3.73663	3.66771	1.88
100.0	-	17.1016	14.0397	13.3657	13.1189	1.88

Table 5.3 Heat dispersivities for $n = 0.38$

(a) Longitudinal $D_L = D_{xx}$

Pe	mesh 1	mesh 2	mesh 3	mesh 4	$\overline{D}_{xx}(0)$	error $e(\%)$
0.1	1.00021	1.00021	1.00022	1.00022	1.00021	7.35e-4
0.2	1.00085	1.00086	1.00086	1.00086	1.00085	6.20e-4
0.3	1.00191	1.00193	1.00194	1.00194	1.00193	6.77e-4
0.5	1.00531	1.00537	1.00539	1.00539	1.00538	1.29e-3
1.0	1.02126	1.02150	1.02156	1.02158	1.02160	1.94e-3
2.0	1.08503	1.0859	1.08623	1.08632	1.08643	9.94e-3
3.0	1.19132	1.19347	1.19402	1.19422	1.19445	1.91e-2
5.0	1.53146	1.53743	1.53895	1.53949	1.54009	3.87e-2
10.0	3.12627	3.14979	3.15581	3.15797	3.16038	7.64e-2
20.0	9.51212	9.60051	9.62361	9.63204	9.64166	9.98e-2
30.0	20.1793	20.3562	20.4045	20.4227	20.4442	.105
50.0	54.5291	54.8123	54.9136	54.9567	55.0134	.103
100.0	221.634	217.136	216.886	216.920	217.072	6.99e-2
200.0	2528.98	885.263	868.472	866.204	824.868	5.01
300.0			1971.29	1953.87		

Table 5.3 (Continued)

(b) Transverse $D_T = D_{yy}$

Pe	mesh 1	mesh 2	mesh 3	mesh 4	$\overline{D}_{yy}(0)$	error $e(\%)$
0.1	1.00000	1.00000	1.00000	1.00000		
0.2	1.00001	1.00001	1.00001	1.00001		
0.3	1.00003	1.00003	1.00003	1.00003		
0.5	1.00008	1.00008	1.00008	1.00008		
1.0	1.00031	1.00031	1.00030	1.00030		
2.0	1.00125	1.00123	1.00122	1.00121	1.00119	2.17e-3
3.0	1.00280	1.00277	1.00274	1.00272	1.00268	3.58e-3
5.0	1.00779	1.00769	1.00761	1.00756	1.00747	8.61e-3
10.0	1.03124	1.03078	1.03045	1.03024	1.02987	3.59e-2
20.0	1.12624	1.12342	1.12191	1.12098	1.11935	.145
30.0	1.28905	1.27880	1.27463	1.27234	1.26857	.297
50.0	1.85145	1.78446	1.76597	1.75774	1.74592	.677
100.0	5.92474	4.34701	4.12426	4.05456	3.97407	2.03
200.0	-	21.2251	14.6632	13.6292	11.9126	3.16

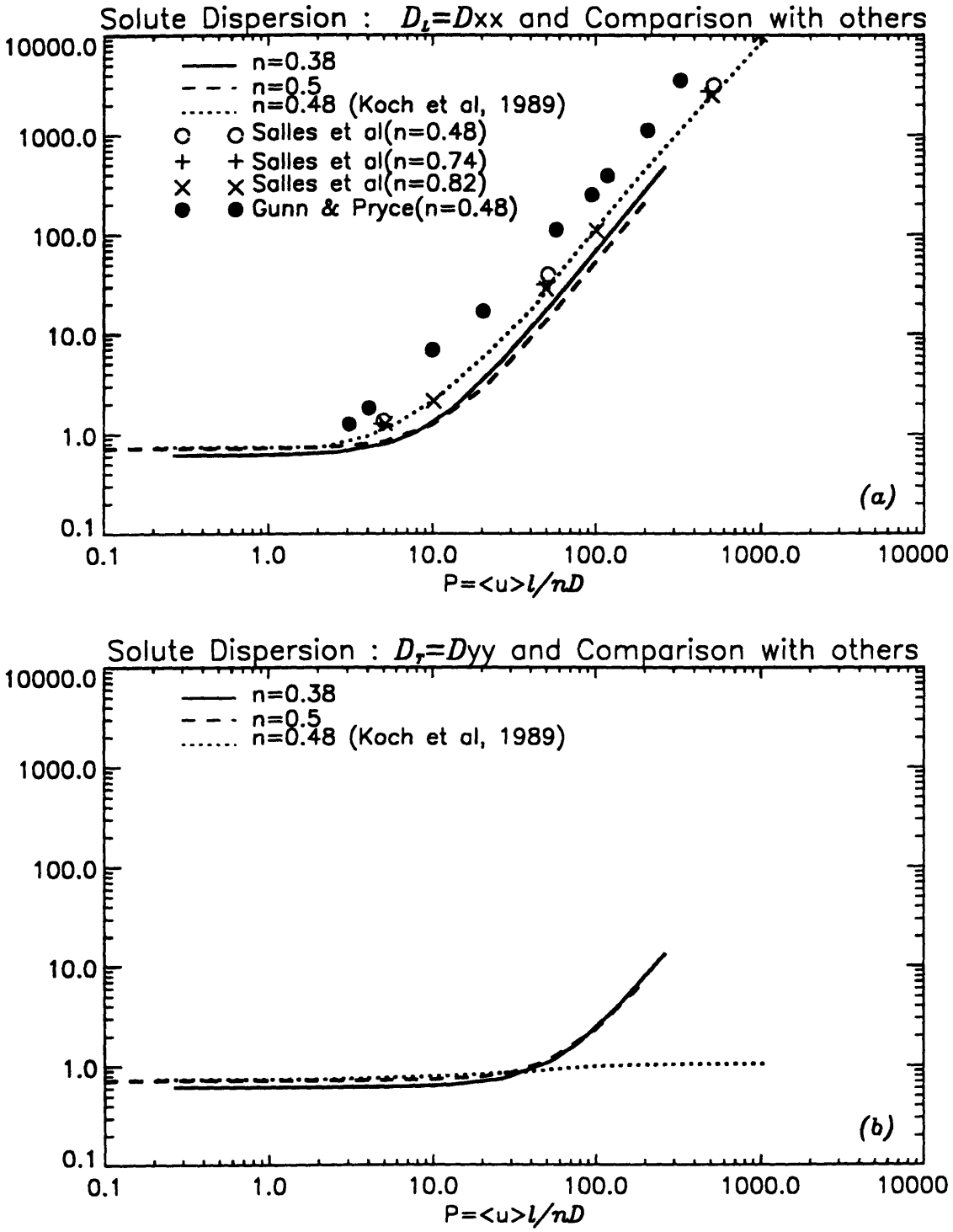

Fig. 5.1 Dispersion coefficients for solute (a) Longitudinal $D_L = D_{xx}$ and (b) Transverse $D_T = D_{yy}$.

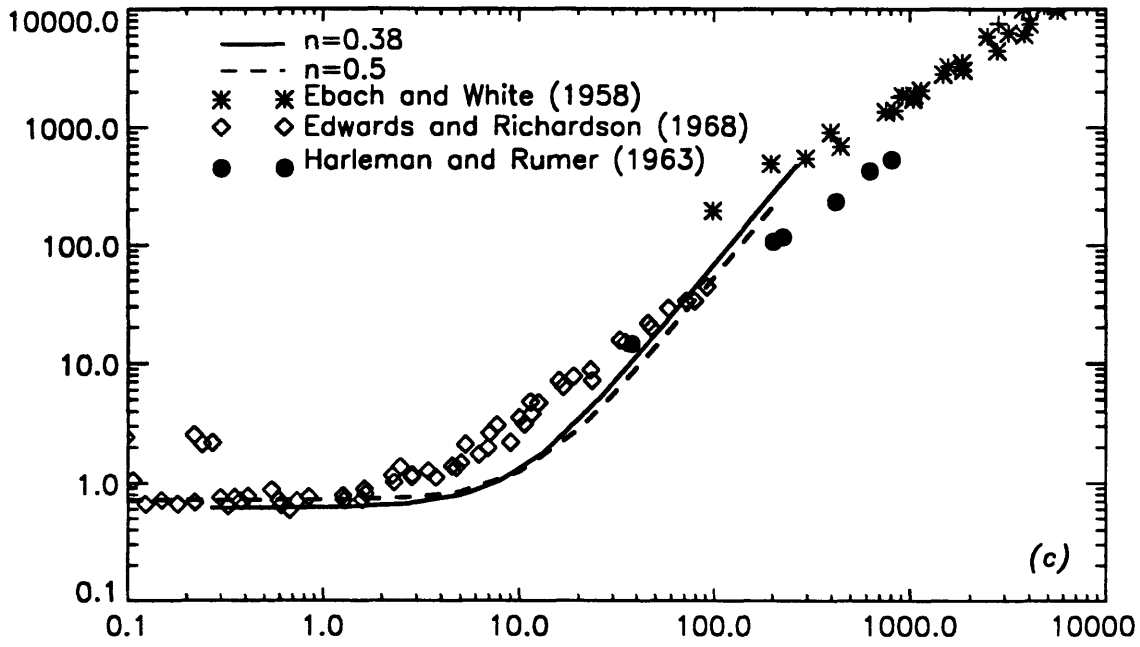

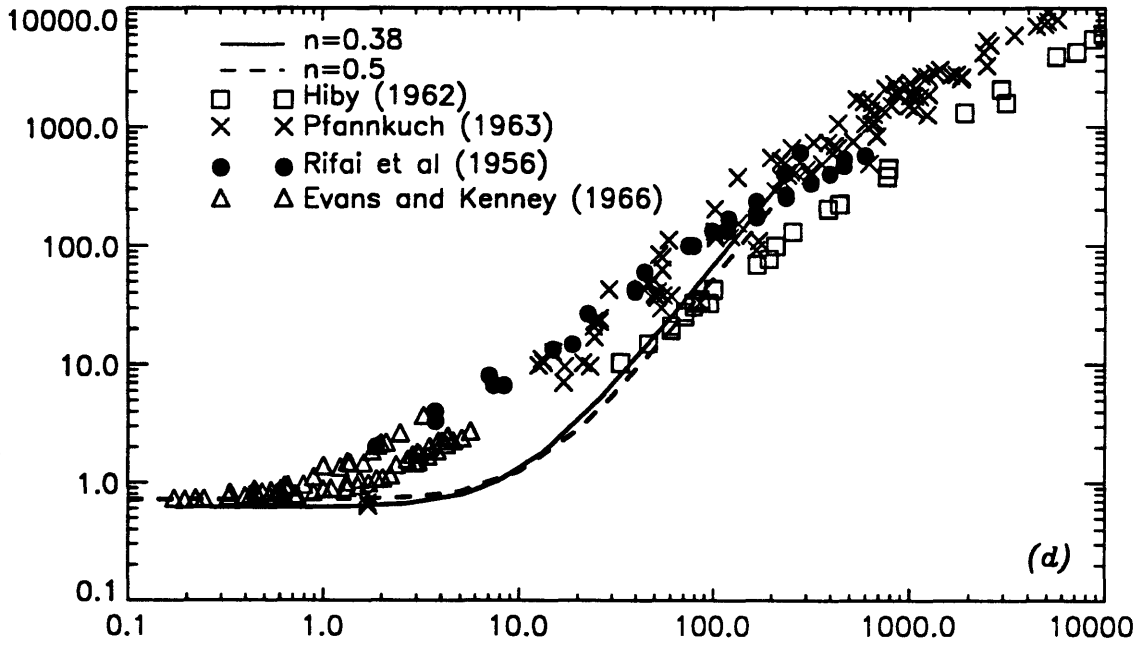

Fig. 5.1 (c) and (d) (continued) Comparison of $D_L = D_{zz}$ for solute with experimental data for natural granular media.

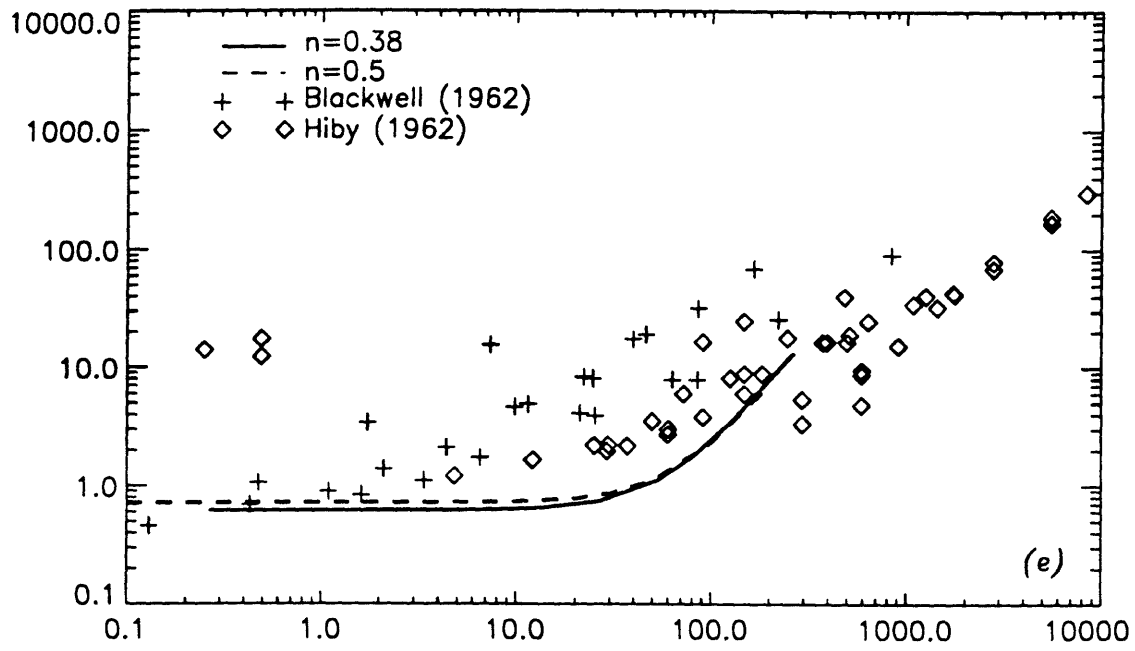

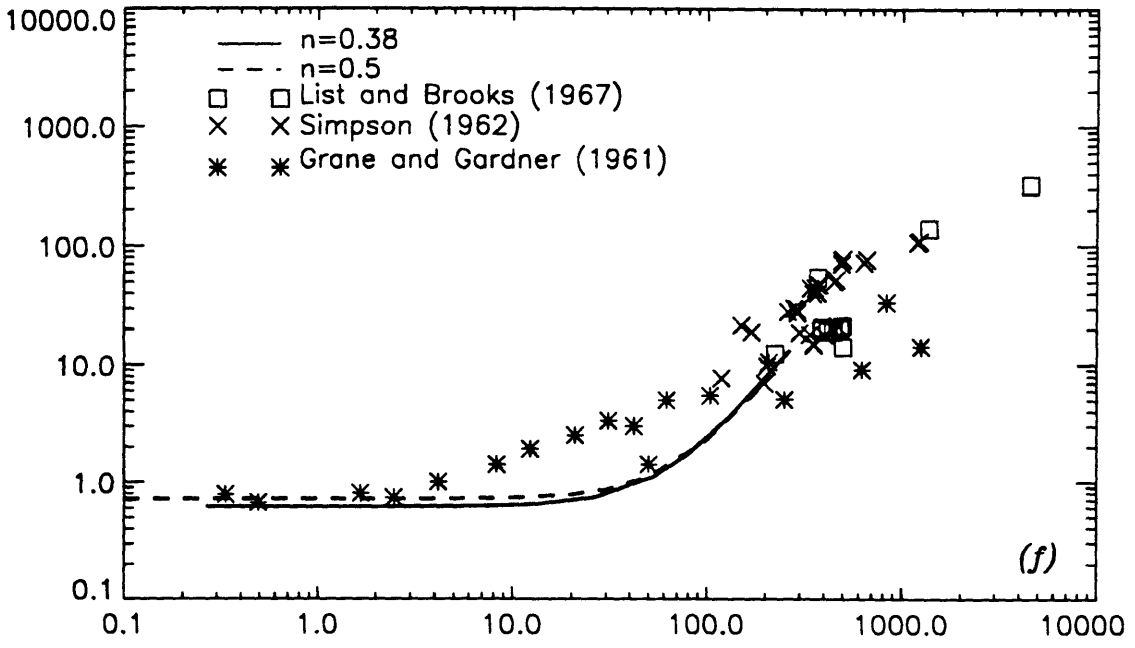

Fig. 5.1 (e) and (f) (continued) Comparison of $D_T = D_{yy}$ for solute with experimental data for natural granular media.

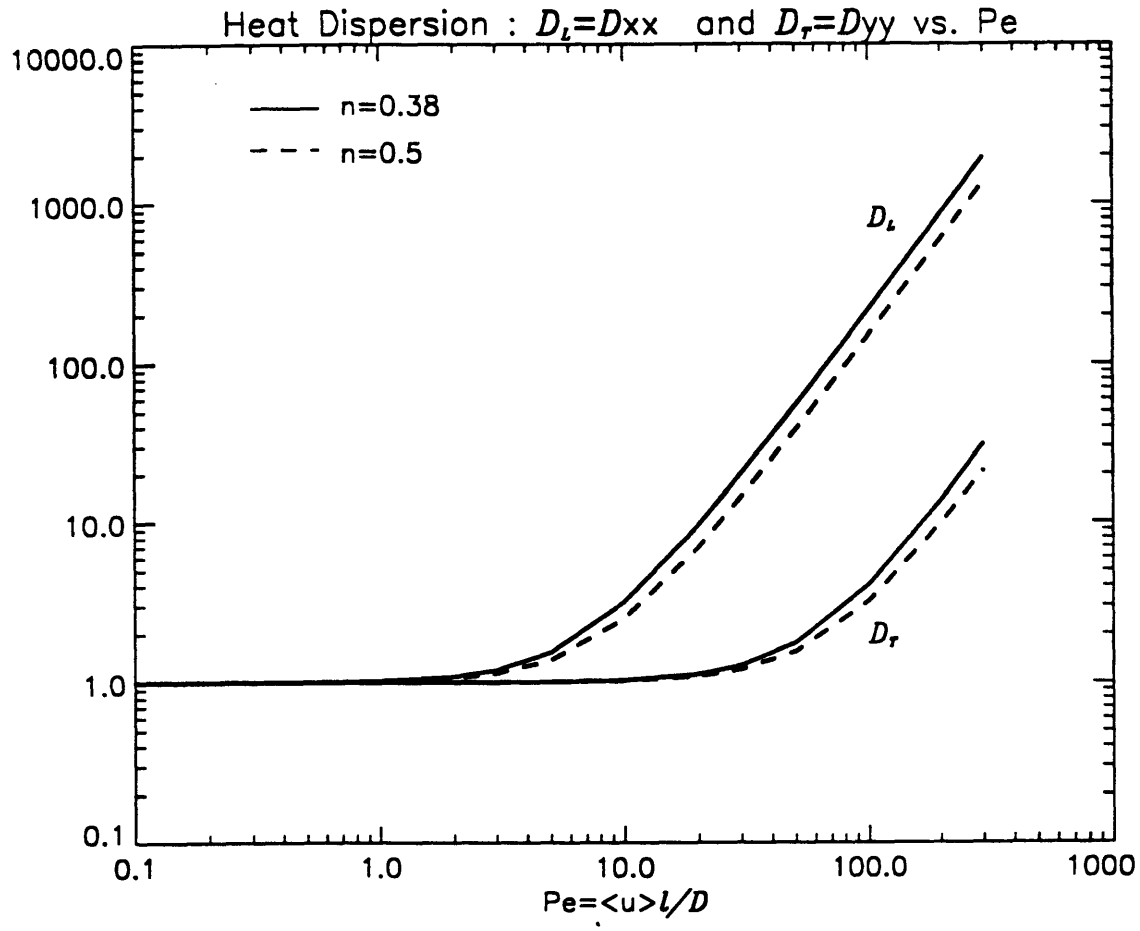

Fig. 5.2 Longitudinal and transverse dispersion coefficients for heat.

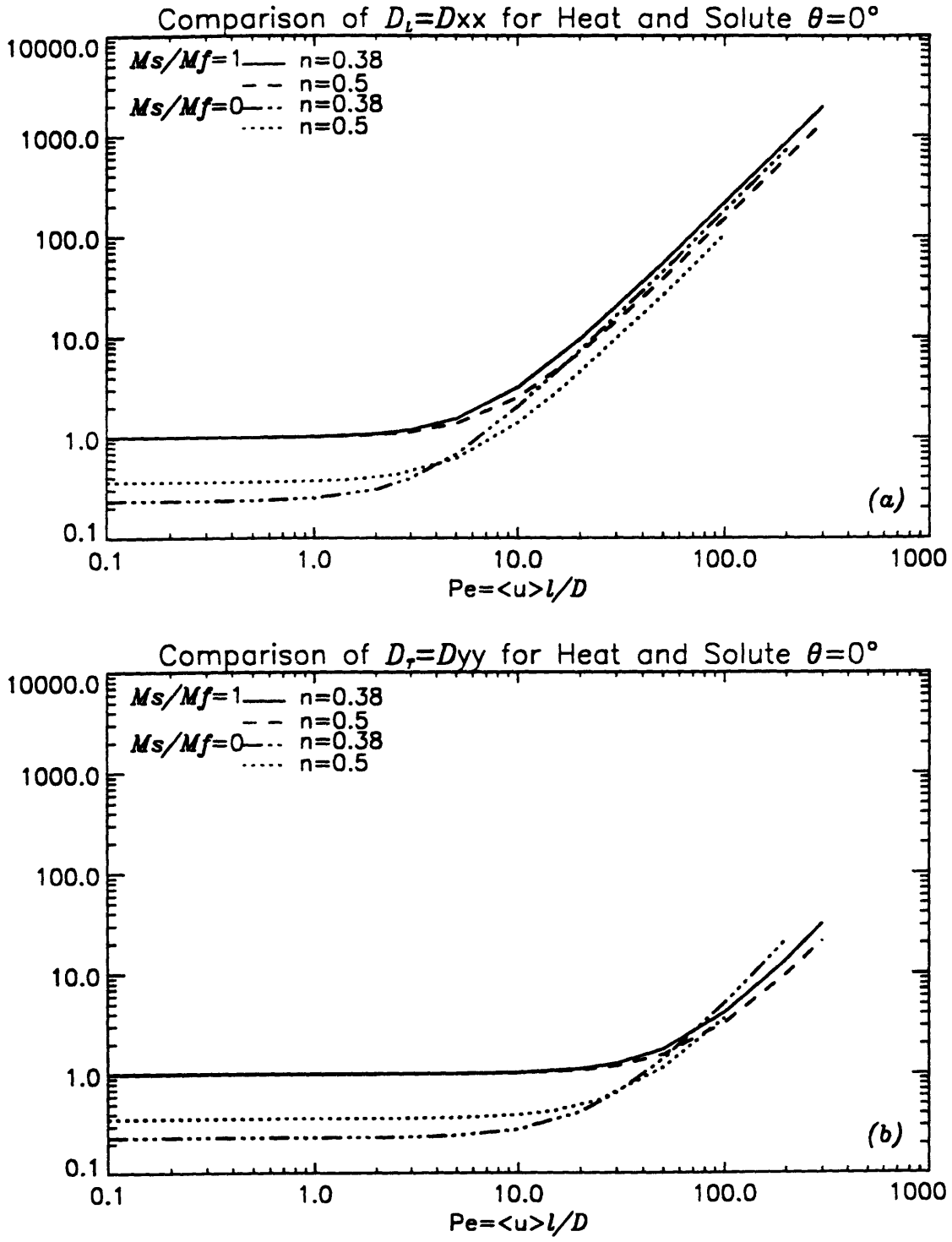

Fig. 5.3 Comparison of dispersion coefficients for heat and solute; (a) longitudinal $D_L = D_{xx}$ and (b) transverse $D_T = D_{yy}$.

6. Concluding Remarks

In this Chapter, we have investigated thermal disperiosn in two-scale periodic porous media by using the theory of homogenization. The microscale Peclét number and the Rayleigh number are assumed to be finite. It is also assumed that the medium is relatively highly permeable and hard. It is shown that heat transport is dominated by convection over the convection time scale. For much longer time scale of heat diffusion, the flow and heat transport are in general nonlinearly coupled because of the effect of weak inertia in fluid. Specifically the first order fluid velocity depends on the pore pressure and the medium temperature hence the convection term in the heat transport equation is nonlinear. However, in a medium which is isotropic and homogeneous on the macroscale, the flow equation is decoupled from heat transport equation which is still nonlinear due to buoyancy in the first order fluid velocity. In any case, the solid deformation is determined from the equilibrium equation by using the pressure and temperature distributions.

For a cubic array of Wigner-Seitz grains, for which the permeability is isotropic, we have calculated the dispersion coefficients for a mean flow direction along one of the symmetry axes by solving a microcell boundary value problem numerically. For the special mean flow direction, it is shown by using the symmetry properties of the solution that there are only two independent nonvanishing coefficients, the longitudianl D_L and transverse D_T coefficients. For both passive solute and heat, the increasing trends of D_L and D_T are proportional to the square of Peclét number. The trend for D_L is consistent with the analytical results for dilute suspensions by Koch et al (1989), the numerical results by Salles et al (1993) and the measurements by Gunn and Pryce (1969) for spheres with cubic packing. However, this behavior is in sharp contrast with data from numerous experiments with natural granular media. These experiments clearly show that, for large Peclét number, the longitudinal dispersion coefficient is proportional to the first power of Peclét number. This discrepancy is likely due to the difference in medium structure between the strictly

periodic microcell and the irregular geometry in natural granular media. The probabilistic approaches by Saffman (1960) and Koch and Brady (1985) in which random nature is taken into account for capillary networks and randomly distributed dilute spheres respectively, the longitudinal dispersion coefficient indeed grows as the first power of Peclét number when the Peclét number is large. Unfortunately no successful theory is known for more general three-dimensional microstructure with densely packed grains.

However, the transverse dispersion coefficient predicted by Koch et al remains almost the same as the molecular diffusion coefficient. To our knowledge there are no reliable measurements of D_T for periodic array of particles.

Chapter II. THERMAL DISPERSION IN THREE-SCALE POROELASTIC MEDIA

1. Introduction

A three-scale porous medium is characterized by the existence of three disparate length scales, the microscale ℓ, the mesoscale ℓ' and the macroscale ℓ'/ϵ. The homogenization theory is now applied to deduce the macroscale governing equations for the flow, heat transport with thermal dispersion and matrix deformation. The mesoscale Peclét number is assumed to be finite whereas the Rayleigh number is assumed to be large. The basic governing equations on the mesoscale are the equilibrium equation, the consolidation equation with buoyancy and heat equation obtained in Part A for relatively highly permeable and hard medium.

On the mesoscale, certain cell boundary value problems are defined whose solutions are necessary to compute the macroscale constitutive coefficients. In particular, it is shown that the mesoscale cell problem for heat transport, whose solution is needed to calculate the dispersion tensor, are nonlinearly coupled to the flow and heat transport on the macroscale. Therfore thermal dispersion with strong buoyancy is an inherently nonlinear problem among the flow, temperature and dispersion tensors. The theory is applied to special case of vertically stratified medium on the mesoscale to derive explicit forms of dispersion tensors. For a medium with two alternating layers assuming that the seepage velocity is known, analytic dispersion tensors are obtained which depend on the inhomogeneities such as permeability, heat capacity and thermal conductivity. In particular, the dependence of dispersion coefficients on the direction of mean flow is examined.

Finally, as an application of the general theory, a thermal cloud released in a uniform seepage flow in a porous layer is considered. The effects of the Peclét number and the Rayleigh number on thermal dispersion are examined.

2. The Governing Equations and Order Estimates

The theory of homogenization is applied to deduce the governing equations for thermal dispersion in porous media with three spatial scales starting from the mesoscale governing equations. The porous medium is assumed to be periodic on the mesoscale so that the medium is composed of periodic arrays of Ω'-cells with periodic length ℓ'. The material coefficients are also assumed to be Ω'-periodic. For this purpose some order estimates are made in §2.1 and it is shown that the mesoscale governing equations at the starting point are those deduced in Part A for thermoconsolidation in two scale porous media with $T_c/T_d \ll 1$. By using the sale estimates the normalized mesoscale giverning equations are obtained in §2.2.

2.1 Order Estimates

The order of magnitude estimates closely follow §2 of Ch. II, Part A. We consider again the flow driven by a pressure difference P'' over the macroscale ℓ''. By using Darcy's law the seepage velocity is scaled by

$$U' = \tilde{k}\frac{P''}{\ell''} \tag{2.1.1}$$

where $\tilde{k}$ is the permeability of the medium.

The stress balance in Hooke's law (3.2.1b) in Ch. I gives

$$\frac{\tilde{\alpha}P''}{\tilde{a} : e(v)} \sim \frac{\tilde{\alpha}P''}{\tilde{a}\delta'} \sim \frac{P''}{\mathcal{D}\delta'} = O(1) \tag{2.1.2}$$

where $\mathcal{D}$ and δ' are the orders of magnitude of the elastic modulus and the strain in the medium and the dimensionless pressure coefficient $\tilde{\alpha}$ is $O(1)$. Since Hooke's law is legitimate only for infinitesimal strain, we assume in (2.1.2) that

$$\delta' \sim \frac{\Delta V''}{\ell''} \sim \frac{P''}{\mathcal{D}} = O(\epsilon) \ll 1 \tag{2.1.3}$$

where $\Delta V''$ is the scale of the medium deformation on the macroscale ℓ''. Equation (2.1.3) implies that $\Delta V''$ is much smaller than the macroscale length ℓ'' but is comparable to the mesoscale,e.g.

$$\Delta V'' = O(\epsilon\ell'') = O(\ell') \tag{2.1.4}$$

If we let P' and $\Delta V'$ be the scales of pressure drop and the medium deformation across the mesoscale ℓ', it follows from (2.1.4) that

$$\frac{\Delta V''}{\ell'} \sim \frac{P'}{\mathcal{D}} \sim \frac{\epsilon P''}{\mathcal{D}} = O(\epsilon^2) \quad ; \quad \Delta V' = O(\epsilon^2 \ell') \tag{2.1.5}$$

There are again three relevant time scales: the consolidation time T'_c, the convection time T'_v and the diffusion time T'_d. They are given by

$$T'_c = \frac{\rho_f g \ell''^2}{\mathcal{D}K}, \quad T'_d = \frac{\ell''^2}{\alpha_f}, \quad T'_v = \frac{\ell''}{U'} \tag{2.1.6}$$

and related by

$$\frac{T'_c}{T'_d} = \frac{\rho_f g \alpha_f}{\mathcal{D}K} \quad \text{and} \quad \frac{T'_v}{T'_d} = \frac{\ell'}{\ell''}\frac{\alpha_f}{U'\ell'} = \frac{\epsilon}{Pe'} \tag{2.1.7a,b}$$

The dimensionless parameter Pe' is the Peclét number which signifies the relative importance of heat convection to heat diffusion over the mesoscale length ℓ' and is assumed to be of order unity:

$$Pe' = \frac{U'\ell'}{\alpha_f} = O(1) \tag{2.1.8}$$

It then follows from (2.1.8) that the microscale Peclét number becomes

$$Pe = \frac{U\ell}{\alpha_f} = \frac{U'\ell'}{\alpha_f}\frac{\ell}{\ell'} = \frac{\ell}{\ell'}Pe' = O\left(\frac{\ell}{\ell'}\right) \ll 1 \tag{2.1.9a}$$

in which ℓ is the microscale length. The microscale to mesoscale length ratio ℓ/ℓ' is not necessarily equal to ℓ'/ℓ'' as long as it is small. For ordering convenience we specifically assume that

$$Pe = O(\epsilon) \tag{2.1.9b}$$

Since Pe' is defined in terms of the mesoscale length, finite Peclét number means that the heat convection is comparable to diffusion over the mesoscale. In view of the time scale ratio (2.1.7b), it is then anticipated that convection will dominate diffusion in the heat transport over the macroscale and lead to dispersion. For

dispersion to be important, the medium must be highly permeable. We shall assume that consolidation is so fast that

$$\frac{T_c'}{T_d'} = O(\epsilon^2) \tag{2.1.10}$$

This is typical of sandy material. Equation (2.1.10) also implies that T_c' is equivalent to the time scale which describes heat diffusion over the mesoscale. Since we are interested in changes over much larger macroscale, the consolidation time T_c' is neglected from the outset. Then the convection time T_v' and the diffusion time T_d' are the fast and slow time scales needed to describe the heat transport on the macroscale.

Another important dimensionless parameter is the Rayleigh number given by

$$Ra' = \frac{\tilde{k}\rho_f g\beta_T \Theta'' \ell''}{\alpha_f} = \frac{K\beta_T \Theta'' \ell''}{\alpha_f} \tag{2.1.11}$$

where $K = \tilde{k}\rho_f g$ has been used. In thermoconsolidation, it has been assumed that $Ra' = O(1)$. In view of the fact that the range of permeability variation is usually $O(10^3)$ or larger even for same type of porous media, we shall assume for highly permeable medium that Ra' is large:

$$Ra' = O(\epsilon^{-1}) \tag{2.1.12}$$

It will be shown in the next section that (2.1.12) implies that the buoyancy becomes important in Darcy's law on the macroscale due to the increase in Rayleigh number.

The above scale assumptions are summarized as follows.

$$\begin{aligned} &\frac{P'}{\mathcal{D}} = O(\epsilon) \quad ; \quad \frac{P}{\mathcal{D}} = O(\epsilon^2); \quad \Delta V'' = O(\epsilon^2 \ell') \\ &Pe' = O(1) \quad ; \quad Pe = O(\epsilon) \quad , \qquad T_v' = \epsilon T_d' \end{aligned} \tag{2.1.13}$$

In view of small Pe, the governing equations at the starting point on the mesoscale are those deduced in Part A for thermoconsolidation. Secondly, the nonlinearly coupled terms which originate from the nonlinear boundary conditions on the fluid-solid interface are negligible because the medium deformation $\Delta V'$ over the mesoscale

is much smaller than the microscale cell size. Lastly, negligibly small consolidation time (cf.(2.1.10)) means that the solid velocity terms in the heat convection and the kinematic boundary condition on the interface are small and accordingly dropped at the outset. Therefore the basic governing equations on the mesoscale are those obtained in §3 of Ch. I, Part A for the special case of $T_c/T_d \ll 1$ and will be used for normalization in the next section.

2.2 Normalized Governing Equations

Under the assumption of (2.1.13), the mesoscale governing equations are (3.5.7) to (3.5.10) in §3 of Ch. I, Part A. In physical variables, we have

$$\nabla \cdot \sigma = \nabla \cdot \left[\tilde{a} : e(v) - \tilde{\alpha} p - \tilde{\beta}_t \theta\right] = -\rho_f g \beta_T n' \theta \mathbf{e}_z \tag{2.2.1}$$

where v, p, θ are the medium displacement, the pore pressure and the temperature variation form the initial state. The right-hand side is the body force due to buoyancy effect in the fluid. Hooke's law is given by

$$\sigma = \tilde{a} : e(v) - \tilde{\alpha} p - \tilde{\beta}_t \theta \tag{2.2.2}$$

Darcy's law is

$$\langle u \rangle = -\tilde{k} \cdot (\nabla p - \rho_f g \beta_T \theta \mathbf{e}_z) \tag{2.2.3}$$

The thermoconsolidation equation is simply

$$\nabla \cdot [\tilde{k} \cdot (\nabla p - \rho_f g \beta_T \theta \mathbf{e}_z)] = 0 \tag{2.2.4}$$

The energy balance is giverned by

$$\overline{\rho C_p} \frac{\partial \theta}{\partial t} + (\rho C_p)_f \langle u \rangle \cdot \nabla \theta = \nabla \cdot (\tilde{m} \cdot \nabla \theta) \tag{2.2.5}$$

where $\overline{\rho C_p}$ and $\tilde{m}$ are the average heat capacity and the thermal conductivity of the medium.

The orders of magnitude of the mesoscale coefficients in (2.2.1) to (2.2.5) are (cf. (2.2.6) of Ch. II, Part A)

$$\begin{aligned} &\tilde{a} \sim \mathcal{D}, \quad \tilde{\alpha} \sim 1, \quad \tilde{\beta}_t \sim B \\ &\tilde{k} \sim \frac{\ell^2}{\mu}, \quad \tilde{m} \sim M_f \end{aligned} \tag{2.2.6}$$

where B is the scale of thermal modulus and α is the linear coefficient of thermal expansion for the solid matrix. The thermal stress $\tilde{\beta}_t\theta$ must be balanced by the strain term in Hooke's law (2.2.2), In view of (2.1.3), it follows that

$$\frac{B\Theta''}{\mathcal{D}} \sim \alpha\Theta'' = O(\epsilon) \tag{2.2.7}$$

With these scale estimates, we introduce the following dimensionless variables denoted by asterisks.

$$\begin{aligned} x &= \ell' x^*, \quad t = T_v t^* \\ \langle u \rangle &= U' \langle u \rangle^* = \tilde{k}\frac{P''}{\ell''}\langle u \rangle^* \\ v &= \Delta V'' v^* = \ell' v^* \\ \theta &= \Theta''\theta^*, \quad \sigma = \mathcal{D}\sigma^* \end{aligned} \tag{2.2.8}$$

Substituting (2.2.8) into (2.2.1) to (2.2.5) and using (2.1.3), (2.1.7) adn (2.1.12), we obtain

$$\nabla^* \cdot \sigma^* = -\epsilon^2 n' \frac{\hat{R}a'}{Pe'}\theta \mathbf{e}_z \tag{2.2.9}$$

$$\sigma^* = a^* : e^*(v^*) - \epsilon\alpha^* p^* - \epsilon\beta_t^*\theta^* \tag{2.2.10}$$

$$\epsilon\langle u \rangle^* = -k^* \cdot \left(\nabla^* p^* - \epsilon\frac{\hat{R}a'}{Pe'}\theta^* \mathbf{e}_z \right) \tag{2.2.11}$$

$$\nabla^* \cdot \left[k^* \cdot \left(\nabla^* p^* - \epsilon\frac{\hat{R}a'}{Pe'}\theta^* \mathbf{e}_z \right) \right] = 0 \tag{2.2.12}$$

$$Pe' \left(\overline{\rho C_p}^* \frac{\partial\theta^*}{\partial t^*} + \langle u \rangle^* \cdot \nabla^*\theta^* \right) = \nabla^* \cdot (m^* \cdot \nabla^*\theta^*) \tag{2.2.13}$$

where

$$\hat{R}a' = \epsilon Ra' = O(1) \tag{2.2.14}$$

Note that (2.2.9) to (2.2.13) are similar to but simpler than (3.1.1) to (3.1.5) in Ch. II, Part A, the normalized governing equations for 3-scale thermoconsolidation. These normalized governing equations are used in the next section to deduce the macroscale governing equations.

3. The Macroscale Governing Equations.

Starting from the normalized governing equations on the mesoscale of §2, the governing equations and constitutive relations on the macroscale are deduced in this section. After introducing the multiple-scales in both space and time in §3.1, the macroscale governing equations are derived for the medium deformation and for the flow in §3.2 and for the heat transport in §3.3. An important new result is that the mesoscale cell boundary value problem, which must be solved to calculate the dispersion tensor and the convection velocity on the macroscale, is nonlinearly coupled to the governing equations for flow and heat on the macroscale. Therefore the dispersion tensor varies with the macroscale heat transport.

3.1 Multiple-Scale Expansions

Since much of the analysis is identical to that in §3 of Ch. II, Part A, only the different features are elaborated here.

Assuming a periodic structure on the mesoscale, we divide the medium into periodic mesoscale cells of length ℓ'. The variables are assumed to be Ω'-periodic.

Introduce the multiple-scale vectors for spatial variables

$$x', \quad x'' = \epsilon x' \tag{3.1.1}$$

and multiple-scale times

$$t_v, \quad t_d = \epsilon t_v \tag{3.1.2}$$

The differential operators are then expanded as

$$\begin{aligned} \nabla^* &= \nabla' + \epsilon \nabla'' \\ e^*(\cdot) &= e'(\cdot) + \epsilon e''(\cdot) \\ \frac{\partial}{\partial t^*} &= \frac{\partial}{\partial t_v} + \epsilon \frac{\partial}{\partial t_d} \end{aligned} \tag{3.1.3a-c}$$

We also introduce the expansion in perturbation series

$$f^* = f^{(0)} + \epsilon f^{(1)} + \epsilon^2 f^{(2)} + \ldots \tag{3.1.4}$$

for

$$f^* = \langle u \rangle^*, v^*, p^* \quad \text{and} \quad \theta^* \tag{3.1.5}$$

where all the perturbation quantities depend on x', x'' and t^* and are Ω'-periodic, but

$$\sigma^* = \sigma^{(-1)} + \epsilon\sigma^{(0)} + \epsilon^2\sigma^{(1)} + \cdots \tag{3.1.6}$$

for the stress. The results which immediately follow from the leading order equations are the same as in §3 of Ch. II, Part A and we simply summarize them as

$$v^{(0)} = v^{(0)}(x'', t_v, t_d), \quad p^{(0)} = p^{(0)}(x'', t_v, t_d), \quad \theta^{(0)} = \theta^{(0)}(x'', t_v, t_d) \tag{3.1.7}$$

Thus the matrix deformation, pore pressure and temperature are independent of the mesoscale at the leading order.

3.2 The Macroscale Equations for Deformation and Flow.

The equilibrium equation is not changed and is the same as (3.2.6) of Ch. II, Part A,e.g.

$$\nabla'' \cdot \langle \sigma^{(0)} \rangle = -n'' \frac{\hat{R}a'}{Pe'} \theta^{(0)} \mathbf{e}_z \tag{3.2.1}$$

The Hooke's law is given by

$$\langle \sigma^{(0)} \rangle = a'' : e''(v^{(0)}) - \alpha'' p^{(0)} - \beta_t'' \theta^{(0)} \tag{3.2.2}$$

in which the coefficients a'', α'' and β_t'' have been given in (3.2.8a-c) in §3 of Ch. II, Part A.

After subsitituting (3.1.5) into (2.2.12) and invoking (3.1.7), the consolidation equation (2.2.12) yields at successive orders of ϵ

$$\begin{aligned}
O(\epsilon) \quad & \nabla' \cdot \left[k^* \cdot \left(\nabla'' p^{(0)} + \nabla' p^{(1)} - \frac{\hat{R}a'}{Pe'} \theta^{(0)} \mathbf{e}_z \right) \right] = 0 \\
O(\epsilon^2) \quad & \nabla'' \cdot \left[k^* \cdot \left(\nabla'' p^{(0)} + \nabla' p^{(1)} - \frac{\hat{R}a'}{Pe'} \theta^{(0)} \mathbf{e}_z \right) \right] \\
& + \nabla' \cdot \left[k^* \cdot \left(\nabla'' p^{(1)} + \nabla' p^{(2)} - \frac{\hat{R}a'}{Pe'} \theta^{(1)} \mathbf{e}_z \right) \right] = 0
\end{aligned} \tag{3.2.3a,b}$$

Equation (3.2.3a) immediately suggests a solution form for $p^{(1)}$

$$p^{(1)} = S' \cdot \left(\nabla'' p^{(0)} - \frac{\hat{R}a'}{Pe'} \theta^{(0)} \mathbf{e}_z \right) \tag{3.2.4}$$

where $S'(x', x'')$ is the same as that in (3.2.10) of Ch. II, Part A and therefore must satisfy the steady seepage flow equation with distributed sources due to mesoscale heterogeneities in permeability,e.g. (3.2.11a,c and d) there. If we substitute (3.2.4) into (3.2.3b), integrate over Ω'-cell and use Ω'-periodicity, there follows the macroscale consolidation equation

$$\nabla'' \cdot \left[k'' \cdot \left(\nabla'' p^{(0)} - \frac{\hat{R}a'}{Pe'} \theta^{(0)} \mathbf{e}_z \right) \right] = 0 \tag{3.2.5}$$

where k'' is the macroscale permeability which is obtained by solving the Ω'-cell problem (3.2.11) of Ch. II, Part A. We note that the first-order pressure $p^{(1)}$, (3.2.4), does not depend on the solid velocity because the consolidation time is so small ($T'_c = \epsilon^2 T'_d$).

From (2.2.11) the velocity of seepage flow through the medium at $O(\epsilon)$ is given by

$$\langle u \rangle^{(0)} = -k^* \cdot \left(\nabla'' p^{(0)} + \nabla' p^{(1)} - \frac{\hat{R}a'}{Pe'} \theta^{(0)} \mathbf{e}_z \right) \tag{3.2.6}$$

Substituting (3.2.4) into (3.2.6) and integrating over Ω'-cell, we obtain Darcy's law as

$$\langle \langle u \rangle^{(0)} \rangle = -k'' \cdot \left(\nabla'' p^{(0)} - \frac{\hat{R}a'}{Pe'} \theta^{(0)} \mathbf{e}_z \right) \tag{3.2.7}$$

In the present problem of thermal dispersion in a 3-scale medium, the seepage velocity is affected by buoyancy. This is due to the increase in Ra' of (2.1.12) by both increased permeability and the length scale change from ℓ' to ℓ''. The seepage velocity at the next order is given by

$$\langle u \rangle^{(1)} = -k^* \cdot \left(\nabla'' p^{(1)} + \nabla' p^{(2)} - \frac{\hat{R}a'}{Pe'} \theta^{(1)} \mathbf{e}_z \right) \tag{3.2.8}$$

after collecting $O(\epsilon^2)$ terms in (2.2.11). It plays the role of convection velocity of heat transfer over much longer diffusion time, as will be shown in the next section.

The first order velocity (3.2.8) will be considered after we obtain the representation of $\theta^{(1)}$ in terms of macroscale thermal gradient $\nabla''\theta^{(0)}$.

3.3 The Macroscale Heat Transport.

In the heat transport, the mesoscale cell boundary value problem involves a convection -diffusion equation whose solution leads to thermal dispersion at the macroscale.

We first obtain the heat equations at various orders of ϵ by substituting (3.1.3) and (3.1.4) into (2.2.13) as

$$
\begin{aligned}
O(1) \qquad & Pe'\langle u\rangle^{(0)}\cdot\nabla'\theta^{(0)} = \nabla'\cdot\left(m^*\cdot\nabla'\theta^{(0)}\right)\\
O(\epsilon)Pe' & \left[\overline{\rho C_p}^*\frac{\partial\theta^{(0)}}{\partial t_v} + \langle u\rangle^{(0)}\cdot\left(\nabla''\theta^{(0)}+\nabla'\theta^{(1)}\right) + \langle u\rangle^{(1)}\cdot\nabla'\theta^{(0)}\right]\\
& \qquad = \nabla'\cdot\left[m^*\cdot\left(\nabla''\theta^{(0)}+\nabla'\theta^{(1)}\right)\right] + \nabla''\cdot\left(m^*\cdot\nabla'\theta^{(0)}\right)\\
O(\epsilon^2)Pe'\overline{\rho C_p}^* & \left(\frac{\partial\theta^{(0)}}{\partial t_d}+\frac{\partial\theta^{(1)}}{\partial t_v}\right) + Pe'\langle u\rangle^{(0)}\cdot\left(\nabla''\theta^{(1)}+\nabla'\theta^{(2)}\right)\\
& \qquad + Pe'\langle u\rangle^{(1)}\cdot\left(\nabla''\theta^{(0)}+\nabla'\theta^{(1)}\right) + Pe'\langle u\rangle^{(2)}\cdot\nabla'\theta^{(0)}\\
& \qquad = \nabla''\cdot\left[m^*\cdot\left(\nabla''\theta^{(0)}+\nabla'\theta^{(1)}\right)\right] + \nabla'\cdot\left[m^*\cdot\left(\nabla''\theta^{(1)}+\nabla'\theta^{(2)}\right)\right]
\end{aligned}
\qquad (3.3.1a-c)
$$

3.3.1 The Canonical Cell Problem for Heat Transport.

At $O(1)$, if we multiply (3.3.1a) by $\theta^{(0)}$ and integrate over Ω'-cell, it follows that

$$
\begin{aligned}
Pe'\int_{\Omega'}&\left[\nabla'\cdot\left(\langle u\rangle^{(0)}\frac{1}{2}\theta^{(0)^2}\right) - \frac{1}{2}\theta^{(0)^2}\nabla'\cdot\langle u\rangle^{(0)}\right]d\Omega'\\
&= \int_{\Omega'}\left[\nabla'\cdot\left(m^*\cdot\nabla'\theta^{(0)}\nabla'\theta^{(0)}\right) - m^*\cdot\nabla'\theta^{(0)}\nabla'\theta^{(0)}\right]d\Omega'
\end{aligned}
\qquad (3.3.2)
$$

The first terms in the integrands of both sides vanish due to Ω'-periodicity whereas the second term on the left-hand side is zero because of (3.2.3a) which is simply $\nabla'\cdot\langle u\rangle^{(0)} = 0$ upon use of (3.2.6). Therefore

$$
\int_{\Omega'} m^*\cdot\nabla'\theta^{(0)}\nabla'\theta^{(0)}d\Omega' = 0
$$

which shows that

$$\theta^{(0)} = \theta^{(0)}(x'', t_v, t_d) \tag{3.3.3}$$

since the thermal conductivity m^* is positive definite. The leading order temperature is independent of the mesoscale coordinate.

After using (3.3.3) at $O(\epsilon)$, (3.3.1b) becomes

$$Pe' \left[\overline{\rho C_p}^* \frac{\partial \theta^{(0)}}{\partial t_v} + \langle u \rangle^{(0)} \cdot \left(\nabla'' \theta^{(0)} + \nabla' \theta^{(1)} \right) \right] = \nabla' \cdot \left[m^* \cdot \left(\nabla'' \theta^{(0)} + \nabla' \theta^{(1)} \right) \right] \tag{3.3.4}$$

Integrating (3.3.4) over Ω'-cell and using the continuity equation (3.3.2a), Gauss theorem and Ω'-periodicity, we get

$$\langle \overline{\rho C_p}^* \rangle \frac{\partial \theta^{(0)}}{\partial t_v} + \langle \langle u \rangle^{(0)} \rangle \cdot \nabla'' \theta^{(0)} = 0 \tag{3.3.5}$$

where

$$\langle \overline{\rho C_p}^* \rangle = \frac{1}{\Omega'} \int_{\Omega'} \overline{\rho C_p}^* d\Omega' \tag{3.3.6}$$

The transport of heat over the time scale T_v is thus by convection only which is correct in view of the definition of T_v. In order to have diffusive effects on the transport of heat, we have to go to the next order. Subtracting (3.3.5) times $Pe' \overline{\rho C_p}^* / \langle \overline{\rho C_p}^* \rangle$ from (3.3.4), we obtain

$$Pe' \left(\widetilde{\langle u \rangle}^{(0)} \cdot \nabla'' \theta^{(0)} + \langle u \rangle^{(0)} \cdot \nabla' \theta^{(1)} \right) = \nabla' \cdot \left[m^* \cdot \left(\nabla'' \theta^{(0)} + \nabla' \theta^{(1)} \right) \right] \tag{3.3.7}$$

where

$$\widetilde{\langle u \rangle}^{(0)} = \langle u \rangle^{(0)} - \frac{\overline{\rho C_p}^*}{\langle \overline{\rho C_p}^* \rangle} \langle \langle u \rangle^{(0)} \rangle \tag{3.3.8}$$

Equation (3.3.7) is convection-diffusion equation for $\theta^{(1)}$ with distributed heat sources on the mesoscale. The source distribution in the Ω'-cell is two-fold. One is from the spatial variation of the seepage velocity $\widetilde{\langle u \rangle}^{(0)}$ which reflects the mesoscale variation of permeability (cf.(3.2.6)). The other is from the heterogeneity in thermal conductivity m^* on the mesoscale. Both effects are proportional to mesoscale-independent thermal gradient $\nabla'' \theta^{(0)}$. On the other hand, (3.3.7) implies nonlinearly coupling between $p^{(0)}$ and $\theta^{(0)}$ since the seepage velocity $\langle u \rangle^{(0)}$ depends on

$\theta^{(0)}$ through (3.2.6) and (3.2.7). Hence $\theta^{(1)}$ depends on $\theta^{(0)}$ nonlinearly. For the moment let us pretend that the seepage velocity is given and express $\theta^{(1)}$ in terms of the macroscale thermal gradient $\nabla''\theta^{(0)}$ which is yet to be determined. Under this assumption, (3.3.7) becomes linear in $\theta^{(1)}$ and $\nabla''\theta^{(0)}$ and we let

$$\theta^{(1)} = B' \cdot \nabla''\theta^{(0)} \tag{3.3.9}$$

and substitute into (3.3.7). This gives the mesoscale cell boundary value problem for the unknown vector $B'(x', x'', t_v, t_d)$ as

$$Pe' \left(\widetilde{\langle u \rangle}^{(0)} + \langle u \rangle^{(0)} \cdot \nabla' B' \right) = \nabla' \cdot [m^* \cdot (I + \nabla' B')] \tag{3.3.10a}$$

and the Ω'-periodicity of $\theta^{(1)}$ requires that

$$B' \quad \text{is } \Omega'\text{-periodic.} \tag{3.3.10b}$$

We also require for uniqueness

$$\langle B' \rangle_{\Omega'} = 0 \tag{3.3.10c}$$

Equation (3.3.10a) is the convection-diffusion equation in Ω'-cell with distributed sources due to the velocity fluctuation about the weighted mean(cf.(3.3.8)). Note that, if the medium is homogeneous on the ℓ' scale, then

$$S' = 0 \qquad \text{and} \qquad \overline{\rho C_p}^* = \langle \overline{\rho C_p}^* \rangle, \quad m^*_{il} = \text{const.} \tag{3.3.11}$$

(see (3.2.11) in Ch. II, Part A for S') so that $\widetilde{\langle u \rangle}^{(0)} = 0$. The homogeneous boundary value problem for B' (3.3.10a-c) has trivial solution i.e., $B' = 0$. The first order correction of temperature, $\theta^{(1)}$, therefore reflects the influence of mesoscale heterogeneity on the distribution of medium temperature. We emphasize that since $\widetilde{\langle u \rangle}^{(0)}$ and $\langle \langle u \rangle^{(0)} \rangle$ depend on $\theta^{(0)}$ which is still unknown, the forcing terms in the boundary value problem for B' (equations (3.3.10a-c)) is not known yet. It can only be solved iteratively together with the heat equation which is derived below.

3.3.2 The Macroscale Heat Transport.

At the next order of $O(\epsilon^2)$, (3.3.1c) may be written after using (3.3.3)

$$
\begin{aligned}
Pe'\overline{\rho C_p}^{*}\left(\frac{\partial\theta^{(0)}}{\partial t_d}+\frac{\partial\theta^{(1)}}{\partial t_v}\right)
&+Pe'\left[\nabla''\cdot\left(\langle u\rangle^{(0)}\theta^{(1)}\right)+\nabla'\cdot\left(\langle u\rangle^{(1)}\theta^{(1)}\right)+\langle u\rangle^{(1)}\cdot\nabla''\theta^{(0)}\right]\\
&+Pe'\left[\nabla'\cdot\left(\langle u\rangle^{(0)}\theta^{(2)}\right)-\theta^{(1)}\left(\nabla''\cdot\langle u\rangle^{(0)}+\nabla'\cdot\langle u\rangle^{(1)}\right)-\theta^{(2)}\nabla'\cdot\langle u\rangle^{(0)}\right]\\
&=\nabla''\cdot\left[m^{*}\cdot\left(\nabla''\theta^{(0)}+\nabla'\theta^{(1)}\right)\right]+\nabla'\cdot\left[m^{*}\cdot\left(\nabla''\theta^{(1)}+\nabla'\theta^{(2)}\right)\right]
\end{aligned}
\tag{3.3.12}
$$

Equations (3.2.3), (3.2.6) and (3.2.8) can be combined to give

$$
\begin{aligned}
\nabla'\cdot\langle u\rangle^{(0)}&=0\\
\nabla''\cdot\langle u\rangle^{(0)}+\nabla'\cdot\langle u\rangle^{(1)}&=0
\end{aligned}
\tag{3.3.13a,b}
$$

Integrating (3.3.12) over Ω'-cell and using (3.3.13a,b), Gauss theorem and Ω'-periodicity, we have

$$
\begin{aligned}
&Pe'\langle\overline{\rho C_p}^{*}\rangle\frac{\partial\theta^{(0)}}{\partial t_d}+Pe'\left\langle\overline{\rho C_p}^{*}\frac{\partial\theta^{(1)}}{\partial t_v}\right\rangle\\
&\quad+Pe'\left[\nabla''\cdot\langle\langle u\rangle^{(0)}\theta^{(1)}\rangle+\langle\langle u\rangle^{(1)}\rangle\cdot\nabla''\theta^{(0)}\right]=\nabla''\cdot\left\langle m^{*}\cdot\left(\nabla''\theta^{(0)}+\nabla'\theta^{(1)}\right)\right\rangle
\end{aligned}
\tag{3.3.14}
$$

The second term on the left-hand side becomes after using (3.3.9)

$$
\begin{aligned}
\left\langle\overline{\rho C_p}^{*}\frac{\partial\theta^{(1)}}{\partial t_v}\right\rangle&=\left\langle\overline{\rho C_p}^{*}B'\cdot\frac{\partial}{\partial t_v}\nabla''\theta^{(0)}\right\rangle\\
&=\left\langle\overline{\rho C_p}^{*}B'\cdot\nabla''\left(\frac{\partial\theta^{(0)}}{\partial t_v}\right)\right\rangle\\
&=\nabla''\cdot\left\langle\overline{\rho C_p}^{*}B'\frac{\partial\theta^{(0)}}{\partial t_v}\right\rangle-\frac{\partial\theta^{(0)}}{\partial t_v}\nabla''\cdot\left\langle\overline{\rho C_p}^{*}B'\right\rangle\\
&=-\nabla''\cdot\left[\frac{\left\langle\overline{\rho C_p}^{*}B'\right\rangle}{\left\langle\overline{\rho C_p}^{*}\right\rangle}\langle\langle u\rangle^{(0)}\rangle\cdot\nabla''\theta^{(0)}\right]+\left[\nabla''\cdot\left\langle\overline{\rho C_p}^{*}B'\right\rangle\right]\frac{\langle\langle u\rangle^{(0)}\rangle}{\left\langle\overline{\rho C_p}^{*}\right\rangle}\cdot\nabla''\theta^{(0)}
\end{aligned}
\tag{3.3.15}
$$

where (3.3.5) has been used for $\partial\theta^{(0)}/\partial t_v$. Substituting (3.3.9) and (3.3.15) into (3.3.14), we finally obtain

$$
Pe'\left(\langle\overline{\rho C_p}^{*}\rangle\frac{\partial\theta^{(0)}}{\partial t_d}+U\cdot\nabla''\theta^{(0)}\right)=\nabla''\cdot\left(D''\cdot\nabla''\theta^{(0)}\right)
\tag{3.3.16}
$$

where

$$U = \langle\langle u\rangle^{(1)}\rangle + \left[\nabla'' \cdot \left\langle \overline{\rho C_p}^{*} B' \right\rangle\right] \frac{\langle\langle u\rangle^{(0)}\rangle}{\left\langle \overline{\rho C_p}^{*} \right\rangle} \tag{3.3.17}$$

$$D'' = \langle m^{*} \cdot (I + \nabla' B')\rangle - Pe' \left\langle \langle\hat{u}\rangle^{(0)} B' \right\rangle + Pe' \frac{\left\langle \overline{\rho C_p}^{*} B' \right\rangle \langle\langle u\rangle^{(0)}\rangle}{\left\langle \overline{\rho C_p}^{*} \right\rangle} \tag{3.3.18}$$

are the velocity for heat convection and the thermal dispersion tensor respectively. In (3.3.18), use has been made of the following relation

$$\langle\langle u\rangle^{(0)} B'\rangle = \left\langle \left(\langle\hat{u}\rangle^{(0)} + \langle\langle u\rangle^{(0)}\rangle \right) B' \right\rangle = \left\langle \langle\hat{u}\rangle^{(0)} B' \right\rangle \tag{3.3.19}$$

in which (3.3.10c) has been used and

$$\langle\hat{u}\rangle^{(0)} = \langle u\rangle^{(0)} - \langle\langle u\rangle^{(0)}\rangle \tag{3.3.20}$$

is the seepage velocity fluctuation about its mean value.

Equation (3.3.16) states that heat is transported not only by convection and diffusion but also by dispersion. The enhancement of diffusion by the mesoscale convection which results in dispersion at the macroscale is obviously caused by the mesoscale heterogeneities of medium in permeability and thermal conductivity. The counterpart of dispersion in the two scale (ℓ, ℓ') medium was due to mixing in the pore fluid at the microsale level.

In addition to the effect of mesoscale fluctuations, the convection velocity U and the dispersion tensor D'' have coupled effects of heterogeneities at both mesoscale and macroscale. For instance, $\left\langle \overline{\rho C_p}^{*} B' \right\rangle$ is the combined effect of heterogeneities in the heat capacity and temperature anomaly at the mesoscale and thus the second term in U is due to the macroscale heterogeneity of $\left\langle \overline{\rho C_p}^{*} B' \right\rangle$. We point out that the term other than $\langle\langle u\rangle^{(1)}\rangle$ in U and the last term in D'' were not present in the two scale analysis (cf. (3.4.22) and (3.4.23) in Ch. I of the present Part). Contributions of the type of the new term in D'' have been obtained previously in stochastic analysis of the effects of porosity and the distribution coefficient K_d by treating

them as stochastic variables (Garabedian et al, 1988). The distribution coefficient is the ratio of the solute concentration in the solid phase to the concentration in the fluid and is analogous to the variable $\overline{\rho C_p}^*$ here. Specifically they allowed the spatial variations of the porosity and K_d to be composed of those correlated to the natural logarithm of permeability and those which are not correlated to permeability. The former gives a correction term in the macrodispersivity as compared to that for the tracer whereas the latter produces some additive effect in the macrodispersivity reflecting the uncorrelated variations of porosity and the distribution coefficient. In view of the fact that B' depends on $p^{(0)}$ and $\theta^{(0)}$, that the macroscale heterogeneity is implicitly reflected in U and D''. If Pe' becomes very small, B' degenerates to A' of (3.3.3) fo Ch. II, Part A and D'' reduces to the effective thermal conductivity of (3.3.6) there.

As a special case, if $\hat{Ra}'$ is small,e.g. $Ra' < O(1)$, the flow velocity becomes independent of $\theta^{(0)}$ due to negligible buoyancy. Equation (3.2.5) is first solve for $p^{(0)}$. Darcy's law (3.2.7) without buoyancy then gives the flow velocity $\langle u\rangle^{(0)}$. Equations (3.3.10a-c) is solved for given velocity filed. The convection-diffusion problem (3.3.10) needs to be solved only once for given flow field to determine the B'-field as a function of Pe'.

The second order tensor D'' of (3.3.18) is, in general, non-symmetric and further decomposition is made as follows.

$$D''_{ij} = m^s_{ij} + m^u_{ij} + D^s_{ij} + D^u_{ij} \tag{3.3.21}$$

where

$$\left\{ \begin{matrix} m^s_{ij} \\ m^u_{ij} \end{matrix} \right\} = \frac{1}{2}\left[\langle m^*\rangle_{ij} \pm \langle m^*\rangle_{ji}\right] \tag{3.3.22}$$

and

$$\begin{aligned} \left\{ \begin{matrix} D^s_{ij} \\ D^u_{ij} \end{matrix} \right\} = &- \frac{Pe'}{2}\left\langle \langle\hat{u}\rangle^{(0)}_i B'_j \pm \langle\hat{u}\rangle^{(0)}_j B'_i \right\rangle \\ &+ \frac{Pe'}{2}\frac{1}{\left\langle \overline{\rho C_p}^* \right\rangle}\left[\left\langle \overline{\rho C_p}^* B'_i \right\rangle \langle\langle u\rangle^{(0)}_j\rangle \pm \left\langle \overline{\rho C_p}^* B'_j \right\rangle \langle\langle u\rangle^{(0)}_i\rangle\right] \\ &+ \frac{1}{2}\left\langle m^*_{i\ell}\frac{\partial B'_j}{\partial x'_\ell} \pm m^*_{j\ell}\frac{\partial B'_i}{\partial x'_\ell}\right\rangle \end{aligned} \tag{3.3.23}$$

The coefficients m^s_{ij} and D^s_{ij} are symmetric and m^u_{ij} and D^u_{ij} are anti-symmetric with respect to the interchange of indices. The arithmetic mean of thermal conductivity is sorted out in m^s_{ij} and m^u_{ij} and its mesoscale variations affect D^s_{ij} and D^u_{ij}.

If we substitute (3.3.17) and (3.3.18) into (3.3.16) and recall that the product of symmetric and anti-symmetric tensors yields zero, (3.3.16) is written

$$Pe'\langle\overline{\rho C_p}^*\rangle\frac{\partial\theta^{(0)}}{\partial t_d}+[Pe'U-\nabla''\cdot(m^u+D^u)]\cdot\nabla''\theta^{(0)}=\nabla''\cdot\left[(m^s+D^s)\cdot\nabla''\theta^{(0)}\right] \tag{3.3.24}$$

in which the anti-symmetric part of heat dispersion modifies heat convection.

The mean heat transport equation which accounts for the leading component of convection and dispersion is now obtained by multiplying (3.3.24) by ϵ and adding it to (3.3.5) and also recalling the scale relation (3.1.2) as

$$\begin{aligned}Pe'\langle\overline{\rho C_p}^*\rangle\frac{\partial\theta^{(0)}}{\partial t^*}+\left[Pe'\langle\langle u\rangle^{(0)}\rangle+\epsilon(Pe'U-\nabla''\cdot(m^u+D^u))\right]\cdot\nabla''\theta^{(0)}\\ =\epsilon\nabla''\cdot\left[(m^s+D^s)\cdot\nabla''\theta^{(0)}\right]\end{aligned} \tag{3.3.25}$$

In summary, the equations (3.2.1), (3.2.5), (3.2.7), (3.3.10) and (3.3.25) are the macroscale governing equations for thermal dispersion in deformable porous media when the mesoscale Peclét number Pe' is finite. The unknowns are $\theta^{(0)}$, $\langle\sigma^{(0)}\rangle$, $v^{(0)}$, $p^{(0)}$, $\langle\langle u\rangle^{(0)}\rangle$ and B'. The flow equation (3.2.5) and the heat transport equation (3.3.25) are coupled via the buoyancy and should be solved together. The process must include the calculation of B' and therefore the convection velocity U and dispersion tensor D^s. Afterwards, the deformation of the medium can be found from the equilibrium equation (3.2.1). The deformation of the porous matrix however does not affect the flow and heat transport.

3.3.3 Alternate Form for the Dispersion Tensor D^s_{ij}

As in the two scale case, another form for D^s_{ij} in (3.3.23) is derived by making use of the mesoscale call problem (3.3.10).

Equation (3.3.10a) is written in indicial form as

$$Pe'\left(\widetilde{\langle u\rangle}_i^{(0)} + \langle u\rangle_\ell^{(0)}\frac{\partial B_i'}{\partial x_\ell'}\right) = \frac{\partial}{\partial x_k'}\left[m_{kn}^*\left(\delta_{ni} + \frac{\partial B_i'}{\partial x_n'}\right)\right] \tag{3.3.26}$$

Multiplying (3.3.26) by B_j' we have

$$\begin{aligned} &Pe'\left(\widetilde{\langle u\rangle}_i^{(0)} B_j' + \langle u\rangle_\ell^{(0)} B_j'\frac{\partial B_i'}{\partial x_\ell'}\right) \\ &\quad = \frac{\partial}{\partial x_k'}\left[B_j' m_{kn}^*\left(\delta_{ni} + \frac{\partial B_i'}{\partial x_n'}\right)\right] - m_{kn}^*\frac{\partial B_j'}{\partial x_k'}\left(\delta_{ni} + \frac{\partial B_i'}{\partial x_n'}\right) \end{aligned} \tag{3.3.27}$$

If indices i and j are exchanged in (3.3.27),

$$\begin{aligned} &Pe'\left(\widetilde{\langle u\rangle}_j^{(0)} B_i' + \langle u\rangle_\ell^{(0)} B_i'\frac{\partial B_j'}{\partial x_\ell'}\right) \\ &\quad = \frac{\partial}{\partial x_k'}\left[B_i' m_{kn}^*\left(\delta_{nj} + \frac{\partial B_j'}{\partial x_n'}\right)\right] - m_{kn}^*\frac{\partial B_i'}{\partial x_k'}\left(\delta_{nj} + \frac{\partial B_j'}{\partial x_n'}\right) \end{aligned} \tag{3.3.28}$$

Adding (3.3.27) and (3.3.28), integrating over Ω'-cell and using Gauss theorem and Ω'-periodicity, we obtain

$$\begin{aligned} Pe'\left\langle \widetilde{\langle u\rangle}_i^{(0)} B_j' + \widetilde{\langle u\rangle}_j^{(0)} B_i'\right\rangle = &-\left\langle m_{ki}^*\frac{\partial B_j'}{\partial x_k'} + m_{kj}^*\frac{\partial B_i'}{\partial x_k'}\right\rangle \\ &-\left\langle m_{kn}^*\left(\frac{\partial B_j'}{\partial x_k'}\frac{\partial B_i'}{\partial x_n'} + \frac{\partial B_i'}{\partial x_k'}\frac{\partial B_j'}{\partial x_n'}\right)\right\rangle \end{aligned} \tag{3.3.29}$$

From (3.3.8) and (3.3.20) we have

$$\begin{aligned} \widetilde{\langle u\rangle}^{(0)} &= \langle u\rangle^{(0)} - \frac{\overline{\rho C_p}^*}{\langle\overline{\rho C_p}^*\rangle}\langle\langle u\rangle^{(0)}\rangle = \langle u\rangle^{(0)} - \langle\langle u\rangle^{(0)}\rangle + \left(1 - \frac{\overline{\rho C_p}^*}{\langle\overline{\rho C_p}^*\rangle}\right)\langle\langle u\rangle^{(0)}\rangle \\ &= \langle\hat{u}\rangle^{(0)} + \left(1 - \frac{\overline{\rho C_p}^*}{\langle\overline{\rho C_p}^*\rangle}\right)\langle\langle u\rangle^{(0)}\rangle \end{aligned} \tag{3.3.30}$$

Substituting (3.3.30) into (3.3.29) and invoking $m_{ij}^* = m_{ji}^*$, we obtain

$$\begin{aligned} Pe'\left\langle \langle\hat{u}\rangle_i^{(0)} B_j' + \langle\hat{u}\rangle_j^{(0)} B_i'\right\rangle = &Pe'\frac{1}{\langle\overline{\rho C_p}^*\rangle}\left[\langle\langle u\rangle_i^{(0)}\rangle\langle\overline{\rho C_p}^* B_j'\rangle + \langle\langle u\rangle_j^{(0)}\rangle\langle\overline{\rho C_p}^* B_i'\rangle\right] \\ &-\left\langle m_{ik}^*\frac{\partial B_j'}{\partial x_k'} + m_{jk}^*\frac{\partial B_i'}{\partial x_k'}\right\rangle - 2\left\langle m_{kn}^*\frac{\partial B_i'}{\partial x_k'}\frac{\partial B_j'}{\partial x_n'}\right\rangle \end{aligned} \tag{3.3.31}$$

where (3.3.10c) has been used.

If (3.3.31) is used in (3.3.23), D^s_{ij} simply becomes

$$D^s_{ij} = \left\langle m^*_{kn} \frac{\partial B'_i}{\partial x'_k} \frac{\partial B'_j}{\partial x'_n} \right\rangle + \left\langle m^*_{ik} \frac{\partial B'_j}{\partial x'_k} + m^*_{jk} \frac{\partial B'_i}{\partial x'_k} \right\rangle \tag{3.3.32}$$

which is identical in its form to two-scale dispersion tensor.

On the other hand, the anti-symmetric dispersion tensor D^u_{ij} of (3.3.23) may be written as

$$D^u_{ij} = -\frac{Pe'}{2} \left(\left\langle \langle \breve{u} \rangle_i B'_j \right\rangle - \left\langle \langle \breve{u} \rangle_i B'_i \right\rangle \right) + \frac{1}{2} \left\langle m^*_{i\ell} \frac{\partial B'_j}{\partial x'_\ell} - m^*_{j\ell} \frac{\partial B'_i}{\partial x'_\ell} \right\rangle \tag{3.3.33}$$

where

$$\begin{aligned} \left\langle \langle \breve{u} \rangle_i B'_j \right\rangle &= \left\langle \left(\langle \hat{u} \rangle_i^{(0)} + \frac{\overline{\rho C_p}^*}{\left\langle \overline{\rho C_p}^* \right\rangle} \langle \langle u \rangle_i^{(0)} \rangle \right) B'_j \right\rangle \\ &= \left\langle \left(\langle u \rangle_i^{(0)} + \frac{\overline{\rho C_p}^*}{\left\langle \overline{\rho C_p}^* \right\rangle} \langle \langle u \rangle_i^{(0)} \rangle \right) B'_j \right\rangle \end{aligned}$$

and therefore

$$\langle \breve{u} \rangle_i = \langle u \rangle_i^{(0)} + \frac{\overline{\rho C_p}^*}{\left\langle \overline{\rho C_p}^* \right\rangle} \langle \langle u \rangle_i^{(0)} \rangle \tag{3.3.34}$$

In the above, the uniqueness requirement (3.3.10c) for B' has been used in replacing $\langle \hat{u} \rangle_i^{(0)}$ by $\langle u \rangle_i^{(0)}$. Comparing (3.3.34) and (3.3.8), we notice that $\langle \breve{u} \rangle_i$ is the flow velocity added to its mean value weighted by the heat capacity of the medium whereas $\widetilde{\langle u \rangle}^{(0)}$ is the fluctuation about the weighted mean.

3.4 First order seepage velocity $\langle \langle u \rangle^{(1)} \rangle$

The first order seepage velocity which contributes to the convection of heat over the diffusion time scale t_d(cf.(3.3.16)) is now obtained in terms of mesoscale independent quantities.

After using (3.2.4) and (3.3.9), the consolidation equation at $O(\epsilon^2)$ (3.2.3b) may be written in indicial form as

$$\nabla''_i \left\{ \left[k^*_{i\ell} \left(\delta_{\ell j} + \nabla'_\ell S'_j \right) \right] \left(\nabla''_j p^{(0)} - \frac{\hat{R}a'}{Pe'} \theta^{(0)} \delta_{jz} \right) \right\}$$
$$+ \nabla'_i \left\{ k^*_{i\ell} \nabla''_\ell \left[S'_j \left(\nabla''_j p^{(0)} - \frac{\hat{R}a'}{Pe'} \theta^{(0)} \delta_{jz} \right) \right] \right\} - \frac{\hat{R}a'}{Pe'} \nabla'_i \left[k^*_{ij} \left(B'_\ell \nabla''_\ell \theta^{(0)} \delta_{jz} \right) \right]$$
$$+ \nabla'_i \left(k^*_{ij} \nabla'_j p^{(2)} \right) = 0 \tag{3.4.1}$$

If the mesoscale-independent terms are factored out, the preceding equation further becomes

$$A_j \left(\nabla''_j p^{(0)} - \frac{\hat{R}a'}{Pe'} \theta^{(0)} \delta_{jz} \right) + B_{ij} \nabla''_i \nabla''_j p^{(0)}$$
$$- (B_{ij} + C_{ij}) \frac{\hat{R}a'}{Pe'} \nabla''_i \theta^{(0)} \delta_{jz} + \nabla'_m \left(k^*_{mn} \nabla'_n p^{(2)} \right) = 0 \tag{3.4.2}$$

where

$$A_j = \nabla''_i \left[k^*_{i\ell} \left(\delta_{\ell j} + \nabla'_\ell S'_j \right) \right] + \nabla'_i \left(k^*_{i\ell} \nabla''_\ell S'_j \right)$$
$$B_{ij} = k^*_{i\ell} \left(\delta_{\ell j} + \nabla'_\ell S'_j \right) + \nabla'_m \left(k^*_{mi} S'_j \right) \tag{3.4.3}$$
$$C_{ij} = \nabla'_m \left(k^*_{mj} B'_i \right)$$

The vector function S'_j has been treated earlier in Ch. II, Part A. We assume that its macroscale variation in (3.4.3) is known.

Equation (3.4.2) is a relationship between $p^{(2)}$ and the mesoscale independent terms, and suggests the following formal representation.

$$p^{(2)} = E'_j \left(\nabla''_j p^{(0)} - \frac{\hat{R}a'}{Pe'} \theta^{(0)} \delta_{jz} \right) + F'_{ij} \nabla''_i \nabla''_j p^{(0)} - G'_{ij} \frac{\hat{R}a'}{Pe'} \nabla''_i \theta^{(0)} \delta_{jz} \tag{3.4.4}$$

where E'_j is an unknown vector, while F'_{ij} and G'_{ij} are unknown tensors of the second rank. By substituting (3.4.4) into (3.4.2) and invoking the Ω'-periodicity we obtain the mesoscale cell boundary value problems for E'_j, F'_{ij}, and G'_{ij} as follows.

$$A_j + \nabla'_m (k^*_{mn} \nabla'_n E'_n) = 0 \quad \text{in} \quad \Omega' \tag{3.4.5}$$

$$B_{ij} + \nabla'_m \left(k^*_{mn} \nabla'_n F'_{ij} \right) = 0 \quad \text{in} \quad \Omega' \tag{3.4.6}$$

$$B_{ij} + C_{ij} + \nabla'_m \left(k^*_{mn} \nabla'_n G'_{ij} \right) = 0 \quad \text{in} \quad \Omega' \tag{3.4.7}$$

and

$$E'_j, \quad F'_{ij}, \quad \text{and} \quad G'_{ij} \quad \text{are} \quad \Omega' - \text{periodic.} \tag{3.4.8}$$

We also require for uniqueness

$$\langle E'_j \rangle = \langle F'_{ij} \rangle = \langle G'_{ij} \rangle = 0 \tag{3.4.9}$$

The governing equations (3.4.5) to (3.4.7) are simply the steady seepage flow equation in heterogeneous medium with distributed source in the mesoscale cell. These cell problems must be solved for a specific mesoscale structure.

The first order seepage velocity $\langle u \rangle^{(1)}$ then becomes

$$\begin{aligned}
\langle u \rangle_i^{(1)} &= -k^*_{ij} \left(\nabla''_j p^{(1)} + \nabla'_j p^{(2)} - \frac{\hat{R}a'}{Pe'} \theta^{(1)} \delta_{jz} \right) \\
&= - \left[k^*_{ij} \left(\nabla''_j S'_\ell + \nabla'_j E'_\ell \right) \right] \left(\nabla''_\ell p^{(0)} - \frac{\hat{R}a'}{Pe'} \theta^{(0)} \delta_{\ell z} \right) \\
&\quad - \left(k^*_{ij} S'_\ell + k^*_{im} \nabla'_m F'_{j\ell} \right) \nabla''_j \nabla''_\ell p^{(0)} \\
&\quad + \left(k^*_{ij} S'_\ell + k^*_{im} \nabla'_m G'_{j\ell} + k^*_{i\ell} B'_j \right) \frac{\hat{R}a'}{Pe'} \nabla''_j \theta^{(0)} \delta_{\ell z}
\end{aligned} \tag{3.4.10}$$

Finally by taking the Ω'-cell average of (3.4.10) we obtain

$$\langle \langle u \rangle_i^{(1)} \rangle = -E''_{i\ell} \left(\nabla''_\ell p^{(0)} - \frac{\hat{R}a'}{Pe'} \theta^{(0)} \delta_{\ell z} \right) - F''_{ij\ell} \nabla''_j \nabla''_\ell p^{(0)} + G''_{ij\ell} \frac{\hat{R}a'}{Pe'} \nabla''_j \theta^{(0)} \delta_{\ell z} \tag{3.4.11}$$

where

$$\begin{aligned}
E''_{i\ell} &= \langle k^*_{ij} \left(\nabla''_j S'_\ell + \nabla'_j E'_\ell \right) \rangle \\
F''_{ij\ell} &= \langle k^*_{ij} S'_\ell + k^*_{im} \nabla'_m F'_{j\ell} \rangle \\
G''_{ij\ell} &= \langle k^*_{ij} S'_\ell + k^*_{im} \nabla'_m G'_{j\ell} + k^*_{i\ell} B'_j \rangle
\end{aligned} \tag{3.4.12}$$

Equation (3.4.11) is the first term of the convection velocity of heat in (3.3.17) when the dispersive effects are important(cf.(3.3.16)). It should be noted that this first order effect, although small by $O(\epsilon)$ as compared to the leading order velocity $\langle \langle u \rangle^{(0)} \rangle$ of (3.3.25), can cause appreciable movement of thermal disturbance over the diffusion time scale.

We now consider a special mesoscale structure.

4. Periodically Stratified Porous Medium

The general theory developed in §3 is now applied to a special case of layered medium. The effective constitutive coefficients at the macroscale will be obtained explicitly by solving the mesoscale cell boundary value problems. The mesoscale coefficients are assumed to have been found for a given microcell geometry. Because of the layered structure, the cell problems are one-dimensional.

On the mesoscale ℓ' the medium is assumed to be stratified along x_3'-axis, while it is homogeneous in $x_1'x_2'$-plane,e.g. material coefficients are uniform in $x_1'x_2'$-plane. The medium is periodically stratified in x_3' direction so that after a period of ℓ' in the x_3'-axis the pattern of stratification is repeated (see Fig. 4.1). The lateral dimension is assumed to be infinite so that the mesoscale cell is an infinite stratum with thickness of ℓ' along x_3'-axis.

Since the elastic coefficients and permeability have been treated in Ch. II of Part A, only the dispersion tensor and heat convection velocity are discussed. The cell boundary value problems defined on the scale ℓ' will be solved analytically for a medium with periodically but otherwise arbitrarily stratified structure in the vertical direction as shown in Fig. 4.1 and then the macroscale coefficients are determined. In a later section, the periodic stratum will be further specialized so that in each layer there are two layers with different material coefficients. Explicit forms of the macroscale dispersion tensor and heat convection velocity are presented. They are expressed only in terms of the mesoscale coefficients and the thickness fraction of layers.

4.1 Thermal Dispersion Tensor D^*_{ij}.

In order to derive thermal dispersion tensor D^*_{ij} for given seepage velocity on the mesoscale, the boundary value problem (4.a-c) must be solved for B'_x, B'_y and

B'_x. For vertically stratified medium of Fig. 4.1, (3.3.10) becomes one-dimensional.

$$Pe'\left(\widetilde{\langle u\rangle}_i + \langle u\rangle_x \frac{\partial B'_i}{\partial z'}\right) = \frac{\partial}{\partial z'}\left(m'_{zj}\delta_{ji} + m'_{zz}\frac{\partial B'_i}{\partial z'}\right) \qquad \text{in } \Omega'.$$

$$B'_i \quad \text{is } \Omega'\text{-periodic} \qquad (4.1.1a-c)$$

$$\langle B'_i\rangle = 0$$

We assume that the thermal conductivity m'_{ij} is isotropic on the scale ℓ', as in the case for the Wigner-Seitz cell (cf. §5 of Ch. I, Part A). Pretending that $\widetilde{\langle u\rangle}_i$ and $\langle u\rangle_x$ are known, equation (4.1.1a) is solved for B'_i subject to the conditions (4.1.1b and c). After using (3.2.4), the seepage velocity $\langle u\rangle_i$ on the mesoscale ℓ' is given by (3.2.6),

$$\langle u\rangle = -\left[k'\cdot(I+\nabla' S')\right]\cdot\left(\nabla'' p^{(0)} - \frac{\hat{R}a'}{Pe'}\theta^{(0)}\mathbf{e}_z\right) \qquad (4.1.2a)$$

in which the vector function S' has been studied in §5 of Ch. II, Part A. It is given by

$$S'_z(z') = k''_{zz}\int_0^{z'}\frac{dz'}{k'} + k''_{zz}\left\langle\frac{z'}{k'(z')}\right\rangle - z' - \frac{\ell'}{2} \quad ; \quad \frac{\partial S'_z}{\partial z'} = \frac{\ell'}{k'\int_0^{\ell'}\frac{dz'}{k'}} - 1 \qquad (4.1.2b)$$

where

$$k''_{zz} = 1\Big/\left\langle\frac{1}{k'}\right\rangle = \left(\frac{1}{\ell'}\int_0^{\ell'}\frac{dz'}{k'(z')}\right)^{-1} \qquad (4.1.2c)$$

If we use (4.1.2b) in (4.1.2a), the seepage velocity becomes

$$\langle u\rangle_x = -k'\frac{\partial p^{(0)}}{\partial x''}, \quad \langle u\rangle_y = -k'\frac{\partial p^{(0)}}{\partial y''}$$

$$\langle u\rangle_z = -\left(k' + k'\frac{\partial S'_z}{\partial z'}\right)\left(\frac{\partial p^{(0)}}{\partial z''} - \frac{\hat{R}a'}{Pe'}\theta^{(0)}\right) = -k''_{zz}\left(\frac{\partial p^{(0)}}{\partial z''} - \frac{\hat{R}a'}{Pe'}\theta^{(0)}\right) = \langle\langle u\rangle_z\rangle \qquad (4.1.3)$$

The velocity in z'-direction (normal to stratifications) is thus constant in the Ω'-cell which must be true by mass conservation. The horizontal components $\langle u\rangle_x$ and $\langle u\rangle_y$ vary with z'.

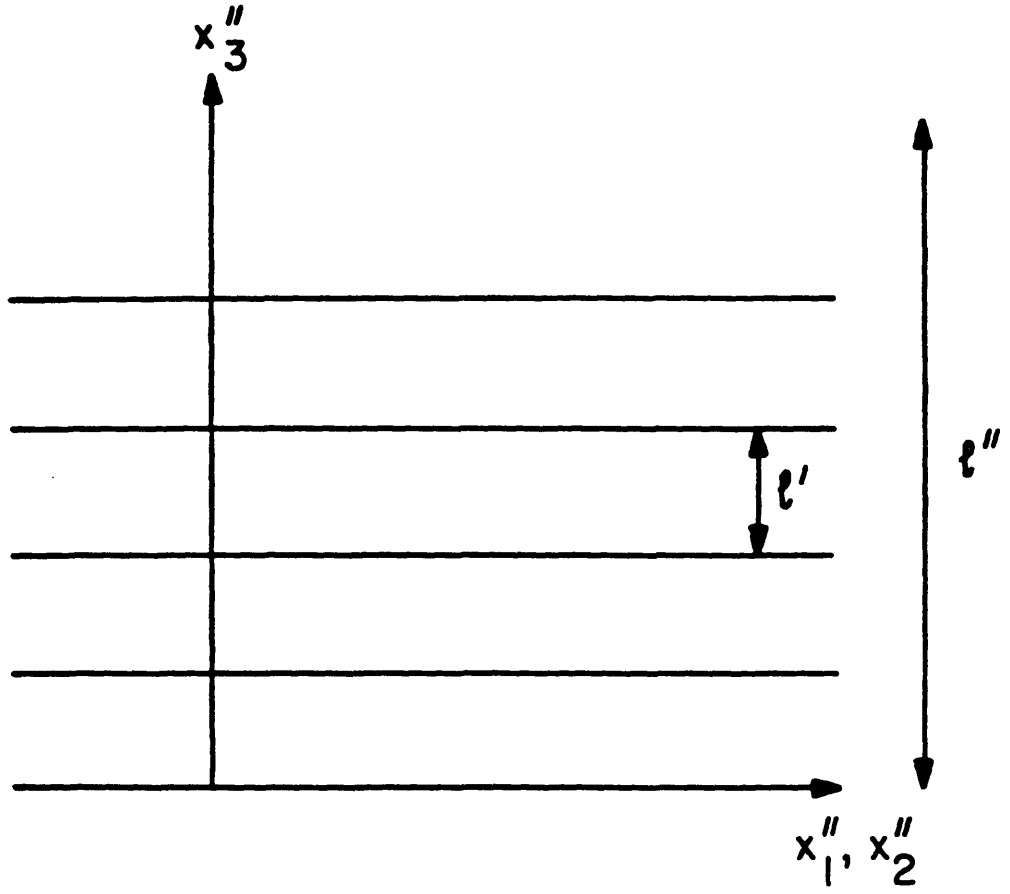

Fig. 4.1 A periodically stratified layers on the mesoscale. The periodic length is ℓ' in x_3'-direction.

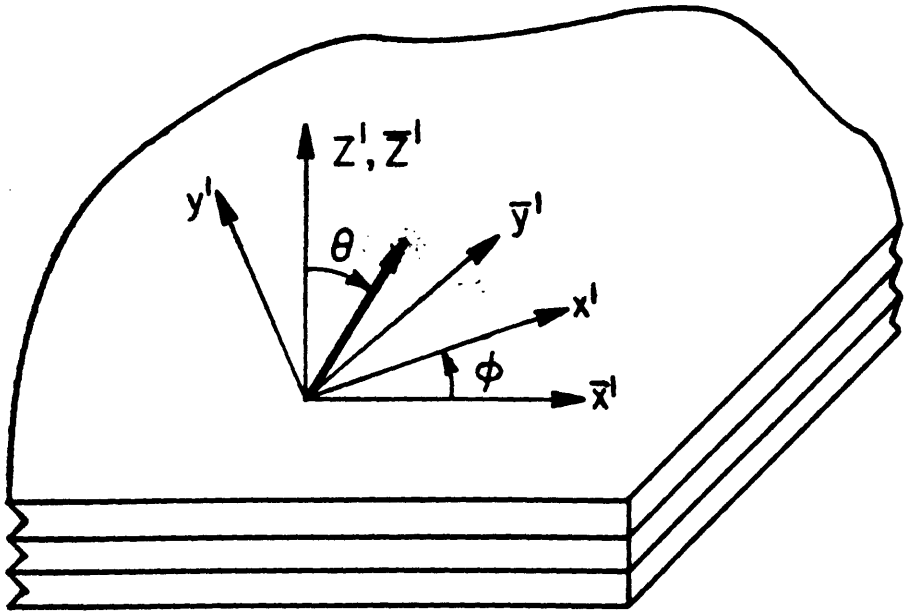

(a)

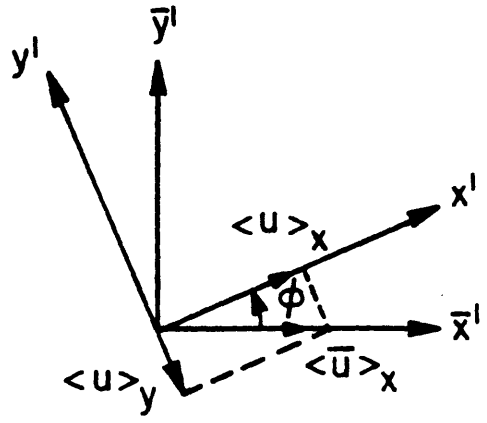

(b)

Fig. 4.2 (a) Two coordinate systems $\bar{x}'\bar{y}'\bar{z}'$ and $x'y'z'$. The system $x'y'z'$ is the one rotated by ϕ counterclockwise from $\bar{x}'\bar{y}'\bar{z}'$ about z' axis. The mean flow is in $x'z'$ plane. (b) The horizontal components of flow in $\bar{x}'\bar{y}'$ plane and $x'y'$ plane.

In terms of the solutions B'_x, B'_y and B'_z which depend on z' only for vertically stratified periodic porous medium, the dispersion tensor D^*_{ij} of (3.3.32) becomes as

$$
\begin{aligned}
D^*_{xx} &= \left\langle m' \frac{\partial B'_x}{\partial z'} \frac{\partial B'_x}{\partial z'} \right\rangle \\
D^*_{xy} = D^*_{yx} &= \left\langle m' \frac{\partial B'_x}{\partial z'} \frac{\partial B'_y}{\partial z'} \right\rangle \\
D^*_{xz} = D^*_{zx} &= \left\langle m' \frac{\partial B'_x}{\partial z'} \frac{\partial B'_z}{\partial z'} \right\rangle + \left\langle m' \frac{\partial B'_x}{\partial z'} \right\rangle \\
D^*_{yy} &= \left\langle m' \frac{\partial B'_y}{\partial z'} \frac{\partial B'_y}{\partial z'} \right\rangle \\
D^*_{yz} = D^*_{zy} &= \left\langle m' \frac{\partial B'_y}{\partial z'} \frac{\partial B'_z}{\partial z'} \right\rangle + \left\langle m' \frac{\partial B'_y}{\partial z'} \right\rangle \\
D^*_{zz} &= \left\langle m' \frac{\partial B'_z}{\partial z'} \frac{\partial B'_z}{\partial z'} \right\rangle + 2 \left\langle m' \frac{\partial B'_z}{\partial z'} \right\rangle
\end{aligned}
\tag{4.1.4}
$$

So far the macroscale pressure gradient $\nabla'' p^{(0)}$ and seepage velocity $\langle \langle u \rangle^{(0)} \rangle$ can be in any direction. It will be shown presently that the dispersion tensor for a mean flow in any direction can be obtained from the dispersion tensor for a mean flow in the $x'z'$-plane. The Ω'-cell problems for the latter is much simpler (see Fig. 4.2).

4.1.1 The Tensor Transformation Property of D^*_{ij} in the $x'y'$-plane

Suppose that the mean flow direction is inclined from the vertical axis z' by an angle θ,e.g. the meridianal angle is θ $(0 < \theta < \pi)$ and is assumed to be constant. Consider two coordinate systems $\bar{x}'\bar{y}'\bar{z}'$ and $x'y'z'$ shown in Fig. 4.2. The seepage flow velocity is denoted by $\overline{\langle u \rangle}_i$ and $\langle u \rangle_i$ respectively in $\bar{x}'\bar{y}'\bar{z}'$ and $x'y'z'$ coordinates. The macroscale coordinates $\bar{x}''\bar{y}''\bar{z}''$ and $x''y''z''$ are parallel to $\bar{x}'\bar{y}'\bar{z}'$ and $x'y'z'$. The coordinate system $\bar{x}'\bar{y}'\bar{z}'$ is oriented in such a way that the mean flow velocity is in $\bar{x}'\bar{z}'$ plane so that $\langle \overline{\langle u \rangle}_y \rangle$=0. The y''-component of Darcy's law (3.2.7) shows that $p^{(0)}$ is independent of y''. It then follows from (4.1.3) that $\overline{\langle u \rangle}_y = 0$. The second coordinate system $x'y'z'$ is the one which is obtained by rotating $\bar{x}'\bar{y}'\bar{z}'$-frame by an azimuthal angle ϕ about $\bar{z}'$-axis in counterclockwise manner. We shall show that

the dispersion tensor in $x'y'z'$-frame is equal to the tensor transformation of $\bar{D}^*_{ij}$ in $\bar{x}'\bar{y}'\bar{z}'$-frame in the horizontal plane.

Let us first write the governing equations for $i = x, y, z$ from (4.1.1a) and (3.3.8) as

$$\frac{d}{dz'}\left(m'\frac{dB'_x}{dz'} - Pe'\langle u\rangle_z B'_x\right) = Pe'\widetilde{\langle u\rangle}_x = Pe'\left(\langle u\rangle_x - \frac{\overline{\rho C_p}^*}{\langle\overline{\rho C_p}^*\rangle}\langle\langle u\rangle_x\rangle\right)$$

$$\frac{d}{dz'}\left(m'\frac{dB'_y}{dz'} - Pe'\langle u\rangle_z B'_y\right) = Pe'\widetilde{\langle u\rangle}_y = Pe'\left(\langle u\rangle_y - \frac{\overline{\rho C_p}^*}{\langle\overline{\rho C_p}^*\rangle}\langle\langle u\rangle_y\rangle\right)$$

$$\frac{d}{dz'}\left[m'\left(1+\frac{dB'_z}{dz'}\right) - Pe'\langle u\rangle_z B'_z\right] = Pe'\widetilde{\langle u\rangle}_z = Pe'\left(1 - \frac{\overline{\rho C_p}^*}{\langle\overline{\rho C_p}^*\rangle}\right)\langle u\rangle_z \qquad (4.1.5a-c)$$

The seepage velocity on the mesoscale in $\bar{x}'\bar{y}'\bar{z}'$-frame is

$$\overline{\langle u\rangle}_x = -k'\frac{\partial p^{(0)}}{\partial \bar{x}''}, \quad \overline{\langle u\rangle}_y = 0, \quad \overline{\langle u\rangle}_z = -k'\left(\frac{\partial p^{(0)}}{\partial \bar{z}''} - \frac{\hat{R}a'}{Pe'}\theta^{(0)}\right) \qquad (4.1.6)$$

Note that the forcing term for B'_y vanishes,e.g. $\widetilde{\langle u\rangle}_y = 0$. Then those in $x'y'z'$-frame will be

$$\langle u\rangle_x = \overline{\langle u\rangle}_x \cos\phi, \quad \langle u\rangle_y = -\overline{\langle u\rangle}_x \sin\phi, \quad \langle u\rangle_z = \overline{\langle u\rangle}_z \qquad (4.1.7)$$

The same holds true for the forcing terms in (4.1.5) so that

$$\widetilde{\langle u\rangle}_x = \widetilde{\overline{\langle u\rangle}}_x \cos\phi, \quad \widetilde{\langle u\rangle}_y = -\widetilde{\overline{\langle u\rangle}}_x \sin\phi, \quad \widetilde{\langle u\rangle}_z = \widetilde{\overline{\langle u\rangle}}_z \qquad (4.1.8)$$

For the flow field (4.1.6) with $\widetilde{\overline{\langle u\rangle}}_y = 0$, it follows from (4.1.5b) with (4.1.1b and c) that $B'_y = 0$. Consequently we have from (4.1.4) in the $\bar{x}'\bar{y}'\bar{z}'$-frame

$$\bar{D}^*_{ij} = \begin{bmatrix} \bar{D}^*_{xx} & 0 & \bar{D}^*_{xz} \\ 0 & 0 & 0 \\ \bar{D}^*_{xz} & 0 & \bar{D}^*_{zz} \end{bmatrix} \qquad (4.1.9)$$

On the other hand, in view of the linear dependence of B'_i on $\widetilde{\langle u\rangle}_i$ in (4.1.5) and the fact that $\langle u\rangle_z = \overline{\langle u\rangle}_z$ is constant, (4.1.8) implies that

$$B'_x = \bar{B}'_x \cos\phi, \quad B'_y = -\bar{B}'_x \sin\phi, \quad B'_z = \bar{B}'_z \qquad (4.1.10)$$

in which the direct proportionality of B'_y to $\bar{B}'_z$ results from the fact that the governing equation for B'_y (4.1.5b) differs from that for B'_x (4.1.5a) by the forcing term only (cf.(4.1.5)). It readily follows from (4.1.4) that

$$\begin{aligned} &D^e_{xx} = \bar{D}^e_{xx}\cos^2\phi, \quad D^e_{xy} = -\bar{D}^e_{xy}\cos\phi\sin\phi, \quad D^e_{xz} = \bar{D}^e_{xz}\cos\phi, \\ &D^e_{yy} = \bar{D}^e_{yy}\sin^2\phi, \quad D^e_{yz} = -\bar{D}^e_{yz}\cos\phi, \quad D^e_{zz} = \bar{D}^e_{zz} \end{aligned} \tag{4.1.11}$$

This relation is simply the transformation rule of tensor $\bar{D}^e_{ij}$ via the transformation matrix A_{ij}

$$D^e_{ij} = A_{ip}A_{jq}\bar{D}^e_{pq} \tag{4.1.12}$$

where

$$A_{ij} = \mathbf{e}_i \cdot \bar{\mathbf{e}}_j = \begin{bmatrix} \cos\phi & \sin\phi & 0 \\ -\sin\phi & \cos\phi & 0 \\ 0 & 0 & 1 \end{bmatrix} \tag{4.1.13}$$

Equation (4.1.12) shows that the dispersion tensor for the mean flow with its horizontal component oriented arbitrarily in the $x'y'$-plane can be obtained by applying the tensor transformation to the mean flow in $\bar{x}'\bar{y}'$-plane for which the dispersion tensor is given by (4.1.9). Therefore it suffices to consider three coefficients $\bar{D}^e_{xx}$, $\bar{D}^e_{xz}$ and $\bar{D}^e_{zz}$ only. For this purpose, (4.1.5) is now solved for B'_x and B'_z in the next section.

4.1.2 The functions B'_x and B'_z.

By taking $i = x$ in (4.1.1) we have, since $\langle u\rangle_z$ is constant,

$$\begin{aligned} \frac{d}{dz'}\left(m'\frac{dB'_x}{dz'} - Pe'\langle u\rangle_z B'_x\right) &= Pe'\widetilde{\langle u\rangle_z} \qquad 0 < z' < \ell' \\ B'_x(z'=0) &= B'_x(z'=\ell') \\ \frac{dB'_x}{dz'}(z'=0) &= \frac{dB'_x}{dz'}(z'=\ell') \\ \langle B'_x\rangle &= 0 \end{aligned} \tag{4.1.14a-d}$$

Note that the expression in parentheses on the left-hand side of (4.51a) is the negative of heat flux due to conduction and convection. If there exists an interface at which two layers are in contact, the temperature is continuous, but the thermal gradient $\partial B'_x/\partial z'$ is discontinuous because of a jump in m' when crossing the interface.

The solution B'_x will be expressed in terms of the Green's function $G(z',\xi)$ as (Appendix A)

$$B'_x(z') = \int_o^{\ell'} G(z',\xi) r(\xi) d\xi \tag{4.1.15}$$

where

$$r(\xi) = Pe' \widetilde{\langle u \rangle_x} = Pe' \left(\langle u \rangle_x - \frac{\overline{\rho C_p}^*}{\langle \overline{\rho C_p}^* \rangle} \langle \langle u \rangle_x \rangle \right) \tag{4.1.16}$$

is the heat source whose strength varies along z' and serves as the forcing term in (4.1.14a). If $r(\xi) = 0$,e.g. the medium is unifrom on the ℓ' scale, (4.1.14) gives the trivial solution $B'_x = 0$. Hence nonvanishing solution B'_x is due directly to the seepage velocity variation in the Ω'-cell. At an interface, the Green's function $G(z',\xi)$ is continuous but its derivative $\partial G/\partial z'$ is discontinuous. We note that the forcing term $r(\xi)$ satisfies the following relation

$$\int_o^{\ell'} r(\xi) d\xi = Pe' \int_o^{\ell'} \widetilde{\langle u \rangle_x} d\xi = Pe' \ell' \left[\langle \langle u \rangle_x \rangle - \frac{\langle \overline{\rho C_p}^* \rangle}{\langle \overline{\rho C_p}^* \rangle} \langle \langle u \rangle_x \rangle \right] = 0 \tag{4.1.17}$$

It can be shown that(Appendix A) the Green's function is given by

$$G(z',\xi) = \left\{ \begin{array}{ll} -\frac{1}{a\ell'} \left[\xi + p(\xi) \int_\xi^{\ell'} \frac{dt}{p(t)} \right] - \frac{1}{a} \left[\langle p^{-1} \rangle - p^{-1}(z') \right] \frac{p(\xi)}{p(\ell')-1} & (z' \le \xi) \\ G(z' \le \xi, \xi) - \frac{1}{a} \left[1 - \frac{p(\xi)}{p(z')} \right] & (z' \ge \xi) \end{array} \right\} \tag{4.1.18}$$

where

$$p(z') = \exp \left[\int_o^{z'} -\frac{a}{m'(z')} dz' \right] \tag{4.1.19}$$

and

$$a = Pe' \langle u \rangle_x \tag{4.1.20}$$

The integrating factor $p(z')$ satisfies the following relation

$$\frac{p(z')}{m'(z')} = -\frac{1}{a} \frac{dp(z')}{dz'} \tag{4.1.21}$$

For reference we also list B'_y. If we choose $j = y$ in (4.1.1), it becomes

$$\begin{aligned} \frac{d}{dz'}\left(m'\frac{dB'_y}{dz'} - Pe'\langle u\rangle_z B'_y\right) &= Pe'\widetilde{\langle u\rangle}_y \qquad 0 < z' < \ell' \\ B'_y(z'=0) &= B'_y(z'=\ell') \\ \frac{dB'_y}{dz'}(z'=0) &= \frac{dB'_y}{dz'}(z'=\ell') \\ \langle B'_y\rangle &= 0 \end{aligned} \tag{4.1.22a-d}$$

Since (4.1.22a) differs from (4.1.14a) by the forcing $\widetilde{\langle u\rangle}_y$, the Green's function must be identical to that for B'_x. Thus

$$B'_y(z') = \int_o^{\ell'} G(z',\xi)s(\xi)d\xi \tag{4.1.23}$$

where

$$s(\xi) = Pe'\widetilde{\langle u\rangle}_y = Pe'\left(\langle u\rangle_y - \frac{\overline{\rho C_p}^*}{\langle\overline{\rho C_p}^*\rangle}\langle\langle u\rangle_y\rangle\right) \tag{4.1.24}$$

4.1.3 The function B'_z.

The function B'_z is also determined by means of the Green's function $G(z',\xi)$. If we take $i = z'$ in (4.1.1), it becomes

$$\begin{aligned} \frac{d}{dz'}\left[m'\left(1+\frac{dB'_z}{dz'}\right) - Pe'\langle u\rangle_z B'_z\right] &= Pe'\widetilde{\langle u\rangle}_z \qquad 0 < z' < \ell' \\ B'_z(z'=0) &= B'_z(z'=\ell') \\ \frac{dB'_z}{dz'}(z'=0) &= \frac{dB'_z}{dz'}(z'=\ell') \\ \langle B'_z\rangle &= 0 \end{aligned} \tag{4.1.25a-d}$$

in which $\widetilde{\langle u\rangle}_z$ is given by

$$\widetilde{\langle u\rangle}_z = \left(1 - \frac{\overline{\rho C_p}^*}{\langle\overline{\rho C_p}^*\rangle}\right)\langle u\rangle_z \tag{4.1.26}$$

because $\langle u\rangle_z = \langle\langle u\rangle_z\rangle$(cf.(4.1.3)) is constant in the Ω'-cell. The forcing is thus due to heterogeneities in the heat capacity and thermal conductivity of the medium on the mesoscale ℓ' and is not caused by nonuniformity of the seepage flow.

We first let

$$B'_x(z') = A'_x(z') + C_x(z') \tag{4.1.27}$$

in which $A'_x(z')$ is the solution of a pure conduction problem treated in (5.3.2) of Ch. 2, Part A and is given by

$$A'_x(z') = m''_{xx}\int_0^{z'} \frac{dz'}{m'(z')} + m''_{xx}\left\langle \frac{z'}{m'(z')}\right\rangle - z' - \frac{\ell'}{2} \quad ; \quad \frac{\partial A'_x}{\partial z'} = \frac{\ell'}{m'\int_0^{\ell'}\frac{dz'}{m'}} - 1 \tag{4.1.28}$$

The thermal conductivity m''_{xx} has been given in (5.3.5) of Ch. 2, Part A as

$$m''_{xx} = \left\langle m'\left(\frac{\partial A'_x}{\partial z'} + 1\right)\right\rangle = 1\Big/\left\langle \frac{1}{m'}\right\rangle \tag{4.1.29}$$

Substituting (4.1.27) into (4.1.26) we obtain the boundary value problem for $C_x(z')$ as

$$\begin{gathered} \frac{d}{dz'}\left(m'\frac{dC_x}{dz'} - Pe'\langle u\rangle_x C_x\right) = t(z') \qquad 0 < z' < \ell' \\ C_x(z'=0) = C_x(z'=\ell') \\ \frac{dC_x}{dz'}(z'=0) = \frac{dC_x}{dz'}(z'=\ell') \\ \langle C_x\rangle = 0 \end{gathered} \tag{4.1.30a-d}$$

where

$$t(z') = -Pe'\langle u\rangle_x\left(\frac{\overline{\rho C_p}^*}{\langle\overline{\rho C_p}^*\rangle} - \frac{m''_{xx}}{m'}\right) \tag{4.1.31}$$

The solution C_x of (4.1.30) is expressed in terms of the Green's function $G(z',\xi)$ as

$$C_x(z') = \int_o^{\ell'} G(z',\xi)t(\xi)d\xi \tag{4.1.32}$$

Combining (4.1.27) and (4.1.31) we get

$$B'_x(z') = A'_x(z') + \int_o^{\ell'} G(z',\xi)t(\xi)d\xi \tag{4.1.33}$$

The solutions B'_x, B'_y and B'_z of the convection-diffusion problem (4.1.1) have been found in terms of the Green's functions. The dispersion tensor in (3.3.32) may now be readily calculated in terms of the functions B'_i above as a matter of quadrature.

4.1.4 Thermal Dispersion Tensor D^s_{ij}.

By using the Green's function representation for B'_x, B'_y, and B'_z of §4.1.2 and §4.1.3, the dispersion tensors are now derived in integral form. They are further reduced to integrals which involve the integrating factor $p(z')$ of (4.1.19) and the forcing terms $r(\xi)$, $s(\xi)$ and $t(\xi)$. Choosing our coordinate system to be $\bar{x}'\bar{y}'\bar{z}'$ mentioned in §4.1.4, only D^s_{xx}, D^s_{zz} and D^s_{zx} need to be considered. For simplicity the overhead symbol is dropped. Recall that thermal conductivity m'_{ij} is isotropic on the mesoscale level but it varies along z'-direction.

We shall consider the effective dispersion coefficients $\langle m'\rangle_{ij} + D^s_{ij}$ (cf. (3.3.25)). Let us consider $\langle m'\rangle_{xx} + D^s_{xx}$ first. Integrating (4.1.4) by parts and using (4.1.14a), D^s_{xx} becomes

$$
\begin{aligned}
&\langle m'\rangle_{xx} + D^s_{xx} \\
&= m''_{xx} + \frac{1}{\ell'}\int_o^{\ell'} m' \frac{dB'_x}{dz'}\frac{dB'_x}{dz'}dz' \\
&= m''_{xx} + \frac{1}{\ell'}\left[B'_x m' \frac{dB'_x}{dz'}\right]_o^{\ell'} - \frac{1}{\ell'}\int_o^{\ell'} B'_x \frac{d}{dz'}\left(m'\frac{dB'_x}{dz'}\right)dz' \\
&= m''_{xx} + \frac{1}{\ell'}\left[B'_x m' \frac{dB'_x}{dz'}\right]_o^{\ell'} - \frac{1}{\ell'}\int_o^{\ell'} B'_x \left[\frac{d}{dz'}(Pe'\langle u\rangle_z B'_x) + Pe'\widetilde{\langle u\rangle}_x\right]dz' \qquad (4.1.34) \\
&= m''_{xx} + \frac{1}{\ell'}\left[B'_x m' \frac{dB'_x}{dz'}\right]_o^{\ell'} - \frac{1}{\ell'}Pe'\langle u\rangle_z\left[\frac{B'^2_x}{2}\right]_o^{\ell'} - \frac{1}{\ell'}Pe'\int_o^{\ell'}\widetilde{\langle u\rangle}_x B'_x dz' \\
&= m''_{xx} - \frac{1}{\ell'}\int_o^{\ell'}\int_o^{\ell'} r(z')G(z',\xi)r(\xi)d\xi dz'
\end{aligned}
$$

where (4.1.14b and c) and (4.1.15) have been used and m''_{xx} is given by (cf. (5.3.1) in Ch. 2, Part A)

$$
m''_{xx} = \frac{1}{\ell'}\int_0^{\ell'} m'(z')dz' \qquad (4.1.35)
$$

By making use of $G(z',\xi)$ in (4.1.18), $\langle m\rangle_{xx} + D^s_{xx}$ can be further reduced to (Appendix B)

$$
\begin{aligned}
&\langle m'\rangle_{xx} + D^s_{xx} = m''_{xx} \\
&-\frac{1}{a\ell'}\left[\frac{1}{p(\ell')-1}\int_o^{\ell'}\frac{r(z')}{p(z')}dz'\int_o^{\ell'} p(\xi)r(\xi)d\xi + \int_o^{\ell'} dz'\frac{r(z')}{p(z')}\int_o^{z'} p(\xi)r(\xi)d\xi\right]
\end{aligned}
\qquad (4.1.36)
$$

It contains the integrating factor $p(\xi)$ and forcing $r(\xi)$ only.

Following the similar procedure(Appendix B), it can be shown that $\langle m' \rangle_{zz} + D^e_{zz}$ becomes as

$$\langle m' \rangle_{zz} + D^e_{zz} = m''_{zz} - \frac{1}{a\ell'} \left[\frac{1}{p(\ell') - 1} \int_o^{\ell'} \frac{t(z')}{p(t')} dz' \int_o^{\ell'} p(\xi) t(\xi) d\xi + \int_o^{\ell'} dz' \frac{t(z')}{p(z')} \int_o^{z'} p(\xi) t(\xi) d\xi \right] \tag{4.1.37}$$

where m''_{zz} and $t(\xi)$ have been given in (4.1.29) and (4.1.31).

The derivation of the off-diagonal entry D^e_{zz} in (4.1.4) is similar (Appendix B). The result is

$$\begin{aligned} 2D^e_{zz} = & - \frac{1}{a\ell'} \left[\frac{1}{p(\ell') - 1} \int_o^{\ell'} \frac{t(z')}{p(z')} dz' \int_o^{\ell'} p(\xi) r(\xi) d\xi + \int_o^{\ell'} dz' \frac{t(z')}{p(z')} \int_o^{z'} p(\xi) r(\xi) d\xi \right] \\ & - \frac{1}{a\ell'} \left[\frac{1}{p(\ell') - 1} \int_o^{\ell'} \frac{r(z')}{p(z')} dz' \int_o^{\ell'} p(\xi) t(\xi) d\xi + \int_o^{\ell'} dz' \frac{r(z')}{p(z')} \int_o^{z'} p(\xi) t(\xi) d\xi \right] \end{aligned} \tag{4.1.38}$$

The symmetric dispersion tensors have been expressed in terms of the source distributions $r(\xi)$, $s(\xi)$ and $t(\xi)$ for the boundary value problems for B'_x, B'_y and B'_z.

In addition to the intrinsic heterogeneities of the medium such as permeability, heat capacity and thermal conductivity, the dispersion tensors are strongly affected by the Peclét number. The larger the Peclét number, the larger the dispersion coefficients as easily seen in the boundary value problems for B'_x, B'_y and B'_z,e.g. In particular, the uneven distribution of heat source in the mesoscale medium is directly amplified by the Peclét number(cf.(4.1.5)). The dependence of D^e_{ij} on Pe' will be discussed quantitatively later for a medium with two alternating layers on the mesoscale.

As a check, we now show that all the dispersion tensor coefficients D^s_{ij} vanish when the medium is homogeneous on the mesoscale. For such a medium, k' and m' are constant, hence we have

$$\begin{aligned} k''_{xx} = k''_{yy} = \langle k' \rangle = k' \quad ; \quad k''_{zz} = k' \\ m''_{xx} = m''_{yy} = \langle m' \rangle = m' \quad ; \quad m''_{zz} = m' \end{aligned} \tag{4.1.39}$$

The heat capacity $\overline{\rho C_p}^*(z')$ is also uniform on the mesoscale. It then follows from (4.1.16), (4.1.24) and (4.1.31) that

$$r(\xi) = s(\xi) = t(\xi) = 0 \tag{4.1.40}$$

It follows from (4.1.5) and (4.1.22) that

$$B'_x(z') = B'_y(z') = C_z(z') = 0 \quad ; \quad B'_z(z') = A'_z(z')$$

which gives right away

$$D^s_{xx} = D^s_{yy} = D^s_{xy} = D^s_{yz} = D^s_{xz} = D^s_{zz} = 0 \tag{4.1.41}$$

Therefore when the medium is homogeneous and the effective diffusion coefficients $(m^s_{ij} + D^s_{ij})$ of (3.3.21) becomes

$$(m^s_{ij} + D^s_{ij}) = m^s_{ij} = m' \tag{4.1.42}$$

which is simply the mesoscale thermal conductivity so that it is like the intermediate scale(the mesoscale) is absent.

4.2 Anti-symmetric Dispersion Tensor D^u_{ij}.

As in the case of D^s_{ij}, the anti-symmetric dispersion tensor D^u_{ij} obeys the tensor transformation rule between the two coordinate systems $\bar{x}'\bar{y}'\bar{z}'$ and $x'y'z'$ of §4.1.1. This is explicitly seen by comparing $\bar{D}^u_{ij}$ in the $\bar{x}'\bar{y}'\bar{z}'$-frame and D^u_{ij} in the $x'y'z'$-frame.

For isotropic thermal conductivity on the mesoscale, from the definition of D^u_{ij} (3.3.23) we have

$$\begin{aligned} D^u_{ij} = &- \frac{Pe'}{2}\left\langle \langle\hat{u}\rangle^{(0)}_i B'_j - \langle\hat{u}\rangle^{(0)}_j B'_i \right\rangle \\ &+ \frac{Pe'}{2}\frac{1}{\left\langle \overline{\rho C_p}^* \right\rangle}\left[\left\langle \overline{\rho C_p}^* B'_i \right\rangle \langle\langle u\rangle^{(0)}_j\rangle - \left\langle \overline{\rho C_p}^* B'_j \right\rangle \langle\langle u\rangle^{(0)}_i\rangle\right] \\ &+ \frac{1}{2}\left\langle m' \frac{\partial B'_j}{\partial x'_i} - m' \frac{\partial B'_i}{\partial x'_j} \right\rangle \end{aligned} \tag{4.2.1}$$

When the flow is viewed from $\bar{x}'\bar{y}'\bar{z}'$-frame, $\overline{\langle u\rangle}_y = \widetilde{\langle u\rangle}_y = 0$ so that $\bar{B}_y = 0$. Then (4.2.1) reduces to

$$\begin{aligned} \bar{D}^u_{xx} =& \bar{D}^u_{yy} = \bar{D}^u_{zz} = 0 \\ \bar{D}^u_{xy} =& \bar{D}^u_{yz} = 0 \\ \bar{D}^u_{xz} =& - \frac{Pe'}{2}\left\langle \langle\hat{\bar{u}}\rangle^{(0)}_x \bar{B}'_z \right\rangle \\ &+ \frac{Pe'}{2}\frac{1}{\left\langle \overline{\rho C_p}^* \right\rangle}\left[\left\langle \overline{\rho C_p}^* \bar{B}'_x \right\rangle \langle\langle \bar{u}\rangle^{(0)}_z\rangle - \left\langle \overline{\rho C_p}^* \bar{B}'_z \right\rangle \langle\langle \bar{u}\rangle^{(0)}_x\rangle\right] - \frac{1}{2}\left\langle m' \frac{\partial \bar{B}'_x}{\partial z'} \right\rangle \end{aligned} \tag{4.2.2}$$

where use has been made of the fact that $\overline{\langle u\rangle}^{(0)}_z$ is constant therefore its fluctuation from the mean $\overline{\langle\hat{u}\rangle}^{(0)}_z = 0$. If the same flow situation is observed from $x'y'z'$-frame, (4.1.7) and (4.1.10) give, the anti-symmetric dispersion tensor

$$D^u_{xy} = 0, \quad D^u_{xz} = \bar{D}^u_{xz}\cos\phi, \quad D^u_{yz} = -\bar{D}^u_{xz}\sin\phi \tag{4.2.3}$$

which is the result of the tensor transformation (4.1.12) applied to D^u_{ij} with A_{ij} as given in (4.1.13). Thus we only need to consider $\bar{D}^u_{xz}$.

Omitting the lengthy algebra, we only give the result here (Appendix C).

$$\begin{aligned} \bar{D}^u_{xz} = &\frac{Pe'}{2}\frac{1}{p(\ell')-1}\frac{1}{\ell'}\int_o^{\ell'}\frac{\langle u\rangle_x}{p(z')}dz'\int_o^{\ell'} p(\xi)\rho C_p(\xi)d\xi \\ &+ \frac{Pe'}{2}\frac{1}{\ell'}\int_o^{\ell'} dz'\frac{\langle u\rangle_x}{p(z')}\int_o^{z'} p(\xi)\rho C_p(\xi)d\xi \\ &- \frac{Pe'}{2}\frac{1}{p(\ell')-1}\frac{1}{\ell'}\int_o^{\ell'} p(\xi)\langle u\rangle_x(\xi)d\xi\int_o^{\ell'}\frac{2-\rho C_p(z')}{p(z')}dz' \\ &- \frac{Pe'}{2}\frac{1}{\ell'}\int_o^{\ell'} dz'\frac{2-\rho C_p(z')}{p(z')}\int_o^{z'} p(\xi)\langle u\rangle_x(\xi)d\xi \end{aligned} \tag{4.2.5}$$

where

$$\rho C_p(\xi) = \overline{\rho C_p}^*(\xi) \Big/ \left\langle \overline{\rho C_p}^* \right\rangle \tag{4.2.6}$$

has been used.

So far both the symmetric and anti-symmetric disperion tensors have been derived in terms of the seepage flow velocities and the material properties of the medium. We now turn to the convection velocity of heat transport in vertically stratified periodic medium.

4.3 The Convection Velocity of Heat Transport.

In the mean heat transport equation (3.3.25), the effective convection velocity is given by

$$\begin{aligned} V_e =& Pe' \langle \langle u \rangle^{(0)} \rangle + \epsilon (Pe' U - \nabla'' \cdot (m^u + D^u)) \\ =& Pe' \langle \langle u \rangle^{(0)} \rangle + \epsilon Pe' \left[\langle \langle u \rangle^{(1)} \rangle + \left(\nabla'' \cdot \left\langle \overline{\rho C_p}^* B' \right\rangle \right) \frac{\langle \langle u \rangle^{(0)} \rangle}{\left\langle \overline{\rho C_p}^* \right\rangle} \right] \\ & - \epsilon \nabla'' \cdot (m^u + D^u) \\ =& Pe' \left(1 + \epsilon \frac{\nabla'' \cdot \left\langle \overline{\rho C_p}^* B' \right\rangle}{\left\langle \overline{\rho C_p}^* \right\rangle} \right) \langle \langle u \rangle^{(0)} \rangle + \epsilon Pe' \langle \langle u \rangle^{(1)} \rangle - \epsilon \nabla'' \cdot (m^u + D^u) \end{aligned} \tag{4.3.1}$$

Clearly the dominant part is the Darcy velocity $Pe' \langle \langle u \rangle^{(0)} \rangle$. However additional terms due to the first order velocity $\langle \langle u \rangle^{(1)} \rangle$ and the anti-symmetric part of thermal dispersion tensor $\nabla'' \cdot (m^u + D^u)$ are also important over long time. It should be noted that the coefficients $\nabla'' \cdot \left\langle \overline{\rho C_p}^* B' \right\rangle$ and $\nabla'' \cdot (m^u + D^u)$ are not the macroscale property of the medium itself but rather induced disturbances by such as seepage flow and temperature just like the dispersion tensor which varies with flow and temperature fields.

It remains to consider $\langle \langle u \rangle^{(1)} \rangle$ only since $\left\langle \overline{\rho C_p}^* B' \right\rangle$ and D^u_{ij} have already been obtained in the previous section. For this purpose, we solve the boundary value

problems (3.4.5) to (3.4.9) for periodically stratified medium along vertical direction. From (3.4.11) we have

$$\langle\langle u\rangle_i^{(1)}\rangle = -E''_{i\ell}\left(\nabla''_\ell p^{(0)} - \frac{\hat{R}a'}{Pe'}\theta^{(0)}\delta_{\ell z}\right) - F''_{ij\ell}\nabla''_j\nabla''_\ell p^{(0)} + G''_{ij\ell}\frac{\hat{R}a'}{Pe'}\nabla''_j\theta^{(0)}\delta_{\ell z} \tag{4.3.2}$$

For periodically stratified medium, the coefficients are given by (Appendix D)

$$\begin{aligned}
&E''_{i\ell} = 0\\
&F''_{zzz} = F''_{zyy} = \frac{k''_{zz}}{\ell'}\int_o^{\ell'}\frac{dz'}{k'(z')}\int_o^{z'}k'(\xi)d\xi + \langle z'k'(z')\rangle - \ell' k''_{zz}\\
&F''_{zxz} = F''_{yyz} = G''_{zxz} = G''_{yyz} = \langle k'S'_z\rangle\\
&F''_{zzz} = G''_{zzz} = k''_{zz}{}^2\left(\left\langle\frac{z'}{k'}\right\rangle - \frac{\ell'}{2k''_{zz}}\right)\\
&F''_{ij\ell} = 0 \qquad \text{otherwise}
\end{aligned} \tag{4.3.3}$$

These coefficients must be determined from $k'(z')$ and $S'_z(z')$. After some algebra we have(Appendix E)

$$\begin{aligned}
F''_{zxz} =&\langle k'S'_z\rangle = \frac{k''_{xz}}{\ell'}\int_o^{\ell'}dz'\left(1-\frac{k''_{zz}}{k'(z')}\right)\int_o^{z'}\left(\frac{k'(\xi)}{k''_{xz}}-1\right)d\xi\\
F''_{zzz} =&k''_{zz}{}^2\left(\left\langle\frac{z'}{k'}\right\rangle - \frac{\ell'}{2k''_{zz}}\right) = \frac{k''_{zz}}{\ell'}\int_o^{\ell'}dz'\int_o^{z'}\left(1-\frac{k''_{zz}}{k'(\xi)}\right)d\xi\\
F''_{zxz} =&\frac{1}{\ell'}\int_o^{\ell'}dz'k'(z')\int_o^{z'}\left(1-\frac{k''_{zz}}{k'(\xi)}\right)d\xi
\end{aligned} \tag{4.3.4}$$

After integration by parts, we also find the following.

$$\begin{aligned}
\frac{k''_{zz}}{k''_{xz}}F''_{zxz} - F''_{zzz} &= \frac{k''_{zz}}{\ell'}\int_o^{\ell'}dz'\left(\frac{k'(z')}{k''_{xz}}-1\right)\int_o^{z'}\left(1-\frac{k''_{zz}}{k'(\xi)}\right)d\xi\\
&= -\frac{k''_{zz}}{k''_{xz}}\left[\frac{k''_{xz}}{\ell'}\int_o^{\ell'}dz'\left(1-\frac{k''_{zz}}{k'(z')}\right)\int_o^{z'}\left(\frac{k'(\xi)}{k''_{xz}}-1\right)d\xi\right]
\end{aligned} \tag{4.3.5}$$

which, inview of F''_{zxz}, gives

$$\frac{k''_{zz}}{k''_{xz}}(F''_{zxz} + F''_{zzz}) = F''_{zzz} \tag{4.3.6}$$

Therefore, there are only two independent coefficients in E''_{ij}, $F''_{ij\ell}$ and $G''_{ij\ell}$.

By using the coefficients E''_{ij}, $F''_{ij\ell}$ and $G''_{ij\ell}$ in (4.3.3), the first order seepage velocity (4.3.2) can now be calculated as follows.

For the horizontal components, we have

$$\begin{aligned}\langle\langle u\rangle_x^{(1)}\rangle &= -F''_{xj\ell}\frac{\partial^2 p^{(0)}}{\partial x''_j \partial x''_\ell} + G''_{xjz}\frac{\hat{R}a'}{Pe'}\frac{\partial\theta^{(0)}}{\partial x''_j} \\ &= -\langle k' S'_z\rangle\left(\frac{\partial^2 p^{(0)}}{\partial x''\partial z''} - \frac{\hat{R}a'}{Pe'}\frac{\partial\theta^{(0)}}{\partial x''}\right) \qquad (4.3.7) \\ \langle\langle u\rangle_y^{(1)}\rangle &= -\langle k' S'_z\rangle\left(\frac{\partial^2 p^{(0)}}{\partial y''\partial z''} - \frac{\hat{R}a'}{Pe'}\frac{\partial\theta^{(0)}}{\partial y''}\right)\end{aligned}$$

Similarly the z''-component becomes

$$\begin{aligned}\langle\langle u\rangle_z^{(1)}\rangle &= -F''_{zj\ell}\frac{\partial^2 p^{(0)}}{\partial x''_j \partial x''_\ell} + G''_{zjz}\frac{\hat{R}a'}{Pe'}\frac{\partial\theta^{(0)}}{\partial x''_j} \\ &= -F''_{zxx}\left(\frac{\partial^2 p^{(0)}}{\partial x''^2} + \frac{\partial^2 p^{(0)}}{\partial y''^2}\right) - F''_{zzz}\left(\frac{\partial^2 p^{(0)}}{\partial z''^2} - \frac{\hat{R}a'}{Pe'}\frac{\partial\theta^{(0)}}{\partial z''}\right) \qquad (4.3.8) \\ &= -\frac{k''_{zz}}{k''_{xx}}\langle k' S'_z\rangle\left(\frac{\partial^2 p^{(0)}}{\partial z''^2} - \frac{\hat{R}a'}{Pe'}\frac{\partial\theta^{(0)}}{\partial z''}\right)\end{aligned}$$

where (4.3.6) and the consolidation equation (3.2.5) have been used. This completes the convection velocity for heat transport.

5. A Medium with Two Alternating Layers on the Mesoscale

The dispersion tensors and the convection velocity of heat derived in §4 for vertically stratified medium are specialized to a medium with two distinct layers in a ℓ' period. After obtaining the dispersion tensors in §5.1 and examining their behavior for small and large Peclét numbers in §5.2, plots are presented in §5.3 for both passive solute and heat. The sensitive variation of dispersion tensors with the flow angle is also discussed. Finally in §5.4, it is shown that the first order convection velocity $\langle u \rangle^{(1)}$ vanishes identically.

5.1 Analytic Dispersion Tensors D^s_{ij} and D^u_{ij}

The explicit forms of dispersion tensors D^s_{ij} and D^u_{ij} are obtained by evaluation of several integrals which involve $p(\xi)$, $r(\xi)$ and $t(\xi)$. The forcing terms $r(\xi)$ and $t(\xi)$ in each layer will be distinguished by employing the superscript symbols $()^-$ and $()^+$ in the lower and upper layers respectively. Other material properties such as thermal conductivity m', heat capacity ρC_p, hydraulic conductivity k', etc will also be distinguished in the same manner. For example, if we let

$$m'(\xi) = \begin{cases} m'^- \\ m'^+ \end{cases} \qquad \begin{matrix} 0 < \xi' < (1-s)\ell' \\ (1-s)\ell' < \xi' < \ell' \end{matrix} \tag{5.1.1}$$

it follows from the definition (4.1.19) that

$$\begin{aligned} p(\xi) &= \exp\left[-\int_o^\xi \frac{a\,dt}{m'(t)}\right] \\ &= \begin{cases} \exp\left[-\frac{a}{m'^-}\xi\right] \\ \exp\left[-\frac{a(1-s)\ell'}{m'^-} - a\frac{\xi-(1-s)\ell'}{m'^+}\right] \end{cases} \qquad \begin{matrix} 0 < \xi' < (1-s)\ell' \\ (1-s)\ell' < \xi' < \ell' \end{matrix} \end{aligned} \tag{5.1.2}$$

where

$$a = Pe'\langle u \rangle_z \tag{5.1.3}$$

After performing evaluation of many integrals(Appendix F), we obatin

$$\langle m' \rangle_{zz} + D^{e}_{zz} = m''_{zz}$$
$$+ \frac{1}{a^2}\left[r^{-^2} m'^{-}(1-s) + r^{+^2} m'^{+} s - \frac{2}{a\ell'}\frac{\sinh x \sinh y}{\sinh(x+y)}\left(r^{-} m'^{-} - r^{+} m'^{+}\right)^2\right]$$
$$\langle m' \rangle_{zz} + D^{e}_{zz} = m''_{zz}$$
$$+ \frac{1}{a^2}\left[t^{-^2} m'^{-}(1-s) + t^{+^2} m'^{+} s - \frac{2}{a\ell'}\frac{\sinh x \sinh y}{\sinh(x+y)}\left(t^{-} m'^{-} - t^{+} m'^{+}\right)^2\right]$$
$$D^{e}_{zz} = \frac{1}{a^2}\left[r^{-} t^{-} m'^{-}(1-s) + r^{+} t^{+} m'^{+} s\right]$$
$$- \frac{2}{a^3 \ell'}\frac{\sinh x \sinh y}{\sinh(x+y)}\left(r^{-} m'^{-} - r^{+} m'^{+}\right)\left(t^{-} m'^{-} - t^{+} m'^{+}\right)$$
$$D^{u}_{zz} = \frac{1}{\langle u \rangle_z}\left[\langle u \rangle^{-}_{x}(1-\rho C^{-}_{p}) m'^{-}(1-s) + \langle u \rangle^{+}_{x}(1-\rho C^{+}_{p}) m'^{+} s\right]$$
$$- \frac{1}{\langle u \rangle_z}\frac{2}{a\ell'}\frac{\sinh x \sinh y}{\sinh(x+y)}\left(\langle u \rangle^{-}_{x} m'^{-} - \langle u \rangle^{+}_{x} m'^{+}\right)\left[(1-\rho C^{-}_{p}) m'^{-} - (1-\rho C^{+}_{p}) m'^{+}\right] \tag{5.1.4}$$

where

$$x = \frac{a(1-s)\ell'}{2m'^{-}}, \qquad y = \frac{as\ell'}{2m'^{+}}$$
$$\rho C^{-}_{p} = \frac{\overline{\rho C^{*-}_{p}}}{\left\langle \overline{\rho C^{*}_{p}} \right\rangle}, \qquad \rho C^{+}_{p} = \frac{\overline{\rho C^{*+}_{p}}}{\left\langle \overline{\rho C^{*}_{p}} \right\rangle} \tag{5.1.5}$$

For the purpose of checking, direct integration of (4.1.14) has also been used to obtain D^{e}_{zz} (Appendix G).

From (4.1.16) and (4.1.31), the source terms $r(\xi)$ and $t(\xi)$ are written as

$$r^{\pm} = Pe'\left(\frac{\langle u \rangle^{\pm}_{x}}{\langle \langle u \rangle_x \rangle} - \rho C^{\pm}_{p}\right)\langle \langle u \rangle_x \rangle = Pe' \langle \langle u \rangle_x \rangle \left(k'^{\pm} - \rho C^{\pm}_{p}\right)$$
$$t^{\pm} = -Pe' \langle u \rangle_z \left(\rho C^{\pm}_{p} - \frac{m''_{zz}}{m'^{\pm}}\right) \tag{5.1.6}$$

Let the angle between the mean flow and the horizontal plane be denoted by θ i.e., the direction of the mean flow is parallel and normal to the layering for $\theta = 0$ and $\theta = 90°$ respectively. Note that θ is equal to 90° minus the meridianal angle in Fig. 4.1. The horizontal and vertical velocity components $\langle \langle u \rangle_x \rangle$ and $\langle u \rangle_z$ of the normalized mean flow are then related by

$$\langle \langle u \rangle_x \rangle = \cos\theta, \quad \langle u \rangle_z = \sin\theta \quad ; \quad \frac{\langle u \rangle_z}{\langle \langle u \rangle_x \rangle} = \tan\theta \tag{5.1.7}$$

Let us introduce the following notations

$$\begin{aligned}\hat{r}^{\pm} &= \frac{r^{\pm}}{Pe'\langle\langle u\rangle_z\rangle} = k'^{\pm} - \rho C_p^{\pm} \\ \hat{t}^{\pm} &= \frac{t^{\pm}}{Pe'\langle u\rangle_z} = -\left(\rho C_p^{\pm} - \frac{m''_{zz}}{m'^{\pm}}\right)\end{aligned} \tag{5.1.8}$$

If we substitute (5.1.6) to (5.1.8) into (5.1.4), the dispersion coefficients become

$$\begin{aligned}\langle m'\rangle_{zz} + D^e_{zz} &= m''_{zz} + \left[\hat{r}^{-2}m'^{-}(1-s) + \hat{r}^{+2}m'^{+}s\right]\frac{1}{\tan^2\theta} \\ &\quad - \frac{2}{Pe'\ell'\sin\theta}\frac{\sinh x \sinh y}{\sinh(x+y)}\left(\hat{r}^{-}m'^{-} - \hat{r}^{+}m'^{+}\right)^2\frac{1}{\tan^2\theta} \\ \langle m'\rangle_{zz} + D^e_{zz} &= m''_{zz} + \left[\hat{t}^{-2}m'^{-}(1-s) + \hat{t}^{+2}m'^{+}s\right] \\ &\quad - \frac{2}{Pe'\ell'\sin\theta}\frac{\sinh x \sinh y}{\sinh(x+y)}\left(\hat{t}^{-}m'^{-} - \hat{t}^{+}m'^{+}\right)^2\end{aligned} \tag{5.1.9}$$

$$\begin{aligned}D^e_{xz} &= \left[\hat{r}^{-}\hat{t}^{-}m'^{-}(1-s) + \hat{r}^{+}\hat{t}^{+}m'^{+}s\right]\frac{1}{\tan\theta} \\ &\quad - \frac{2}{Pe'\ell'\sin\theta}\frac{\sinh x \sinh y}{\sinh(x+y)}\left(\hat{r}^{-}m'^{-} - \hat{r}^{+}m'^{+}\right)\left(\hat{t}^{-}m'^{-} - \hat{t}^{+}m'^{+}\right)\frac{1}{\tan\theta} \\ D^u_{xz} &= \left[k'^{-}(1-\rho C_p^{-})m'^{-}(1-s) + k'^{+}(1-\rho C_p^{+})m'^{+}s\right]\frac{1}{\tan\theta} \\ &\quad - \frac{2}{Pe'\ell'\sin\theta}\frac{\sinh x \sinh y}{\sinh(x+y)}\left(k'^{-}m'^{-} - k'^{+}m'^{+}\right) \\ &\quad \times \left[(1-\rho C_p^{-})m'^{-} - (1-\rho C_p^{+})m'^{+}\right]\frac{1}{\tan\theta}\end{aligned}$$

For the moment let us assume that $\theta \neq 0$. Equation (5.1.9) shows that the dispersion coefficients strongly depends on θ. Especially $\langle m'\rangle_{zz} + D^e_{zz}$ varies more rapidly. If $\theta = 90°$, $\tan\theta \to \infty$ and $\langle m'\rangle_{zz} + D^e_{zz} \to m''_{zz}$ and $D^e_{zz}, D^u_{zz} \to 0$. They are discussed in more detail in the following sections.

5.2 Asymptotic Behavior of Dispersion Tensors

In this section, the asymptotic behavior of dispersion tensors is investigated for small and large Peclét numbers. Also comparison with earlier results for anisotropic medium is made.

5.2.1 Behavior for Small Peclét Number

As the Peclét number Pe' goes to zero, $a = Pe'\langle u\rangle_z$ in (5.1.3) and x and y in (5.1.5) become smaller. Upon expanding the hyperbolic functions in Taylor series in (5.1.4), we get

$$\begin{aligned}\frac{\sinh x \sinh y}{\sinh(x+y)} =& \frac{(x+x^3/6+\cdots)(y+y^3/6+\cdots)}{x+y+(x+y)^3/6+\cdots} \\ =& \frac{xy}{x+y}\left[1+\frac{1}{6}(x^2+y^2)+\cdots\right]\left[1-\frac{1}{6}(x+y)^2+\cdots\right] \\ =& \frac{xy}{x+y}\left(1-\frac{1}{3}xy+\cdots\right)\end{aligned} \tag{5.2.1}$$

where

$$xy = \frac{Pe'^2(1-s)s\ell'^2\sin^2\theta}{4m'^-m'^+}, \quad \frac{xy}{x+y} = \frac{Pe'\ell'\sin\theta}{2}\frac{(1-s)s}{(1-s)m'^+ + sm'^-} \tag{5.2.2}$$

If we substitute (5.2.1) into D^*_{zz} in (5.1.9) and use (5.2.2), there follows

$$\begin{aligned}&\langle m'\rangle_{zz} + D^*_{zz} = m''_{zz} + \frac{1}{\tan^2\theta}\times \\ &\left[\hat{r}^{-2}m'^-(1-s)+\hat{r}^{+2}m'^+s - \frac{2}{a\ell'}\frac{xy}{x+y}\left(1-\frac{1}{3}xy+\cdots\right)\left(\hat{r}^-m'^- - \hat{r}^+m'^+\right)^2\right] \\ &= m''_{zz} + \frac{1}{\tan^2\theta}\times \\ &\left[\hat{r}^{-2}m'^-(1-s)+\hat{r}^{+2}m'^+s - \frac{(1-s)s}{(1-s)m'^+ + sm'^-}\left(\hat{r}^-m'^- - \hat{r}^+m'^+\right)^2\right] \\ &+ \frac{Pe'^2\sin^2\theta}{12}\frac{\ell'^2(1-s)^2s^2}{m'^-m'^+[(1-s)m'^+ + sm'^-]}\left(\hat{r}^-m'^- - \hat{r}^+m'^+\right)^2\frac{1}{\tan^2\theta} + O(a^3) \\ &= m''_{zz} + \frac{m'^-m'^+}{(1-s)m'^+ + sm'^-}[(1-s)\hat{r}^- + s\hat{r}^+]^2\frac{1}{\tan^2\theta} \\ &\quad + \frac{Pe'^2\cos^2\theta}{12}\frac{\ell'^2(1-s)^2s^2}{m'^-m'^+[(1-s)m'^+ + sm'^-]}\left(\hat{r}^-m'^- - \hat{r}^+m'^+\right)^2 + O(a^3)\end{aligned} \tag{5.2.3}$$

The second term in (5.2.3) vanishes because of (4.1.17) i.e.,

$$\int_0^{\ell'} r(\xi)d\xi = (1-s)r^- + sr^+ = 0 \tag{5.2.4}$$

The effective dispersion coefficient ($\langle m'\rangle + D^*_{zz}$) then becomes

$$\begin{aligned}&\langle m'\rangle + D^*_{zz} = m''_{zz} \\ &+ \frac{Pe'^2\cos^2\theta}{12}\frac{\ell'^2(1-s)^2s^2}{m'^-m'^+[(1-s)m'^+ + sm'^-]}\left(\hat{r}^-m'^- - \hat{r}^+m'^+\right)^2\end{aligned} \tag{5.2.5}$$

It is maximum when $\theta = 0$ and reduces to m''_{zz} when $\theta = 90°$.

Similarly for small a, D^s_{zz} becomes

$$\begin{aligned}
&\langle m' \rangle_{zz} + D^s_{zz} = m''_{zz} \\
&\quad + \left[\hat{t}^{-2} m'^{-}(1-s) + \hat{t}^{+2} m'^{+} s - \frac{(1-s)s}{(1-s)m'^{+} + sm'^{-}} \left(\hat{t}^{-} m'^{-} - \hat{t}^{+} m'^{+} \right)^2 \right] \\
&\quad + \frac{Pe'^2 \sin^2\theta}{12} \frac{\ell'^2 (1-s)^2 s^2}{m'^{-} m'^{+} [(1-s)m'^{+} + sm'^{-}]} \left(\hat{t}^{-} m'^{-} - \hat{t}^{+} m'^{+} \right)^2 + O(a^3) \\
&= m''_{zz} + \frac{1}{12} Pe'^2 \sin^2\theta \frac{\ell'^2 (1-s)^2 s^2}{m'^{-} m'^{+} [(1-s)m'^{+} + sm'^{-}]} \left(\rho C_p{}^{-} m'^{-} - \rho C_p{}^{+} m'^{+} \right)^2 \\
&\quad + O(Pe'^3)
\end{aligned} \tag{5.2.6}$$

The dispersion coefficient $\langle m' \rangle_{zz} + D^s_{zz}$ thus reaches its maximum when $\theta = 90°$ and reduces to m''_{zz} when $\theta = 0$. Following the same procedure, we also obtain

$$\begin{aligned}
D^s_{zz} = \frac{1}{12} Pe'^2 \sin\theta\cos\theta \frac{\ell'^2 (1-s)^2 s^2}{m'^{-} m'^{+} [(1-s)m'^{+} + sm'^{-}]} \\
\times \left(\hat{r}^{-} m'^{-} - \hat{r}^{+} m'^{+} \right) \left(\rho C_p{}^{+} - \rho C_p{}^{-} \right) + O(Pe'^3)
\end{aligned} \tag{5.2.7}$$

$$\begin{aligned}
D^u_{zz} = \frac{1}{12} Pe'^2 \sin\theta\cos\theta \frac{\ell'^2 (1-s)^2 s^2}{m'^{-} m'^{+} [(1-s)m'^{+} + sm'^{-}]} \\
\times \left(k'^{-} m'^{-} - k'^{+} m'^{+} \right) \left[(1 - \rho C_p{}^{-}) m'^{-} - (1 - \rho C_p{}^{+}) m'^{+} \right]
\end{aligned} \tag{5.2.8}$$

From the above it is readily shown that

$$\begin{aligned}
&\langle m' \rangle + D^s_{zz} \to m''_{zz}, \quad \langle m' \rangle + D^s_{zz} \to m''_{zz} \\
&D^s_{zz} \to 0, \quad D^u_{zz} \to 0 \qquad\qquad \text{as} \quad Pe' \to 0
\end{aligned} \tag{5.2.9}$$

Thus the effective dispersion coeffcients reduce to the macroscale thermal conductivies which are anisotropic due to the layered structure. But, as Pe' increases, they increase in proportion to Pe'^2. In a study of dispersion tensor, Poreh(1965) used dimensional and symmetry arguments about the plane of layering to obtain a general form for dispersivity tensor for transversely isotropic medium. For small Pe' his result reduces to a form similar to (5.2.5) and (5.2.6) in that the dependence on Pe' is quadratic. But they contain several coeffcients which depend on the geometric characteristics of the medium and must be determined experimentally.

In the case of dispersion of passive solute for which heterogeneity due to the permeability variation in the medium is important, one may assume for other normalized coefficients that

$$\rho C_p{}^- = \rho C_p{}^+ = 1, \quad m'^- = m'^+ = 1 \tag{5.2.10}$$

which implies in (5.1.8) that

$$\hat{r}^\pm = k'^\pm, \quad t^\pm = 0, \quad m''_{xx} = m''_{zz} = 1 \tag{5.2.11}$$

It then follows from (5.2.5) to (5.2.8) that

$$\begin{aligned}
&\langle m' \rangle + D^e_{xx} = 1 + \frac{1}{12} Pe'^2 \ell'^2 \cos^2\theta (1-s)^2 s^2 \left(k'^- - k'^+\right)^2 + O(Pe'^3) \\
&\langle m' \rangle + D^e_{zz} = 1 \\
&D^e_{xz} = 0 \\
&D^u_{xz} = 0
\end{aligned} \tag{5.2.12}$$

Therefore, for alternating layers with distinct permeability, $\langle m' \rangle + D^e_{xx}$ and $\langle m' \rangle + D^e_{zz}$ are important and others vanish. However, the vanishing of D^e_{xz} and D^u_{xz} in a layered medium with the property of (5.2.10) is valid for all Peclét number(cf.(5.1.4)).

5.2.2 Behavior for Large Peclét Number

When the Peclét number becomes large, the dispersion tensor is strongly affected by the angle between the flow direction and that of layering. We shall distinguish the case when $\langle u \rangle_z \equiv 0 (\theta \equiv 0)$ and the general case $\langle u \rangle_z \neq 0 (\theta \neq 0)$.

Let us first consider the case $\langle u \rangle_z \neq 0$. For large Pe', in view of (5.1.3) and (5.1.5), we have

$$\frac{\sinh x \sinh y}{\sinh(x+y)} = \frac{1}{\coth x + \coth y} \simeq \frac{1}{2} \qquad Pe' \to \infty \tag{5.2.13}$$

so that terms involving hyperbolic functions in (5.1.4) are negligibly small. It readily follows then from (5.1.9) that

$$
\begin{aligned}
&\langle m' \rangle + D^e_{zz} \simeq m''_{zz} + \left[\hat{r}^{-2} m'^{-}(1-s) + \hat{r}^{+2} m'^{+} s\right] \frac{1}{\tan^2\theta} \\
&\langle m' \rangle + D^e_{zz} \simeq m''_{zz} + \hat{t}^{-2} m'^{-}(1-s) + \hat{t}^{+2} m'^{+} s \qquad \text{as} \quad Pe' \to \infty \\
&D^e_{zz} \simeq -\left[\hat{r}^{-}\hat{t}^{-} m'^{-}(1-s) - \hat{r}^{+}\hat{t}^{+} m'^{+} s\right] \frac{1}{\tan\theta} \\
&D^u_{zz} \simeq \left[k'^{-}(1-\rho C_p{}^{-}) m'^{-}(1-s) + k'^{+}(1-\rho C_p{}^{+}) m'^{+} s\right] \frac{1}{\tan\theta}
\end{aligned}
\tag{5.2.14}
$$

in which $\hat{r}^{\pm}$ and $\hat{t}^{\pm}$ have been given in (5.1.8). Note that the dispersion coefficients approach to finite values in the case of $\langle u \rangle_z \neq 0$ as $Pe' \to \infty$. Also the large Pe' limit values are highly dependent upon θ and thus the flow direction relative to layering.

When $\langle u \rangle_z$ is identically zero, the large Pe' behavior of dispersion coefficients are found from the asymptotic formulas for $a = Pe' \langle u \rangle_z = Pe' \sin\theta \ll 1$ treated in §5.2.1. Specifically (5.2.5) to (5.2.8) give

$$
\begin{aligned}
&\langle m' \rangle + D^e_{zz} = m''_{zz} + \frac{1}{12} Pe'^2 \frac{\ell'^2 (1-s)^2 s^2}{m'^{-} m'^{+} [(1-s) m'^{+} + s m'^{-}]} \left(\hat{r}^{-} m'^{-} - \hat{r}^{+} m'^{+}\right)^2 \\
&\langle m' \rangle + D^e_{zz} = m''_{zz} \\
&D^e_{zz} = 0 \\
&D^u_{zz} = 0
\end{aligned}
\tag{5.2.15}
$$

The differences between (5.2.14) and (5.2.15) are quite drastic. The longitudinal coefficient ($\langle m' \rangle + D^e_{zz}$) is proportional to Pe'^2 whereas the transverse coefficient ($\langle m' \rangle + D^e_{zz}$) remains at the pure diffusion value when $\theta = 0$. The coefficients D^e_{zz} and D^u_{zz} are identically zero. From (5.2.14) and (5.2.15), it is readily seen that for given Pe' the variation of the dispersion coefficients change sharply with $\langle u \rangle_z$.

For periodic medium with alternating layers, Moranville et al (1977a,b) and Tyvand(1980) have studied the dispersion coefficients for large Peclét number by employing the general formulas for anisotropic medium due to Scheidegger(1961)

and Poreh(1965). The dispersion coefficient along the mean flow direction is proportional to the mean velocity, since they assumed that the dispersion coefficients on the mesoscale are proportional to the velocity. It should be noted that the form of dispersion tensor employed by Scheidegger and Poreh, and thus by Moranville et al, is based on physical postulates inferred from experimental observations that dispersion coefficients are linearly proportional to the velocity. Our results (5.2.18) for general non-zero $\langle u \rangle_z$ do not make use of any empirical information and have been deduced from the basic governing equations on the mesoscale.

5.3 Dispersion Tensors for Passive Solute and Heat

The analytic expressions of dispersion tensors in §5.1 are now used to calculate the coefficients for passive solute and heat. Their dependence on the Peclét number Pe' and the effects of varying medium properties such as the permeability, heat capacity and thermal conductivity are discussed. The layers are assumed to be of equal thickness i.e., $s = 0.5$.

5.3.1 Passive Solute

In the study of the transport of passive solute through porous media, the effects of the permeability difference between layers are most important. Accordingly we assume that the normalized thermal properties are equal to unity.

$$\rho C_p{}^- = \rho C_p{}^+ = 1, \quad m'^- = m'^+ = 1 \quad ; \quad m''_{xx} = m''_{zz} = 1 \tag{5.3.1a}$$

Accordingly the Peclét number is defined by

$$Pe' = \frac{U'\ell'}{M} \tag{5.3.1b}$$

where U' and M are the velocity of mean flow and the diffusivity of solute matter on the mesoscale. The angle between the mean flow and the horizontal plane is again denoted by θ. It then follows from (5.1.6) to (5.1.8) that

$$\begin{aligned} r^{\pm} &= Pe'\langle\langle u\rangle_z\rangle \left(k'^{\pm} - 1\right) \quad ; \quad \hat{r}^{\pm} = \frac{r^{\pm}}{Pe'\langle\langle u\rangle_z\rangle} = k'^{\pm} - 1 \\ t^{\pm} &= -\, Pe'\langle u\rangle_z \left(\rho C_p^{\pm} - 1\right) \quad ; \quad \hat{t}^{\pm} = 0 \\ x &= \frac{1}{2} Pe'(1-s)\ell' \sin\theta, \quad y = \frac{1}{2} Pe' s\ell' \sin\theta \end{aligned} \tag{5.3.2}$$

The dispersion coefficients in (5.1.9) reduce to

$$\begin{aligned}
&\langle m' \rangle + D^s_{xx} \\
&\quad = 1 + \left[\hat{r}^{-2}(1-s) + \hat{r}^{+2} s - \frac{2}{Pe' \ell' \sin\theta} \frac{\sinh x \sinh y}{\sinh(x+y)} \left(\hat{r}^- - \hat{r}^+ \right)^2 \right] \frac{1}{\tan^2 \theta} \\
&\langle m' \rangle + D^s_{zz} = 1 \\
&D^s_{zx} = D^u_{zx} = 0
\end{aligned} \tag{5.3.3}$$

so that there are only two nonvanishing dispersion coefficients. Obviously the coefficient $(\langle m' \rangle + D^s_{zz})$ is unity because the seepage velocity $\langle u \rangle_z$ is constant and $m'^- = m'^+ = 1$. Note that the off-diagonal and anti-symmetric components D^s_{zx} and D^u_{zx} vanish for the present porous medium with two alternating layers.

In Fig. 5.1(a)-(d), the dispersion coefficients $(\langle m' \rangle + D^s_{xx})$ and $(\langle m' \rangle + D^s_{zz})$ are plotted against Pe' for various mean flow directions. The contrasts in permeability k'^+/k'^- are 2, 5, 10 and 100 in (a),(b), (c) and (d) respectively. We first note as shown in §5.2 that, for high Pe', $(\langle m' \rangle + D^s_{xx})$ increases as $O(Pe'^2)$ when $\theta = 0$. For nonzero θ, it reaches finite limit value which decreases with θ since $\langle u \rangle_z = \sin\theta$ increases. In high Pe' region, $(\langle m' \rangle + D^s_{xx})$ changes drastically with θ. As is shown in Fig. 5.1, even for mean flow direction slightly off the plane parallel to the layers, the coefficient does not grow indefinitely with Pe' and approaches to the limit value. This kind of behavior has been observed in different approaches (Gupta and Bhattacharya, 1986; Güven and Moltz, 1986). It is very unlikely that the flow direction is perfectly in plane with the layers. In the case of $\theta = 90°$,i.e. the mean flow direction is normal to the layers, $r^{\pm} = 0$ and there is no spreading of solute caused by mixing. Thus $(\langle m' \rangle + D^s_{xx})$ and $(\langle m' \rangle + D^s_{zz})$ are identically equal to unity. Also note that the value of Pe', beyond which dispersion becomes significant, decreases with the permeability contrast from Fig. 5.1(a) to Fig. 5.1(d). In order to show that effect, $(\langle m' \rangle + D^s_{xx})$ for $\theta = 10°$ is plotted for the same set of k'^+/k'^- values in Fig. 5.2. As k'^+/k'^- changes from 2 to 100, the high Pe' limit is noticeably increased.

5.3.2 Heat

Thermal dispersion coefficients are influenced not only by the permeability but also by the heat capacity and the thermal conductivity. The effects of permeability have been studied in §5.3.1 for the particular case of passive solute. We consider the case when the permeability and thermal conductivities are equal : But the heat capacityies are different between the layers so that

$$m'^{-} = m'^{+} = 1, \quad k'^{-} = k'^{+} = 1 \tag{5.3.4a}$$

But the heat capacities are different between the layers so that

$$\rho C_p^{+} / \rho C_p^{-} = 10 \tag{5.3.4b}$$

The anti-symmetric dispersison coefficient D^u_{zz} then vanishes(cf.(5.1.4)). The coefficients $(\langle m' \rangle + D^s_{zz})$, $(\langle m' \rangle + D^s_{zz})$ and D^s_{zz} are shown in Fig. 5.3. Even if the layers have the same permeability ($k'^{-} = k'^{+}$), the heterogeneity in the heat capacity causes significant dispersion. We also note that D^s_{zz} becomes appreciable. It is smaller than $(\langle m' \rangle + D^s_{zz})$ but is larger than $(\langle m' \rangle + D^s_{zz})$. The effect of different thermal conductivity is also expected to increase dispersion as the contrast increases (cf.(5.2.14)) but they are not as pronounced as those by heat capacity since $(\langle m' \rangle + D^s_{zz})$ is proportional to the square of $\hat{r} = k' - \rho C_p$ but is linearly proportional to m'.

The thermal dispersison tensors are also plotted in Fig. 5.4 for a porous medium with $\rho C_p{}^{+} / \rho C_p{}^{-} = 2$, $m'^{+}/m'^{-} = 10$ and $k'^{+}/k'^{-} = 100$. The heat capacity does not change much from soil to soil whereas the thermal conductivity does to some extent.They increase with Pe' as before. The anti-symmetric dispersison coefficient does not vanish although it is small, but it is much larger than $(\langle m' \rangle + D^s_{zz})$. The dependence on the mean flow direction is presented in Fig. 5.5(a)-(d). The sharp changes are clearly shown when θ increases from zero. The coefficients D^s_{zz} and D^u_{zz} are zero when θ is identically zero. They first increase rapidly and then decrease as θ increases.

5.4 The Convection Velocity of Heat Transport

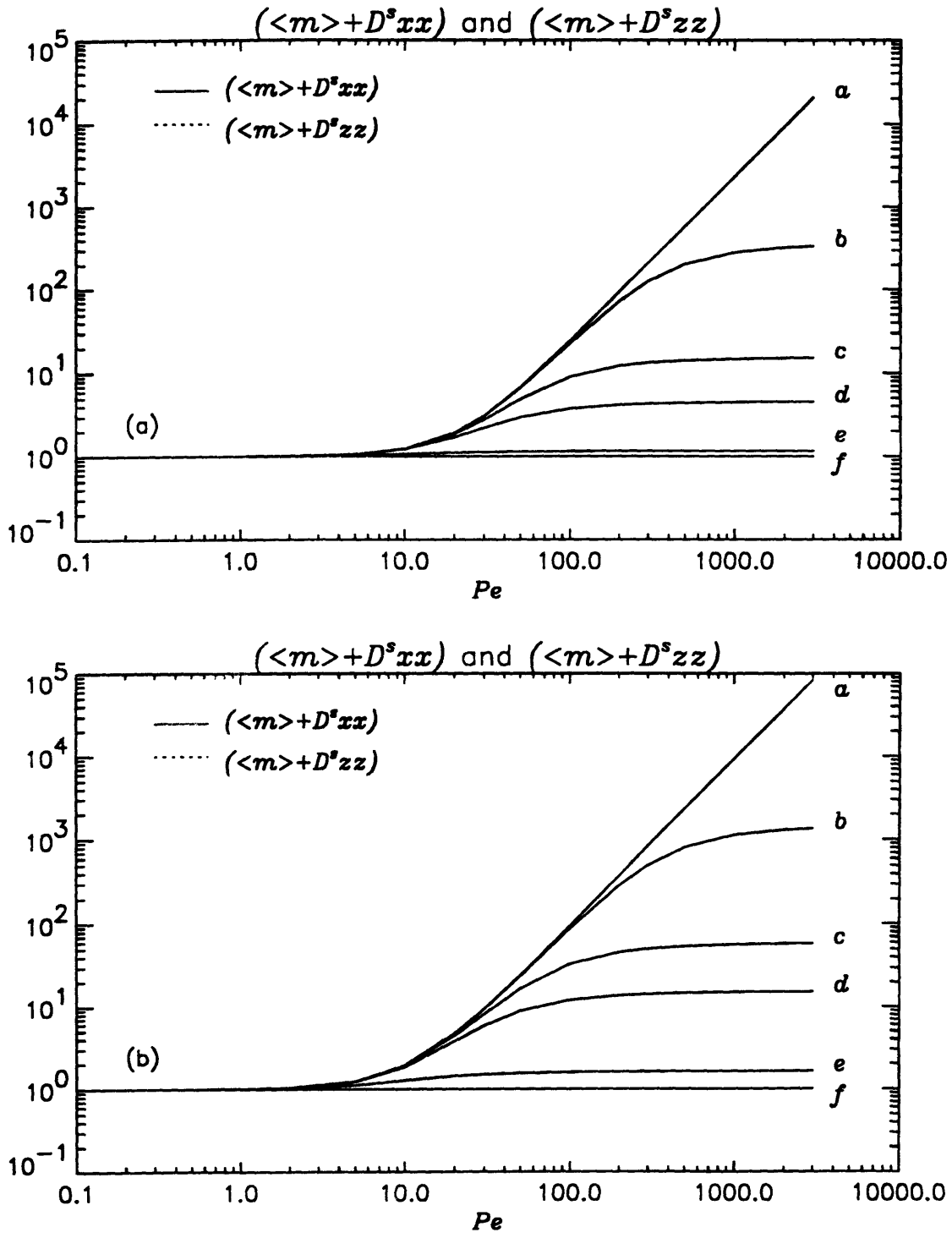

Fig. 5.1 Dispersion coefficients $(\langle m' \rangle + D^e_{zz})$ and $(\langle m' \rangle + D^e_{xz})$ for passive solute in a layered medium. The angle for mean flow direction is $a(\theta = 0°)$, $b(\theta = 1°)$, $c(\theta = 5°)$, $d(\theta = 10°)$, $e(\theta = 40°)$, and $f(\theta = 90°)$. The permeability ratios are (a) $k'^{+}/k'^{-} = 2$ and (b) $k'^{+}/k'^{-} = 5$. $(\langle m' \rangle + D^e_{zz})$ is the straight line marked by f.

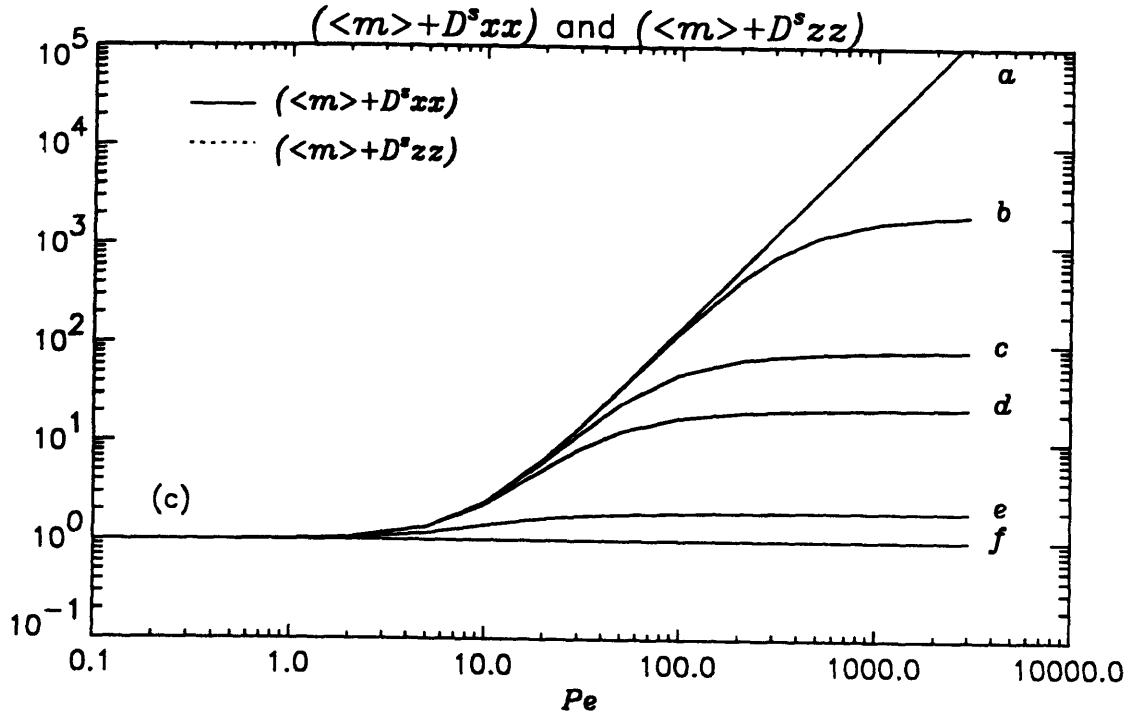

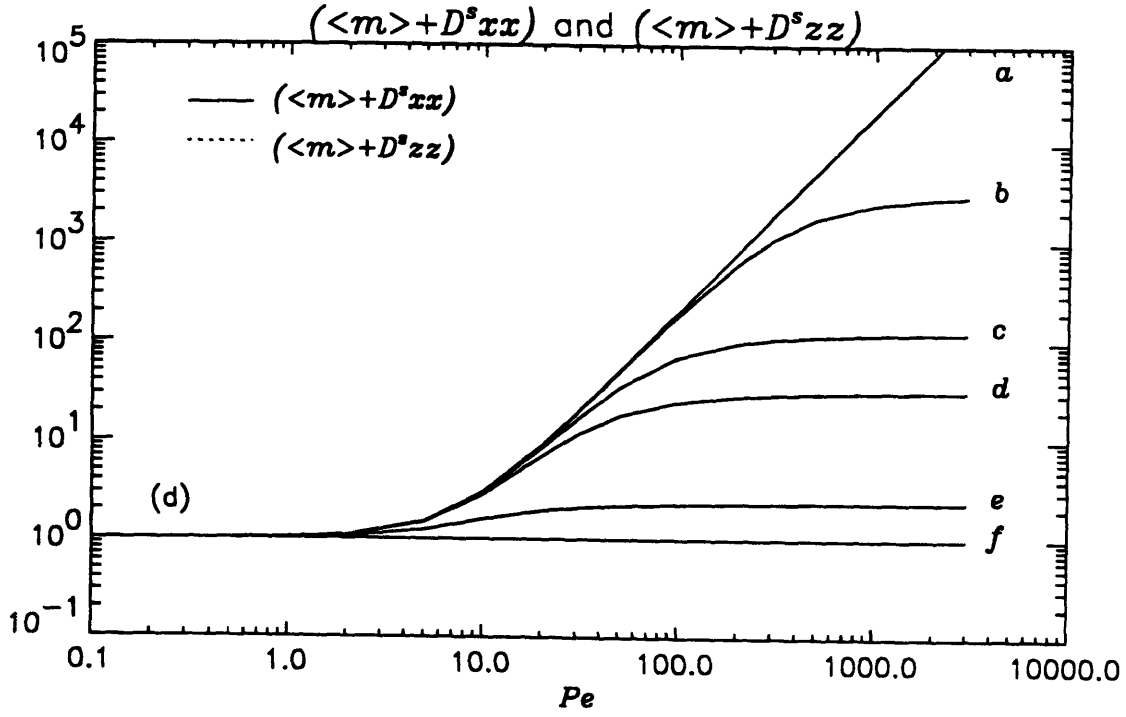

Fig. 5.1 (continued) The permeability ratios are (c) $k'^{+}/k'^{-} = 10$ and (d) $k'^{+}/k'^{-} = 100$.

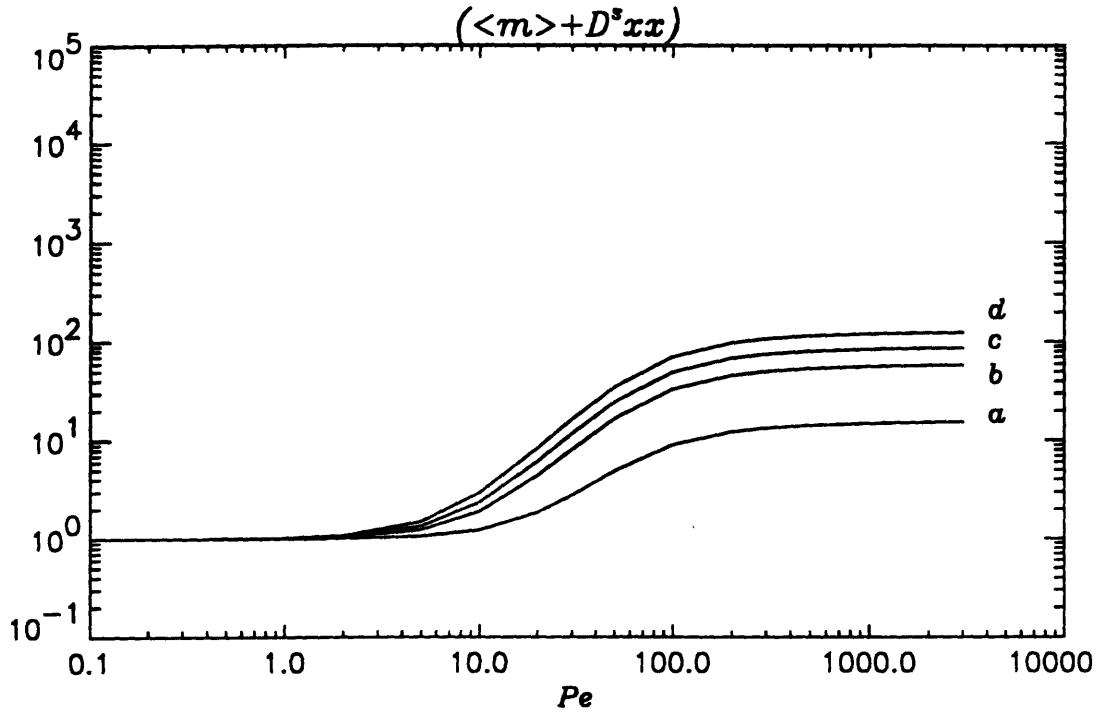

Fig. 5.2 Dispersion coefficient ($\langle m' \rangle + D^s_{zz}$) for passive solute in a layered medium with $\theta = 10°$. The permeability ratios are $a(k'^+/k'^- = 2)$, $b(k'^+/k'^- = 5)$, $c(k'^+/k'^- = 10)$ and $d(k'^+/k'^- = 100)$.

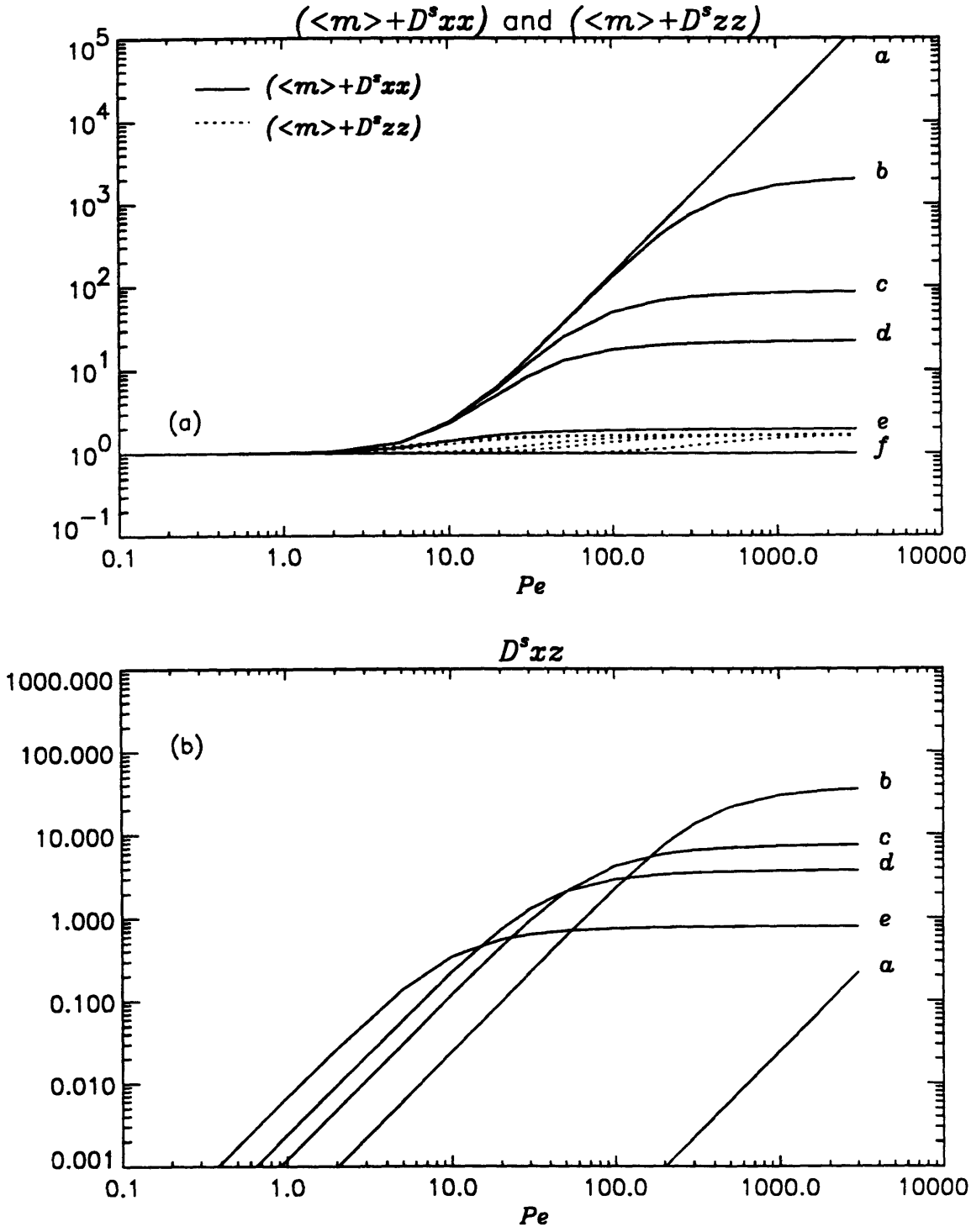

Fig. 5.3 Dispersion coefficients (a) $(\langle m' \rangle + D^s_{xx})$, $(\langle m' \rangle + D^s_{zz})$ and (b) D^s_{xz} for heat with $k'^+/k'^- = m'^+/m'^- = 1$ and $\rho C_p^+/\rho C_p^- = 10$. For the flow angle θ see the caption of Fig. 5.1.

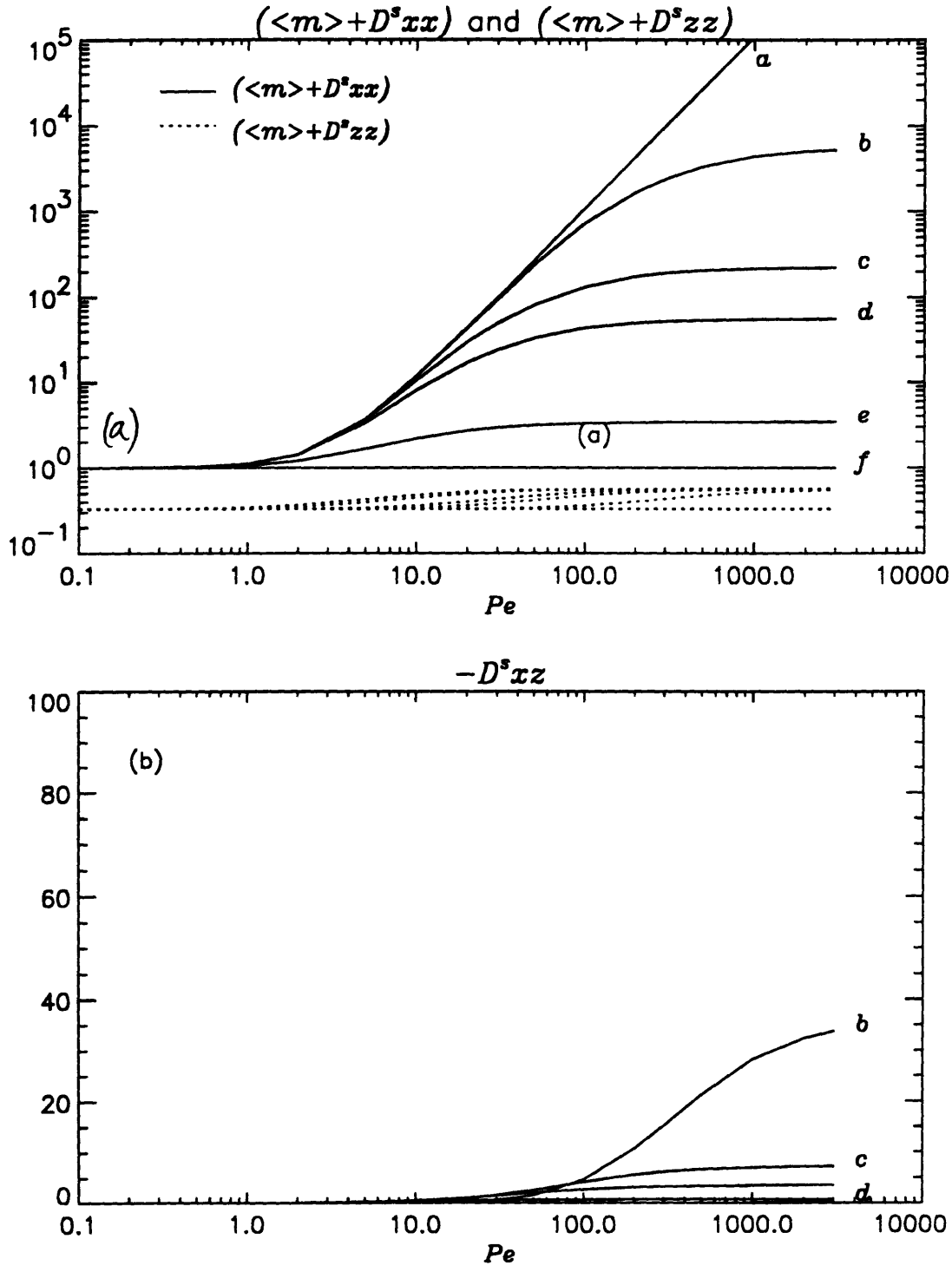

Fig. 5.4 Dispersion coefficients (a) $(\langle m' \rangle + D^s_{xx})$, $(\langle m' \rangle + D^s_{zz})$ and (b) $-D^s_{xz}$ for heat with $\rho C_p^+ / \rho C_p^- = 2$, $m'^+ / m'^- = 10$ and $k'^+ / k'^- = 100$. For the flow angle θ see the caption of Fig. 5.1.

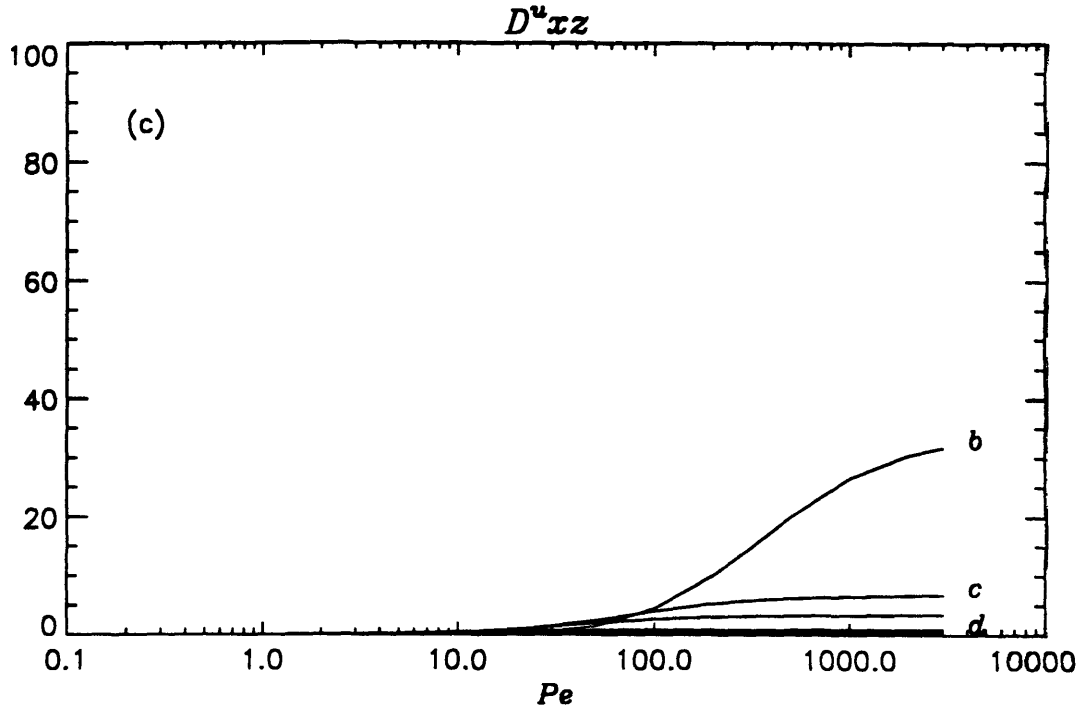

Fig. 5.4 (continued.) (c) D^u_{xz}. For the flow angle θ see the caption of Fig. 5.1.

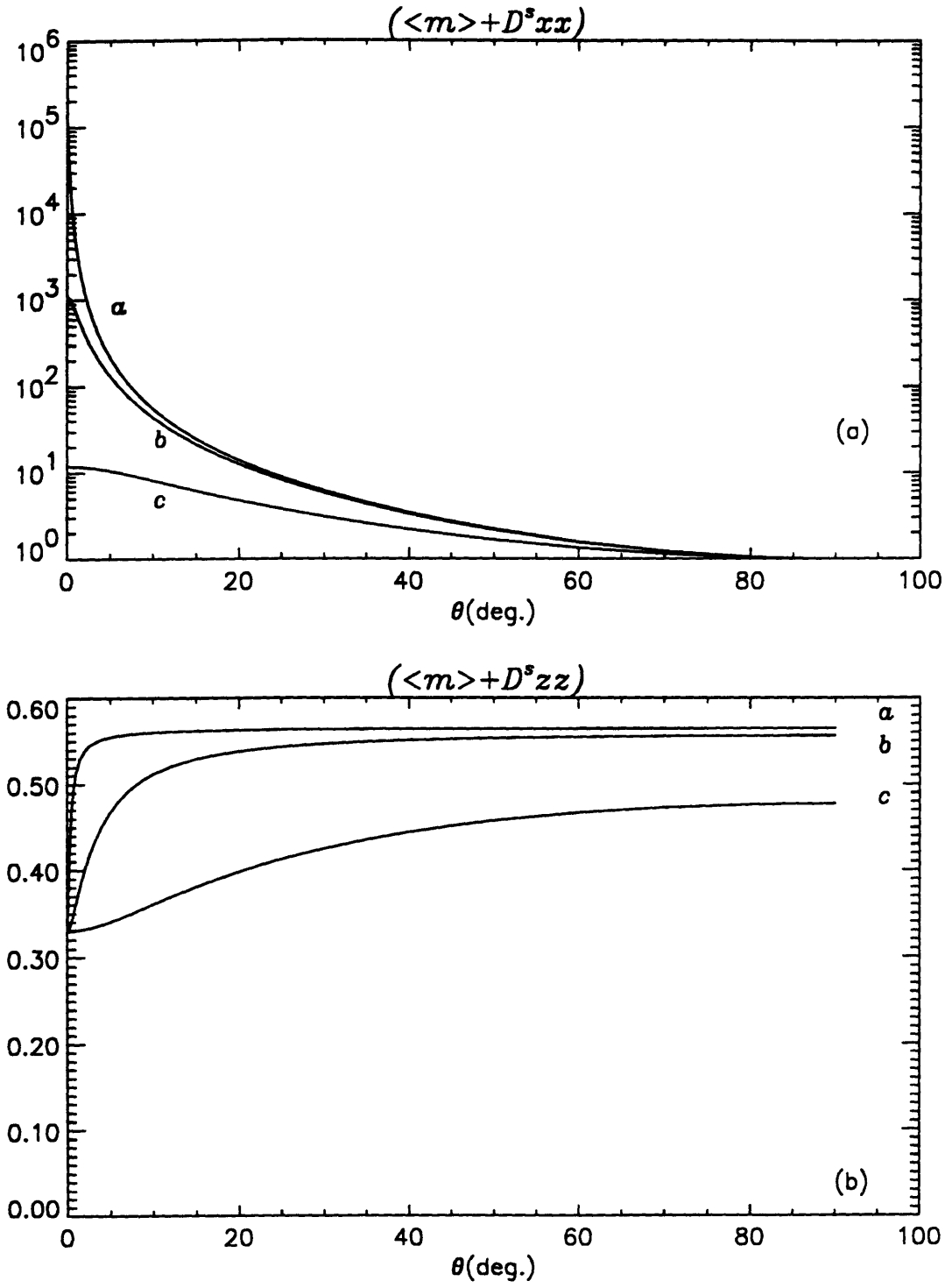

Fig. 5.5 Variation of dispersion coefficients (a) $(\langle m' \rangle + D^s_{xx})$ and (b) $(\langle m' \rangle + D^s_{zz})$ with flow angle. The Peclét numbers are *a*: $Pe' = 1000$, *b*: $Pe' = 100$ and *c*: $Pe' = 10$.

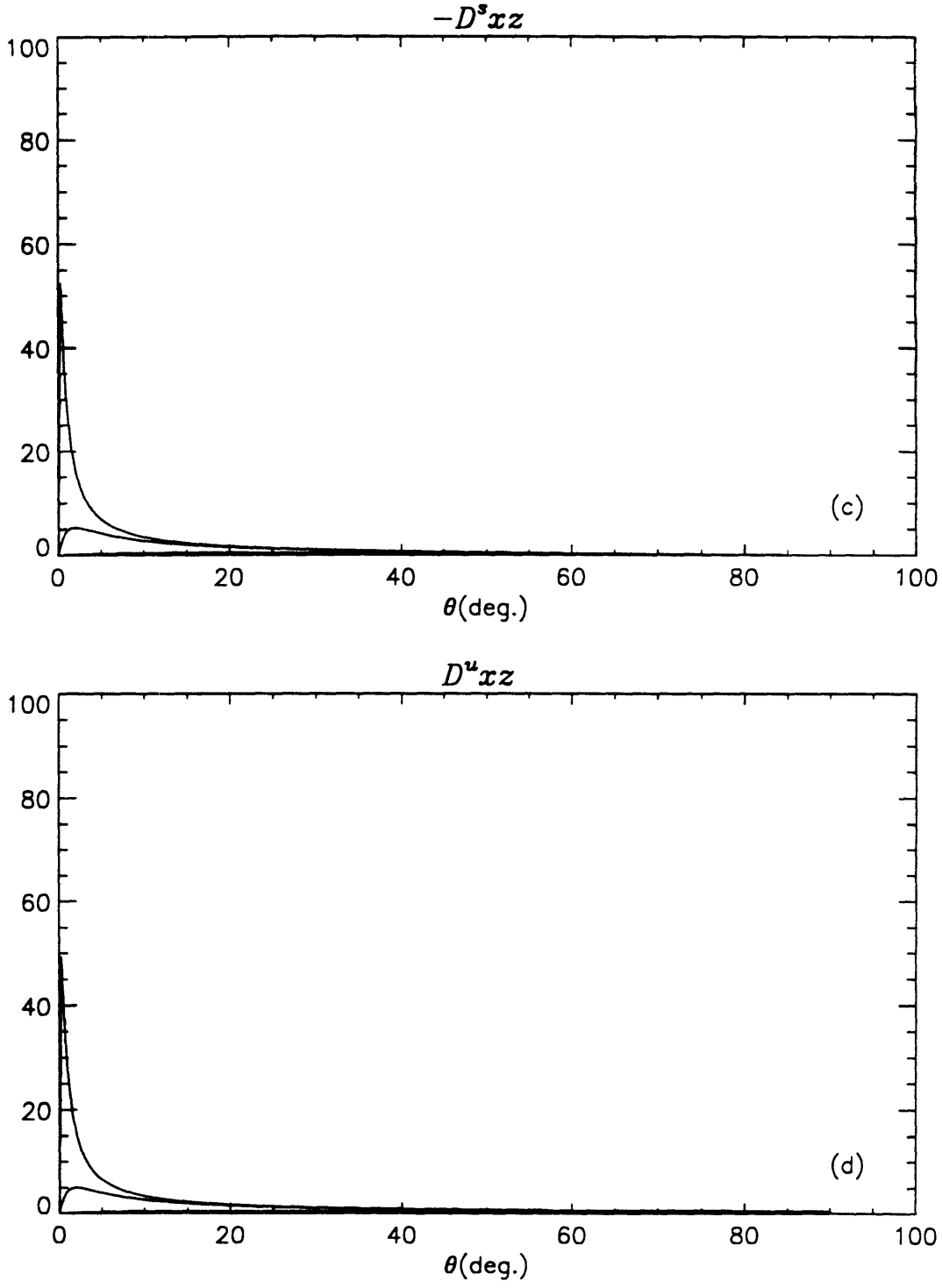

Fig. 5.5 (continued.) (c) $-D^s_{zz}$ and (d) D^u_{zz}. As Pe' decreases, the curves become lower.

The leading order convection velocity is the Darcy velocity and it requires only the macroscale permeability k''_{ij} wich has been treated in Ch. II, Part A.

The convection velocity of $O(\epsilon)$ is composed of several terms(cf.(4.3.1)). They are the Darcy type velocity weighted by $\nabla'' \cdot \left\langle \overline{\rho C_p}^* B' \right\rangle / \left\langle \overline{\rho C_p}^* \right\rangle$ which depends on induced disturbances on the macroscale, the first order seepage velocity $\langle\langle u \rangle^{(1)}\rangle$ and the spatial variation of the anti-symmetric dispersion tensor $\nabla'' \cdot (m^u + D^u)$. Each of these will be examined and the explicit forms of the coefficients are determined for the alternating layers.

The $O(\epsilon)$ correction to the Darcy velocity in (4.3.1) requires the following coefficient which can be obtaianed by using $\nabla'' \cdot \left\langle \overline{\rho C_p}^* B'_x \right\rangle$ and $\nabla'' \cdot \left\langle \overline{\rho C_p}^* B'_z \right\rangle$ in D^u_{xz} (Appendix F) as

$$\frac{\nabla'' \cdot \left\langle \overline{\rho C_p}^* B' \right\rangle}{\left\langle \overline{\rho C_p}^* \right\rangle} = \frac{\partial I_x}{\partial x''} + \frac{\partial I_y}{\partial y''} + \frac{\partial I_z}{\partial z''} \tag{5.4.1}$$

where

$$\begin{aligned}
I_x =& -\frac{\ell'}{a}\left[(1-\rho C_p^-)r^- - (1-\rho C_p^+)r^+\right]\frac{(1-s)^2}{2} \\
&- \frac{\ell'}{a}(1-\rho C_p^+)\left[(r^- - r^+)(1-s)s + \frac{r^+}{2}\right] \\
&- \frac{1}{a^2}\left[r^- m'^-(\rho C_p^- - 1)(1-s) + r^+ m'^+(\rho C_p^+ - 1)s\right] \\
&+ \frac{2}{a^3\ell'}\frac{\sinh x \sinh y}{\sinh(x+y)}\left(r^- m'^- - r^+ m'^+\right)\left[(\rho C_p^- - 1)m'^- - (\rho C_p^+ - 1)m'^+\right] \\
I_y =& I_x \quad \text{with } r^\pm \text{ replaced by } s^\pm \\
I_z =& \frac{1}{a^2}\left[\rho C_p^- m'^-(\rho C_p^- - 1)(1-s) + \rho C_p^+ m'^+(\rho C_p^+ - 1)s\right] \\
&- \frac{2}{a^3\ell'}\frac{\sinh x \sinh y}{\sinh(x+y)}\left(\rho C_p^- m'^- - \rho C_p^+ m'^+\right)\left[(\rho C_p^- - 1)m'^- - (\rho C_p^+ - 1)m'^+\right]
\end{aligned} \tag{5.4.2}$$

in which $s^\pm$ is the forcing term for the convection-diffusion equation (4.1.33) for B'_y. Thus nonuniform velocity field reflected in $r^\pm$, $s^\pm$ and $t^\pm$ and the heterogeneity in the heat capacity, thermal conductivity and permeability produce Darcy velocity correction in the convection part.

Next the first order seepage velocity requires calculation of the coefficient $\langle k' S'_z \rangle$ as shown in (4.3.7) and (4.3.8). For a medium with two alternating layers, it vanishes as shown below. We first note that

$$\int_o^{z'} \left(\frac{k'(\xi)}{k''_{zz}} - 1 \right) d\xi = \begin{cases} -s[\![k']\!]z'/k''_{zz} & 0 < z' < (1-s)\ell' \\ -[\![k']\!](1-s)(\ell' - z')/k''_{zz} & (1-s)\ell' < z' < \ell' \end{cases} \tag{5.4.3}$$

where

$$[\![k']\!] = k'^{+} - k'^{-} \tag{5.4.4}$$

It then follows from (4.3.4) that

$$\begin{aligned} \frac{\ell'}{k''_{zz}} \langle k' S'_z \rangle &= \int_o^{\ell'} dz' \left(1 - \frac{k''_{zz}}{k'(z')} \right) \int_o^{z'} \left(\frac{k'(\xi)}{k''_{zz}} - 1 \right) d\xi \\ &= -\int_o^{(1-s)\ell'} dz' \frac{k'^{-} - k''_{zz}}{k'^{-}} \frac{s[\![k']\!]}{k''_{zz}} z' dz' \\ &\quad - \int_{(1-s)\ell'}^{\ell'} dz' \frac{k'^{+} - k''_{zz}}{k'^{+}} \frac{(1-s)[\![k']\!]}{k''_{zz}} (\ell' - z') dz' \\ &= -\frac{[\![k']\!]\ell'^2}{2k''_{zz}} s(1-s) \left[\frac{k'^{-} - k''_{zz}}{k'^{-}} (1-s) + \frac{k'^{+} - k''_{zz}}{k'^{+}} s \right] \\ &= -\frac{[\![k']\!]\ell'^2}{2k''_{zz}} s(1-s) \frac{k'^{-}k'^{+} - k''_{zz}[k'^{+}(1-s) + k'^{-}s]}{k'^{-}k'^{+}} \\ &= 0 \end{aligned} \tag{5.4.5}$$

where the following has been used

$$k''_{zz} = \left(\frac{1}{\ell'} \int_o^{\ell'} \frac{1}{k'(z')} dz' \right)^{-1} = \frac{k'^{-}k'^{+}}{k'^{+}(1-s) + k'^{-}s} \tag{5.4.6}$$

As mentioned earlier, the vanishing of $\langle k' S'_z \rangle$ is the consequence of the distribution of the integrand for the alternating uniform layers and is seen from (4.3.31). The integrand $1 - k''_{zz}/k'(\xi)$ is the deviation of $k''_{zz}/k'(\xi)$ from its average value unity because $k''_{zz} = \langle k'^{-1} \rangle^{-1}$. Similarly $k'(\xi)/k''_{zz} - 1$ is the deviation of $k'(\xi)/k''_{zz}$ from the average. Their distributions are identical in a medium with two layers. Then the double integral of the type as F'''_{zzz} in (4.3.4) can be shown to be zero after an

integration by parts (cf. (B.2) in Appendix B). It readily follows from (4.3.34) and (4.3.35) that

$$\langle\langle u\rangle_x^{(1)}\rangle = \langle\langle u\rangle_y^{(1)}\rangle = \langle\langle u\rangle_z^{(1)}\rangle = 0 \tag{5.4.7}$$

Therefore the first order seepage velocity vanishes for a medium with two alternating uniform layers.

Lastly in the anti-symmetric dispersion tensor term in the convection velocity of (4.3.1), we note that $m' = 0$ is of diagonal form. We then have

$$\nabla'' \cdot (m^u + D^u) = J_x \mathbf{e}_x + J_y \mathbf{e}_y + J_z \mathbf{e}_z \tag{5.4.8}$$

where

$$\begin{aligned} J_x &= \nabla_i'' D_{ix}^u = \frac{\partial D_{yx}^u}{\partial y''} + \frac{\partial D_{zx}^u}{\partial z''} \\ J_y &= \nabla_i'' D_{iy}^u = \frac{\partial D_{xy}^u}{\partial x''} + \frac{\partial D_{zy}^u}{\partial z''} \\ J_z &= \nabla_i'' D_{iz}^u = \frac{\partial D_{xz}^u}{\partial x''} + \frac{\partial D_{yz}^u}{\partial y''} \end{aligned} \tag{5.4.9}$$

in which D_{ij}^u are calculated from $\bar{D}_{xz}^u$ of (4.2.2) by using (4.1.12). For the present two layer medium, $\bar{D}_{xz}^u$ is given by (5.1.4).

6. Thermal Dispersion in a Uniform Seepage Flow Through a Layered Medium

As an application of the general theory for 3-scale medium, we study the dispersion of a thermal cloud of finite size released in a porous layer with uniform background flow in the longitudinal direction. The medium is assumed to be composed of uniform layers alternating periodically on the mesoscale. Material properties on the macroscale such as elastic coefficients, permeability and dispersion coefficients are then anisotropic and have been analyzed in §5 of Ch.II, Part A and in §5 of the current chapter. The normalized governing equations and boundary conditions are summarized in §6.1 and then the macroscale coefficients and dimensionless parameters are discussed in §6.2. The numerical scheme based on finite differences and iterations is explained in §6.3. Numerical results for various dimensionless parameters are discussed in §6.4.

6.1 The Normalized Governing Equations and Boundary Conditions

Consider a stratum of porous medium with thickness h shown in Fig. 6.1 in which a uniform background flow in the x-direction exists. The medium is initially at uniform temperature. The lower boundary at $z = 0$ is rigid and impermeable and is maintained at the initial temperature. At the upper boundary ($z = h$), it is assumed that the pressure and temperature are kept at the initial values. It is also assumed that the upper surface is stress free.

Suppose that a thermal cloud is released in the lower part of the layer at $t = 0$. Since there exists a uniform seepage flow in the longitudinal direction, the thermal cloud is convected by the flow and spreads due to diffusion and dispersion which strongly depends on the Peclét number. If the Rayleigh number is sufficiently large, buoyancy causes upward convection which in turn modifies the flow and dispersion tensor and the transport process and flow are coupled with full nonlinearity.

At the initial state, the temperature is uniform and the solid matrix is at rest. Let the uniform seepage velocity be denoted by U. Since the x-component of the

convection velocity in the heat transport equation (3.3.25) has U, it is convenient to introduce the moving coordinate (ξ, τ) which are related to the space-fixed ones (x, t) by

$$\xi = x - \frac{(\rho C_p)_f}{\langle \rho C_p \rangle} U t, \quad \tau = t \tag{6.1.1}$$

in which $(\rho C_p)_f$ and $\langle \rho C_p \rangle$ are the heat capacities of the fluid in the convection term and the medium in the local derivative. Accordingly, the derivatives are transformed by the following relations

$$\begin{aligned} \frac{\partial}{\partial t} &= \frac{\partial}{\partial \tau} - \frac{(\rho C_p)_f}{\langle \rho C_p \rangle} U \frac{\partial}{\partial \xi} \\ \frac{\partial}{\partial x} &= \frac{\partial}{\partial \xi} \end{aligned} \tag{6.1.2}$$

Equations (6.1.1) and (6.1.2) are used to rewrite the governing equations in the moving frame.

6.1.1 The Governing Equations

In the moving frame, the uniform background flow is absent. For simpler notation, the macroscale Darcy velocity is denoted by a single pair of brackets. The consolidation equation (3.2.5) and the heat transport equation (3.3.25) then become in physical variables

$$\frac{\partial \langle u \rangle_x}{\partial \xi} + \frac{\partial \langle u \rangle_z}{\partial z} = 0 \tag{6.1.3}$$

$$\begin{aligned} &\langle \rho C_p \rangle \frac{\partial \theta}{\partial \tau} + (\rho C_p)_f \left(V_x \frac{\partial \theta}{\partial \xi} + V_z \frac{\partial \theta}{\partial z} \right) = \\ &\frac{\partial}{\partial \xi} \left[(\langle m' \rangle + D^e_{xx}) \frac{\partial \theta}{\partial \xi} + D^e_{xz} \frac{\partial \theta}{\partial z} \right] + \frac{\partial}{\partial z} \left[D^e_{xz} \frac{\partial \theta}{\partial \xi} + (\langle m' \rangle + D^e_{zz}) \frac{\partial \theta}{\partial z} \right] \end{aligned} \tag{6.1.4}$$

where the Darcy velocities $\langle u \rangle_x$ and $\langle u \rangle_z$ in (6.1.3) are given from (3.2.7) in physical variables by

$$\begin{aligned} \langle u \rangle_x &= - k''_{xx} \frac{\partial p}{\partial \xi} \\ \langle u \rangle_z &= - k''_{zz} \left(\frac{\partial p}{\partial z} - \rho_f g \beta_T \theta \mathbf{e}_z \right) \end{aligned} \tag{6.1.5}$$

They are the Darcy velocities observed in the moving frame. From (4.3.1) the convection velocity in (6.1.4) is given by

$$\begin{aligned} V_x &= \langle u \rangle_x + \left[\langle u \rangle_x^{(1)} + (\nabla \cdot \langle \rho C_p B' \rangle) \langle u \rangle_x - \frac{1}{(\rho C_p)_f} \frac{\partial D_{xz}^u}{\partial z} \right] \\ V_z &= \langle u \rangle_z + \left[\langle u \rangle_z^{(1)} + (\nabla \cdot \langle \rho C_p B' \rangle) \langle u \rangle_z - \frac{1}{(\rho C_p)_f} \frac{\partial D_{zz}^u}{\partial z} \right] \end{aligned} \tag{6.1.6}$$

Recall that D_{ij}^e and D_{ij}^u depend on the local macroscale flow velocity and the flow direction, which are affected by temperature. The part $\langle u \rangle_i^{(1)}$ is the first order seepage velocity considered in §5 and vanishes for the present medium with alternating layers on the mesoscale, as shown before. The coefficient $\nabla \cdot \langle \rho C_p B' \rangle$ has been given in (5.4.1). The convection velocities in brackets in (6.1.6) are very small,e.g. $O(\epsilon)$ as compared with the first terms. It should be noted that the dispersion tensor depends on the sum of uniform velocity U and the Darcy velocity of (6.1.5) induced by introducing thermal cloud.

The equilibrium equation (3.2.1) becomes in physical variables as

$$\begin{aligned} \frac{\partial \sigma_{xx}}{\partial \xi} + \frac{\partial \sigma_{xz}}{\partial z} &= 0 \\ \frac{\partial \sigma_{xz}}{\partial \xi} + \frac{\partial \sigma_{zz}}{\partial z} &= -n'' \rho_f g \beta_T \theta \end{aligned} \tag{6.1.7}$$

in which the stress components are given by Hooke's law as

$$\begin{aligned} \sigma_{xx} &= a_1 \frac{\partial u}{\partial \xi} + a_4 \frac{\partial w}{\partial z} - \alpha_{xx}'' p - (\beta_t'')_{xx} \theta \\ \sigma_{xz} &= a_6 \left(\frac{\partial u}{\partial z} + \frac{\partial w}{\partial \xi} \right) \\ \sigma_{zz} &= a_2 \frac{\partial w}{\partial z} + a_4 \frac{\partial u}{\partial \xi} - \alpha_{zz}'' p - (\beta_t'')_{zz} \theta \end{aligned} \tag{6.1.8}$$

The elastic coefficients a_1, a_2, a_4 and a_6 are equal to a''_{xxxx}, a''_{zzzz}, a''_{xxzz} and a''_{xzxz} studied in §6 in Ch.II of Part A. Because of the cubic symmetry of the Wigner-Seitz grains on the microscale the medium is orthotropic on the macroscale. Also the anisotropic pressure coefficients and thermal moduli have been considered there.

In the present problem of thermal dispersion in uniform seepage flow, the disturbances are induced by thermal cloud. The scales of the macroscale variables then

must be estimated from the governing equations (6.1.3) to (6.1.5) and (6.1.7) and (6.1.8) based on the temperature variation in the medium. Also the anisotropy of the macroscale permeability is taken into consideration in the scaling of the seepage velocity and the spatial coordinates. Let the temperature of thermal cloud introduced be higher than the initial value by Θ''. Taking Θ'' as the normalization scale for θ, the pore pressure is scaled by $P = \rho_f g \beta_T \Theta'' h$ in the z-component of Darcy's law (6.1.5). The indeced seepage velocities are then $\langle u \rangle_x = O(k''_{xx} \rho_f g \beta_T \Theta'')$ and $\langle u \rangle_z = O(k''_{zz} \rho_f g \beta_T \Theta'')$ respectively. From Hooke's law (6.1.8), the medium displacement is then scaled by $u, w = O(B\Theta'' h/\mathcal{D})$ where $\mathcal{D}$ and B are the scales of elastic coefficient and thermal modulus. We summarize the normalization scales as

$$\begin{aligned}
&\xi \sim \sqrt{\frac{k''_{xx}}{k''_{zz}}} h = k_r^{1/2} h, \quad z \sim h, \quad t \sim \frac{h^2}{\alpha_m} \\
&\theta \sim \Theta'', \quad p \sim \rho_f g \beta_T \Theta'' h \\
&\langle u \rangle_x \sim k''_{xx} \rho_f g \beta_T \Theta'', \quad \langle u \rangle_z \sim k''_{zz} \rho_f g \beta_T \Theta'' \\
&u, w \sim \frac{B\Theta'' h}{\mathcal{D}}
\end{aligned} \tag{6.1.9}$$

in which α_m is the thermal diffusivity of the medium. The ratio

$$k_r = \frac{k''_{xx}}{k''_{zz}} \tag{6.1.10}$$

is a measure of permeability anisotropy. The normalization scales for the spatial coordinates have been chosen differently to make the consolidation equation and thus the convection velocity of heat expressed in terms of p be of isotropic form. The symmetric and anti-symmetric dispersion tensors are normalized by the thermal conductivity M_m of the medium so that

$$\langle m' \rangle, \quad D^s_{ij}, \quad D^u_{ij} \sim M_m \tag{6.1.11}$$

These scale estimates are used to normalize the governing equations and boundary conditions.

By substituting (6.1.9) into (6.1.3), the consolidation equation becomes in dimensionless variables

$$\frac{\partial^2 p}{\partial \xi^2} + \frac{\partial}{\partial z}\left(\frac{\partial p}{\partial z} - \theta\right) = 0 \tag{6.1.12}$$

The Darcy's law (6.1.5) then becomes

$$\begin{aligned} \langle u \rangle_x &= -\frac{1}{k_r^{1/2}} \frac{\partial p}{\partial \xi} \\ \langle u \rangle_z &= -\left(\frac{\partial p}{\partial z} - \theta\right) \end{aligned} \tag{6.1.13}$$

The normalized heat transport equation is similarly obtained by using (6.1.9) to (6.1.11) in (6.1.4) to (6.1.6). While the normalization of the local derivative and dispersion terms is simple, the convection terms are treated as follows. For example, the ratio of x-direction term to dispersion term $\langle m' \rangle \Theta''/h^2$ becomes

$$\begin{aligned} \frac{(\rho C_p)_f V_x \partial\theta/\partial\xi}{\langle m' \rangle \Theta''/h^2} &\simeq \frac{(\rho C_p)_f}{M_m} \frac{k''_{xx} \rho_f g \beta_T \Theta'' h}{k_r^{1/2}} = \sqrt{\frac{k''_{xx}}{k''_{zz}}} \frac{k''_{zz} \rho_f g \beta_T \Theta'' h}{\alpha_f} \frac{M_f}{M_m} \\ &= \frac{M_f}{M_m} k_r^{1/2} Ra' \end{aligned} \tag{6.1.14}$$

where

$$Ra' = \frac{k''_{zz} \rho_f g \beta_T \Theta'' h}{\alpha_f} \tag{6.1.15}$$

is the Rayleigh number defined in terms of the vertical permeability of the medium and the macroscale length h. It is of $O(\epsilon^{-1})$ and is large. For the convection term in z-direction, since $V_z = V_x/k_r$ and $\xi = k_r^{1/2} z$, the ratio simply becomes $Ra' M_f/M_m$. The normalized heat equation then becomes

$$\begin{aligned} &\frac{\partial \theta}{\partial \tau} + \frac{M_f}{M_m} Ra' \left(k_r^{1/2} V_x \frac{\partial \theta}{\partial \xi} + V_z \frac{\partial \theta}{\partial z}\right) \\ &\quad = \frac{\partial}{\partial \xi}\left(\frac{\langle m' \rangle + D^*_{xx}}{k_r} \frac{\partial \theta}{\partial \xi} + \frac{D^*_{xz}}{k_r^{1/2}} \frac{\partial \theta}{\partial z}\right) + \frac{\partial}{\partial z}\left(\frac{D^*_{xz}}{k_r^{1/2}} \frac{\partial \theta}{\partial \xi} + (\langle m' \rangle + D^*_{zz}) \frac{\partial \theta}{\partial z}\right) \end{aligned} \tag{6.1.16}$$

If we invoke (6.1.11) and Darcy's law (6.1.13) and the fact that $\langle u\rangle_z^{(1)}$ vanishes in (6.1.6), the convection terms further become as follows.

$$
\begin{aligned}
&k_r^{1/2} V_z \frac{\partial \theta}{\partial \xi} \\
&\quad = \left\{ -\left[1 + \epsilon \left(\frac{1}{k_r^{1/2}} \frac{\partial \langle \rho C_p B_z' \rangle}{\partial \xi} + \frac{\partial \langle \rho C_p B_z' \rangle}{\partial z} \right) \right] \frac{\partial p}{\partial \xi} + \frac{M_m}{M_f} \frac{1}{k_r^{1/2}} \frac{\partial D_{zz}^u}{\partial z} \right\} \frac{\partial \theta}{\partial \xi} \\
&V_z \frac{\partial \theta}{\partial z} = \frac{\partial \theta}{\partial z} \times \\
&\left\{ -\left[1 + \epsilon \left(\frac{1}{k_r^{1/2}} \frac{\partial \langle \rho C_p B_z' \rangle}{\partial \xi} + \frac{\partial \langle \rho C_p B_z' \rangle}{\partial z} \right) \right] \left(\frac{\partial p}{\partial z} - \theta \right) - \frac{M_m}{M_f} \frac{1}{k_r^{1/2}} \frac{\partial D_{zz}^u}{\partial \xi} \right\}
\end{aligned}
\tag{6.1.17}
$$

in which ϵ is the ratio of the mesoscale ℓ' to the macroscale ℓ'' and is much smaller than unity. Notice that, due to buoyancy, the heat transport equation (6.1.16) is coupled to the consolidation equation (6.1.12). In addition to the full nonlinearity of the convection terms in (6.1.17), the dispersion terms on the right-hand side of (6.1.16) are also nonlinearly coupled to the flow field because of the dependence of dispersion tensors on the flow.

Recall that the dispersion coefficients depend not only on the Peclét number but also on the local macroscale flow direction in the layered medium. We now express these in terms of the normalized variables. Let $\overline{Pe}_f$ and Pe_m be the Peclét numbers of the initial uniform flow U and the combined flow of the uniform flow and the induced flow respectively i.e.,

$$
\overline{Pe}_f = \frac{Uh}{\alpha_f}, \qquad Pe_m = \frac{1}{\alpha_m} \left[(U + \langle u\rangle_z)^2 + \langle u\rangle_z^2 \right]^{\frac{1}{2}} h \tag{6.1.18}
$$

where α_f and α_m are the thermal diffusivities of the fluid and the medium respectively. Note that Pe_m varies with time and in space. It follows that

$$
Pe_m = \frac{Uh}{\alpha_m} \left[\left(1 + \frac{\langle u\rangle_z}{U} \right)^2 + \left(\frac{\langle u\rangle_z}{U} \right)^2 \right]^{\frac{1}{2}} \tag{6.1.19}
$$

If we substitute (6.1.9) and (6.1.18) into (6.1.19), it becomes in dimensionless variables

$$
Pe_m = \overline{Pe}_m \left[\left(1 + \frac{k_{zz}''}{k_{zz}''} \frac{Ra'}{\overline{Pe}_f} \langle u\rangle_z \right)^2 + \left(\frac{Ra'}{\overline{Pe}_f} \langle u\rangle_z \right)^2 \right]^{\frac{1}{2}} \tag{6.1.20}
$$

where

$$\overline{Pe}_m = \frac{\alpha_f}{\alpha_m}\overline{Pe}_f \tag{6.1.21}$$

and $\langle u\rangle_x$ and $\langle u\rangle_z$ are given by Darcy's law (6.1.13).

Let the angle between the local flow and x-axis, which is measured positive counterclockwise in xz-plane, be denoted by θ (which is different from that used to denote the temperature). It readily follows from (6.1.18) and (6.1.20) that

$$\theta = \arctan\left(\frac{\langle u\rangle_z}{U+\langle u\rangle_x}\right) = \arctan\left[\frac{Ra'}{\overline{\overline{Pe}}_f}\langle u\rangle_z \Big/ \left(1+\frac{k''_{xz}}{k''_{zz}}\frac{Ra'}{\overline{\overline{Pe}}_f}\langle u\rangle_x\right)\right] \tag{6.1.22}$$

We note again that both Pe_m and θ vary and so do the dispersion coefficients. Since U and θ are coupled, equations (6.1.19) and (6.1.22) show that the thermal dispersion in (6.1.16) is inherently a nonlinear phenomenon.

Finally by substituting the normalization scales of (6.1.9) into (6.1.7) and (6.1.8), the equilibrium equation becomes in dimensionless variables

$$\begin{aligned}
&\frac{1}{k_r^{1/2}}\frac{\partial \sigma_{xx}}{\partial \xi} + \frac{\partial \sigma_{xz}}{\partial z} = 0\\
&\frac{1}{k_r^{1/2}}\frac{\partial \sigma_{xz}}{\partial \xi} + \frac{\partial \sigma_{zz}}{\partial z} = -n''c\theta
\end{aligned} \tag{6.1.23}$$

where

$$c = \frac{\rho_f g \beta_T h}{B} \tag{6.1.24}$$

is the ratio of the body force due to buoyancy to thermal stress. Hooke's law similarly becomes

$$\begin{aligned}
\sigma_{xx} =& \frac{a_1}{k_r^{1/2}}\frac{\partial u}{\partial \xi} + a_4\frac{\partial w}{\partial z} - c\alpha''_{xx}p - (\beta''_t)_{xx}\theta\\
\sigma_{xz} =& a_6\left(\frac{\partial u}{\partial z} + \frac{1}{k_r^{1/2}}\frac{\partial w}{\partial \xi}\right)\\
\sigma_{zz} =& a_2\frac{\partial w}{\partial z} + \frac{a_4}{k_r^{1/2}}\frac{\partial u}{\partial \xi} - c\alpha''_{zz}p - (\beta''_t)_{zz}\theta
\end{aligned} \tag{6.1.25}$$

6.1.2 The Stream Function

Let ψ be the stream function which is defined by

$$\langle u \rangle_x = \frac{\partial \psi}{\partial z}, \qquad \langle u \rangle_z = -\frac{\partial \psi}{\partial \xi} \tag{6.1.26}$$

The mass conservation equation (6.1.3) is then automatically satisfied by ψ. Combining (6.1.5) and (6.1.26), we have in physical variables

$$\begin{aligned} \frac{\partial \psi}{\partial z} &= -k''_{xx}\frac{\partial p}{\partial \xi} \\ \frac{\partial \psi}{\partial \xi} &= k''_{zz}\left(\frac{\partial p}{\partial z} - \rho_f g \beta_T \theta \mathbf{e}_z\right) \end{aligned} \tag{6.1.27}$$

If we take the curl of (6.1.27), it becomes

$$\frac{1}{k''_{xx}}\frac{\partial^2 \psi}{\partial z^2} + \frac{1}{k''_{zz}}\frac{\partial^2 \psi}{\partial \xi^2} = -\rho_f g \beta_T \frac{\partial \theta}{\partial \xi} \tag{6.1.28}$$

In view of different velocity scales for $\langle u \rangle_x$ and $\langle u \rangle_z$ in (6.1.9), we let the scale of ψ be

$$\psi \sim \sqrt{k''_{xx} k''_{zz}}\rho_f g \beta_T \Theta'' h \tag{6.1.29}$$

After using (6.1.9) and (6.1.29), (6.1.28) is written in dimensionless variables as

$$\frac{\partial^2 \psi}{\partial \xi^2} + k_r \frac{\partial^2 \psi}{\partial z^2} = -\frac{\partial \theta}{\partial \xi} \tag{6.1.30}$$

6.1.3 The Initial and Boundary Conditions

On the lower boundary at $z = 0$, the solid displacements, temperature variation and normal flux of seepage flow are zero so that

$$u = w = \theta = \frac{\partial p}{\partial z} = 0 \qquad \text{at} \quad z = 0 \tag{6.1.31}$$

On the upper boundary at $z = 1$, the excessive pore pressure, the temperature variation and the traction forces are zero and thus the following conditions are imposed.

$$\begin{aligned} p &= \theta = 0 \\ \sigma_{zz} &= a_2 \frac{\partial w}{\partial z} + \frac{a_4}{k_r^{1/2}}\frac{\partial u}{\partial \xi} = 0 \qquad \text{at } z = 1 \\ \sigma_{xz} &= a_6\left(\frac{\partial u}{\partial z} + \frac{1}{k_r^{1/2}}\frac{\partial w}{\partial \xi}\right) = 0 \end{aligned} \tag{6.1.32a-c}$$

in which (6.1.32a) has been used in (6.1.32b and c). Note that neither u nor w is known a priori at $z = 1$. At infinity all disturbances vanish so that

$$u = w = p = \theta = 0 \qquad \text{as} \quad \xi \to \pm\infty \tag{6.1.33}$$

At $t = 0$, a thermal cloud of finte size and uniform temperature is released at $\xi = 0$. For numerical convenience, the cloud is of diamond shape (Fig. 6.1) and the distances along the diagonals are equal in ξ and z directions They are chosen as 0.4. The actual shape in the xz plane is much elongated because of the strained coordinate in (6.1.9). The initial condition in normalized temperature is then

$$\theta = \begin{cases} 1 & (\xi, z) \in \Omega_h, \quad t = 0 \\ 0 & (\xi, z) \notin \Omega_h, \quad t = 0 \end{cases} \tag{6.1.34}$$

where Ω_h is the region for thermal cloud at $t = 0$.

The boundary conditions for the stream function ψ are obtained by using (6.1.31) to (6.1.33). In (6.1.30), ψ is arbitrary upto a constant and we choose the value of ψ at the lower impermeable boundary to be zero. It then follows from (6.1.26) that

$$\begin{aligned} \psi &= 0 && \text{at} \quad z = 0 \\ \frac{\partial \psi}{\partial z} &= 0 && \text{at} \quad z = 1 \\ \frac{\partial \psi}{\partial \xi} &= 0 && \text{as} \quad \xi \to \pm\infty \end{aligned} \tag{6.1.34}$$

The above boundary conditions must be incorporated into the governing equations of the previous section.

6.2 The Macroscale Coefficients and Dimensionless Parameters

On the mesoscale, the two layers are assumed to be of equal thickness so that we have $s = 0.5$. The porosity values were chosen as 0.284 and 0.716 for the lower and upper layers respectively. Assuming that the microcell is of Wigner-Seitz type

studied in two-scale medium, we summarize the coefficients from §5 of Ch.I, Part A as follows.

$$\begin{array}{ll} 1-s=0.5 & s=0.5 \\ n'^{-}=0.284 & n'^{+}=0.716 \\ a_I^{-}=0.62428 & a_I^{+}=0.088977 \\ a_{II}^{-}=0.19218 & a_{II}^{+}=0.0063776 \\ a_{III}^{-}=0.17576 & a_{III}^{+}=0.015477 \\ \alpha'^{-}=0.59654 & \alpha'^{+}=0.95931 \\ \beta_t'^{-}=1.00864 & \beta_t'^{+}=0.101732 \end{array} \tag{6.2.1}$$

Also for the permeability k', heat capacity ρC_p and thermal conductivity m', in view of the fact that k' varies widely but ρC_p and m' do only mildly, we choose

$$\begin{array}{ll} k'^{-}=100 & k'^{+}=1 \\ m'^{-}=10 & m'^{+}=1 \\ \rho C_p^{-}=1 & \rho C_p^{+}=1.14 \end{array} \tag{6.2.2}$$

Assuming relatively highly porous medium, some typical values for sandy material (Jumikis, 1977 ; see also §7.4 in Ch.I, Part A) have been chosen for the following ratios.

$$(\rho C_p)_m/(\rho C_p)_f=0.79, \quad M_m/M_f=1.924 \quad ; \quad \alpha_m/\alpha_f=2.44 \tag{6.2.3}$$

Employing the explicit forms for the macroscale coefficients derived in §6 of Ch.II, Part A, we obtain

$$\begin{array}{ll} a_1=a''_{zzzz}=0.33243 & a_2=a''_{zzzz}=0.15575 \\ a_4=a''_{zzzz}=0.02956 & a_6=a''_{zzzz}=0.02845 \\ \alpha''_{zz}=0.82518 & \alpha''_{zz}=0.91405 \\ (\beta''_t)_{zz}=0.43706 & (\beta''_t)_{zz}=0.21487 \\ k''_{zz}=1 & k''_{zz}=0.03921 \\ m''_{zz}=1 & m''_{zz}=0.33058 \end{array} \tag{6.2.4}$$

These values have been used in the computations. From the values of k''_{zz} and k''_{zz}, the anisotropy ratio k_r of permeability becomes

$$k_r=\frac{k''_{zz}}{k''_{zz}}=25.5 \quad ; \quad k_r^{\frac{1}{2}}=5.05 \tag{6.2.5}$$

so that the width of the thermal cloud in Fig. 6.1 is 5 times larger than the height in the actual shape.

There are two important dimensionless parameters, the Peclét and Rayleigh numbers. We estimate their order of magnitudes by using some typical values for groundwater flow. The hydraulic gradient in field situations lies in the range of $O(10^{-3}-10^{-2})$ (Gelhar, 1986). By using the hydraulic conductivity values for sands in the range $K = O(10^{-4} - 10^{-7}m/s)$, we obtain that the seepage velocity is of $O(10^{-5}m/s)$ or less which is at most $1(m/\text{day})$. Taking $\alpha_f = 10^{-7}(m^2/s)$ typical of water and $h < O(10^2 m)$, the Peclét number $\overline{Pe_f}$ (cf.(6.1.18)) for the uniform background flow is estimated to be $\overline{Pe_f} \leq O(10^3)$. If the scale ratio $\epsilon = 10^{-2}$ is used, the mesoscale Peclét number $Pe' = \epsilon\overline{Pe_f}$ becomes $O(10)$ or less which is in the range assumed earlier in §3. On the other hand, if we use $\beta_T = 10^{-4}(1/°C)$ and allow $\Theta'' < O(10^2 °C)$, the Rayleigh number in (6.1.15) is estimated to be in the range $O(10 - 10^4)$. Since Ra' is defined in terms of the permeability in the vertical direction, it is expected to be in the lower region of the range i.e., $O(10^2)$ or less. Based on these estimates, we consider the following cases

	Ra'	$\overline{Pe_f}$
Case(i)	10	1000, 2000
Case(ii)	100	1000, 2000
Case(iii)	200	1000, 2000

(6.2.6)

As Ra' increases, the buoyancy effect also increases causing thermal cloud to rise fast. For two different $\overline{Pe_f}$ values, the effect of dispersion will also be examined. The ratio of buoyant force to thermal stress c in (6.1.24) has been chosen to be unity. We now move the numerical scheme.

6.3 Numerical Scheme

Finite differences are used to solve the initial boundary value problem defined in §6.1. Choosing the location at which thermal cloud is released as $\xi = 0$, the horizontal extent of the computational domain is truncated at large distances in both positive and negative ξ directions, which were sufficiently large to ensure that the numerical results are not affected by further increase in ξ. Specifically centered difference for spatial derivatives and implicit time marching scheme have been used in approximating the governing equations and boundary conditions. Basic finite

difference approximations were shown in Appendix D of Part A. The finite difference forms of the equations are listed in Appendix G. We only describe the computational procedure.

At each time step, the computation is performed in two steps. In the first step, the nonlinearly coupled consolidation equation (6.1.12) and the heat transport equation (6.1.16) are solved for p and θ. In the next step, the pressure and temperature field determined in the first step is used to calculate the matrix deformation by solving the equilibrium equation (6.1.23) together with Hooke's law (6.1.25). Both steps require a number of iterations.

Suppose that computations have been completed upto n-th time step. Advancing to $(n+1)$-th time step is performed as follows.

(i) Take n-th time step results for $f^n(f = p, \theta', D^s_{ij}, D^u_{ij})$ as the trial values for the first iteration values for ${}^1\theta^{n+1}$ in the heat transport equation where the superscript on the left shoulder denotes the iteration count.

(ii) Use ${}^1\theta^{n+1}$ in the consolidation equation to solve for the first iteration values ${}^1p^{n+1}$.

(iii) Use ${}^1\theta^{n+1}$ and ${}^1p^{n+1}$ to calculate the convection velocity and dispersion tensors ${}^1D^s_{ij}{}^{n+1}$ and ${}^1D^u_{ij}{}^{n+1}$.

(iv) Repeat steps (i) to (iii) until the difference in the solution values of two consecutive iterations becomes negligibly small,e.g.

$$|{}^{k+1}f^{n+1} - {}^kf^{n+1}|/|{}^kf^{n+1}| < \delta \tag{6.3.1}$$

(v) Use θ^{n+1} to solve for the stream function in (6.1.28).

(vi) Use θ^{n+1} and p^{n+1} and take $f^n(f = u, w)$ as the trial values on the upper boundary $(z = 1)$ to solve for the first iteration valus of ${}^1f^{n+1}(f = u, w)$.

(vii) Repeat step (vi) until satisfactory convergence is achieved in ${}^kf^{n+1}(f = u, w)$ by the criterion of (6.3.1). The computation for $(n+1)$-th time step is now

complete and ready to move to the next time step. In real computations, $\delta = 10^{-6}$ has been used.

We note that the use of centered difference in the convection term can cause instability of numerical scheme leaving some oscillations in the results. In order to prevent such behavior, it is recommended by Roache(1977) and Pinder and Gray(1977) in one-dimensional problem that the grid Peclét number $Pe_g = V\Delta/\alpha$ be less than 2. The quantities V, Δ and α are the convection velocity, grid spacing and diffusion coefficient and correspond to roughly $Ra'M_f/M_m$, $\Delta\xi$ (or Δz), and $(\langle m' \rangle + D^s_{xz})/k_r$ in (6.1.16). Care has been taken to avoid oscillations in the computation. Finite difference meshes of $\Delta\xi = \Delta z = 0.05$ for $Ra' \leq 100$ and $\Delta\xi = \Delta z = 0.0333$ for $Ra' = 200$ were fine enough to avoid such oscillations.

6.4 Numerical Results and Discussions

The numerical results for Cases (i), (ii) and (iii) specified in (6.2.6) are presented. In Case (i), the medium response are discussed in terms of temperature, streamlines, pore pressure and displacements. Cases (ii) and (iii) are then examined with primary emphasis on the increased effects of nonlinear coupling between the flow and heat transport as the Rayleigh number increases. In particular, it is shown for sufficiently large Rayleigh number that the thermal cloud does not only travels downstream with the background uniform seepage flow but also rises vertically. It is also shown that, in the early stage when the Rayleigh number is large, the variation of the horizontal dispersion coefficient becomes large and is comparable to the value of the unifrom flow itself and thus the rising pattern is not symmetric about the centerline.

The three case of (6.2.6) are now examined. The scale ratio has been chosen as $\epsilon = 0.01$ in all cases.

Case(i) $Ra' = 10$; $\overline{Pe_f}$=1000, 2000

The mesoscale Peclét number $Pe' = \epsilon\overline{Pe_f}$ is 10 and 20 respectively. For the uniform background seepage flow before the thermal cloud is introduced, the longitudinal dispersion coefficient is $\langle m' \rangle + D^e_{zz} = 41.6$ for $\overline{Pe_f} = 1000$ and 163.5 for $\overline{Pe_f} = 2000$.

The case with $\overline{Pe_f} = 1000$ is discussed first. The distributions of the temperature θ, the streamlines ψ=constant, the pressure p, the vertical displacement w and the horizontal displacement u in the moving frame are presented in Fig. 6.2(a)-(e). The actual horizontal distance is 5 times larger than shown because of (6.2.5). Since the Rayleigh number is not sufficiently large*, the thermal cloud stays very close where it is released as is shown in Fig. 6.2(a). Beyond $t = 0.1$, the buoyancy effect becomes too weak and the temperature becomes evenly distributed in the layer. However, due to local heating, the pore fluid flows through the medium as shown in the plot of streamlines in Fig. 6.2(b) even if the motion is very weak. A pair of counter rotating cells is formed symmetrically about $\xi = 0$. The upward velocity $\langle u \rangle_z$ in the central region above $\xi = 0$ is 0.35, 0.2 and 0.05 at t=0.004, 0.01 and 0.04 respectively. At the upper boundary, the pressure variation is zero. Thus the fluid flows out of the layer in the central region due to buyant convection but recharges the layer in the outer region, affected by the rotating motion in the layer. In Fig.6.2(c), as the pore fluid rises along the centerline, the pressure becomes negative in the lower region because of the impermeable boundary at the bottom whereas it becomes slightly positive above the cloud since the pore fluid is being pushed upward by the flow. The medium deformation is dominantly affected by thermal stress so that the vertical displacement w becomes positive symmetrically in the center region but the horizontal displacement u is anti-symmetric in Figs. 6.2(d) and (e). The maximmum values occur on the upper traction free boundary. In Fig. 6.3, the displacements on the upper boundary are shown. At the early time, there are little compacting bowls next to the sharp swelling peak and as time

* As a heuristic reference, the critical Rayleigh number in Lapwood problem is 40.

increases they flatten out. The compacting bowls are created because of pressure variation. In the region outside the thermal cloud, the counter-rotating flow directs downwards as shown in Fig. 6.2(b). Since the buoyancy effect is negligibly small there, the flow is driven mostly by pressure gradient. Thus the body force term due to pore pressure change in the z-component of the equilibrium equation (cf.(6.1.7) and (6.1.8)) acts downwards and its effect shows as subsidence at the upper boundary. The time-varying distribution of the dispersion coefficient $\langle m' \rangle + D^e_{zz}$ is shown in Fig. 6.4. Recall that its value is 41.6 for the uniform seepage flow for $\overline{Pe}_f = 1000$. In the lower left part, the rotational convection of pore fluid tends to increase the downstream seepage velocity but decrease in the lower right part. At the early time in the upper region, the flow pattern is opposite due to the counter-rotating flow. Thus the dispersion coefficient is smaller and larger respectively in the left and right regions to $\xi = 0$. As a result, the dispersion coefficient changes to 41.9 to 41.4 respectively. We note that the spatial variation of $\langle m' \rangle + D^e_{zz}$ is from the nonlinear coupling between the flow and temperature in the equations of consolidation and heat transport since the dispersion coefficient depends on the flow which in turn depends on the temperature. As the temperature decreases with time, the dispersion coefficient approaches that of the uniform flow.

For $\overline{Pe}_f = 2000$, the numerical results are presented for θ, ψ, p, w and u in Fig. 6.5(a)-(e). While the vertical dispersion coefficient $\langle m' \rangle + D^e_{zz}$ remains very close to the value $m''_{zz} = 0.33$ because of the layered structure of the medium (cf.§5.3)), the horizontal dispersion coefficient $\langle m' \rangle + D^e_{zz}$ becomes 4 times larger than $\overline{Pe}_f = 1000$ case. It is then anticipated that the spreading of thermal cloud is twice as fast as in the ξ direction. The computation has been performed in the region $-8 < \xi < 8$ but the results are shown only over $-4 < \xi < 4$. It is clearly shown that the region over which noticeable changes occur is almost doubled in the horizontal extent for θ, ψ, p, w and u. Note that the peak temperature is only half of the previous case at all times. The upward velocity $\langle u \rangle_z$ along $\xi = 0$ is 0.2 and 0.08 at t=0.004 and 0.01 respectively and is smaller than the case of $\overline{Pe}_f = 1000$ due to fast spreading of θ. It continues to decrease as t increases. The displcements at the upper boundary are

shown in Fig. 6.6 for several discrete times. Recall that the equilibrium equation is decoupled from others and is linear. Because of the dominant effect of thermal stress, the deformation is almost one half of the case with $\overline{Pe_f} = 1000$ except the very early time $t = 0.04$. The spatial variation of the dispersion coefficient is very minor as shown in Fig. 6.7.

Case(ii) $Ra' = 100$; $\overline{Pe_f}$=1000, 2000

The Rayleigh number is now increased to 100 and more pronounced nonlinear coupling effect in the convection of heat is anticipated.

The distributions of θ, ψ, p, w and u at discrete times are shown in Fig. 6.8(a)-(e) for the case of $\overline{Pe_f} = 1000$. Due to increased buoyancy, the thermal cloud rises from $z = 0.2$ to $z = 0.4$ for t upto 0.04. Note the slight asymmetry of cloud temperature at early times ($t \leq 0.01$). It is due to the nonlinear coupling between flow and themperature and the reason is as follows. Because of counter-rotating motion of of fluid shown in Fig. 6.8(b), the downstream seepage velocity (flowing to the right) is reduced in the upper left corner of the thermal cloud and is increased in the upper right corner as compared to the initial uniform flow. The horizontal dispersion coefficient is then decreased in the upper left and is increased in the upper right which means that heat is more conserved in the left than in the right. Consequently the buoyancy-induced convection is stronger on the left. This causes the asymmetry. But as time increases the medium temperature decreases and the nonlinear coupling effect becomes weak. Thus the distribution becomes symmetric about $\xi = 0$. The same discussions appliy to pressure and displacements. The buoyancy-induced upward velocity $\langle u \rangle_z$ along $\xi = 0$ is 0.4, 0.25 and 0.07 at t=0.004, 0.01 and 0.04 respectively and is larger than the case of $Ra' = 10$ and $\overline{Pe_f} = 1000$. In Fig. 6.9, the displacements on the upper boundary are shown. The actual magnitudes are 10 times larger than the case of $Ra' = 10$ because of the normalization (cf.(6.1.9)). The spatial distribution of the horizontal dispersion coefficient $\langle m' \rangle + D^s_{zz}$ is shown in Fig. 6.10. As a result of increased convection

explained above, the coefficient varies from 33 to 50 across the thermal cloud at the very early time $t = 0.04$ and the range narrows as time increases.

The case of $\overline{Pe_f} = 2000$ is shown in Fig. 6.11(a)-(e) for θ, ψ, p, w and u. As compared to the case of $\overline{Pe_f} = 1000$, the spreading is faster in the ξ direction, due to the increase in the horizontal dispersion coefficient. This weakens the effect of nonlinear convection fast. Accordingly the thermal cloud does not rise as much as in the case of $\overline{Pe_f} = 1000$ and the temperature, streamlines and pressure flatten out in the horizontal direction promptly. The upward velocity $\langle u \rangle_z$ along $\xi = 0$ is 0.2, 0.08 and 0.015 at t=0.004, 0.01 and 0.04 respectively and is obviously smaller than the case of $\overline{Pe_f} = 1000$. The displacements on the upper boundary presented in Fig. 6.12 also, as in Case (i), show about half magnitudes of the case with $\overline{Pe_f} = 1000$. The variation of the horizontal dispersion coefficient is not as pronounced as shown in Fig. 6.13.

Case(iii) $Ra' = 200$; $\overline{Pe_f}$=1000, 2000

The Rayleigh number is further increased to 200. The nonlinear coupling effect is the strongest of the three cases.

For $\overline{Pe_f} = 1000$, the temperature, streamlines, pressure and displacements are presented in Fig. 6.14(a)-(e). It is clearly demonstrated in Fig. 6.14(a) that the upward convection due to buoyancy is strong enough to carry the thermal cloud to the upper boundary by the time $t = 0.08$. Afterwards the thermal cloud spreads out in the medium due to dispersion. The asymmetry at the early time is more pronounced in Fig. 6.14(a) and (b). The isotherms are denser in the upper part of the cloud because of faster upward movement of the hot peak. The upward velocity $\langle u \rangle_z$ along $\xi = 0$ is 0.46, 0.25, 0.08 and 0.03 at t=0.004, 0.01, 0.04 and 0.01 respectively. The recharge and upward leakage of the fluid at the upper boundary start as early as $t = 0.04$. The displacements at the upper boundary are shown in Fig. 6.15 and the distribution is qualitatively same as other cases. The variations of the horizontal dispersion coefficient $\langle m' \rangle + D^*_{xx}$ is presented in Fig. 6.16. At the widest,e.g. at the earliest time, it ranges from 28 to 56. Because the cloud reaches

the upper boundary soon, so does the distribution of dispersion coefficient and after $t = 0.04$ it is simply divided into the upstream region with larger values and the downstream region with smaller values.

When $\overline{Pe}_f$ is increased to 2000, the convection due to buoyancy becomes weak fast and the thermal cloud does not reach the upper boundary as shown in Fig. 6.17(a). The streamlines , pressure, vertical and horizontal displacements shown in Fig. 6.17(b)-(e) are quite similar to the case with $\overline{Pe}_f = 2000$ in Case (ii). Also the deforamtion on the upper boundary is shown in Fig. 6.18 and is about one half of the case with $\overline{Pe}_f = 1000$ as before. The dispersion coefficient $\langle m' \rangle + D^s_{zz}$ variation is as plotted in Fig. 6.19. At $t = 0.04$, the range of variation is from 142 in the lower right to 184 in the lower left. Comparing with the value of 163.5 for uniform flow, the deviations are as high as 13% toward both sides. As time increases the distribution also becomes more and more uniform approaching to that of the uniform stream.

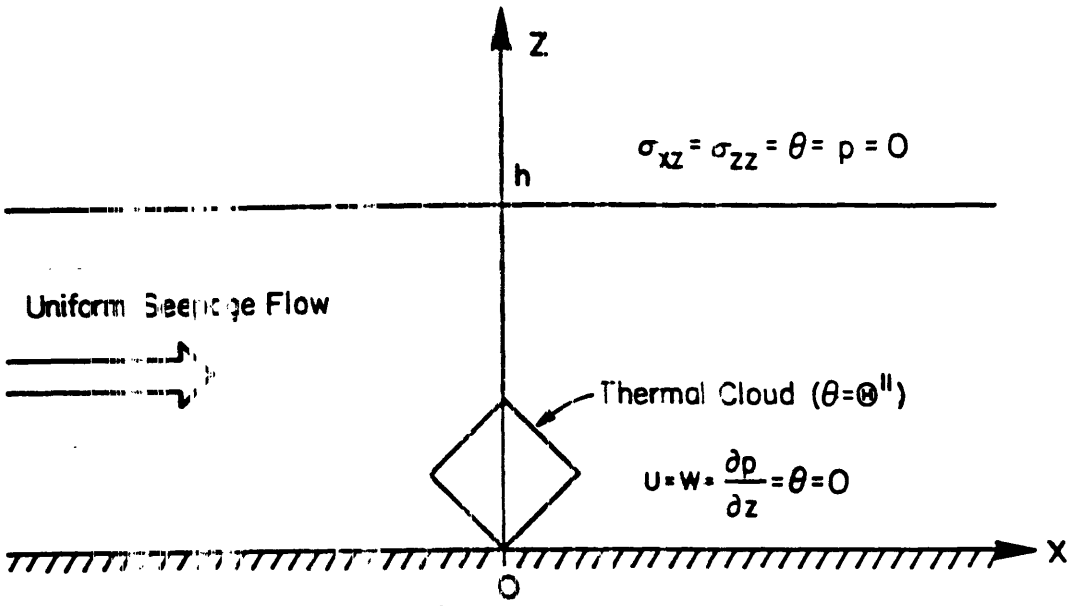

Fig. 6.1 A thermal cloud released in a uniform seepage flow through layered porous layer.

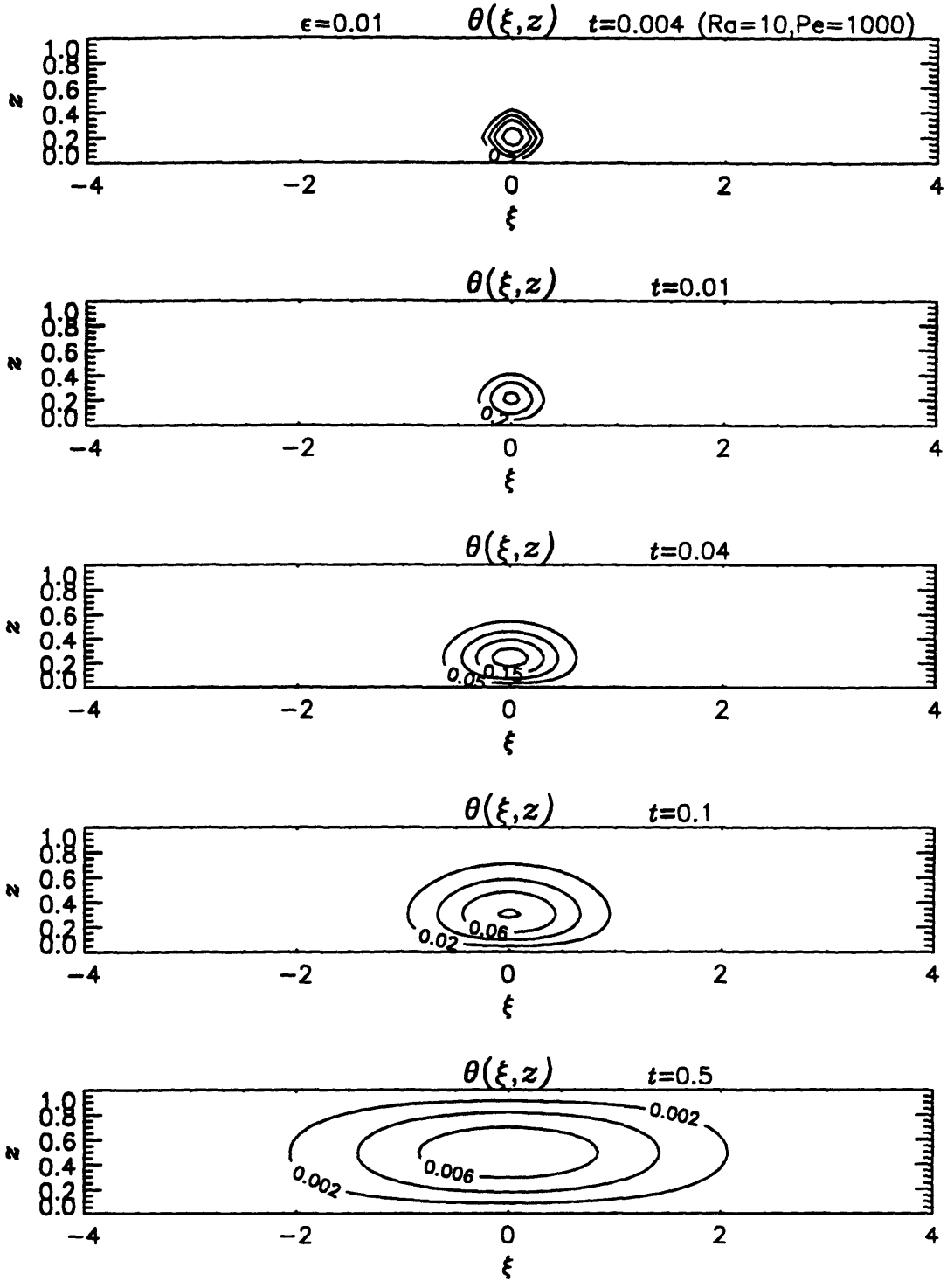

Fig. 6.2(a) Temperature distribution $\theta(\xi, z)$ for $Ra' = 10$ and $\overline{Pe_f} = 1000$ at various times.

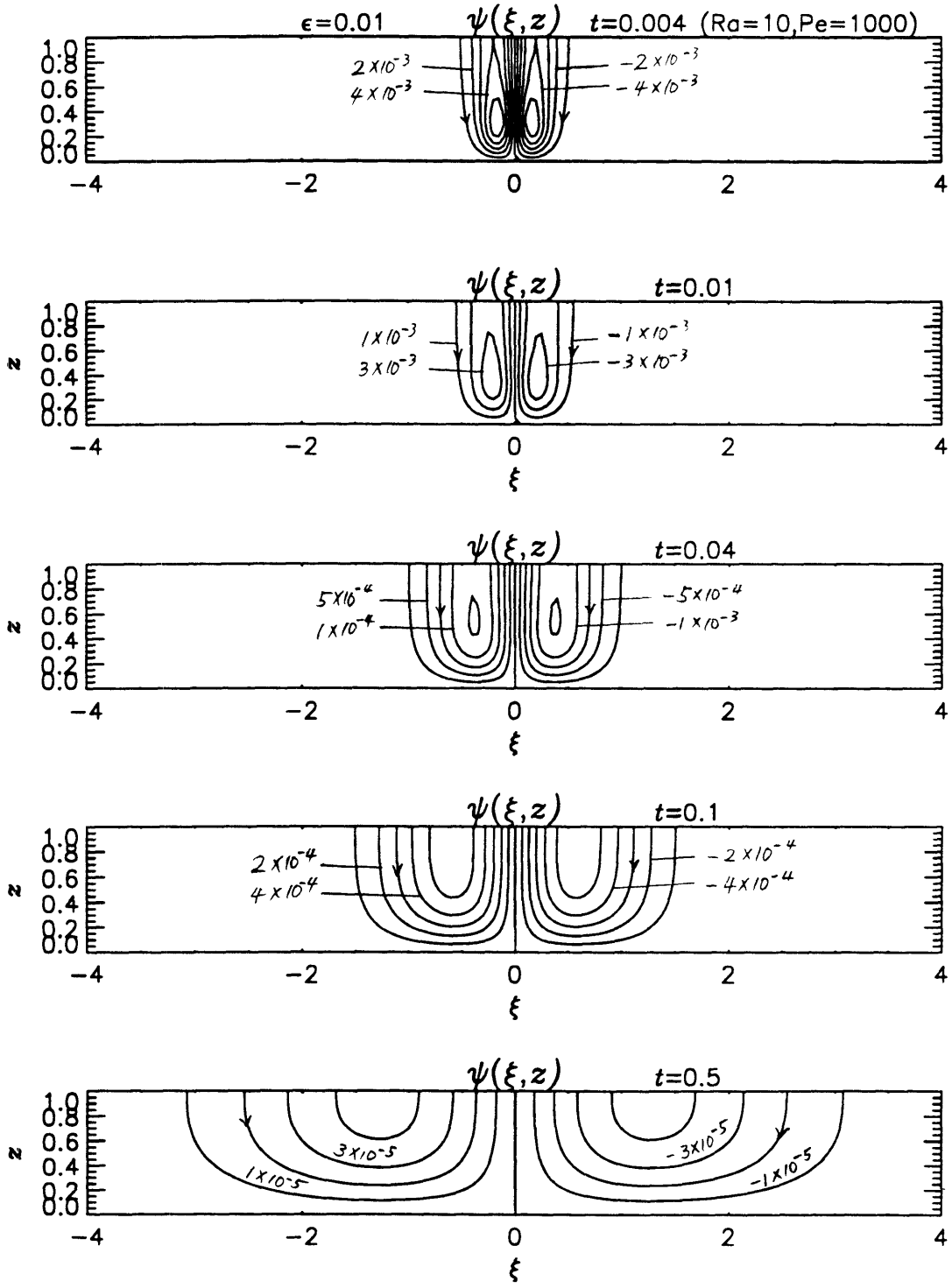

Fig. 6.2(b) Streamlines $\psi(\xi, z)$ for $Ra' = 10$ and $\overline{Pe_f} = 1000$ at various times.

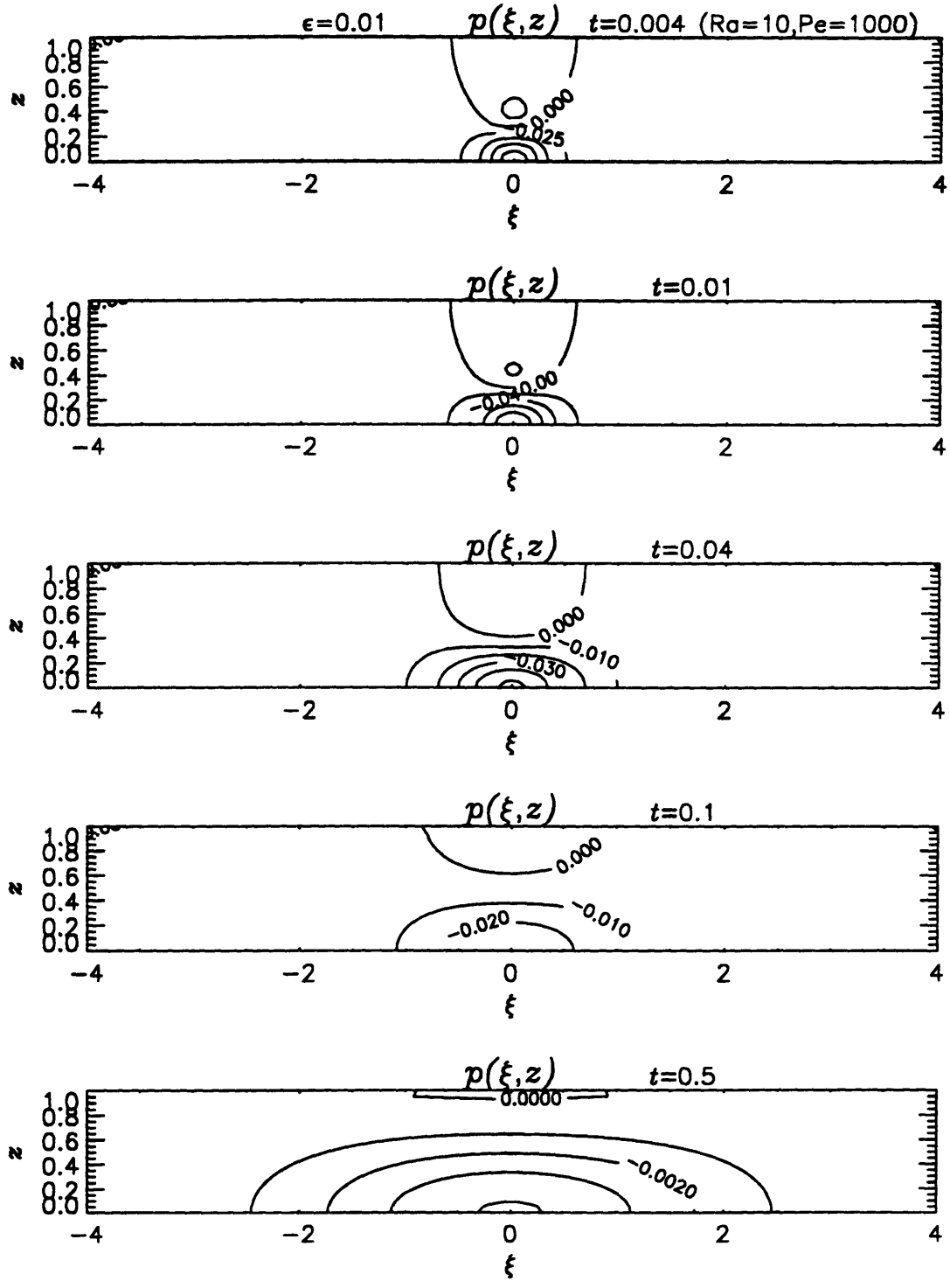

Fig. 6.2(c) Pressure distribution $p(\xi, z)$ for $Ra' = 10$ and $\overline{Pe_f} = 1000$ at various times.

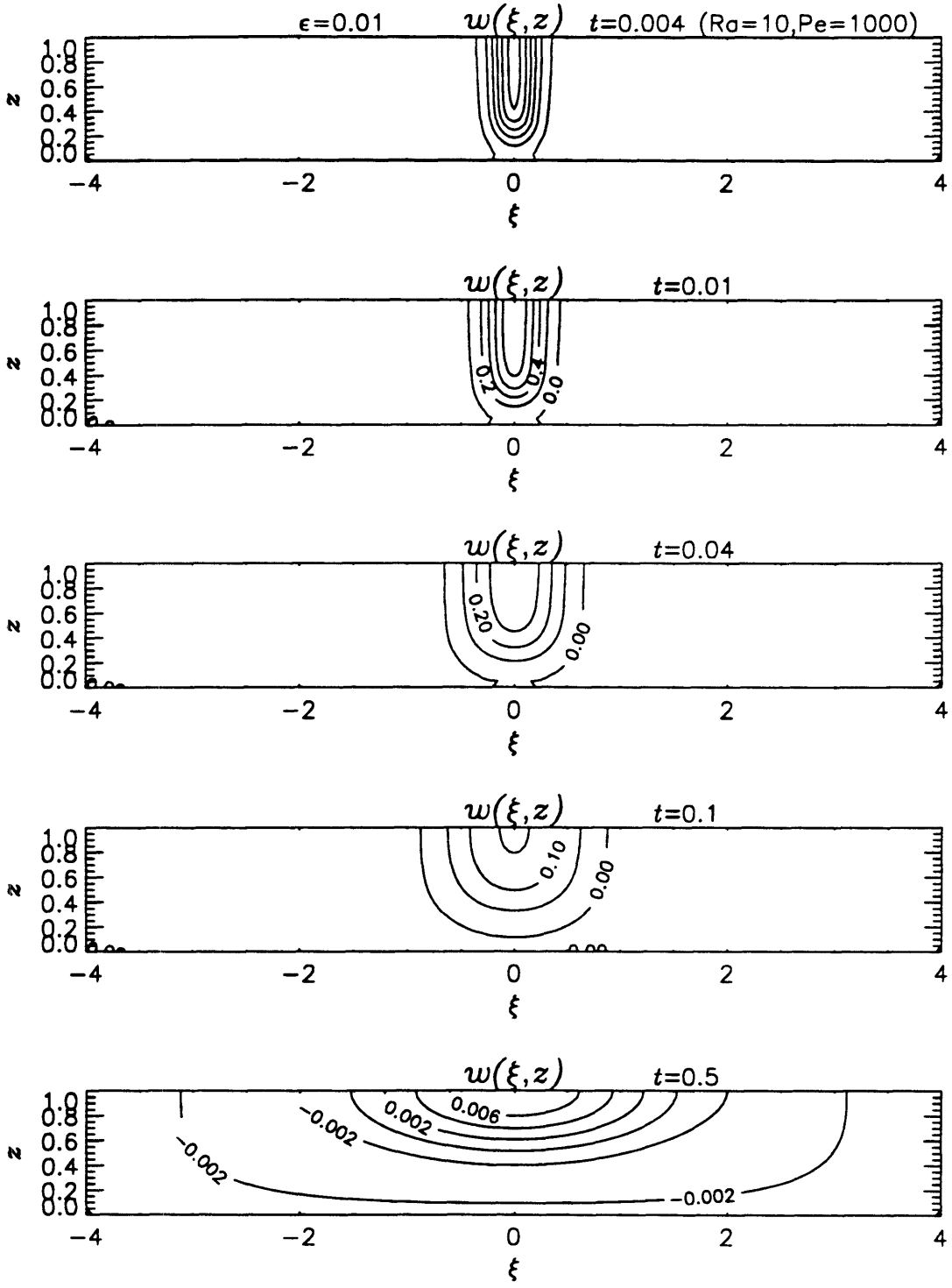

Fig. 6.2(d) Vertical displacement $w(\xi, z)$ for $Ra' = 10$ and $\overline{Pe_f} = 1000$ at various times.

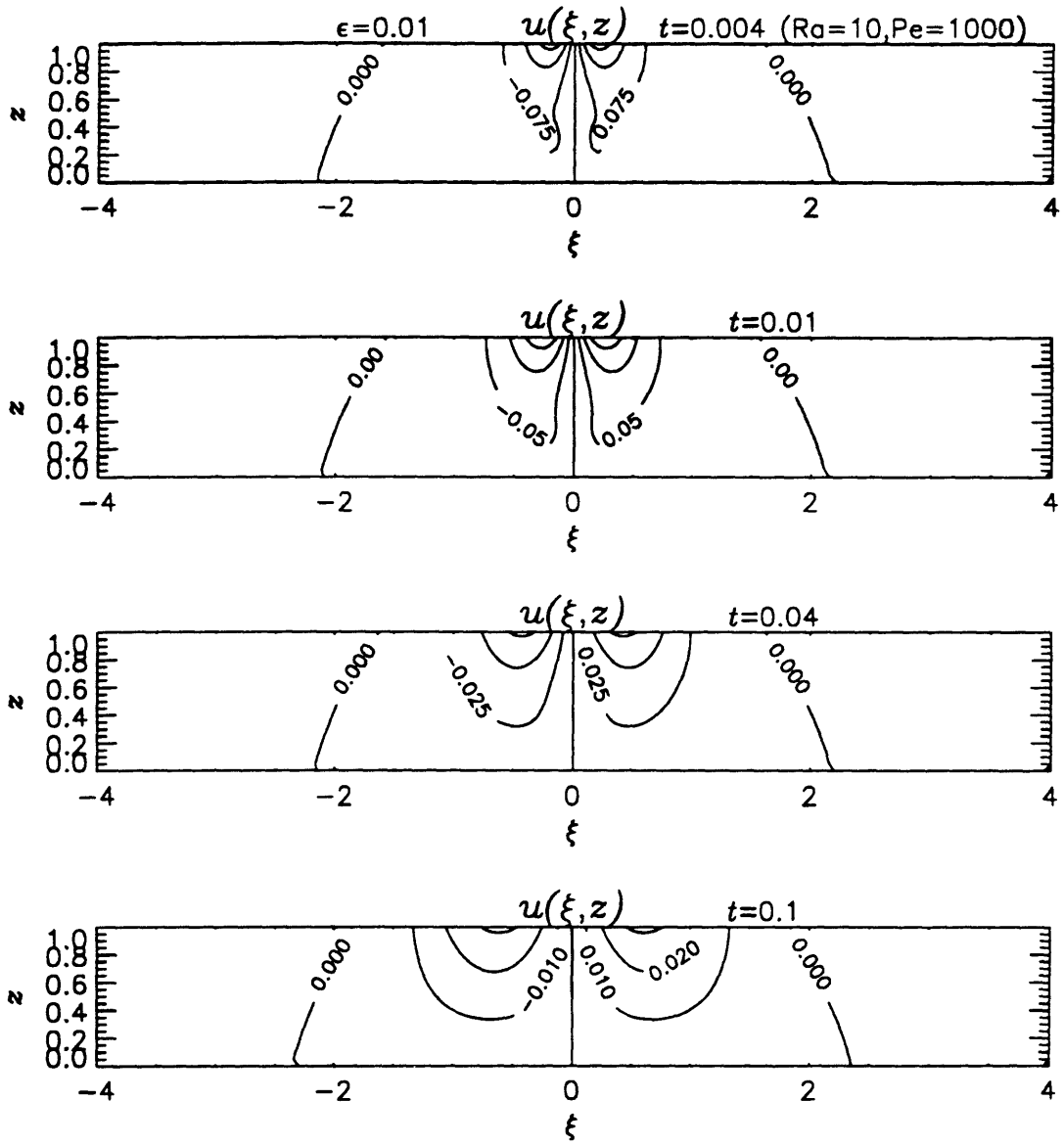

Fig. 6.2(e) Horizontal displacement $u(\xi, z)$ for $Ra' = 10$ and $\overline{Pe_f} = 1000$ at various times.

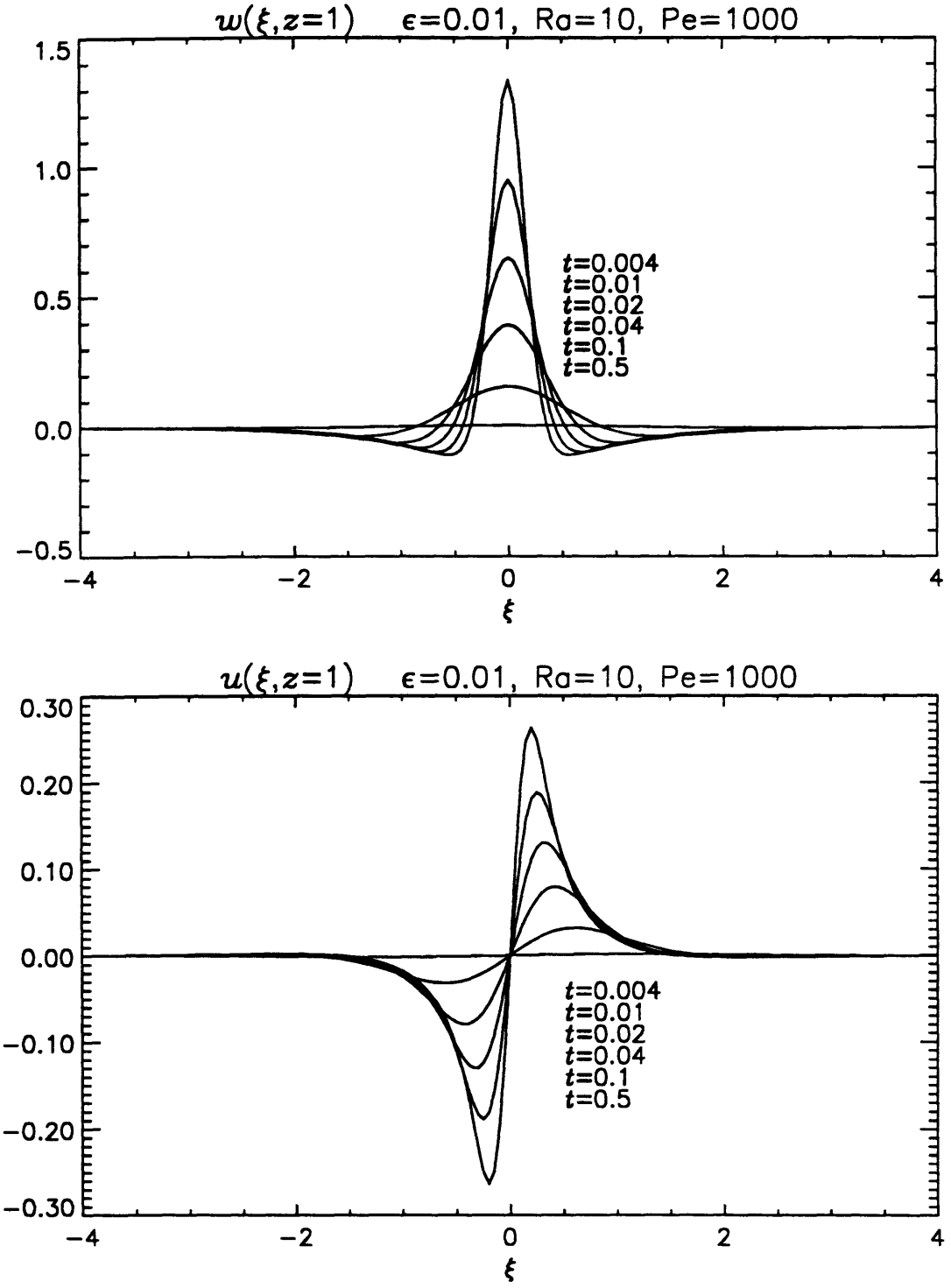

Fig. 6.3 Matrix displacements at the upper surface (a) $w(\xi, z = 1)$ and (b) $u(\xi, z = 1)$ for $Ra' = 10$ and $\overline{Pe_f} = 1000$ at various times. The magnitude decreases with t.

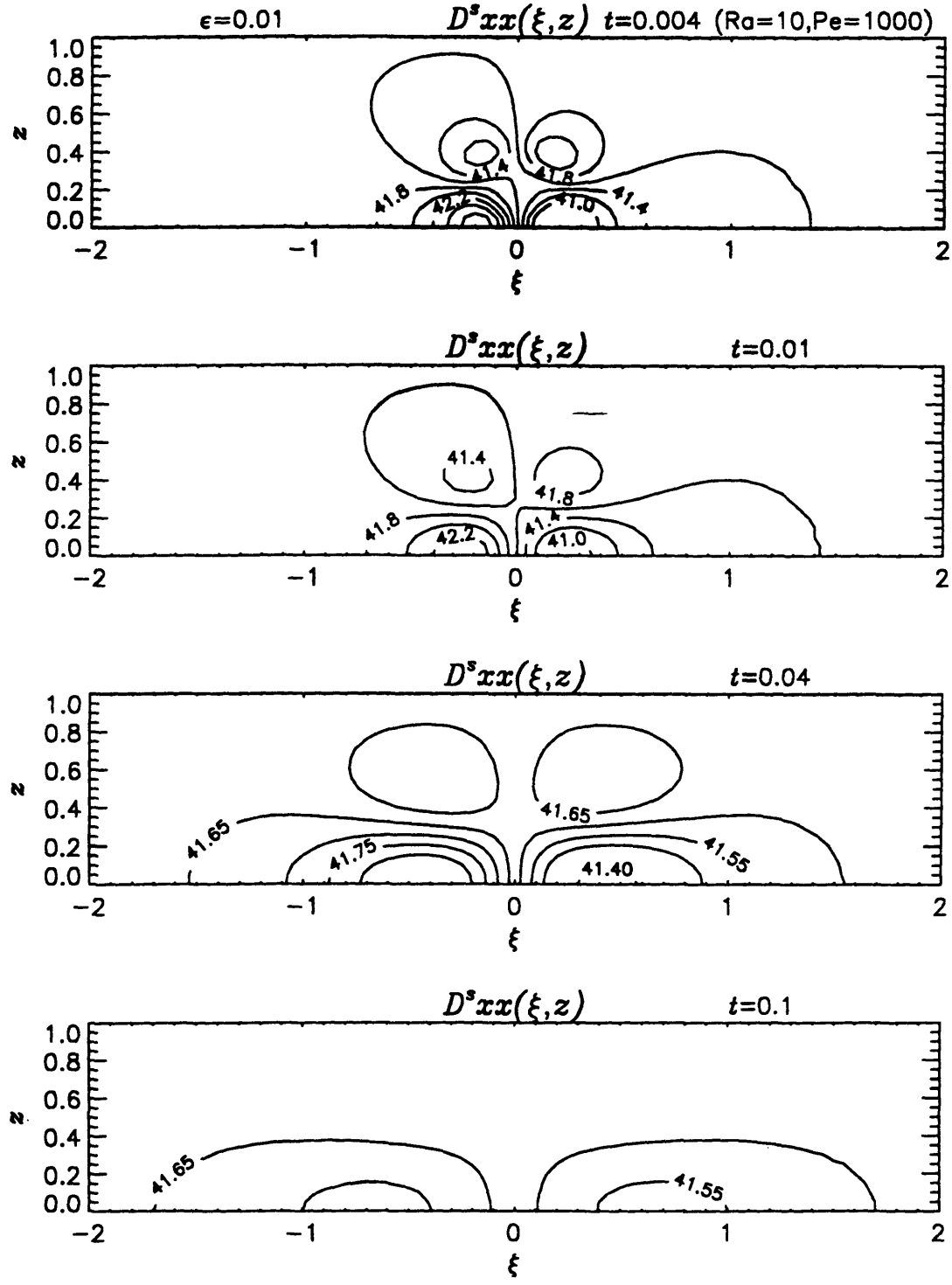

Fig. 6.4 Distribution of the dispersion coefficient $\langle m' \rangle + D^s_{zz}$ for $Ra' = 10$ and $\overline{Pe_f} = 1000$ at various times.

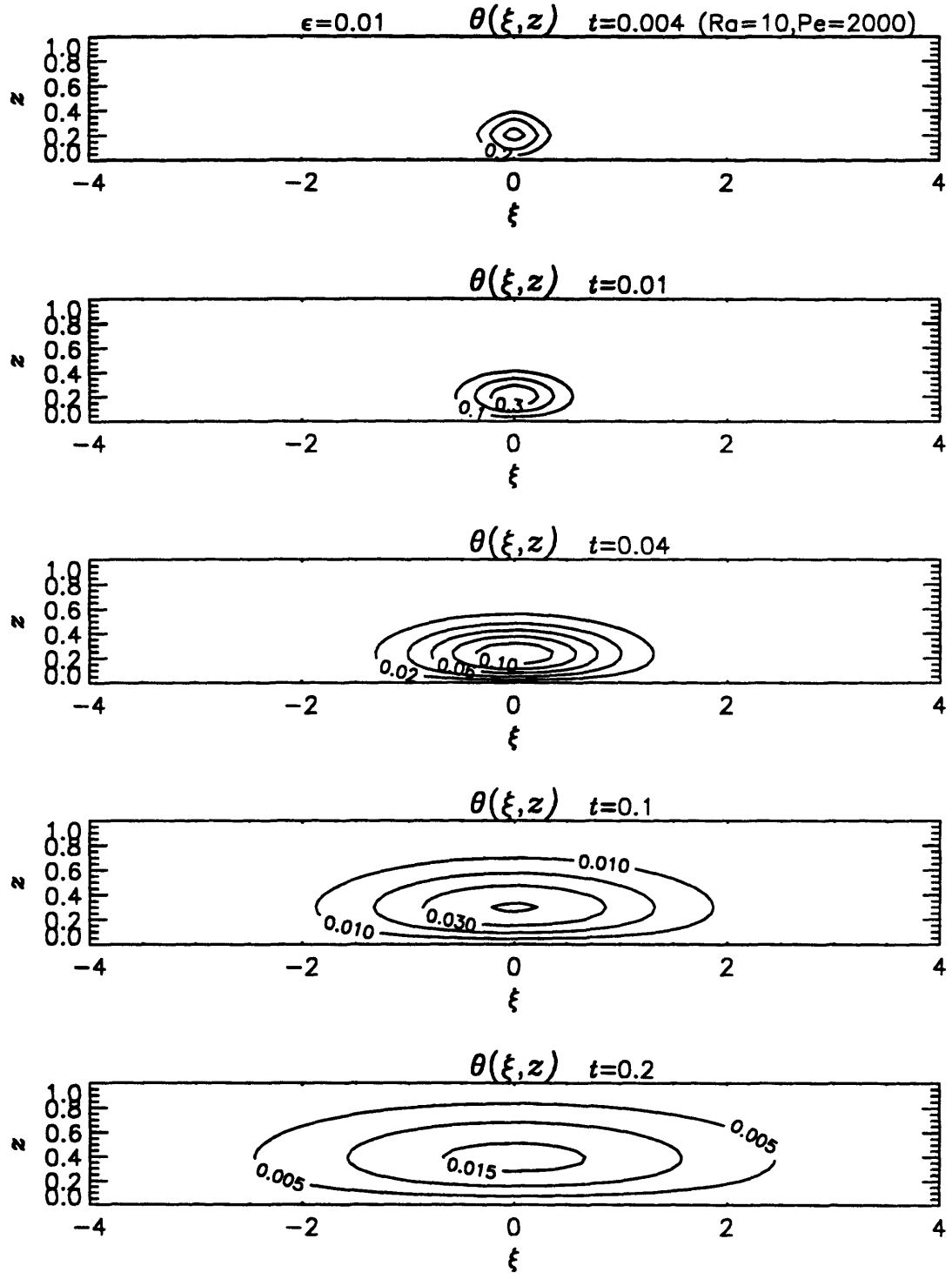

Fig. 6.5(a) Temperature distribution $\theta(\xi, z)$ for $Ra' = 10$ and $\overline{Pe_f} = 2000$ at various times.

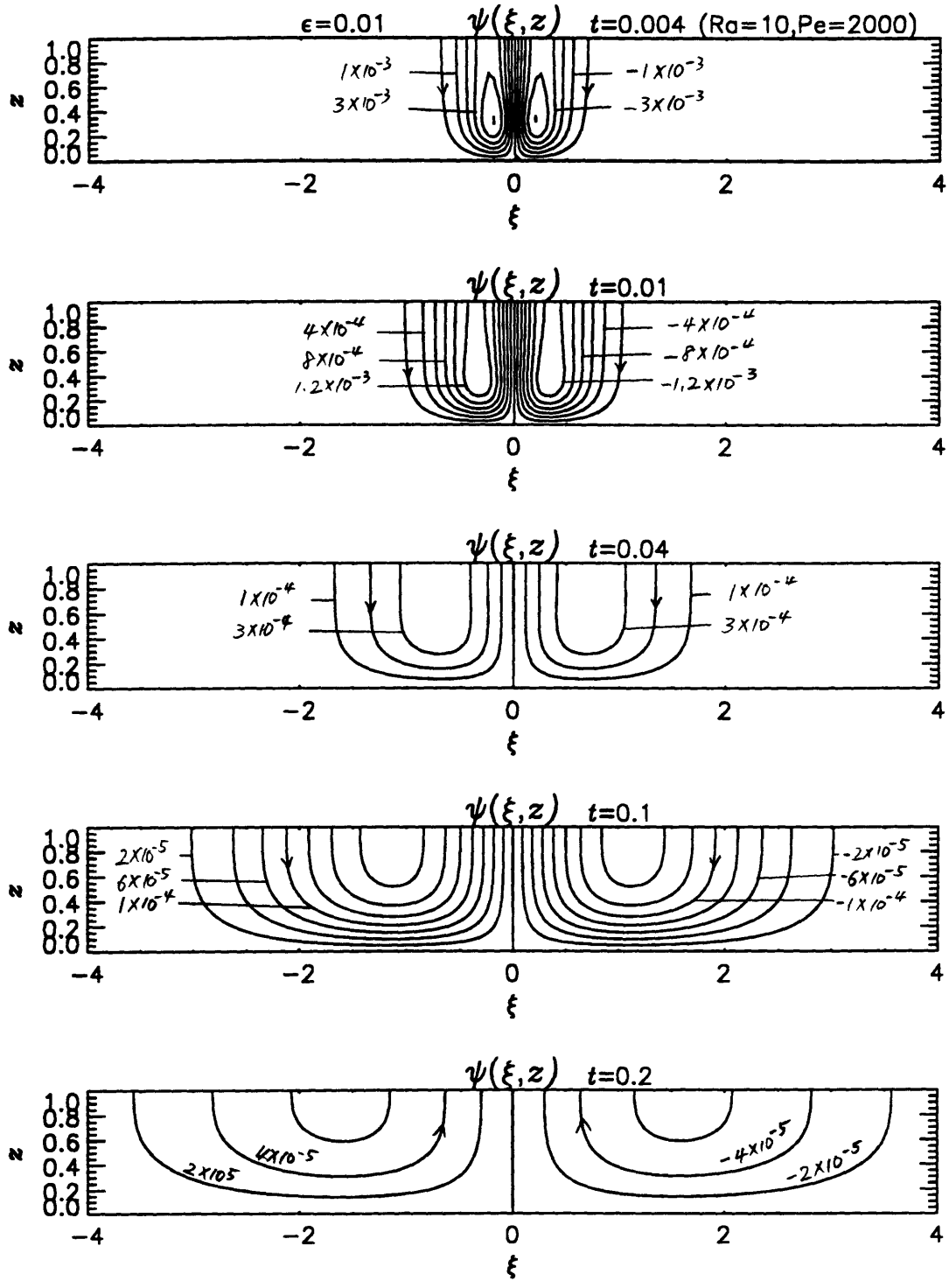

Fig. 6.5(b) Streamlines $\psi(\xi, z)$ for $Ra' = 10$ and $\overline{Pe_f} = 2000$ at various times.

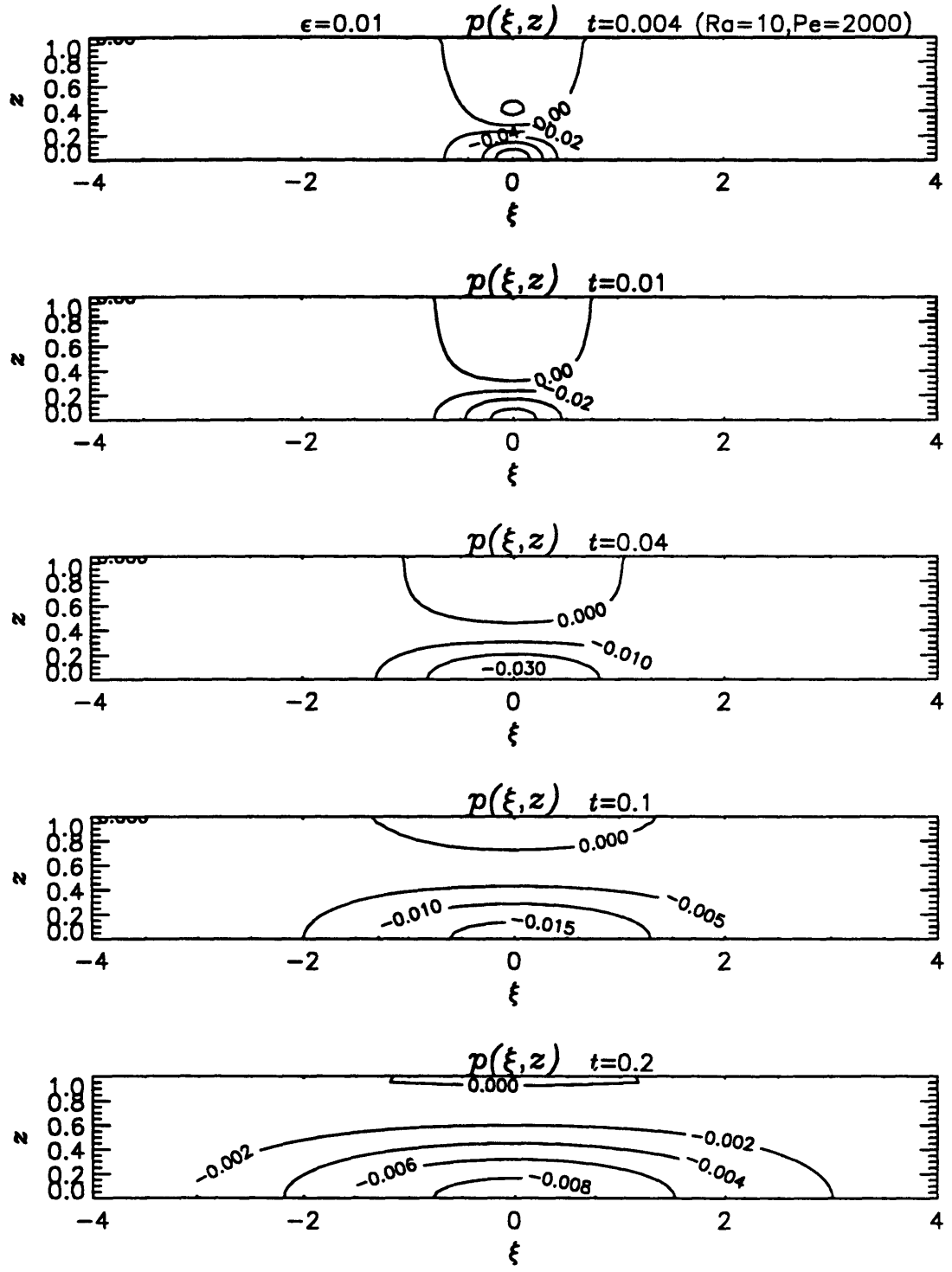

Fig. 6.5(c) Pressure distribution $p(\xi, z)$ for $Ra' = 10$ and $\overline{Pe_f} = 2000$ at various times.

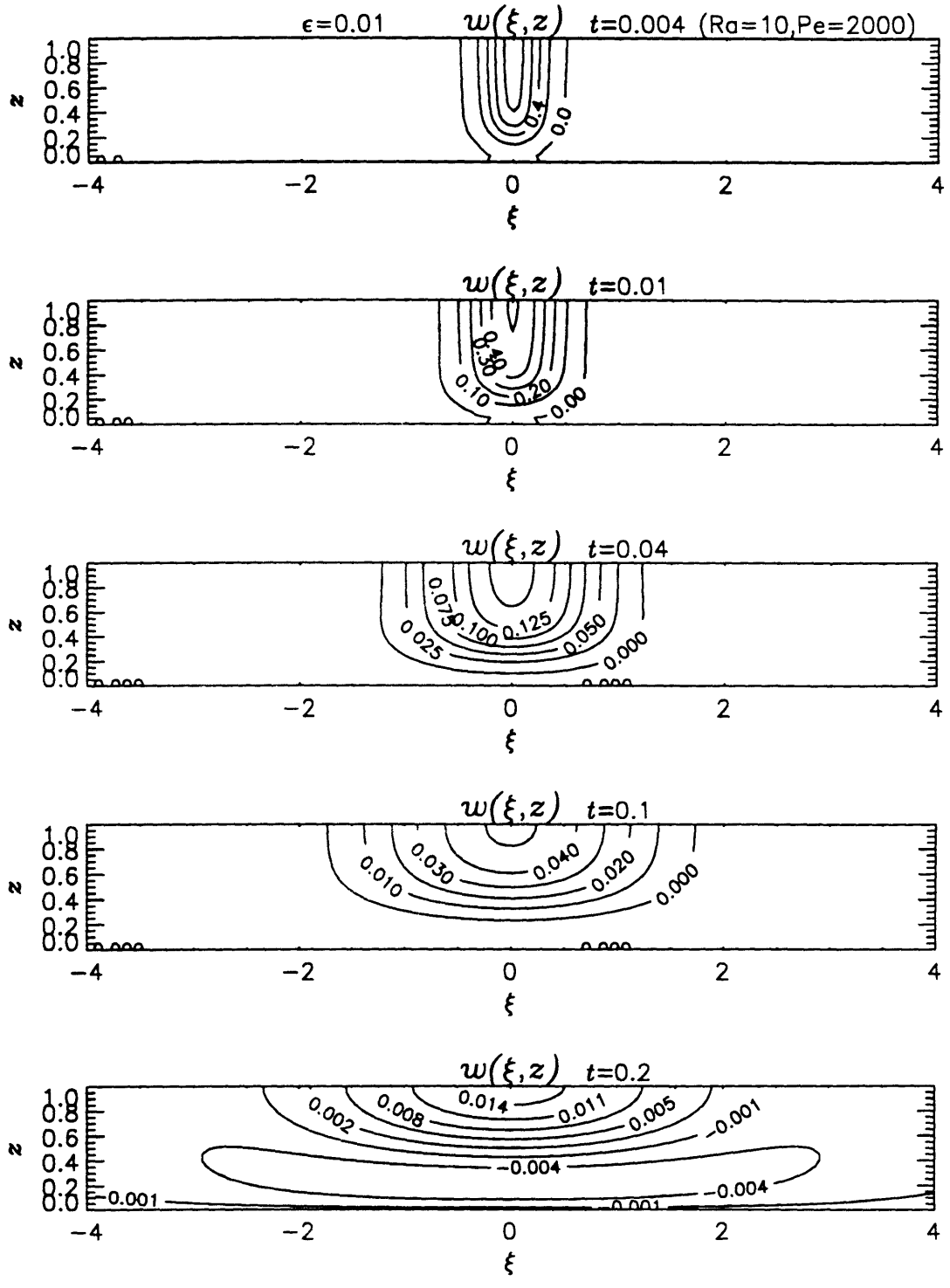

Fig. 6.5(d) Vertical displacement $w(\xi, z)$ for $Ra' = 10$ and $\overline{Pe_f} = 2000$ at various times.

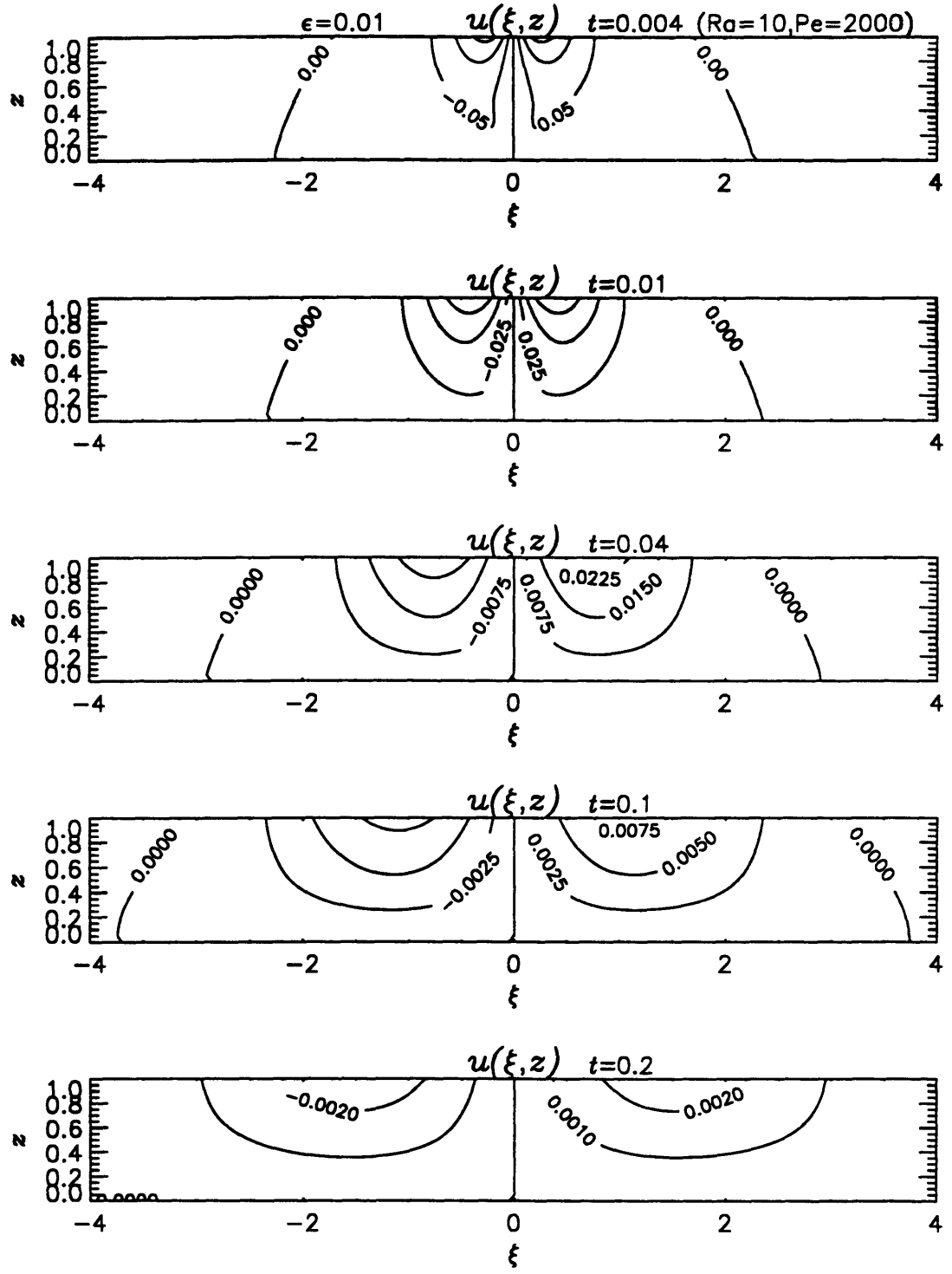

Fig. 6.5(e) Horizontal displacement $u(\xi, z)$ for $Ra' = 10$ and $\overline{Pe_f} = 2000$ at various times.

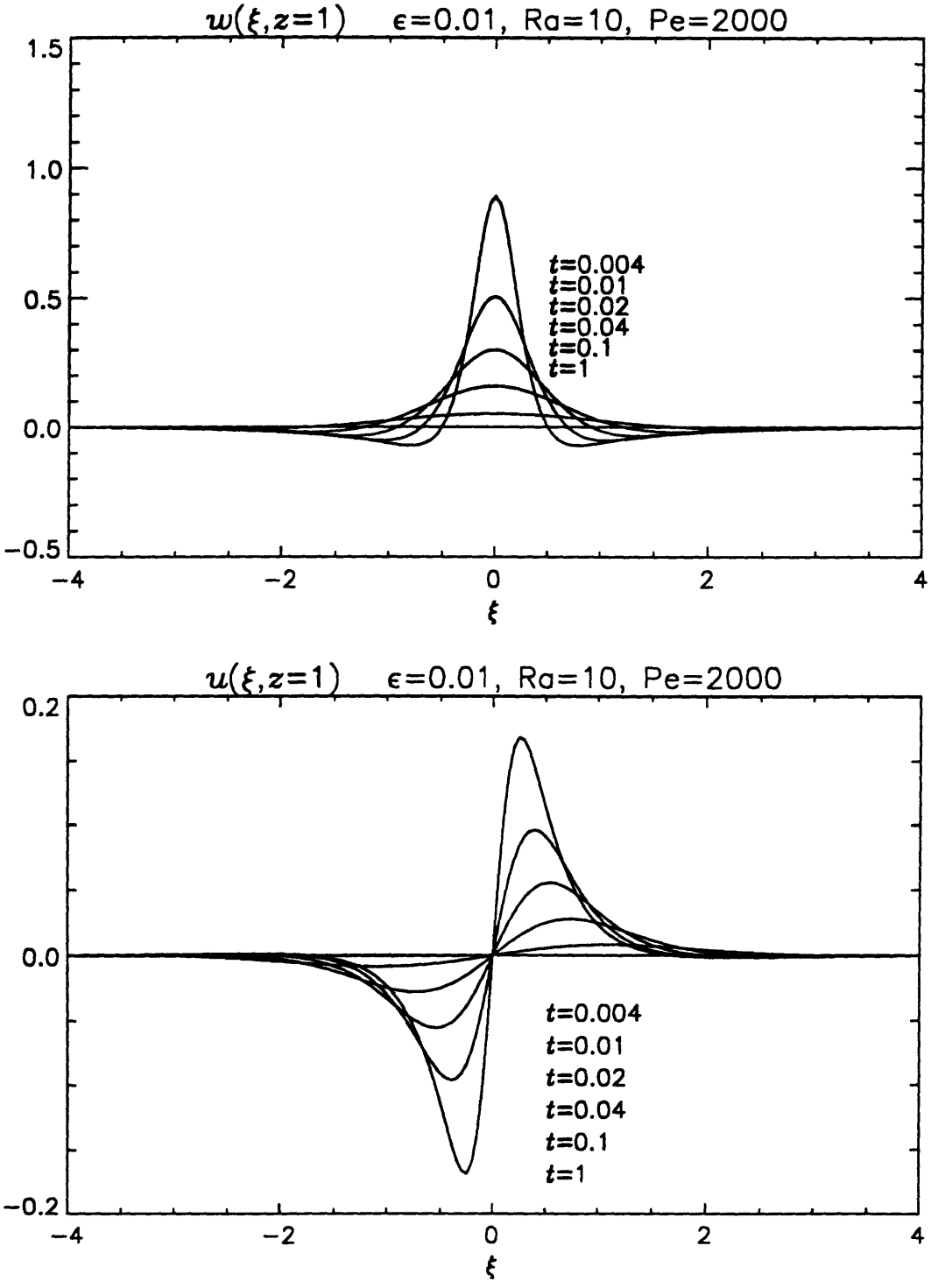

Fig. 6.6 Displacements at the upper surface (a) $w(\xi, z = 1)$ and (b) $u(\xi, z = 1)$ for $Ra' = 10$ and $\overline{Pe_f} = 2000$ at various times. The magnitude decreases with t.

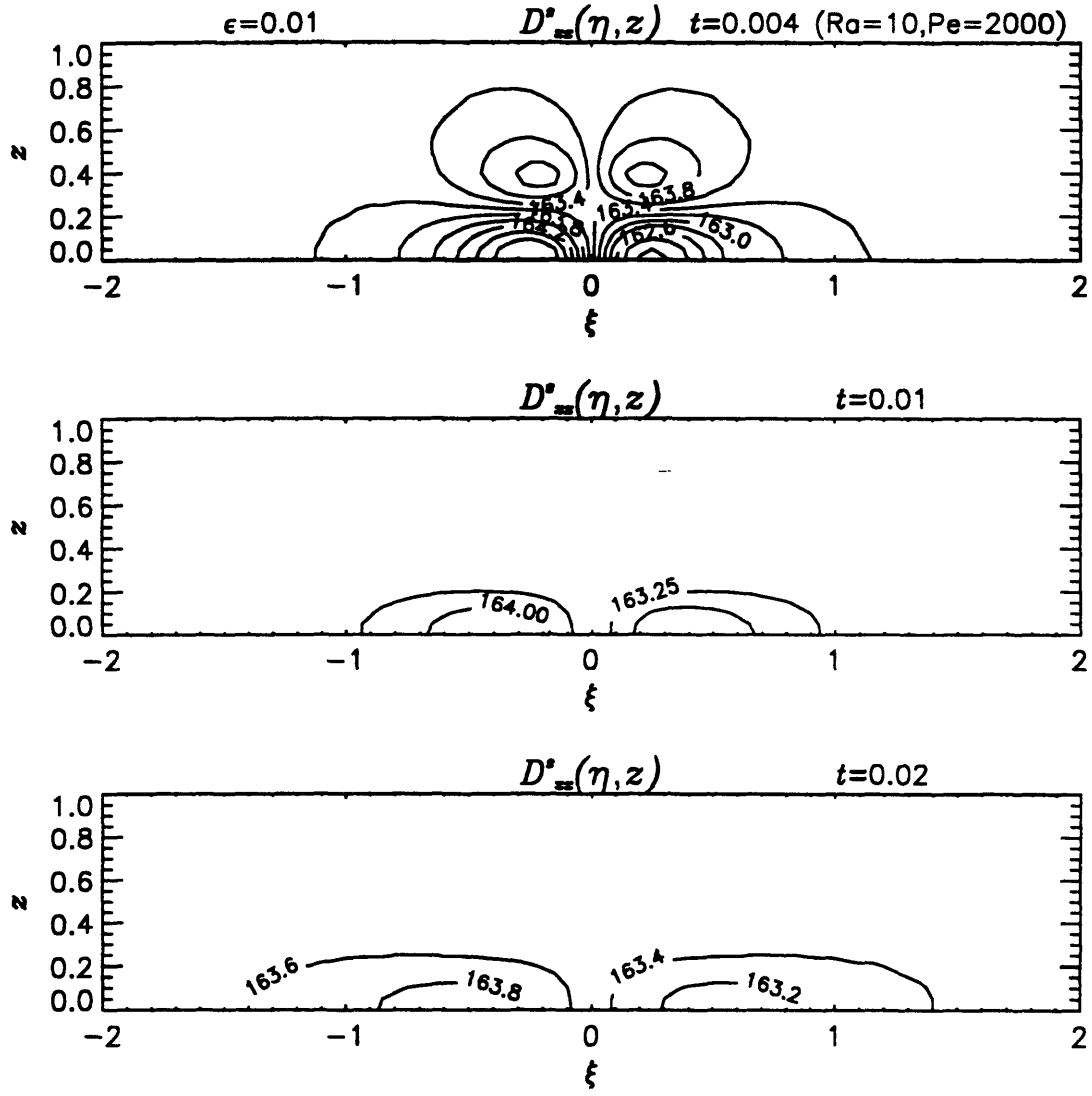

Fig. 6.7 Distribution of the dispersion coefficient $\langle m' \rangle + D^e_{zz}$ for $Ra' = 10$ and $\overline{Pe_f} = 2000$ at various times.

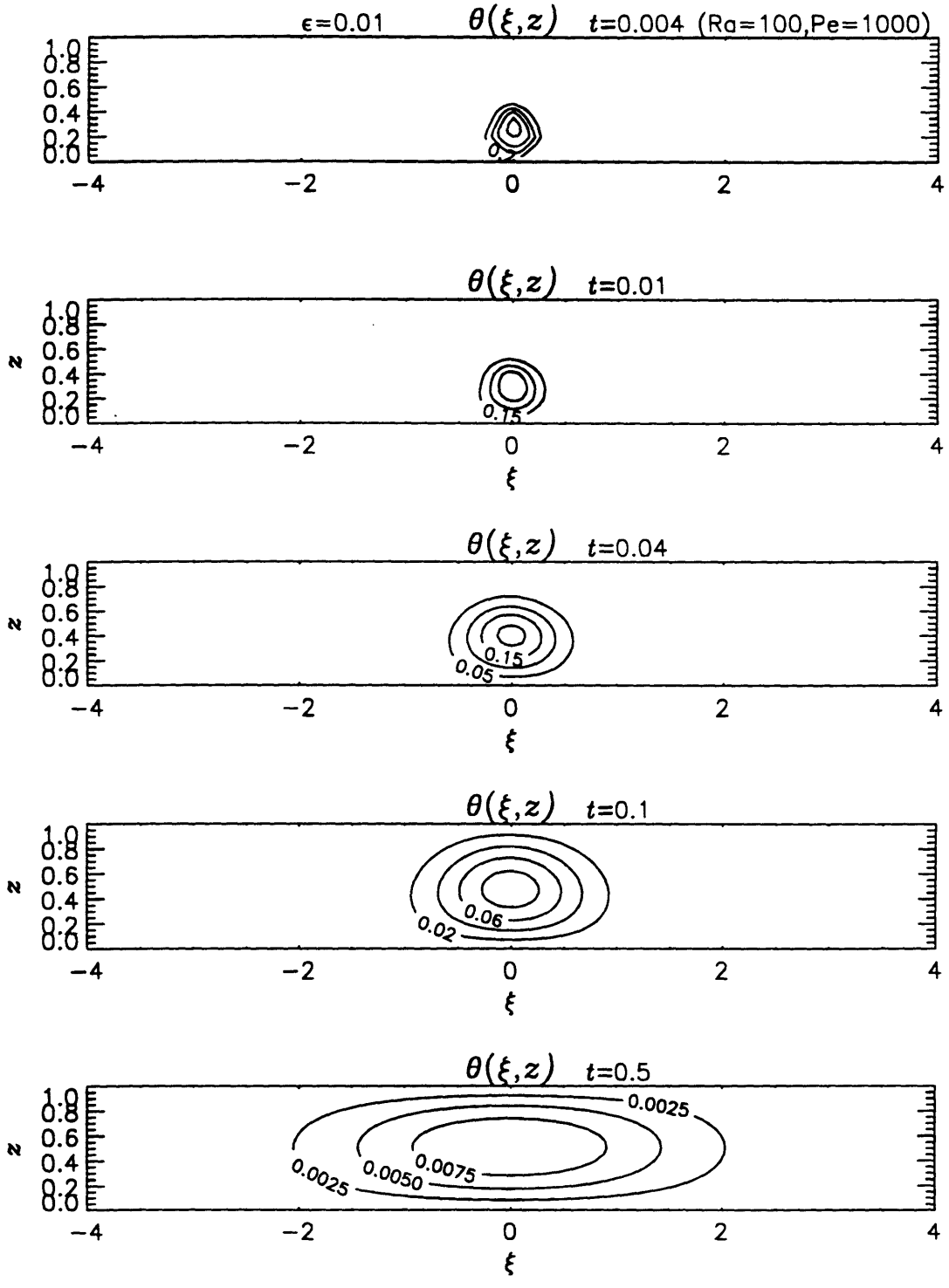

Fig. 6.8(a) Temperature distribution $\theta(\xi, z)$ for $Ra' = 100$ and $\overline{Pe_f} = 1000$ at various times.

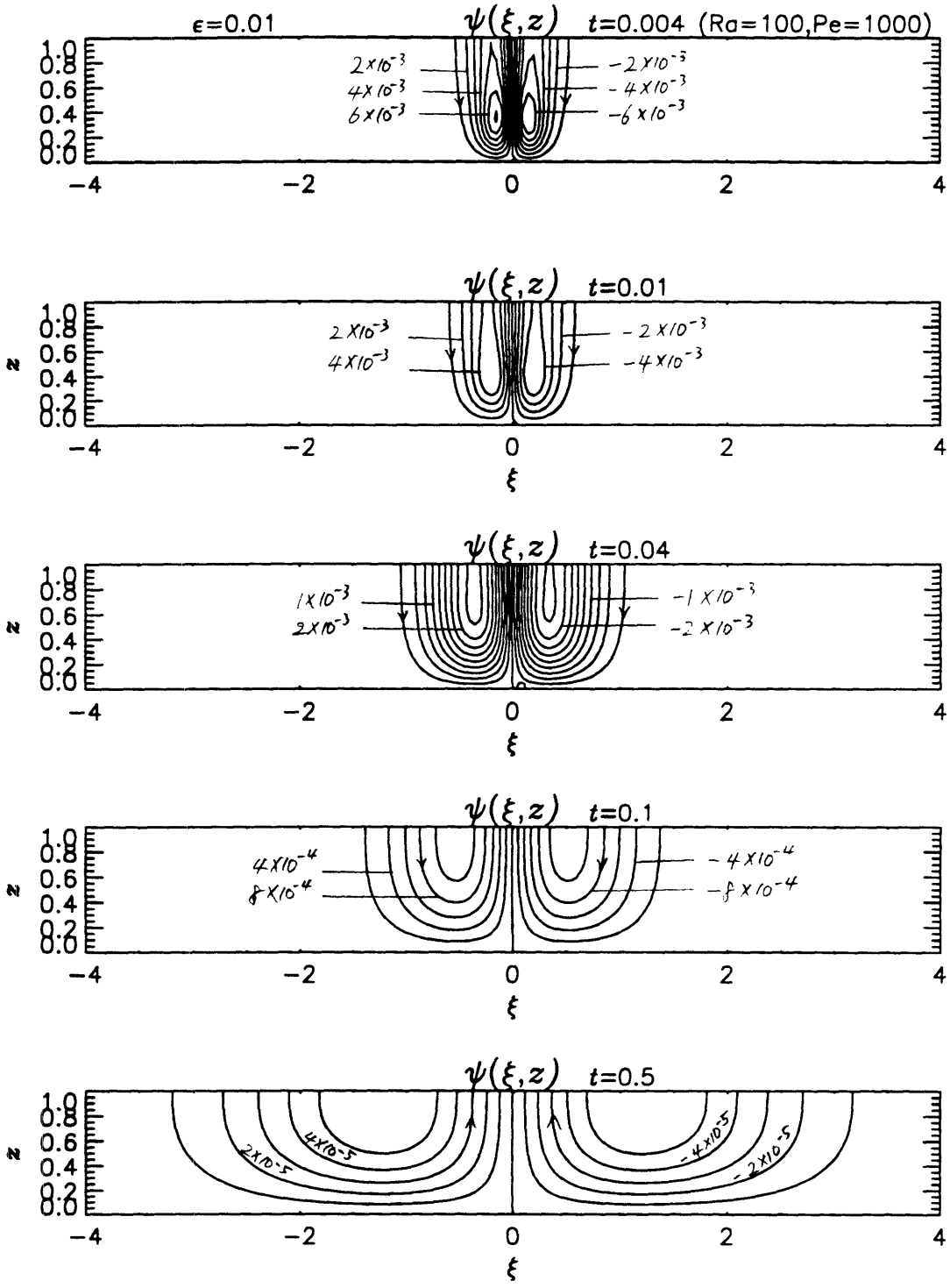

Fig. 6.8(b) Streamlines $\psi(\xi, z)$ for $Ra' = 100$ and $\overline{Pe_f} = 1000$ at various times.

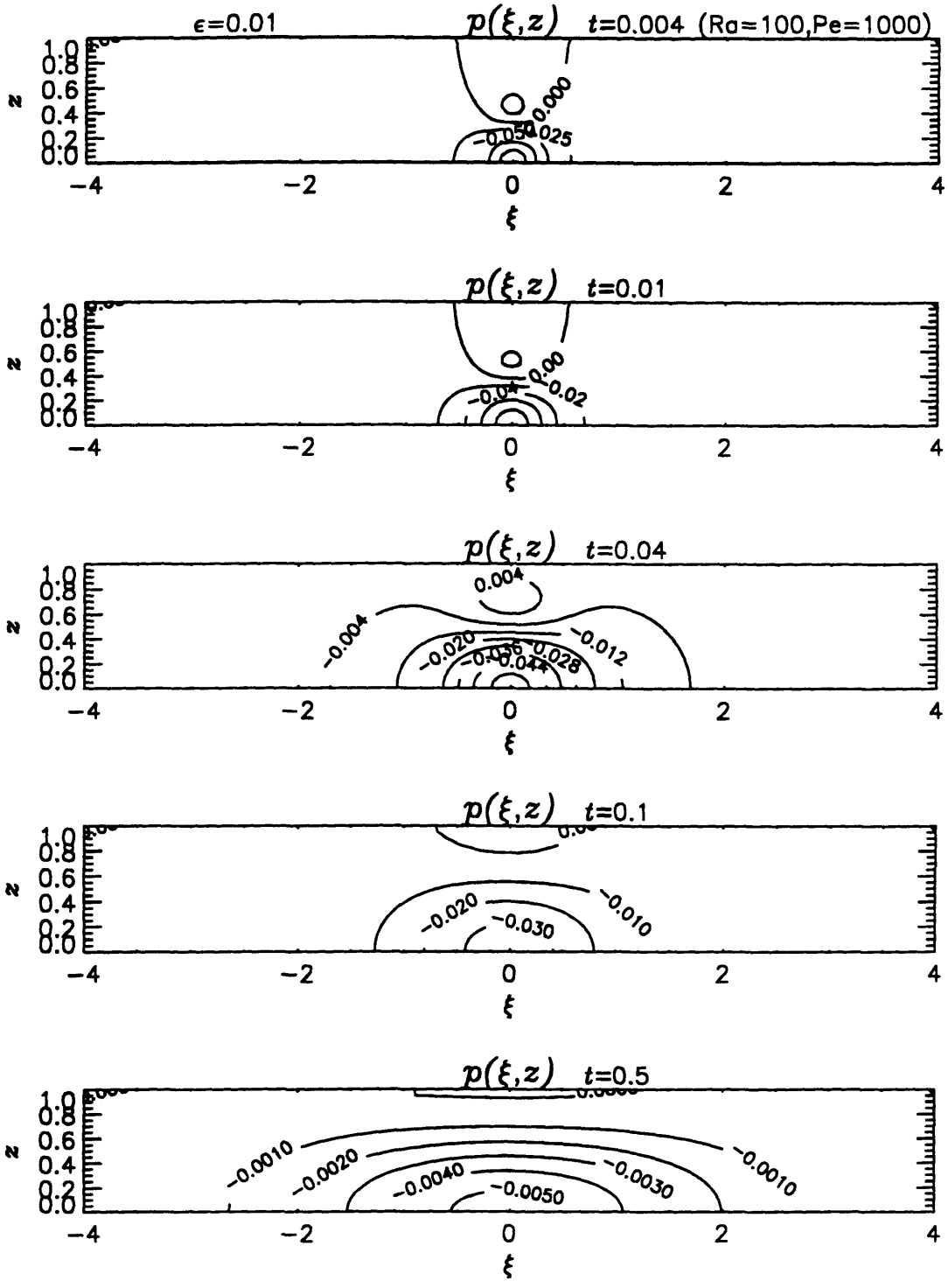

Fig. 6.8(c) Pressure distribution $p(\xi, z)$ for $Ra' = 100$ and $\overline{Pe_f} = 1000$ at various times.

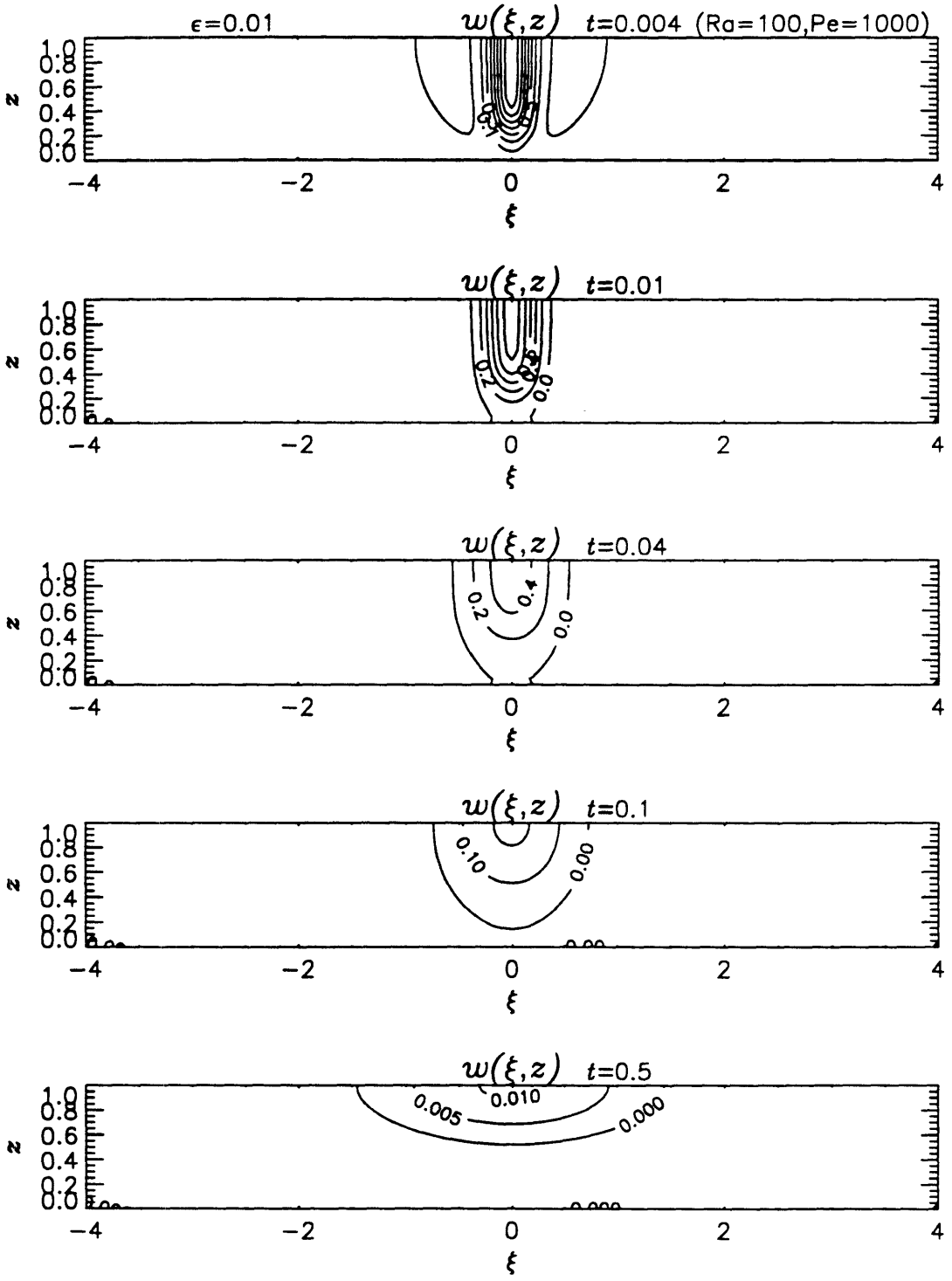

Fig. 6.8(d) Vertical displacement $w(\xi, z)$ for $Ra' = 100$ and $\overline{Pe_f} = 1000$ at various times.

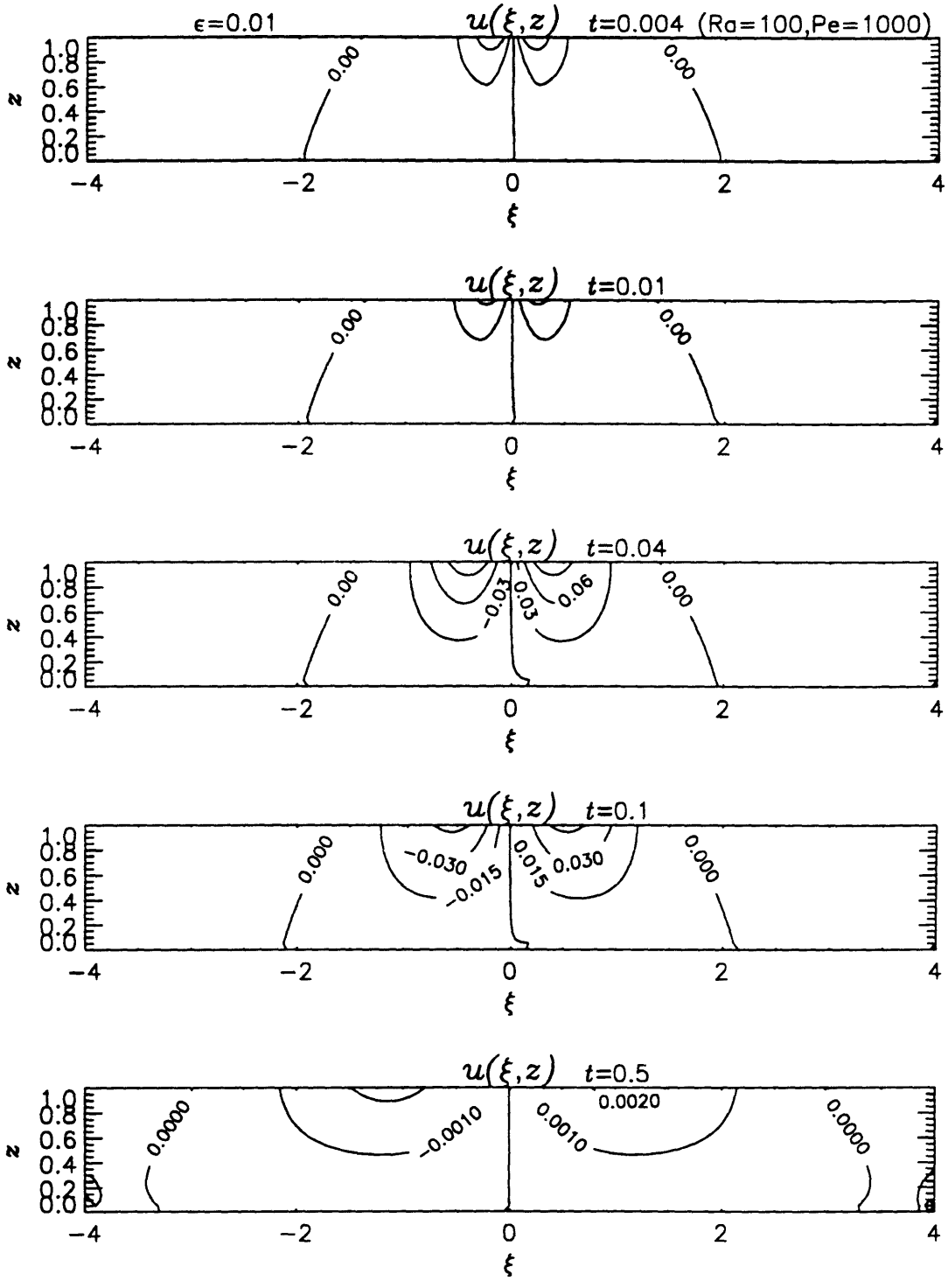

Fig. 6.8(e) Horizontal displacement $u(\xi, z)$ for $Ra' = 100$ and $\overline{Pe_f} = 1000$ at various times.

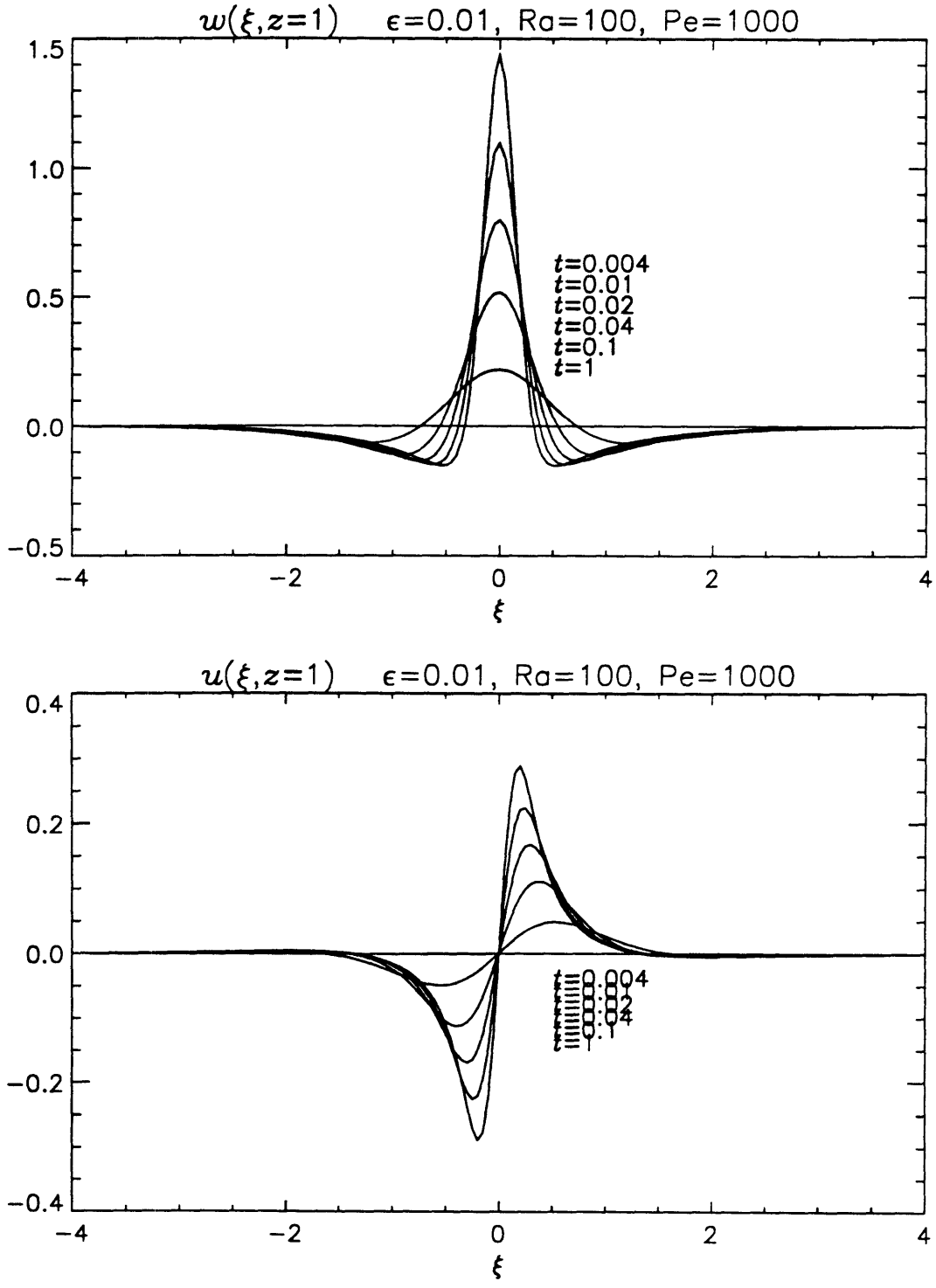

Fig. 6.9 Displacements at the upper surface (a) $w(\xi, z = 1)$ and (b) $u(\xi, z = 1)$ for $Ra' = 100$ and $\overline{Pe_f} = 1000$ at various times. The magnitude decreases with t.

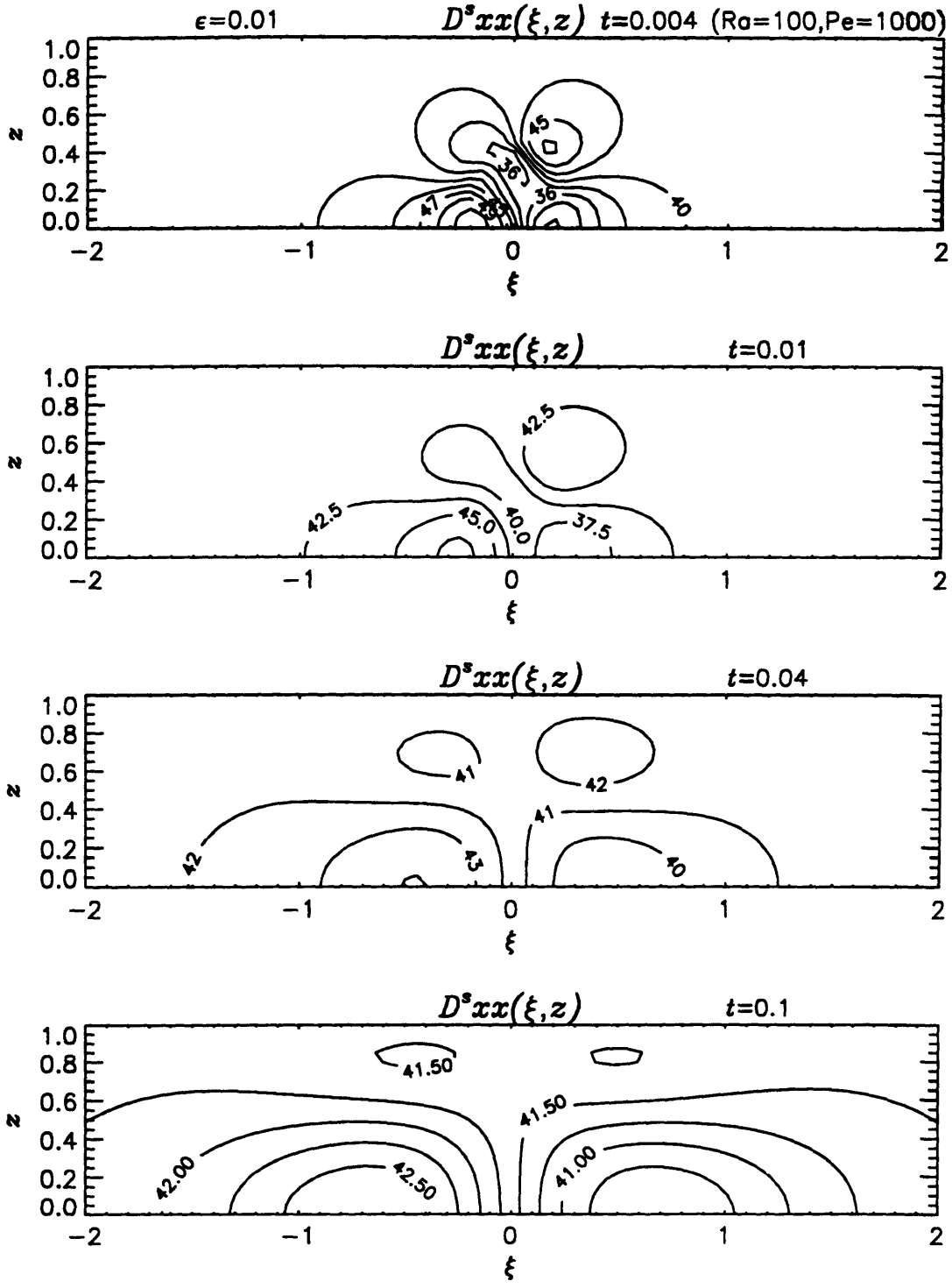

Fig. 6.10 Distribution of the dispersion coefficient $\langle m' \rangle + D^s_{xx}$ for $Ra' = 100$ and $\overline{Pe_f} = 1000$ at various times.

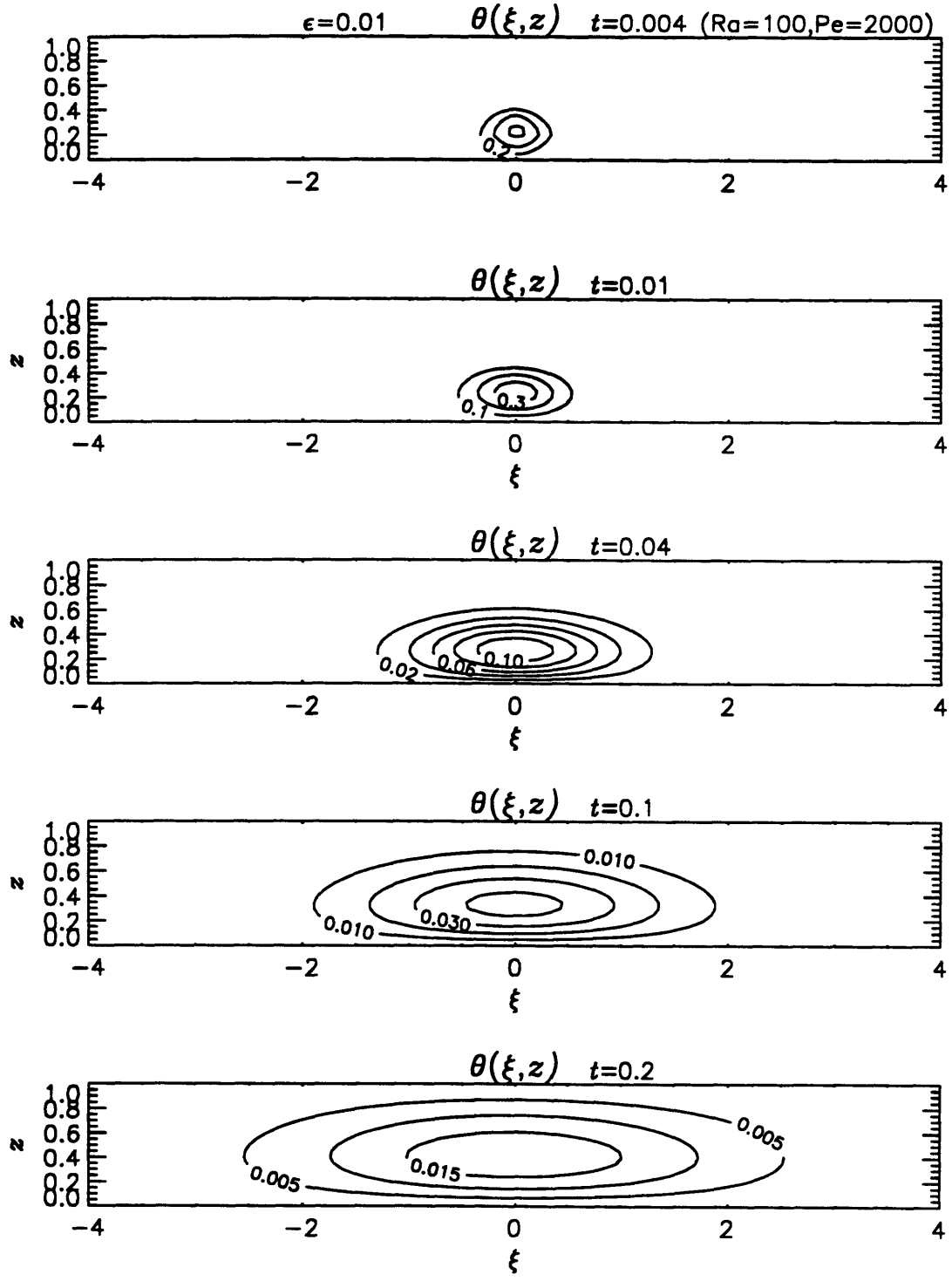

Fig. 6.11(a) Temperature distribution $\theta(\xi, z)$ for $Ra' = 100$ and $\overline{Pe_f} = 2000$ at various times.

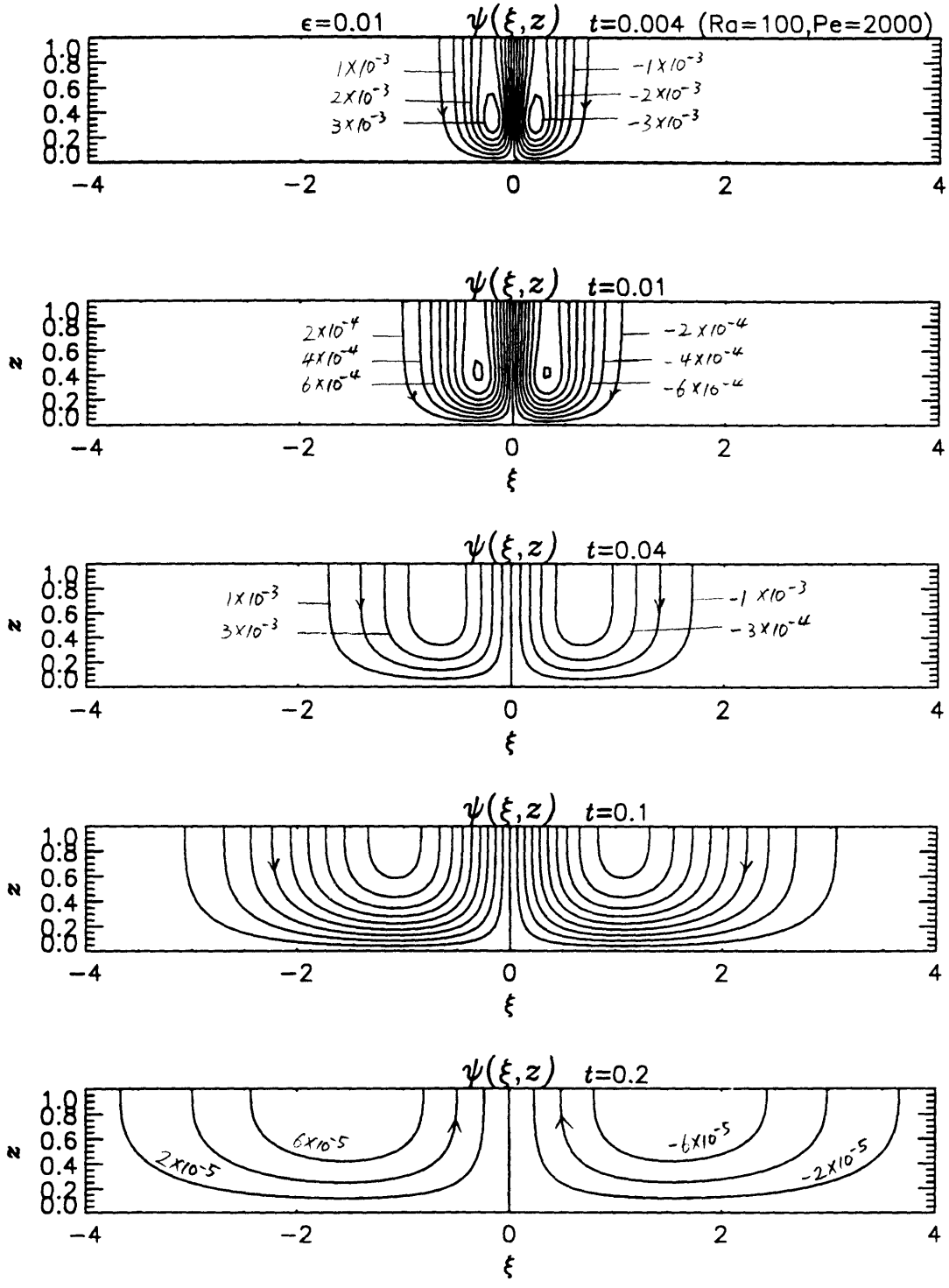

Fig. 6.11(b) Streamlines $\psi(\xi, z)$ for $Ra' = 100$ and $\overline{Pe_f} = 2000$ at various times.

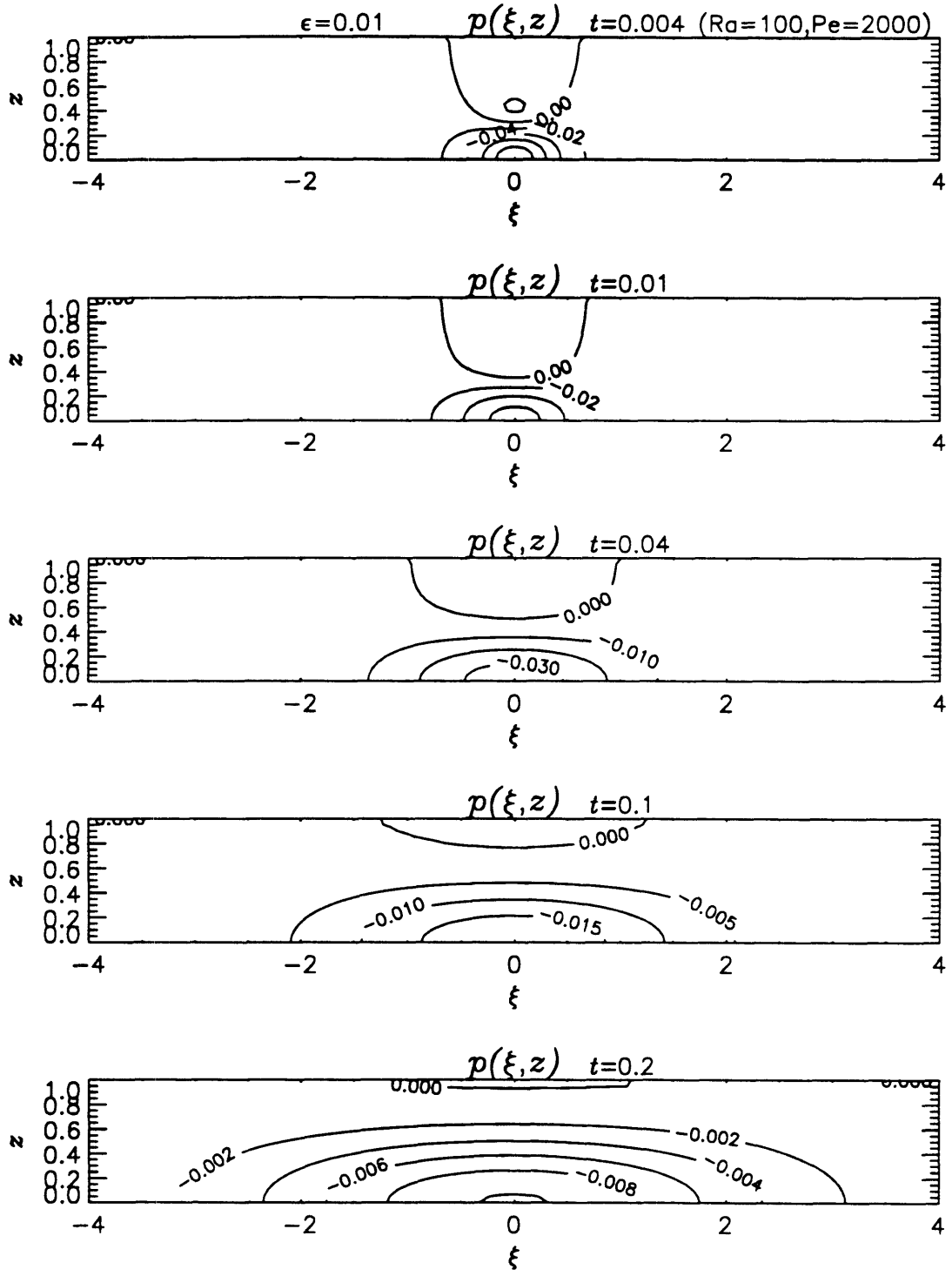

Fig. 6.11(c) Pressure distribution $p(\xi, z)$ for $Ra' = 100$ and $\overline{Pe_f} = 2000$ at various times.

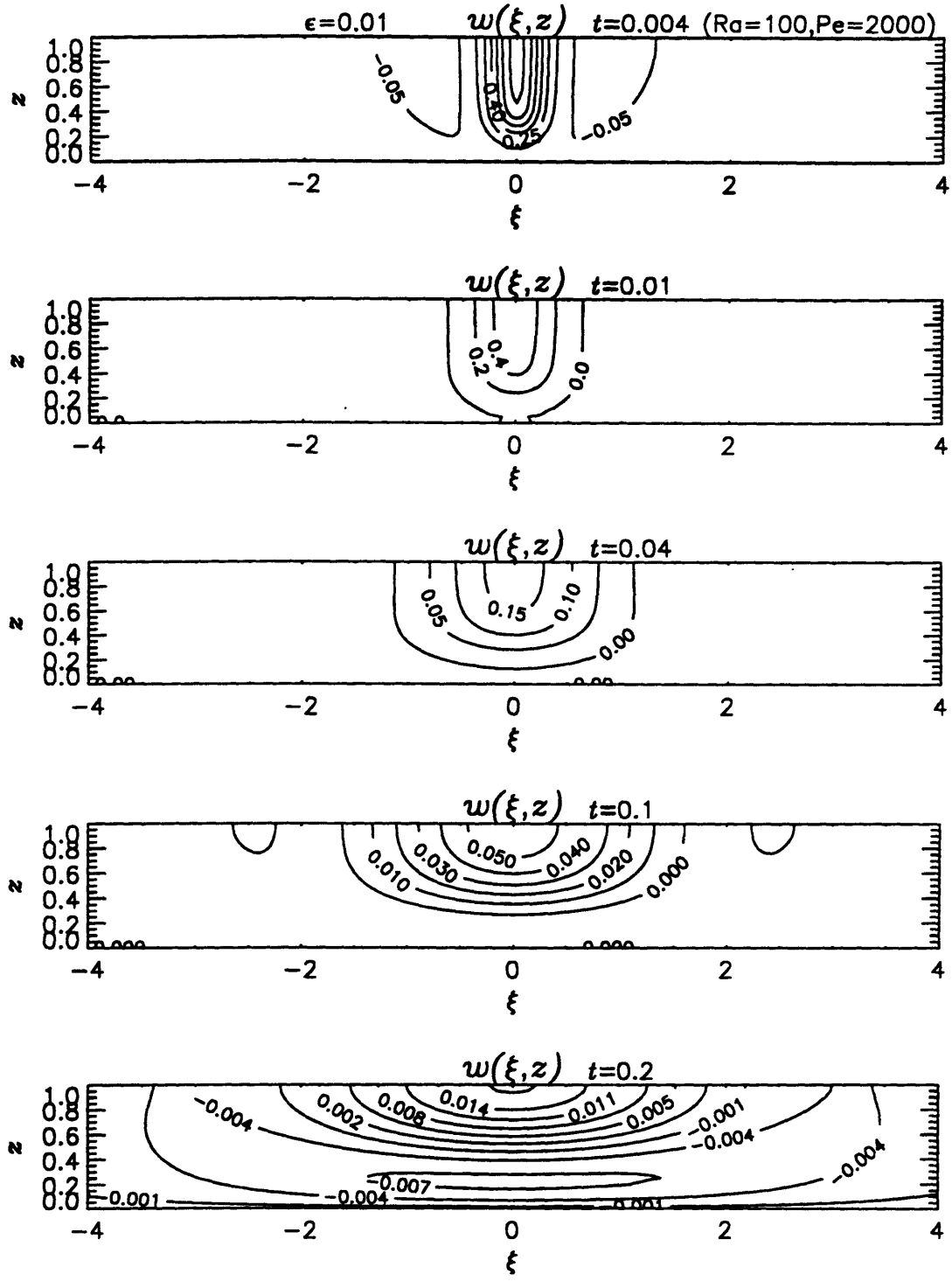

Fig. 6.11(d) Vertical displacement $w(\xi, z)$ for $Ra' = 100$ and $\overline{Pe_f} = 2000$ at various times.

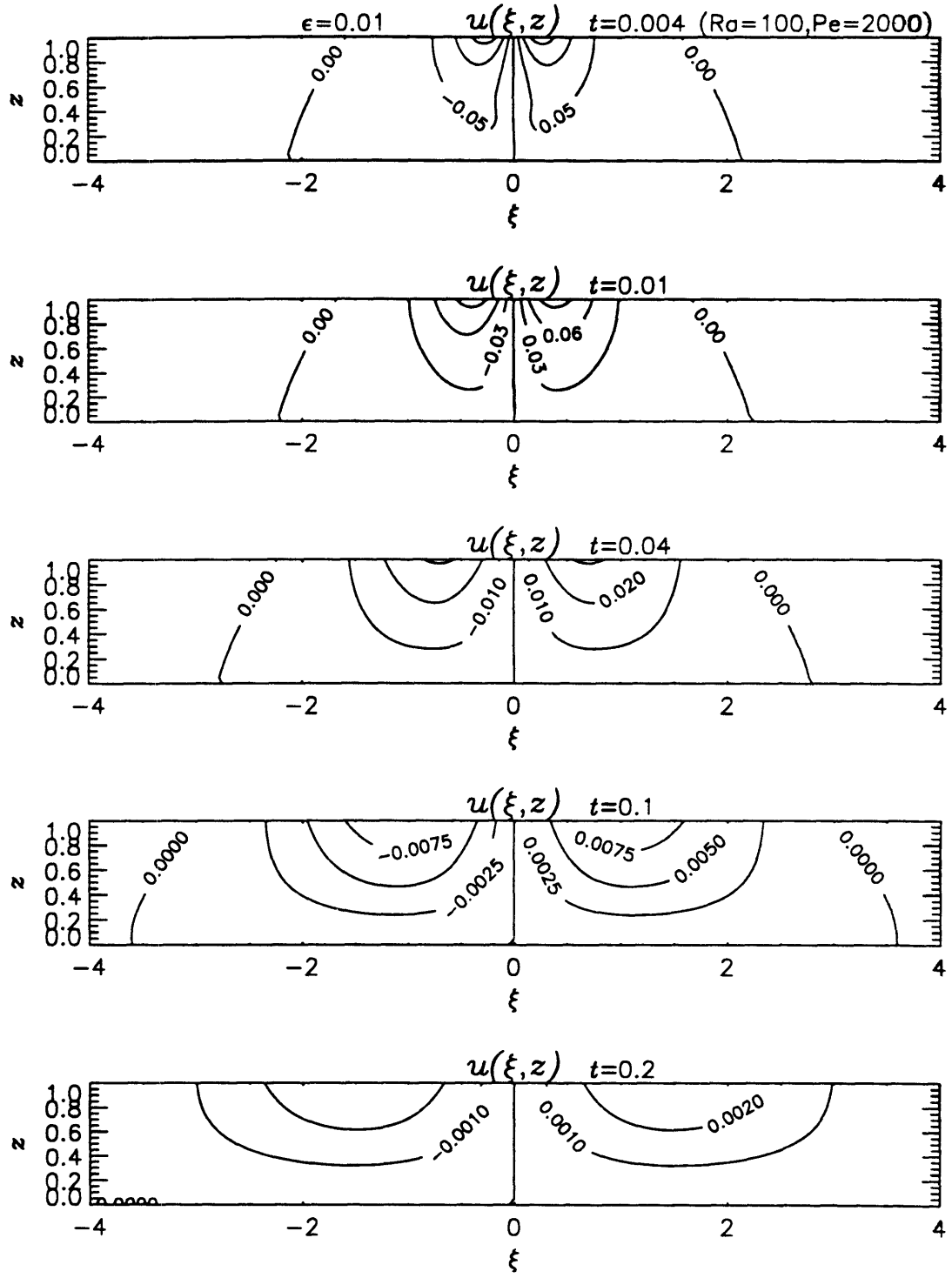

Fig. 6.11(e) Horizontal displacement $u(\xi, z)$ for $Ra' = 100$ and $\overline{Pe_f} = 2000$ at various times.

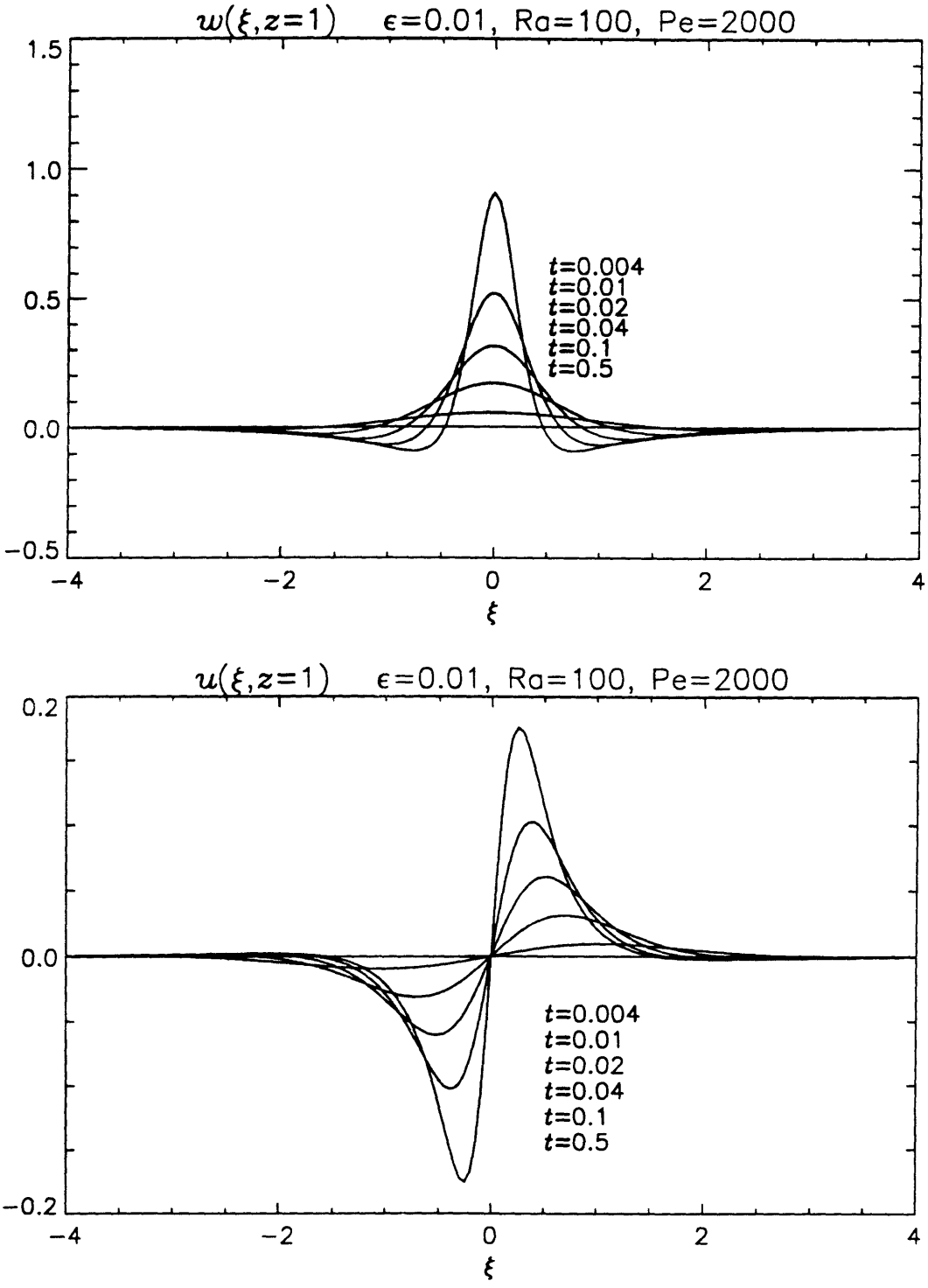

Fig. 6.12 Displacements at the upper surface (a) $w(\xi, z = 1)$ and (b) $u(\xi, z = 1)$ for $Ra' = 100$ and $\overline{Pe_f} = 2000$ at various times. The magnitude decreases with t.

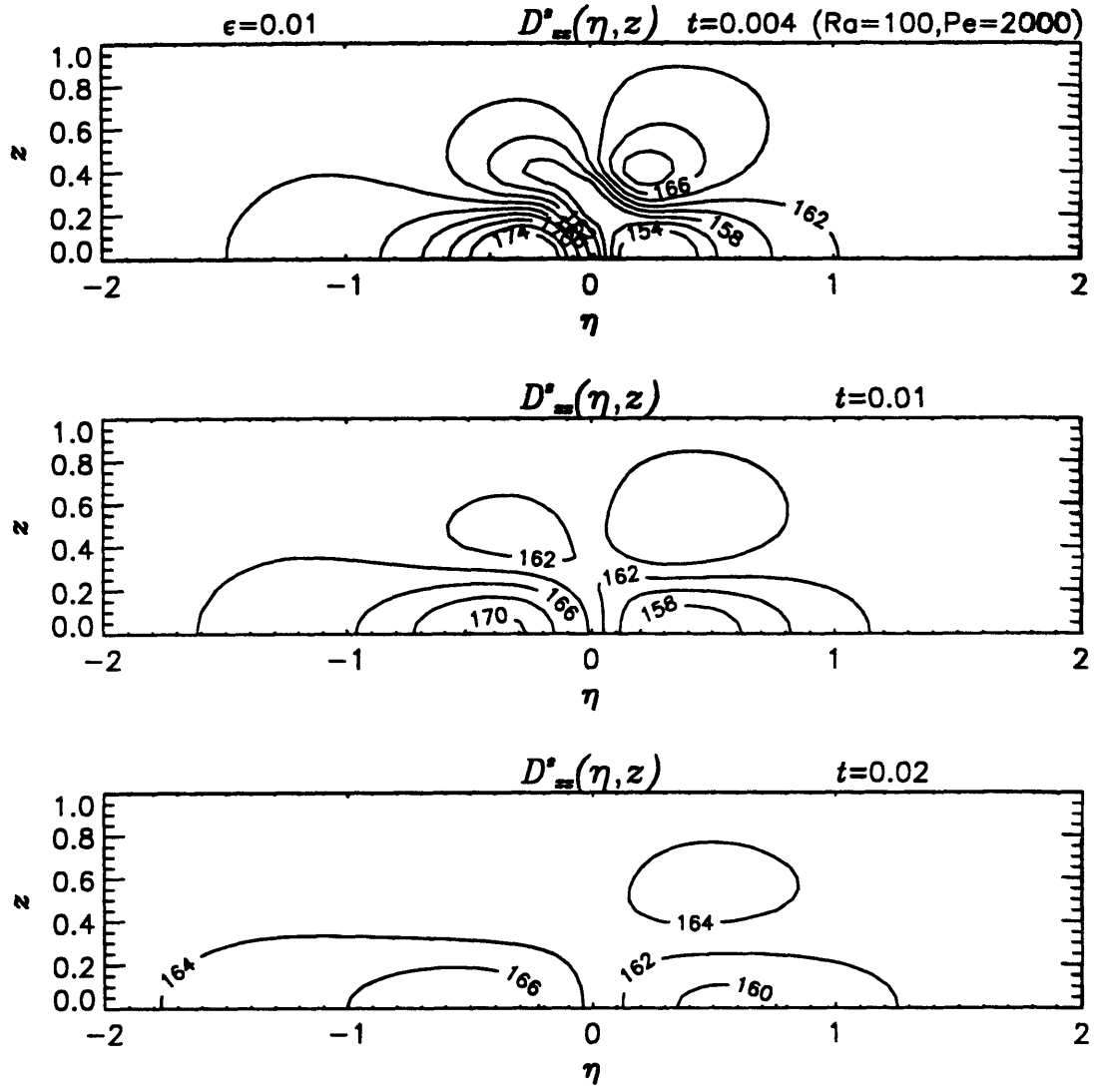

Fig. 6.13 Distribution of the dispersion coefficient $\langle m' \rangle + D^e_{zz}$ for $Ra' = 100$ and $\overline{Pe_f} = 2000$ at various times.

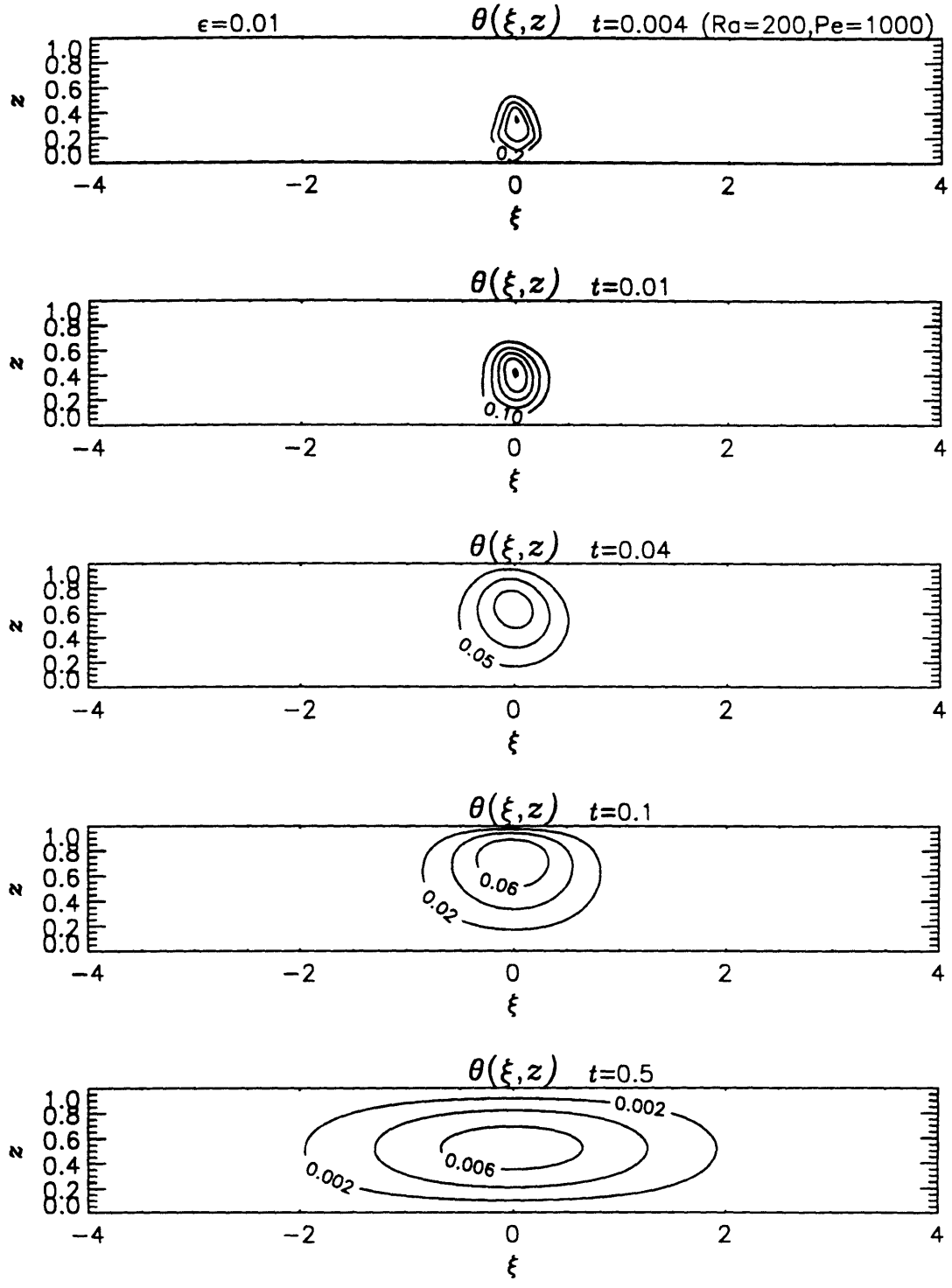

Fig. 6.14(a) Temperature distribution $\theta(\xi, z)$ for $Ra' = 200$ and $\overline{Pe_f} = 1000$ at various times.

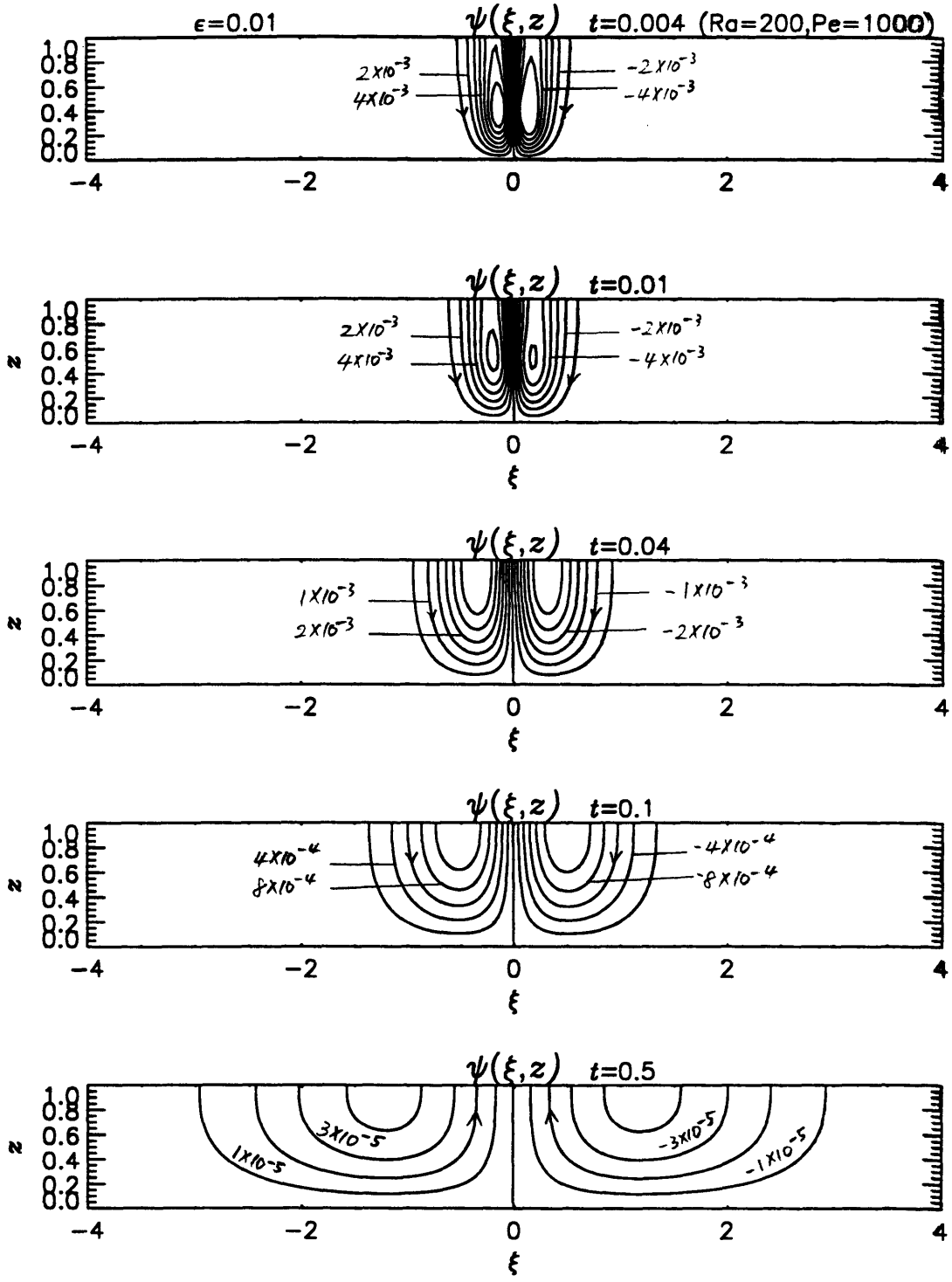

Fig. 6.14(b) Streamlines $\psi(\xi, z)$ for $Ra' = 200$ and $\overline{Pe_f} = 1000$ at various times.

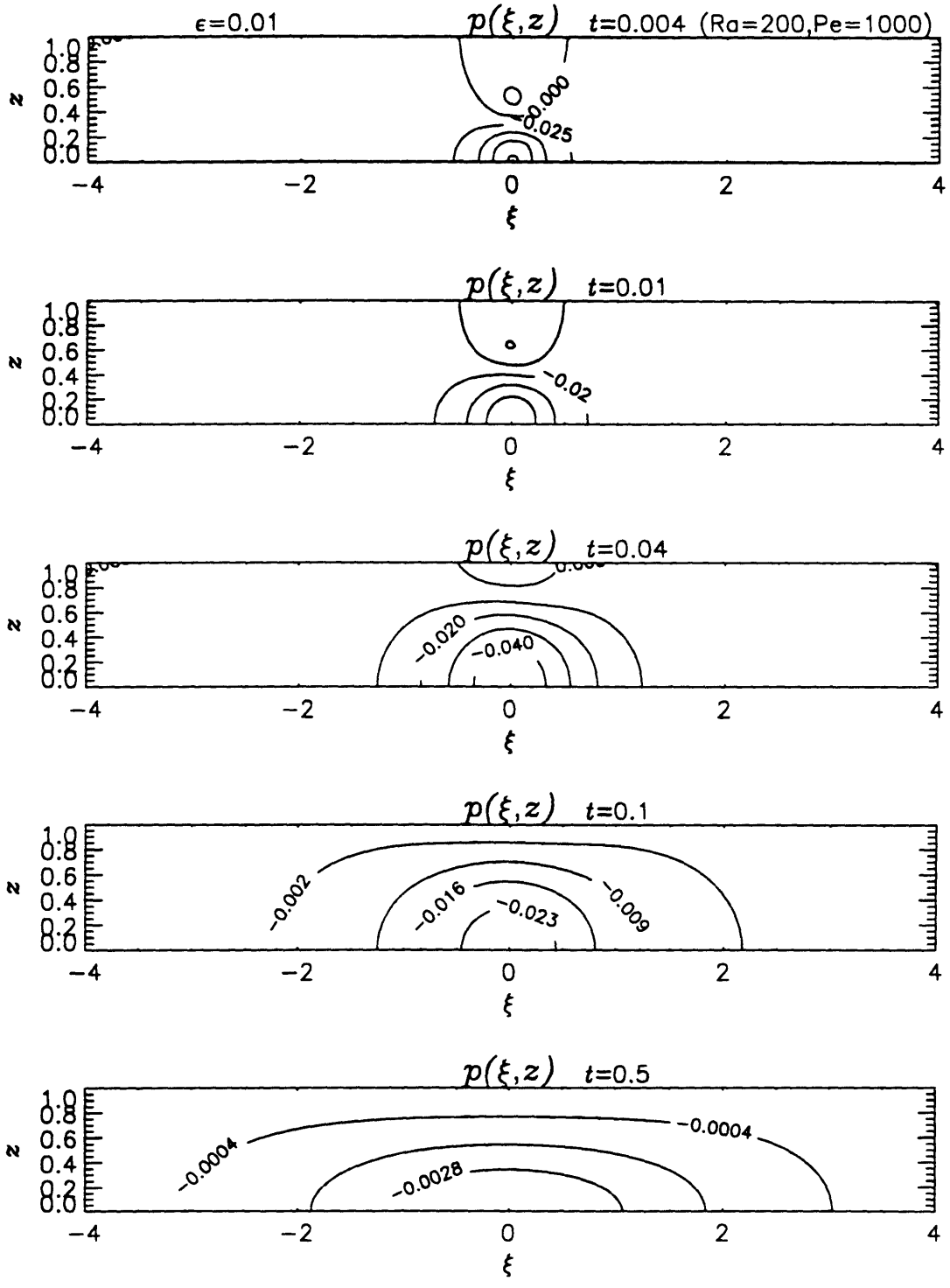

Fig. 6.14(c) Pressure distribution $p(\xi, z)$ for $Ra' = 200$ and $\overline{Pe_f} = 1000$ at various times.

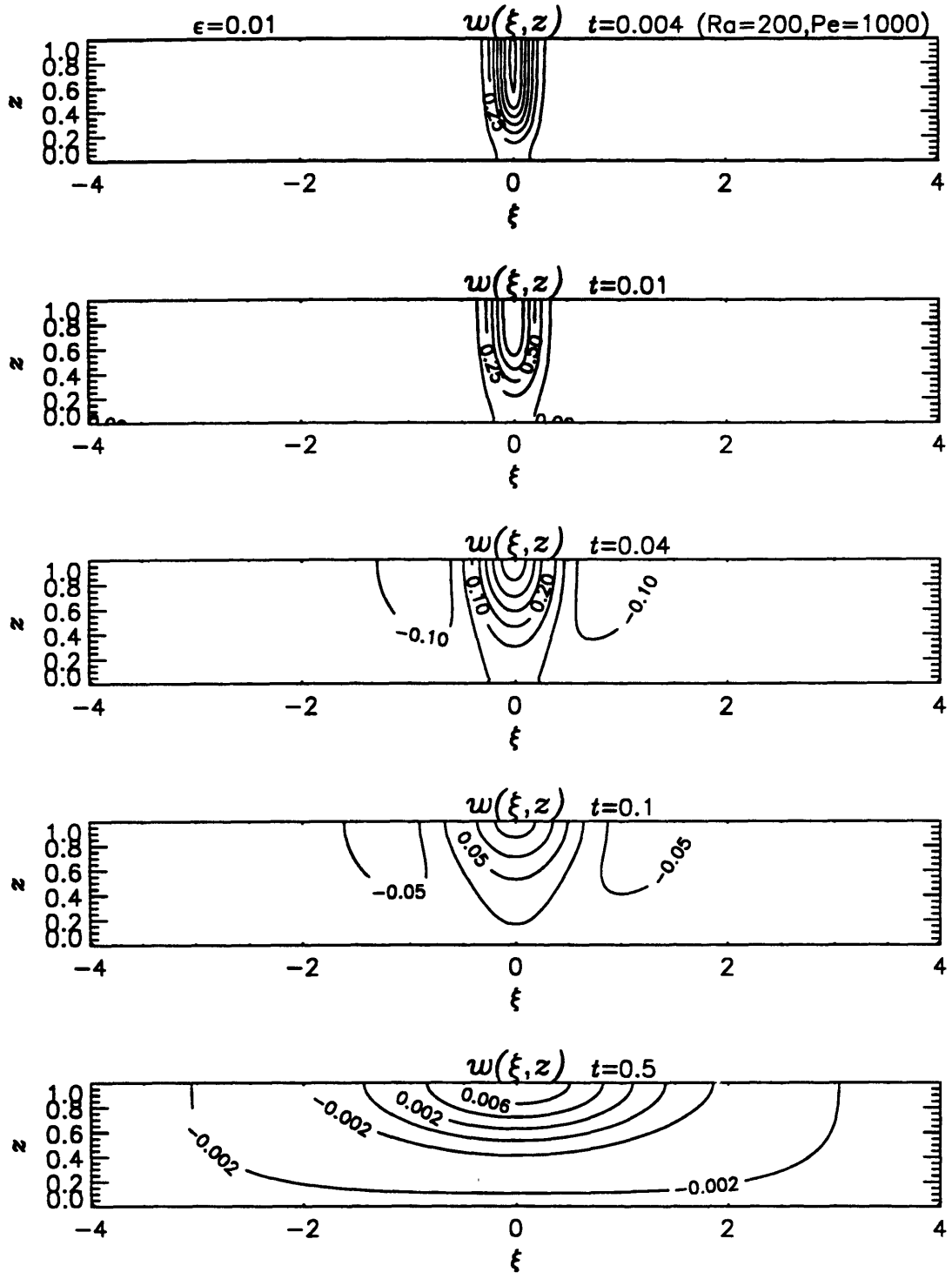

Fig. 6.14(d) Vertical displacement $w(\xi, z)$ for $Ra' = 200$ and $\overline{Pe_f} = 1000$ at various times.

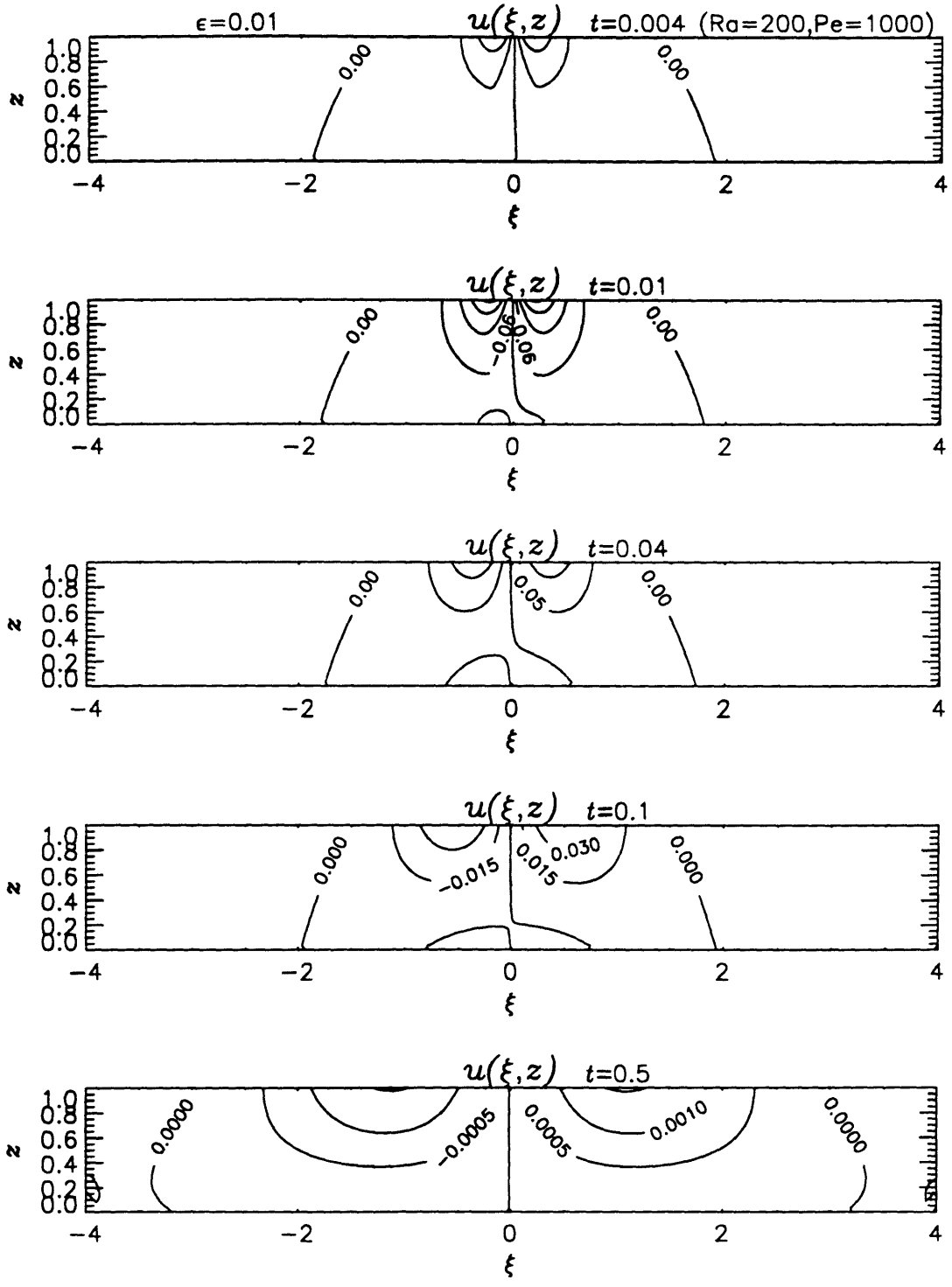

Fig. 6.14(e) Horizontal displacement $u(\xi, z)$ for $Ra' = 200$ and $\overline{Pe_f} = 1000$ at various times.

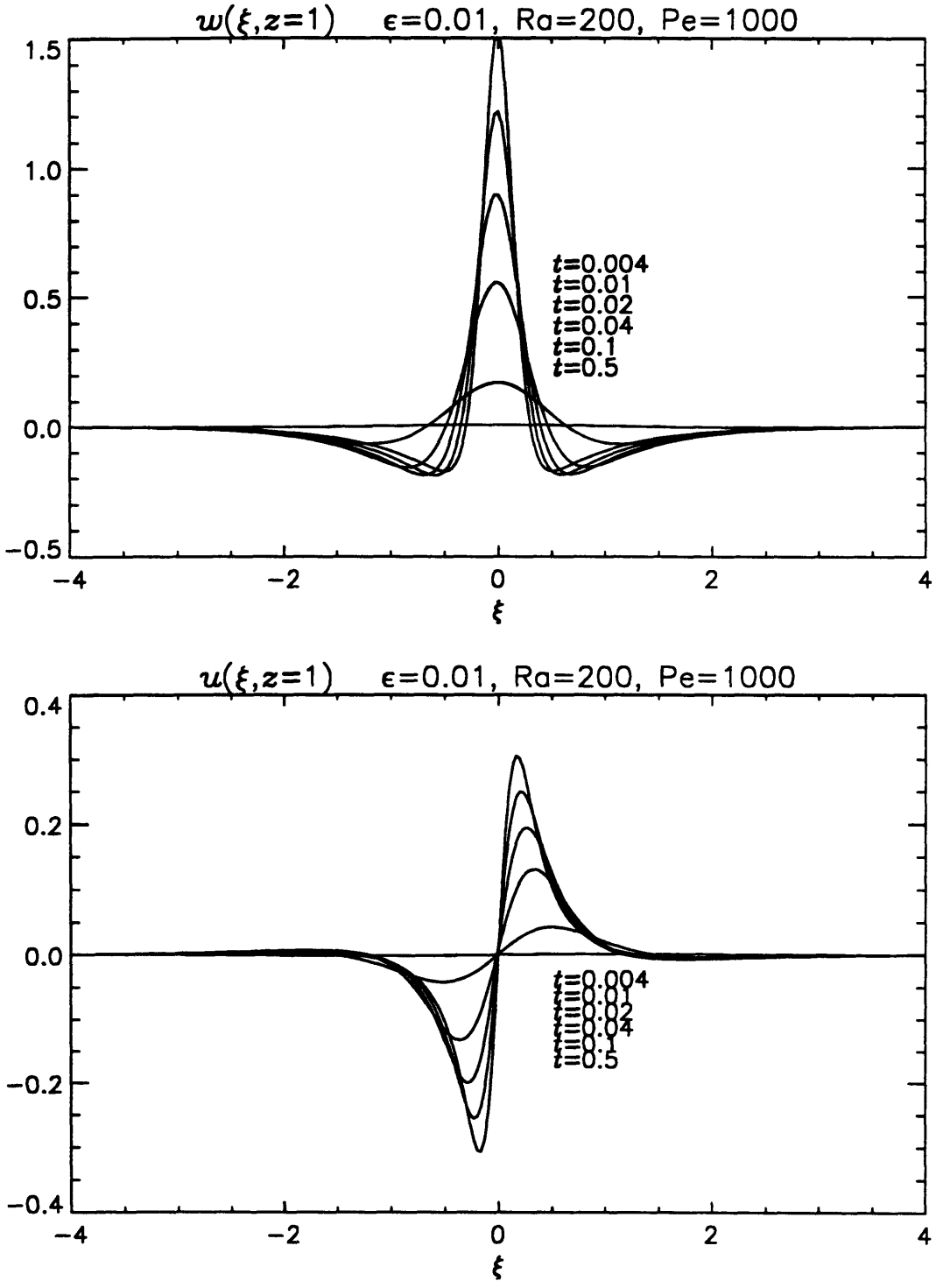

Fig. 6.15 Displacements at the upper surface (a) $w(\xi, z = 1)$ and (b) $u(\xi, z = 1)$ for $Ra' = 200$ and $\overline{Pe_f} = 1000$ at various times. The magnitude decreases with t.

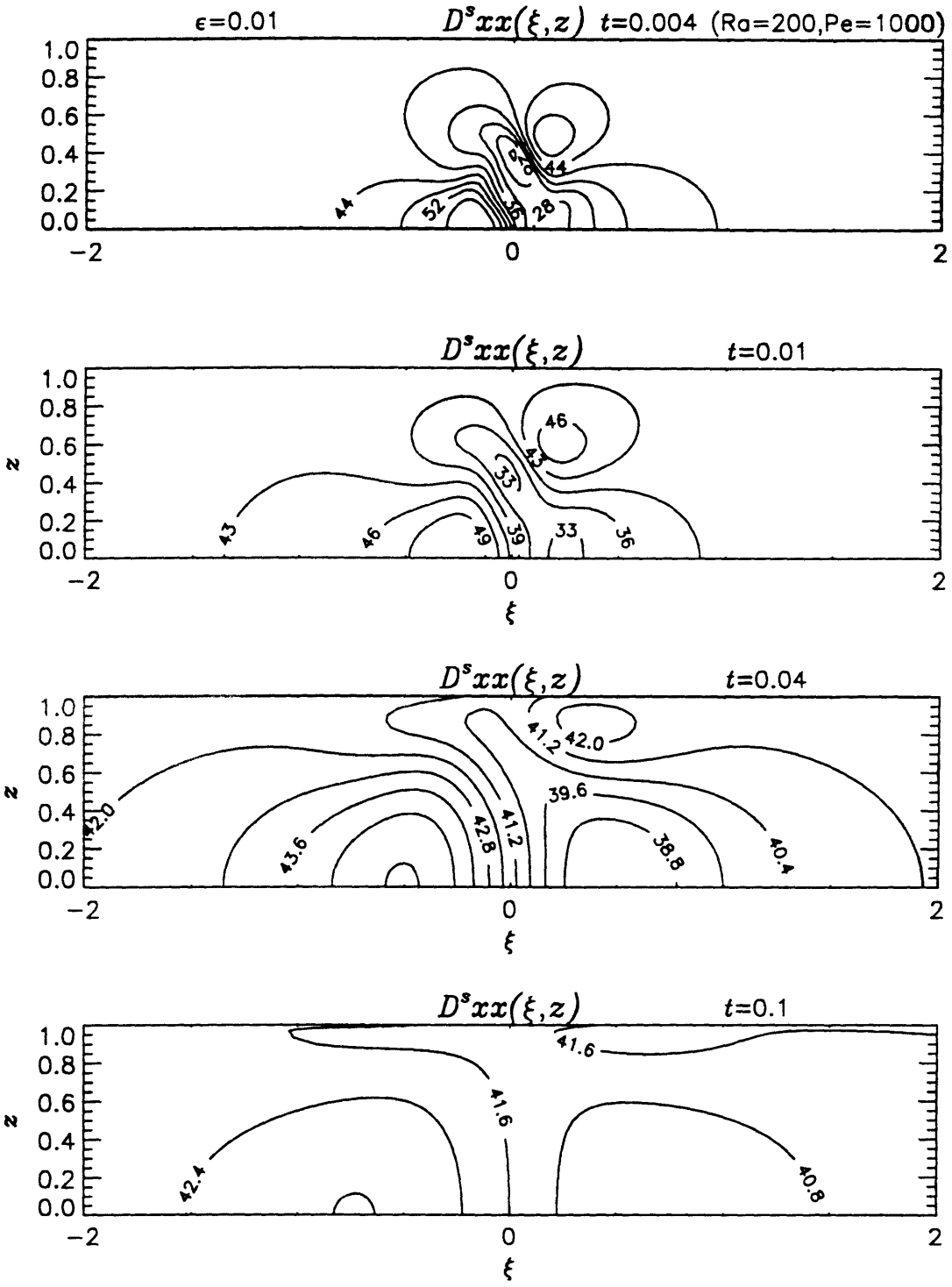

Fig. 6.16 Distribution of the dispersion coefficient $\langle m' \rangle + D^s_{xx}$ for $Ra' = 200$ and $\overline{Pe_f} = 1000$ at various times.

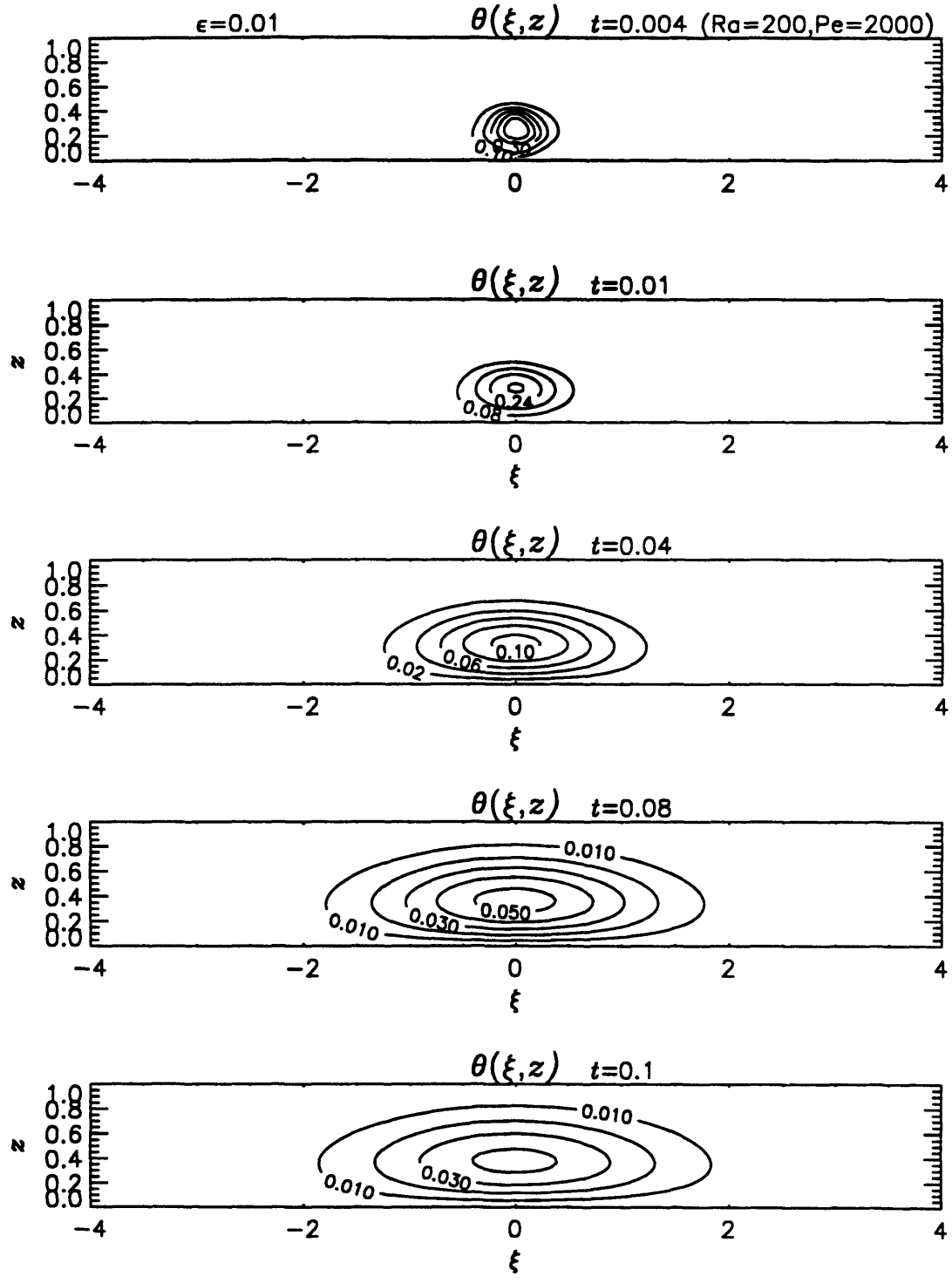

Fig. 6.17(a) Temperature distribution $\theta(\xi, z)$ for $Ra' = 200$ and $\overline{Pe_f} = 2000$ at various times.

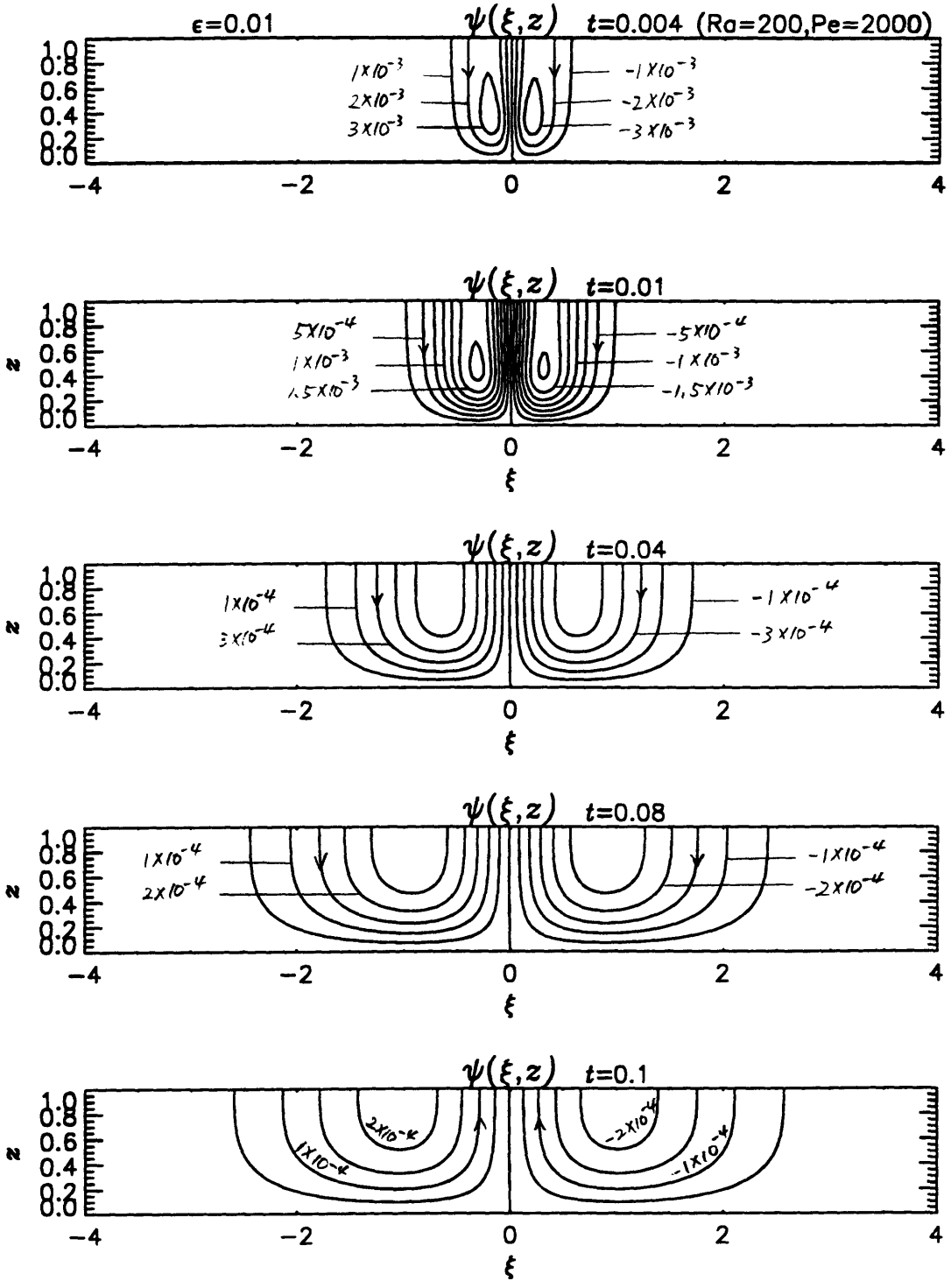

Fig. 6.17(b) Streamlines $\psi(\xi, z)$ for $Ra' = 200$ and $\overline{Pe_f} = 2000$ at various times.

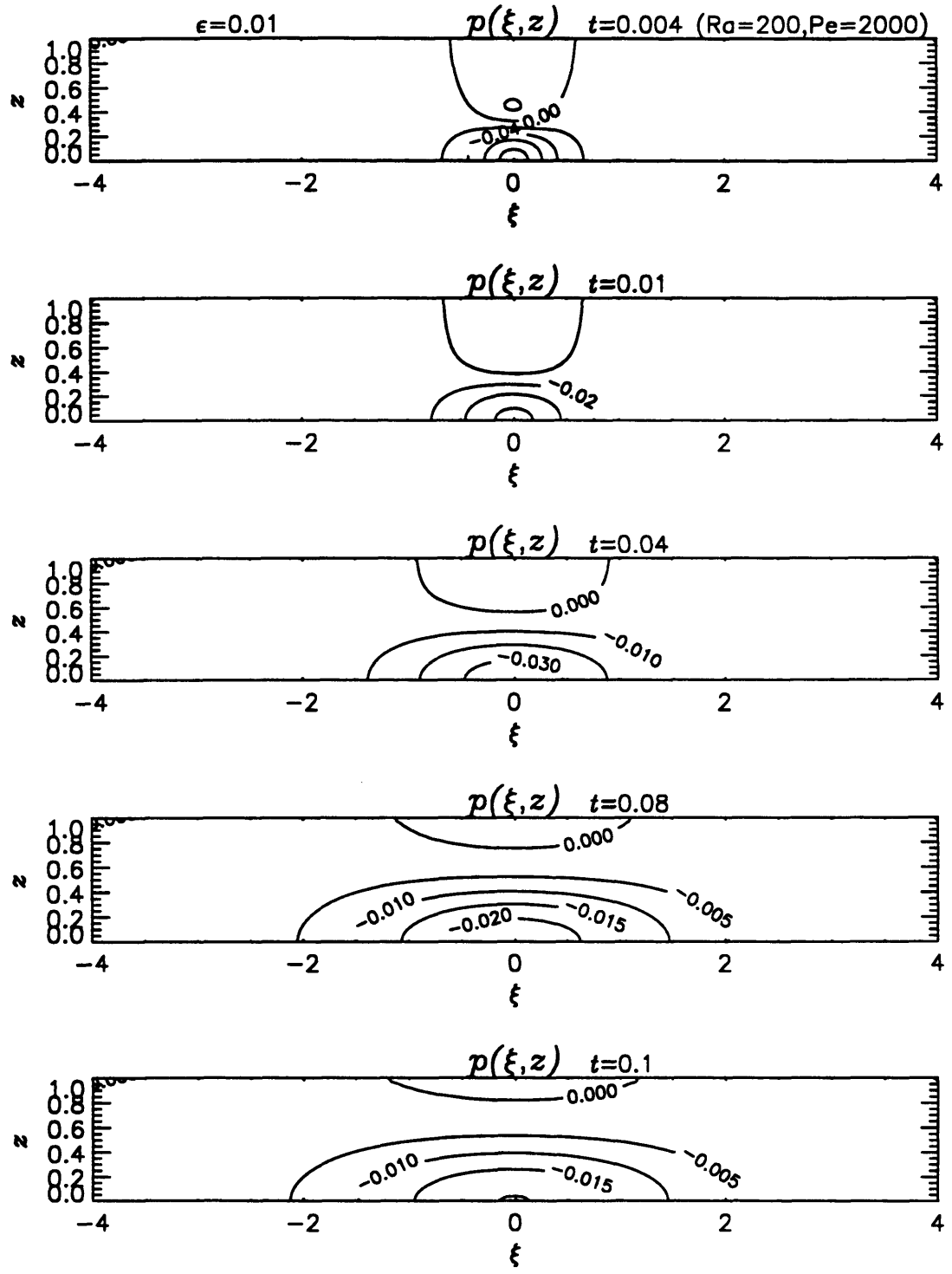

Fig. 6.17(c) Pressure distribution $p(\xi, z)$ for $Ra' = 200$ and $\overline{Pe_f} = 2000$ at various times.

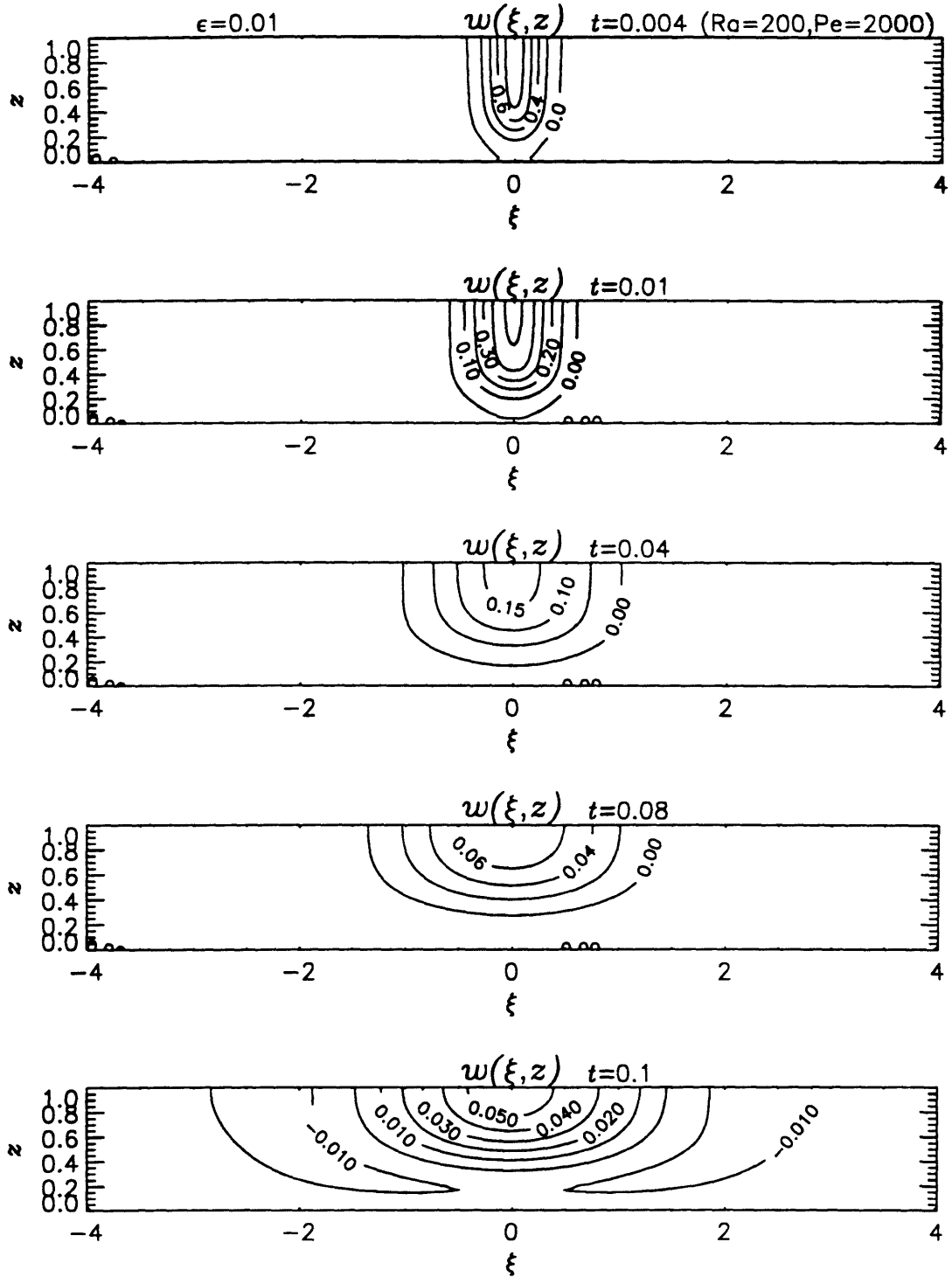

Fig. 6.17(d) Vertical displacement $w(\xi, z)$ for $Ra' = 200$ and $\overline{Pe_f} = 2000$ at various times.

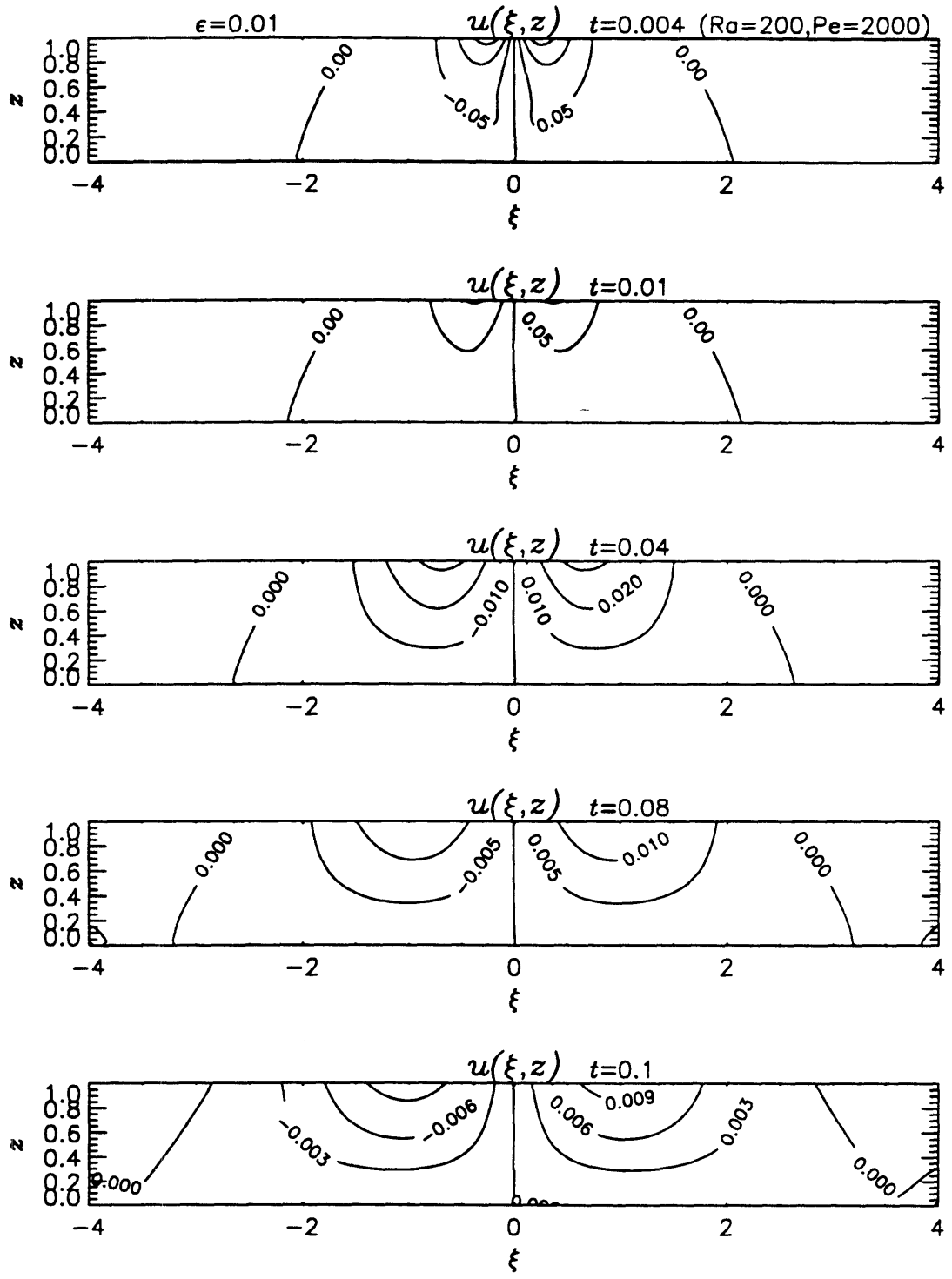

Fig. 6.17(e) Horizontal displacement $u(\xi, z)$ for $Ra' = 200$ and $\overline{Pe_f} = 2000$ at various times.

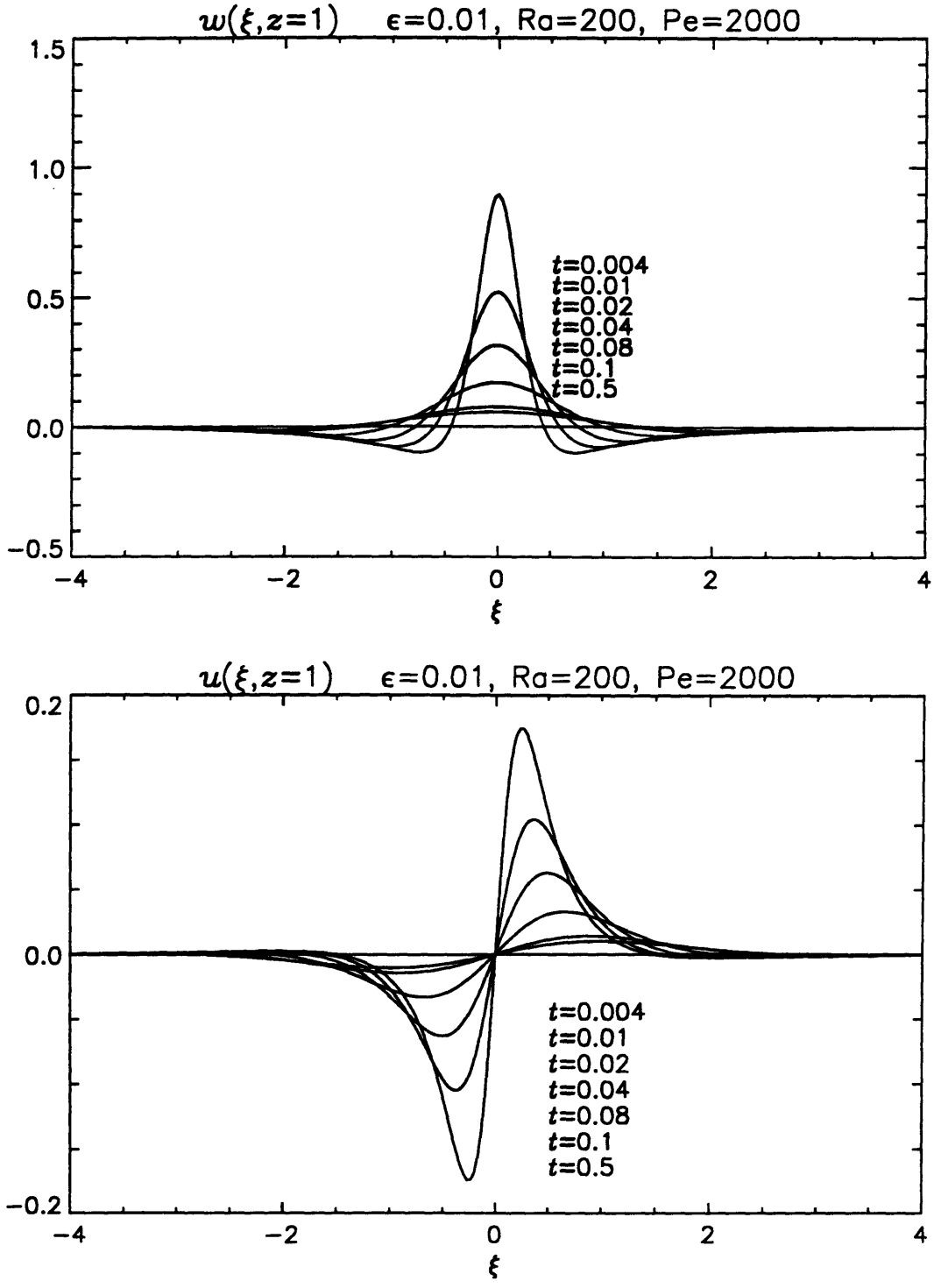

Fig. 6.18 Displacements at the upper surface (a) $w(\xi, z = 1)$ and (b) $u(\xi, z = 1)$ for $Ra' = 200$ and $\overline{Pe_f} = 2000$ at various times. The magnitude decreases with t.

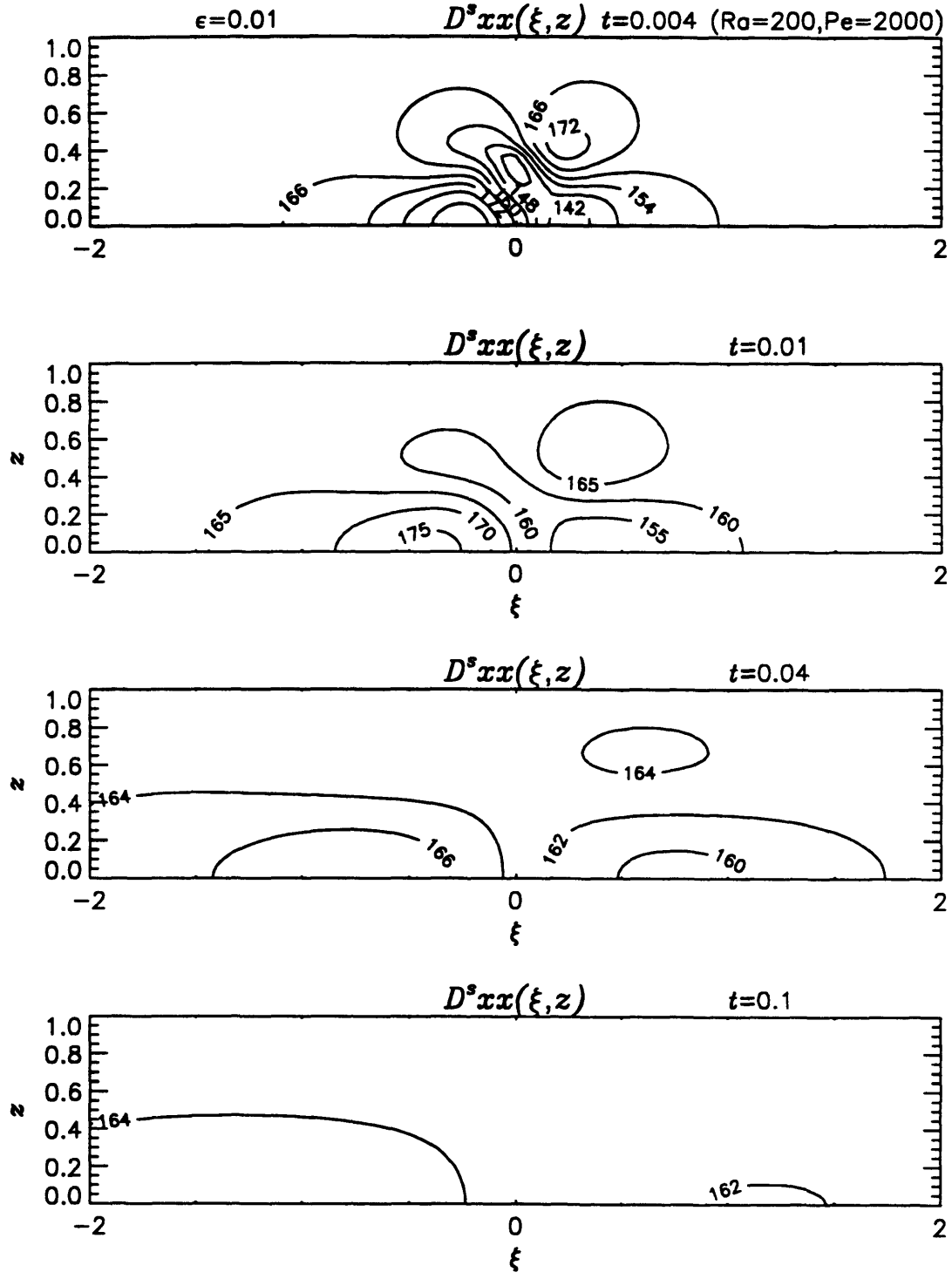

Fig. 6.19 Distribution of the dispersion coefficient $\langle m' \rangle + D^s_{zz}$ for $Ra' = 200$ and $\overline{Pe_f} = 2000$ at various times.

7. Conclusions

In this Chapter, we have studied thermal dispersion in three-scale poroelastic media. The mesoscale Peclét number is assumed to be finite but the Rayleigh number defined in terms of macroscale length is allowed to be large. The governing equations on the macroscale are deduced from those on the intermediate mesoscale by using the theory of homogenization. They are the equilibrium equation for matrix deformation, the consolidation equation for flow and the heat transport equation. Because of finite Peclét number heat convection induces dispersion on the macroscale. Due to buoyancy the flow and heat transport equations are coupled with full nonlinearity and can only be solved in iterative manner. The dispersion tensor can be calculated for a given seepage flow distribution by solving a mesoscale cell boundary value problem, which is a convection-diffusion equation with distributed sources. An important new result is that the mesoscale cell boundary value problem is nonlinearly coupled to the governing equations for flow and heat on the macroscale.

The general theory is applied to a special case of vertically stratified medium. By assuming that the velocity field is know, the symmetric and anti-symmetric dispersion tensors are obtained explicitly. It is shown that the dispersion tensors possess the tensor transformation property in the horizontal plane so that the dispersion tensors for any mean flow direction can be obtained from those for a mean flow in a vertical coordinate plane. Consequently it is only necessary to calculate D^s_{xx}, D^s_{zx} and D^s_{xz} for symmetric part and D^u_{xz} for anti-symmetric part for a mean flow in xz plane. Also the convection velocity of heat is explicitly obtained. It is composed of the Darcy velocity, the first order seepage velocity and the anti-symmetric dispersion tensor. It is shown that there are only two independent coefficients for the first order seepage velocity. They are determined by solving certain mesoscale cell boundary value problems which are seepage flow equations with distributed sources. However, if the medium is homogeneous on the mesoscale

all the macroscale coefficients reduce to those on the mesoscale since the medium is then two-scale medium.

The results for vertically stratified medium is further specialized to a medium with two alternating layers on the mesoscale. Analytic dispersion tensors and convection velocity of heat are obtained. In particular, the symmetric dispersion tensor depends strongly on the mean flow direction. When the mean flow is perfectly parallel to the layers, the longitudinal dispersion coefficient $\langle m' \rangle + D^s_{zz}$ increases with Pe'^2 where Pe' is the mesoscale Peclét number. For flow directions not parallel to the layers (even for mean flow directions slightly off the horizontal plane), $\langle m' \rangle + D^s_{zz}$ first increases with Pe' but soon reaches finite limit value which decreases as $\cot^2 \theta$ where θ is the angle between the mean flow direction and the layers. Similar results have been shown in different approaches,e.g. stochastic random walk and moment method (Matheron and de Marsily, 1980; Gupta and Bhattacharya, 1986; Güven and Moltz, 1986). The transverse dispersion coefficient $\langle m' \rangle + D^s_{zz}$ increases only by a small amount as θ increases. For passive solute D^s_{zz} and D^u_{zz} are zero. For heat D^s_{zz} and D^u_{zz} are not zero although they are much smaller than $\langle m' \rangle + D^s_{zz}$ but larger than $\langle m' \rangle + D^s_{zz}$.

The theory is applied to dispersion of a thermal cloud released in a uniform seepage flow through a layered medium. As the Peclét number of the uniform flow increases, the thermal cloud spreads faster in the longitudinal direction because the dispersion coefficient $\langle m' \rangle + D^s_{zz}$ increases. It is also shown for large Rayleigh number that the thermal cloud does not only convected by the uniform flow but also rises vertically due to strong buoyancy. As mentioned above, thermal dispersion is nonlinearly coupled among the flow, temperature and dispersion coefficients. The buoyancy induced flow modifies the downstream seepage flow. Consequently the dispersion coefficients vary in space. It is shown for large Rayleigh number that, at the early stage when the temperature is high, the variation of the longitudinal dispersion coefficient $\langle m' \rangle + D^s_{zz}$ is comparable to that of the uniform background seepage flow. The matrix deformation is dominated by thermal stress. Inparticular,

the upper surface swells up with neighboring compaction bowls. The compaction bowls are due to rotating flow in the layer and is caused by the downward seepage flow underneath.

SUMMARY AND CONCLUSIONS

We have investigated thermal dispersion in poroelastic media by using the theory of homogenization : in Chapter I for two-scale media and in Chapter II for three-scale media. The medium is assumed to be relatively highly permeable and hard. The homogenization theory makes two key assumptions. One is the existence of disparate length scales. Secondly the medium structure, the unknowns and the material properties are assumed to be periodic at all scales but the largest one. Specifically, in two-scale medium there are the microscale ℓ and the macroscale ℓ' such that $\ell/\ell' \ll 1$ and the microscale ℓ, the mesoscale ℓ' and the macroscale ℓ'' in three-scale medium which are related by $\ell/\ell' \ll 1$ and $\ell'/\ell'' \ll 1$. By choosing $\epsilon = \ell/\ell' = \ell/\ell'$ as ordering parameter, the multiple-scale analysis is then used to deduce the governing equations and constitutive coefficients on the macroscale without empirical assumptions. Certain microcell and meoscale cell boundary value problems are defined which must be solved for given cell geometries to calculate the macroscale coefficients. It is a methematically rigorous scheme and the macroscale inhomogeneities are easily incorporated.

In Chapter I, the macroscale governing equations are deduced from the basic conservation laws in the fluid and solid phases. Both the microscale Peclét number and the Rayleigh number are assumed to be finite. Under this assumption, buoyancy is not important in Darcy's law and appears only as first order contribution. The governing equations are the quasi-static equilibrium equation, the consolidation equation and the heat transport equation. Because of the assumption of relatively hard porous medium, the equilibrium equation is decoupled from the rest. On the other hand, the consolidation equation and the heat transport equation are nonlinearly coupled via the first order seepage velocity due to the effect of weak inertia in the fluid momentum equation. The dispersion tensor is in general not symmetric. It is determined in terms of the leading order fluid velocity. For solute transport as shown by Mei and Auriault(1991) and Mei(1992), if the medium is isotropic and homogeneous on the macroscale, the first order seepage velocity is

identically zero so that the flow and heat transport are decoupled. In this study, it is shown that for heat transport, even if the medium is isotropic and homogeneous, the first order seepage velocity depends on the medium temperature due to buoyancy. Consequently the heat transport is still nonlinear equation for the temperature although it is very weak. In any case, the solid deformation is determined from the equalibrium equation by using the pressure and temperature distributions.

As a model microcell geometry, we have chosen a cubic array of Wigner-Seitz grains and calculated the dispersion tensor by solving a microcell boundary value problem numerically. The cell boundary value problem is a convection-diffusion equation with distributed sources and is identical to that defined in Mei(1991) for rigid medium. For solute transport, it reduces to Brenner's(1980). The Wigner-Seitz cell has three planes of symmetry and the mean flow direction is chosen to be in one of the symmetry axes. For the chosen flow direction, it is shown by using the symmetry properties of the solution that there are only two independent nonvanishing coefficients, the longitudianl D_L and transverse D_T coefficients. Also D_L and D_T are isotropic in the plane normal to the mean flow direction, as pointed out by Brenner(1980). However for other flow directions this does not hold.

Computed D_L and D_T show growth as Pe^2 where $Pe = U\ell/\alpha_f$ is the microscale Peclét number with U, ℓ and α_f being the mean flow velocity, microcell size and thermal diffusivity of fluid. The tendency of Pe^2 for D_L has been previously shown in the approximate analytical results for dilute periodic suspensions of spheres by Koch et al (1989) and is consistent with the numerical results by Salles et al (1993) and the measurements by Gunn and Pryce (1969). However, the prediction for D_T by Koch et al does not grow with Pe and remains almost the same as the molecular diffusion coefficient. For dilute suspension they assume that the convection velocity in the pores to be equal to that of the ambient mean flow. As a result, the pore fluid velocity variations are discarded. On the other hand, the randomly distributed particles approach by Koch and Brady(1985) indicates that D_T also grows with Pe. Their analysis is based on the assumption that the medium is dilute and the

disturbances are basically induced by a single particle. For large Pe, the following three mechanisms are accounted : purely mechanical contribution, hold up of solute in particles, and boundary layer effect. None of these produces non-zero contribution to D_T. However, by adding correction due to particle interactions, they were able to obtain the behavior of D_T proportional to Pe. This shows that, especially for densely packed particles like Wigner-Seitz grains, the interactions among the particles are important. Numerical results for D_T are not available in Salles et al and to our knowledge there are no reliable measurements of D_T for periodic arrays of particles. It should ne noted however that the Pe^2 growing tendency is in contrast with data from numerous experiments with natural granular media for which linearly increasing dispersion coefficients are observed. The discrepancy is likely due to the difference in the medium structure of the Wigner-Seitz grain and the natural media.

In Chapter II, thermal dispersion in three-scale deformable porous media is studied by extending the two-scale analysis of Ch. I. The scale ℓ' which was called the macroscale in two-scale medium is now called the mesoscale. The macroscale ℓ'' is much larger than ℓ'. The mesoscale Peclét number is assumed to be finite, but the Rayleigh number is large. The macroscale governing equations and effective coefficients are deduced by using the homogenization theory from the mesoscale equations. Because of large Rayleigh number, buoyancy becomes important in Darcy's law and heat convection. Accordingly, the flow and heat transport equations are nonlinearly coupled. An important new result is that the mesoscale cell boundary value problem, which is a convection-diffusion equation, is nonlinearly coupled to the governing equations for flow and heat on the macroscale. This shows that the dispersion tensor can be calculated only for a given seepage velocity distribution by solving the mesoscale boundary value problem. The dependence of dispersion tensor on temperature has been recognized in the study of the effect of thermal dispersion on the stability of steady convection in porous layer (Rubin, 1974; Tyvand, 1977,1981).

As a special class of periodic media, we have chosen periodically stratified medium in the vertical direction. Assuming that the seepage velocity field is known, we derive explicit expressions for the symmetric and anti-symmetric dispersion tensors and also the heat convection velocity. In particular, it is shown that the dispersion tensors for a mean flow direction rotated in the horizontal plane are obtained from those for the mean flow direction in a coordinate plane by using tensor transformation rule. This simplifies the calculation of dispersion tensors for stratified medium. Consequently it is only necessary to calculate D^s_{xx}, D^s_{zx} and D^s_{zz} for the symmetric part and D^u_{zx} for the anti-symmetric part.

For a medium with two alternating layers on the mesoscale, the analytic dispersion tensors are used to calculate $\langle m' \rangle + D^s_{xx}$, D^s_{zx}, $\langle m' \rangle + D^s_{zz}$ and D^u_{zx} where $\langle m' \rangle$ is the depth average of the mesoscale thermal conductivity. For solute dispersion by allowing the variation of permeability only, we show that $D^s_{zx} = D^u_{zx} = 0$ and $\langle m' \rangle + D^s_{zz} = m''_{zz}$ where m''_{zz} is the harmonic mean of m' along depth. It is particularly shown that the longitudinal dispersion coefficient $\langle m' \rangle + D^s_{xx}$ strongly depends on the mean flow direction. If the mean flow direction is perfectly parallel to the layers, $\langle m' \rangle + D^s_{xx}$ increases as Pe'^2 where Pe' is the mesoscale Peclét number. For flow directions not parallel to the layers, $\langle m' \rangle + D^s_{xx}$ first increases with Pe' but soon reaches finite limit value which decreases with $\cot^2 \theta$ where θ is the angle between the mean flow direction and the layers. Similar results have been shown previously by different approaches (Matheron and de Marsily, 1980; Gupta and Bhattacharya, 1986; Güven and Moltz, 1986). Since it is very unlikely that the flow direction is perfectly parallel to the layers, $\langle m' \rangle + D^s_{xx}$ is expected to reach finite limit as Pe' increases in most situations. On the other hand, the tranverse dispersion coefficient $\langle m' \rangle + D^s_{zz}$ increases only by a small amount as θ increases.

Thermal dispersion tensors depend on the mesoscale inhomogeneities of not only permeability but also the heat capacity and thermal conductivity. The dependence of the longitudinal dispersion coefficient $\langle m' \rangle + D^s_{xx}$ on the flow direction is

the same as in solute transport. It is further shown in this study that the symmetric dispersion tensor is quadratically proportional to the heat capacity whereas linearly proportional to the thermal conductivity. Inhomogeneities in heat capacity therefore can cause dispersion comparable to that due to inhomogeneities in permeability. It is also shown that D^s_{xz} and D^u_{xz} are non-zero in thermal -dispersion. They are much smaller than $\langle m' \rangle + D^s_{xz}$ but larger than $\langle m' \rangle + D^s_{zz}$. For two alternating layers, Moranville et al (1977a,b) and Tyvand (1980) considered the dispersion tensor by employing the general formulas for anisotropic medium due to Scheidegger(1961) and Poreh(1965). By considering several special directions of flow and concentration gradient, they only obtain some constraints for the coefficients which must be determined from experiments. We stress that the dispersion tensor form employed by Scheidegger and Poreh is based on physical postulates inferred from experimental observations that dispersion coefficients are linearly proportional to the velocity. Our results have been deduced from the basic governing equations on the mesoscale.

As an application of the macroscale equations, dispersion of a thermal cloud released in a uniform seepage flow through a layered medium is studied. For the uniform flow disprsion coefficients are constant. While the thermal cloud is convected downstream by the uniform flow, buoyancy-induced flow modifies the uniform flow. As a result the dispersion coefficients vary both in space and time. If the cloud is solute matter, the uniform flow is not altered and dispersion coefficients remain constant. The spreading of solute is affected only by the Peclét number of the uniform flow and the solute transport equation becomes linear. In thermal dispersion, the flow, temperature and dispersion coefficients are nonlinearly coupled. As the Rayleigh number increases, buoyancy becomes stronger and the spatial variation of the longitudinal dispersion coefficient becomes large. For sufficiently large Rayleigh number, the thermal cloud rises across the layer thickness before it spreads out due to dispersion. The Peclét number tends to weaken the buoyancy effects since the longitudinal dispersion coefficient increases with Peclét number. The medium deformation is dominated by thermal stress so that the upper surface swells up with

neighboring compaction bowls. The appearance of compaction bowls is due to rotating motion of pore fluid induced by buoyancy. As time increases, all disturbances die out. We note that the dispersion coefficient is determined as a part of solution for the coupled flow and heat transport.

Rubin(1974) and Tyvand(1977,1981) have considered the effect of thermal dispersion on the stability of uniform flow in a porous layer with temperature gradient across the layer. They take into account the dependence of dispersion coefficient on the temperature and thus the flow and heat equations are nonlinearly coupled. However the dispersion tensor used is based on the form due to Poreh(1965) and, as mentioned above, contains some coeffcients which must be determined experimentally. This leads to additional parameters.

Extensions of the present work are worthwhile in the following directions.

First, as a continuation of the present study, calculation of dispersion tensor for mean flow directions other than along the symmetry axis of the Wigner-Seitz cell is needed to investigate the dependence of dispersion tensor on the direction of the mean flow. For two-dimensional arrays of cylinders some results are available for flow directions other than the crystallographic axes,e.g. Edwards et al(1989) and Salles et al (1993). For three diemnsional array of spheres, the results by Koch et al show that the dispersion coefficients increase and then reach finite limit values even for a flow direction slightly off the crystallographic axis as the Peclét number increases. Examination of the relationship between dispersion tensor and flow direction will help understand dispersion characteristics of spatially periodic medium.

We have assumed, at the outset, that the porous medium is relatively highly permeable and hard. As a result, the solid deformation is decoupled from the flow and heat transport. More specifically the criterion is the ratio of the consolidation time to heat diffusion time $T_c/T_d = \rho_f g \alpha_f / \mathcal{D} K$ is very small where $\rho_f g$, α_f, $\mathcal{D}$ and K are the specific weight of fluid, thermal diffusivity of fluid, elastic modulus of medium and hydraulic conductivity.While $\rho_f g$ and α_f do not change much, $\mathcal{D}$ and

K vary widely depending on the medium. Hence in moderately permeable and hard medium, the time scale ratio may become finite. This will lead to an interesting problem in view of the interactions among the medium deformation, pressure and heat.

In realistic field situations, porous medium usually does not show the scale disparity clearly. In fact, the medium structure appears to be rather complicated and it is not easy to identify the length scales by the appearance of the medium. To describe a natural medium adequately is a problem of characterization. The more difficult the medium is to characterize, the less likely can the theory be free of empiricism. The homogenization theory used in this work does not deal with the medium characterization but aims at complete analysis of all scales. In the stochastic approaches, this issue of characterization is addressed but the microscale is largely overlooked. In view of this and the goal of improving the capability of the homogenization theory towards the applicability to realistic porous media, efforts should be made to incorporate the problem of characterizing porous media in terms of hydrologic, mechanical and thermal properties of the medium, and to perform computations for more complex microcells.

Heat transport and solute transport occur together in many situations such as double diffusive convection in porous media, thermohaline convection in gorundwater flow and disposal of toxic or nuclear wastes (Griffiths, 1981; Rubin and Roth, 1983; Henseley and Savvidou, 1993). They belong to the subject of double diffusion. Application of the homogenization theory to double diffusion would be straightforward and requires simultaneous consideration of solute and heat. Interesting features due to interactions among the pressure, solute and heat are expected.

REFERENCES

Adler, P.M. and Brenner, H. (1984), Transport processes in spatially periodic capillary networks, PhysicoChem. Hydrodyn., 5, 245-285.

Bear, J. (1972), Dynamics of fluids in porous media, Elsevier, New York.

Bear, J. and Bachmat, Y. (1990), Introduction to Modeling of Transport Phenomena in Porous Media, Kluwer Academic Pub.

Blackwell, R.J. (1962), Laboratory studies of microscopic dispersion phenomena, Soc. Pet. Eng. J., 2, 1-8.

Brenner, H. (1980), Dispersion resulting from flow through spatially periodic porous media, Phil. Trans. Roy. Soc. Lond., A297, 81-133.

Brenner, H. and Adler (1982), Dispersion resulting from flow through spatially periodic porous media, II Surface and intraparticle transport, Phil. Trans. Roy. Soc. Lond., A307, 149-200.

Brenner, H. and Edwards, D.A. (1993), Macrotransport Processes, Butterworth-Heinemann.

Carbonel, R.G. and Whitaker, S. (1983), Dispersion in pulsed systems- II. Theoretical development for passive dispersion in porous media, Chem. Eng. Sci., 38, 1795-1802.

Dagan, G. (1984), Solute transport in heterogeneous porous formation, J. Fluid Mech., 145, 151-177.

Dagan, G. (1989), Flow and Transport in porous Formations, Speinger-Verlag.

de Jong, d. J. (1958), Longitudinal and transverse diffusion in granular deposites, Trans. Am. Geophy. Union, 39, 67-74.

Dungan, S.R., Shapiro, M. and Brenner, H. (1990), Convective-diffusive-reactive dispersion processes in particulate multiphase systems, Proc. Roy. Soc Lond., A429, 639-671.

Ebach, E.A. and White, R.R. (1958), Mixing of fluids flowing through beds of packed solids, AIChE J., 4(2): 161-169.

Eckert, E.R.G. and Drake, R.M. (1987), Analysis of Heat and Mass Transfer.

Edwards, M.F. and Richardson, J.F. (1968), Gas dispersion in packed beds, Chem. Eng. Sci., 23, 109-123.

Edwards, D.A., Shapiro, M., Brenner, H. and Shapira, M. (1991), Dispersion of inert solutes in spatially periodic, two-dimensional model porous media, Transp. in Porous Media, 6, 337-358.

Eidsath, A., Carbonel, R.G. , Whitaker, S. and Herman, L.R. (1982), Dispersion in pulsed systems - III. Comparison between theory and experiment for packed beds, Chem. Eng. Sci., 38, 1803-1816.

Evans, E.V. and Kennedy, C.N. (1966), Gaseous dispersion in packed beds at low Reynolds numbers, Trans Inst. Chem. Engrs., 44, T189-T197.

Fried, J.J. and Combarnous, M.A. (1971), Dispersion in porous media, Adv. in Hydrosci., 7, 169-282.

Garabedian, S.P., Gelhar, L.W., and Celia, M.A. (1988), Large-scale dispersive transport in aquifers: Field experiments and reactive transport theory, Parsons Lab. Rep. 315, Massachusetts Institute of Technology, Cambridge, Massachusetts.

Garabedian, S.P., LeBlanc, D.R., Gelhar, L.W. and Celia, M.A. (1991), Large-scale natural gradient tracer test in sand and gravel, Cape Cod, Massachusetts, 2. Analysis of spatial moments for a nonreactive tracer, Water Resources Research, 27(5), 911-924.

Gelhar, L.W. (1986), Stochastic subsurface hydrology from theory to applications, Water Resources Research, 135S-145S.

Gelhar, L.W. (1987), Stochastic analysis of solute transport in saturated and unsaturated porous media, NATO ASI Ser., Ser. E, 128, 657-700.

Gelhar, L.W. (1993), Stochastic Subsurface Hydrology, Prentice Hall.

Gelhar, L.W. and Axness, C.L. (1983), Three-dimensional stochastic analysis of macrodispersion in aquifers, Water Resources Research, 19(1), 161-180.

Gelhar, L.W., Gutjar, A.L. and Naff, R.L. (1979), Stochastic analysis of macrodiapersion in a stratified aquifer, Water Resources Research, 15(6): 1387-1397.

Gelhar, L.W., Welty, C. and Rehfeldt, K.R. (1992), A critical review of data on field-scale dispersion in aquifers, Water Resources Research, 28(7), 1955-1974.

Grane, F.E. and Gardner, G.H.F. (1961), Measurements of transverse dispersion in granular media, J. Chem Eng. and Data, 6, 283-287.

Griffiths, R.W. (1981), Layered double-diffusive convection in porous media, J Fluid Mech., 102, 221-248.

Gunn, D.L. and Pryce, C. (1969), Dispersion in packed beds, Trans. Inst. Chem. Engrs., 47, T341-T350.

Gupta, V.K. and Bhattacharya, R.N. (1986), Solute diapersion in multidimensional periodic saturated porous media, Water Resources Research, 22(2): 156-164.

Güven, O. and Moltz, F.J. (1986), Detreministic and stochastic analyses of dispersion in an unbounded stratified porous medium, Water Resources Research, 22(11): 1565-1574.

Güven, O., Moltz, F.J. and Melville, J.G. (1984), An analysis of dispersion in a stratified aquifer, Water Resources Research, 20(10): 1337-1354.

Haring, R.E. and Greenkorn, R.A. (1970), A statistical model of a porous media with nonuniform pores, AIChE J., 16, 477-483.

Harleman, D.R.F. and Rumer, R.R. (1963), Longitudinal and lateral dispersion in an isotropic porous medium, J. Fluid Mech., 16(3), 385-394.

Henseley, P.J. and Savvioudou, C. (1993), Modeling coupled heat and contaminant transport in groundwater, Int. J. Num. analy. Meth. Geomech., 17, 493-527.

Hiby, J.W. (1962), Longitudinal and transverse mixing during single-phase flow through granular beds, Proc. Symp. Interaction between fluids and particles, London, 312-325.

Hsu, C.T. and Cheng, P. (1990), Thermal disperion in a porous medium, Int. J. Heat Mass Transfer, 33, 1587-1597.

Kaviany, M (1991), Principles of Heat Transfer in Porous Media, Springer-Verlag.

Kays and Crawford (1980), Convective Heat and Mass Transfer.

Koch, D.L. and Brady, J.F. (1985), Dispersion in fixed beds, J. Fluid Mech., 154, 399-427.

Koch, D.L. and Brady, J.F. (1987), The symmetry properties of the effective diffusivity tensor in anisotropic porous media, Phys. Fluid, 30, 642-650.

Koch, D.L., Cox, R.G., Brenner, H. and Brady, J.F. (1989), The effect of order on dispersion in porous media, J. Fluid Mech., 200, 173-188.

LeBlanc, D.R., Garabedian, S.P., Hess, K.M., Gelhar, L.W., Quadri, R.D., Stollenwerk, K.G. and Wood, W.W. (1991), Large-scale natural gradient tracer test in sand and gravel, Cape Cod, Massachusetts, 1. Experimental design and observed tracer movement, Water Resources Research, 27(5), 895-910.

Lienhard, J.H. (1984), A Heat Transfer Textbook.

List, E.J. and Brooks, N.H. (1967), Lateral dispersion in saturated porous media, J. Geophys. Res., 72, 2531-2541.

Matheron, G. and de Marsily, G. (1980), Is transport in porous media always diffusive ? A counterexample, Water Resources Research, 16(5): 901-917.

Mei, C.C. (1991), Dispersion of heat in periodic porous media by homogenization method, in T. Miloh(ed.), Mathematical Spproaches in Hydrodynamics, Soc. indust. Appl. Math.

Mei, C.C. (1992), Method of homogenization applied to dispersion in porous media, Transp. in Porous Media, 9, 261-274.

Mei, C.C. and Auriault, J.-L. (1991), The effect of weak inertia on flow through a porous medium, J. Fluid Mech., 222, 647-663.

Moranville, M.B., Kessler, D.P. and Greenkorn, R.A. (1977a), Directional dispersion coefficients in ansotropic porous media, Ind. Eng. Chem., Fundam., 16(3):327-332.

Moranville, M.B., Kessler, D.P. and Greenkorn, R.A. (1977b), Dispersion in layered porous media, AIChE J., 23 (6): 786-794.

Pinder, G.F. and Gray, W.G. (1977), Finite Element Simulations in Surface and Subsurace Hydrology, Academic Press.

Pfannkuch, H.O. (1963), Contribution a L'Etude des deplacements de Fluides Miscibles dans un milieu poreux, Revue de L'Institut Francais du Petrole, 215-270.

Poreh, M., (1965), The dispersivity tensor in isotropic and sxisymmetric medium, J. Geophys. Res., 70(16). 3909-3913.

Rifai, M., Kaufman, W.J. and Todd, D.K. (1956), Dispersion phenomena in laminar flow through porous media, Sanitary engineering Res. Lab. and Div Civil Eng., Univ. Calif., Berkeley, Rep. no. 2, I.E.R. Ser. 93.

Roache, P.J. (1977), Computational Fluid Dynamics, Hermosa Publishers.

Rubin, H. (1974), Heat dispersion effect on thermal convection in a porous medium layer, J. Hydrology, 21, 173-185.

Rubin, H. and Roth, C. (1983), Thermohaline convection in flowing groundwater, Adv. Water Res., 6, 146-155.

Rubinstein, J. and Mauri, R. (1986), Dispersion and convection in periodic porous media, SIAM J. Appl. Math., 46, 1018-1023.

Saffman, P.G. (1959), A theory of dispersion in a porous medium, J. Fluid Mech., 6, 321-349.

Saffman, P.G. (1960), Dispersion due to molecular diffusion and macroscopic mixing in flow through a network of capillaries, J. Fluid Mech., 7, 194-208.

Salles, J., Thovert, J.-F., Delannay, R., Prevors, L., Auriault, J.-L. and Adler, P.M. (1993), Taylor dispersion in porous media. Determination of the dispersion tensor, Phys. Fluids, 5, 2348-2376.

Sangani, A.S. and Acrivos, A. (1983), The effective conductivity of a periodic array of spheres, Proc. Roy. Soc. Lond., A386, 263-275.

Scheidegger, A.E. (1961), General theory of dispersion in porous media, J. Geophys. Res., 66, 3273-3278.

Simpson, E.S. (1962), Transverse dispersion in liquid flow through porous media, USGS Prof. Paper 411-C.

Slattery, J.C. (1972), Momentum, Energy and Mass Transfer in Continuum, McGraw - Hill Book Co.

Tyvand, P.A. (1977), Heat dispersion effect on thermal convection in anisotropic media, J. Hydrology, 21, 173-185.

Tyvand, P.A. (1980), Approximate formulae for the dispersion coefficients of layered porous media, AIChE J., 26(3): 513-517.

Tyvand, P.A. (1981), Influence of heat dispersion on steady convection in anisotropic porous media, J. Hydrology, 52, 13-23.

Welty, C. and Gelhar, L.W. (1991), Stochastic analysis of the effects of fluid density and viscosity variability on macrodispersion in heterogeneous media, Water Resources Research, 27(8), 2061-2075.

Welty, C. and Gelhar, L.W. (1992), Simulation of large-scale transport of variable density and viscosity fluids using a stochastic mean model, Water Resources Research, 28(3), 815-827.

Whitaker, S. (1967), Diffusion and dispersion in porous media, AIChE J., 13(3), 420-427.

FIGURE CAPTIONS and TABLES

Chapter I

Fig. 4.1 A Wigner-seitz microcell. The interiot of the soccer ball shape is fluid and the rest is solid. The mean flow is shown in the x-direction.

Fig. 4.2 Sign and symmetry relations of the velocity components at points symmetric about the planes $x = 0$, $y = 0$ and $z = 0$ in (a) the region $z > 0$ and (b) the region $x > 0$. Mean flow is in the x-direction.

Fig. 4.3 Sign and symmetry properties of B_j^f and related quanties in sectors A, D, E and H when the mean flow is in the x-direction. (a) B_j^f and its derivatives, (b) I_{ij}^f and (c) $e_{ij}(B_j^f)$.

Fig. 4.4 A typical cross-section of the microcell parallel to yz-plane and points on the interface symmetric about $y = 0$ and $z = 0$.

Fig. 4.5 A rotational coordinate transformation by 90 degrees about x-axis counterclockwise.

Fig. 5.1 Dispersion coefficients for solute (a) Longitudinal $D_L = D_{xx}$ and (b) Transverse $D_T = D_{yy}$.

Fig. 5.2 Longitudinal and transverse dispersion coefficients for heat.

Fig. 5.3 Comparison of dispersion coefficients for heat and solute; (a) longitudinal $D_L = D_{xx}$ and (b) transverse $D_T = D_{yy}$.

Chapter II

Fig. 4.1 A periodically stratified layers on the mesoscale. The periodic length is ℓ' in x_3'-direction.

Fig. 4.2 (a) Two coordinate systems $\bar{x}'\bar{y}'\bar{z}'$ and $x'y'z'$. The system $x'y'z'$ is the one rotated by ϕ counterclockwise from $\bar{x}'\bar{y}'\bar{z}'$ about z' axis. The mean flow is in $x'z'$ plane. (b) The horizontal components of flow in $\bar{x}'\bar{y}'$ plane and $x'y'$ plane.

Fig. 5.1 Dispersion coefficients $(\langle m' \rangle + D_{xx}^*)$ and $(\langle m' \rangle + D_{zz}^*)$ for passive solute in a layered medium. The angle for mean flow direction is $a(\theta = 0°)$, $b(\theta = 1°)$, $c(\theta = 5°)$, $d(\theta = 10°)$, $e(\theta = 40°)$, and $f(\theta = 90°)$. The permeability ratios are (a) $k'^+/k'^- = 2$ and (b) $k'^+/k'^- = 5$. $(\langle m' \rangle + D_{zz}^*)$ is the straight line marked by f.

Fig. 5.1 (continued) The permeability ratios are (c) $k'^+/k'^- = 10$ and (d) $k'^+/k'^- = 100$.

Fig. 5.2 Dispersion coefficient $(\langle m' \rangle + D^s_{zz})$ for passive solute in a layered medium with $\theta = 10°$. The permeability ratios are $a(k'^+/k'^- = 2)$, $b(k'^+/k'^- = 5)$, $c(k'^+/k'^- = 10)$ and $d(k'^+/k'^- = 100)$.

Fig. 5.3 Dispersion coefficients (a) $(\langle m' \rangle + D^s_{zz})$, $(\langle m' \rangle + D^s_{xz})$ and (b) D^s_{xz} for heat with $k'^+/k'^- = m'^+/m'^- = 1$ and $\rho C_p^+/\rho C_p^- = 10$. For the flow angle θ see the caption of Fig. 5.1.

Fig. 5.4 Dispersion coefficients (a) $(\langle m' \rangle + D^s_{zz})$, $(\langle m' \rangle + D^s_{xz})$ and (b) $-D^s_{xz}$ for heat with $\rho C_p^+/\rho C_p^- = 2$, $m'^+/m'^- = 10$ and $k'^+/k'^- = 100$. For the flow angle θ see the caption of Fig. 5.1.

Fig. 5.4 (continued.) (c) D^u_{xz}. For the flow angle θ see the caption of Fig. 5.1.

Fig. 5.5 Variation of dispersion coefficients (a) $(\langle m' \rangle + D^s_{zz})$ and (b) $(\langle m' \rangle + D^s_{xz})$ with flow angle. The Peclét numbers are *a*: $Pe' = 1000$, *b*: $Pe' = 100$ and *c*: $Pe' = 10$.

Fig. 5.5 (continued.) (c) $-D^s_{xz}$ and (d) D^u_{xz}. As Pe' decreases, the curves become lower.

Fig. 6.1 A thermal cloud released in a uniform seepage flow through layered porous layer.

Fig. 6.2(a) Temperature distribution $\theta(\xi, z)$ for $Ra' = 10$ and $\overline{Pe_f} = 1000$ at various times.

Fig. 6.2(b) Streamlines $\psi(\xi, z)$ for $Ra' = 10$ and $\overline{Pe_f} = 1000$ at various times.

Fig. 6.2(c) Pressure distribution $p(\xi, z)$ for $Ra' = 10$ and $\overline{Pe_f} = 1000$ at various times.

Fig. 6.2(d) Vertical displacement $w(\xi, z)$ for $Ra' = 10$ and $\overline{Pe_f} = 1000$ at various times.

Fig. 6.2(e) Horizontal displacement $u(\xi, z)$ for $Ra' = 10$ and $\overline{Pe_f} = 1000$ at various times.

Fig. 6.3 Matrix displacements at the upper surface (a) $w(\xi, z = 1)$ and (b) $u(\xi, z = 1)$ for $Ra' = 10$ and $\overline{Pe_f} = 1000$ at various times. The magnitude decreases with t.

Fig. 6.4 Distribution of the dispersion coefficient $\langle m' \rangle + D^s_{xz}$ for $Ra' = 10$ and $\overline{Pe_f} = 1000$ at various times.

Fig. 6.5(a) Temperature distribution $\theta(\xi, z)$ for $Ra' = 10$ and $\overline{Pe_f} = 2000$ at various times.

Fig. 6.5(b) Streamlines $\psi(\xi, z)$ for $Ra' = 10$ and $\overline{Pe_f} = 2000$ at various times.

Fig. 6.5(c) Pressure distribution $p(\xi, z)$ for $Ra' = 10$ and $\overline{Pe_f} = 2000$ at various times.

Fig. 6.5(d) Vertical displacement $w(\xi, z)$ for $Ra' = 10$ and $\overline{Pe_f} = 2000$ at various times.

Fig. 6.5(e) Horizontal displacement $u(\xi, z)$ for $Ra' = 10$ and $\overline{Pe_f} = 2000$ at various times.

Fig. 6.6 Displacements at the upper surface (a) $w(\xi, z = 1)$ and (b) $u(\xi, z = 1)$ for $Ra' = 10$ and $\overline{Pe_f} = 2000$ at various times. The magnitude decreases with t.

Fig. 6.7 Distribution of the dispersion coefficient $\langle m' \rangle + D^*_{xx}$ for $Ra' = 10$ and $\overline{Pe_f} = 2000$ at various times.

Fig. 6.8(a) Temperature distribution $\theta(\xi, z)$ for $Ra' = 100$ and $\overline{Pe_f} = 1000$ at various times.

Fig. 6.8(b) Streamlines $\psi(\xi, z)$ for $Ra' = 100$ and $\overline{Pe_f} = 1000$ at various times.

Fig. 6.8(c) Pressure distribution $p(\xi, z)$ for $Ra' = 100$ and $\overline{Pe_f} = 1000$ at various times.

Fig. 6.8(d) Vertical displacement $w(\xi, z)$ for $Ra' = 100$ and $\overline{Pe_f} = 1000$ at various times.

Fig. 6.8(e) Horizontal displacement $u(\xi, z)$ for $Ra' = 100$ and $\overline{Pe_f} = 1000$ at various times.

Fig. 6.9 Displacements at the upper surface (a) $w(\xi, z = 1)$ and (b) $u(\xi, z = 1)$ for $Ra' = 100$ and $\overline{Pe_f} = 1000$ at various times. The magnitude decreases with t.

Fig. 6.10 Distribution of the dispersion coefficient $\langle m' \rangle + D^*_{xx}$ for $Ra' = 100$ and $\overline{Pe_f} = 1000$ at various times.

Fig. 6.11(a) Temperature distribution $\theta(\xi, z)$ for $Ra' = 100$ and $\overline{Pe_f} = 2000$ at various times.

Fig. 6.11(b) Streamlines $\psi(\xi, z)$ for $Ra' = 100$ and $\overline{Pe_f} = 2000$ at various times.

Fig. 6.11(c) Pressure distribution $p(\xi, z)$ for $Ra' = 100$ and $\overline{Pe_f} = 2000$ at various times.

Fig. 6.11(d) Vertical displacement $w(\xi, z)$ for $Ra' = 100$ and $\overline{Pe_f} = 2000$ at various times.

Fig. 6.11(e) Horizontal displacement $u(\xi, z)$ for $Ra' = 100$ and $\overline{Pe_f} = 2000$ at various times.

Fig. 6.12 Displacements at the upper surface (a) $w(\xi, z = 1)$ and (b) $u(\xi, z = 1)$ for $Ra' = 100$ and $\overline{Pe_f} = 2000$ at various times. The magnitude decreases with t.

Fig. 6.13 Distribution of the dispersion coefficient $\langle m' \rangle + D^s_{zz}$ for $Ra' = 100$ and $\overline{Pe_f} = 2000$ at various times.

Fig. 6.14(a) Temperature distribution $\theta(\xi, z)$ for $Ra' = 200$ and $\overline{Pe_f} = 1000$ at various times.

Fig. 6.14(b) Streamlines $\psi(\xi, z)$ for $Ra' = 200$ and $\overline{Pe_f} = 1000$ at various times.

Fig. 6.14(c) Pressure distribution $p(\xi, z)$ for $Ra' = 200$ and $\overline{Pe_f} = 1000$ at various times.

Fig. 6.14(d) Vertical displacement $w(\xi, z)$ for $Ra' = 200$ and $\overline{Pe_f} = 1000$ at various times.

Fig. 6.14(e) Horizontal displacement $u(\xi, z)$ for $Ra' = 200$ and $\overline{Pe_f} = 1000$ at various times.

Fig. 6.15 Displacements at the upper surface (a) $w(\xi, z = 1)$ and (b) $u(\xi, z = 1)$ for $Ra' = 200$ and $\overline{Pe_f} = 1000$ at various times. The magnitude decreases with t.

Fig. 6.16 Distribution of the dispersion coefficient $\langle m' \rangle + D^s_{zz}$ for $Ra' = 200$ and $\overline{Pe_f} = 1000$ at various times.

Fig. 6.17(a) Temperature distribution $\theta(\xi, z)$ for $Ra' = 200$ and $\overline{Pe_f} = 2000$ at various times.

Fig. 6.17(b) Streamlines $\psi(\xi, z)$ for $Ra' = 200$ and $\overline{Pe_f} = 2000$ at various times.

Fig. 6.17(c) Pressure distribution $p(\xi, z)$ for $Ra' = 200$ and $\overline{Pe_f} = 2000$ at various times.

Fig. 6.17(d) Vertical displacement $w(\xi, z)$ for $Ra' = 200$ and $\overline{Pe_f} = 2000$ at various times.

Fig. 6.17(e) Horizontal displacement $u(\xi, z)$ for $Ra' = 200$ and $\overline{Pe_f} = 2000$ at various times.

Fig. 6.18 Displacements at the upper surface (a) $w(\xi, z = 1)$ and (b) $u(\xi, z = 1)$ for $Ra' = 200$ and $\overline{Pe_f} = 2000$ at various times. The magnitude decreases with t.

Fig. 6.19 Distribution of the dispersion coefficient $\langle m' \rangle + D^s_{zz}$ for $Ra' = 200$ and $\overline{Pe_f} = 2000$ at various times.

TABLES

Chapter I

Appendix A. The Green's function $G(z',\xi)$

Let the differential operator of (4.1.14a) be denoted by L i.e.,

$$L = \frac{\partial}{\partial z'}\left(m'\frac{\partial}{\partial z'}\right) - a\frac{\partial}{\partial z'} \tag{A.1}$$

where

$$a = Pe'\langle u\rangle_z \tag{A.2}$$

It is non-self adjoint. Let us define the adjoint operator L^* by

$$L^* = \frac{\partial}{\partial z'}\left(m'\frac{\partial}{\partial z'}\right) + a\frac{\partial}{\partial z'} \tag{A.3}$$

and the Green's function $G^*(z',\xi)$ by

$$\begin{aligned} L^*G^* &= \delta(z'-\xi) \qquad 0 < z' < \ell' \\ G^*(0,\xi) &= G^*(\ell',\xi) \\ \left.\frac{\partial G^*}{\partial z'}\right|_{z'=0} &= \left.\frac{\partial G^*}{\partial z'}\right|_{z'=\ell'} \\ \int_o^{\ell'} G^*(z',\xi)dz' &= 0 \end{aligned} \tag{A.4a-d}$$

It then follows that

$$\begin{aligned} &\int_o^{\ell'} (B'_z L^*G^* - G^*LB'_z)\,dz' \\ &= \int_o^{\ell'} \left\{ B'_z\left[\frac{\partial}{\partial z'}\left(m'\frac{\partial G^*}{\partial z'}\right) + a\frac{\partial G^*}{\partial z'}\right] - G^*\left[\frac{\partial}{\partial z'}\left(m'\frac{\partial B'_z}{\partial z'}\right) - a\frac{\partial B'_z}{\partial z'}\right]\right\} dz' \\ &= \int_o^{\ell'} \left[\frac{\partial}{\partial z'}\left(m'B'_z\frac{\partial G^*}{\partial z'} - m'G^*\frac{\partial B'_z}{\partial z'}\right) + a\frac{\partial}{\partial z'}(B'_zG^*)\right] dz' \\ &= \left[m'B'_z\frac{\partial G^*}{\partial z'} - m'G^*\frac{\partial B'_z}{\partial z'}\right]_o^{\ell'} + a\,[B'_zG^*]_o^{\ell'} \\ &= 0 \end{aligned} \tag{A.5}$$

where the Ω'-periodicity has been used. Hence we have

$$\int_o^{\ell'} [B'_z(z')\delta(z'-\xi) - G^*(z',\xi)r(z')]\,dz' = 0$$

or

$$B'_x(\xi) = \int_o^{\ell'} G^*(z',\xi) r(z') dz' \tag{A.6}$$

Let us define $G(z',\xi)$ be the Green's function of the operator L:

$$\begin{aligned} LG &= \delta(z'-\xi) \qquad 0 < z' < \ell' \\ G(0,\xi) &= G(\ell',\xi) \\ \left.\frac{\partial G}{\partial z'}\right|_{z'=0} &= \left.\frac{\partial G}{\partial z'}\right|_{z'=\ell'} \\ \int_o^{\ell'} G(z',\xi) dz' &= 0 \end{aligned} \tag{A.7a-d}$$

It is easy to show that

$$G(z',\xi) = G^*(\xi, z') \tag{A.8}$$

Equation (A.6) then becomes

$$B'_x(z') = \int_o^{\ell'} G(z',\xi) r(\xi) d\xi \tag{A.9}$$

The Green's function $G(z',\xi)$ is now derived.

Integrating (A.7a) with respect to z', we get

$$m'(z') \frac{\partial G}{\partial z'} - aG = f(z',\xi) \tag{A.10}$$

where

$$f(z',\xi) = \left\{ \begin{array}{ll} c(\xi) & z' \le \xi \\ 1 + c(\xi) & z' \ge \xi \end{array} \right\} \tag{A.11}$$

is a step function which has a discontinuity at $z' = \xi'$. Note that, although (A.10) is discontinuous at $z' = \xi'$, the heat flux at $z' = \xi'$

$$m'(z') \frac{dB'_x}{dz'} - aB'_x = \int_o^{\ell'} \left(m'(z') \frac{\partial G}{\partial z'} - aG \right) r(\xi) d\xi = \int_o^{\ell'} f(z',\xi) r(\xi) d\xi \tag{A.12}$$

is continuous. The general solution of (A.10) then becomes

$$G(z',\xi) = \frac{1}{p(z')} \int_o^{z'} p(z') \frac{f(z',\xi)}{m'(z')} dz' + \frac{G(z'=0,\xi)}{p(z')} \tag{A.13}$$

where

$$p(z') = \exp\left[\int_o^{z'} -\frac{a}{m'(z')}dz'\right] \tag{A.14}$$

is the integrating factor. It satisfies the following relation

$$\frac{p(z')}{m'(z')} = -\frac{1}{a}\frac{dp(z')}{dz'} \tag{A.15}$$

In the region $z' \leq \xi$, if we substitute (A.14) into (A.13) and use (A.11) and (A.15), it follows that

$$\begin{aligned} G(z' \leq \xi, \xi) &= \frac{1}{p(z')}\int_o^{z'} p(z')\frac{c(\xi)}{m'(z')}dz' + \frac{G(0,\xi)}{p(z')} \\ &= -\frac{c(\xi)}{a}\frac{1}{p(z')}\left[p(z') - 1\right] + \frac{G(0,\xi)}{p(z')} \qquad (z' \leq \xi) \\ &= -\frac{c(\xi)}{a}\left[1 - p^{-1}(z')\right] + \frac{G(0,\xi)}{p(z')} \end{aligned} \tag{A.16}$$

Similarly, in the region $z' \geq \xi$, we have

$$\begin{aligned} G(z' \geq \xi, \xi) &= \frac{1}{p(z')}\left[\int_o^{\xi} p(z')\frac{c(\xi)}{m'(z')}dz' + \int_\xi^{z'} p(z')\frac{1+c(\xi)}{m'(z')}dz'\right] + \frac{G(0,\xi)}{p(z')} \\ &= -\frac{1}{p(z')}\left\{\frac{c(\xi)}{a}\left[p(\xi) - 1\right] + \frac{1+c(\xi)}{a}\left[p(z') - p(\xi)\right]\right\} + \frac{G(0,\xi)}{p(z')} \quad (z' \geq \xi) \\ &= -\frac{c(\xi)}{a}\left[1 - p^{-1}(z')\right] - \frac{1}{a}\left[1 - \frac{p(\xi)}{p(z')}\right] + \frac{G(0,\xi)}{p(z')} \end{aligned} \tag{A.17}$$

We now impose the Ω'-periodicity condition (A.7b). At $z' = 0$, (A.9) automatically gives $G(0,\xi)$. At $z' = \ell'$, we have from (A.17)

$$G(\ell', \xi) = -\frac{c(\xi)}{a}\left[1 - p^{-1}(\ell')\right] - \frac{1}{a}\left[1 - \frac{p(\xi)}{p(\ell')}\right] + \frac{G(0,\xi)}{p(\ell')}$$

which becomes after using (A.7b)

$$\left[1 - p^{-1}(\ell')\right] G(0,\xi) = -\frac{c(\xi)}{a}\left[1 - p^{-1}(\ell')\right] - \frac{1}{a}\left[1 - \frac{p(\xi)}{p(\ell')}\right]$$

or

$$G(0,\xi) = -\frac{c(\xi)}{a} - \frac{1}{a}\frac{p(\ell') - p(\xi)}{p(\ell') - 1} \tag{A.18}$$

The integration constant $c(\xi)$ is determined from the zero average condition (A.7d). Integrating $G(z',\xi)$ from $z'=0$ to $z'=\ell'$, we obtain from (A.16) and (A.17)

$$\begin{aligned}
&\int_o^{\ell'} G(z',\xi)dz' = \int_o^{\xi} G(z'\le\xi,\xi)dz' + \int_{\xi}^{\ell'} G(z'\ge\xi,\xi)dz' \\
&= -\frac{c(\xi)}{a}\int_o^{\xi}\left[1-p^{-1}(z')\right]dz' - \frac{c(\xi)}{a}\int_{\xi}^{\ell'}\left[1-p^{-1}(z')\right]dz' - \frac{1}{a}\int_{\xi}^{\ell'}\left[1-\frac{p(\xi)}{p(z')}\right]dz' \\
&\quad + G(0,\xi)\int_o^{\ell'}\frac{dz'}{p(z')} \\
&= -\frac{c(\xi)}{a}\left[\ell' - \int_o^{\ell'}\frac{dz'}{p(z')}\right] - \frac{1}{a}\left[\ell'-\xi-p(\xi)\int_{\xi}^{\ell'}\frac{dz'}{p(z')}\right] \\
&\quad - \left[\frac{c(\xi)}{a} + \frac{1}{a}\frac{p(\ell')-p(\xi)}{p(\ell')-1}\right]\int_o^{\ell'}\frac{dz'}{p(z')} \\
&= 0
\end{aligned} \tag{A.19}$$

where (A.18) has been used for $G(0,\xi)$. The function $c(\xi)$ thus becomes

$$\frac{c(\xi)}{a} = -\frac{1}{a}\left[1-\frac{\xi}{\ell'} - \frac{p(\xi)}{\ell'}\int_{\xi}^{\ell'}\frac{dt}{p(t)}\right] - \frac{\langle p^{-1}\rangle}{a}\frac{p(\ell')-p(\xi)}{p(\ell')-1} \tag{A.20}$$

where

$$\langle p^{-1}\rangle = \frac{1}{\ell'}\int_0^{\ell'}\frac{dt}{p(t)}$$

is the Ω'-cell average of $1/p(z')$. Equation (A.18) then gives

$$G(0,\xi) = \frac{1}{a}\left[1-\frac{\xi}{\ell'} - \frac{p(\xi)}{\ell'}\int_{\xi}^{\ell'}\frac{dt}{p(t)}\right] + \frac{\langle p^{-1}\rangle - 1}{a}\frac{p(\ell')-p(\xi)}{p(\ell')-1} \tag{A.21}$$

Finally by substituting (A.20) and (A.21) into (A.16) and (A.17) and rearranging, the Green's function becomes

$$G(z',\xi) = \begin{cases} \frac{1}{a}\left[1-\frac{\xi}{\ell'}-\frac{p(\xi)}{\ell'}\int_{\xi}^{\ell'}\frac{dt}{p(t)}\right] + \frac{1}{a}\left[\langle p^{-1}\rangle - p^{-1}(z')\right]\frac{p(\ell')-p(\xi)}{p(\ell')-1} & (z'\le\xi) \\ G(z'\le\xi,\xi) - \frac{1}{a}\left[1-\frac{p(\xi)}{p(z')}\right] & (z'\ge\xi) \end{cases} \tag{A.22}$$

The Green's function $G(z',\xi)$ can be further reduced as follows. Equation (4.1.16) implies that the parts which are independent of ξ and present in both

regions $z' \leq \xi$ and $z' \geq \xi$ in (A.22) make no contribution to $B'_z(z')$(cf.(A.9)). Thus $G(z', \xi)$ is reduced to

$$G(z',\xi) = \left\{ \begin{array}{cc} -\frac{1}{a\ell'}\left[\xi + p(\xi)\int_\xi^{\ell'} \frac{dt}{p(t)}\right] - \frac{1}{a}\left[\langle p^{-1}\rangle - p^{-1}(z')\right]\frac{p(\xi)}{p(\ell')-1} & (z' \leq \xi) \\ G(z' \leq \xi, \xi) - \frac{1}{a}\left[1 - \frac{p(\xi)}{p(z')}\right] & (z' \geq \xi) \end{array} \right\} \tag{A.23}$$

which is (4.1.18).

Appendix B. The Dispersion Coefficients $\langle m' \rangle_{xx} + D^*_{xx}$, $\langle m' \rangle_{zz} + D^*_{zz}$ and D^*_{xz}

The symmetric dispersion coefficients are determined in terms of the integrating factor $p(\xi)$ and forcing terms $r(\xi)$ and $t(\xi)$ for B'_x and B'_z respectively.

We first substitute $G(z', \xi)$ from (4.1.18) into (4.1.34) and recall the relation (4.1.17). Since the integrand in (4.1.34) has $r(z')$, the part of $G(z', \xi)$ which is function of ξ only will produce zero upon integration with respect to z' by virtue of (4.1.17). It follows immediately that

$$D^*_{xz} = -\frac{1}{a\ell'}\frac{1}{p(\ell')-1}\left(\int_o^{\ell'} \frac{r(z')}{p(z')}dz'\right)\left(\int_o^{\ell'} p(\xi)r(\xi)d\xi\right) + \frac{1}{a\ell'}\left[\int_o^{\ell'} dz'\left(r(z')\int_o^{z'} r(\xi)d\xi\right) - \int_o^{\ell'} dz'\left(\frac{r(z')}{p(z')}\int_o^{z'} p(\xi)r(\xi)d\xi\right)\right] \tag{B.1}$$

After integration by parts, the first term in the bracketed expression becomes

$$\int_o^{\ell'} dz'r(z')\int_o^{z'} r(\xi)d\xi = \int_o^{\ell'} r(t)dt\int_o^{\ell'} r(\xi)d\xi - \int_o^{\ell'} dz'\left(r(z')\int_o^{z'} r(\xi)d\xi\right) = -\int_o^{\ell'} dz'r(z')\int_o^{z'} r(\xi)d\xi \tag{B.2}$$

where (4.1.17) has been used. Thus the integral is identically zero and (4.1.34) becomes

$$\langle m' \rangle_{xx} + D^*_{xx} = m''_{xx} - \frac{1}{a\ell'}\left[\frac{1}{p(\ell')-1}\int_o^{\ell'} \frac{r(z')}{p(z')}dz'\int_o^{\ell'} p(\xi)r(\xi)d\xi + \int_o^{\ell'} dz'\frac{r(z')}{p(z')}\int_o^{z'} p(\xi)r(\xi)d\xi\right] \tag{B.3}$$

For $\langle m' \rangle_{zz} + D^*_{zz}$ by using (4.1.14) and (4.1.27), we get

$$\begin{aligned}\langle m' \rangle_{zz} + D^*_{zz} &= \langle m' \rangle + \left\langle m'\frac{dB'_z}{dz'}\frac{dB'_z}{dz'}\right\rangle + 2\left\langle m'\frac{dB'_z}{dz'}\right\rangle \\ &= \langle m' \rangle + \left\langle m'\frac{dA'_z}{dz'}\frac{dA'_z}{dz'}\right\rangle + 2\left\langle m'\frac{dA'_z}{dz'}\frac{dC_z}{dz'}\right\rangle + \left\langle m'\frac{dC_z}{dz'}\frac{dC_z}{dz'}\right\rangle \\ &\quad + 2\left\langle m'\left(\frac{dA'_z}{dz'} + \frac{dC_z}{dz'}\right)\right\rangle\end{aligned} \tag{B.4}$$

From (4.1.28) we have

$$A'_z(z') = m''_{zz}\int_0^{z'}\frac{dz'}{m'(z')} + m''_{zz}\left\langle\frac{z'}{m'(z')}\right\rangle - z' - \frac{\ell'}{2} \quad ; \quad \frac{\partial A'_z}{\partial z'} = \frac{\ell'}{m'\int_0^{\ell'}\frac{dz'}{m'}} - 1 \tag{B.5}$$

By using (B.5) the third term in (B.4) may be written as

$$2\left\langle m'\frac{dA'_z}{dz'}\frac{dC_z}{dz'}\right\rangle = 2\left\langle m'\left(\frac{m''_{zz}}{m'} - 1\right)\frac{dC_z}{dz'}\right\rangle = -2\left\langle m'\frac{dC_z}{dz'}\right\rangle \tag{B.6}$$

where the Ω'-periodicity (4.1.30b) has been used. Also from (B.5) it follows that

$$\begin{aligned} 2\left\langle m'\frac{dA'_z}{dz'}\right\rangle &= 2\left\langle m'\left(\frac{m''_{zz}}{m'} - 1\right)\right\rangle = 2m''_{zz} - 2\langle m'\rangle \\ &= -2\left\langle m'\frac{dA'_z}{dz'}\frac{dA'_z}{dz'}\right\rangle \end{aligned} \tag{B.7}$$

where (4.25) in Ch. 2, Part A has been used for m''_{zz} in the last step i.e.,

$$m''_{zz} = \langle m'\rangle - \left\langle m'\frac{dA'_z}{dz'}\frac{dA'_z}{dz'}\right\rangle \tag{B.8}$$

Substituting (B.6) and (B.7) into (B.4) we obtain

$$\begin{aligned} \langle m'\rangle_{zz} + D^*_{zz} &= \langle m'\rangle - \left\langle m'\frac{dA'_z}{dz'}\frac{dA'_z}{dz'}\right\rangle + \left\langle m'\frac{dC_z}{dz'}\frac{dC_z}{dz'}\right\rangle \\ &= m''_{zz} + \left\langle m'\frac{dC_z}{dz'}\frac{dC_z}{dz'}\right\rangle \end{aligned} \tag{B.9}$$

after using (B.8). The second term is readily obtained upon replacing $r(\xi)$ by $t(\xi)$ in (B.1). Thus we have

$$\begin{aligned} &\langle m'\rangle_{zz} + D^*_{zz} = m''_{zz} \\ &-\frac{1}{a\ell'}\left[\frac{1}{p(\ell')-1}\int_o^{\ell'}\frac{t(z')}{p(t')}dz'\int_o^{\ell'}p(\xi)t(\xi)d\xi + \int_o^{\ell'}dz'\frac{t(z')}{p(z')}\int_o^{z'}p(\xi)t(\xi)d\xi\right] \end{aligned} \tag{B.10}$$

which is (4.1.37).

The off-diagonal entry D^*_{zz} of (4.1.4) becomes

$$\begin{aligned} D^*_{zz} &= \left\langle m'\frac{dB'_z}{dz'}\frac{dB'_z}{dz'}\right\rangle + \left\langle m'\frac{dB'_z}{dz'}\right\rangle \\ &= \left\langle m'\frac{dB'_z}{dz'}\left(\frac{dA'_z}{dz'} + \frac{dC_z}{dz'}\right)\right\rangle + \left\langle m'\frac{dB'_z}{dz'}\right\rangle \\ &= \left\langle m'\frac{dB'_z}{dz'}\frac{dC_z}{dz'}\right\rangle \end{aligned} \tag{B.11}$$

where (B.5) and the Ω'-periodicity have been used. Integrating by parts, (B.11) further becomes

$$\begin{aligned} D^e_{xz} =& \frac{1}{\ell'} \int_o^{\ell'} \left[\frac{d}{dz'} \left(m' C_z \frac{dB'_x}{dz'} \right) - C_z \frac{d}{dz'} \left(m' \frac{dB'_x}{dz'} \right) \right] dz' \\ =& -\frac{1}{\ell'} \int_o^{\ell'} C_z \left(Pe' \langle u \rangle_z \frac{dB'_x}{dz'} + r(z') \right) dz' \end{aligned} \tag{B.12}$$

If the integration by parts is taken alternatively, we have

$$D^e_{xz} = -\frac{1}{\ell'} \int_o^{\ell'} B'_x \left(Pe' \langle u \rangle_z \frac{dC_z}{dz'} + t(z') \right) dz' \tag{B.13}$$

Adding (B.12) and (B.13) and invoking the Ω'-periodicity, we readily obtain

$$\begin{aligned} 2D^e_{xz} =& -\frac{1}{\ell'} \int_o^{\ell'} \left(r(z') C_z(z') + t(z') B'_x(z') \right) dz' \\ =& -\frac{1}{\ell'} \int_o^{\ell'} \int_o^{\ell'} \left[r(z') G(z', \xi) t(\xi) + t(z') G(z', \xi) r(\xi) \right] d\xi dz' \end{aligned} \tag{B.14}$$

where (4.1.15) and (4.1.32) have been used. Because of symmetry, it then follows from (B.3) that

$$\begin{aligned} & 2D^e_{xz} = \\ & -\frac{1}{a\ell'} \left[\frac{1}{p(\ell') - 1} \int_o^{\ell'} \frac{t(z')}{p(z')} dz' \int_o^{\ell'} p(\xi) r(\xi) d\xi + \int_o^{\ell'} dz' \frac{t(z')}{p(z')} \int_o^{z'} p(\xi) r(\xi) d\xi \right] \\ & -\frac{1}{a\ell'} \left[\frac{1}{p(\ell') - 1} \int_o^{\ell'} \frac{r(z')}{p(z')} dz' \int_o^{\ell'} p(\xi) t(\xi) d\xi + \int_o^{\ell'} dz' \frac{r(z')}{p(z')} \int_o^{z'} p(\xi) t(\xi) d\xi \right] \end{aligned} \tag{B.15}$$

which is (4.1.38).

Appendix C. The Anti-symmetric Dispersion Coefficient D^u_{zz}

For brevity the overhead bars and the leading order symbol '(0)' are omitted in (4.2.2) for D^u_{zz}. We shall use $\langle\langle u\rangle^{(0)}_z B'_z\rangle$ instead of $\langle\hat{\langle u\rangle}^{(0)}_z B'_z\rangle$ in the first term of D^u_{zz} since it does not alter D^u_{zz} because of the condition $\langle B'_z\rangle = 0$(cf.(4.1.25d)).

For algebraic convenience, we write $C_z(z')$ in (4.1.32) as follows.

$$C_z(z') = C^o(z') + C^A(z') \tag{C.1}$$

where

$$\begin{aligned} C^o(z') &= \int_o^{\ell'} G(z',\xi) t^o(\xi) d\xi \\ C^A(z') &= \int_o^{\ell'} G(z',\xi) t^A(\xi) d\xi \end{aligned} \tag{C.2}$$

in which

$$\begin{aligned} &t^o(\xi) = -Pe'\langle u\rangle_z \rho C_p(\xi), \qquad \rho C_p(\xi) = \overline{\rho C_p}^*(\xi) \Big/ \left\langle \overline{\rho C_p}^* \right\rangle \\ &t^A(\xi) = Pe'\langle u\rangle_z \frac{m''_{zz}}{m'(\xi)} \end{aligned} \tag{C.3}$$

The function $B'_z(z')$ then becomes

$$B'_z(z') = A'_z(z') + C^o(z') + C^A(z') \tag{C.4}$$

where $A'_z(z')$ has been given in (4.1.28).

Substituting (C.4) into (4.2.2), we have

$$\begin{aligned} D^u_{zz} = &- \frac{Pe'}{2}\left(\langle\langle u\rangle_z A'_z\rangle + \langle\langle u\rangle_z C^A\rangle\right) \\ &- \frac{Pe'}{2}\left(\langle\rho C_p A'_z\rangle\langle\langle u\rangle_z\rangle + \langle\rho C_p C^A\rangle\langle\langle u\rangle_z\rangle\right) \\ &- \frac{Pe'}{2}\langle\langle u\rangle_z C^o\rangle + \frac{Pe'}{2}\left[\langle\rho C_p B'_z\rangle\langle u\rangle_z - \langle\rho C_p C^o\rangle\langle\langle u\rangle_z\rangle\right] - \frac{1}{2}\left\langle m' \frac{dB'_z}{dz'}\right\rangle \end{aligned} \tag{C.5}$$

Each term is now considered. From $G(z',\xi)$ in (4.1.18) and $t^A(\xi)$ in (C.3) after integration by parts, we obtain

$$\begin{aligned} C^A(z') &= \int_o^{\ell'} G(z',\xi) Pe' \langle u \rangle_x \frac{m''_{xz}}{m'(\xi)} d\xi \\ &= -\frac{1}{a}\langle \xi t^A(\xi)\rangle - \frac{1}{a\ell'}\int_o^{\ell'} \frac{d\xi}{p(\xi)} \int_o^{\xi} p(t) t^A(t) dt \\ &\quad - \frac{\ell'}{a}\frac{\langle p^{-1}\rangle - p^{-1}(z')}{p(\ell')-1}\langle p(\xi) t^A(\xi)\rangle - \frac{1}{a}\int_o^{z'} \left[1 - \frac{p(\xi)}{p(z')}\right] t^A(\xi) d\xi \end{aligned} \tag{C.6}$$

where a pair of angle brackets denotes the Ω'-cell average. It then follows that

$$\begin{aligned} &\langle \langle u \rangle_x C^A \rangle \\ &= \langle \langle u \rangle_x \rangle \left[-\frac{1}{a}\langle \xi t^A(\xi)\rangle - \frac{1}{a\ell'}\int_o^{\ell'} \frac{dz'}{p(z')} \int_o^{z'} p(\xi) t^A(\xi) d\xi - \frac{\ell'}{a}\frac{\langle p^{-1}\rangle}{p(\ell')-1}\langle p(\xi) t^A(\xi)\rangle \right] \\ &\quad + \frac{1}{a}\frac{\langle p(\xi) t^A(\xi)\rangle}{p(\ell')-1}\int_o^{\ell'} \frac{\langle u \rangle_x(z')}{p(z')} dz' \\ &\quad - \frac{1}{a\ell'}\int_o^{\ell'} dz' \langle u \rangle_x(z') \int_o^{z'} \left[1 - \frac{p(\xi)}{p(z')}\right] t^A(\xi) d\xi \end{aligned} \tag{C.7}$$

We also have from (4.1.28) that

$$\langle \langle u \rangle_x A'_x \rangle = \left(m''_{xz} \left\langle \frac{z'}{m'(z')} \right\rangle - \frac{\ell'}{2} \right) \langle \langle u \rangle_x \rangle + \frac{1}{\ell'}\int_o^{\ell'} dz' \langle u \rangle_x(z') \left(\int_o^{z'} \frac{m''_{xz}}{m'(\xi)} d\xi - z' \right) \tag{C.8}$$

If we substitute $t^A(\xi)$ from (C.3) into (C.7) and (C.8), it follows after some cancellations that

$$\begin{aligned} &\langle \langle u \rangle_x C^A \rangle + \langle \langle u \rangle_x A'_x \rangle \\ &= \frac{m''_{xz}}{\ell'}\int_o^{\ell'} dz' \frac{\langle u \rangle_x(z') - \langle \langle u \rangle_x \rangle}{p(z')} \int_o^{z'} \frac{p(\xi)}{m'(\xi)} d\xi - \frac{\ell'}{2}\langle \langle u \rangle_x \rangle - \frac{1}{\ell'}\int_o^{\ell'} z' \langle u \rangle_x(z') dz' \\ &\quad + \frac{m''_{xz}}{\ell'}\frac{1}{p(\ell')-1}\int_o^{\ell'} \frac{\langle u \rangle_x(z') - \langle \langle u \rangle_x \rangle}{p(z')} dz' \int_o^{\ell'} \frac{p(\xi)}{m'(\xi)} d\xi \end{aligned} \tag{C.9}$$

Similarly after replacing $\langle u\rangle_z$ and $\langle\langle u\rangle_z\rangle$ by ρC_p and 1 in (C.9), we have

$$\begin{aligned}
&\langle \rho C_p C^A\rangle + \langle \rho C_p A'_z\rangle \\
&= \frac{m''_{zz}}{\ell'}\int_o^{\ell'} dz' \frac{\rho C_p(z')-1}{p(z')}\int_o^{z'}\frac{p(\xi)}{m'(\xi)}d\xi - \frac{\ell'}{2} - \frac{1}{\ell'}\int_o^{\ell'} z'\rho C_p(z')dz' \\
&+ \frac{m''_{zz}}{\ell'}\frac{1}{p(\ell')-1}\int_o^{\ell'}\frac{\rho C_p(z')-1}{p(z')}dz'\int_o^{\ell'}\frac{p(\xi)}{m'(\xi)}d\xi
\end{aligned} \tag{C.10}$$

The first two lines in (C.5) then become

$$\begin{aligned}
&-\frac{Pe'}{2}\left(\langle\langle u\rangle_z C^A\rangle + \langle\langle u\rangle_z A'_z\rangle\right) - \frac{Pe'}{2}\left(\langle \rho C_p C^A\rangle + \langle \rho C_p A'_z\rangle\right)\langle\langle u\rangle_z\rangle \\
&= -\frac{Pe'}{2}\langle\langle u\rangle_z\rangle\left[\frac{m''_{zz}}{\ell'}\int_o^{\ell'} dz'\frac{\langle u\rangle_z/\langle\langle u\rangle_z\rangle - 2 + \rho C_p}{p(z')}\int_o^{z'}\frac{p(\xi)}{m'(\xi)}d\xi\right] \\
&-\frac{Pe'}{2}\langle\langle u\rangle_z\rangle\left[m''_{zz}\frac{\ell'}{p(\ell')-1}\int_o^{\ell'} dz'\frac{\langle u\rangle_z/\langle\langle u\rangle_z\rangle - 2 + \rho C_p}{p(z')}\int_o^{\ell'} d\xi\frac{p(\xi)}{m'(\xi)}\right] \\
&+\frac{Pe'}{2}\langle\langle u\rangle_z\rangle\left[\ell' + \int_o^{\ell'} z'(\langle u\rangle_z/\langle\langle u\rangle_z\rangle + \rho C_p)dz'\right]
\end{aligned} \tag{C.11}$$

From (4.1.21) we have

$$\int_o^{z'}\frac{p(\xi)}{m'(\xi)}d\xi = -\frac{1}{a}\int_o^{z'}\frac{dp(\xi)}{d\xi}d\xi = -\frac{1}{a}[p(z')-1] \tag{C.12}$$

If we substitute (C.12) into (C.11), it simply reduces to

$$\begin{aligned}
&-\frac{Pe'}{2}\left(\langle\langle u\rangle_z C^A\rangle + \langle\langle u\rangle_z A'_z\rangle\right) - \frac{Pe'}{2}\left(\langle \rho C_p C^A\rangle + \langle \rho C_p A'_z\rangle\right)\langle\langle u\rangle_z\rangle \\
&\qquad = \frac{Pe'}{2}\langle\langle u\rangle_z\rangle\left[\ell' + \int_o^{\ell'} z'(\langle u\rangle_z/\langle\langle u\rangle_z\rangle + \rho C_p)dz'\right]
\end{aligned} \tag{C.13}$$

Following the same procedure, we also obtain

$$\begin{aligned}
&-\frac{Pe'}{2}\left(\langle\langle u\rangle_z C^o\rangle + \langle \rho C_p C^o\rangle\langle\langle u\rangle_z\rangle\right) \\
&= -\frac{Pe'}{2}\langle\langle u\rangle_z\rangle\left[-\frac{2}{a}\langle \xi t^o(\xi)\rangle + \frac{1}{a}\frac{\langle p(\xi)t^o(\xi)\rangle}{p(\ell')-1}\int_o^{\ell'} + \frac{\langle u\rangle_z/\langle\langle u\rangle_z\rangle - 2 + \rho C_p}{p(z')}dz'\right] \\
&+\frac{Pe'}{2}\frac{1}{a\ell'}\int_o^{\ell'} dz'\left(\langle u\rangle_z/\langle\langle u\rangle_z\rangle + \rho C_p\right)\int_o^{z'} t^o(\xi)d\xi \\
&-\frac{Pe'}{2}\frac{1}{a\ell'}\int_o^{\ell'} dz'\frac{\langle u\rangle_z/\langle\langle u\rangle_z\rangle - 2 + \rho C_p}{p(z')}\int_o^{z'} p(\xi)t^o(\xi)d\xi
\end{aligned} \tag{C.14}$$

Similarly

$$
\begin{aligned}
&\frac{Pe'}{2}\langle \rho C_p B'_x\rangle\langle u\rangle_z \\
=&\frac{Pe'}{2}\langle u\rangle_z\left[-\frac{1}{a}\langle \xi r(\xi)\rangle - \frac{\ell'}{a}\frac{\langle p^{-1}\rangle}{p(\ell')-1}\langle p(\xi)r(\xi)\rangle\right] \\
&+\frac{Pe'}{2}\langle u\rangle_z\left[-\frac{1}{a\ell'}\int_o^{\ell'} dz'\rho C_p\int_o^{z'} r(\xi)d\xi + \frac{1}{a}\frac{\langle p(\xi)r(\xi)\rangle}{p(\ell')-1}\int_o^{\ell'}\rho C_p\frac{dz'}{p(z')}\right] \\
&-\frac{Pe'}{2}\langle u\rangle_z\frac{1}{a\ell'}\int_o^{\ell'}\frac{dz'}{p(z')}(1-\rho C_p)\int_o^{z'} p(\xi)r(\xi)d\xi
\end{aligned}
\tag{C.15}
$$

From (4.1.18), we also obtain

$$
-\frac{1}{2}\left\langle m'\frac{\partial B'_x}{\partial z'}\right\rangle = -\frac{1}{2}\left(\frac{\langle p^{-1}\rangle}{p(\ell')-1}\int_o^{\ell'} p(\xi)r(\xi)d\xi + \frac{1}{\ell'}\int_o^{\ell'}\frac{dz'}{p(z')}\int_o^{z'} p(\xi)r(\xi)d\xi\right) \tag{C.16}
$$

Finally by substituting (C.13) to (C.16) into (C.5), the anti-symmetric dispersion coefficient D^u_{xz} becomes

$$
\begin{aligned}
&D^u_{xz} \\
&=\frac{Pe'}{2}\langle\langle u\rangle_z\rangle\left[\ell' + \int_o^{\ell'} z'(\langle u\rangle_z/\langle\langle u\rangle_z\rangle + \rho C_p)dz'\right] \\
&-\frac{Pe'}{2}\langle\langle u\rangle_z\rangle\left[-\frac{2}{a}\langle \xi t^o(\xi)\rangle - \frac{1}{a}\frac{\langle p(\xi)t^o(\xi)\rangle}{p(\ell')-1}\int_o^{\ell'} + \frac{\langle u\rangle_z/\langle\langle u\rangle_z\rangle - 2 + \rho C_p}{p(z')}dz'\right] \\
&+\frac{Pe'}{2}\frac{1}{a\ell'}\int_o^{\ell'} dz'\left(\langle u\rangle_z/\langle\langle u\rangle_z\rangle + \rho C_p\right)\int_o^{z'} t^o(\xi)d\xi \\
&-\frac{Pe'}{2}\frac{1}{a\ell'}\int_o^{\ell'} dz'\frac{\langle u\rangle_z/\langle\langle u\rangle_z\rangle - 2 + \rho C_p}{p(z')}\int_o^{z'} p(\xi)t^o(\xi)d\xi \\
&+\frac{1}{2}\left[-\langle \xi r(\xi)\rangle - 2\frac{\langle p^{-1}\rangle}{p(\ell')-1}\langle p(\xi)r(\xi)\rangle - \frac{1}{\ell'}\int_o^{\ell'} dz'\rho C_p\int_o^{z'} r(\xi)d\xi\right] \\
&+\frac{1}{2}\left[\frac{\langle p(\xi)r(\xi)\rangle}{p(\ell')-1}\int_o^{\ell'} dz'\frac{\rho C_p(z')}{p(z')} - \frac{1}{\ell'}\int_o^{\ell'} dz'\frac{2-\rho C_p(z')}{p(z')}\int_o^{z'} p(\xi)r(\xi)d\xi\right]
\end{aligned}
\tag{C.17}
$$

From (4.1.16) $r(\xi)$ is given by

$$
r(\xi) = Pe'(\langle u\rangle_z(\xi) - \rho C_p\langle\langle u\rangle_z\rangle) \tag{C.18}
$$

If we substitute (C.18) and (C.3) into (C.17), equation (4.2.5) follows after some cancellations.

Appendix D. The Coefficients $E''_{i\ell}$, $F''_{ij\ell}$ and $G''_{ij\ell}$

In this Appendix, the coefficients in the first order seepage velocity $\langle\langle u\rangle_i^{(1)}\rangle$ are derived by solving the boundary value problems (3.4.5) to (3.4.9).

D.1 The Coefficient $E''_{i\ell}$.

Let us first consider (3.4.5),(3.4.8) and (3.4.9) for the function E'_j. For the medium under consideration, they may be written as

$$\begin{aligned} A_j + \frac{\partial}{\partial z'}\left(k'\frac{\partial E'_j}{\partial z'}\right) &= 0 \qquad 0 < z' < \ell' \\ E'_j(0) &= E'_j(\ell') \\ \left.\frac{\partial E'_j}{\partial z'}\right|_0 &= \left.\frac{\partial E'_j}{\partial z'}\right|_{\ell'} \\ \langle E'_j\rangle &= 0 \end{aligned} \qquad (D.1a-d)$$

where the forcing term A_j becomes from (3.4.3)

$$A_j = \nabla''_i\left[k'\left(\delta_{ij} + \nabla'_i S'_j\right)\right] + \nabla'_i\left(k'\nabla''_i S'_j\right) \qquad (D.2)$$

It is assumed that $k'(z')$ and $S'_j(z')$ are homogeneous on the macroscale x''. We recall from (5.2.4) in Ch.2, Part A that

$$\frac{\partial S'_x}{\partial z'} = \frac{\partial S'_y}{\partial z'} = 0, \quad \frac{\partial S'_z}{\partial z'} = \frac{1}{k'\left\langle\frac{1}{k'}\right\rangle} - 1 \qquad (D.3)$$

Then (D.2) becomes for each component as follows.

$$A_x = \frac{\partial k'}{\partial x''} + \frac{\partial}{\partial x'}\left(k'\frac{\partial S'_x}{\partial x''}\right) = 0 \qquad (D.4a)$$

and similarly

$$A_y = A_z = 0 \qquad (D.4b)$$

Since the source term A_j vanishes, it readily follows from (D.2) that

$$E'_x = E'_y = E'_z = 0 \qquad (D.5)$$

and therefore (3.4.12) becomes

$$E''_{i\ell} = \langle k' \nabla'_i E'_\ell \rangle = 0 \qquad (D.6)$$

Recall that the coefficient $E''_{i\ell}$ accounts for precisely the Darcy type velocity in $\langle\langle u \rangle^{(1)}\rangle$ which is zero. This is the consequence of the uniqueness condition (D.1d) imposed on E'_j.

D.2 The Coefficient $F''_{ij\ell}$.

From (3.4.6),(3.4.8) and (3.4.9) we have

$$\begin{aligned} B_{ij} + \frac{\partial}{\partial z'}\left(k' \frac{\partial F'_{ij}}{\partial z'}\right) &= 0 \qquad 0 < z' < \ell' \\ F'_{ij}(0) &= F'_{ij}(\ell') \\ \left.\frac{\partial F'_{ij}}{\partial z'}\right|_0 &= \left.\frac{\partial F'_{ij}}{\partial z'}\right|_{\ell'} \\ \langle F'_{ij} \rangle &= 0 \end{aligned} \qquad (D.7a-d)$$

For isotropic k' on the mesoscale the source term B_{ij} reduces to

$$B_{ij} = k' \left(\delta_{ij} + \nabla'_i S'_j\right) + \nabla'_i \left(k' S'_j\right) \qquad (D.8)$$

For vertically stratified medium (D.3) holds, hence (D.8) becomes

$$\begin{aligned} B_{xx} &= B_{yy} = k'(z') \\ B_{zz} &= k''_{zz} + \frac{\partial}{\partial z'}\left(k' S'_z\right) \\ B_{ij} &= 0 \qquad \text{otherwise} \end{aligned} \qquad (D.9)$$

where $k''_z = \langle k'(1 + \partial S'_z/\partial z')\rangle$ has been used for B_{zz}. In view of (D.9), it is necessary to consider only diagonal terms of F'_{ij}. If we choose $i = j = x$ in (D.7) and integrate, it becomes

$$k' \frac{dF'_{xx}}{dz'} - \left[k' \frac{dF'_{xx}}{dz'}\right]_{z'=0} + \int_o^{z'} k' dz' = 0 \qquad (D.10)$$

Another integration gives

$$F'_{xx}(z') - F'_{xx}(0) = \left[k' \frac{dF'_{xx}}{dz'}\right]_{z'=0} \int_o^{z'} \frac{dz'}{k'(z')} - \int_o^{z'} \frac{dz'}{k'(z')} \int_o^{z'} k'(\xi) d\xi \qquad (D.11)$$

Imposing the Ω'-periodicity (D.7b), we get

$$\left[k' \frac{dF'_{xz}}{dz'}\right]_{z'=0} = \frac{\int_o^{\ell'} \frac{dz'}{k'(z')} \int_o^{z'} k'(\xi) d\xi}{\ell' \left\langle \frac{1}{k'} \right\rangle} = \frac{k''_{xz}}{\ell'} \int_o^{\ell'} \frac{dz'}{k'(z')} \int_o^{z'} k'(\xi) d\xi \qquad (D.12)$$

where k''_{xz} is the harmonic depth mean of k'.

$$k''_{xz} = \frac{\ell'}{\int_o^{\ell'} \frac{dz'}{k'(z')}} = 1 \Big/ \left\langle \frac{1}{k'} \right\rangle \qquad (D.13)$$

Substituting (D.12) into (D.10), we obtain

$$\frac{dF'_{xz}}{dz'} = \frac{k''_{xz}}{\ell' k'(z')} \int_o^{\ell'} \frac{dz'}{k'(z')} \int_o^{z'} k'(\xi) d\xi - \frac{1}{k'(z')} \int_o^{z'} k'(\xi) d\xi \qquad (D.14)$$

Since $B_{xz} = B_{yy}$, it is obvious that

$$\frac{dF'_{yy}}{dz'} = \frac{dF'_{xz}}{dz'} \qquad (D.15)$$

For $i = j = z$ in (D.7), we readily obtain by following the same procedure

$$k' \left(S'_z + \frac{dF'_{zz}}{dz'} \right) - \left[k' \left(S'_z + \frac{dF'_{zz}}{dz'} \right) \right]_{z'=0} + k''_{zz} z' = 0 \qquad (D.16)$$

Another integration gives

$$F'_{zz}(z') - F'_{zz}(0) = - \int_o^{z'} S'_z dz' + \left[k' \left(S'_z + \frac{dF'_{zz}}{dz'} \right) \right]_{z'=0} \int_o^{z'} \frac{dz'}{k'(z')} - k''_{zz} \int_o^{z'} \frac{z'}{k'(z')} dz'$$

Imposing the Ω'-periodicity (D.7b) and using the uniqueness condition for S'_z, $\langle S'_z \rangle = 0$, we obtain

$$\left[k' \left(S'_z + \frac{dF'_{zz}}{dz'} \right) \right]_{z'=0} = \frac{k''_{zz}}{\left\langle \frac{1}{k'} \right\rangle} \left\langle \frac{z'}{k'} \right\rangle = k''^{\,2}_{zz} \left\langle \frac{z'}{k'} \right\rangle \qquad (D.17)$$

It then follows from (D.16) that

$$\frac{dF'_{zz}}{dz'} = -S'_z + \frac{k''^{\,2}_{zz}}{k'(z')} \left\langle \frac{z'}{k'} \right\rangle - k''_{zz} \frac{z'}{k'(z')} \qquad (D.18)$$

The coefficient $F''_{ij\ell}$ of (3.4.12) now becomes

$$F''_{ij\ell} = \langle k' S'_\ell \rangle \delta_{ij} + \langle k' \nabla'_i F'_{j\ell} \rangle \qquad (D.19)$$

It is straightforward to find $F''_{ij\ell}$ by using S'_z, (D.14), (D.15) and (D.19) and we only list the nonvanishing coefficients here.

$$\begin{aligned}
F''_{zxx} &= F''_{zyy} = \left\langle k' \frac{dF'_{xz}}{dz'} \right\rangle = \frac{k''_{xz}}{\ell'} \int_o^{\ell'} \frac{dz'}{k'(z')} \int_o^{z'} k'(\xi) d\xi + \langle z' k'(z') \rangle - \ell' k''_{xz} \\
F''_{xzx} &= F''_{yyz} = \langle k' S'_z \rangle \\
F''_{zzz} &= \left\langle k' S'_z + k' \frac{dF'_{zz}}{dz'} \right\rangle = k''^{\,2}_{zz} \left(\left\langle \frac{z'}{k'} \right\rangle - \frac{\ell'}{2k''_{zz}} \right) \\
F''_{ij\ell} &= 0 \qquad \text{otherwise}
\end{aligned} \qquad (D.20)$$

where k''_{xz} is the depth average of $k'(z')$ i.e., $k''_{xz} = (\int_o^{\ell'} k'(z') dz')/\ell'$.

D.3 The Coefficient $G''_{ij\ell}$.

These coefficients represent the buoyancy effect of macroscale thermal gradient in z'-direction on $\langle \langle u \rangle_i^{(1)} \rangle$ (cf.(3.4.11)) and may be written from (3.4.12) as

$$G''_{ijz} = \left\langle k' S'_z + k' \frac{dG'_{jz}}{dx'_i} + k' B' \delta_{iz} \right\rangle \qquad (D.21)$$

Accordingly we only need G'_{jz}.

From (3.4.7),(3.4.8) and (3.4.9) we have

$$\begin{aligned}
B_{iz} + C_{iz} + \frac{d}{dz'} \left(k' \frac{dG'_{iz}}{dz'} \right) &= 0 \qquad 0 < z' < \ell' \\
G'_{iz}(0) &= G'_{iz}(\ell') \\
\left. \frac{dG'_{iz}}{dz'} \right|_0 &= \left. \frac{dG'_{iz}}{dz'} \right|_{\ell'} \\
\langle G'_{iz} \rangle &= 0
\end{aligned} \qquad (D.22a-d)$$

From (3.4.3) the new source term C_{iz} is given by

$$C_{iz} = \frac{d}{dz'} (k' B'_i) \qquad (D.23)$$

Note that B'_i is the vector function used in $\theta^{(1)} = B'_i \nabla''_i \theta^{(0)}$ which has been studied earlier.

For $i = x$, we have from (D.22), (D.9) and (D.23)

$$\frac{d}{dz'}\left[k'\left(B'_x + \frac{dG'_{iz}}{dz'}\right)\right] = 0 \tag{D.24}$$

which gives right away

$$\frac{dG'_{xz}}{dz'} = -B'_x(z') \tag{D.25}$$

By analogy it immediately follows for $i = y$ that

$$\frac{dG'_{yz}}{dz'} = -B'_y(z') \tag{D.26}$$

For $i = z$ after using (D.9) and (D.23), (D.22) becomes

$$k''_{zz} + \frac{d}{dz'}\left[k'\left(S'_z + B'_z + \frac{dG'_{zz}}{dz'}\right)\right] = 0 \tag{D.27}$$

By its analogy to (D.16) we readily have

$$\frac{dG'_{zz}}{dz'} = -S'_z - B'_z + \frac{k''^{\,2}_{zz}}{k'(z')}\left\langle\frac{z'}{k'}\right\rangle - k''_{zz}\frac{z'}{k'(z')} \tag{D.28}$$

In terms of (D.25),(D.26) and (D.28), we obtain from (D.21) that

$$\begin{aligned} G''_{zzz} &= G''_{yyz} = \langle k'S'_z\rangle \\ G''_{zzz} &= k''^{\,2}_{zz}\left(\left\langle\frac{z'}{k'}\right\rangle - \frac{\ell'}{2k''_{zz}}\right) \\ G''_{ijz} &= 0 \qquad \text{otherwise} \end{aligned} \tag{D.29}$$

From (D.20) and (D.29) it may be summarized that

$$\begin{aligned} G''_{zzz} &= G''_{yyz} = F''_{zzz} = F''_{yyz} = \langle k'S'_z\rangle \\ G''_{zzz} &= F''_{zzz} = k''^{\,2}_{zz}\left(\left\langle\frac{z'}{k'}\right\rangle - \frac{\ell'}{2k''_{zz}}\right) \\ F''_{zzz} &= F''_{zyy} = \frac{k''_{zz}}{\ell'}\int_o^{\ell'}\frac{dz'}{k'(z')}\int_o^{z'} k'(\xi)d\xi + \langle z'k'(z')\rangle - \ell' k''_{zz} \end{aligned} \tag{D.30}$$

Appendix E. The Coefficients F''_{zzz}, F''_{zzz} and F''_{zzz}

The coefficients which are necessary to compute the first order seepage velocity in the periodically layered medium, e.g. G''_{zzz}, G''_{zzz} and F''_{zzz}, are now obtained completely in terms of the medium permeability.

From (5.2.9) in Ch.2, Part I, we have

$$S'_z(z') = k''_{zz}\int_0^{z'}\frac{dz'}{k'} + k''_{zz}\left\langle\frac{z'}{k'(z')}\right\rangle - z' - \frac{\ell'}{2}$$

from which it follows that

$$\langle k'S'_z\rangle = \frac{k''_{zz}}{\ell'}\left(\int_o^{\ell'} dz'k'\int_o^{z'}\frac{d\xi}{k'} + k''_{zz}\int_o^{\ell'} dz'\frac{z'}{k'}\right) - \frac{1}{\ell'}\int_o^{\ell'} dz'k'z' - \frac{\ell'}{2}k''_{zz} \quad (E.1)$$

Each integral except the first one further becomes

$$\begin{aligned}
\frac{k''_{zz}k''_{zz}}{\ell'}\int_o^{\ell'} dz'\frac{z'}{k'} &= \frac{k''_{zz}k''_{zz}}{\ell'}\left(\ell'\int_o^{\ell'}\frac{dz'}{k'} - \int_o^{\ell'} dz'\int_o^{z'}\frac{d\xi}{k'}\right)\\
&= \ell'k''_{zz} - \frac{k''_{zz}k''_{zz}}{\ell'}\int_o^{\ell'} dz'\int_o^{z'}\frac{d\xi}{k'}\\
-\frac{1}{\ell'}\int_o^{\ell'} dz'k'z' &= -\frac{1}{\ell'}\left(\ell'\int_o^{\ell'} dz'k' - \int_o^{\ell'} dz'\int_o^{z'} k'd\xi\right) \qquad (E.2a-c)\\
&= -\ell'k''_{zz} + \frac{1}{\ell'}\int_o^{\ell'} dz'\int_o^{z'} k'd\xi\\
-\frac{\ell'}{2}k''_{zz} &= -\frac{1}{\ell'}\int_o^{\ell'} dz'k''_{zz}z' = -\frac{1}{\ell'}\int_o^{\ell'} dz'\int_o^{z'} k''_{zz}d\xi
\end{aligned}$$

Substituting (E.2a-c) into (E.1) we have

$$\langle k'S'_z\rangle = \frac{k''_{zz}}{\ell'}\int_o^{\ell'} dz'\,(k'-k''_{zz})\int_o^{z'}\frac{d\xi}{k'} + \frac{1}{\ell'}\int_o^{\ell'} dz'\int_o^{z'}(k'-k''_{zz})\,d\xi \quad (E.3)$$

The first term further becomes

$$\begin{aligned}
&\frac{k''_{zz}}{\ell'}\int_o^{\ell'} dz'\,(k'-k''_{zz})\int_o^{z'}\frac{d\xi}{k'}\\
&\quad = \frac{k''_{zz}}{\ell'}\left[\int_o^{\ell'}\frac{d\xi}{k'}\int_o^{\ell'}(k'-k''_{zz})\,dz' - \int_o^{\ell'}\frac{dz'}{k'}\int_o^{z'}(k'-k''_{zz})\,d\xi\right]
\end{aligned} \quad (E.4)$$

From the definition of k''_{zz} it follows that

$$\int_o^{\ell'} (k' - k''_{zz})\, dz' = \int_o^{\ell'} k' dz' - k''_{zz}\ell' = 0 \qquad (E.5)$$

By using (E.5) and (E.4) in (E.3), we have

$$F''_{zzz} = \langle k' S'_z \rangle = \frac{k''_{zz}}{\ell'} \int_o^{\ell'} dz' \left(1 - \frac{k''_{zz}}{k'(z')}\right) \int_o^{z'} \left(\frac{k'(\xi)}{k''_{zz}} - 1\right) d\xi \qquad (E.6)$$

Also by using (E.2a) we may write

$$\begin{aligned} F''_{zzz} = k''^{\,2}_{zz} \left(\left\langle \frac{z'}{k'} \right\rangle - \frac{\ell'}{2k''_{zz}}\right) &= k''^{\,2}_{zz} \left(\frac{\ell'}{2k''_{zz}} - \frac{1}{\ell'} \int_o^{\ell'} dz' \int_o^{z'} \frac{d\xi}{k'}\right) \\ &= \frac{k''^{\,2}_{zz}}{\ell'} \left(\int_o^{\ell'} dz' \frac{z'}{k''_{zz}} - \int_o^{\ell'} dz' \int_o^{z'} \frac{d\xi}{k'}\right) \\ &= \frac{k''_{zz}}{\ell'} \int_o^{\ell'} dz' \int_o^{z'} \left(1 - \frac{k''_{zz}}{k'(\xi)}\right) d\xi \end{aligned} \qquad (E.7)$$

If we use (E.2b) for F''_{zzz} in (4.3.4), there follows

$$\begin{aligned} F''_{zzz} &= \frac{1}{\ell'} \int_o^{\ell'} dz' \left(\frac{k''_{zz}}{k'} - 1\right) \int_o^{z'} k' d\xi \\ &= \frac{1}{\ell'} \left[\int_o^{\ell'} dz' \left(\frac{k''_{zz}}{k'} - 1\right) \int_o^{\ell'} k' dz' - \int_o^{\ell'} dz' k' \int_o^{z'} \left(\frac{k''_{zz}}{k'} - 1\right) d\xi\right] \\ &= \frac{1}{\ell'} \int_o^{\ell'} dz' k' \int_o^{z'} \left(1 - \frac{k''_{zz}}{k'}\right) d\xi \end{aligned} \qquad (E.8)$$

where $1/k''_{zz} = \langle 1/k' \rangle$ has been used.

Appendix F. The Dispersion Tensors D^*_{ij} and D^u_{ij} for Alternating Uniform Layers.

The analytic forms of D^*_{ij} and D^u_{ij} are derived for periodic medium with alternating uniform layers.

F.1 Evaluation of Integrals.

By using (5.1.1) and (5.1.2) we obtain

$$\int_o^\xi p(\xi)r(\xi)d\xi = -A^-\left[\exp\left(-\frac{a\xi}{m'^-}\right)-1\right] \quad \text{for} \quad 0<\xi'<(1-s)\ell'$$
$$\int_o^\xi p(\xi)r(\xi)d\xi = -(A^- - A^+)\exp\left(-\frac{a(1-s)\ell'}{m'^-}\right) + A^- - A^+\exp\left[-a(1-s)\ell'\left(\frac{1}{m'^-}-\frac{1}{m'^+}\right)-\frac{a\xi}{m'^+}\right] \quad \text{for} \quad (1-s)\ell'<\xi'<\ell' \tag{F.1}$$

where

$$A^\pm = \frac{r^\pm m'^\pm}{a}, \quad a = Pe'\langle u|ra_z \tag{F.2}$$

From now on whenever a pair of curly brackets as in (F.1) is used, it is meant that the domain of definition is as indicated in (F.1). It then follows from (F.1) after replacing a by $-a$ (cf. (5.1.2)) that

$$\int_o^\xi \frac{r(\xi)}{p(\xi)}d\xi = \left\{\begin{array}{c} A^-\left[\exp\left(\frac{a\xi}{m'^-}\right)-1\right] \\ (A^- - A^+)\exp\left(\frac{a(1-s)\ell'}{m'^-}\right) - A^- \\ +A^+\exp\left[a(1-s)\ell'\left(\frac{1}{m'^-}-\frac{1}{m'^+}\right)+\frac{a\xi}{m'^+}\right] \end{array}\right\} \tag{F.3}$$

If we take the upper limit ξ to be ℓ', (F.1) and (F.3) become

$$\int_o^{\ell'} p(\xi)r(\xi)d\xi = 2\left(A^-e^{-x}\sinh x + A^+e^{-2x-y}\sinh y\right)$$
$$\int_o^{\ell'} \frac{r(\xi)}{p(\xi)}d\xi = 2\left(A^-e^{x}\sinh x + A^+e^{2x+y}\sinh y\right) \tag{F.4}$$

where

$$x = \frac{a(1-s)\ell'}{2m'^-}, \qquad y = \frac{as\ell'}{2m'^+} \tag{F.5}$$

were used for simpler notation. They are related to $m''_{zz} = \ell' / \int_o^{\ell'} m' dz$ by

$$x + y = \frac{a\ell'}{2m''_{zz}} \tag{F.6}$$

It follows from (F.1) that

$$\frac{r(\xi)}{p(\xi)} \int_o^{\xi} p(t)r(t)dt$$
$$= \left\{ \begin{array}{c} -r^- A^- \left[1 - \exp\left(-\frac{a\xi}{m'^-}\right)\right] \\ -r^+(A^- - A^+) \exp\left(a\frac{\xi-(1-s)\ell'}{m'^+}\right) \\ +r^+ A^- \exp\left[a(1-s)\ell'\left(\frac{1}{m'^-} - \frac{1}{m'^+}\right)\right] \exp\left(\frac{a\xi}{m'^+}\right) - r^+ A^+ \end{array} \right\} \tag{F.7}$$

which yields after integration

$$\int_o^{\ell'} d\xi \frac{r(\xi)}{p(\xi)} \int_o^{\xi} p(t)r(t)dt = -\left[r^- A^-(1-s)\ell' + r^+ A^+ s\ell'\right]$$
$$+ 2A^{-^2} e^x \sinh x + 2A^{+^2} e^y \sinh y + 4A^- A^+ e^{x+y} \sinh x \sinh y \tag{F.8}$$

We also have from (5.1.2) that

$$\frac{1}{p(\ell') - 1} = \frac{1}{e^{-2x-2y} - 1} = -\frac{e^{x+y}}{2\sinh(x+y)} \tag{F.9}$$

F.2 Dispersion Coefficients D^s_{xx}, D^s_{zz}, D^s_{xz} and D^u_{zz}

The dispersion coefficient D^s_{xx} given in (4.1.36) becomes after combining (F.4), (F.8) and (F.9) as

$$D^s_{xx} = \frac{1}{a^2}\left[r^{-^2} m'^-(1-s) + r^{+^2} m'^+ - \frac{2}{a\ell'}\frac{\sinh x \sinh y}{\sinh(x+y)}\left(r^- m'^- - r^+ m'^+\right)^2\right] \tag{F.10}$$

After inserting $t^{\pm}$ for $r^{\pm}$ in (F.10), the coefficient D^s_{zz} in (4.1.37) is then given as

$$D^s_{zz} = \frac{1}{a^2}\left[t^{-^2} m'^-(1-s) + t^{+^2} m'^+ - \frac{2}{a\ell'}\frac{\sinh x \sinh y}{\sinh(x+y)}\left(t^- m'^- - t^+ m'^+\right)^2\right] \tag{F.11}$$

For the off-diagonal coefficient D^s_{xz}, the procedure is the same and only slight modifications are necessary. For example, we have from (F.8)

$$\int_o^{\ell'} d\xi \frac{t(\xi)}{p(\xi)} \int_o^{\xi} p(t)r(t)dt = -\left[t^- A^-(1-s)\ell' + t^+ A^+ s\ell'\right] + 2A^- B^- e^x \sinh x + 2A^+ B^+ e^y \sinh y + 4A^- B^+ e^{x+y} \sinh x \sinh y \tag{F.12}$$

where

$$B^{\pm} = \frac{t^{\pm} m'^{\pm}}{a} \tag{F.13}$$

Similarly

$$\int_o^{\ell'} dz' \frac{r(z')}{p(z')} \int_o^{z'} p(\xi)t(\xi)d\xi = -\left[r^- B^-(1-s)\ell' + r^+ B^+ s\ell'\right] + 2A^- B^- e^x \sinh x + 2A^+ B^+ e^y \sinh y + 4A^+ B^- e^{x+y} \sinh x \sinh y \tag{F.14}$$

By using (F.4), its equivalent form for $t(\xi)$ and (F.12) and (F.14), we readily have

$$D^s_{xz} = \frac{1}{a^2} r^- t^- m'^-(1-s) + r^+ t^+ m'^+ s - \frac{2}{a^3 \ell'} \frac{\sinh x \sinh y}{\sinh(x+y)} \left(r^- m'^- - r^+ m'^+\right)\left(t^- m'^- - t^+ m'^+\right) \tag{F.15}$$

The anti-symmetric dispersion coefficient D^u_{xz} derived also by making use of analogy. Rewriting D^u_{xz} from (4.2.5)

$$D^u_{xz} = (D^u_{xz})_1 + (D^u_{xz})_2 \tag{F.16}$$

where

$$(D^u_{xz})_1 = \frac{Pe'}{2\ell'}\left[\frac{1}{p(\ell')-1}\int_o^{\ell'} \frac{\langle u\rangle_x}{p(z')}dz' \int_o^{\ell'} p(\xi)\rho C_p(\xi)d\xi + \int_o^{\ell'} dz' \frac{\langle u\rangle_x}{p(z')} \int_o^{z'} p(\xi)\rho C_p(\xi)d\xi\right] + \frac{Pe'}{2\ell'}\left(\frac{1}{p(\ell')-1}\int_o^{\ell'} \frac{\rho C_p(z')}{p(z')}dz' \int_o^{\ell'} p(\xi)\langle u\rangle_x(\xi)d\xi\right) + \frac{Pe'}{2\ell'} + \int_o^{\ell'} dz' \frac{\rho C_p(z')}{p(z')} \int_o^{z'} p(\xi)\langle u\rangle_x(\xi)d\xi \tag{F.17a}$$

$$(D^u_{zz})_2 = -\frac{Pe'}{\ell'}\left(\frac{1}{p(\ell')-1}\int_o^{\ell'}\frac{dz'}{p(z')}\int_o^{\ell'} p(\xi)\langle u\rangle_z(\xi)d\xi\right)$$
$$-\frac{Pe'}{\ell'}+\int_o^{\ell'}\frac{dz'}{p(z')}\int_o^{z'} p(\xi)\langle u\rangle_z(\xi)d\xi \qquad (F.17b)$$

The first part $(D^u_{zz})_1$ is readily obtained by replacing $r(\xi)$ and $t(\xi)$ by $\langle u\rangle_z(\xi)$ and $\rho C_p(\xi)$ in (F.15) and then multiplying by $-aPe'$ (cf. (4.1.38)). Thus we have

$$(D^u_{zz})_1 = -\frac{Pe'}{a}\langle u\rangle_z^- \rho C_p^- m'^-(1-s)+\langle u\rangle_z^+\rho C_p^+ m'^+ s$$
$$+\frac{2Pe'}{a^3\ell'}\frac{\sinh x\sinh y}{\sinh(x+y)}\left(\langle u\rangle_z^- m'^- - \langle u\rangle_z^+ m'^+\right)\left(\rho C_p^- m'^- - \rho C_p^+ m'^+\right) \qquad (F.18)$$

Similarly the second part $(D^u_{zz})_2$ is obtained from D^s_{zz} in (F.10) by replacing one $r(\xi)$ by $\langle u\rangle_z^-(\xi)$ and another $r(\xi)$ by unity and then multiplying by aPe' i.e.,

$$(D^u_{zz})_2 = \frac{Pe'}{a}\langle u\rangle_z^- m'^-(1-s)+\langle u\rangle_z^+ m'^+ s$$
$$+\frac{2Pe'}{a^3\ell'}\frac{\sinh x\sinh y}{\sinh(x+y)}\left(\langle u\rangle_z^- m'^- - \langle u\rangle_z^+ m'^+\right)\left(m'^- - m'^+\right) \qquad (F.19)$$

If we add (F.18) and (F.19) and use the relation $a = Pe'\langle u\rangle_z$, D^u_{zz} in (5.1.4) readily follows.

Appendix G. Direct Integration of (4.1.14) for Two Layer Medium

As in §5.1, the variables in the lower and upper layers are denoted by the superscript symbols $()^-$ and $()^+$. For convenience the prime is omitted. In the lower and upper layers, (4.1.14a) becomes

$$\frac{d}{dz}\left(\frac{dB_x^-}{dz} - q^- B_x^-\right) = \frac{r^-}{m^-} \qquad 0 < z < (1-s)\ell \tag{G.1}$$

$$\frac{d}{dz}\left(\frac{dB_x^+}{dz} - q^+ B_x^+\right) = \frac{r^+}{m^+} \qquad 0 < z < (1-s)\ell \tag{G.2}$$

where

$$q^\pm = \frac{Pe\langle u\rangle_z}{m^\pm}, \qquad r^\pm = Pe\left(\langle u\rangle_x^\pm - \rho C_p^\pm \langle\langle u\rangle_x\rangle\right) \tag{G.3a}$$

The source terms $r^\pm$ satisfy (cf. (4.1.17))

$$\int_o^{(1-s)\ell} r^- dz + \int_{(1-s)\ell}^{\ell} r^+ dz = 0 \tag{G.3b}$$

The boundary conditions are

$$\begin{aligned} B_x^-(0) &= B_x^+(\ell) \\ \left[m^- \frac{dB_x^-}{dz} - Pe\langle u\rangle_z B_x^-\right]_o &= \left[m^+ \frac{dB_x^+}{dz} - Pe\langle u\rangle_z B_x^+\right]_\ell \\ B_x^-((1-s)\ell) &= B_x^+((1-s)\ell) \\ \int_o^{(1-s)\ell} B_x^- dz + \int_{(1-s)\ell}^{\ell} B_x^+ dz &= 0 \end{aligned} \tag{G.4a-d}$$

in which (G.3a and b) are from the Ω'-periodicity and (G.3c) is the continuity of temperature at the interface. The last condition is imposed for uniqueness.

Integrating (G.1) from o to $z(< (1-s)\ell)$, we have

$$e^{q^- z}\frac{d}{dz}\left(e^{-q^- z} B_x^-\right) - \left[\frac{dB_x^-}{dz} - q^- B_x^-\right]_o = \frac{r^-}{m^-} z \tag{G.5}$$

Another integration gives

$$\begin{aligned} B_x^- - B_x^-(0)e^{q^- z} + \left[\frac{dB_x^-}{dz} - q^- B_x^-\right]_o \frac{1}{q^-}\left(1 - e^{q^- z}\right) \\ = \frac{r^-}{m^-}\left[-\frac{z}{q^-} - \frac{1}{q^{-2}}\left(1 - e^{q^- z}\right)\right] \end{aligned} \tag{G.6}$$

Similarly if we integrate (G.2) from ℓ to $z(>(1-s)\ell)$ twice, there follows

$$B_z^+ - B_z^+(\ell)e^{q^+(z-\ell)} + \left[\frac{dB_z^+}{dz} - q^+B_z^+\right]_\ell \frac{1}{q^+}\left(1-e^{q^+(z-\ell)}\right) = \frac{r^+}{m^+}\left[-\frac{z-\ell}{q^+} - \frac{1}{q^{+2}}\left(1-e^{q^+(z-\ell)}\right)\right] \tag{G.7}$$

After using (G.4a and b) in (G.6) and (G.7), the condition (G.4c) yields

$$B_z^-(0)\left(e^{2x}-e^{-2y}\right) + \left[\frac{dB_z^-}{dz} - q^-B_z^-\right]_o \frac{e^{2x}-e^{-2y}}{q^-} = \frac{1}{Pe^2\langle u\rangle_z{}^2}\left[r^-m^-(1-e^{2x}) - r^+m^+(1-e^{-2y})\right] \tag{G.8}$$

where

$$x = \frac{(1-s)\ell}{2m^-}, \qquad y = \frac{s\ell}{2m^+} \tag{G.9}$$

and (G.3b) has been used. Thus

$$m^-\left[\frac{dB_z^-}{dz} - q^-B_z^-\right]_o = -Pe\langle u\rangle_z B_z^-(0) + \frac{r^-m^-(1-e^{2x}) - r^+m^+(1-e^{-2y})}{Pe\langle u\rangle_z(e^{2x}-e^{-2y})} \tag{G.10}$$

Substituting (G.10) into (G.6) and (g.7), we obtain

$$\begin{aligned} B_z^- &= B_z^-(0) - \frac{r^-m^-(1-e^{2x}) - r^+m^+(1-e^{-2y})}{(Pe\langle u\rangle_z)^2(e^{2x}-e^{-2y})}(1-e^{q^-z}) - \frac{r^-}{Pe\langle u\rangle_z}z \\ &\quad - \frac{r^-m^-}{(Pe\langle u\rangle_z)^2}(1-e^{q^-z}) \\ B_z^+ &= B_z^-(0) - \frac{r^-m^-(1-e^{2x}) - r^+m^+(1-e^{-2y})}{(Pe\langle u\rangle_z)^2(e^{2x}-e^{-2y})}(1-e^{q^+(z-\ell)}) - \frac{r^+}{Pe\langle u\rangle_z}(z-\ell) \\ &\quad - \frac{r^+m^+}{(Pe\langle u\rangle_z)^2}(1-e^{q^-(z-\ell)}) \end{aligned} \tag{G.11}$$

The dispersion coefficient D_{zz}^e is given by (cf. (4.1.34))

$$D_{zz}^e = \left\langle m\frac{dB_z}{dz}\frac{dB_z}{dz}\right\rangle = -\frac{1}{\ell}\int_o^\ell r(z)B_z(z)dz \tag{G.12}$$

Note , in view of (G.3b), that $B_x^-(0)$ in B_x^- and B_x^+ produces zero. Then D_{xx}^s becomes

$$
\begin{aligned}
D_{xx}^s &= -\frac{1}{\ell}\left(\int_o^{(1-s)\ell} B_x^-(z)dz + \int_{(1-s)\ell}^{\ell} B_x^+(z)dz\right) \\
&= -\frac{1}{\ell}\left\{\frac{m^-r^-}{a^3}H(e^{2x}-1) - \frac{r^{-2}}{a}\frac{(1-s)^2\ell^2}{2}\right\} \\
&+ \frac{1}{\ell}\left\{\frac{r^{-2}m^-(1-s)\ell}{a^2} + \frac{r^{-2}m^{-2}}{a^3}(e^{2x}-1)\right\} \\
&- \frac{1}{\ell}\left\{\frac{m^+r^+}{a^3}H(1-e^{-2y}) + \frac{r^{+2}}{a}\frac{s^2\ell^2}{2} - \frac{r^{+2}m^+s\ell}{a^2} + \frac{r^{+2}m^{+2}}{a^3}(1-e^{-2y})\right\}
\end{aligned}
$$

$$
\begin{aligned}
=&\frac{1}{2a\ell}\left[r^-(1-s)\ell + r^+s\ell\right]\left[r^-(1-s)\ell - r^+s\ell\right] \\
&+ \frac{1}{a^2\ell}\left[r^{-2}m^-(1-s)\ell + r^{+2}m^+s\ell\right] \\
&- \frac{1}{a^3\ell}H\left[r^-m^-(e^{2x}-1) + r^+m^+(1-e^{-2y})\right] \\
&- \frac{1}{a^3\ell}\left[r^{-2}m^{-2}(e^{2x}-1) + r^{+2}m^{+2}(1-e^{-2y})\right]
\end{aligned}
\qquad (G.13)
$$

where

$$
H = \frac{r^-m^-(1-e^{2x}) - r^+m^+(1-e^{-2y})}{e^{2x}-e^{-2y}} \qquad (G.14)
$$

The first line vanishes because of (G.3b). Let the last two lines in (G.13) be denoted by I. It may be written as

$$
\begin{aligned}
I =& -\frac{r^{-2}m^{-2}}{a^3\ell}(e^{2x}-1)\left[\frac{e^{-x+y}-e^{x+y}}{2\sinh(x+y)}+1\right] \\
&+ \frac{r^{+2}m^{+2}}{a^3\ell}(1-e^{-2y})\left[\frac{e^{-x+y}-e^{-x-y}}{2\sinh(x+y)}-1\right] \\
&+ \frac{r^-m^-r^+m^+}{a^3\ell}\left[\frac{e^{-x+y}-e^{-x-y}}{2\sinh(x+y)}(e^{2x}-1) - \frac{e^{-x+y}-e^{x+y}}{2\sinh(x+y)}(1-e^{-2y})\right] \\
=& -\frac{2}{a^3\ell}\frac{\sinh x\sinh y}{\sinh(x+y)}\left(r^{-2}m^{-2} - 2r^-m^-r^+m^+ + r^{+2}m^{+2}\right) \\
=& -\frac{2}{a^3\ell}\frac{\sinh x\sinh y}{\sinh(x+y)}\left(r^-m^- - r^+m^+\right)^2
\end{aligned}
\qquad (G.15)
$$

Finally by substituting (G.14) and (G.15), we get

$$D^s_{xx} = \frac{1}{a^2}\left[r^{-2}m^-(1-s) + r^{+2}m^+s - \frac{2}{a\ell}\frac{\sinh x \sinh y}{\sinh(x+y)}\left(r^-m^- - r^+m^+\right)^2\right] \tag{G.16}$$

which is the same as D^s_{xx} in (5.1.4) obtained from the Green's function.

For the medium with two layers, other dispersion coefficients D^s_{zz}, D^s_{xz} and D^u_{xz} can be calculated in the same manner by direct integration of the governing equations. They are omitted.

Appendix H. The Coefficients $\langle \overline{\rho C_p}^{*} B_i' \rangle$

They have been considered for D_{zz}^{u} in Appendix C. Analogies are made use of to calculate them for alternating uniform layers.

The coefficient $\langle \overline{\rho C_p}^{*} B_z' \rangle / \langle \overline{\rho C_p}^{*} \rangle$ has been given in (C.15) for vertically stratified periodic medium. Its first term may be written after integration by parts

$$\langle \xi r(\xi) \rangle = \frac{1}{\ell'} \left[z' \int_o^{z'} r(z') dz' \Big|_{z'=0}^{z'=\ell'} - \int_o^{\ell'} dz' \int_o^{z'} r(\xi) d\xi \right] = -\frac{1}{\ell'} \int_o^{\ell'} dz' \int_o^{z'} r(\xi) d\xi \tag{H.1}$$

in which (4.1.17) has been used. If we substitute (H.1) into (C.15) and rearrange the result, it follows that

$$\begin{aligned} \frac{\langle \overline{\rho C_p}^{*} B_z' \rangle}{\langle \overline{\rho C_p}^{*} \rangle} &= -\frac{1}{a\ell'} \int_o^{\ell'} dz' \left(1 - \rho C_p(z')\right) \int_o^{z'} r(\xi) d\xi \\ &\quad - \frac{1}{a\ell'} \left[\frac{1}{p(\ell') - 1} \int_o^{\ell'} \frac{dz'}{p(z')} \int_o^{\ell'} p(\xi) r(\xi) d\xi + \int_o^{\ell'} \frac{dz'}{p(z')} \int_o^{z'} p(\xi) r(\xi) d\xi \right] \\ &\quad + \frac{1}{a\ell'} \left(\frac{1}{p(\ell') - 1} \int_o^{\ell'} \frac{\rho C_p(z')}{p(z')} dz' \int_o^{\ell'} p(\xi) r(\xi) d\xi \right) \\ &\quad + \frac{1}{a\ell'} \int_o^{\ell'} dz' \frac{\rho C_p(z')}{p(z')} \int_o^{z'} p(\xi) r(\xi) d\xi \end{aligned} \tag{H.2}$$

where the reduced symbol $\rho C_p(z') = \overline{\rho C_p}^{*}(z') / \langle \overline{\rho C_p}^{*} \rangle$ has been used. Each line in (H.2) is designated by I, II and III from the first to the third respectively. The integral I becomes

$$\begin{aligned} I &= \int_o^{\ell'} dz' \left(1 - \rho C_p(z')\right) \int_o^{z'} r(\xi) d\xi \\ &= \int_o^{\ell'} \left\{ \begin{matrix} \left(1 - \rho C_p{}^{-}\right) r^{-} z' \\ \left(1 - \rho C_p{}^{+}\right) \left[(r^{-} - r^{+})(1 - s)\ell' + r^{+} z' \right] \end{matrix} \right\} dz' \\ &= -\frac{\ell'}{a} \left[(1 - \rho C_p{}^{-}) r^{-} - (1 - \rho C_p{}^{+}) r^{+} \right] \frac{(1 - s)^2}{2} \\ &\quad - \frac{\ell'}{a} (1 - \rho C_p^{+}) \left[(r^{-} - r^{+})(1 - s)s + \frac{r^{+}}{2} \right] \end{aligned} \tag{H.3}$$

The second line II has the same form as D^s_{zz} except that one $r(z')$ in (4.1.36) is replaced by unity. The result readily follows from (F.10) :

$$II = -\frac{\ell'}{a}\times$$
$$\left[r^- m'^-(1-s) + r^+ m'^+ s - \frac{2}{a\ell'}\frac{\sinh x \sinh y}{\sinh(x+y)}\left(r^- m'^- - r^+ m'^+\right)\left(m'^- - m'^+\right)\right] \tag{H.4}$$

Similarly, upon replacing one $r(z')$ by $\rho C_p(z')$, we get

$$\begin{aligned} III = &-\frac{\ell'}{a}\left[r^- m'^- \rho C_p{}^-(1-s) + r^+ m'^+ \rho C_p{}^+ s\right] \\ &+ \frac{2}{a^2}\frac{\sinh x \sinh y}{\sinh(x+y)}\left(r^- m'^- - r^+ m'^+\right)\left(\rho C_p{}^- m'^- \rho C_p{}^+ - m'^+\right) \end{aligned} \tag{H.5}$$

If we substitute (H.3) - (H.5) into (H.2), it gives I_x of (5.4.2).

The coefficient $\langle\overline{\rho C_p}^* B'_y\rangle/\langle\overline{\rho C_p}^*\rangle$ requires the replacement of forcing terms $r^\pm$ by $S^\pm$ for B'_y in $\langle\overline{\rho C_p}^* B'_x\rangle/\langle\overline{\rho C_p}^*\rangle$.

Similarly after invoking (C.3) and (C.4), the coefficient $\langle\overline{\rho C_p}^* B'_z\rangle/\langle\overline{\rho C_p}^*\rangle$ can be calculated from (C.10) and (C.14) as follows.

$$\begin{aligned} &\langle\rho C_p B'_z\rangle = \langle\rho C_p A'_z\rangle + \langle\rho C_p C^A\rangle + \langle\rho C_p C^o\rangle \\ &= \frac{m''_{zz}}{\ell'}\int_o^{\ell'} dz' \frac{\rho C_p(z')-1}{p(z')}\int_o^{z'}\frac{p(\xi)}{m'(\xi)}d\xi - \frac{\ell'}{2} - \frac{1}{\ell'}\int_o^{\ell'} z'\rho C_p(z')dz' \\ &+ \frac{m''_{zz}}{\ell'}\frac{1}{p(\ell')-1}\int_o^{\ell'}\frac{\rho C_p(z')-1}{p(z')}dz'\int_o^{\ell'}\frac{p(\xi)}{m'(\xi)}d\xi \\ &-\frac{1}{a}\langle\xi t^o(\xi)\rangle - \frac{\ell'}{a}\frac{\langle p^{-1}\rangle}{p(\ell')-1}\langle p(\xi)t^o(\xi)\rangle - \frac{1}{a\ell'}\int_o^{\ell'} dz'\rho C_p(z')\int_o^{z'} t^o(\xi)d\xi \\ &-\frac{1}{a}\frac{\langle p(\xi)t^o(\xi)\rangle}{p(\ell')-1}\int_o^{\ell'} dz'\frac{\rho C_p(z')}{p(z')} \\ &-\frac{1}{a\ell'}\int_o^{\ell'}\frac{dz'}{p(z')}(1-\rho C_p)\int_o^{z'} p(\xi)t^o(\xi)d\xi \end{aligned} \tag{H.6}$$

Note in view of (C.12) that

$$\begin{aligned}
&\frac{m''_{zz}}{\ell'}\left(\frac{1}{p(\ell')-1}\int_o^{\ell'}\frac{\rho C_p(z')-1}{p(z')}dz'\int_o^{\ell'}\frac{p(\xi)}{m'(\xi)}d\xi\right)\\
&+\frac{m''_{zz}}{\ell'}\left(\int_o^{\ell'}dz'\frac{\rho C_p(z')-1}{p(z')}\int_o^{z'}\frac{p(\xi)}{m'(\xi)}d\xi\right)\\
=&\frac{m''_{zz}}{\ell'}\left(-\frac{1}{a}\int_o^{\ell'}\frac{\rho C_p(z')-1}{p(z')}dz'-\frac{1}{a}\int_o^{\ell'}\left[\rho C_p(z')-1\right]dz'\right)\\
&+\frac{m''_{zz}}{\ell'}\left(\frac{1}{a}\int_o^{\ell'}\frac{\rho C_p(z')-1}{p(z')}dz'\right)\\
=&0
\end{aligned}\tag{H.7}$$

because $\int_o^{\ell'}\rho C_p(z')dz'=\ell'$. Also upon recalling $t^o(\xi)$ from (C.3), we have

$$-\frac{1}{a}\langle\xi t^o(\xi)\rangle=\frac{1}{\ell'}\int_o^{\ell'}z'\rho C_p(z')dz'\tag{H.8}$$

and

$$-\frac{1}{a\ell'}\int_o^{\ell'}dz'\rho C_p(z')\int_o^{z'}t^o(\xi)d\xi=\frac{1}{\ell'}\int_o^{\ell'}dz'\rho C_p(z')\int_o^{z'}\rho C_p(\xi)d\xi\tag{H.9}$$

The latter becomes after integration by parts

$$\begin{aligned}
\frac{1}{\ell'}\int_o^{\ell'}dz'\rho C_p(z')\int_o^{z'}\rho C_p(\xi)d\xi=&\frac{1}{\ell'}\int_o^{\ell'}dz'\rho C_p(z')\int_o^{\ell'}\rho C_p(\xi)d\xi\\
&-\frac{1}{\ell'}\int_o^{\ell'}dz'\rho C_p(z')\int_o^{z'}\rho C_p(\xi)d\xi
\end{aligned}$$

which gives

$$\frac{1}{\ell'}\int_o^{\ell'}dz'\rho C_p(z')\int_o^{z'}\rho C_p(\xi)d\xi=\frac{\ell'}{2}\tag{H.10}$$

Finally upon substituting (H.7) to (H.10) into (H.6) and rearranging, we obtain

$$\begin{aligned}
&\langle\rho C_pB'_z\rangle\\
&=-\frac{1}{a\ell'}\frac{1}{p(\ell')-1}\int_o^{\ell'}\frac{\rho C_p(z')-1}{p(z')}dz'\int_o^{\ell'}\rho C_p(\xi)p(\xi)d\xi\\
&\quad-\frac{1}{a\ell'}\int_o^{\ell'}\frac{\rho C_p(z')-1}{p(z')}dz'\int_o^{z'}\rho C_p(\xi)p(\xi)d\xi
\end{aligned}\tag{H.11}$$

By it resemblance to D^s_{xx} in (4.1.36), I_z in (5.4.2) follows right away.

Appendix I. Finite Difference Equations for Thermal Dispersion

Finite difference forms of the governing equations and boundary conditions are derived here. For a scalar variable f its spatial derivatives are approximated by using centered difference for which the truncation error is $O(\Delta^2)$ where Δ is grid spacing. Let $f_{i,j}$ be the value of f at node (i,j) which is located at $\xi = (i-1)\Delta\xi$ and $z = (j-1)\Delta z$. The derivatives then become

$$\begin{aligned}\left(\frac{\partial f}{\partial \xi}\right)_{i,j} &= \frac{1}{2\Delta\xi}(f_{i+1,j} - f_{i-1,j}) + O(\Delta\xi^2) \\ \left(\frac{\partial^2 f}{\partial \xi^2}\right)_{i,j} &= \frac{1}{\Delta\xi^2}(f_{i+1,j} - 2f_{i,j} + f_{i-1,j}) + O(\Delta\xi^2)\end{aligned} \tag{I.1}$$

in which the error terms are the consistency of the finite difference approximations and are from the truncation of Taylor expansion of f. For z derivatives one simply replaces $\Delta\xi$,i and j by Δz,j and i. Similarly the cross derivatives are approximated by

$$\begin{aligned}\left(\frac{\partial^2 f}{\partial \xi \partial z}\right)_{i,j} = &\frac{1}{4\Delta\xi\Delta z}(f_{i+1,j+1} - f_{i-1,j+1} - f_{i+1,j-1} + f_{i-1,j-1}) \\ &+ O(\Delta\xi^2, \Delta z^2, \Delta\xi\Delta z)\end{aligned} \tag{I.2}$$

By employing the implicit scheme, the heat transport equation (6.1.10) is written as

$$\frac{{}^k\theta_{i,j}^{n+1} - \theta_{i,j}^n}{\Delta\tau} = {}^kR_{i,j}^{n+1} + O(\Delta\tau) \tag{I.3}$$

where ${}^kR_{i,j}^{n+1}$ is the rest of (6.1.16) at the current time step $(n+1)$ and iteration number k and is given by

$$\begin{aligned}{}^kR_{i,j}^{n+1} = &{}^kCX_{i,j}^{n+1}\frac{\partial\theta}{\partial\xi} + {}^kCZ_{i,j}^{n+1}\frac{\partial\theta}{\partial z} + \frac{{}^{k-1}(\langle m'\rangle + D_{xz}^e)_{i,j}^{n+1}}{R}\ {}^k\left(\frac{\partial^2\theta}{\partial\xi^2}\right)_{i,j}^{n+1} \\ &+ 2\frac{{}^{k-1}(D_{xz}^e)_{i,j}^{n+1}}{R^{1/2}}\ {}^k\left(\frac{\partial^2\theta}{\partial\xi\partial z}\right)_{i,j}^{n+1} + {}^{k-1}(\langle m'\rangle + D_{zz}^e)_{i,j}^{n+1}\ {}^k\left(\frac{\partial^2\theta}{\partial z^2}\right)_{i,j}^{n+1}\end{aligned} \tag{I.4}$$

where R is the anisotropy ratio of permeability R_k in (6.1.10) and

$$
\begin{aligned}
CX =& \frac{M_f}{M_m} CVX + \frac{\partial}{\partial \xi}\left(\frac{\langle m' \rangle + D^e_{xz}}{R}\right) + \frac{\partial}{\partial z}\left(\frac{D^e_{xz}}{R^{1/2}}\right) \\
CZ =& \frac{M_f}{M_m} CVZ + \frac{\partial}{\partial \xi}\left(\frac{D^e_{xz}}{R^{1/2}}\right) + \frac{\partial D^e_{zz}}{\partial z}
\end{aligned}
\tag{I.5}
$$

in which CVX and CVZ are from the convection terms and the rest are from the dispersion terms. In (I.5), CVX and CVZ are further given by

$$
\begin{aligned}
CVX =& \left[1 + \epsilon\left(\frac{1}{R^{1/2}}\frac{\partial \langle \rho C_p B'_x \rangle}{\partial \xi} + \frac{\partial \langle \rho C_p B'_z \rangle}{\partial z}\right)\right]\frac{\partial p}{\partial \xi} - \frac{M_m}{M_f}\frac{1}{R^{1/2}}\frac{\partial D^u_{xz}}{\partial z} \\
CVZ =& \left[1 + \epsilon\left(\frac{1}{R^{1/2}}\frac{\partial \langle \rho C_p B'_x \rangle}{\partial \xi} + \frac{\partial \langle \rho C_p B'_z \rangle}{\partial z}\right)\right]\left(\frac{\partial p}{\partial z} - \theta\right) + \frac{M_m}{M_f}\frac{1}{R^{1/2}}\frac{\partial D^u_{xz}}{\partial \xi}
\end{aligned}
\tag{I.6}
$$

in which ϵ is the ratio of the mesoscale to the macroscale. The quantities CX, CZ, CVX and CVZ are all computed by uisng the results from the previous iteration step $(k-1)$. The consistency of (I.3) is $O(\Delta\tau)$. In the actual computations, $\Delta\tau = 0.002$ and $\Delta\xi = \Delta z \leq 0.05$ have been used. Accordingly both of the consistencies $O(\Delta\xi^2, \Delta z^2, \Delta\xi\Delta z)$ and $O(\Delta\tau)$ are $O(10^{-3})$.

If we substitute the finite difference formulas (I.1) - (I.2) and (I.4) to (I.6) into (I.3), multiply by $(\Delta\xi)^2/{}^k[(\langle m' \rangle + D^e_{xz})/R]^{n+1}_{i,j}$ and rearrange, the following algebraic equations is obtained.

$$
\begin{aligned}
&{}^{k-1}H11^{n+1}_{i,j} \quad {}^k\theta^{n+1}_{i-1,j-1} + {}^{k-1}H12^{n+1}_{i,j} \quad {}^k\theta^{n+1}_{i-1,j} + {}^{k-1}H13^{n+1}_{i,j} \quad {}^k\theta^{n+1}_{i-1,j+1} \\
&{}^{k-1}H21^{n+1}_{i,j} \quad {}^k\theta^{n+1}_{i,j-1} + {}^{k-1}H22^{n+1}_{i,j} \quad {}^k\theta^{n+1}_{i,j} + {}^{k-1}H23^{n+1}_{i,j} \quad {}^k\theta^{n+1}_{i,j+1} \\
&{}^{k-1}H31^{n+1}_{i,j} \quad {}^k\theta^{n+1}_{i+1,j-1} + {}^{k-1}H32^{n+1}_{i,j} \quad {}^k\theta^{n+1}_{i+1,j} + {}^{k-1}H33^{n+1}_{i,j} \quad {}^k\theta^{n+1}_{i+1,j+1} \\
&= {}^kHR^{n+1}_{i,j} \quad {}^k\theta^n_{i,j}
\end{aligned}
\tag{I.7}
$$

where the coefficients are given by

$$
\begin{aligned}
&H11 = -H13 = \frac{(\Delta\xi)^2}{(\Delta z)^2} D^e_{zz}\left(\frac{D^e_{xz}}{R}\right), \quad H12 = 1 - H121 \\
&H21 = H211 - H212, \quad H22 = -2 - 2H211 - H221, \quad H23 = H211 + H212 \\
&H31 = -H11, \quad H32 = 1 + H121, \quad H33 = H11, \quad HR = H221
\end{aligned}
\tag{I.8}
$$

in which

$$H121 = \frac{\Delta\xi}{2} CX \Big/ \left(\frac{D^s_{zz}}{R}\right), \quad H211 = \frac{(\Delta\xi)^2}{(\Delta z)^2} D^s_{zz} \left(\frac{D^s_{zz}}{R}\right)$$
$$H212 = \frac{(\Delta\xi)^2}{2\Delta z} CZ \Big/ \left(\frac{D^s_{zz}}{R}\right), \quad H221 = \frac{(\Delta\xi)^2}{\Delta\tau} \Big/ \left(\frac{D^s_{zz}}{R}\right) \tag{I.9}$$

The coefficients in (I.8) and (I.9) are determined in terms of the previous iteration step $(k-1)$ values.

The consolidation equation (6.1.12) becomes after using (I.1) and (I.2) in finite difference form as

$$\begin{aligned} {}^k p^{n+1}_{i-1,j} + C21\, {}^k p^{n+1}_{i,j-1} + C22\, {}^k p^{n+1}_{i,j} + C23\, {}^k p^{n+1}_{i,j+1} + {}^k p^{n+1}_{i+1,j} \\ = CR\left({}^{k-1}\theta^{n+1}_{i,j+1} - {}^{k-1}\theta^{n+1}_{i,j-1}\right) \end{aligned} \tag{I.10}$$

where

$$C21 = C23 = \frac{(\Delta\xi)^2}{(\Delta z)^2}, \quad C22 = -2 - 2\frac{(\Delta\xi)^2}{(\Delta z)^2}, \quad CR = \frac{(\Delta\xi)^2}{2\Delta z} \tag{I.11}$$

The finite difference equation for the stream function ψ in (6.1.28) is the same as (I.10) and (I.11) except that $CR = -(\Delta\xi)/2$ and is omitted.

The equilibrium equation (6.1.23) is similarly written in finite difference form. For the x-component, after using (I.1) and (I.2), multiplying by $(\Delta\xi)^2$ and collecting temrs at the same nodes, we obtain

$$\begin{aligned} &XU12 \quad u^{n+1}_{i-1,j} + XW11 \quad w^{n+1}_{i-1,j-1} + XW13 \quad w^{n+1}_{i-1,j+1} \\ &+XU21 \quad u^{n+1}_{i,j-1} + XU22 u^{n+1}_{i,j} + XU23 \quad u^{n+1}_{i,j+1} \\ &+XU32 \quad u^{n+1}_{i+1,j} + XW31 \quad w^{n+1}_{i+1,j-1} + XW33 \quad w^{n+1}_{i+1,j+1} = XR \end{aligned} \tag{I.12}$$

where

$$XU12 = XU32 = \frac{a_1}{R}, \quad XW11 = -XW13 = -XW31 = XW33 = \frac{a_4 + a_6}{R}\frac{\Delta\xi}{4\Delta z}$$
$$XU21 = XU23 = a_6 \frac{(\Delta\xi)^2}{(\Delta z)^2}, \quad XU22 = -2XU12 - 2XU21$$
$$XR = \frac{c\alpha''_{zz}}{Ra' R^{1/2}} \frac{\Delta\xi}{2}(p^{n+1}_{i+1,j} - p^{n+1}_{i-1,j}) + \frac{c\beta''_{zz}}{Ra' R^{1/2}} \frac{\Delta\xi}{2}(\theta^{n+1}_{i+1,j} - \theta^{n+1}_{i-1,j}) \tag{I.13}$$

The z-component also becomes

$$\begin{aligned} & ZU11 \quad u^{n+1}_{i-1,j-1} + ZU13 \quad u^{n+1}_{i-1,j+1} + ZW12 \quad w^{n+1}_{i-1,j} \\ & +ZW21 \quad w^{n+1}_{i,j-1} + ZW22 \quad w^{n+1}_{i,j} + ZW23 \quad w^{n+1}_{i,j+1} \\ & +ZU31 \quad u^{n+1}_{i+1,j-1} + ZU33 \quad u^{n+1}_{i+1,j+1} + ZW32 \quad w^{n+1}_{i+1,j} = ZR \end{aligned} \tag{I.14}$$

where

$$\begin{aligned} & ZU11 = -ZU13 = -ZU31 = ZU33 = \frac{a_4 + a_6}{R} \frac{\Delta z}{4\Delta \xi} \\ & ZW12 = ZW32 = \frac{a_6}{R} \frac{(\Delta z)^2}{(\Delta \xi)^2} \\ & ZW21 = ZW23 = a_2, \quad ZW22 = -2ZW21 - 2ZW12 \end{aligned} \tag{I.15}$$

The boundary conditions also should be written in finite difference form. They have been given in Appendix D of Part I and are not repeated here.